Doctoral Dissertation
Doctoral Program in Energetics (34th Cycle)

Urban-Scale Energy Modeling to Promote Smart Solutions for Sustainable and Resilient Cities

Valeria Todeschi
* * * * * *

Supervisors
Prof. Guglielmina, Mutani, Supervisor
Prof. Marco Carlo, Masoero, Co-Supervisor

Doctoral Examination Committee:
Prof. Dr. Davide Astasio Garcia, Università degli studi di Roma 'La Sapienza', Italy
Dr. Pietro Florio, Joint Research Centre (JRC), Italy

Politecnico di Torino
March 5, 2022

I hereby declare that, the contents and organisation of this dissertation constitute my own original work and does not compromise in any way the rights of third parties, including those relating to the security of personal data.

Valeria Todeschi
Turin, March 5, 2022

"*All models are wrong,*
but some are useful."
George E. P. Box

Summary

The development of Urban-Scale Energy Models (USEMs) at the district level is currently the goal of many research groups due to the increased interest in evaluating the impact of energy efficiency measures in cities. These models are useful to explore energy efficiency solutions at urban scale and to quantitatively assess retrofit strategies and energy supply options. This can lead to more effective energy policies and management of energy supply and demand. USEMs can be used to obtain lower energy demand identifying the available renewable energy sources (RESs) that meet the actual and future energy demand. Since the relationship between urban form and buildings affects energy performances (EPs), the combined use of urban planning, retrofit interventions, and RESs can optimize the EP in cities.

A review of the literature reveals that USEMs can consider a few of the variables that influence energy consumption, especially as regards big urban contexts. Research needs to be dedicated to the construction of data-driven and process-driven models that consider several possible factors to describe the urban environment, and an approach needs to be developed that is flexible and can easily be applied to different contexts.

Overall, USEMs are complex and they need simplifying to be an effective decision-making tool. The aim of this doctoral research is to investigate and develop new energy models at urban scale to promote a smarter use of energy and to meet energy demand with more efficient renewable energy systems, especially to help public administrations define policies suited to existing built environments.

Within this research, energy models at urban scale were designed for different European cities. Through the use of a place-based approach, these models can estimate energy consumption, energy production and energy productivity from RESs related to a specific territory, considering their spatial distribution and local environmental impact. Depending on the availability of data and on the type of analysis needed, different methods and techniques can be used to develop USEMs.

Firstly, simplified data-driven models, which use bottom-up and top-down approaches, were designed using highly detailed data at building level and aggregated data at municipal level, respectively. Annual energy models based on the Geographic Information System (GIS) were created and applied to different territorial contexts in order to evaluate the main energy-related variables and to characterize the energy performance of buildings.

Subsequently, new engineering models (i.e., process-driven model) at district scale were created by considering variables at building, block of buildings and neighborhood scale, and the morphology of the built environment. Urban energy balance models were introduced at monthly and hourly time-steps using the support of GIS tools. The energy consumption for space heating and space cooling was estimated by considering the thermal balance of the built environment for different territorial contexts and climate conditions.

A monthly engineering model was created to evaluate the EP of the buildings connected to the district heating network in Turin, Italy. In order to evaluate the thermal peak loads, an hourly model was developed. A dynamic urban-scale energy model was designed according to the current standards used for the EP of buildings. Applying this dynamic model, the optimal shape of the buildings with low energy consumption for space heating and cooling and high solar energy production has been defined for different urban neighborhoods.

Based on the dynamic urban-scale energy model, a hybrid model was designed using a data-driven correction with a Random Forest algorithm. The new model was used to study the impact of the COVID-19 pandemic on the energy performance of the residential buildings in three neighborhoods in the Canton of Geneva, Switzerland.

Place-based energy models were also used to evaluate the feasibility of establishing energy communities, grouping producers, users and prosumers. A methodology to promote self-consumption and self-sufficiency using the integration of solar energy with photovoltaic-battery systems and considering the new economic incentives in Italy was developed.

The shape of cities, the characteristics of outdoor surfaces and the EP of the built environment also influence the thermal comfort conditions and the livability of urban spaces. Smart solutions for the city of Turin were identified in order to mitigate the urban heat island effect and improve thermal comfort conditions. The applicability of smart solutions was analyzed to support the review of the Building Annex Energy Code of Turin. This analysis was performed within the 'Re-Coding' project aimed at updating the current building code of the city, undertaken by the Research Centre Future Urban Legacy Lab.

In conclusion, this doctoral research proposes different place-based approaches to design energy models. These models can investigate energy consumption, productivity from RESs and energy retrofit scenarios. The goal is to help stakeholders, urban planners and policy makers to plan sustainable cities and smart energy systems taking into account the real built environment, the socio-economic characteristics of the population, financial incentives and energy polices.

Acknowledgments

I would first to thank my supervisor Guglielmina Mutani for her continuous support and for granting me the possibly of pursuing my research interests in the energy modeling field. Special thanks also go to my co-supervisor Marco Masoero for his guidance throughout the PhD period.

I am grateful to the doctoral examination committee Prof. Dr. Davide Astasio Garcia and Dr. Pietro Florio for their detailed, constructive, and useful review.

I am thankful to the Future Urban Legacy Lab (FU*LL*). In particular to Matteo Robiglio for giving me the opportunity to develop my doctoral research within the laboratory, and to the whole team of FU*LL* for the scientific support.

I am really thankful to the Joint Research Centre (JRC) and to the Energy Efficiency and Renewable team. In particular to Christian Thiel for giving me the opportunity to do the internship, to Paolo Bertoldi for his support and guidance, and to Marina Economidou for her scientific support, the friendly discussion and valuable advice.

It is my pleasure to thank to *École Polytechnique Fédérale de Lausanne* (EPFL) and to the Solar Energy and Building Physics Laboratory (LESO-PB). I am thankful to Jean-Louis Scartezzini for giving me the opportunity to carry on my doctoral research at the LESO-PB, to the whole team of LESO-PB, in particular to Kavan Javanroodi, Roberto Castello, Nahid Mohajeri Pour Rayeni for the scientific support and the profuse expertise.

I am grateful to the district heating company of the city of Turin, IREN, in particular to Marco Gorzegno and the whole district heating team, for their collaboration in collecting the energy data.

I would like to thank my officemates Marco and Paolo, and my colleague Gabriele, for the everyday-life support and confrontations.

And finally, the most important acknowledgment goes to my parents and my brother Andrea for their daily support and for always helping me achieve my goals.

Contents

Chapter 4

Chapter 5

Nomenclature

Symbols and units

A	Area	m^2
ach	Air changes per hour	h^{-1}
A_{NIR}	Near infrared albedo	-
b	Correction factor for an unconditioned adjacent space	-
BCR	Building coverage ratio	m^2/m^2
BD	Building density	m^3/m^2
BH	Building height	m
C	Effective heat capacity of a conditioned space	J/K
c	Specific heat capacity	J/kg/K
d	Layer/wall thickness	m
EER	Energy efficiency ratio	-
E_r	Percentage relative error	%
F	Reduction factor	-
fn	Conversion coefficient for the gross-net floor area	-
G	Number of days of the considered calculation period	-
g	Total solar energy transmittance	-
H	Heat transfer coefficient	W/K
H/H_{avg}	Relative height	m/m
H/W	Height-to-width ratio or canyon effect	m/m
h	Heat transfer surface coefficient	$W/m^2/K$
I_{sol}	Solar irradiance	W/m^2
LST	Land surface temperature	°C, K
MAE	Mean absolute error	-
MAPE	Mean absolute percentage error	%

MOS	Main orientation of the streets	-
NDVI	Normalized difference vegetation index	-
P	Installed electric power	kW
PET	Physiologically equivalent temperature	°C
PMV	Predicted mean vote	-
PPD	Predicted percentage dissatisfied	%
Q	Energy	Wh
q_v	Volumetric airflow rate	m^3/s
R	Thermal resistance	m^2K/W
R^2	Coefficient of determination	-
RE	Relative error	-
SET	Standard effective temperature	°C
Su	Heated floor area per dwelling	m^2
S/V	Surface-to-volume ratio	m^2/m^3
SVF	Sky view factor	-
T	temperature	°C, K
U	Thermal transmittance	$W/m^2/K$
UTCI	Universal thermal climate index	°C
V	Volume	m^3
WWR	Window-to-wall ratio	%
α	Solar radiation absorption coefficient	-
β	Solar declination	◦
ξ	Percentage of shadow on the vertical wall	%
ε	Emissivity of a surface for long-wave thermal radiation	-
η	Efficiency for space heating and/or domestic hot water, utilization factor	-
ρ	Density	kg/m^3
τ	Time	h or s
Φ	Heat flow rate, thermal power	W

Subscripts

a	Air
adj	Adjusted
avg	Average
B	Internal structures of the building, furniture, and air
e	External
E	Opaque envelope
er,i	Hot water supply
F	Frame
f	Floor
g	Ground
G	Transparent envelope
gl	Glazing, glazed element
gn	Gains
ht	Heat transfer
H	Heating
H,nd	Energy needs for space heating
i	Internal
int	Internal heat gains
m	Mass-related
mrt	Mean radiant
nd	Needs
o	Incoming cold water
ob	Obstacles
op	Opaque
r	Radiative
se	External surface
sh	Shading
sol	Solar

tr	Transmission
v	Volume
ve	Ventilation
W	Water
w	Window
W,nd	Energy needs for domestic hot water

Acronyms

AL	Appliances and lighting
CDD	Cooling degree days
CEC	Citizens energy community
CS	CitySim
DBT	Territorial database
DHN	District heating network
DHW	Domestic hot water
DSM	Digital surface model
DTM	Digital terrain model
EC	Energy community
EE	Energy efficiency
EEM	Energy efficient mortgage
EEOs	Energy efficiency obligations
EN	Engineering model
EP	Energy performance
EPC	Energy performance certificate
EPG	Energy performance guarantee
ES	Energy savings
ESCO	Energy services company
EE FITs	Energy efficiency feed-in tariffs

GA	Green areas
GHG	Greenhouse gas
GIS	Geographic information system
HDD	Heating degree days
ID	Identification code
Ind	Industrial buildings
LGBM	Light gradient boosting machine
ML	Machine learning
Mun	Municipal buildings
NZEBs	Nearly zero-energy buildings
OP	Over-production
OSM	Open street map
OSSs	One-stop-shops
PACE	Property assessed clean energy
PV	Photovoltaic
PVGIS	Photovoltaic geographical information system
RECs	Renewable energy communities
Res	Residential buildings
RES	Renewable energy source
RF	Random forest
RVT	Relief visualization toolbox
SC	Space cooling
SCI	Self-consumption index
SEAP	Sustainable energy action plan
SH	Space heating
SQ	Squares
SSI	Self-sufficiency index
ST	Solar thermal
TC	Total consumption

Ter	Tertiary buildings
TP	Total production
TS	Thermodynamic system
UC	Urban courtyards
UD	Uncovered demand
USEM	Urban-scale energy modeling
UHI	Urban heat island
VAT	Value added tax
WS	Weather station

List of Tables

List of Figures

Chapter 1

Introduction

1.1 Research background

1.1.1 Context

Today 54% of the world's population resides in urban areas and in 2050 the projections are for 66%. In Italy this percentage is 68%, and is expected to increase in the future [1]. While the transportation and industrial activities can differ among cities, buildings are a common and key-contributor to reducing greenhouse gas (GHG) emissions and promoting a more sustainable use of energy [2]. The energy consumption of buildings has a significant impact on urban sustainability and climate change, and these phenomena are more pronounced in high-density urban contexts. Cities are responsible for 75% of GHG emissions, and the building and transport sectors are the main contributors [3].

New urban development is an opportunity to combat climate change, and to create new livable and energy efficient urban areas in order to obtain better environmental sustainability [4]. Cities around the world have begun to set targets for the reduction of GHG emissions in order to achieve low environmental impacts and to address climate change [5].

In recent years, the obtained data have showed that global energy-related CO_2 emissions rose in 2018, increasing by 1.7%, following a 1.6% increase in 2017 from the previous year. The building sector accounted for about 28% of the total energy-related CO_2 emissions [6]. The 97% of the EU building stock not being energy efficient and only 0.2% of EU residential buildings having undergone important retrofitting measures. To achieve energy and climate targets for 2030, the improvement of energy performance (EP) of buildings and the reduction of energy consumptions is a fundamental point in European policies [7].

With the European Green Deal, the European Union is increasing its climate ambition and the aim is to make its economy sustainable. Some key actions are the decarbonization of the energy sector and ensuring the buildings are more energy

efficient by promoting low-carbon strategies and energy-efficient technologies. Therefore, cities have to encourage a resilient development improving building EP and encouraging policy makers, planners and architects to work together in delivering a sustainable built environment [8,9].

In Italy, and in most European countries, energy policies are focused on two prior actions to reduce energy consumption and GHG emissions: an improvement in energy efficiency (EE) and an exploitation of the available renewable energy sources (RESs) [10]. A number of solutions may be adopted, such as the distribution of heat through a district heating network (DHN), the use of building envelopes and urban spaces to produce energy from RESs and a mix of user types with a different daily energy load in the same areas. The limited availability of RESs in urban contexts leads to the need for a combination of these solutions, with strategies to reduce, manage and monitor energy uses [11]. The balance of energy demand and supply should be at the smallest scale possible: at a building, block of buildings or district scale rather than at an urban or territorial scale [12]. However, there is no one-solution strategy in energy planning at an urban or territorial scale, because cities, built environments and population are different.

Urban-scale energy models (USEMs) can be of help in describing the use of energy in a real context, and they can take into account cultural differences that may influence the choice of energy retrofitting measures or the use of RESs. These models can also be used to evaluate future scenarios, and the impact of potential retrofitting measures as well as to identify the critical areas where a priority of interventions is required [13].

The EP of buildings is influenced by several factors, such as the building shape and their typological characteristics, the heating and cooling system efficiencies, the type of users and the behaviour of the people therein, but also by the urban context and the local climate [14]. The USEMs are fundamental to simulate energy consumption at urban scale taking into account not only characteristics at buildings level, but also the built-up urban context [15]. USEMs usually utilize three methods: process-driven (physical), data-driven (statistical and artificial intelligence) and hybrid [16]. It is possible to identify a reliable energy model if the input database is accurate and complete, and if the results can be compared with wide-ranging data on measured energy consumptions to validate the model [5]. The main problem of these models is that they need to manage a large number of data which may have different levels of accuracy and scales. Furthermore, they should also process data quickly [17].

Geographic Information Systems (GIS) can georeference all the information on energy-related variables at a territorial scale, and they can play a key role in the identification and application of energy models at an urban scale [18]. GIS tools can also help decision-makers and urban planners by offering them the opportunity to visualize realistic and multilayer representations of urban energy consumptions and spatiotemporal parameters, as well as of performing qualitative and quantitative

analysis with different scenarios for future smart and more sustainable cities [19,20].

1.1.2 Existing energy models and tools

The research is moved from building to urban scale and the development of USEMs is currently the goal of many research groups. Different energy and climate tools exist in the literature capable of running simulations at urban level, simulating space heating (SH) and space cooling (SC) energy consumptions, assessing energy productivity, and quantifying the outdoor thermal comfort conditions [21–23].

The most common tools able to estimate the building stock energy demand considering the building characteristics, the local climate conditions and the urban morphology are: CEA (City Energy Analyst), CityBES (City Building Energy Saver), CitySim, UMI (Urban Modeling Interface) and SimStadt [24–27]. UMI and CitySim are also able to investigate the outdoor urban comfort conditions. Some of the tools allow for city-scale simulations to be performed, enabling the impact of large-scale energy policies to be assessed. The analysis detail is less than other tools that simulate energy consumption at a district scale, providing more detailed information [23].

CityBES is an open web platform based on City Building Energy Saver that uses EnergyPlus. It allows to quickly simulate city-scale building energy consumption and to support EE analysis [25,28].

CitySim is a large-scale building energy simulation tool developed at EPFL (Ecole Polytechnique Fédérale de Lausanne) that includes a solver module (CitySim Solver) and a graphical interface (CitySim Pro) [11]. The simulation is based on a simplified thermal-electrical analogy and the aim is to support the more sustainable planning of urban environment [29,30]. It is used to quantify the energy consumption of buildings at district scale and the cooling effect of vegetation on SC consumption in urban environment by shadowing and evapotranspiration. CitySim is also able to estimate the mean radiant temperature (T_{mrt}) at urban level [31].

UMI is a building energy performance simulation tool based on the EnergyPlus engine that considers the mutual shading of buildings and the daylighting at neighbourhood scale. With the support of UWG (Urban Weather Generator) tool is able to evaluate outdoor thermal comfort conditions [32,33].

SimStadt is an urban modeling platform based on a dynamic physical energy model of building for simulating the energy demand of cities based on CityGML standard [34–36].

In conjunction with the reduction of the use of energy in urban spaces, there are improvements in the outdoor thermal comfort conditions. Today, there are several climate tools able to quantify the outdoor thermal comfort conditions in an urban environment, the main ones are: ENVI-met, RayMan, SOLWEIG (SOlar and

LongWave Environmental Irradiance Geometry model), UMI and CitySim [37–39].

ENVI-met is a tool that simulates local climate and thermal comfort conditions in urban environment using a holistic approach. Biomet is a post-processing tool used to calculate human thermal comfort indexes based on ENVI-met simulation results (e.g., T_{mrt}). Biomet can evaluate the impact of green infrastructures by calculating the following thermal comfort indexes: the predicted mean vote (*PMV*), the predicted percentage dissatisfied (*PPD*), the physiologically equivalent temperature (*PET*), the standard effective temperature (*SET*), and the universal thermal climate index (*UTCI*).

RayMan is a free tool able to evaluate thermal indicators used in the assessment of thermal comfort conditions (i.e., T_{mrt} *PET* and *PMV*) [40].

SOLWEIG is a free tool of QGIS based on shortwave and longwave radiative flows model able to simulate outdoor thermal comfort conditions [39]. It is an extension of UMEP (Urban Multi-scale Environmental Predictor), an urban multi-scale environmental predictor used for a variety of applications related to outdoor thermal comfort, energy consumption at urban scale, and climate changes mitigation [41]. SOLWEIG estimates spatial variations of 3D radiation fluxes and T_{mrt} in complex urban settings by calculating *PET* and *UTCI*.

Following a few studies regarding approaches (top-down, bottom-up, statistical), instruments (CityGML, Rhino, Ladybug tools for Grasshopper) and tools (CitySim, GIS, UMI) used to support the creation of USEMs are reported. Chen et al. [25] investigated the energy consumption considering buildings characteristics and shading buildings, shared walls and wheatear conditions. They introduced the CityBES tool to assess energy retrofit analysis, identifying EE measures to improve EP of a large number of buildings in cities. A bottom-up modeling approach for urban-scale analysis was developed by Hedegaard et al. [42], and the district heating consumptions of residential buildings were investigated using smart-meter data, building characteristics, and climate conditions. Their model was able to analyse the demand response potential investigating how to reduce the peak. USEMs have to be also take into consideration the presence of vegetation and trees, which affect the urban microclimate. Perera et al. [43] proposed an approach that, with the use of CitySim tool, allows to analyse the peak and the annual demand related to the urban climate. They found that neglecting the urban climate could cause a drop in power reliability. Buckley et al. [44] used GIS data to defined input data needed to simulate energy use with the UMI tool. The authors tested the impact of energy retrofitting policies at neighbourhood level considering 9,000 residential buildings in a Dublin. The methodology presented is reproducible elsewhere in Europe where building archetypes are available.

The main problem of these tools is that frequently require a large amount of input data, which is not always available, or a detailed model of each building is

needed. Additionally, these tools tend to have long simulation times, which can grow rapidly as more elements are added to the scene.

1.2 Research gap

A review of the literature reveals that the problem of existing energy models tools is that they require a large amount of input data and often some information are not available. In addition, these energy tools only consider a few of the variables that influence consumption, especially as regards the urban context [16]. USEMs should consider not only building and climate characteristics, but also the urban morphology, occupancy behaviour, social and economic conditions, and local regulation. In addition, existing tools are able to simulate a group of buildings, this is not possible for an entire city due to excessive simulation times.

Therefore, existing models and tools have limitations in representing a realistic urban energy distribution able to assess the EP at neighbourhood scale [45]. The simulation programs consist of an assemblage of different sub-models [21] and are time-consuming processes. Research should be dedicated to the construction of place-based models that considers several possible factors to describe the urban environment, to have a flexible, fast and easy approach that may be applied to different contexts.

Another limit in the design of USEMs is the model validation. Due to privacy concerns, energy data, especially hourly data, are not available. So the trend is to use simulated data from other existing tools that have already been validated.

In summary, the difficulty is to create models that are simple and easily applicable to different urban contexts, but at the same time sufficiently accurate to provide reliable results.

1.3 Research objectives and novelty

The aim of this doctoral research is to investigate and design new energy models at urban scale. It proposes new methods for energy simulation on an urban scale, with the aim of overcoming the main limitations of existing energy models and tools. The place-based models presented use GIS tools and, as they are simplified models, the simulation times are significantly lower than with existing models and tools. Even if they are simplified models, they are sufficiently accurate and able to simulate energy consumption from the building block scale to the city scale. They use open data available for urban planning purposes, so are easily applicable to different urban contexts. To sum up, the main objectives of this research are the following:

- To evaluate energy consumption driven variables by using sensitivity analysis in order to assess the EP of buildings at the urban level. Some variables can be defined as fundamental and other variables can be added to improve the accuracy of the energy simulations.

- To define a procedure to harmonize and process the input data using the existing open-source databases available for almost every city in the world (e.g. municipal technical maps and digital elevation models).
- To design and optimize new energy-use models at urban scale using data-driven and process-driven methods.
- To assess the accuracy of the models using the real energy consumption data available for different European cities regarding a variety of building stocks, users and climates, and to test their flexibility.
- To analyze the relationship between urban morphology and the EP of buildings with implications for solar availability in urban areas, to optimize solar gains and to harness solar energy as a renewable resource for local energy production in densely built-up contexts.
- To promote the use of smart green solutions (e.g. green roofs) with financial mechanisms and incentives, and to identify effective energy policies, considering the real characteristics of the buildings, the population and the urban morphology (e.g. for building codes).
- To develop an "Energy Platform" for cities as a support decision-making tool, able to quantitatively assess retrofit strategies and their impacts on the territory.

1.4 Thesis structure

The doctoral thesis is divided into seven chapters and structured as follows. This chapter introduces the research background and gap. An overview of the existing urban-scale energy tools are presented. The second part describes the objectives, novelty and contributions of this research. Part of the work related to this chapter is published in the journals *Energy Efficienc*y [46] and *Sustainability* [47].

Chapter two introduces place-based energy models for energy consumption, production, productivity from RESs and energy efficiency scenarios. Approaches, methods and data used to design these models are described. The work related to this chapter is published in the journals *Energy Efficienc*y [13,46] *International Journal of Heat and Technology* [15], and in the report edited by *ENEA* (*Italian National Agency for New Technologies, Energy and Sustainable Economic Development*) [48].

Chapter three describes in detail place-based energy consumption models designed for different cities. "Annual data-driven model" section introduces simplified statistical models applied to the city of Turin in Italy. The work related to this section is presented at the *International Scientific Conference CISBAT* on *Future Buildings & Districts – Energy Efficiency from Nano to Urban Scale* in September 2017 [12]. The annual model for Turin was compared with other energy simulation tools applied to Essen in Germany and to Geneva in Switzerland [11]. The main topic of this doctoral research is the development of engineering models

that are more complex. Engineering monthly models for SH and domestic hot water (DHW) consumptions are designed for Turin and presented in "Monthly process-driven model" section. The work related to this section is published in the journal *Energy Efficienc*y [46]. Hourly models are designed distinguishing process-driven (i.e., engineering) models, data-driven models and hybrid models. Regarding process-driven models, a first version of a place-based dynamic engineering model is presented at the *38th International Conference UIT* on *Heat Transfer Conference* in June 2021 [49]. The model is optimize by introducing three thermodynamic systems in the urban thermal balance. "Hourly process-driven models" section presents the last version of this model for SH and SC published in the journal *Sustainability* [50] and presented at the *38th International Conference UIT on Heat Transfer Conference* in June 2021 [49]. "Hourly data-driven models" section introduces machine learning techniques and a light gradient boosting machine (LGBM) model is designed for the city of Fribourg in Switzerland. The work related to this section is published in the journal *Sustainability* [47]. Finally, a hybrid model that combines the place-based engineering model and machine learning techniques is described in "Hourly hybrid models" section. The work related to this section is submitted to the journal *Sustainable Cities and Society* [51].

Chapter four introduces place-based energy production and productivity models from RESs. A focus on solar energy is carried out, and the main tools used to investigate the solar energy potential in cities are described. Consumption models are implemented with productivity models to evaluate the potential use of solar thermal (ST) and photovoltaic (PV) technologies. A monthly model is presented in the first part of the chapter, and some scenarios are assessed using ST collectors and PV technologies. The work related to this section is published in the journal *Tecnica Italiana - Italian Journal of Engineering Science* [52]. Subsequently, hourly models are developed by analyzing the feasibility of PV technologies and storage systems. In this context, the possibility of establishing energy communities is investigated. The work related to this part is published in the journals *Energies* [53] and *International Journal of Heat and Technology* [54].

Chapter five introduces EE models and low-carbon scenarios for Turin. Energy retrofit measures are defined and the energy savings is evaluated by applying monthly data-driven and process-driven models. "Energy retrofit models" section is presented at the *10th International Conference IEECB&SC on Improving Energy Efficiency in Commercial Buildings and Smart Communities* in March 2018 [55] and is published in the journal *Energy Efficiency* [13]. "Smart rooftop solutions and green infrastructures" section describes the impact of green and cool roofs in terms of energy and environmental benefits. The work related to this section is published in the journal *Applied Sciences* [56], and in the journal *International Journal of Sustainable Development and Planning* [57]. The last section on "Building shape and urban form" investigates how the urban form affect the EP of buildings and the solar potential. The results of this assessment are presented at the *3rd International IEEE Conference AND workshop in Óbuda CANDO on Electrical and Power*

Engineering in November 2020 [58] and at the *38th International Conference UIT on Heat Transfer Conference* in June 2021 [49]. Finally, the outdoor thermal comfort conditions are investigated as a function of the urban form, and this analysis is published in the journal *Tecnica Italiana - Italian Journal of Engineering Science* [59].

Chapter six introduces EE policies and financial instruments for buildings. The first part describes in detail EE policies of EU starting from the 70s until today. In the second part, financial and fiscal instruments are described distinguishing loans, grants, subsidies and fiscal instruments. Finally an overview of public and private schemes in Europe is provided. The work related to this chapter is published in the journals. *Energy & Buildings* [60] and *WIREs Energy & Environment* [61], and in the report edited by JRC (Joint Research Center) [62].

Chapter seven summaries the main results of this doctoral research and introduces the future outlook.

The author would like to acknowledge the co-authors for their contributions. Special thanks are addressed to Roberto Boghetti, PhD student in Electrical Engineering at the EPFL, for his help in the energy simulations carried out in CitySim and in the development of the machine learning model for the city of Fribourg presented in Chapter 3; to Paolo Marocco, assistant professor in Energetics at the Politecnico di Torino, for designing the optimization model using grid connected PV-battery systems applied to the city of Turin presented in Chapter 4; to Elisa Guelpa, assistant professor in Energetics at the Politecnico di Torino, for designing and applying the fluid-dynamic model of the DHN to the city of Turin presented in Chapter 5; to Silvia Santantonio PhD student in Energetics at the Politecnico di Torino, for her help in the energy simulations carried out in CitySim presented in Chapter 5; to Simone Beltramino PhD student in Urban and Regional Development at the Politecnico di Torino, for his help in the outdoor thermal comfort simulations carried out in Envi-met presented in Chapter 5; to the whole team of the JRC for supporting the review and investigation on energy efficiency policies and financial instruments in Chapter 6.

Chapter 2

Overview of place-based energy models

2.1 Chapter overview

Energy consumption, production and productivity models allow to evaluate the distribution of energy at different territorial scales. With the use of the place-based methodology supported by GIS tools, it is possible to consider not only the variables at building scale, but also the urban context, which significantly affects the EP of buildings. In addition to these factors, the climatic conditions and the characteristics of the population are taken into consideration.

There are two approaches used to design USEMs: top-down and bottom-up. Depending on the availability of the data and the type of analysis to be carried out, the proper approach is selected. Secondly, the technique to be used is identified, either data-driven methods or process-driven methods, or hybrid methods which combine both.

There are a number of simulation energy tools and models, such as CEA, CityBES, CitySim, SimStadt, UMI, that are able to estimate building stock energy demand considering the weather data and urban parameters [25,26].

The existing models and tools can accurately simulate the EP at the block of buildings or neighbourhood scale, but not at the city level. In general, these models need the support of other combined tools, do not interact with the existing open databases and are also paid for. They used Rhino and/or EnergyPlus, which are much more complex and time consuming especially at urban scale (these tools were developed for application at building scale). Instead, the use of place-based methodologies supported by GIS tools is very flexible consenting to easily manage data at different territorial levels.

Therefore, this doctoral research investigates how to design USEMs with a GIS-based approach. Figure 1 describes the structure of Chapter 2. This chapter defines how to design place-based energy models using different approaches (i.e.,

top-down and bottom-up) with the support of GIS tools. These models give an important contribution in the assessment of the EP of buildings at urban scale, by analysing the energy consumption, production, productivity from RESs and future scenarios. The energy-related variables used as input data and the main output of these models are described in the last part of the chapter.

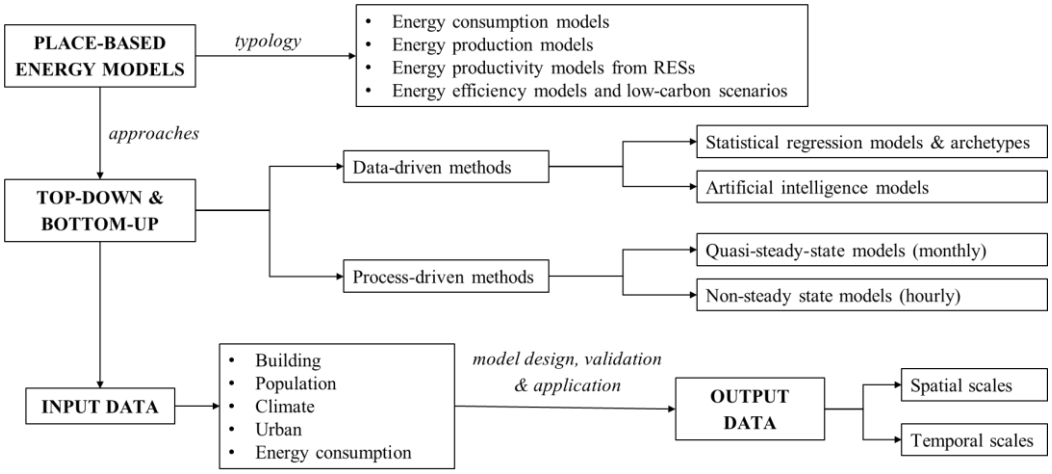

Figure 1. Flowchart of Chapter 2.

2.2 Place-based energy models

USEMs have to manage a large amount of data, which is generally inaccurate compared to the data of building scale models. On a territorial scale, information is not always available and it is usually provided on heterogeneous scales. Place-based models, that use GIS tools, allow to manage information from different sources and scale by overlapping databases and creating a complete territorial database (DBT). Using GIS tools, it is possible to quantify the energy consumption related to human activities in a specific territory, considering socio-economic features of local population. Energy demand of a territory can be compared with the thermal and electrical energy productivity from RESs available locally. Future scenarios based on EE measures can be defined, selecting the most effective energy policies and financial instruments able to promote the sustainable development of the territory.

Place-based energy models can be classified as energy consumption models, energy production models, and energy productivity models from RESs. It is possible, with a combined use of energy consumption, production and productivity models, to design EE models and define low-carbon scenarios in which energy security, sustainability and affordability are promoted for a more resilient city [15].

Figure 2 describes the main steps necessary to create place-based models. The first phase is the collection of input data regarding buildings, climate conditions, characteristics of the terrain and population, characteristics of energy production systems/plants, and the identification of energy sources available locally. According to the type of input data, two approaches (i.e., top-down and bottom-up) can be used to create energy models at city scale (phase 2). Through the use of GIS

tools, all constrains on the territory are taken into consideration to assess the applicability of EE measures and the use of RESs. In the last phase, different EE scenarios are investigated and their impact from an energy, environmental and economic point of view can be analysed.

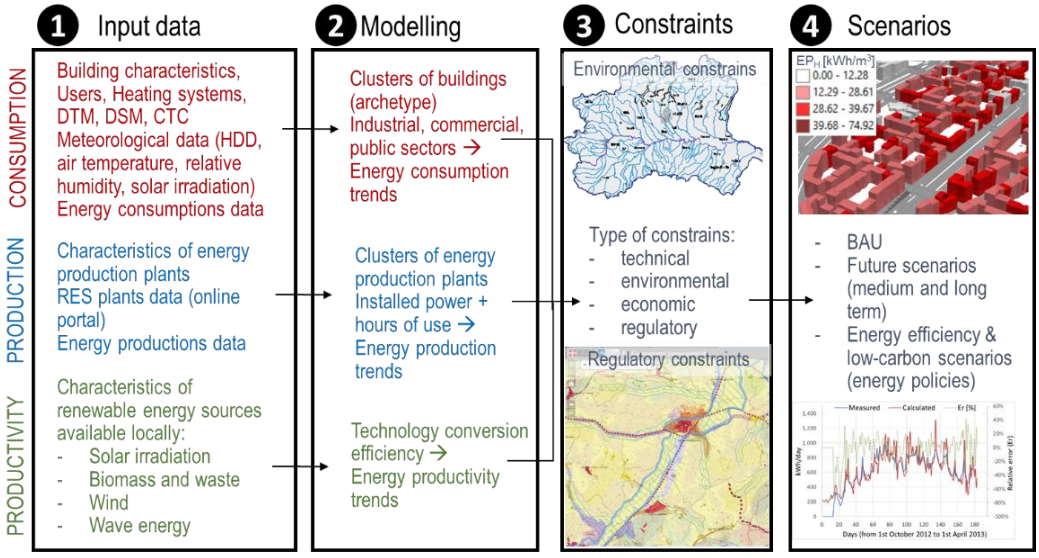

Figure 2. Place-based methodology to design energy consumption, production, productivity from RESs and energy efficiency models [15].

Figure 3 shows the comparison between energy demand and supply which is carried out through the definition of hourly, daily, monthly, and annual energy consumption and production profiles. Especially in the analysis of the energy that can be produced from RESs, which are related to the climatic conditions of the territory, it is necessary to make a balance between daily and monthly energy supply and demand, also because the storage systems available on the market do not have yet a seasonal capacity.

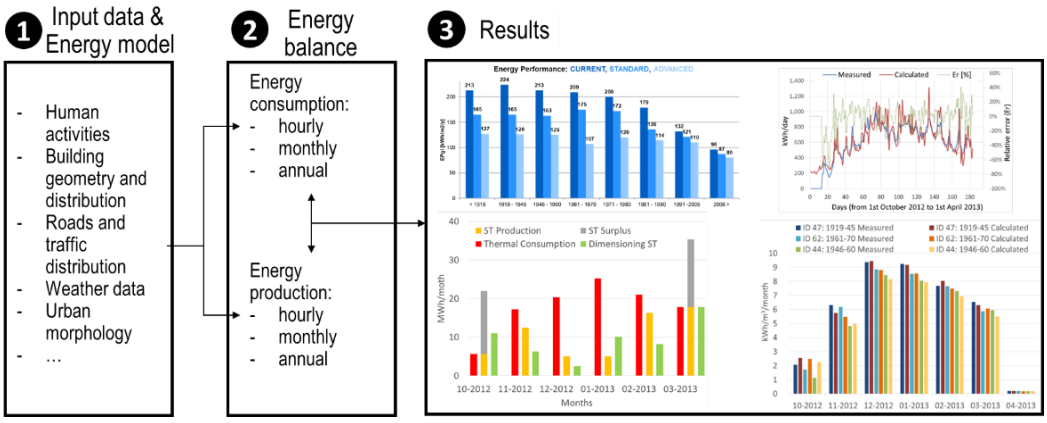

Figure 3. Place-based energy models with hourly, monthly and annual details [48].

The aim of these models is to investigate energy trends (historical, current, and future) on a large scale to understand how urban environment affect energy consumption, make assumptions on energy retrofit interventions and promoting

sustainable development through the exploitation of RESs. Therefore, place-based models are tools that can evaluate the distribution of the energy demand and supply of buildings at city scale by applying energy saving scenarios [21,22]. Since these models take into consideration the real characteristics of an urban environment, they can be used to support territorial energy planning, through the promotion of a sustainable development of cities towards energy transition [22].

2.2.1 Energy consumption models

Place-based energy consumption models can predict the energy demand in buildings by distinguishing different users. The results can be aggregated at different scales and GIS tools can be used to assess the distribution of energy at territorial level. These models are used to simulate energy for (i) space heating (SH) and space cooling (SC), that is the energy required to maintain the internal temperature of the building at a comfortable temperature and air quality conditions, (ii) domestic hot water (DHW) that is the energy required to heat water to a comfortable temperature for users, (iii) appliances and lighting (AL) that is the energy consumed to operate appliances and for the lighting.

These models can be designed using real data, such as monitoring campaign, questionnaires or bills. After validation, they can be applied to other case studies to predict hourly, daily, monthly, and/or annual energy from building up to city level. For example, D'Alonzo et al. [63] proposed a place-based methodology to assess the SH data of the residential building stock, knowing the measured SH demand. An energy balance at the building level was applied to a case study in Italy, and the energy consumption of almost 42,000 buildings was calculated. Buffat et al. [64] developed a model based on GIS data able to consider shadowing due to the topography and climatic conditions. The model was validated using the real data of 1,845 buildings in the city of St. Gallen, Switzerland and 120 buildings in the Alpine village of Zernez, Switzerland.

It is also possible to define the EP of buildings by consulting existing energy databases. The energy performance certificate (EPC) database is an important tool that gives information of the energy-use of buildings. Hjortling et al. [65] assessed building energy consumption in Sweden with reference to 186,021 EPCs, and the authors identified the main energy-related variables, such as the type of users, the construction period and the climate zone.

Energy use can also be predicted using simulation techniques.

2.2.2 Energy production and productivity models from RESs

As the consumption models, the energy production models can be processed with a monitoring campaign that allows to predict the hourly, daily, monthly, and annual production according to the technology used and the climatic conditions. It is necessary to know the existing production system, for example by consulting online portals. It is possible to evaluate the thermal and electrical energy annually

produced from RESs by multiplying the installed power by the equivalent hours provided by the online portals. By consulting EPC databases, information on the installation of RESs technologies, such as ST collectors and PV panels, can be collected. Through the use of GIS tools it is possible to map the existing production sources and evaluate energy scenarios.

So, considering the existing production systems, the energy that can be produced from RESs on a specific territory mainly depends on the availability of the sources, on their technical accessibility and on the existing constraints that can hinder their exploitation. In the assessment of the use of RESs, it is important to consider: (i) available and emerging technologies; (ii) energy potential available; (iii) planning of the infrastructures necessary for the prospective management of emerging technologies; (iv) investment and management costs, through a cost-benefit analysis to ensure an adequate return on investments; (v) assessment of risks and environmental impacts; (vi) interactions, synergies, and competitions with other sectors economically relevant to the island.

The productivity models take into account all constraints (territorial, environmental, technical, etc.) that limit the installation of production plants from RES. Groppi et al. [66] developed a GIS-based model to assess buildings energy consumption, production and productivity from solar energy in two urban areas in Rome, in Italy. The suitability of building rooftops for the installation of solar technologies considers regulatory constraints and building barriers. Pillot et al. [67] developed a model able to compute the optimal geographical location and size of PV technologies. The methodology was applied to a case study of French Guiana, and consider geographical and technical constraints.

The new plants should also include environmental redevelopment interventions in the areas adjacent to the plants, to also create greater acceptance of these interventions by the population.

2.2.3 Energy efficiency models and low-carbon scenarios

Place-based energy models can be applied in future climate scenarios, to evaluate the impact of climate change in the energy demand and supply of buildings, as well as in the potential retrofit scenarios. The EPC database can be used to define EE scenarios and to evaluate the impact of EE measures on the existing EP of buildings [68–70]. Camporeale and Mercader-Moyano [71] and Gupta and Gregg [72] proposed a GIS-based methodology to identify areas suitable for energy refurbishment. EE scenarios were defined using EPCs. Exner et al. [73] proposed a number of energy-saving scenarios considering different renovation levels. The analysis was carried out for two case studies in northern Italy. With these models it was possible to assess the effect of different energy retrofitting measures on the improvement of the EP of buildings [74]. Meha et al. [75] investigated the impact of EE measures on the SH using a GIS-based methodology. According to the energy policies, three scenarios were applied to the case study of

Prishtina, Kosovo. Droutsa et el. [76] analysed 650,000 EPCs to understand the EP of existing residential buildings in Greece. They found that the most common retrofitting actions were the replacement of windows and the installation of solar collectors. Moreover, Ali et al. [77] proposed a methodology to identify retrofitting solutions by analysing a case study of Dublin. The authors investigated the EP of the building stock using an EPC dataset of the Irish residential stock.

EPCs can also be used to improve the energy simulations by improving the detail of input data. Cozza et al. [78] examined the performance gap of retrofitted buildings located in Switzerland using the Cantonal Energy Certificate for Buildings database. The authors analysed 1,172 buildings for which both simulated and measured consumptions were known, and they found a gap of -23% in the EP of building (pre-retrofitted). This gap became positive (2%) for buildings that had been renovated. Ahern and Norton [79] performed a similar analysis and found that, for Ireland's single-family housing, the adoption of thermal default values (U-values) underestimated the EP of about 90% of the dwellings. The authors introduced a methodology, based on an Irish EPC database that is able to assess a realistic energy savings, after building retrofitting, using default U-values. Fan and Xia [80] optimized building energy retrofitting models using the EPCs of a few buildings in South Africa. The optimization was conducted using a grouping method and verifying the energy savings of the sample of retrofits. In general, the performance gap between predicted and measured energy use was found to deviate by 34%, and to depend on the model approach (impact of 20-60% on energy use), occupant behaviour (impact of 10-80%), and poor operational practices (impact of 15-80%) [81].

In conclusion, these models can support the urban planning of new and existing neighbourhoods, to promote retrofit analysis of building stock, to improve the EP of buildings using smart green technologies, and to design and optimize district energy networks [82,83]. They are fundamental tools to identify effective energy policies in order to promote a sustainable development of cities. For example, Oberegger et al. [84] after the application of energy retrofit models, summarized the results using an EE cost curve allowing policy makers to estimate potential costs and energy savings.

2.3 Approaches and methods

Currently, there are a variety of methods, tools and techniques used to design USEMs [85]. Depending on the type of input data (i.e., availability, accuracy and level) and on the type of analysis to be performed, there are different energy simulation approaches that can be grouped into two categories: top-down and bottom-up [12,35,86]. The main techniques used to simulate the energy consumption with these approaches are data-driven methods (i.e., statistical regression and artificial intelligence models) and process-driven methods (i.e., archetypes and physical models) [45]. Specifically, data-driven methods require

disaggregated historical consumption data to have a sample of a group of buildings, while process-driven methods use as input data building geometries and thermo-physical characteristics.

USEMs can be also categorized as white-box, gray-box and black-box methods, where: (i) white-box models, based on physics approach, need detailed information on the thermo-physical characteristics of buildings; (ii) gray-box models are an adjustment of white-box models and use also a statistical approach, the main input data refer to historical data and to the simplified physical information; (iii) and black-box models simulates the phenomenon using historical data without the detailed information about physical phenomena [16,87–89].

It is also possible to classify USEMs according to the type of energy simulation, as: non-steady state models [90] based on dynamic simulations, quasi-steady state models based on monthly or daily data sets [91] and steady-state models that do not consider the element of time [92]. The time resolution can vary, from an hourly to an annual precision, with different simulation times and different accuracy levels.

Depending on the methodology used, the input data required for energy analyzes are different, the simulation techniques are more or less complex with different simulation times, and the results are more or less accurate with different territorial levels of analysis [93].

2.3.1 Top-down approach

Top-down models (disaggregation of energy consumption from higher scale) use energy-related variables and statistical data to describe EP of urban areas. This approach provides aggregated energy information at large-scale [94].

Regarding energy consumption models, top-down approaches start from energy consumption data at municipal scale and allow to determine an average consumption of buildings, relating them with the climatic conditions and the socio-economic characteristics.

These models do not need specific data for each building. Variables refer to historic aggregate energy data at municipal or national level and other energy-related variables, such as heated volumes, income, climate conditions, in order to attribute the energy use to the users of the entire building stock.

2.3.2 Bottom-up approach

The bottom-up approach (aggregation of energy consumption to higher scale) calculates the energy consumption of a single building or groups of buildings, and then elaborates the results to describe the distribution of energy consumption at municipal or territorial level [93].

The biggest challenge is collecting and processing a large amount of building data and then apply it to the entire city [95]. Variables used are at building scale and are more detailed than that used in the top-down approach. Input data refers to the geometric characteristics of the buildings, the properties of the construction

materials, the climatic conditions, technological systems, the type of users, the occupant behaviour and the urban morphology.

Once validated, these models can be used to calculate energy consumption without the information of energy historical data. Simulation techniques are more complex than top-down methods, but they are more flexible, accurate and it is possible to model EE scenarios [96].

According to the literature, there are two main categories that use the bottom-up approach: data-driven methods and process-driven methods. Nouvel et al. [97] compared a statistical (data-driven) and engineering (process-driven) models for urban heat consumption simulation of 1,000 buildings in Rotterdam, Netherlands. The accuracy of these models is strongly influenced by the lack of information on renovated buildings, occupants' behaviour, and unoccupied buildings. A combined used of both methods (i.e., hybrid approach), allowed to improve the model accuracy.

2.3.3 Data-driven method

Data-driven methods can be classified in statistical regression models and artificial intelligence models.

Statistical regression models involve regression techniques and are widely used due to their simple structure and fast processing time. These models analyse the relation between historical information of energy consumption and energy-related variables by defining different combinations of parameters. Input variables that have negligible impact are removed from the model to simplify it. Models based on these relations can be applied to calculate energy consumption. A statistical model was designed by Caldera et al. [98] using as a case study 50 residential buildings in Turin. Simplified correlations between the construction year of the building and main geometric and thermo-physical properties were observed. This statistical model was able to estimate the energy demand for SH.

Statistical analyses can also be performed to define archetypes. Buildings are classified according to their dimension, orientation, construction year, location, operating parameters, etc. Referring to these archetypes, input data is identified and energy consumption is simulated for each cluster of buildings. In Netherlands, Yang et al. [99] have developed a model based on GIS data and archetypes to simulate SH and DHW consumption of residential buildings. Archetypes were defined according to building geometries, thermal properties, and heating systems. In a similar work [100], residential archetypes were defined by geometrical and thermophysical properties of the building, heating and cooling system type, geographical-climatic zone. This model was tested at territorial level in Sicily region, Italy. Streicher et al. [70] defined archetypes using the SH demand of 54 Swiss residential buildings. Their bottom-up model uses as input data EPCs.

Artificial intelligence models uses algorithms, and allow to define correlations between input data and output, in this case building energy-uses, considering

complex phenomena. The most used algorithms are decision trees, random forest, deep learning, gradient boosted trees, and support vector regression [89]. For example, Ali et al. [77] have designed a GIS-based energy model to predict the EP of buildings on a large scale. A data-driven approach, that uses 650,000 Irish EPCs, was used train the model. Using deep learning algorithms, the accuracy of the prediction was 88%.

2.3.4 Process-driven method

Process-driven methods are based on engineering models able to simulate energy consumption as a results of an energy balance. At urban scale less data are needed, but all information about each heat exchange are fundamental to complete the energy balance equations. One of the problems of these models is to collect correct information on the thermal properties of buildings, and to define occupational profiles as faithful as possible to reality. In fact, these models require a complete dataset to define the characteristics of a building, or a group of buildings, but they are very flexible and allow the identification of effective strategies to improve the EP at urban scale. Through process-driven models, it is possible to modify the various variables in the energy models, to obtain future scenarios of energy consumption and production. They can be used to optimize the urban energy system, by improving demand and supply.

These models can be simple if they calculate the annual or monthly consumption, or they are more complex models based on hourly heat transfers between the building and the outdoor environment. For example, a simplified building stock model was designed for 20 European countries using TABULA database [101]. In this investigation archetypes were used to define input data, and a monthly engineering balance was applied at building level.

Compared to other methods, with this approach it is possible to simulate the energy use with greater temporal detail (i.e., daily or hourly) [23].

2.4 Input and output data

A city building dataset is a fundamental component to design and apply USEMs. In an urban context, the energy consumption, production and productivity of a building stock is affected by several factors, such as the design of the built environment, the relationship between the buildings and open spaces, the type of materials used for the external surfaces, the socio-economic characteristics of the population, the type of obstructions and, naturally, the climate and local climate conditions [102–104].

The accuracy of USEMs depends on the reliability of the databases and the amount of missing data. Models at city scale are simplified models, and not all data are always available for the entire city. With the use of a sensitivity analysis the main variables that influence energy in buildings can be identified, and some

variables are fundamental such as building characteristics and climate data and other variables can be added to improve the accuracy of the energy simulation.

The main input datasets include building and system data, building operational data, whether data, GIS data, EE measures, codes and standards, availability of RESs, policy and regulations.

After the collection and processing of input data, USEMs can be designed and used to simulate energy consumption, production, and productivity from RESs.

The output can be mapped using a place-based methodology and it is possible to create energy maps. The results can have different scales, from the building scale to the city scale, and different time resolution with annual, monthly, and hourly details.

2.4.1 Input data

The main energy-dependent variables are building characteristics such as the building envelope and utility systems' efficiencies, local climate conditions and variations around buildings, the people's behaviour, social and economic conditions, local and national regulations, the characteristics of energy production plants, the availability of energy sources, but also the urban morphology that significantly affects the energy consumption and productivity from RESs [105,106].

To process the input data, it is necessary to use tools able to collect data from different sources and to manage city building dataset. The most common tools are CityGML model which uses a standardized geometrical format and GIS tools [107]. The place-based models designed in this research use open databases available for most of the territories and cities that describe the municipal/regional master plan and the land use.

With CityGML it is possible to create and design 3D city models using an open standard format to support the energy simulation at city level [11,108–111].

GIS tools allow to capture, process, storage, and display of in-depth information of the real characteristics of the building stock, and this data is used to simulate energy demand and supply at city level. For example, Ferrari et al. [112] elaborated a database to map energy-related features in order to estimate the energy demand of urban buildings in the city of Milano in Italy. In addition, GIS tools can play a significant role in the analysis of RESs available locally [18,19,66,113]. In several researches [66,114–116] GIS tools were used to determine the potential of solar energy in cities, by investigating the available rooftop area, the obstructions and shadow effects on buildings, and by evaluating and mapping solar irradiation in urban areas.

Building data

At building level, there are three main groups of input data, which are used to describe the sample of buildings to be analysed.

The first group refers to the building geometry, including the building shape and height, the number of floors, the heated and gross volume, the heat loss surfaces, the quota of transparent and opaque envelope, the type of roof and the orientation. GIS tools are of significant importance to investigate these variables. The main data used to assess the building geometry refers to municipal technical maps and digital elevation models. Municipal technical maps give information on the building's footprint, the type of users and the construction year. Information of building footprints can be used to quantify the number of floors, the building height [m] the roof area [m^2], the net heated volume [m^3] and the usable area [m^2] useful to understand the quota of heated building and the occupancy (if a building is fully or partially heated), the surface-to-volume (*S/V*) ratio [m^2/m^3] that is the ratio between the heat loss surface and the gross heated volume of a building, it indicates how compact a building is identifying the building typology (e.g. detached house or big condominiums), the building orientation and the roof typology that indicate the surface of the roofs exposed to solar radiation to understand their capturing capacity and the solar potential. Elevation models can be used to assess shadows' effects on buildings and the surrounding's urban context to quantify the solar radiation, considering the sun and sky models, and to evaluate the building characteristics such as roof slope and orientation. There are two types of digital elevation model: the digital terrain model (DTM) that describes the natural terrain, and represents the bare-Earth surface without natural or built features, and the digital surface model (DSM) that represents the Earth's surface including trees and buildings.

The second group refers to the thermophysical properties such as the thermal transmittances, the total solar energy transmittance, the absorption coefficient for solar radiation and the emissivity for thermal radiation of opaque and transparent envelope, and the thermal capacities of heated zones. For existing buildings, thermophysical properties and building elements can be defined according to the construction year and using values indicated in standards and literature. It is possible to assign to each building its construction materials such as thermal transmittance, resistance, and thermal capacity. If the construction year is used to define the characteristics of the building, it is not considered whether the buildings have been retrofitted. To overcome this problem, EPC databases can be used to update the building data. From the EPC it is possible to identify the buildings that have been retrofitted.

The third group refers to the type of energy systems and their operation conditions, such as SH, SC, ventilation and DHW systems [117]. Knowing the type of energy system and its efficiency, it is possible to quantify the energy supplied for SH, SC and DWH. Usually this data can be defined according to standards, literature and census data. From census data (e.g., Italian National Institute of Statistics – ISTAT which are open data) it is possible to have information at block-of-building scale on the type of heating system (central or autonomous), and on the type of energy vector (e.g., natural gas).

Population data

Population data are important for defining socio-economic characteristics and occupant behaviour.

Socio-economic and demographic characteristics influence the energy use in buildings. From census data (e.g., Italian National Institute of Statistics – ISTAT which are open data) it is possible to have information at block-of-building scale on people occupancy, number of inhabitants, number of families and family members, percentage of foreigners, gender, age, income, employment rate, economic data (annual income). All these parameters allow to optimize energy models, and to define effective energy policies according not only to the existing building stock, but above all to socio-economic and demographic characteristics of the population.

Occupancy profiles of buildings play an important role in the energy consumption and in the optimization of the energy demand and supply [118]. The human behaviour, different occupancy densities and variations in thermal and lighting preferences contribute significantly to the gap between simulated and real EP in buildings [119–121]. When real data is not available, these variables can be defined according to standards and literature.

Climate data

Climate and local climate conditions can be assessed using weather stations' measurements and climate tools such as Meteonorm that is able to extract climate data for a specific location.

The main variables used in the energy simulations are the Heating Degree Days (HDD), the Cooling Degree Days (CDD), and the hourly data on temperature, relative humidity, vapor pressure, and wind velocity of the outdoor air.

There are also portals that can provide information on climate data. For example, the Photovoltaic Geographical Information System (PVGIS) portal gives information on the solar radiation and temperature, with monthly, daily and hourly profiles of a specific location.

Urban data

The spatial configuration of the built environment can be described using several energy-related parameters able to express the compactness of the built environment and the type of the surrounding open spaces. Urban parameters can be classified in variables used to describe the urban morphology and the outdoor urban surfaces. Table 1 summarizes the main urban parameters that affect the energy demand and supply of buildings.

Urban morphology can be assessed with GIS tools using municipal technical maps and elevation models (i.e., DTM and DSM). The main variables are the building density (*BD*), the building height (*BH*), the building coverage ratio (*BCR*), the relative buildings' height (H/H_{avg}), the canyon effect or aspect ratio (*H/W*), the

sky view factor (*SVF*), the solar exposition, and main orientation of the streets (*MOS*).

The main data used to investigate urban surfaces are satellite images and orthophotos. Satellite images can be used to analyse the land cover types and to calculate the albedo (*A*) of the outdoor spaces, the presence of vegetation, and the land surface temperature (*LST*). Orthophotos with RGB (red, green, blue) and IR (infrared) spectral bands can be used to identify green areas and to evaluate albedo values of outdoor urban spaces and buildings' roofs, as a function of colour tones.

Table 1. Urban parameters that affect the energy performance of buildings [46].

Type	Parameter		Description	Unit	References
Urban morphology	Building coverage ratio	*BCR*	It is defined as the percentage of built area	m^2/m^2	[70,102,122,123]
	Building density	*BD*	It is the ratio of the building volume to the sample area	m^3/m^2	
	Canyon effect or height-to-width ratio	*H/W*	The canyon effect can be measured by means of the aspect ratio, that is, the ratio between the height of the urban canyon and its width	m/m	[102,124,125]
	Main orientation of streets	*MOS*	The main orientation of buildings at an urban scale may be calculated using *MOS* from 0 (north) to 1 (south)	-	[126,127]
	Relative height	H/H_{avg}	Describes the solar exposition in relation to the building heights	m/m	[102,123,126]
	Sky view factor	*SVF*	Measures the portion of sky visible from a given location or point	-	[128,129]
Urban surfaces	Albedo	*A*	It is used to describes the characteristics of outdoor surfaces, and it is the percentage of solar incident irradiation reflected by a surface	-	[123,130–132]
	Normalized difference vegetation index	*NDVI*	Describes the presence of vegetation. Low values (-1) for barren rock and sand areas or urban/built-up areas, 0 values for water and high values (+1) for vegetation.	-	[133]
	Land-surface temperature	*LST*	Describes the temperature of horizontal surface	°C	[134,135]
	Urban heat island effect	*UHI*	Is used to evaluate the factors that have the most influence on the urban climate	-	[43,136]

Energy consumption data

Measured energy data are necessary to design, calibrate and/or validate USEMs. The measured consumption data are sensitive data, so it is not always possible to collect it and use to develop energy consumption models. Usually, energy data are provided by the energy distribution companies of the cities. They can give

information on heat and electricity consumption. The detail of energy data can be annual, monthly, or hourly, from the apartment/building scale to the neighbourhood/district scale. Energy data should refer to at least two or three consecutive years in order to carry out accurate statistical analysis and to develop/validate the models.

Depending on the information scale of the energy data, top-down or bottom-up models can be developed. Bottom-up approach uses energy consumption data of measured energy-needs at building scale. Top-down approach elaborates energy data at municipal or urban scale. For example, data from Sustainable Energy Action Plans (SEAPs) of the cities give information on the distribution of energy use and how to achieve energy and climate goals using RESs and EE measures.

Energy data can also be collected from bills or questionnaires, this approach takes more time to process the information.

Another tool that provides information on energy data of building are the EPCs. This database can also be used to evaluate the type of EE action and the impact retrofit interventions.

With the use of GIS tools, it is possible to process and georeference the energy data for an entire city. The real characteristics of the territory can be associated to the energy data.

2.4.2 Output data

USEMs aim to consider the urban context by simulating the EP of a group of buildings at multiple temporal and spatial scales. They can map the energy demand with: (i) annual or monthly detail from time-aggregated energy data [137]; (ii) hourly detail from consumption profiles' data [138,139]. USEMs are also able to visualize and replicate the effects of the surrounding urban area on the buildings. GIS tools can be used for mapping and planning the distribution of energy at different scales. The outputs of USEMs allow to visualize the distribution of energy consumption, identifying for example the most critical areas (high consumption) and, in these urban areas, the thermal comfort conditions are scares compared to other ones. USEMs can therefore support energy retrofit strategies by assessing their impact on the territory [140]. Below are indicated some studies that, after the application of USEMs, map energy consumption at territorial scale, using 3D-city models.

Johansson et al. [82] created an energy atlas of the multifamily building stock in Sweden to enable estimations of the costs, the effects on energy-use and the socio-economic features associated with possible retrofit strategies. The atlas was developed using the extract transform and load technology to aggregate information on the energy building performance, ownership, retrofit status, and socio-economic characteristics of inhabitants from various data sources. Belussi et al. [141] mapped the energy consumption of buildings, at an urban scale, using a bottom-up and top-down methodology, which was based on information provided by an open-source

database on geometrical, morphological and typological characteristics (TABULA and EPCs data). A statistical approach was adopted, and the energy performances were calculated according to the building characteristics (volume, *S/V*, thermal transmittance).

More recently, Sokol et al. [5] introduced an urban building energy modelling using a new Bayesian approach. Their model allows calibrating building archetypes to model small residential and commercial building stocks and the results were mapped using a 3D city-model. Monteiro et al. [142] developed a 3D model, and the energy simulation was made to identify the reference value for different building types and estimate the total urban energy consumption. Li et al. [143] classified residential building archetypes developing a bottom-up energy modeling at district level. With the support of UMI (Urban Modeling Interface) [32], the distribution of energy consumptions has been investigated at territorial scale.

Chapter 3

Place-based energy consumption models

3.1 Chapter overview

This chapter describes how to design place-based energy consumption models using different approaches and methods (Figure 4). The models presented were developed within this doctoral research. Depending on the availability of data and on the type of analysis needed, one approach or methodology is better than another. The simplest models are the annual data-driven ones. In the first part of this chapter, annual top-down and bottom-up models based on GIS-tools, that use statistical techniques, are designed for the city of Turin using data with high detail at the building level (bottom-up) and data at the municipal level (top-down) [12].

To consider the urban morphology in the EP assessment, a new place-based monthly process-driven model is designed according to the standards on the energy balance of buildings. It is an urban energy balance created for the residential sector. The model is validated using the energy consumption data for SH and DHW of residential buildings connected to the DHN in Turin [46].

In order to evaluate the thermal peak loads, an hourly process-driven model is developed. Starting from the monthly model, new urban parameters are added to the thermal balance of the built environment in order to improve the accuracy [144]. Subsequently, the thermal balance is improved considering three thermodynamic systems that exchange heat with each other. This model is able to simulate SH and SC demand of residential users. It is applied to the city of Turin and validated using the real data for the heating season [50] and simulated data for the cooling season [49].

As already mentioned, the different methods used have strengths and weaknesses in terms of simulation times, flexibility, and applicability. An hourly data-driven model that uses a machine learning (ML) technique is developed for the city of Fribourg in Switzerland. The accuracy and flexibility of this model is

compared with the hourly process-driven model that uses an engineering technique [47].

Finally, a hybrid model is designed for some neighbourhoods in the Canton of Geneva in Switzerland. The hourly engineering model is optimized by adopting a data-driven correction with a Random Forest (RF) algorithm [51].

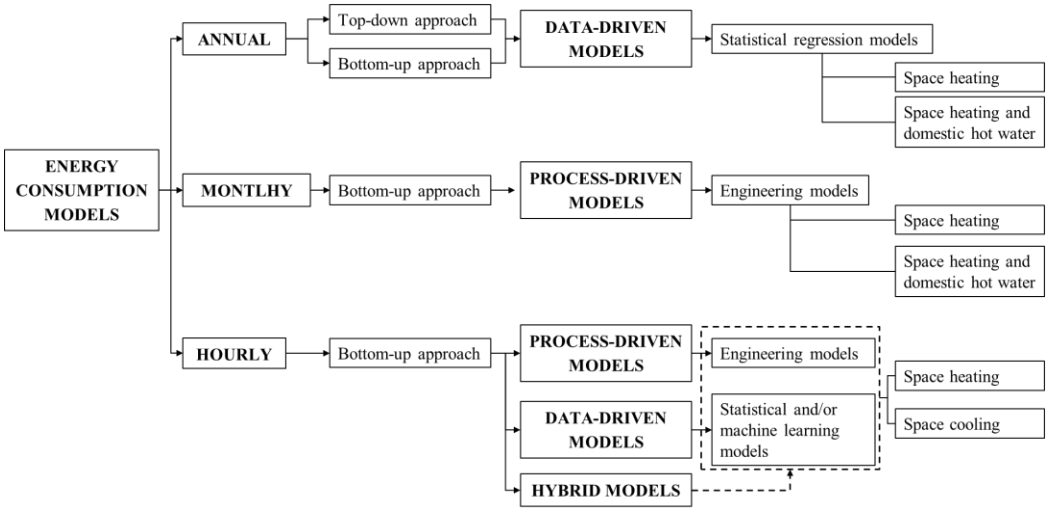

Figure 4. Flowchart of Chapter 3

The accuracy of the models presented in this chapter is investigated using: the relative error (*RE*), the percentage relative error (E_r), the mean absolute error (*MAPE*), the mean absolute percentage error (*MAPE* or $|E_r|$) and the coefficient of determination (R^2).

3.2 Annual data-driven models

The purpose of this section is to define statistical models at urban scale using top-down and bottom-up approaches. Energy consumption models are designed for the city of Turin considering the built environment, high population densities, anthropogenic activities, energy demands, and environmental impacts. Figure 5 shows the methodology used to design the models at urban scale.

These models are used to calculate annual SH and DHW consumption for both residential and non-residential buildings using GIS tools. Top-down and bottom-up approaches consider established statistical methods as well as the introduction of energy-dependent urban-scale variables. The main variables are assessed considering sampling more than 2,000 buildings. For these buildings, the data measured for over three heating seasons in the city are known. Normal distribution, average and variance of energy consumptions are used to discard anomalous data. The described GIS-based methodology can be used to manage and represent buildings' energy consumptions from building level to city scale.

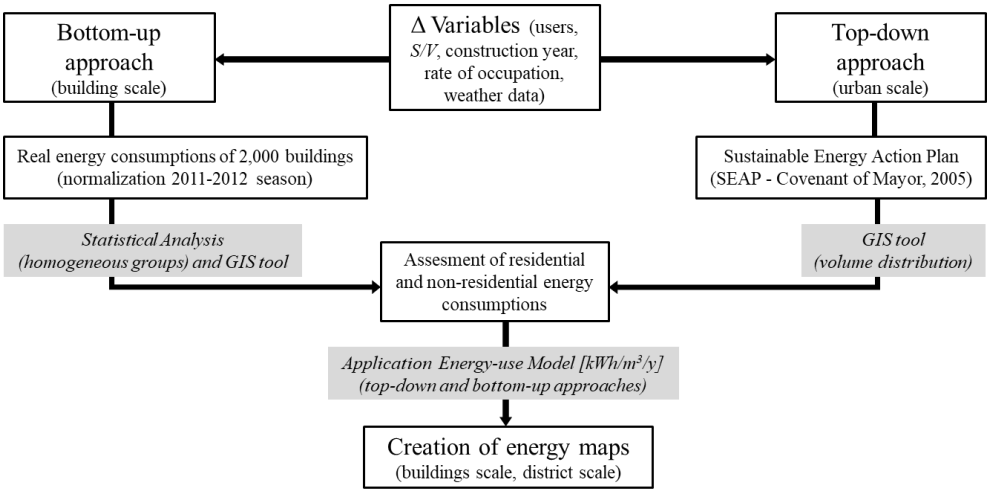

Figure 5. Methodological flowchart of the space heating models at urban scale for buildings in the city of Turin [12].

3.2.1 Input data

To design annual statistical top-down and bottom-up models the following databases are elaborated: the municipal technical map of the city, the census database of population (ISTAT, National Institute of Statistics; in Italian: *Istituto Nazionale di Statistica*, 2011), the DSM, building data (height, *S/V* ratio, roof type, etc.) processed from the municipal technical map (open database) and the DSM, and local climate conditions (e.g., outdoor air temperatures, HDD).

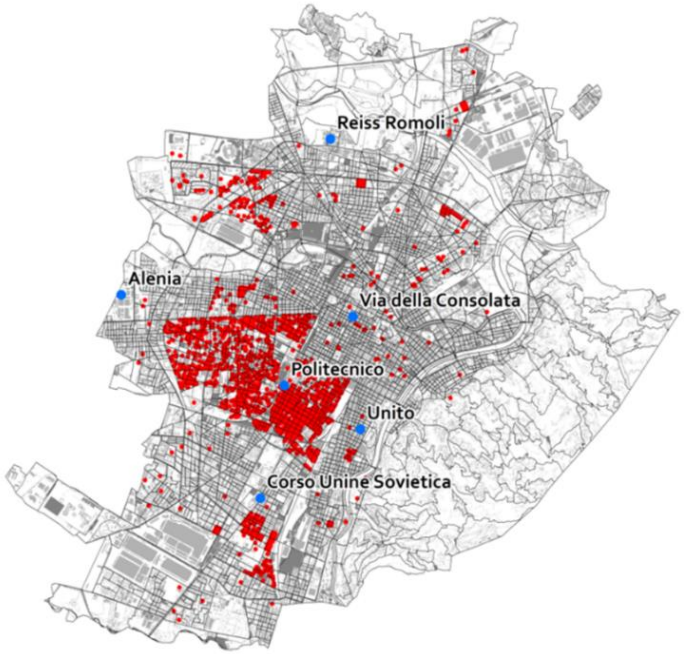

Figure 6. The data sample of 2,092 buildings georeferenced (in red) and the six weather stations considered (in blue) [12].

The main energy-use related variables used for residential buildings refer to construction year, compactness (or *S/V* ratio) and heated/gross volume; for non-residential buildings data refer to the type of user, and heated/gross volume.

The statistical bottom-up model is designed using data at building level. The energy consumption of about 2,000 residential buildings and 130 schools and public buildings connected to the DHN is georeferenced using GIS tools. Energy data is normalized according to the 2011-2012 heating season (with a relative deviation of 1.5% on the medium value of HDD in the last 10 years). Local climate data of six weather stations in the city are used (Figure 6).

In the design of the statistical top-down model, the SEAP (Covenant of Mayor, 2005) is used. The energy consumption of the city is analysed for all sectors at the aggregated municipal scale for the year 2005.

3.2.2 Statistical model

Buildings are subdivided into homogeneous groups according to the type of user and the geometrical characteristics. For each homogeneous group, a statistical analysis is performed to evaluate the normal distribution of energy consumption data. This allowed to discard anomalous data that differed too much from the average consumption. After the analysis of the trend of the consumptions for each homogeneous group, an average value of energy consumption and its standard deviation is determined.

Table 2. Homogeneous groups of buildings identified considering type of use, class of construction year and *S/V* values [12].

Type of use	**Construction year**	**Classes of *S/V* [m²/m³]**					**Buildings analysed**	**Buildings selected**
		1	**2**	**3**	**4**	**5**		
Residential	(1-2)	<0.32	0.32-0.41	0.41-0.59	0.59-0.78	>0.78	409	325
	(3)	<0.38	0.38-0.58	0.58-0.68	>0.68		366	288
	(4)	<0.32	0.32-0.38	0.38-0.50	>0.50		553	433
	(5)	<0.37	0.37-0.57	0.57			238	187
	(6)	<0.33	0.33-0.36	0.36			41	33
	(7)	<0.30	0.30-0.40	0.40-0.82	>0.82		12	10
	(8-9)	<0.40					2	2
Type of use								
Schools	Nurseries and kindergartens						41	28
	Primary and secondary						46	30
	Grammar schools or lyceums						22	20
	Technical institutes						33	31
Offices							39	27

In Table 2, homogeneous groups of buildings subdivided by the type of use, the construction year, and the *S/V* ratio, are reported. Regarding the residential sector, buildings are classified using nine classes of construction year: before 1918 (class

1), between 1919 and 1945 (class 2), between 1946 and 1960 (class 3), between 1961 and 1970 (class 4), between 1971 and 1980 (class 5), between 1981 and 1990 (class 6), between 1991 and 2000 (class 7), between 2001 and 2005 (class 8), after 2006 (class 9). Most of the analysed buildings (87.5%) were built before the first Italian Law on energy savings in buildings (L. 373/1976). In particular, 29% of residential buildings were built in 1946-1960, 20% in 1919-1945, and 20% in 1961-1970.

Figure 7 shows an example of the normal distribution for specific SH energy consumption considering the heating season 2011-2012 with about 2,221 HDD at 20 °C according to "Via della Consolata" weather station. This homogenous group refers to residential buildings with *S/V* lower than 0.32 m^2/m^3 and buildings built before 1945. In green is indicated 68% of the selected data and in red the anomalous data with consumptions lower or higher than the average energy-use ± its standard deviation.

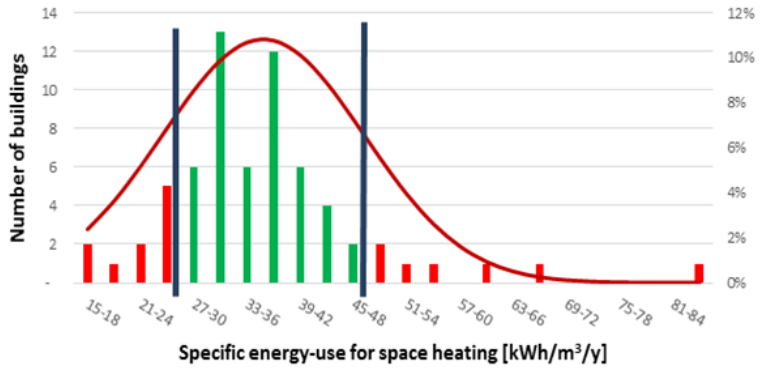

Figure 7. Normal distribution of specific space heating energy consumption for a homogeneous group [12].

Comparing the results of the bottom-up approach at buildings scale and the top-down approach at municipal scale, a correction factor is determined. This is necessary to improve the accuracy of the bottom-up model, that is a simplified model and does not consider important factors such as the spatial variability in solar gains, indoor/outdoor air temperatures, the use of RESs and, mainly, the level of buildings' retrofit those changes building energy consumption. To consider these variables and to adapt the model to real energy consumption data at building and municipal scales, the energy simulations of the bottom-up model are multiplied by a correction factor. This factor takes into account the type of environment in which the building is located, so it is typical for Turin.

3.2.3 Model results and validation

Regarding the bottom-up model, the analysed residential buildings are mainly compact and big condominiums with low *S/V* values. On average the S/*V* is 0.38 m^2/m^3, and the value for all residential buildings in Turin is of 0.6 m^2/m^3 with lower

closes to 0.5 m^2/m^3 in the historical centre. For each construction year, the analysis on different classes of *S/V* ratio is conducted, as reported in Table 2.

In Figure 8 the average and standard deviation (with the vertical line) values for SH consumption (*EPh* in $kWh/m^3/y$) are indicated for each construction year. Buildings built between 1961 and 1990 consumed more energy for SH than old and recent ones, probably due to the thinner structures of the envelopes built during the economic boom after the end of the Second World War. After 1991, the average energy consumption decreased due to the consequences of the Italian Laws on building energy savings (L. 373/76 and L. 10/91).

Differences in energy consumption, represented by the standard deviation, are mainly due to the compactness of the envelope, the heating system efficiency, the solar exposition, and other energy-related variables of the buildings. The trend of energy consumptions increased after 1960 and decreased after 1991.

For a higher robustness of the statistical analysis more data on energy consumptions are needed, especially for recent buildings built after 2001 (as can be observed by the number of buildings in Table 2).

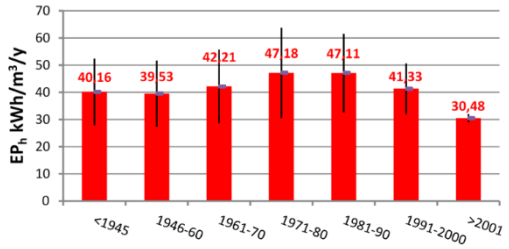

Figure 8. Average values of specific space heating consumptions (*EPh*) and standard deviations (vertical lines) of residential buildings by construction year for the heating season 2011-12 [12].

For public buildings, consumptions data of 233 buildings are collected. 61% of them are schools (142 buildings) and, for this type of public sector, some distinctions are made according to the type of school. In Figure 9 it can be observed that: (i) nursery and kindergarten buildings consumed more energy, as they require warmer environments than primary and secondary schools; (ii) high schools are divided into grammar schools and technical institutes because they have different timetables and various types of laboratories and activities with consequently different energy demands.

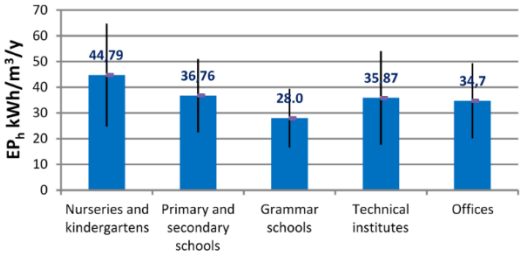

Figure 9. Average values of specific space heating consumptions (*EPh*) and standard deviations (vertical lines) of non-residential buildings by type of users for the heating season 2011-12 [12].

In Figure 10 the average energy consumption for SH of residential buildings is represented for each homogeneous group according to the construction year and *S/V* values. SH consumption increases with higher values of *S/V*, and the intensity of the increase depends on the construction year.

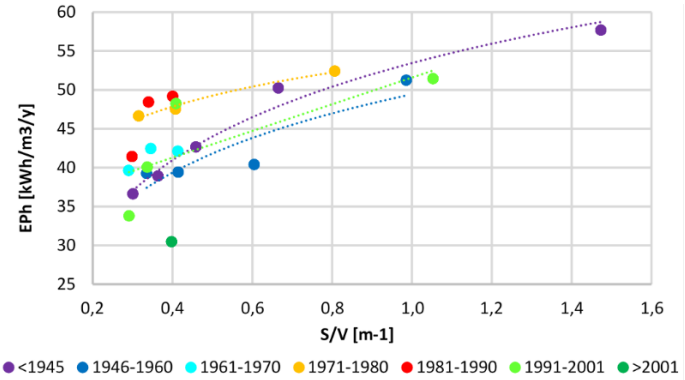

Figure 10. Specific space heating consumptions (*EPh*) of residential buildings according to the *S/V* and construction year [12].

As already observed in Figure 10, the older buildings have similar consumptions to newer buildings. Therefore, other different clusters are investigated. As seen in Figure 11, the buildings built before 1970 and between 1991 and 2001 can be grouped together, as for the buildings built between 1971 and 1990. Lower energy consumptions can be noted for newer buildings (built after 2001) and similar EPs can be observed for buildings with high values of *S/V*.

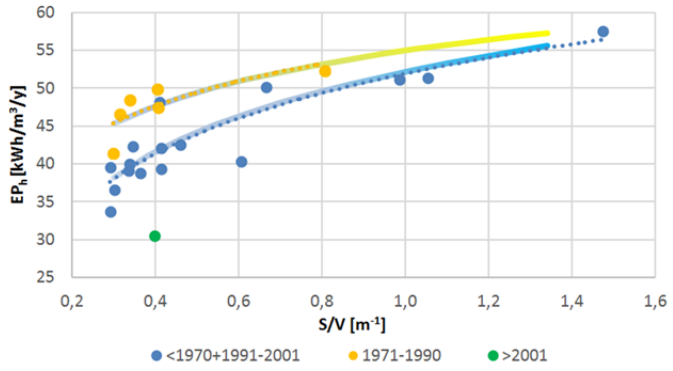

Figure 11. *EPh* of residential buildings according to the *S/V,* grouped into three homogeneous classes for different construction years [12].

In the development of top-down model, the information of heated volumes in the SEAP and in the municipal technical map of the city are compared for all the buildings. The average specific energy-use value is deducted from the overall consumption for the different type of buildings. In Table 3 the average consumptions data used for the buildings in Turin are reported. In brackets the corrected heated volumes (that is defined by comparing GIS and SEAP databases) and the relative specific energy-uses data is indicated.

Table 3. Gross heated volumes of buildings and the relative specific energy-uses for space heating and hot water (*EPgl*) consumption considering the reference heating season of 2011-2012 with 2,221 HDD at 20°C [12].

Type of user	**N. of buildings**	**Volume (at 2005) km^3**	***EPgl* (kWh/m^3/y)**
Churches	306	25.52 (510.41)	27.73 (4.45)
Commercial buildings	2,818	11,691.18 (8,993.22)	17.06 (22.18)
Hospitals	606	2,508.01	53.03
Hotels	260	849.21 (424.60)	57.62 (28.81)
Industrial buildings	4,519	29,713.93	88.70
Offices	918	3,232.15	22.08
Residential buildings	44,803	160,548.12	31.09
Recreational buildings	108	593.94	23.14
Schools	1,754	5,340.73	25.35
Services buildings	1,985	5,315.57	30.55
Sport facilities	397	512,415.11	36.82
Swimming pools	93	271.89	69.02
Universities	403	2,147.47 (3,376.43)	41.20 (26.20)

In Table 4, the statistical comparison between bottom-up and top-down models using GIS tools is reported. The bottom-up models for residential and non-residential buildings in Turin are applied using with a correction factor of 1.02 to match the results of statistical models of buildings consumption and the SEAP municipal energy consumption reported for the year 2005. This value shows the good quality and accuracy of buildings database. The correction factor considers: the different types of heating systems across the city's neighbourhoods, the percentage of centralized and autonomous systems, the presence of the DHN, and the different level of buildings retrofit [145].

Table 4. Gross heated volume of residential buildings, HDD, percentage of space heated and the correction factor applied to Turin [12].

City	Turin
Volume of residential buildings in 2005 (10^{3}m^3)	160,548
Volume of residential buildings in 2015 (10^{3}m^3)	163,362
Standard HDD at 20°C UNI 10349-3: 2016	2,648
HDD at 20°C year 2005	2,703
HDD at 20°C for last 10 years (last 5 years)	2,449 (2,150)
Thermal energy-use at 2005 (MWh/y)	5,846,863
Thermal energy-use from District Heating at 2005 (MWh/y)	1,000,104
% Of heated volumes from ISTAT 2011 database (-)	0.845
Correction factor (-)	1.02

With these models, the energy-consumption for SH and DHW production can be represented with the possibility to also correlate these data with the spatial distribution of buildings CO_2 emissions.

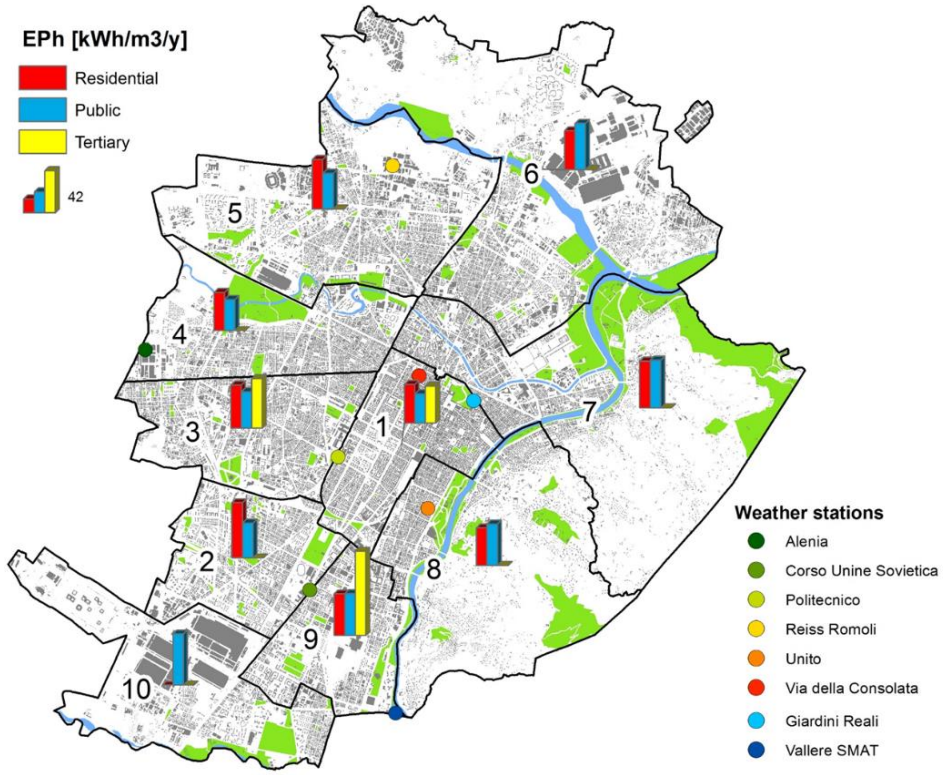

Figure 12. The 10 districts in Turin with the considered weather stations and the average specific energy-use EP_{gl} (the scale can be observed in the legend for tertiary sector) [12].

In Figure 12 the average specific energy-consumption is represented for the different districts with the vertical bar chart (scaled on the value of 42 kWh/m^3/y for the tertiary sector in yellow). It is possible to observe how specific energy-use (EP_{gl}) depends upon neighbourhood as outdoor air temperature may be influenced by the UHI effect, in addition to other local climate variations. Notably, lower values of EP_{gl} are observed in the city centre (where the effect of UHI higher) regardless of whether the neighbourhood is residential, public, or tertiary.

To sum up, a bottom-up statistical model was designed using measured energy data of 2000 residential buildings and a top-down model was designed for the whole city (residential, municipal, commercial and industrial sectors). The main energy-depended variables (e.g., construction period, type of users, *S/V*) were elaborated for the city. Finally, the models were validated against SEAP aggregated city-level data.

To have more accurate analyzes both in terms of precision of the model and in terms of temporal analysis, it is necessary to use other techniques and input data, such as process-driven models. The main limitation of the models presented in this section is that they are not very flexible and do not allow to evaluate how consumption changes according to the urban form.

3.3 Monthly process-driven models

This section presents a new bottom-up engineering model at urban scale with monthly detail. The model is designed by means of a quasi-steady state method. The calculation method refers to ISO 52016-1:2017 [146], ISO 52017-1:2017 [147] and ISO 13790:2008 [148] standards. Starting from the existing energy balance at building scale, the model is designed by introducing three urban variables elaborated with the support of GIS tools. The urban energy balance model is designed using as a case study the city of Turin. This place-based methodology is applied to thirty-three meshes (districts) with a dimension of 1 km x 1 km. The model is validated using the monthly SH and DHW consumption data of three consecutive heating seasons. The results showed that the model is very accurate for old built areas. The *MAPE* is 10% for buildings built before 1970, while the error reaches 20% for newer buildings.

The novelty of this energy model is that it adds three urban parameters to the energy balance to take into account the urban context. The thermal radiation lost to the sky of the built environment is quantified through the use of the *SVF*, the solar exposition is described considering the *MOS* and the relative height of the district with respect to its surroundings H/H_{avg}.

3.3.1 Methodology

The presented model is an energy balance at neighbourhood scale that simulates monthly thermal energy consumptions of residential buildings connected to the DHN. The measured energy data used for the validation refer to three consecutive heating seasons (2012-2013, 2013-2014 and 2014-2015). Monthly data about the energy consumption for SH and DHW were provided by the IREN district heating company for forty-eight meshes (districts) with a dimension of 1 km x 1 km. The energy model is set up considering the energy balance indicated in the ISO 52016-1:2017 and ISO 52017-1:2017 standards for residential buildings. The thermal energy demand for humidification and dehumidification is not considered.

The residential buildings of the city are classified according to the type of consumption: space heating “H” or space heating and domestic hot water “H+DHW” consumptions. This distinction was made after having analysed the consumption data: the meshes in which consumption was known in the summer months are identified as H+DHW, while the meshes in which consumption was only known for the winter season are classified as H.

Only residential buildings are considered in this model. The percentage of residential buildings located in each mesh is calculated and this percentage is applied to the total energy consumption data to consider only the residential quota. This methodology hypothesizes that, in each area of the city, residential buildings have a certain consumption depending on the characteristics of the buildings, on the construction year, and on the shape and orientation of the built context. Since the

main quota of energy consumption is due to residential buildings, it is assumed that the other buildings have a constant specific consumption [12].

Two parameters are used to evaluate the distribution of users related to the quota connected to the DHN:

- The percentage of residential, commercial, municipal and industrial sectors. These values were calculated using the municipal technical map of the city with GIS tools through the information of buildings' volume (net and gross), area, number of floors and type of users.
- The percentage of volumes connected to the DHN. This value was calculated using the data from IREN district heating company (net volume) compared to the total volume (from GIS database) of the area.

Most of the residential buildings were built before 1990 and their shape is quite uniform, with only large condominiums being connected to the DHN.

As previous mentioned, the adopted approach is a bottom-up engineering model of the heat and mass flow balance which may be used to predict thermal energy-use at a district scale. The model is based on simplified heat transfer equations, and three urban variables that affect the thermal consumption of buildings are introduced. Existing standards do not consider these parameters, but this methodology has introduced them in order to analyse how the orientation of the building and how the relationship between a building and its surrounding context influence its energy performances. The heat and mass flows of the thermodynamic system are represented in Figure 13 with the control surface and the main characteristics of the building stock and the surroundings.

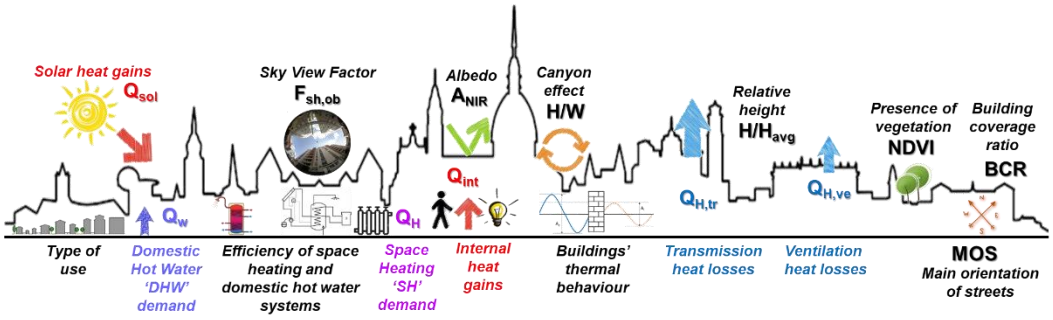

Figure 13. Scheme of heat and mass flows of the thermodynamic system of the building stock at a neighbourhood scale with the control surface (black line) between the building stock and the outdoor environment [46].

The EP of buildings is strongly influenced by the climatic conditions. The weather data (air temperature, relative humidity, and solar radiation) have been associated to each mesh (district), and they refer to the average climatic data of the city and to the nearest weather station (WS).

For each homogeneous group of buildings, the following monthly energy balance for SH and DHW production is carried out:

- The thermal energy demand of the building envelopes, with heat dispersion for transmission and ventilation, and the solar and internal heat gains, considering the thermal transmittance values of the envelope, the air flow rate, the solar shadings, and the internal heat gains.
- The energy supplied to the buildings, considering the efficiency of SH and DHW systems. The distribution losses of the DHN are not considered because the energy meters are located near each building. Therefore, the efficiency of the systems considers the generation and utilization components, respectively from the point of delivery of the building to the distribution system and from the distribution system to the emission system.

This place-based method involves the calculation of the energy demand and supply of residential buildings necessary to guarantee internal air temperature comfort conditions at a temperature of 20°C during the heating season. This methodology adapts the energy balance equations at a building scale. Some variables used in the standards are modified to describe the phenomenon at a larger scale. Three urban variables were added to the energy balance equations: the *SVF*, the *MOS* and H/H_{avg}. These urban parameters were introduced to evaluate the solar exposition (solar heat gains) and heat dispersion (radiative extra-flux to the sky) of each mesh. The laminar coefficients (i.e., convective and radiative) of the heat losses on the building façade, were selected according to the wind velocities recorded by local weather stations and the Italian Standards (i.e., UNI/TS 11300). These coefficients were identified by experimental campaigns and CFD analyses.

Figure 14 shows the process from the input data and pre-processing to the simulation procedure:

- Input data refers to the buildings, climate conditions, and urban morphology. Only a number of the indicated urban parameters (with an 'x') are considered in this version of the model.
- In the pre-processing phase, the input data are elaborated and associated to each mesh.
- The simulation results are compared with the measured data, for validation purposes, and the model was calibrated with a number of urban variables to optimize it and reduce the error.

The input data are elaborated with GIS tools and a database is created using: the municipal technical map, the territorial database of the region, the socio-economic data, the WS measurements (HDD, air temperature, relative humidity, solar radiation), satellite images (Landsat 8) with a precision of 30 meters available from USGS website, the DSM with a precision of 5 meters provided by Piedmont

region, and the monthly energy consumptions data provided by the IREN district heating company.

An iterative procedure is performed on excel spreadsheets to reduce the error of the energy simulations, using the following quality measures: (i) the error (E) is used to compare the results of the model (forecast values) with the measured data; (ii) the relative error (E_r) and the absolute relative error ($|E_r|$). E_r is calculated as the difference between measured and forecast value, divided by the measured value. $|E_r|$ is the measure of the prediction accuracy of the model and is the absolute value of the relative error; (iii) the coefficient of determination (R^2), which is a key output to compare calculated and measured data, and it was used as a guideline to establish the accuracy of the model.

The joint use of these types of error allows to consider both the absolute values and the percentage differences between calculated and measured data but also to consider 'acceptable' higher percentage errors if the absolute consumption value is very low.

In the last part of this analysis, to understand how the urban form influences the energy consumption of residential buildings, some simulations are made using the variability of two urban parameters: *SVF* and *MOS*. Four scenarios are investigated considering different levels of unfavorable and favourable conditions.

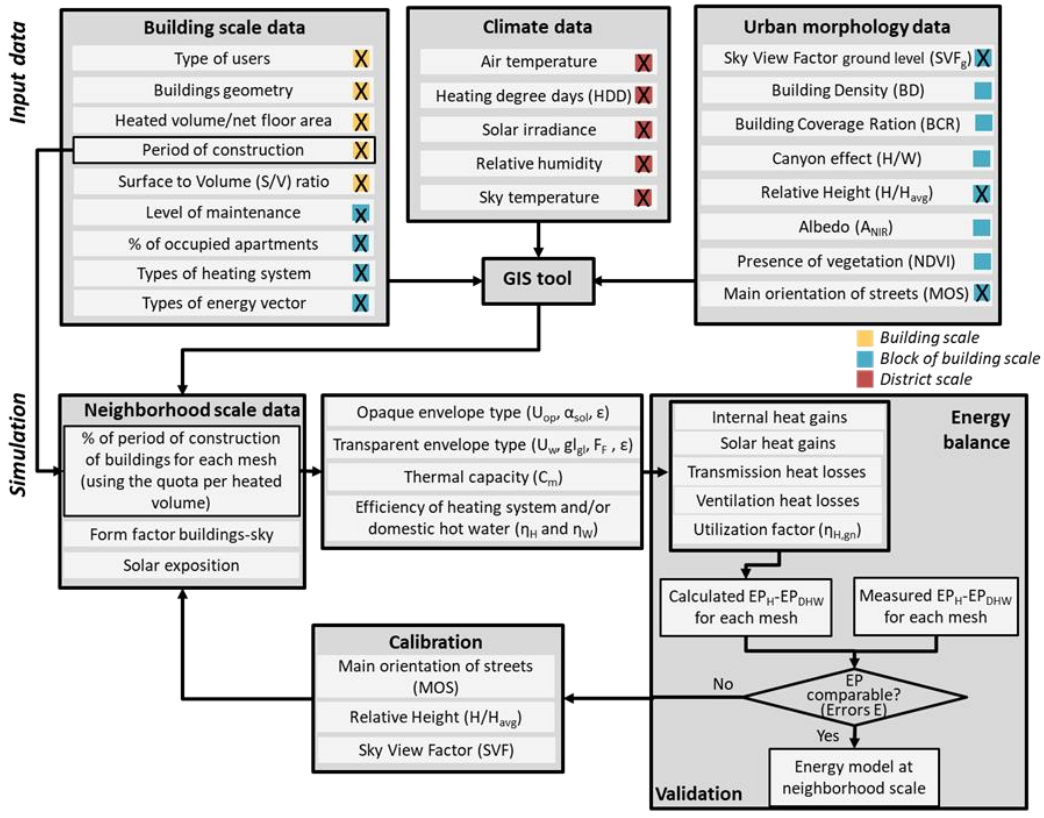

Figure 14. Flowchart of the methodology: data input (building data, climate data and urban morphology data), pre-processing (mesh scale data) and simulation (calibration and validation at mesh scale) [46].

3.3.2 Input data

The following data is elaborated by means of GIS tools at a building and district scale:

- Climate conditions (air temperature and relative humidity, solar irradiance, HDD), distinguishing between the average monthly data for Turin and the monthly data of the nearest WS in order to characterize the local climate of the different urban built-up areas.
- Building characteristics (heated volume, type of building, construction year, *S/V* ratio, net floor surface, opaque and transparent envelope type and area).
- Characteristics of the heating system (centralized or autonomous system, system efficiencies, type of energy vector).
- Urban morphology (solar exposition, streets orientation and *SVF*).

Climate data

The local climate conditions are influenced to a great extent by such environmental context factors as the urban morphology, the solar exposition, the type of materials of the outdoor spaces and the presence of vegetation and/or water.

In this analysis, the data of five WSs are used to evaluate how the urban characteristics influenced the local climate and the energy consumptions. Two models are elaborated. The first one considers the average climatic conditions of the entire city, and the second one uses the local climate data registered by the nearest WS. As shown in Figure 15, the WSs data (air temperature) are very similar even if, in the heating season 2013-2014 with 1,962 HDD ("Via della Consolata" WS), a difference of 1°C could influence the energy consumption of about 10%.

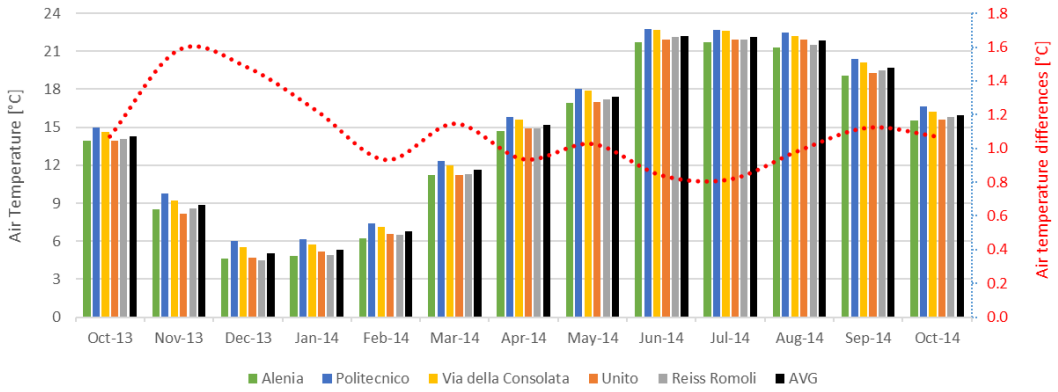

Figure 15. Distribution of the monthly WS air temperatures for the 2013-2014 season in the city of Turin (using data from five WSs) [46].

The local climate data used as input data refer to: monthly average values of the outdoor air temperature [°C] and monthly average solar irradiance [W/m^2] on the horizontal plane taken from the WSs in Turin.

Building data

The thermophysical and geometric parameters of the buildings in the analysed forty-eight meshes, are characterized using information from the municipal technical map of the city (2015), ISTAT census data (2011), European standards and data from the literature review [149]. Because of missing data and/or anomalies, only a certain number of meshes are analysed to develop the monthly energy models. The unused meshes are lacking in data for a few months of the three considered seasons. Therefore, to avoid errors in the model due to a lack of data for some months and/or due to the presence of erroneous data, only thirty-three of the original forty-eight meshes were selected.

The following data are calculated for each mesh to characterize the residential buildings connected to the DHN. The geometrical data are calculated using the attribute of a 2D footprint. The territorial database is implemented with other official information, such as the characteristics of the territory (using the DSM) and the distribution of the population (ISTAT data).

The typological characteristics of the building used as input data are: (i) net and gross heated volume [m^3] of the buildings; (ii) net and gross floor surface [m^2] of the buildings, the net area is obtained by multiplying the gross area by the f_n coefficient as a function of a typical wall thickness (d_m) of the construction period; (iii) heat transmission surfaces [m^2] of the inferior or ground slab, of the roof or the upper slab and of the vertical walls, but the walls adjacent to other heated buildings are not considered in the calculation; a transparent surface equal to 1/8 of the floor is assumed for the windows (equally distributed among all external wall orientations), according to [149]; (iv) solar exposure and orientation, the *MOS* is evaluated considering an average value at a census section scale (at a block of buildings scale); (v) shading elements, using the DSM of Turin and the equations on solar geometry in GIS (i.e., area solar radiation in spatial analyst tool); (vi) solar reflectance of the external outdoor surfaces taken from satellite images (the near-IR albedo calculated from Landsat 8 images was used in this work [151]).

The thermal properties of the building used as input data are: (i) thermal transmittance [$W/m^2/K$] of the envelope; a specific value is selected for each construction year for all the heat transmission surfaces, and an average value is associated to each district (1 km^2) considering the percentage distribution of the buildings with different construction periods [149]; (ii) total solar transmittance (g_{gl}) of the transparent envelope; only two values of g_{gl} are considered, with reference to the standard (ISO 52016-1:2017): for single glass and for double glass, and the construction period and the maintenance level of the buildings are also taken into consideration; (iii) the solar radiation absorption coefficient (α_{sol}) of the opaque envelope is determined considering the main colour of the building envelope; (iv) emissivity (ε) of the envelope is assumed constant for opaque and transparent elements; (v) reduction frame factor (F_F) of the windows is supposed constant; (vi) thermal capacity (C_m) [$kJ/m^2/K$] is determined as a function of the construction year; (vii) system efficiencies (η) are determined for the different construction years

for the SH and DHW systems, considering the typical centralized and autonomous systems that are connected to the DHN (ISO 52017-1:2017, [149]).

Below is the list of the use of the buildings used: (i) type of use, the buildings are classified as residential, municipal, tertiary, and industrial (the municipal and tertiary ones are further sub-categorized); (ii) type of ventilation, natural or mechanical; (iii) heating season period, which depends on the Italian climatic zone; (iv) internal heat gains (Q_{int}), which depend on the use of the of building types (ISO 52016-1:2017).

Urban data

Each mesh is categorized by analysing different urban variables. These variables are evaluated using the municipal technical map (2015), ISTAT census data (2011), remote satellite images (2015) and the DSM with a precision of 5 meters. A georeferenced territorial database was created. Average values of urban morphology factors are identified for each mesh.

The H/W, the H/H_{avg}, the BCR and BD are calculated using GIS tools.

The SVF is calculated with the support of Relief Visualization Toolbox (RVT) software [150], an average value of SVF is elaborated and associated to each mesh with a GIS tool. The SVF is used to quantify the shading reduction factor ($F_{sh,ob}$) resulting from external obstacles and the form factor (F_r) between the buildings and the sky. The SVF is considered at a mid-height of the buildings (considering an SVF = 1 at the building roof level) and this value is constant for each month of the year.

Albedo near infrared (A_{NIR}) is considered in order to investigate different materials used for the urban surfaces can influence the microclimate in the surrounding building context. The A_{NIR} is calculated from remote sensing images (Landsat 8) referring to November 2nd, 2015, at 10 a.m. with a percentage of cloud cover of only 3.9%; three bands (α4, α5 and α7) are used to predict the A_{NIR} [130]. These data were assumed constant for each month of the year.

The presence of vegetation is evaluated with the $NDVI$ using Landsat 8 satellite images (for November 2nd, 2015, at 10 a.m.) [151]. Turin is mainly East-South oriented, following the course of the Po River and facing the hills.

The main orientation of the buildings is calculated using the MOS. The optimal condition of solar exposition is the East-West axis (with MOS = 1), while the worst condition is the North-South axis (MOS = 0).

3.3.3 Engineering model

This section describes the method used to define the monthly energy balance for a group of residential buildings, adapting the energy balance from a building to a district scale. Usually, these standards specify calculation methods that can be used to assess the sensible energy needs for SH, based on monthly calculations at building scale. This calculation method can be used for residential or non-

residential buildings and can be applied to buildings at the design stage, to new buildings after construction and to existing buildings in the use phase.

Space heating energy demand

Equation (1) defines the monthly energy balance of the building stock envelope, considering the total heat transfer ($Q_{H,ht}$) and total heat gains (Q_{gn}) for SH under different climatic conditions:

$$Q_{H,nd} = Q_{H,ht} - \eta_{H,gn} \cdot Q_{gn} = \left(Q_{H,tr} + Q_{H,ve}\right) - \eta_{H,gn} \cdot (Q_{int} + Q_{sol}) \quad (1)$$

The total heat transfer ($Q_{H,ht}$) is composed of the sum of the heat transfer due to transmission ($Q_{H,tr}$) and ventilation ($Q_{H,ve}$), while the heat gains are due to the internal (Q_{int}) and solar (Q_{sol}) heat components.

The transmission heat transfer, between the heated space of the building stock and the external environment, is driven by the difference between the air temperature inside the heated buildings (T_i) and the external air temperature (T_e) is assumed constant at 20°C. This methodology introduces a monthly model, and the temperature during the day varies slightly, but on average always remains constant. Two outdoor air temperature values are considered for T_e: the average monthly temperature of five WSs in the city and the monthly air temperature of the nearest WS in each mesh. The utilization factor ($\eta_{H,gn}$) is a function of the heat flow balance through the building envelope and the thermal inertia of the building stock; it is evaluated for each month and for each mesh, according to the internal heat capacity characteristics of the building stock, considering the different construction years.

The construction characteristics of the building stocks are assumed, in consideration of the different construction years and the geometric features of the buildings, as evaluated with the support of GIS tools.

Equations (2) and (3) describe the total heat loss as a result of transmission and ventilation of the building stock, respectively, and considering a uniform inside air temperature of 20°C during the heating season (τ is the number of hours).

$$Q_{H,tr} = H_{tr,adj} \cdot (T_i - T_e) \cdot \tau + \left\{\sum_k F_{r,k} \cdot \phi_{r,k}\right\} \cdot \tau - Q_{sol,op} \quad (2)$$

The transmission heat transfer coefficient ($H_{tr,adj}$) is calculated considering: the thermal transmittance values (U) of the buildings for different construction years (before 1918, 1919-1945, 1946-1960, 1961-1970, 1971-1980, 1981-1990 and 1991-2005) for each mesh using the percentage quota per heated volume [149]; the opaque and transparent heat dispersing areas (A), calculated by means of GIS tools

(with a constant transparent area equal to 1/8 of the building floor surface); and the unheated volumes of the attics and cellars.

The extra heat transfer, considering the thermal radiation lost to the sky, depends on the form factor between the building stock and the sky ($F_{r,k}$) and on the thermal radiation lost to the sky ($\phi_{r,k}$).

$$F_{r,k} = F_{sh,ob} \cdot \frac{1 - cos\alpha}{2} = \left(\mathbf{1} + \boldsymbol{SVF_g}\right)/\mathbf{2} \cdot \frac{1 - cos\alpha}{2} \quad (2.1)$$

$$\phi_{r,k} = R_{se} \cdot U_{op} \cdot h_r \cdot (T_e - T_{sky}) \quad (2.2)$$

The form factor $F_{r,k}$ depends on the *SVF* of the building stock and on the inclination α of the control surface. The *SVF* is calculated at the ground level (SVF_g) for each mesh and an average value of *SVF* is considered at the mid-height of the buildings (considering an *SVF* of 1 at the building roof level).

The thermal radiation $\phi_{r,k}$ is calculated considering the control surface with a constant external thermal surface resistance (R_{se}), which is a function of the outdoor air velocity, and an external radiative heat transfer coefficient (h_r), which is a function of the control surface emissivity and of the sky temperatures.

Moreover, to consider the influence of the direct solar radiation component, $Q_{sol,op}$ is multiplied by the *MOS* value, as indicated in Equation (2.3), for zones with low relative heights ($H/H_{avg} < 1$) and with unfavorable orientation of the streets (with $MOS < 0.5$). In this way it is possible to consider a non-optimal solar exposure and, as a result, lower solar heat gains.

$$Q_{sol,op} = \left\{\sum_k \phi_{sol,op,k}\right\} \cdot \tau \quad (2.3)$$

with:

$$\phi_{sol,op,k} = F_{sh,ob,op} \cdot A_{sol,op} \cdot I_{sol,op} = \boldsymbol{\omega} \cdot \left(\mathbf{1} + \boldsymbol{SVF_g}\right)/\mathbf{2} \cdot A_{sol,op} \cdot I_{sol,op}$$

$$\boldsymbol{\omega} = \begin{cases} \boldsymbol{MOS} \; if \; \dfrac{\boldsymbol{H}}{\boldsymbol{H_{avg}}} < 1 \; and \; \boldsymbol{MOS} < 0.5 \\ 1 \; if \; \dfrac{\boldsymbol{H}}{\boldsymbol{H_{avg}}} \geq 1 \; or \; \boldsymbol{MOS} \geq 0.5 \end{cases}$$

(*MOS* = 0 for a building axis with a North-South orientation and *MOS* = 1 for a building axis with a West-East orientation)

$$A_{sol,op} = \alpha_{sol,op} \cdot R_{se} \cdot U_{op} \cdot A_{op}$$

The shading reduction factor ($F_{sh,ob,op}$) is a function of the external obstacles and is equal to the average value of *SVF* at the mid-height of the buildings; solar irradiance ($I_{sol,op}$) is the amount of incident solar irradiance on the opaque envelope; the absorption coefficient ($\alpha_{sol,op}$) of the opaque envelope is supposed constant and depends by the average color of the buildings walls; thermal surface resistance (R_{se}) is a function of the outdoor air velocity; the thermal transmittance of the opaque envelope (U_{op}) depends on the different periods of construction; the opaque envelope area (A_{op}) is calculated by means of GIS tools.

The total heat transfer ($Q_{H,ht}$) in Equation (1) is also influenced by the ventilation heat losses ($Q_{H,ve}$):

$$Q_{H,ve} = H_{ve,adj} \cdot (T_i - T_e) \cdot \tau \quad (3)$$

with:

$$H_{ve,adj} = \rho_a \cdot c_a \cdot \left\{ \sum_k q_{ve,k} \right\} = \rho_a \cdot c_a \cdot \frac{n \cdot V}{3600}$$

The value of the heat transfer coefficient resulting from ventilation $H_{ve,adj}$ depends on the heat capacity of the air per volume ($\rho_a \cdot c_a$ = 1,200 J/m^3/K), on the air flow rate volumes ($q_{ve,k}$) or on the hourly air exchange volumes (n).

Equations (4) and (5) describe the total heat gains (Q_{gn}), which are obtained by summing the internal heat gains (Q_{int}) and the solar heat gains ($Q_{sol,w}$).

$$Q_{int} = \left\{ \sum_k \phi_{int,k} \right\} \cdot \tau = \{5.294 \cdot S_f - 0.01577 \cdot S_f^2\} \cdot \tau \quad (4)$$

The internal heat gains Q_{int} are calculated considering the floor area of residential buildings and the average area per dwelling (with the geometrical characteristics of the building stock calculated with GIS tools and ISTAT census data for 2011).

The global value of the internal heat gains is obtained for residential buildings with a net floor area (S_f) less than or equal to 120 m^2 (UNI/TS 11300-1:2014 issued to implement the European Directive 2002/91/CE).

$$Q_{sol,w} = \boldsymbol{\omega} \cdot \left\{ \sum_k \phi_{sol,w,k} \right\} \cdot \tau \quad (5)$$

with:

$$\phi_{sol,w,k} = F_{sh,ob,w} \cdot A_{sol,w} \cdot I_{sol,w} = \left(\mathbf{1} + \boldsymbol{SVF_g}\right)/\mathbf{2} \cdot A_{sol,w} \cdot I_{sol,w}$$

$$A_{sol,w} = g_{gl} \cdot (1 - F_F) \cdot A_w$$

The solar heat gains $Q_{sol,w}$ are calculated by multiplying the heat flow rate, due to the solar heat sources $\phi_{sol,w,k}$ by ω considering the solar exposition (as mentioned above); the shading reduction factor, due to the external obstructions ($F_{sh,ob,w}$), is calculated considering the *SVF*; the effective glazing area ($A_{sol,w}$) pertains to the window area (A_w), the window frame factor (F_F) and the total solar energy transmittance of the glasses (g_{gl}) for the different construction years of the buildings.

Domestic hot water demand

The energy demand for domestic hot water ($Q_{W,nd}$) is calculated according to Equation (6).

$$Q_{W,nd} = \rho_w \cdot c_w \cdot \sum_i V_{w,i} \cdot \left(T_{er,i} - T_o\right) \cdot G \quad (6)$$

with:

$$V_{w,i} = 1.067 \cdot S_f + 36.67$$

Where ρ_w and c_w are the density and the specific heat of water, respectively; $V_{w,i}$ is the required daily volume of hot water; $\left(T_{er,i} - T_o\right)$ is the difference between the hot water supply temperature (assumed equal to 40°C, with reference to the standard ISO 52017-1:2017 condition) and the incoming cold water temperature (assumed equal to the annual air temperature); G is the number of days of the considered calculation period (year) which, in this case, is equal to 365 days; $V_{w,i}$ is the required daily hot water volume as a function of the average floor area per dwelling in each mesh; for residential buildings, $V_{w,i}$ is obtained by the standard (ISO 52017-1:2017) for apartments with net floor surfaces (S_f) between 50 and 200 m^2.

Heat energy consumption

The energy need ($Q_{H,nd}$ and $Q_{W,nd}$) being known, annual average values of the system efficiencies (η_H and η_W) are used to quantify the energy supplied for space heating (Q_H) and domestic hot water (Q_W) at district scale for each 1 km^2 mesh:

$$Q_H = \frac{Q_{H,nd}}{\eta_H} \qquad Q_W = \frac{Q_{W,nd}}{\eta_W} \quad (7)$$

To exclude the quota of non-residential energy consumption, it is assumed that the non-residential users have a constant specific consumption (expressed in $kWh/m^3/y$) [12]. This hypothesis can be considered acceptable since the consumption provided by the IREN district heating company is mainly for residential buildings.

Theoretical backgrounds

In this subsection the comparison between the standard energy balance at building scale and the new energy balance at neighbourhood scale is explained in detail. Referring to the energy balance equations for residential buildings of the new model, the various variables introduced in the urban-scale model are summarized in Table 5.

Table 5. Comparison between energy balances at building scale with the new model at neighbourhood scale [46].

Standard energy balance at building scale	**New energy balance at neighbourhood scale (mesh scale)**	**Eq.**
The energy needs $Q_{H,nd}$ and all terms of the energy balance refer to a single residential building.	$Q_{H,nd}$ and all terms of Eq. 1 refer to the residential buildings in a neighbourhood; the quota of residential buildings is calculated by the percentage in volume.	(1)
The transmission heat transfer coefficient ($H_{tr,adj}$) is calculated with thermal transmittances and heat-dispersing areas of the building envelope.	$H_{tr,adj}$ is calculated knowing: the areas and the thermal transmittances, by average values weighted on the volumes of buildings of different construction periods.	(2)
The outdoor climatic variable (as the air temperature T_e) is the monthly average value recorded locally.	For a district, T_e is the monthly average value recorded by the nearest WS; for the city, the average value is calculated considering all WSs. The same applies to all other climatic variables.	(2), (2.2), (3), (6)
The form factor between the building surfaces and the sky ($F_{r,k}$) is calculated knowing the shading reduction factor $F_{sh,ob}$ and the surfaces inclination.	The form factor between the buildings and the sky ($F_{r,k}$) is calculated with the average values of *SVF* on the envelope surfaces (e.g., for the vertical walls at the mid-height of the buildings).	(2.1)
The solar heat gains through the envelope elements (Q_{sol}) are calculated knowing $F_{sh,ob}$, A, $\alpha_{sol,op}$, U_{op}, g_{gl} and F_F of each opaque and transparent surface.	The $F_{sh,ob}$ is equal to the average value of *SVF* on the envelope surfaces multiplied by the solar exposition of the district *ω;* the solar exposition ω considers the height of the buildings compared with their surroundings and their main orientation. The envelope area is calculated with GIS tools and for $\alpha_{sol,op}$, U_{op} and g_{gl}an average value is utilized depending by the period of construction.	(2.3), (5)
The ventilation heat losses ($Q_{H,ve}$) are calculated knowing the air volume of a buildings and the air flow rate of the type of user (residential).	The air volume and the air flow rate of all buildings are calculated with GIS tools knowing the: gross volume of buildings, envelope thickness, percentage of occupied volume and percentage of residential buildings in the districts.	(3)
The internal heat gains (Q_{int}) depends by the useful floor area and by the type of user (residential).	Q_{int} is calculated with GIS tools knowing the: gross area of buildings, envelope thickness, percentage of occupied volume and average floor area of dwellings.	(4)
The energy demand for domestic hot water ($Q_{W,nd}$) depends by the required volume of hot water and the water temperature gradient.	$Q_{W,nd}$ at depends by the: number of dwellings, average dwelling floor area, percentage of DHW systems connected to the DHN and the water temperature supplied by the aqueduct (T_e= average annual external air temperature).	(6)
The energy supplied for space heating (Q_H) and domestic hot water (Q_W) for each district depends by the energy needs and the efficiency of the systems η).	The efficiencies of the systems η were obtained by average annual values weighted on the volumes of buildings of different construction periods.	(7)

3.3.4 Model application

The model is applied to the city of Turin that is in the North-Western part of Italy, in the climate zone E with 2,648 HDD (according to UNI 10349-3:2016). Averaging over the five WSs considered, the HDD for the three consecutive heating seasons analysed are: 2,388 HDD for 2012-2013, 2,028 HDD for 2013-2014 and 2,054 HDD for 2014-2015.

There are about 60,000 heated buildings, of which 45,000 are residential, and the quota of heated gross volume is 232 Mm^3. The residential sector is mainly made up of large and compact condominiums. More than 24,000 residential buildings (55%) have the *S/V* less than 0.45 m^2/m^3 (average value of Turin is 0.55 m^2/m^3). The 57% of residential buildings were built before 1960, 80% of the buildings were built before 1970 (before the first Italian Law 373/1976 on buildings energy savings), 15% of the residential buildings were built between 1970 and 2000 and only 2% were built after 2006.

This methodology has investigated residential buildings connected to the DHN and the territorial analysis unit is a 1 km^2 mesh. A total of 28,186 heated buildings are analysed in the 48 meshes, of which 78% (22,007) are residential buildings.

The main construction year of the residential sector is between 1946 and 1970 (52%): 7% of the residential buildings were built before 1918, 19% were built between 1919 and 1945, 11% between 1971 and 1980 and 10% after 1981 (only 2% were built after 2006).

The average *S/V* value is 0.54 m^2/m^3 and the median value is 0.44 m^2/m^3. The shapes of the buildings are quite homogenous in the considered areas. The residential buildings have a somewhat constant height of 18.5 m, and they are mainly large condominiums with low *S/V* values. The occupancy ratio of the residential buildings is close to 0.93, and this value is typical of the residential sector.

The quota of DHW of the buildings connected to the DHN is low, around 10% and the percentage of buildings connected to the DHN is on average 55%, but this value varies a lot depending by the zone. Some meshes are excluded in this analysis because the type of energy consumption changed in the analysed period (only H in some seasons and H+DHW in other seasons).

Since the model is based on the energy consumption of residential buildings connected to DH, the accuracy of the model depends on the number of buildings connected to the DHN.

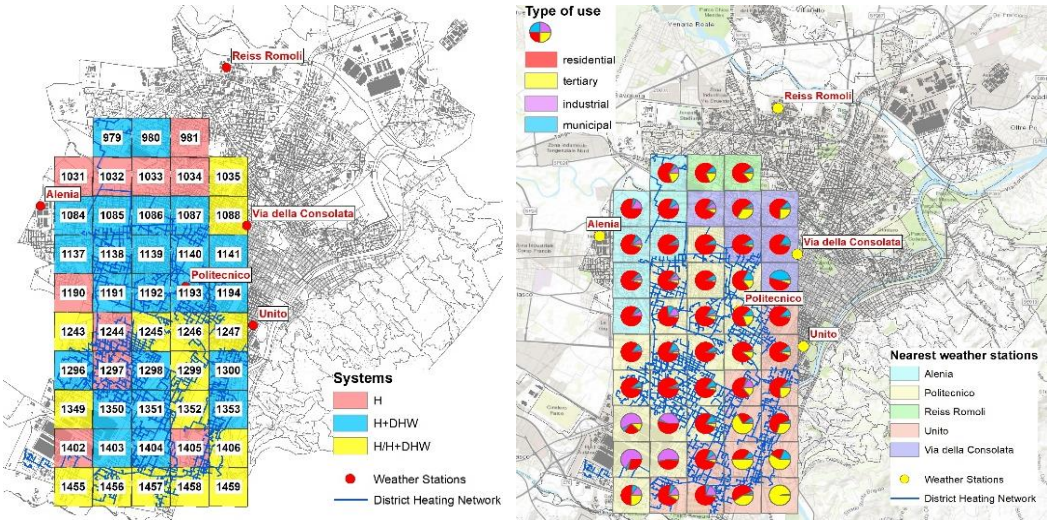

(a) (b)

Figure 16. Case study: (a) Distribution of the 48 meshes (1 km^2) and classification of the type of energy consumption: space heating 'H' in red, space heating and domestic hot water 'H+DHW' in blue, 'H' and/or 'H+DHW' in yellow (the identification code (ID) is inside the meshes); (b) Identification of the nearest WS for each mesh and distribution of the different types of user considering 4 sectors: residential (red), tertiary (yellow), municipal (blue) and industrial (violet) [46].

Figure 16 shows the location of the 48 meshes analysed and information about the types of energy consumption, the nearest WS and the different type of users at a district scale. Figure 16a shows the 15 yellow meshes that are excluded from the analysis because they had some season with only H and others with H+DHW, 10 meshes with only H and 23 meshes with H+DHW. Figure 16b shows the five WSs considered in this work: it can be observed that, for some meshes, the nearest WS does not describe the real weather conditions of the area (the station is too far away). The average Turin weather data are also used to design the model, and the result of two models are compared to evaluate how the urban characteristics influence the local climate and the energy consumption. The comparison of the two models allows to understand how much the precision of the models varies according to the climate and local climate characteristics.

Assumptions

Some assumptions have been made to apply the monthly energy model at a neighbourhood scale. Most of Turin's residential building stock is built before 1970 (80%), and the structural characteristics of the buildings are quite homogeneous. Therefore, it is assumed that the analysed residential buildings had certain factors in common (calculated using the European standards in force):

- The gross heated volumes connected to the DHN are calculated from the net volumes divided by 0.75, as specified by the IREN district heating company.
- The U-values are calculated for each mesh considering the percentage of building volumes for each construction year, and an average value

was identified by distinguishing between transmittance vertical walls, a transparent envelope, a floor with a basement (with an adjustment factor for unconditioned spaces, btr_{floor} = 0.8) and a ceiling with an unheated attic and an uninsulated roof (btr_{roof} = 0.9). In Table 6 the data about the thermal transmittance for the different construction years are reported.

- The f_n coefficient, which is used to obtain the net usable floor area from the gross area, is calculated considering the construction year of the buildings.
- The thermal capacity is assumed constant, with C_m = 165 kJ/m^2/K for buildings with no or external thermal insulation, with a medium or heavy envelope and a greater number of floors than 3.
- The average colour of the opaque envelope is an average one, neither dark nor clear, with a solar radiation absorption coefficient of α_{sol} = 0.6 and an emissivity ε = 0.9.
- The external surface heat resistance R_{se} is taken as 0.04 m^{2}K/W, considering that the contribution of wind to the different areas in Turin is negligible (about 1.4 m/s, according to UNI 10349:2016).
- The window area is calculated considering 1/8 of the net floor area (according to the indications of the Italian hygienic standards for buildings D.M. 5/7/1975). The frame factor F_F was assumed constant and equal to 0.8; the total solar energy transmittance values of the glasses g_{gl}, are defined as a function of the construction year of the buildings and their level of maintenance referring to single glass (g_{gl} = 0.85) or to double glass (g_{gl} = 0.75).
- An air exchange rate of n = 0.5-0.3 h^{-1} is assumed for natural ventilation in residential buildings, depending on their construction year and level of maintenance.
- The heating season for the city of Turin is from October 15th to April 15th and covers a period of 183 days. The full months of October and April are considered in the energy simulations because the systems are switched on before this date in order to have all the heating systems active on October 15th; the same procedure takes place for the shutdown: the systems are gradually switched off from April 15th and the heating period is therefore generally longer.
- The average value of the usable floor area per dwelling (Sf) is used to evaluate the DHW consumption of each mesh and it was always less than 200 m^2 (with an average value of 88 m^2).
- The internal heat gains are calculated for each mesh, considering the average floor area per dwelling as 3.9-5.2 W/m^2 (with an average value of 4.9 W/m^2).
- The system efficiencies of the SH and DHW are calculated for each mesh, considering the connection to the DHN (in Table 6, [149]).

For SH systems an average value is calculated for the different construction years as "multi-unit housing" building classes; a typical heating system is considered to consist of a radiator emission system on uninsulated walls with a climate control system, a vertical distribution system with about 4 floors and a heat exchanger as the generation system; according to construction year, the overall system efficiency was taken on average equal to 0.67-0.81 taking into account that the old boilers have been partially replaced with the district heating heat exchangers (according to the percentage of buildings connected to the DHN).

For DHW systems the overall system efficiency is assumed to be about 0.60; the percentage of buildings connected to the DHN for this service was calculated for the consumption of DHW.

Table 6. U (W/m^2/K) and η_H (%) values for buildings with different construction years [46].

Variable	<1918	1919-45	1946-60	1961-70	1971-80	1981-90	1991-2005
U_{window},	4.85	4.75	4.40	4.90	4.57	3.80	2.15
U_{roof}	1.80	1.80	1.80	2.20	2.20	1.18	0.68
U_{wall}	1.45	1.35	1.18	1.13	1.04	0.78	0.70
U_{slab}	1.75	1.58	1.23	1.30	1.21	1.95	0.80
η_H (with gas boiler)	67			67 (1961-76)		69 (1977-93)	75
η_H (connected to DHN)	78			79 (1961-76)		82 (1977-93)	84

Homogenous groups

33 meshes with complete data on energy consumption for H and DHW from October 2012 to January 2016 are selected to apply and validate the monthly energy model. A consistent quota of residential buildings is found in most of the meshes, and the model is therefore studied for this type of user as the percentage in volume of the heated residential buildings in each mesh is known. The IREN district heating company supplied the monthly energy consumption data for each mesh, and the total of the heated volumes connected to the DHN.

Two types of energy balance models are created based on the type of consumption: group 1 (H+DHW) had 23 meshes with information on the SH and DHW consumptions, and group 2 (H) is composed of 10 meshes with only consumption information for SH consumption.

The data on energy consumption are available for each mesh and for three consecutive heating seasons: 2012-2013, 2013-2014 and 2014-2015. The meshes with low percentages of residential buildings, especially in the peripheral areas, may yield less accurate energy performance results.

The group 1, H+DHW, is divided into three homogenous groups of buildings, according to their construction year: H+DHW|$_1$ construction year < 1960, H+DHW|$_2$ construction year 1961-1970, H+DHW|$_3$ construction year 1971-1990. The S/V of the residential buildings in these areas is constant, with an average value

of 0.53 m^2/m^3 and a standard deviation of 0.07 (i.e., large condominiums). The energy-use model of the residential buildings is analysed considering the energy consumption of all the buildings and the proportion of residential buildings connected to the DHN. The meshes showed a high percentage of residential buildings (an average value of 72%), but there are some meshes (ID: 979, 1141, 1300, 1350, 1353 and 1403) that had a smaller percentage, and the energy simulations could be less accurate. The state of maintenance of the buildings is generally good, with higher values for new buildings, and the average U-values are higher for the meshes with older buildings. Systems efficiency is about 72-75 % depending on the percentage of buildings connected to the DHN and the different construction years. The *BCR* is higher for the residential buildings built before 1960 than for the buildings built later on, and the building density is in general greater in the central historical urban area of Turin. The *H/W* is also higher in the meshes with buildings built before 1960, while the H/H_{avg} is basically equal for all the built-up areas. The SVF_g is lower for the high-density areas and higher in the areas with a lower *BCR* (ID: 1296, 1350, 1403, 1404) and in zones with a high presence of vegetation (high *NDVI* in ID: 979, 980).

The second homogenous group, H, is composed of 10 meshes. Due to the limited number of meshes, no subdivisions are made for the building construction years, consequently the accuracy of this model is lower. In this group, residential buildings were mainly built between 1961 and 1970 (6 meshes), the level of maintenance is more than sufficient, and the *S/V* was similar, with an average value of 0.58 m^2/m^3 and a standard deviation of 0.05. The percentage of residential buildings is in general above 77% (median value), with an average value of 69 %; only three meshes (ID: 1034, 1402 and 1405) had a lower percentage. As already mentioned, the *U* and the systems efficiency (≅ 72 %) depend on the construction year. SVF_g is relatively constant, with an average value of 0.54. The presence of vegetation is somewhat scarce since the analysed areas are in a consolidated urban context. Three meshes (ID: 1031, 1032 and 1033) had a slightly high *NDVI* value, because they are near a park or a green area. The other urban variables showed that the areas are densely built, and the buildings had similar heights (with H/H_{avg} of 1).

Table 7. Variability of the building characteristics [46].

Group	**Period**	***S/V***	**Maint. level**	***BCR***	***H/W***	H/H_{avg}	***MOS***	SVF_g	A_{NIR}	***NDVI***
-	-	m^2/m^3		-	-	-	-	-	-	-
$H+DHW\|_1$	< 1960	0.47-0.76	2-4	0.20-0.43	0.29-0.56	0.92-1.02	0.34-0.53	0.34-0.53	0.1-0.13	0.08-0.18
$H+DHW\|_2$	1961-70	0.43-0.61	2-4	0.27-0.40	0.31-0.47	0.98-1.03	0.35-0.45	0.40-0.60	0.11-0.14	0.13-0.22
$H+DHW\|_3$	1971-90	0.37-0.53	3-4	0.15-0.29	0.25-0.42	1.01-1.08	0.35-0.48	0.55-0.73	0.12-0.16	0.14-0.29
H	-	0.47-0.64	3-4	0.19-0.36	0.24-0.46	0.95-1.03	0.29-0.56	0.47-0.6	0.12-0.17	0.11-0.32

Table 7 describes the field of application of the models according to the variability of the data. The variability of *S/V*, level of maintenance (1 = very bad, 4 = optimal), *BCR*, *H/W*, H/H_{avg}, *MOS*, SVF_g, A_{NIR} and *NDVI* are indicated for each group. It can be observed that: (i) the variability of *BCR* and A_{NIR} is low, because the urban context is consolidated, and the territory is densely built up; (ii) *H/W* has a similar range for each group; (iii) the H/H_{avg} is close to 1, with the exception of the H+DHW|$_3$ group (in which the buildings have more solar gains); (iv) *MOS* has a less variability, because most of the blocks of buildings have a North-South orientation; (v) meshes located in the peripheral areas have higher *SVF* and *NDVI* values, due to the lower urban density and the greater presence of green areas and parks. These data are used in the model to evaluate how energy consumption varies for different solar exposition values (*SVF*, H/H_{avg} and *MOS*). The homogeneous H group shows a lower EP than the H+DHW groups, and the consumptions are lower in the centre of the city (high-density areas). Decreasing values of *BCR* have be observed from the centre to the peripheral areas, while rising values can be perceived for the SVF_g and H/H_{avg}. Regarding the *MOS*, the main streets in the historical centre of Turin are about 30° from the North-South axis along the Po River and face the hills.

3.3.5 Model results and validation

This section presents and discusses the results obtained for each mesh from the application of the monthly energy balance models to the residential buildings. The data are divided into two groups: group 1, referring to the energy-use for H+DHW in 23 meshes, and group 2, referring to the energy-use for H in 10 meshes. The following steps summarize the main phases for the definition of the model:

- Identification of the input data of the built environment. At first, data about the main characteristics of the built environment were used for each mesh together with the calculation the geometric variables with GIS tool. The buildings were grouped for construction years and therefore at each group the characteristics of those buildings have been associated with a weight equal to the percentage quota in volume. Many attempts have been made to reduce model errors; for example, entering the maintenance level to reduce the thermal transmittance of the windows, but this evaluation did not lead to a significant improvement of the model.
- Introduction of the *SVF* to describe the solar exposition and the thermal radiation lost to the sky of the built environment.
- To consider the paths of the sun (and to reduce errors), in the calculation of solar exposure, the *MOS* and the H/H_{avg} have been added.
- Comparison of the simulation results using between the average climate data in the city of Turin and the data of the nearest WS to each mesh.

After identifying the main variables that affect energy consumption, the model is optimized to improve accuracy. Different types of errors are considered. With the support of the iterative procedure on excel spreadsheets, the errors are reduced by introducing new data and urban variables. Since in almost all the meshes the share of residential buildings connected to the DHN is prevalent, a constant specific consumption has been assumed for non-residential buildings. For the industrial activity, only in three meshes there are high percentages of this activity: 1350, 1403 and 1402; this area is the industrial zone (called "Mirafiori"). From the analysis it has emerged that:

- 29 meshes have consumption related to residential users, with a high percentage of residential buildings of on average 76%.
- In the meshes 979, 1034, 1141, 1300, 1353 and 1405 there is a high percentage of municipal and commercial buildings; as already mentioned, the energy consumption for SH of commercial buildings was considered constant with an annual specific consumption of 22-30 kWh/m^3/y [12].
- In the meshes 1350, 1402 and 1403 half of the buildings are residential and the other half industrial; mainly residential buildings are connected to the DHN and, for the remaining industrial portion (e.g., "Mirafiori"), a constant specific consumption was used.

Figure 17 shows some examples of the monthly consumptions for SH and the DHW profile with reference to the following meshes: 1350 (Figure 17a), for residential buildings built between 1946 and 1960; 1351 (Figure 17b), for residential buildings built between 1961 and 1970; 1296 (Figure 17c), for residential buildings built between 1971 and 1980. The higher relative errors that can be observed in the mid-seasons are due to different utilization factors or types of regulation system.

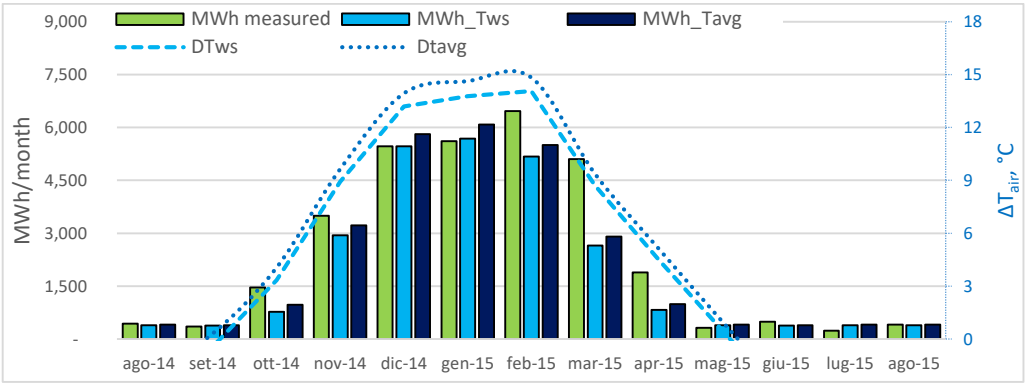

(a)

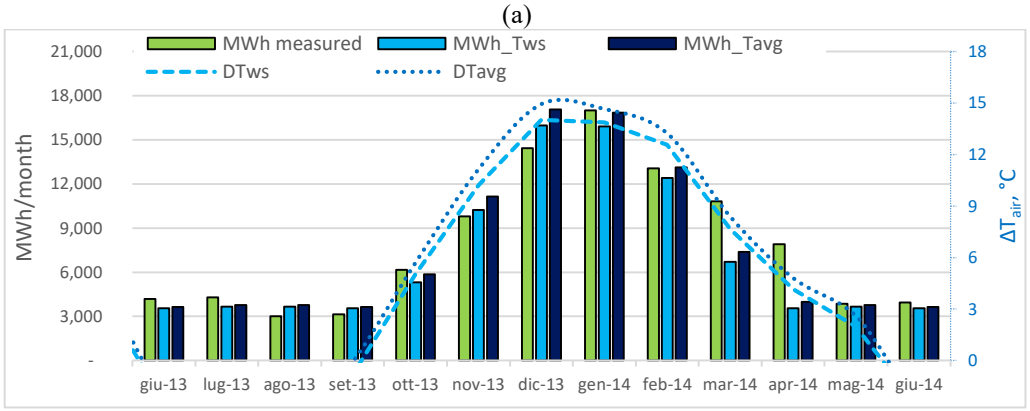

(b)

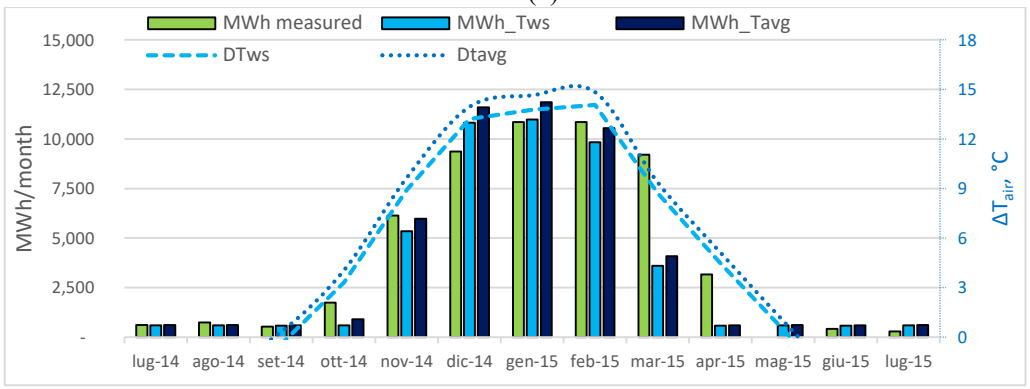

(c)

Figure 17. Monthly space heating and domestic hot water profile [MWh/month] for the August 2014 - August 2015 period: comparison between measured and simulated consumptions using the nearest WS 'Politecnico' and the average weather data were used: (a) mesh '1350'; (b) mesh '1351'; (c) mesh '1296' [46].

The energy consumptions are compared considering the average weather data from five WSs in Turin (T_{avg}) and the weather data from the nearest WSs (T_{ws}). The results show that the air temperatures T_{ws} are slightly higher than the average air temperatures T_{avg} in Turin and the results of the calculated energy consumptions in these cases are consequently higher. The data regarding DHW use are quite constant during spring and summer, but this trend depends on the number of buildings that have hot water systems connected to the DHN in each mesh.

The absolute relative errors $|E_r|$ are reported in Figure 18. The $|E_r|$ is chosen to present the results because it is more significant and the difference between the monthly measured values and the calculated values add up because they are always positive. In this work, the absolute relative errors are considered not significant when the energy consumptions are low. To take into account any final balance adjustments of the effective energy consumptions made by the IREN energy company, the global consumption is measured for the three heating seasons and compared with the result of the model.

In general, $|E_r|$ values are variable between 4-17% but higher values (e.g., meshes: 979, 1190 and 1402) can be observed when the number of buildings connected to the DHN is very low (% of DH and number of buildings). Moreover, the meshes 1402 and 1403 have and high percentage of industrial buildings and

then the accuracy of this model is lower. The E_r and $|E_r|$ increased when the T_{avg} was used, although no significant differences were observed.

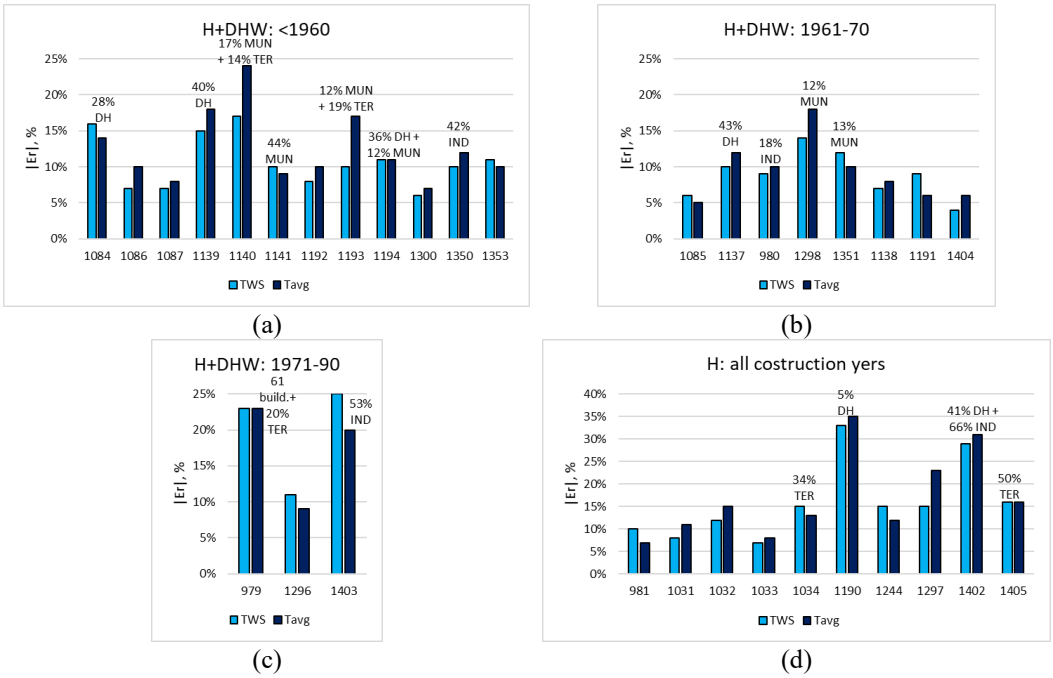

Figure 18. Absolute relative errors $|E_r|$: (a) H+DHW: <1960; (b) H+DHW: 1961-70; (c) H+DHW: 1971-90; (d) H: for all construction years [46].

The absolute relative errors $|E_r|$ of the model are mapped at a mesh scale, as shown in Figure 19. As previously mentioned, there are no major error differences between the model with the average Turin air temperatures data and the data from the nearest WS. These results, which have similar errors, are because the analysis is made on large neighbourhoods of 1 km^2 or maybe Turin is not a very large city. Consequently, there are no high variations in air temperature, since the analysed areas are all urbanized, and there are limited microclimatic variations.

Comparing errors with the information in Figure 17 and Figure 18, higher $|E_r|$ can be observed in meshes with: (i) a low percentage of buildings connected to the DHN (meshes: 1033, 1034, 1190, 1402); (ii) a low percentage of residential buildings (meshes: 1141, 1034 and 1402), for example, there is a significant quota of municipal buildings in mesh 1141; (iii) high values of *NDVI* (more green areas) and/or high values of albedo *ANIR* (meshes: 979, 1033, 1034, 1190); (iv) high *BCR* (meshes: 1034, 1086, 1190, 1298, 1353, 1402); (v) low SVF_g (meshes: 1033, 1034, 1141, 1244, 1297); (vi) low values of H/H_{avg} (meshes: 1033, 1034, 1141, 1190, 1402).

Mesh 979 is considered as a particular case because it is the only mesh with most buildings built during the 1981-1990 period. As not enough data are available for this construction year, it is not possible to optimize the model for this group. However, further evaluations could be made with more data to understand whether and if so, what other urban parameters affect the energy consumption of buildings built between 1981 and 1990.

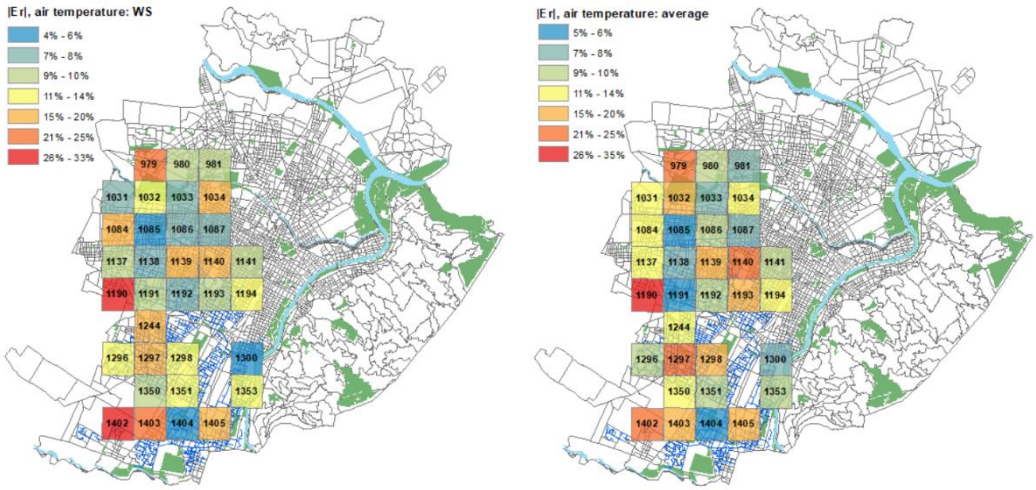

(a) (b)

Figure 19. Absolute relative error with reference to the monthly energy balance model using data from the nearest WS; (b) Absolute relative error with reference to the monthly energy balance model using the average Turin data [46].

Figure 20 below refers to a comparison of the measured data (y-axis) with the calculated data (x-axis). The global consumptions (of three consecutive heating seasons) are indicated for each mesh and the H+DHW group (Figure 20a) is distinguished from the H group (Figure 20b).

Some simulations are conducted to understand how the urban form influences the energy consumption of residential buildings. Using the variability of the data (Table 7), four scenarios are hypothesized considering different levels of solar exposition: (i) unfavorable low solar exposition, with an *SVF* of 0.34 and *MOS* of 0.35; two intermediate conditions, with (ii) an *SVF* of 0.34 and *MOS* of 0.56 and (iii) an *SVF* of 0.73 and *MOS* of 0.35 (iv) favourable conditions with high solar exposition, with an *SVF* of 0.73 and MOS of 0.56.

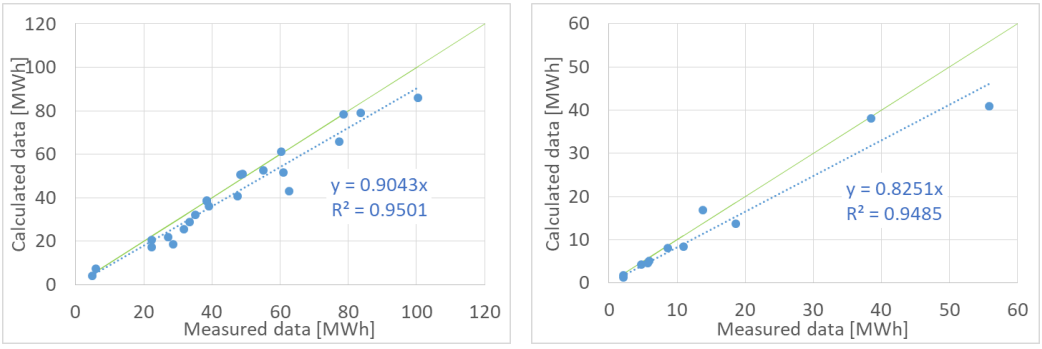

(a) (b)

Figure 20. The calculated energy consumption value on the x-axis were compared with the measured value on the y-axis: (a) the 'H+DHW' group and (b) the 'H' group [46].

The results of scenarios (ii), (iii) and (iv) are compared in Figure 21. Comparison of the energy consumptions for different solar exposition scenarios: (i) *SVFg* = 0.34 and *MOS* = 0.35; (ii) *SVFg* = 0.73 and *MOS* = 0.35; (iii) *SVFg* = 0.34 and *MOS* = 0.56; (iv) *SVFg* = 0.73 and *MOS* = 0.56 [46]. with the most unfavorable

scenario (i) for all the H and H+DHW groups. The results show that the energy consumptions with the more favourable conditions of solar exposition (scenario (iv)) decreased by 10.9% compared with the most unfavorable conditions (scenario (i)). These results are the average values of the 33 analysed meshes.

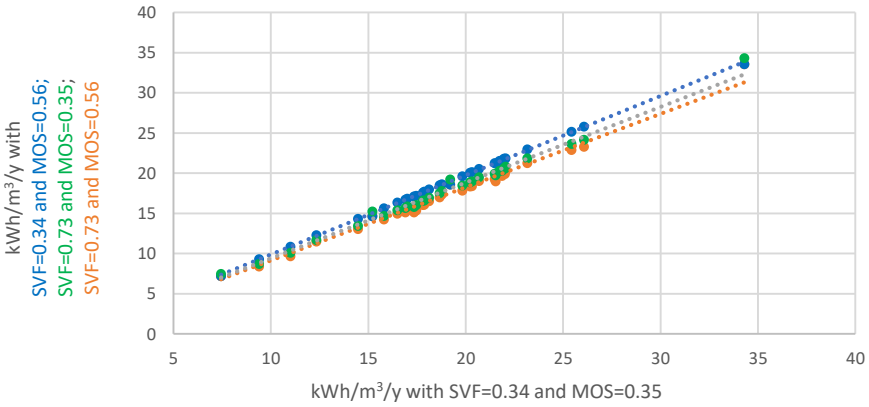

Figure 21. Comparison of the energy consumptions for different solar exposition scenarios: (i) SVF_g = 0.34 and MOS = 0.35; (ii) SVF_g = 0.73 and MOS = 0.35; (iii) SVF_g = 0.34 and MOS = 0.56; (iv) SVF_g = 0.73 and MOS = 0.56 [46].

Two examples of meshes with buildings from different periods of construction are compared in Figure 22 with different solar expositions. Again, in this case, the most unfavorable condition (scenario (i)) is compared with the more favourable solar expositions (scenarios (ii), (iii) and (iv)). The results show a few differences: there are lower energy consumptions for the 1300 mesh with older buildings and the energy consumptions could be reduced by as much as 10.1% with better solar conditions, while this difference is 8.4%.

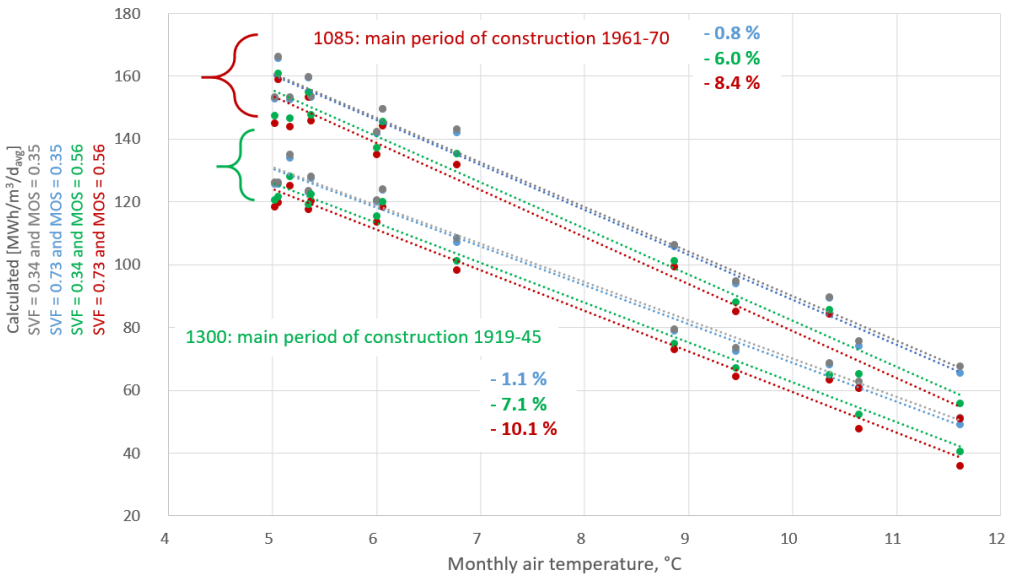

Figure 22. The energy consumption trends with the outdoor air temperature for two meshes with different construction periods and different solar expositions: mesh no. 1300 (1919-45 period) and mesh no.1085 (1961-70 period) [46].

In summary, several district in the city of Turin were selected, in which the DH energy demand was available. The energy demand for SH and DHW in these districts was simulated using monthly process-driven models, based on a quasi-stationary methods corrected by some urban parameters (i.e., *SVF*, H/H_{avg}, *MOS*). Models were validated against measured DH data. The impact of urban parameters on the EP of buildings was investigated, and it has emerged that the *SVF* is more influential than the *MOS*. In the next sections, a sensitivity analysis investigates more in depth the effect of urban morphology and the other energy variables on consumptions.

3.4 Hourly process-driven models

In order to evaluate the thermal peak loads, an hourly model is developed. A dynamic energy model to be applied at the urban scale is created starting from the energy balance equations at a building scale (according to ISO 13786:2018, ISO 52016-1:2017, ISO 52017-1:2017, and ISO 13790:2008 standards). One of the novelties of this urban energy model is that it can be applied to groups of buildings considering the energy-related variables that describe the urban morphology. These variables are introduced in the incoming and outgoing energy flows of the energy balance equations. The aim of the development of the dynamic engineering model is to investigate the following topics:

- Why should we use hourly models? The DHN is dimensioned according to the peak of hourly energy demand. Therefore, the evaluation of the morning peak of consumption is a key factor related to the capacity of the energy distribution network. Moreover, hourly models can be also used to evaluate the optimization of the energy supply/demand, especially boosting renewable technologies.
- Is this hourly model accurate? How precise would the results be if the model is applied at an urban-territorial scale and to a group of buildings? The novelty of this model is its application to homogeneous groups of buildings using urban morphology variables. The model has been simplified so that it can use the data available for all the buildings in a city; it must provide results quickly, but these results should be accurate.
- Starting from the consideration that the model will be used to calculate the hourly consumption of buildings in a city, it is better to consider the temperature inside the buildings to be constant (e.g., set-point range) or variable according to the weather conditions?

Summing up, it is a simplified engineering model that uses a bottom-up approach applied at the urban scale. It uses existing territorial databases and a place-based assessment through GIS tools. The model is studied to consider the interactions between buildings introducing new urban variables. Furthermore, with

this energy model it is possible to evaluate the future energy efficiency or renewable energy scenarios, representing the spatial distribution of the energy demand/supply to achieve energy and climate targets [55,152].

3.4.1 Methodology

This section describes the input data and explains the equations that regulate the energy balance of buildings and groups of buildings.

In this first part of this analysis, residential buildings with different energy consumptions are characterized according to the main variables that influence their energy consumptions. Subsequently, the buildings are characterized into archetypes and grouped into clusters according to their typologies and consumptions.

The energy model is applied to the different clusters, identifying the most effective input data. Finally, to further reduce the errors, the buildings' temperature profiles are corrected, considering climatic conditions.

The accuracy of this hourly energy balance model is evaluated by comparing the forecast energy supplied with the measured consumptions for the 2013-2014 heating season. The development of this model can be divided into three parts (Figure 23):

1. Input data have been collected and processed using existing databases and the energy consumption provided by the IREN district heating company. The data have been processed and georeferenced with the support of a GIS tool.
2. The energy balance with an iterative procedure is designed, dividing residential buildings into four clusters (homogenous groups) according to the hourly consumption profiles and the construction periods. The profiles of the building temperature, simulated using the energy balance equations, are compared with the indoor comfort temperature (according to ISO 7730: 2005 and EN 16798-1:2019). To further optimize the model, the internal temperature of the buildings is corrected, considering the climatic conditions (external air temperature and sol-air temperature).
3. The energy consumptions are simulated using optimized energy balance equations and have been compared with the measured energy consumptions to test the accuracy of the model and validate it.

This place-based methodology is able to calculate the time series of internal temperature and the heat loads, using equations for the transient heat and mass transfer between the external and internal environment through the opaque and transparent elements bounding the building, as a function of internal and external heat flow and temperature. The thermal balance of building is made up at an hourly time interval. The main goal of this kind of model is to consider the influence of

hourly and daily variation in weather, operation, and their dynamic interactions for heating.

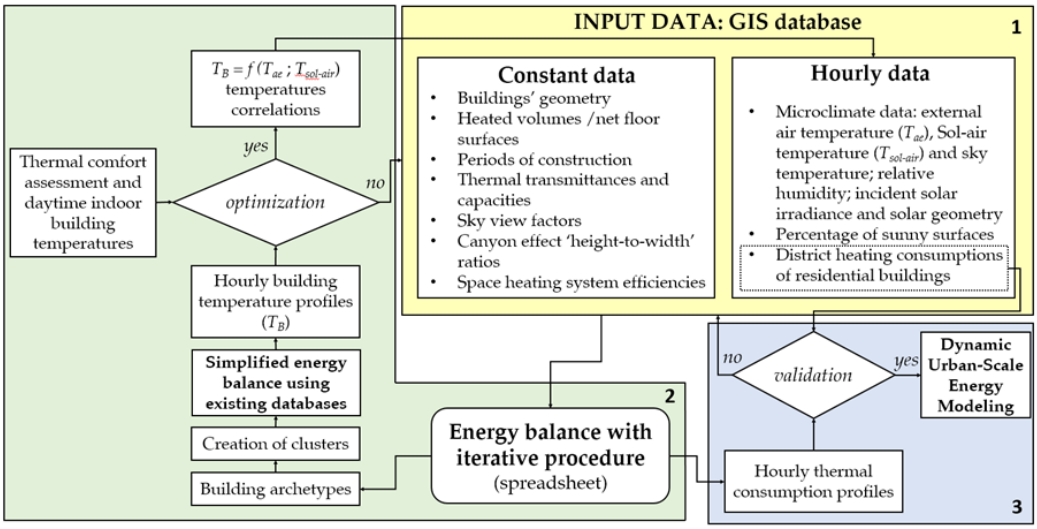

Figure 23. Flowchart of the methodology [50].

3.4.2 Input data

This section describes the input data, how they are analysed, and the tools that were used for their management and processing. A georeferenced database is created using the data presented in the following sub-sections (see Table 8).

The input data refers to: geometrical data calculated using municipal technical maps with the support a GIS tool; thermophysical parameters of the building and building elements estimated according to construction year and using values indicated in standards and literature; operating and boundary condition described using urban and morphological parameters; constants and physical data; hourly local climatic data. The main steps in the management of data are indicated below:

- A sorting algorithm is used in the pre-processing phase to elaborate the DH energy consumption data. The raw data of the energy consumptions were interpolated with a constant time interval equal to 1 hour; building data with too many errors or missing data (more than 10%) are discarded.
- GIS tools are used to locate each building, identifying its characteristics according to the availability of data at the urban scale. The input data were processed to evaluate the geometrical and typological characteristics of buildings and groups of buildings and all energy-related variables; at the block of buildings scale, also the sky view factor (*SVF*), urban canyon height-to-distance ratio (*H/W*), building orientation, and solar exposition were evaluated to characterize the buildings' surrounding context.

Table 8. Main input data of buildings and urban morphology characteristics [50].

	Input data	Source	GIS tool	Scale
Known data	Net and gross area, usable area, heated volume, dispersing surfaces (geometric characteristics)	Municipal Technical Map	Calculate geometry	Building
	Period of construction, type of user (typological characteristics)	Municipal Technical Map	Select by attributes	Building
	Type of roof	Municipal Technical Map, DSM, orthophotos	Aspect, Slope, Solar radiation	Building
	Solar exposition	Municipal Technical Map, Digital Surface Model (DSM)	Calculate Polygon Main Angle	Building/Urban
	Sky view factor	Municipal Technical Map, DSM	Relief Visualization Toolbox software	Urban
	Height-to-distance ratio	Building footprints	Generate near table	Urban
	Weather data	ARPA and Politecnico di Torino weather stations	Select by attributes	District
Hypothesized data	Percentage of transparent envelope	National Ministerial Decree of July 5th, 1975 (in Italian)	Calculate geometry, Join by attributes	Building
	Thermal transmittance, resistance, system efficiency	ISO 52016-1:2017, ISO 52017-1:2017, UNI-TR 11552:2014, [149]	Join by attributes	Building
	Thermal capacity	ISO 13786:2018, UNI-TR 11552:2014 and UNI 11300-1:2014	Calculate geometry, Join by attributes	Building

Climate data

Hourly climate data are used to simulate the hourly energy consumption for the space heating and cooling of buildings. The local climate data are processed with reference to the nearest weather station (WS), the ENEA portal (Italian National Agency for New Technologies, Energy, and Sustainable Economic Development: http://www.solaritaly.enea.it/), and to the PVGIS portal (Photovoltaic Geographical Information System: https://re.jrc.ec.europa.eu/pvg_tools/en/tools.html).

The hourly air and sky temperature, relative humidity, and incident solar radiation data from the nearest ARPA WS (Regional Environmental Protection Agency; in Italian: Agenzia Regionale per la Protezione Ambientale) were elaborated.

The direct and diffuse components of solar irradiation are obtained from WS measurements and the PVGIS portal. The solar azimuth (a) and the solar height (h) were obtained from solar geometry correlations. According to [153,154], the relation between these parameters can be written as follows:

$$h = sin^{-1} \cdot (\sin\varphi \cdot \sin\beta + \cos\varphi \cdot \cos\beta \cdot \cos z) \quad (8)$$

$$a = sin^{-1} \cdot (\cos\beta \cdot sin\, z \,/\, cos\, h) \quad (9)$$

$$\beta = sin^{-1} \cdot \{0.398 \cdot \sin[0.9863 \cdot (d - 82)]\} \quad (10)$$

Where h is the solar height, φ is the latitude, β is the solar declination, $z = 15 \cdot (t - 12)$ is the hour angle, t is the solar hour, and d is the day.

The incident solar irradiance on walls ($I_{sol,wall}$) is assessed considering the hourly variation in the shadow percentage for each building (ξ) as a function of the solar height h and the canyon height to distance ratio H/W (Figure 24). When h is less than the urban canyon angle $\arctan(H/W)$, the shadow quota of the building wall is equal to the $\frac{\tan(h)}{H/W}$; instead, if $\arctan(H/W)$ is greater than/equal to 1, there is no shadow on the building wall.

$$\xi = \begin{cases} \dfrac{\tan(h)}{H/W} & if \quad h < \arctan(H/W) \\ 1 & if \quad h \geq \arctan(H/W) \end{cases} \quad (11)$$

ξ is the percentage of shadow on the vertical wall, h is the solar height, H is the urban canyon height, and W is the urban canyon width.

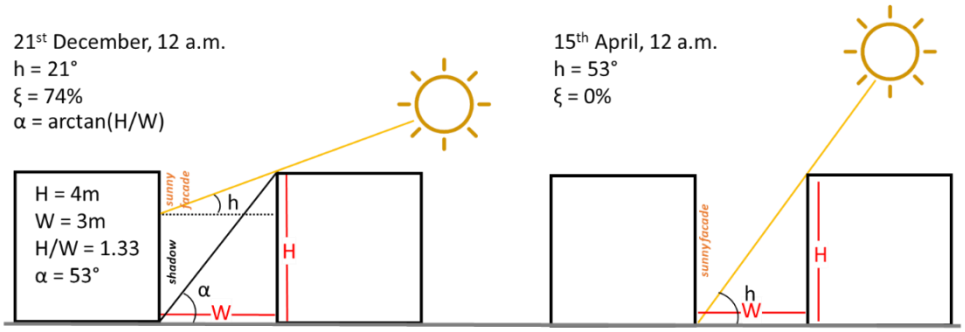

Figure 24. Shadow percentage assessment (an example for two days in April and December) [50].

Building data

The thermophysical and geometric parameters of the residential buildings are evaluated using information from the municipal technical maps, ISTAT census data for the year 2011, European standards, and the literature. The DBT is implemented with other official information (e.g., DSM and satellite images).

The typological characteristics of residential buildings are calculated using the attributes of a 2D footprint derived from the municipal technical map using GIS tools: net and gross heated volume; net and gross floor surface; a transparent surface equal to 1/8 of the floor is assumed for the glazing (air-lighting ratio of D.M., July 7th, 1975, and Turin building regulations); solar exposure and orientation, and shading elements, using the DSM and the solar geometry; the presence of uninhabited cellars and attics (very common in large Italian cities) has been hypothesized.

The thermal and construction characteristics of the residential buildings are assessed by identifying archetypes according to the construction year. The main input data are (ISO 52016-1:2017): the thermal transmittance (U) and resistance (R) of the building envelope elements; the total solar transmittance (g_G) of the transparent envelope; the solar radiation absorption coefficient (α_E) of the opaque envelope, which is determined considering the average colour; the emissivity (ε_E *and* ε_G) of the envelope, which is assumed to be constant for opaque and transparent elements; a reduction frame factor (F_F) of the windows, which is hypothesized as being constant; thermal capacities (C) and system efficiencies (η); the type of system management (i.e., intermittent with night shutdown).

The data concerning the use of the buildings mainly refer to (i) the type of ventilation and (ii) the type of internal heat gains:

(i) As far as the type of ventilation is concerned, three scenarios are assessed to evaluate the quota of heat losses due to natural ventilation. First, an air exchange per hour (*ach*) of 0.5 h^{-1} is assumed to be constant for all residential buildings during the day (24 h) resulting from infiltration. In the second scenario, *ach* is assumed to be variable during the daytime (with *ach* equal to 0.62 h^{-1}) from 7 a.m. to 9 p.m. and the nighttime (with *ach* equal to 0.30 h^{-1}) from 10 p.m. to 6 a.m. due to the use of shutters. In the last scenario, the thermal balance is implemented and the *ach* is assumed to be variable, considering a quota for infiltrations (3/4 h) and a quota for window opening (1/4 h) when the temperature inside the buildings exceeded the comfort temperature ($T_B > 22$ °C).

(ii) According to ISO 52016-1:2017, the internal heat gains are assumed with daytime and nighttime profiles.

Urban data

The morphological parameters are calculated using the municipal technical map, ISTAT census data, remote satellite images, and a DSM with a precision of 0.5 meters. The urban characteristics that were calculated at block of buildings scale are: the *SVF*, which measures the visible portion of the sky from a given location; the albedo, which is the percentage of solar incident irradiation reflected from a surface, and varies mainly according to the characteristics of the materials; the presence of vegetation, which is evaluated with the normalized difference vegetation index; the main orientation of the buildings; the urban canyon effect, which influences the outside air temperature and wind velocity, and which can be quantified considering the ratio between the urban canyon height "H" and its width "W"; the relative building height (H/H_{avg}), which describes the solar exposition in relation to the height of the surrounding buildings; the building coverage ratio (*BCR*) and the building density (*BD*), which describe the percentage of built area and the ratio of the building volumes to the sample area, respectively.

In this model, *SVF* is used to describe the solar exposition and the thermal radiation lost to the sky from the built environment and *H/W* was used to quantify the effect of direct solar irradiation on the building envelope at hourly time-steps.

3.4.3 Engineering model

Starting from the thermal balance at the building scale (according to ISO 52016-1:2017 and ISO 52017-1:2017), the thermal flux equations have been simplified using the available data at the urban scale. The EP of buildings is based on the following statements:

- The buildings internal environments are considered with uniform thermal conditions to enable a thermal balance calculation (during the heating season, the heated space has a daily temperature of 20 ± 2°C, during the cooling season 26 ± 2°C).
- To evaluate the heat flow between two environments, the heat transfer coefficients by transmission and ventilation are used.
- The energy need for humidification or dehumidification is neglected, as the heating systems of residential buildings are mainly central water systems with radiators and without mechanical ventilation systems; they can control only the temperature and not the relative humidity.
- The calculation time interval is one hour.
- Compared to the monthly method, the main goal of the hourly calculation is to be able to consider the influence of hourly and daily variation in weather and operation.

In Figure 25 the heat fluxes during the heating season have been indicated. In this energy balance model, three thermodynamic systems (TSs) are considered:

E) The opaque envelope, which is composed of all opaque surfaces separating the heated internal volume of the building from the external environment or other unheated spaces.

G) The glazing, which consists of all transparent surfaces separating the heated internal volume of the building from the external environment or other unheated spaces.

B) The building, which is the inside part of a building with internal structures, furniture, and air.

The energy balance equations on the three systems make it possible to assess the temperatures of the three systems per hour using an iterative method. The maximum number of iterations and the acceptable error were set at 1000 and 0.001, respectively.

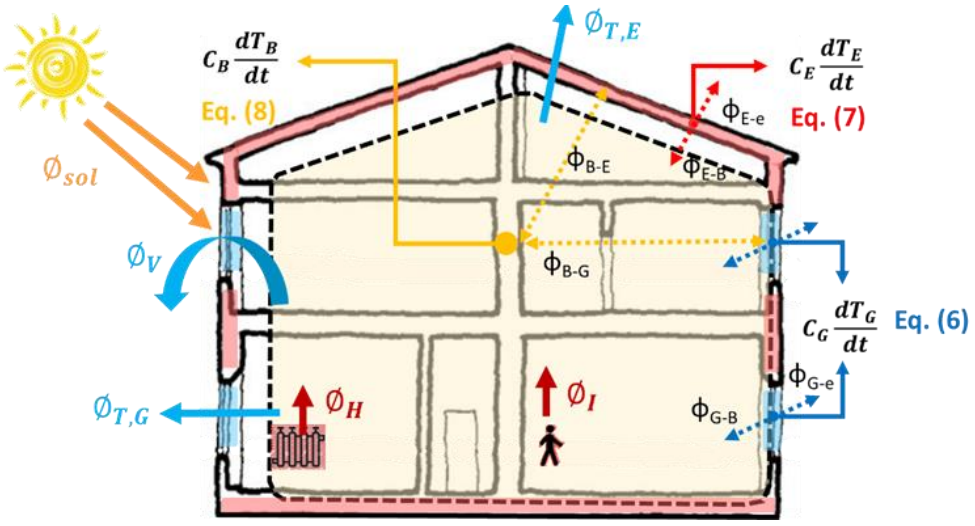

Figure 25. The three thermodynamic systems of the dynamic engineering model for the heating season: B = internal structures of the building, furniture, and air; E = opaque envelope; G = transparent envelope (glass) [50].

Equations (12) and (13) explain the heat flux components for a generic TS for the heating and cooling season.

$$C_{TS}\frac{dT_{TS}}{dt} = \emptyset_{sol} + \emptyset_I + \emptyset_H - (\emptyset_t + \emptyset_v) \tag{12}$$

$$C_{TS}\frac{dT_{TS}}{dt} = \emptyset_{sol} + \emptyset_I - (\emptyset_t + \emptyset_v + \emptyset_C) \tag{13}$$

The equations of the three thermodynamic systems G, E, and B are shown below.

$$\begin{aligned} C_G\frac{dT_G}{dt} = &\sum \alpha_{G,k}\cdot I_{sol,k}\cdot \xi_k \cdot F_k \cdot A_{G,k} \\ &- \sum \frac{A_{G,k}}{\frac{1}{2}\cdot R_{G,k} + R_{se}}\cdot (T_G - T_{ae}) \\ &- \sum \frac{A_{G,k}}{\frac{1}{2}\cdot R_{G,k} + R_{si}}\cdot (T_G - T_B) \\ &- \sum F_r \cdot R_{se}\cdot U_{G,k}\cdot A_{G,k}\cdot h_{r,G,k}\cdot \left(T_{ae} - T_{sky}\right) \end{aligned} \tag{14}$$

$$\begin{aligned} C_E\frac{dT_E}{dt} = &\sum \alpha_{W,k}\cdot I_{sol,k}\cdot \xi_k \cdot F_k \cdot A_{W,k} \\ &- \sum \frac{A_{E,k}}{\frac{1}{2}\cdot R_{E,k} + R_{se}}\cdot b\cdot (T_E - T_{ae}) \\ &- \sum \frac{A_{E,k}}{\frac{1}{2}\cdot R_{E,k} + R_{si}}\cdot (T_E - T_B) \\ &- \sum F_r \cdot R_{se}\cdot U_{W,k}\cdot A_{W,k}\cdot h_{r,W,k}\cdot \left(T_{ae} - T_{sky}\right) \end{aligned} \tag{15}$$

$$C_B \frac{dT_B}{dt} = \sum \tau_{G,k} \cdot I_{sol,k} \cdot \xi_k \cdot F_k \cdot A_{G,k} + \emptyset_I + \emptyset_{H-C} - \sum \frac{A_{E,k}}{\frac{1}{2} \cdot R_{E,k} + R_{si}} \cdot (T_B - T_E) - \sum \frac{A_{G,k}}{\frac{1}{2} \cdot R_{G,k} + R_{si}} \cdot (T_B - T_G) - c_a \cdot \dot{m}_a \cdot (T_{ai} - T_{ae}) \quad (16)$$

For each TS, C is the heat capacity (JK^{-1}); T is the temperature of the TS, air or sky (K); t is the time (s); ϕ_{sol} is the heat flow rate from solar gains; ϕ_I is the heat flow rate from internal gains; ϕ_H is the heat flow rate from the heating system; ϕ_C is the heat flow rate from the cooling system; ϕ_T is the heat flow rate dispersed by transmission; ϕ_V is the heat flow rate dispersed by ventilation; α is the solar absorption coeff. (-); τ is the total solar energy transmittance (-); I_{sol} is the solar irradiance (Wm^{-2}); ξ is the envelope sunny quota (-); F is the reduction factor (-); A is the envelope area (m^2); R is the thermal resistance (m^2KW^{-1}); U is the thermal transmittance ($Wm^{-2}K^{-1}$); F_r is the form factor buildings-sky (-); h_r is the radiative heat flux coeff. ($Wm^{-2}K^{-1}$); c_a is the air specific heat ($Jkg^{-1}K^{-1}$); and $\dot{m}_a$ is the air mass flow rate (kgm^{-3}).

The hourly temperatures of the glazing (T_G) are obtained with Equation (14) from a balance of the thermal flows between the glazing and the building (T_B) and the glazing and the outdoor environment (T_{ae}); similarly, the hourly temperatures of the envelope (T_E) are calculated using Equation (15), and the hourly temperatures of the buildings are calculated using Equation (16).

The definitions of the equations and the input data of the model have been realized to have a building temperature equal to the set-point range during the heating season 20 ± 2 °C and during the cooling season 26 ± 2 °C. Then, it is observed that the building temperature (T_B) varied according to the outdoor climatic conditions, and therefore correlations were found with T_{ae} and $T_{sol\text{-}air}$.

$T_{sol\text{-}air}$ is introduced because it allows one to consider not only the outside air temperature but also the solar irradiation absorbed by the opaque envelope:

$$T_{sol-air} = T_{ae} + \left(\alpha_E \cdot \frac{I_{sol}}{h_e}\right) \quad (17)$$

Where T_{ae} is the outside air temperature (°C), α_E is the absorption coefficient (-), I_{sol} is the incident solar irradiance (Wm^{-2}), and h_e is the external thermal adductance ($Wm^{-2}K^{-1}$).

The output of the model are:

- In case the *heat load is given as input*, the outputs are the building indoor air temperature (T_B).
- In case *indoor temperature set points are given as input*, the output is the heating/cooling load ($\Phi_{H\text{-}C}$).

The following subsections explain the different components of the energy balance in detail.

Heat flow rate from solar gains

The heat flow rate from solar gains (Φ_{sol}) is obtained directly by transmission or indirectly by absorption considering the solar irradiation through the building element (k). In accordance with standards ISO 13790:2008, ISO 52016-1:2017, and ISO 52017-1:2017, the heat flow rate from solar gains is given by:

$$\emptyset_{sol} = \emptyset_{sol,\alpha} + \emptyset_{sol,\tau}$$
$$\emptyset_{sol,\alpha} = \sum \alpha_k \cdot I_{sol} \cdot \xi \cdot F_k \cdot A_k \qquad \emptyset_{sol,\tau} = \sum \tau_G \cdot I_{sol} \cdot \xi \cdot F_k \cdot A_k \tag{18}$$

Where ϕ_{sol} is the heat flow rate from solar gains, α is the solar absorption coefficient (-), τ is the total solar energy transmittance (-), I_{sol} is the solar irradiance (Wm^{-2}), ξ is the envelope sunny quota (-), F is the reduction factor (-) and A is the envelope area (m^2).

The heat flow rate from solar gains $\phi_{sol,\alpha}$ is used for the envelope and glazing TSs, and $\Phi_{sol,\tau}$ is used for the building TS. In this model, the following data are used:

- I_{sol} is calculated considering the orientation and the inclination of the surfaces of the building envelope.
- ξ is calculated with hourly time steps, since the height of the sun (h) and the urban canyon height-to-distance ratio (H/W) were known [155].
- α_k is assumed equal to 0.6 for an opaque envelope (α_E), considering an intermediate color (not dark or light), while, for a transparent envelope, α_G depended on the type of glass used in the different periods of construction (e.g., 0.06 for single glass in buildings built before 1976).
- τ_G depended on the type of glass used in the different periods of construction (e.g., 0.72 for single glass in buildings built before 1976).
- The obstruction factor F_k has been calculated through the view factor and the SVF (on a grid of points at the street level and on the roof of buildings with the Relief Visualization Toolbox).
- A_k is calculated as all geometrical characteristics, with the support of the GIS software, considering the area of the walls (A_W), the glazing area (A_G), and the opaque envelope area (A_E), considering the non-dispersive walls between adjacent buildings.

Heat flow rate from internal heat sources

The heat flow rate of residential buildings, resulting from internal heat sources (ϕ_I), depends on the average floor area per dwelling (S_f):

$$\emptyset_I = q_{int} \cdot S_f \cdot n \quad (19)$$

Where q_{int} is the internal heat flow rate (W/m^2), S_f is the average floor area of a dwelling (m^2), and n is the number of dwellings in a building (-).

The heat flow rate ϕ_I is calculated using the hourly profiles of q_{int} for daytime and nighttime due to occupants and equipment for residential buildings, according to the standards UNI/TS 11300-1:2014 and ISO 13790:2008.

Heat flow released from the heating/cooling system

In Turin, the most widely used heating system is a centralized water heating system consisting of radiators and a climate control unit; only recently have room controllers been installed. In this model, the heat flow rate released from the heating system (ϕ_H) guarantees the set-point range in the buildings; then, when the comfort temperature is reached (i.e., 20 ± 2 °C in the daytime), the heating system is switched off.

If the heat flow rate supplied to the heating system $\phi_{S,H}$ is known, it is possible to calculate ϕ_H by multiplying $\phi_{S,H}$ by the system efficiency η_H:

$$\emptyset_H = \emptyset_{S,H} \cdot \eta_H \quad (20)$$

Where ϕ_H is the heat flow released into the building by the heating system (W); $\phi_{S,H}$ is the heat flow supplied by the DH network (W); and η_H is the system efficiency (-), which depends on the period of construction of the buildings.

Heat flow rate lost by transmission

The heat flow rate lost by transmission through the building envelope can be calculated considering the heat flow lost by transmission due to temperature differences and the extra heat flow due to the infrared radiation lost to the sky. The heat flow rate due to temperature differences through walls, the roof, slabs, and windows was calculated considering the thermal transmittances (U) and the thermal resistances (R) of the building element k, according to the thermal properties of common building elements for the different periods of construction (UNI-TR 11552:2014). $\phi_{T,t}$ was calculated in accordance with ISO 13790:2008, and it is given by:

$$\emptyset_{T,t} = \sum \frac{A_k}{\frac{1}{2} \cdot R_k + R_{se}} \cdot b \cdot (T_{TS} - T_{ae}) - \sum \frac{A_k}{\frac{1}{2} \cdot R_k + R_{si}} \cdot (T_{TS} - T_B) \quad (21)$$

Where $\phi_{T,t}$ is the heat flow rate lost by transmission (W), k is the envelope element (-), A_k is the area of the element k (m^2), R_k is the thermal resistance (m^{2}KW^{-1}) of the building element k, R_s is the surface thermal resistance (m^{2}KW^{-1}) (R_{se}=0.04 m^{2}KW^{-1}, R_{si}= 0.13 m^{2}KW^{-1} for a horizontal heat flow, 0.17 m^{2}KW^{-1} for

a downward heat flow, and 0.10 $m^2K^{-1}W$ for an upward heat flow), b is the correction factor for unconditioned adjacent spaces (b=1 for external surfaces, b=*0.5* for cellars, and b=*0.9* for unheated attics), and T is the temperature of the thermodynamic system (K).

The extra heat flow due to thermal radiation lost to the sky ($\phi_{T,r}$), for opaque and transparent building elements is given by:

$$\emptyset_{T,r} = F_r \cdot R_{se} \cdot U_k \cdot A_k \cdot h_{r,k} \cdot (T_{ae} - T_{sky}) \quad (22)$$

Where F_r is the form factor between a building element and the sky (-), R_{se} is the external surface thermal resistance (m^2KW^{-1}), U_k is the thermal transmittance of the element k ($Wm^{-2}K^{-1}$), A_k is the projected area of the element k (m^2), $h_{r,k}$ is the radiative heat transfer coefficient ($Wm^{-2}K^{-1}$), and T is the temperature of the external air and sky (K).

The form factor F_r depends on the presence of obstructions ($F_{sh,ob}$) and it is calculated as a function of the sky view factor (*SVF*) and the view factor that depends on the surface inclination (γ). The radiative heat transfer coefficient $h_{r,k}$ was calculated according to ISO 13790:2008, with the emissivity (ε) of the external surfaces assumed to be equal to 0.9 for opaque elements and 0.873 for glass without low-emission coatings.

Heat flow rate from ventilation

The heat flow rate from ventilation (ϕ_V) depends on the heat capacity of the air per volume ($\rho_a \cdot c_a$), the number of air changes per hour (*ach*), and the temperature differences of the air:

$$\emptyset_V = c_a \cdot \dot{m}_a \cdot (T_{ai} - T_{ae}) = \rho_a \cdot c_a \cdot \frac{ach \cdot V}{3600} \cdot (T_{ai} - T_{ae}) \quad (23)$$

Where ρ_a is the air density (kgm^{-3}), c_a is the air specific heat ($Jkg^{-1}K^{-1}$), $\rho_a \cdot c_a$ the heat capacity of air per volume ($Jm^{-3}K^{-1}$), $\dot{m}_a$ is the air mass flow rate (kgm^{-3}), *ach* are the number of air changes per hour (h^{-1}), V is the volume of air (m^3), and T_a is the air temperature inside and outside the building (K).

Firstly, a constant air change rate *ach* = 0.5 h^{-1} is assumed during the day (24 h), considering natural ventilation through infiltrations (widely used in Italy in residential buildings). In the second phase of this model, to improve the accuracy, *ach* is assumed to be variable during the daytime and nighttime; ventilation heat losses are minimal during the night due to the presence of shutters. Finally, *ach* is calculated considering that when the building temperature exceeds the set-point range, users can open windows; therefore, the air change rate can be calculated considering a quota for infiltrations and a quota for window openings. Then, the number of *ach* for the window openings is calculated according to [156] (in Figure 26).

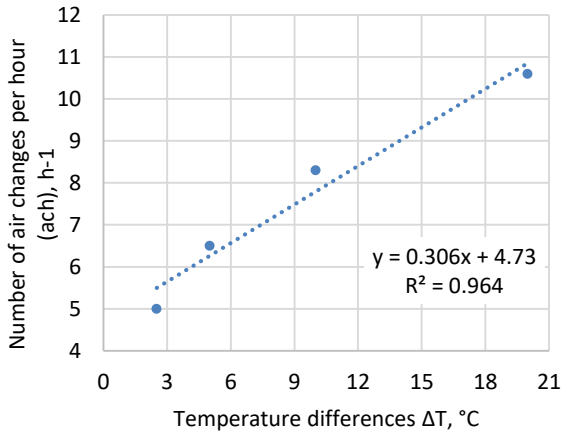

Figure 26. Correlation between ΔT = (Tai – Tae) (°C) and the number of air exchanges per hour; measured data for typical Italian windows with a height = 1.5 m [50].

Further considerations on ventilation loads at urban scale are made in [157]. In this application of the model, the monthly air change per hours are investigated as a function of the climatic data, the air permeability, shape and orientation of the building and the urban morphology. Considering only the natural infiltrations, the monthly ach has been assessed. Four scenarios of *ach* have been assessed to ensure Indoor Air Quality (IAQ) requirements, have been compared and applied to the place-based energy model. The methodology has been applied to two building located in a central district in Turin. They are representative of the urban building stock with two typical orientations. Monthly prevailing wind direction and speed have been considered to assess average monthly pressure coefficients that mainly vary according to the height of the building floor. The results of this investigation, show how the air change rates vary with the building floor and with the wind direction and velocity.

3.4.4 Space heating energy demand

This section presents the engineering model used to simulate the hourly energy demand for SH in residential buildings at neighbourhood scale (Equation 24).

$$C_{TS}\frac{dT_{TS}}{dt} = \emptyset_{sol} + \emptyset_I + \emptyset_H - (\emptyset_t + \emptyset_v) \quad (24)$$

The dynamic urban-scale energy model has been calibrated and optimized through an iterative procedure in excel spreadsheets on about 100 residential buildings in a district of the city of Turin. The results show how a place-based dynamic energy balance methodology can also be sufficiently accurate at an urban scale with seasonal *MAPE* of 14%. To achieve this accuracy, the model has been optimized by correcting the typological and geometrical characteristics of the buildings and the typologies of ventilation and heating system. In addition, the

indoor temperatures of the buildings, which are initially estimated as constant, have been correlated to the climatic variables.

Model application

The thermal balance model is applied to a district in the city of Turin. The energy consumption for space heating in Turin is rather important due to the high building density, the low level of energy efficiency of the buildings, and the cold climate; therefore, a DHN was built in 2000 to distribute energy effectively and reduce the high emissions of individual boilers; the DHN is currently connected to 60.3 Mm^3 of buildings with about 600,000 inhabitants in Turin [15].

The DH energy consumptions are used to optimize and validate the dynamic urban-scale energy model. The definition of the model is carried out by choosing the input data and defining the balance equations to have comfortable temperatures in the buildings.

Subsequently, the model is optimized by finding correlations between the temperature of the building and the climatic conditions. The validation is carried out using the model to calculate energy consumptions, setting the internal temperature of the building according to the external climatic conditions. The model is applied to a total of 92 residential buildings grouped in four clusters of various periods of construction in a central district of Turin.

Input data

All the input data were geo-referenced, and a DBT for the city of Turin is created with the support of GIS tools.

The energy consumptions of the buildings are provided by the IREN district heating company and elaborated at hourly time steps. Starting from 102 residential buildings (whose thermal consumption was known for the 2013–2014 heating season), 92 were selected for the model application. The first selection is made considering only buildings with the heating system switched off during the night (typical of Italian buildings). Other six buildings are excluded from this analysis due to anomalous/missing data. The local climate conditions are elaborated using hourly data (i.e., air temperature, relative humidity, solar irradiation) measured at the Politecnico di Torino WS.

The main thermophysical and geometric parameters of the building elements are indicated in Table 9 and Table 10. Data on the thermal transmittances (U) and relative thermal resistances (R) of the building elements for different periods of construction are reported in Table 9. The U data in the GIS database are calculated for each building according to its period of construction, distinguishing U values for vertical walls, glass, cellar slabs (with an adjustment factor b equal to 0.5), and ceiling slabs in unheated attics with un-insulated roofs (with an adjustment factor b of 0.9). The heat capacities of the building elements are reported in Table 10 according to the period of construction. For the envelope elements, the thermal capacity reported considers the recurring stratigraphies for the different

construction periods (UNI/TR 11552:2014). For the building, we started from the value of 165,000 J/m^2/K (per m^2 of envelope, from UNI/TS 11300-1:2014), which considers the inside part of the building plus 10 cm of the internal envelope; subtracting this last quota, the value of 30,496 J/m^2/K is obtained (per m^2 of net heated surface, considering that air and furniture have a heat capacity of 10,000 J/m^2/K, ISO 52016-1:2017).

Table 9. Thermal transmittances (U, Wm^{-2}K^{-1}) and resistances (R, m^{2}KW^{-1}) of the building elements and the TSs (E and G) [50].

Building element	1919–1945			1946–1960			1961–1970			1971–1980		
	U	***1/2·Rk +Rse***	***1/2·Rk +Rsi***	***U***	***1/2·Rk +Rse***	***1/2·Rk +Rsi***	***U***	***1/2·Rk +Rse***	***1/2·Rk +Rsi***	***U***	***1/2·Rk+Rse***	***1/2·Rk +Rsi***
Slab in cellar	0.79	0.63		0.62	0.81		0.65	0.77		0.61	0.83	
Slab in attic	1.76	0.28		1.35	0.37		1.49	0.34		1.35	0.37	
Wall	1.35	0.41	0.32	1.18	0.47	0.38	1.13	0.49	0.40	1.04	0.53	0.44
Envelope (E)	1.32	0.42	0.33	1.11	0.50	0.41	1.11	0.50	0.41	1.02	0.54	0.45
Glazing (G)	4.75	0.15	0.06	4.40	0.16	0.07	4.90	0.15	0.06	4.57	0.15	0.06

Table 10. Thermal capacities (C, Jm^{-2}K^{-1}) of the building elements and thermodynamic systems (E, G, B) [50].

Building elements	< 1945	1946–1960	1961–1970	> 1971
Slab in cellar	317,867			
Slab in attic	434,400			
Wall	574,560	574,560	574,560	574,560
Envelope (E)	497,888	503,490	282,871	242,030
Glazing (G)	7314			
Building (B): air, furniture, and internal partitions	30,496*			

Values of the thermal capacities are expressed per m^2 of envelope area.

*The reference area [m^2] for the building (B) is its net heated surface and not the envelope area.

Building clusters

To represent the average energy behaviour of residential buildings, groups of buildings with similar characteristics are identified. This analysis can simplify the application of the model on an urban scale. Building archetypes are defined by analyzing the energy consumption profiles, the thermophysical and geometric parameters, and the typology of the heating systems. The main energy-related variables identified for the building archetypes are the volume, the area of dispersing surfaces, the envelope technology, the percentage of windowed area, and the type and efficiency of the heating system [15]. The *S/V* ratio is not considered because is quite constant, with an average value of 0.28 m^{-1} and a standard deviation of 0.04 (i.e., large apartment buildings). After analyzing the trend in heating consumption, the buildings are grouped into four construction periods and with different envelope technologies, percentages of windowed area, and types and efficiencies of the heating system. Table 11 indicates the characteristics of each cluster and the main input data that are used to analyse the energy balance model. The following discussion is on the four clusters, which have similar volumes (only

cluster 4 has different values of net heated volume and floor due to low values of occupancy) and therefore allow a comparison of their results.

Table 11. Cluster characteristics [50].

Data	Cluster 1	Cluster 2	Cluster 3	Cluster 4
Period of construction	1919–1945	1946–1960	1961–1970	1971–1980
No. of buildings	27	32	22	11
Gross heated volume [m3]	131,219 (−9%)*	140,014 (−2%)*	159,195 (+11%)*	91,909 (−36%)*
Net heated floor [m2]	37,983	40,634	41,816	25,066
DH consumption [kWh/m3/y]	29.20	27.48	26.88	21.21
CE [MJ/K]	23,884	25,996	10,896	5980
CG [MJ/K]	46	50	48	28
CB [MJ/K]	1262	1463	1403	799
No. of dwelling units	494	504	506	240
Heated surface/unit [m2]	93.31	91.13	93.46	97.06
System efficiency [-]	0.783	0.783	0.794	0.816

* Percentage with respect to the average volume of buildings in the three first clusters.

Typical monthly days

The hourly data on the external air, solar-air and sky temperatures, relative humidity, solar irradiation, and position of the sun from the Politecnico WS are elaborated, and 34 typical days are identified for the 2013–2014 heating season. These days are selected to identify all the possible climate conditions during a heating season, with daily T_{ae} = 1.70–7.97°C and $I_{sol,d}$ = 169–5774 Wh/m^2/d.

Table 12 indicates the characteristics of the 34 typical days that are identified. Date 1 and date 2 are chosen with similar outdoor air temperatures but different solar irradiation conditions.

Table 12. Typical days of a heating season [50].

Date 1	Tae [°C]	Isol,d [Wh/ m2/d]	hsol [h]	Tsol-air [°C]	Date 2	Tae [°C]	Isol,d [Wh/m2/d]	hsol [h]	Tsol-air [°C]
30/01/2014	1.70	214	9.17	2.05	**29/01/2014**	1.81	397	9.17	2.49
09/12/2013	3.42	1232	8.67	5.24	**22/11/2013**	3.70	507	9.47	4.39
01/01/2014	4.33	1610	9.17	6.60	**27/11/2013**	4.44	1939	9.47	7.25
07/02/2014	5.17	324	8.67	5.71	**26/11/2013**	5.32	2077	9.47	8.37
22/02/2014	6.24	1003	10.27	8.04	**16/12/2013**	6.30	1644	8.67	8.64
07/01/2014	7.30	1233	9.17	8.99	**15/02/2014**	7.39	1860	10.27	10.36
15/11/2013	8.32	370	9.47	8.89	**10/01/2014**	8.69	993	9.17	10.09
25/02/2014	9.21	2706	8.67	15.01	**18/11/2013**	9.36	169	9.47	9.58
21/01/2014	9.86	1732	9.17	12.45	**22/02/2014**	10.00	3633	8.67	16.46
04/11/2013	11.19	1336	9.47	13.40	**05/03/2014**	11.20	4015	11.73	17.23
08/03/2014	12.48	4225	11.73	18.78	**13/11/2014**	12.63	2151	9.47	16.33
15/10/2013	12.99	1864	10.88	16.08	**01/11/2013**	13.22	2027	9.47	17.00
06/11/2013	14.68	2451	9.47	19.07	**19/10/2013**	14.16	1020	10.88	15.90
18/10/2013	15.02	2547	10.88	19.30	**18/03/2014**	15.31	4488	11.73	21.89
31/03/2014	16.22	5102	11.73	23.44	**30/10/2013**	16.22	1205	10.88	18.11
28/10/2013	17.08	1692	10.88	19.81	**09/04/2014**	17.32	5774	13.28	24.37
08/04/2014	17.97	2890	13.28	21.39	**14/04/2014**	17.68	5754	13.28	24.57

Model results

The main results pertaining to the analyses of the energy consumptions of buildings and clusters of buildings, the heat flow components of the energy balance, the trends of the temperatures of the three thermodynamic systems, and the application of the hourly energy balance model to clusters of buildings are reported in the following sections. This hourly energy balance model is validated by comparing the forecast energy supplied with the measured consumptions for the 2013–2014 heating season.

Hourly district heating consumption data

Space heating consumption data at the building scale (in Wh) with different time intervals (from 20 minutes to 1 hour) are provided by the IREN district heating company of Turin for the 2013-2014 heating season. The database, which has a large extension (5 GB), has been elaborated, and in the pre-processing phase a sorting algorithm in python language has been used to extract and organize the data for each building with hourly time-steps according to the following actions:

- The raw data (from 20 minutes to 1 hour) are interpolated with a constant time interval equal to 1 h, the missing data are computed from the available measurements, data with too many errors or missing data (with no information of 10%) are discarded (the useful sample of buildings decreased from 102 to 92 buildings).
- Space heating consumptions are georeferenced at the building scale according to the coordinates/address of each energy meter using GIS tools.

Building cluster identification

Hourly consumption profile for the SH of buildings depends on the type of building, its level of energy efficiency, and the local climate conditions. For this case study on compact residential buildings, these characteristics can be represented by grouping the buildings by periods of construction.

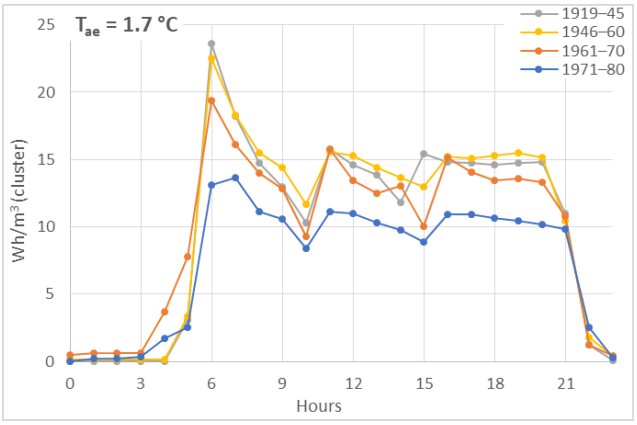

(a)

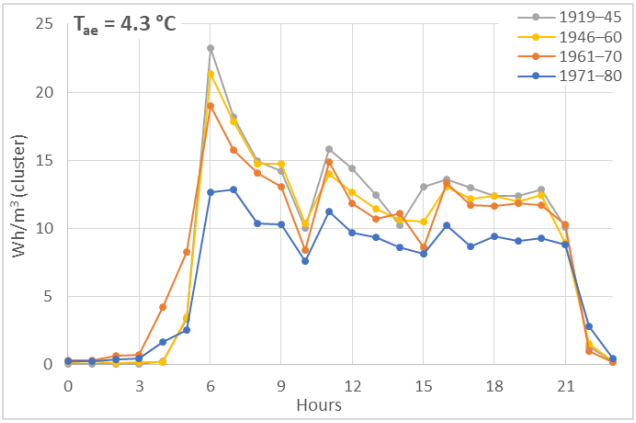

(b)

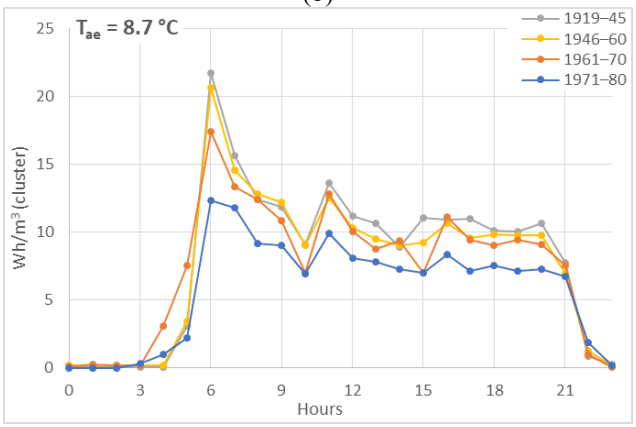

(c)

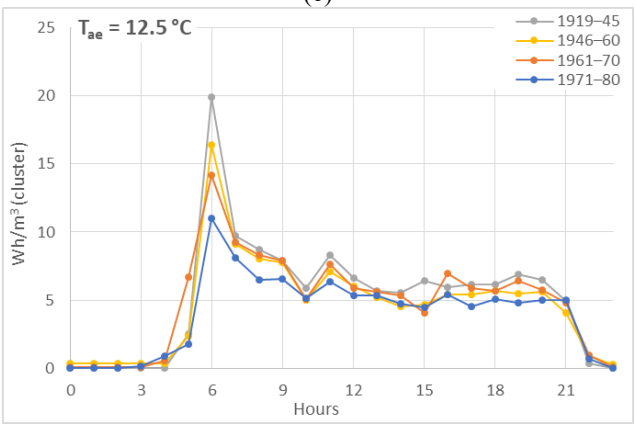

(d)

Figure 27. Space heating hourly consumptions (Wh/m3) with different Tae—(a) 1.7 °C, (b) 4.3 °C, (c) 8.7 °C, (d) 12.5 °C—for four clusters of buildings: cluster 1—1919–1945; cluster 2—1946–1960; cluster 3—1961–1970; cluster 4—1971–1980 [50].

Four periods have been identified with different geometrical and material characteristics, envelopes, and types of energy systems: 1919–1945, 1946–1960, 1961–1970, and 1971–1980 (new buildings in the urban environment are few and therefore it is more difficult to make this analysis). The specific energy consumptions of the four clusters of buildings for four typical days are represented in Figure 27. It can be observed that the hourly energy consumption profiles of the clusters have a typical trend—the buildings have a night-time heating interruption, with a peak at 6 in the morning and a quite constant consumption up to 8 p.m. In

general, the energy peak of the clusters decreases as the outdoor temperature (T_{ae}) increases. If the percentage of energy consumed daily is represented, the opposite would be observed: the percentage of energy consumed at 6 a.m. is higher if the outside temperature increases. In addition, with the percentage of daily consumption, buildings that consume less have a higher peak at the same outdoor temperature: from 10% to 16% for the 1919–1945 period, from 9% to 15% for 1945–1960, from 8% to 12% for 1961–1970, and from 8% to 11% for 1971–1980. Moreover, consumption is constant at 6% from 9 a.m. to 8 p.m., regardless of the temperature and period of construction. The specific consumption per m^3 has been represented because the four clusters do not have the same heated volume (see Table 11).

Heat fluxes components and building temperatures

Figure 28, Figure 29, Figure 30 and Figure 31 show the trend of all the heat fluxes components and consequently the resulting trends of the temperatures of the three TSs: building, opaque envelope, and glazing.

The heat flux components in Equation (12) can be observed on the left; the heat flux through ventilation, ϕ_V (light blue), is quite constant. The temperatures of the three thermodynamic systems (B, E, and G) are represented, with the outside air temperature and the solar irradiance, on the right. These representations allowed us to control the input data and the weight of the energy balance components.

Figure 28 shows the results of the energy balance model with a number of constant air changes per hour of 0.5 h^{-1} over 24 hours for the typical day of February 22nd, 2014, with a T_{ae}= 6.24 °C. It can be observed that the temperature of the building, $T_{B,}$ (in green), has a constant diurnal and nighttime trend; the set-point range (20 ± 2 °C) is reached during the day.

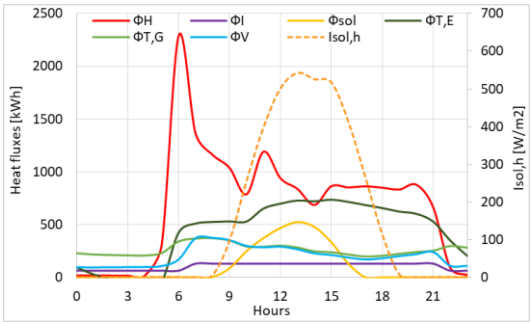

(**a**) Cluster 1 (1919–1945).

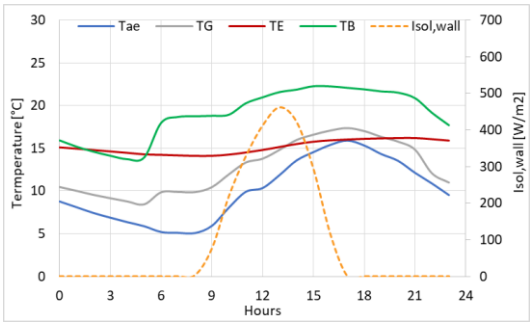

(**b**) Cluster 1 (1919–1945).

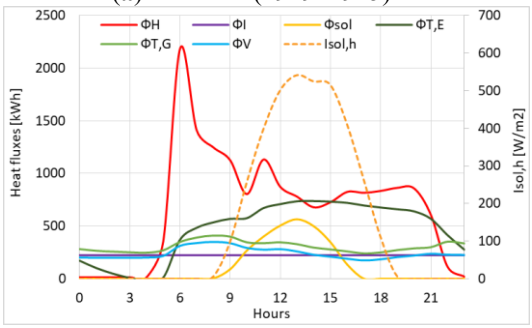

(**c**) Cluster 2 (1946–1960).

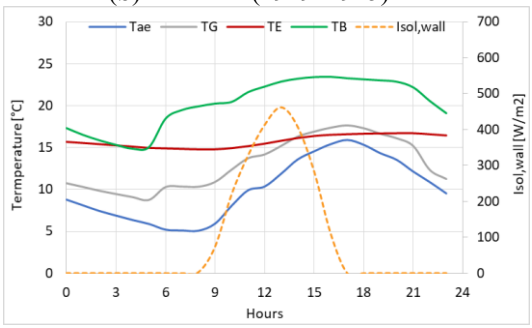

(**d**) Cluster 2 (1946–1960).

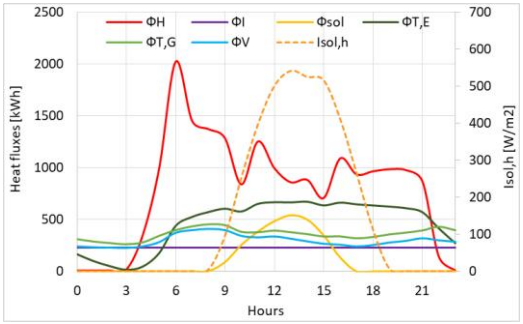

(**e**) Cluster 3 (1961–1970).

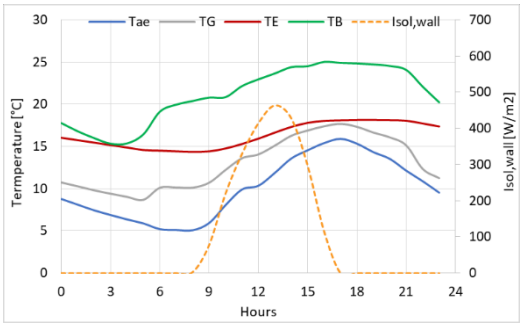

(**f**) Cluster 3 (1961–1970).

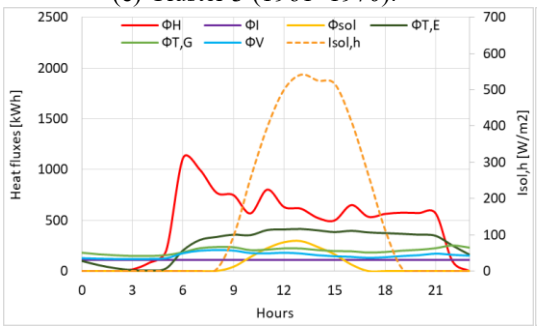

(**g**) Cluster 4 (1971–1980).

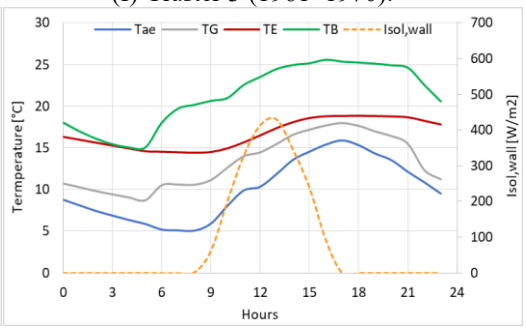

(**h**) Cluster 4 (1971–1980).

Figure 28. Heat flux components and building temperatures (with constant ach = 0.5 h−1) for a typical day: February 22nd, 2014, with a Tae= 6.24 °C (clusters for the four construction periods) [50].

Similar results have been obtained applying the energy balance model with variable ventilation between daytime (*ach* = 0.62 h^{-1}) and nighttime (0.3 h^{-1}) in Figure 29. Compared to the previous model (with constant ventilation), during the day the dispersions due to ventilation are slightly higher, and consequently the temperature B is lower.

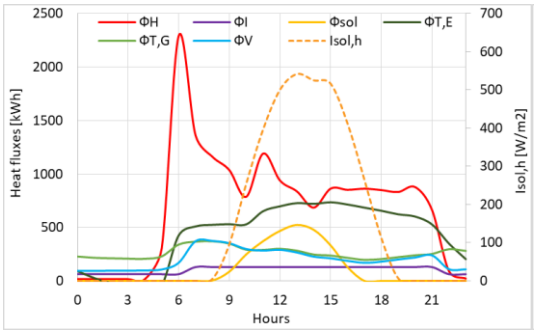

(**a**) Cluster 1 (1919–1945).

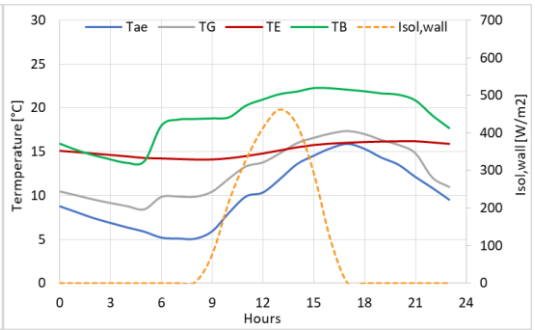

(**b**) Cluster 1 (1919–1945).

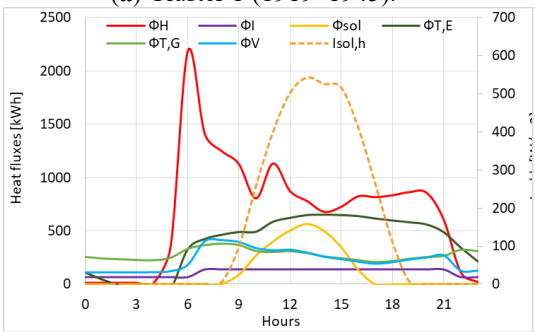

(**c**) Cluster 2 (1946–1960).

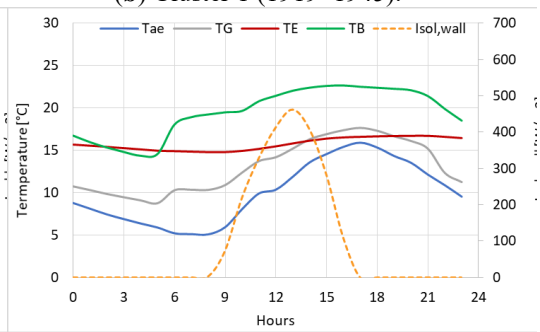

(**d**) Cluster 2 (1946–1960).

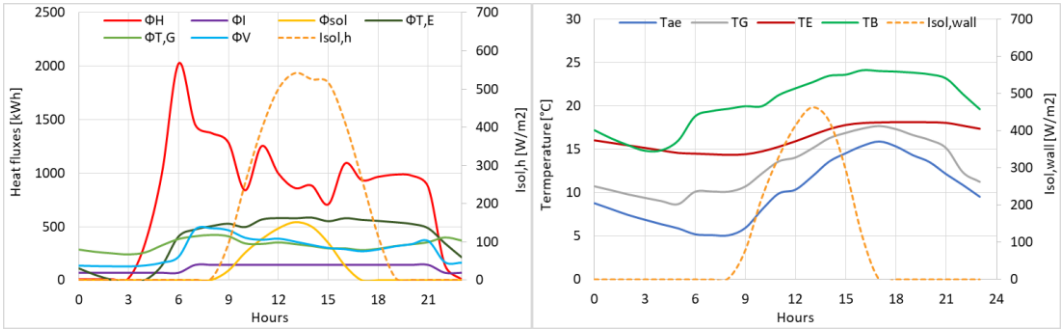

(**e**) Cluster 3 (1961–1970). (**f**) Cluster 3 (1961–1970).

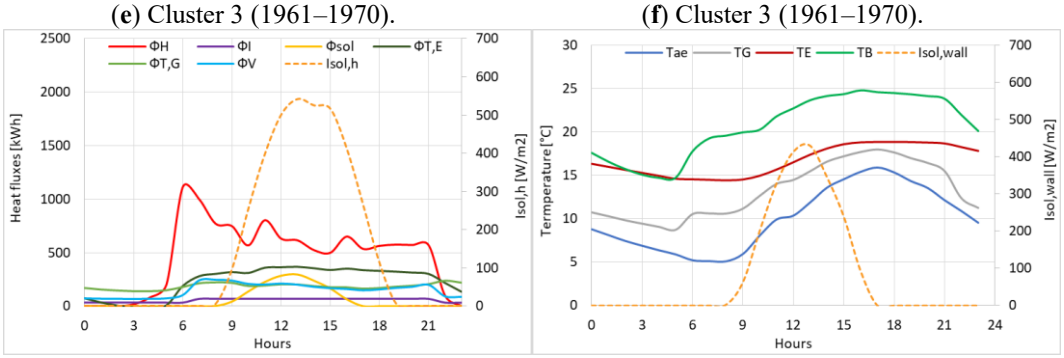

(**g**) Cluster 4 (1971–1980). (**h**) Cluster 4 (1971–1980).

Figure 29. Heat flux components and building temperatures with a variable number of air changes per hour (in daytime ach = 0.62 h−1, and in nighttime ach = 0.3 h−1) for a typical day: February 22nd, 2014, with a Tae= 6.24 °C (clusters for the four construction periods) [50].

Figure 30 and Figure 31 show results considering a variable number of *ach* and the opening of windows for typical days in February and October (the windows have been opened when the building temperature exceeds 23 °C). In Figure 30, the heat fluxes for February 22nd, 2014, can be observed on the left with a clear difference in the heat flux from ventilation between the day and night and the high variation due to window openings. The temperature trend on the right is similar, but the temperature of the buildings does not exceed 23 °C.

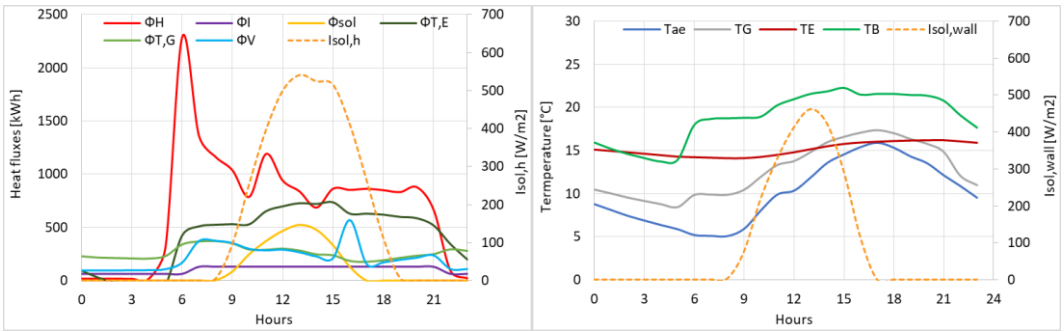

(**a**) Cluster 1 (1919–1945). (**b**) Cluster 1 (1919–1945).

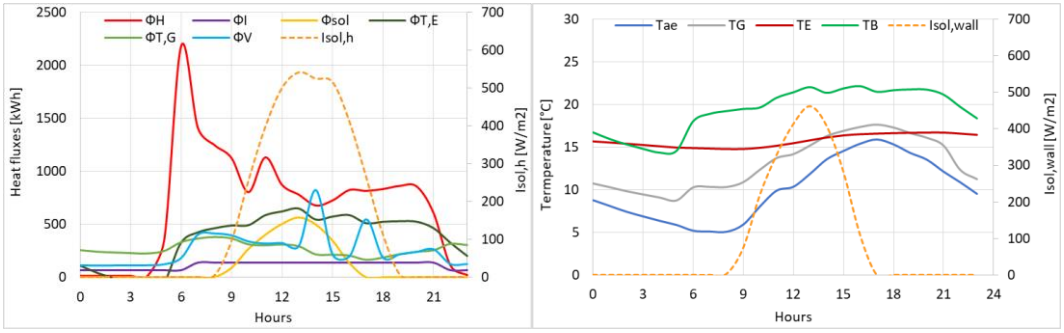

(**c**) Cluster 2 (1946–1960). (**d**) Cluster 2 (1946–1960)

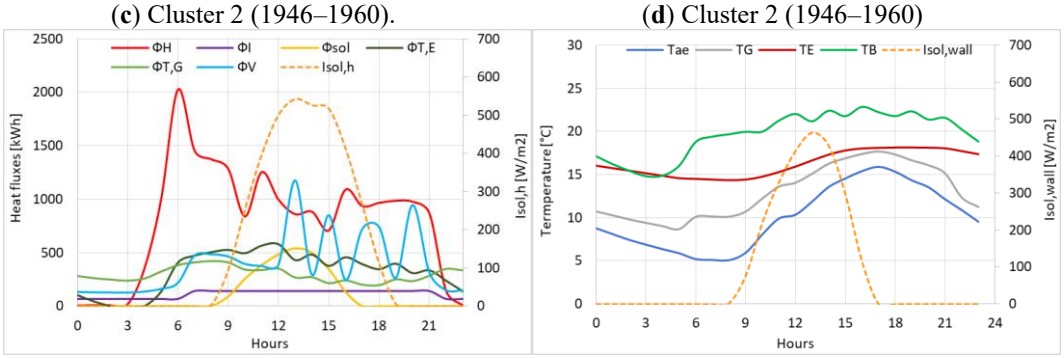

(**e**) Cluster 3 (1961–1970). (**f**) Cluster 3 (1961–1970).

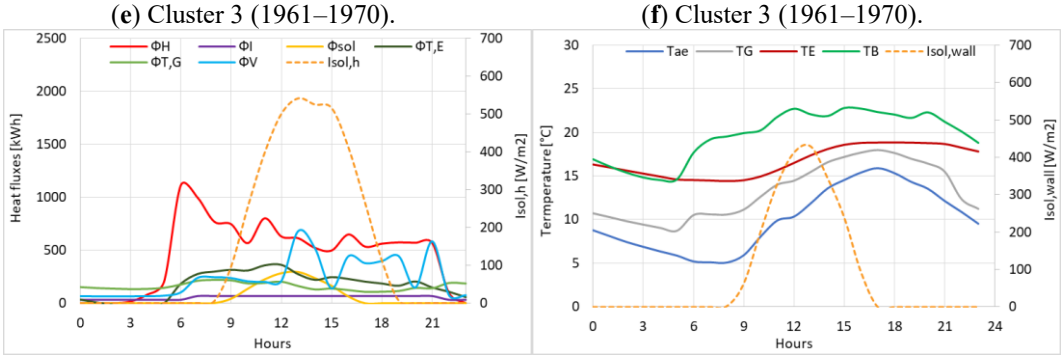

(**g**) Cluster 4 (1971–1980). (**h**) Cluster 4 (1971–1980).

Figure 30. Heat flux components and building temperatures (with a variable number of air changes per hour and windows opening) for a typical day: February 22nd, 2014, with a Tae= 6.24 °C (clusters for the four construction periods) [50].

The results of the energy balance model with a variable number of *ach* and the opening of windows have been presented also for a typical day in October, that is, October 24th, 2013, with T_{ae} = 16.3 °C (Figure 31). In general, it is possible to see, on the left, the increase in the ϕ_V, due to the windows opening at 2 p.m. A similar trend can be seen for clusters 3 and 4, where the windows are opened more times, with a consequent stabilization of the building temperature.

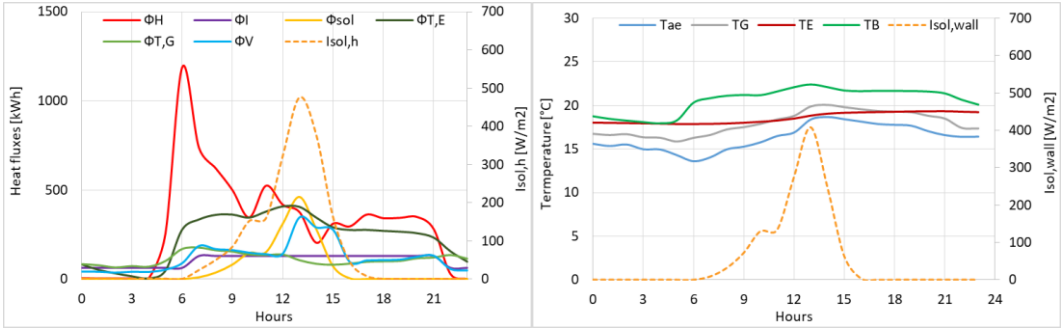

(**a**) Cluster 1 (1919–1945). (**b**) Cluster 1 (1919–1945).

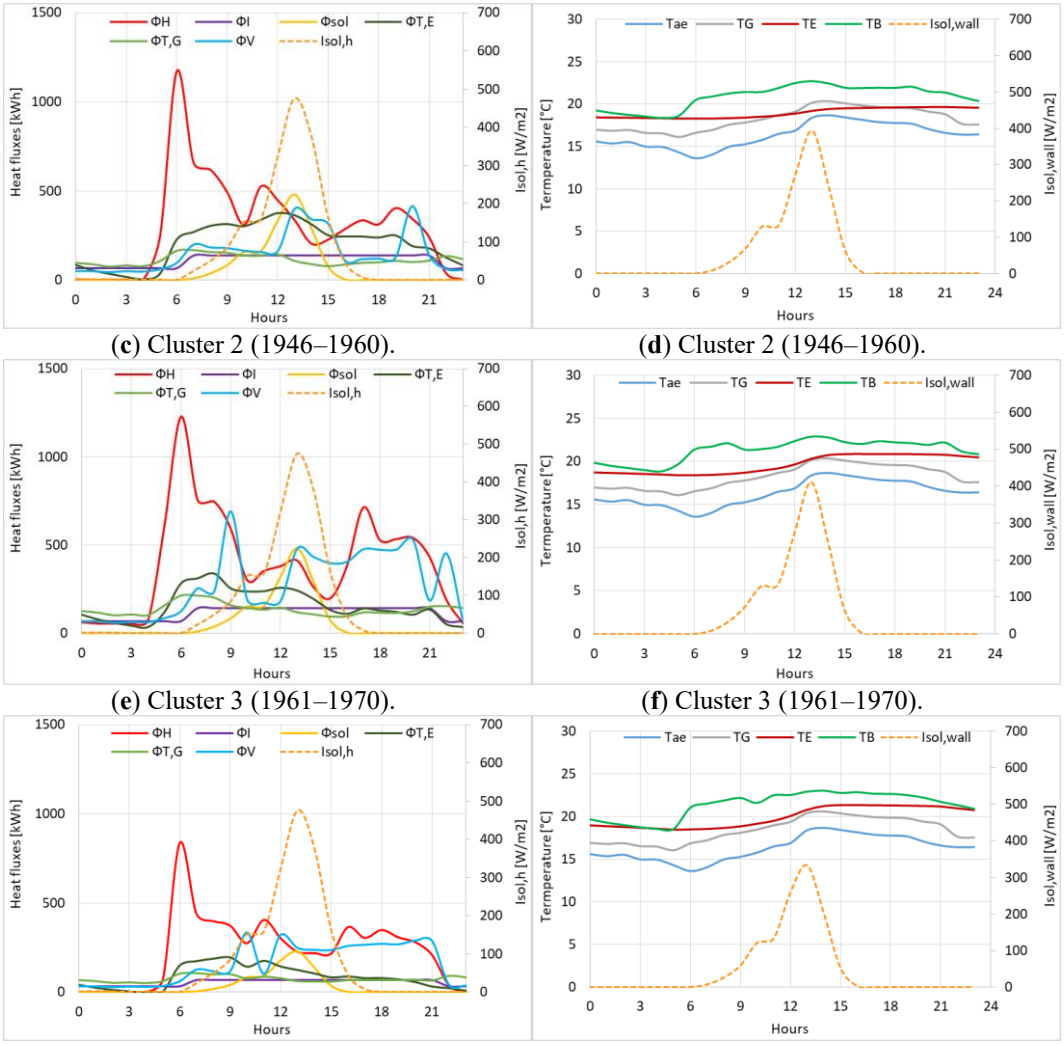

(**c**) Cluster 2 (1946–1960). (**d**) Cluster 2 (1946–1960).

(**e**) Cluster 3 (1961–1970). (**f**) Cluster 3 (1961–1970).

(**g**) Cluster 4 (1971–1980). (**h**) Cluster 4 (1971–1980).

Figure 31. Heat flux components and building temperatures (with a variable *ach* per hour and windows opening) for a typical day: October 24th, 2013, with a Tae = 16.3 °C (clusters with solid lines and buildings with dashed lines for the three construction periods) [50].

Figure 32 shows a representation of the positive and negative heat flux contributions for seven typical days that have been selected from Table 12 (remember that cluster 4 has a smaller useful surface area and volume). It is possible to observe that the heat flux for space heating is higher in the cold months of December and January, the thermal losses by transmission through opaque envelope and glazing and by ventilation vary according to the external climate conditions and are higher in cold months, internal gains are constant, and solar gains through windows are higher in the warmer months (October, March, and April).

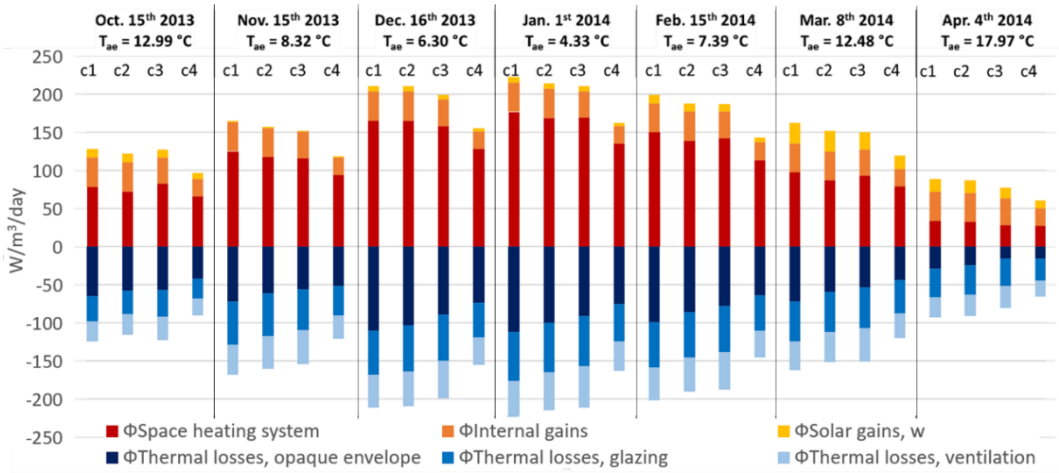

Figure 32. Positive and negative heat flux contributions with constant ventilation (ach = 0.5 h^{-1}) for the typical monthly days ($T_{ae,day}$), distinguishing by clusters (c1, c2, c3, c4) [50].

The building temperatures, T_B, are represented in Figure 33, where the climate conditions for four typical days are shown, with T_{ae} = 3.7, 7.4, 11.2, and 15.3 °C.

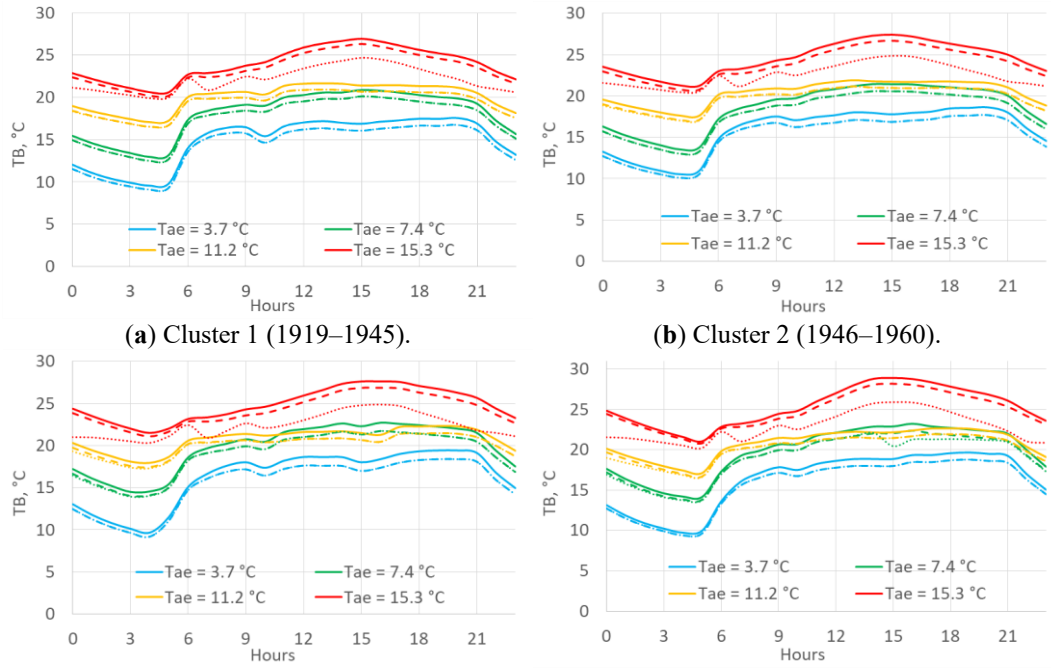

(**a**) Cluster 1 (1919–1945). (**b**) Cluster 2 (1946–1960).

(**c**) Cluster 3 (1961–1970). (**d**) Cluster 3 (1971–1980).

Figure 33. Building temperatures, TB, with an ach = 0.5 h−1 (solid lines), with a variable *ach* during the daytime (0.62 h−1) and nighttime (0.3 h−1) (dashed line), and with a variable *ach* plus window openings (dotted lines) for four typical days (clusters of the 4 construction periods) [50].

The solid lines represent the results of T_B with constant ventilation with *ach* = 0.5 h^{-1}, the dashed lines refer variable ventilation between daytime (*ach* = 0.62 h^{-1}) and nighttime (0.3 h^{-1}), and the dotted lines represent the *ach* variable and windows opening. The temperature of the three ventilation models is very similar for colder days. The difference with window openings can be observed only for higher temperatures (dotted lines). Comparing the four clusters of buildings with different periods of construction, is possible to observe that the night and daytime building temperatures are quite stable and depend on both the characteristics of the buildings

and on the external climatic conditions. This behaviour suggests that it would be possible to hypothesize some correlations between the climatic conditions and the day and night temperatures of the building, T_B.

Correlations between temperatures

The linear correlations between T_B, T_{air}, and $T_{sol\text{-}air}$ are reported in Figure 34 for the different ventilation conditions.

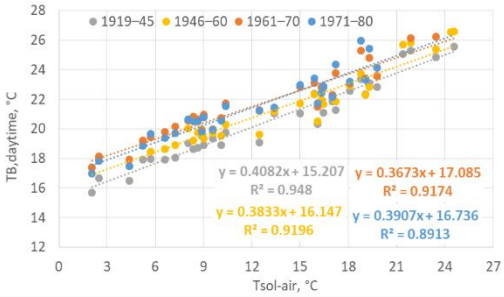

(**a**) *ach* = 0.5 h^{-1} day.

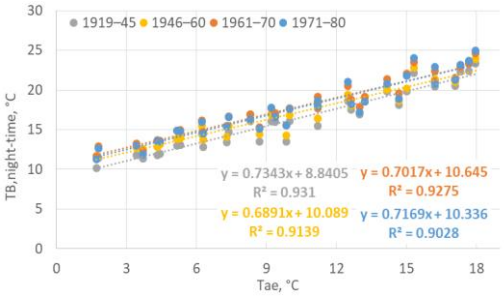

(**b**) *ach* = 0.5 h^{-1} day.

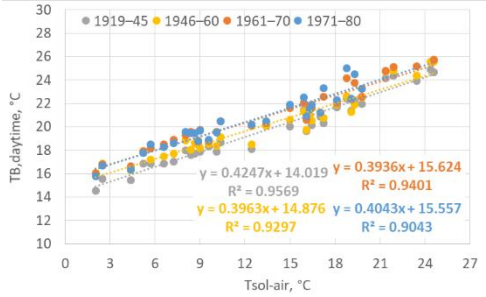

(**c**) *ach* = 0.62 h^{-1} daytime, *ach* = 0.3 h^{-1} nighttime.

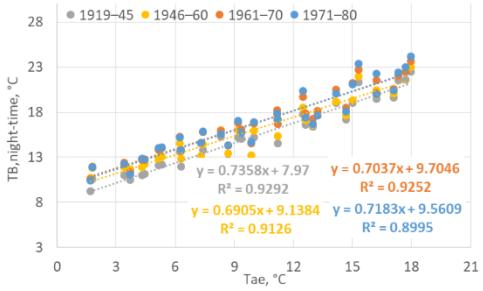

(d) *ach* = 0.62 h^{-1} daytime, *ach* = 0.3 h^{-1} nighttime.

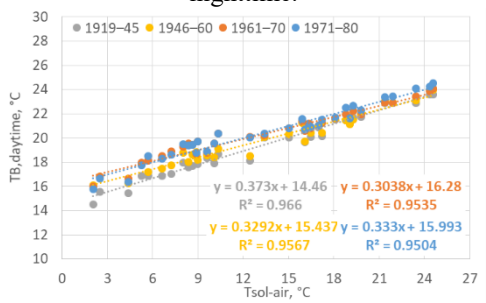

(**e**) *ach* variable with window openings.

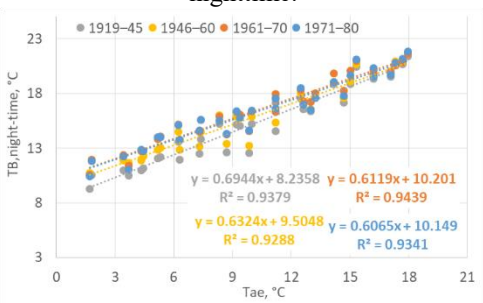

(**f**) *ach* variable with window openings.

Figure 34. Correlations between the TB and Tsol-air throughout the daytime from 6 a.m. to 9 p.m. (left column): TB and Tae during the nighttime, from 10 p.m. to 5 a.m. (right column). Distinguishing constant (a, b) and variable ventilation (c, d) and variable ventilation with window openings (e, f) [50].

Figure 34a,b presents the correlations with a constant *ach* = 0.5 h^{-1}, Figure 34c,d considers a variable *ach*, and Figure 34e,f considers a variable *ach* with window opening. The main results are the following:

- Good correlations with T_B are obtained for $T_{sol\text{-}air}$ throughout the day (24 h) and daytime, while T_{ae} is used for the nighttime (when solar irradiance cannot influence T_B).
- Linear correlations are obtained with a good R^2 coefficient of determination.
- Different correlations are obtained for the different clusters of buildings built in the four construction periods; the correlations with older buildings have a higher R^2 and the values deviate less from the line of correlation with lower external temperatures. Lower values of R^2 for new buildings may be due to either the sample of buildings being smaller than the old ones or that newer buildings may be more dependent on human occupancy variables than on climate.

Different correlations are obtained for the different ventilation typologies; with variable *ach* and window openings, the lines of the correlation change the slope.

Model validation

Figure 35 shows the comparison between the simulated and measured daily thermal consumptions applying the model with the correlations for the building temperature and the three different ventilation conditions.

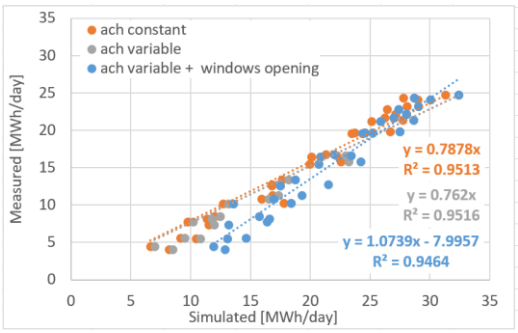

(**a**) Cluster 1 (1919–1945).

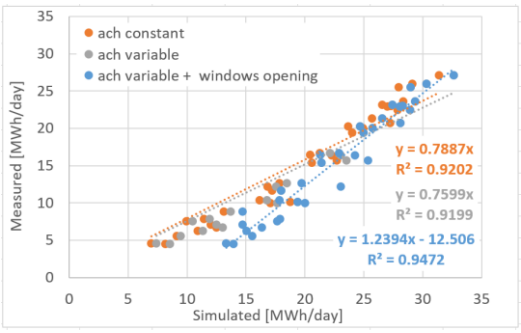

(**b**) Cluster 2 (1946–1960).

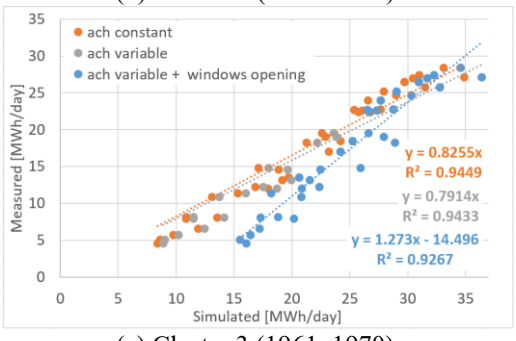

(**c**) Cluster 3 (1961–1970).

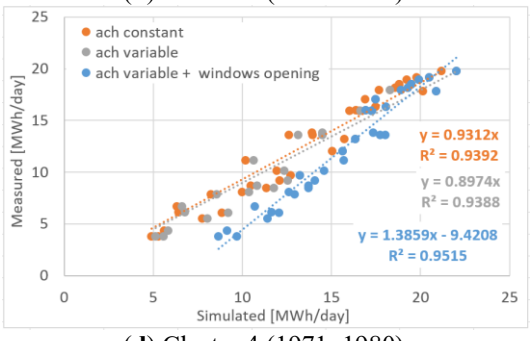

(**d**) Cluster 4 (1971–1980).

Figure 35. Comparison between simulated and measured typical daily thermal consumptions, distinguishing ach = 0.5 h−1 (in orange), ach = 0.62 h−1 during the daytime, ach = 0.3 h−1 during the nighttime (in grey), and a variable ach with window openings (in blue) [50].

A very good accuracy can be observed by comparing the simulated and measured values for each period of construction for the model with *ach* constant; the accuracy decreases with a variable *ach* and the last model with a variable *ach* and window openings is not accurate enough. This result attests that, in Turin, the

ventilation load depends on natural infiltration influenced by the permeability and local climate conditions; then, the *ach* can be represented with the model of constant infiltration (during the analysed heating period).

Comparing the calculated and measured monthly energy consumption data, the main conclusions are the same: the model that best represents the results is the one with constant ventilation; this model with a constant air change rate *ach* of 0.5 h^{-1} is chosen.

This type of model can be applied at the urban scale to represent the distribution of energy consumptions, evaluate the heat peak in every zone of a city, access the potential of renewable energy technologies that can be useful to meet that energy demand profile, and analyse the further expansion of a district heating network. All these applications can improve the security, sustainability, and affordability of the energy system and therefore the energy resilience of an urban environment.

In Figure 36, an example of the hourly model application to the city is represented. By changing the building attributes on the right, the results of this solution can be obtained.

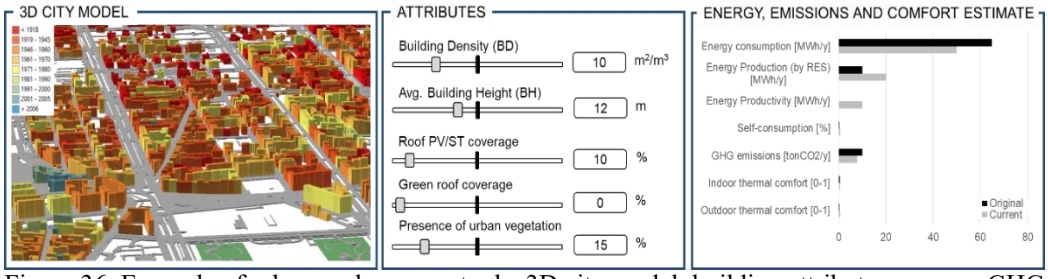

Figure 36. Example of urban-scale energy tools: 3D city model; building attributes; energy, GHG emissions, and comfort estimation [50].

3.4.5 Space cooling energy demand

This section presents the engineering model used to simulate the hourly energy demand for SC in residential buildings at neighbourhood scale (Equation 25).

$$C_{TS}\frac{dT_{TS}}{dt} = \emptyset_{sol} + \emptyset_I - (\emptyset_t + \emptyset_v + \emptyset_C) \tag{25}$$

A place-based methodology is applied to six neighbourhoods in the city of Turin, identified as homogeneous zones with different building characteristics and urban contexts [58]. The hourly cooling demand of residential buildings is studied starting from the energy balance at building scale, and then is applied at block of buildings scale with the support of GIS tools. This model is validated with a comparison of the results using CitySim tool and ISO 52016 assessment.

Model application

The GIS-based engineering model has been calibrated and validated at urban scale by comparing the cooling demand simulated at a block of buildings scale. Figure 37 shows the five blocks of buildings investigated. It is possible to observe different urban form: open-court buildings-Block 1, row-Block 2, tower-Block 3, and courtyard-Block 4-5. Blocks 4 and 5 represent the typical courtyards in the city of Turin with high-building density and different orientations.

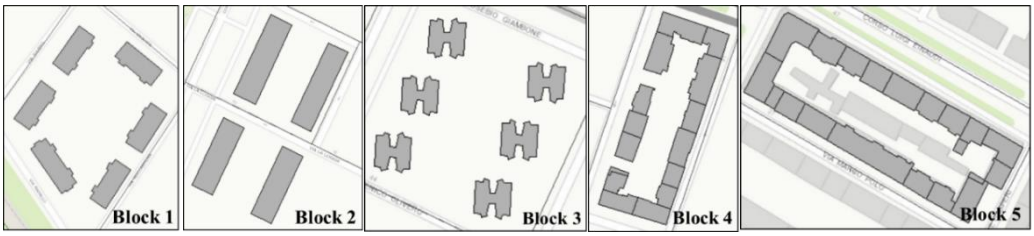

Figure 37. Blocks of buildings [49].

Input data

The place-based engineering model is applied considering the construction year as a reference to identify different thermophysical properties of the buildings. Table 13 shows the thermal transmittances ($W/m^2/K$) and the thermal capacities ($kJ/m^2/K$) of the opaque and transparent building components for nine construction years used as input data.

Table 13. Thermophysical properties of the buildings [49].

Period	U_g	U_{wall}	U_{roof}	U_{floor}	$g_{\perp}$	$C_{envelope}$
	$W/m^2/K$					-
< 1918	5.9	1.45	1.8	1.75	0.82	504
1919-45	5.9	1.35	1.8	1.58	0.82	504
1946-60	5.9	1.18	1.8	1.23	0.82	283
1961-70	5.9	1.13	2.2	1.3	0.82	283
1971-80	5.9	1.04	2.2	1.21	0.82	257
1981-90	3.3	0.78	1.18	1.95	0.70	264
1991-00	2.7	0.7	0.68	0.8	0.70	274
2001-05	2.7	0.7	0.68	0.8	0.70	274
> 2006	1.8	0.46*	0.43*	0.43*	0.62	267
*Legislative Decree Dgls 311, 29 December 2006						

The main input data at block of buildings scale are reported in Table 14.

Table 14. Blocks of buildings' characteristics [49].

Block of Buildings		Block 1	Block 2	Block 3	Block 4	Block 5
Neighborhood (name)		Arquata	Villaggio Olimpico		Mediterraneo	Crocetta
N. of buildings	-	6	4	6	15	20
Surface of flat	m^2/flat	62	114	90	79	117
Components per family	Inh/fam	1.63	2.16	2.09	1.85	2.05
Prevalent Period	-	1961-1970	1971-1980	1961-1970	1946-1960	1961-1970
U_{wall}	$W/m^2/K$	1.13	0.93	1.13	1.16	1.2

U_{roof}		2.2	1.73	2.2	1.73	2.02
U_{floor}		1.3	1.55	1.3	1.20	1.40
$U_{glazing}$		5.9	4.72	5.9	5.74	5.9
$g_{\perp}$	-	0.82	0.77	0.82	0.81	0.82
$C_{envelope}$	J/m²/K	282,518	260,199	282,518	282,094	345,277
Window-to-wall ratio	%	14	20	12	21	23
S/V	m²/m³	0.41	0.29	0.38	0.28	0.27
Prevalent Azimut	°	N/W=+125	N/W=+155	N/W=+165	N/W=+110	N/E=-150
		S/E=-55	S/E=-65	S/E=-85	S/E=-70	S/W=+30
BCR	m²/m²	0.16	0.31	0.12	0.31	0.38
BD	m³/m²	2.58	7.99	3.88	8.63	7.78
H/W	m²/m²	0.22	0.35	0.37	0.73	0.58
SVF	-	0.77	0.74	0.82	0.68	0.67

Energy simulations are carried out according to the cooling season 2014 (same period used for the heating simulations [50]). Since in Turin the cooling energy consumptions is quite low, the warmer day of each month has been chosen to analyse the results of the GIS-based model in the summer season: May 30th, June 12th, July 18th, August 5th, and September 1st. In Table 15 the average ($T_{ae,avg}$) and maximum daily ($T_{ae,max}$) air temperature (°C), and the global horizontal irradiation (*GHI*, kWh/m²) have been indicated.

Table 15. The warmer day of each month for the cooling season 2014 [49].

	May 30th	**June 12th**	**July 18th**	**August 5th**	**September 1st**
$T_{ae,avg}$,°C	21.4	28.7	27.6	24.3	23.0
$T_{ae,max}$,°C (hour)	25.9 (4 p.m.)	33.6 (5 p.m.)	32.1 (7 p.m.)	29.6 (6 p.m.)	28.1 (5 p.m.)
GHI, kWh/m²/day	6.91	7.36	6.98	7.08	6.23

Model results and validation

This section presents the GIS-based engineering model validation by analyzing the monthly, daily, and hourly results. The cooling energy demand simulated is compared:

(i) At building scale, considering five typical residential buildings for each of the six neighbourhoods (30 buildings), and the comparison has been carried out with CitySim tool and ISO 52016 standard assessment.

(ii) At block of buildings scale, five blocks of buildings with different urban shapes have been selected among the neighbourhoods, and the simulations have been carried out with CitySim tool.

The results of the hourly simulation at building scale of three residential buildings are shown in Figure 38: 'ED-5' built in 1919-46 in Crocetta neighbourhood; 'ED-5' built in 1946-60 in Mediterraneo neighbourhood; and 'ED-5' built in 1981-90 in Villaggio Olimpico neighbourhood. The hourly cooling energy profiles assessed with the GIS-based model (in red), the CitySim tool (in blue) and the ISO 52016 standard (in green) are compared.

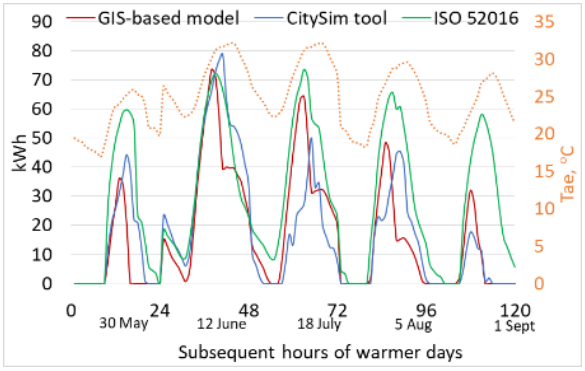

(a) 'ED-5': 1919-46, NW-SE

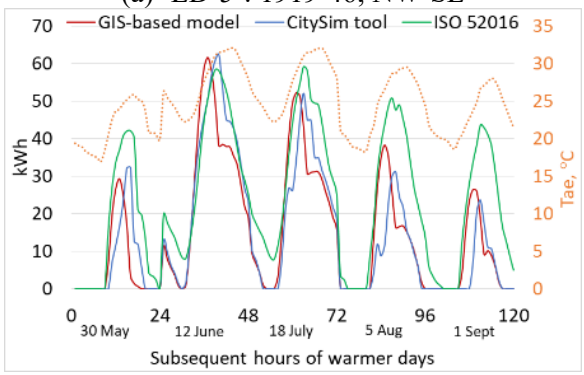

(b) 'ED-5: 1946-60, E-W

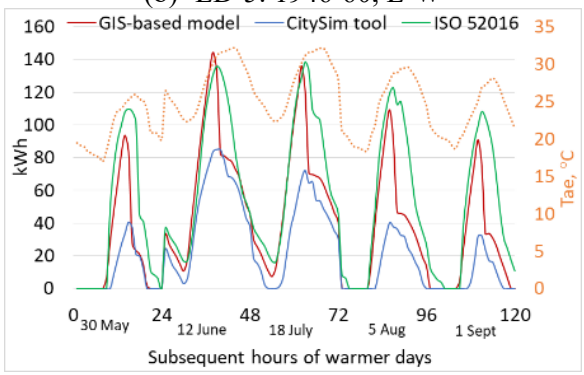

(c) 'ED-5: 1981-90, NE-SW

Figure 38. Crocetta neighbourhood: comparison of hourly cooling demand for the five warmer days: GIS-based model, CitySim tool and hourly method ISO 52016 [49].

It can be observed that the hourly energy profiles have a typical trend related to the external air temperature T_{ae} (and to the solar irradiation). The GIS-based model and the CitySim results are very similar: the hourly energy peaks for the five days, and for both buildings are very close. The ISO 52016 standard simulates higher consumption than the other two tools, especially for month with lower external air temperature (May and September). These differences are mainly because local climate conditions refer to the typical meteorological year (TMY was adapted to monthly air temperatures and solar irradiations of 2014, instead CitySim and the GIS-based model used real weather data). In this case, correlations between air temperature/global horizontal irradiance and cooling demand have been used to compare the results according to the weather data used in the CitySim tool and in the GIS-based engineering model. The annual absolute relative error for the cooling season (April 15th - October 15th) calculated at building level is on average 30%

(median 26%). There are minimum values of 21 and 22%, respectively in Raffaello and Crocetta neighbourhoods, and a maximum value of 70% in Villaggio Olimpico neighbourhoods. These results are compatible with the application of the GIS-based model which is on an urban scale and not on a building scale. The precision of the GIS-based model depends on the urban form, and it has been designed for the typical district of the city of Turin, the courtyard. Raffaello and Crocetta represent the typical neighbourhood of the city with compact condominiums built between 1946 and 1980, while Villaggio Olimpico was built more recently, and it is characterized by towers and big isolated condominiums. It is necessary to consider that the relative error has less meaning when it refers to very low energy demands such as 2 to 6 kWh/m^3/year. Figure 39 shows the comparison of the daily cooling demand between the GIS-based model and the CitySim calculated for the five warmer days. In Figure 39a, the results refer to the energy simulations of the 30 residential buildings analysed, while Figure 39b reports the cooling energy demand calculated for the five blocks of buildings. The GIS-based model shows a good accuracy in both cases, especially on June 12th and July 18th thanks to the highest daily temperatures, 33.6 and 32.1 °C, respectively.

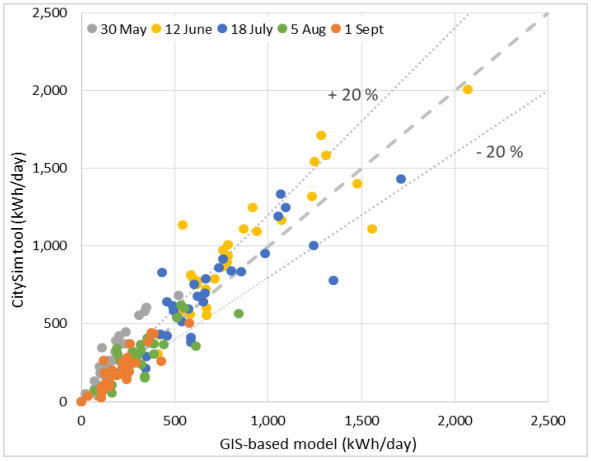

(a) Building scale: 30 buildings

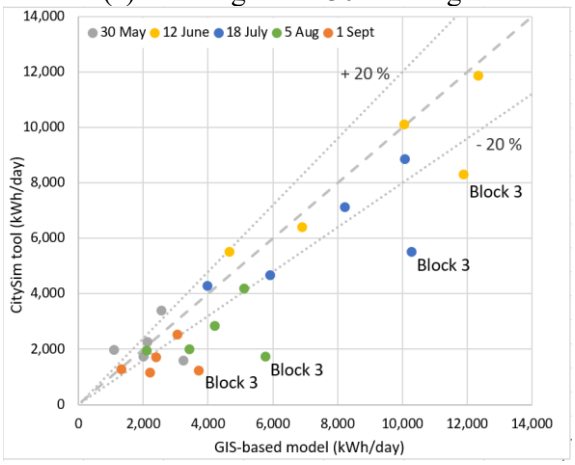

(b) Block of buildings scale: 5 blocks

Figure 39. Comparison of daily cooling demand for the five warmer days: (a) GIS-based model and CitySim tool at building (b) and block of building scale [49].

Figure 40 shows the comparison of the hourly SC demand between the GIS-based model (in red) and the CitySim tool (in blue) calculated for the five warmer days at block of buildings scale. As already observed in Figure 38 and Figure 39, the model is less accurate for Villaggio Olimpico block 2 and especially for block 3. The precision also depends on the number of buildings in each block and on the scale of application [15], this is another reason why the GIS model is more accurate in blocks 4 and 5 with 15-20 buildings, compared to blocks 2 and 3 with 4-6 isolated buildings.

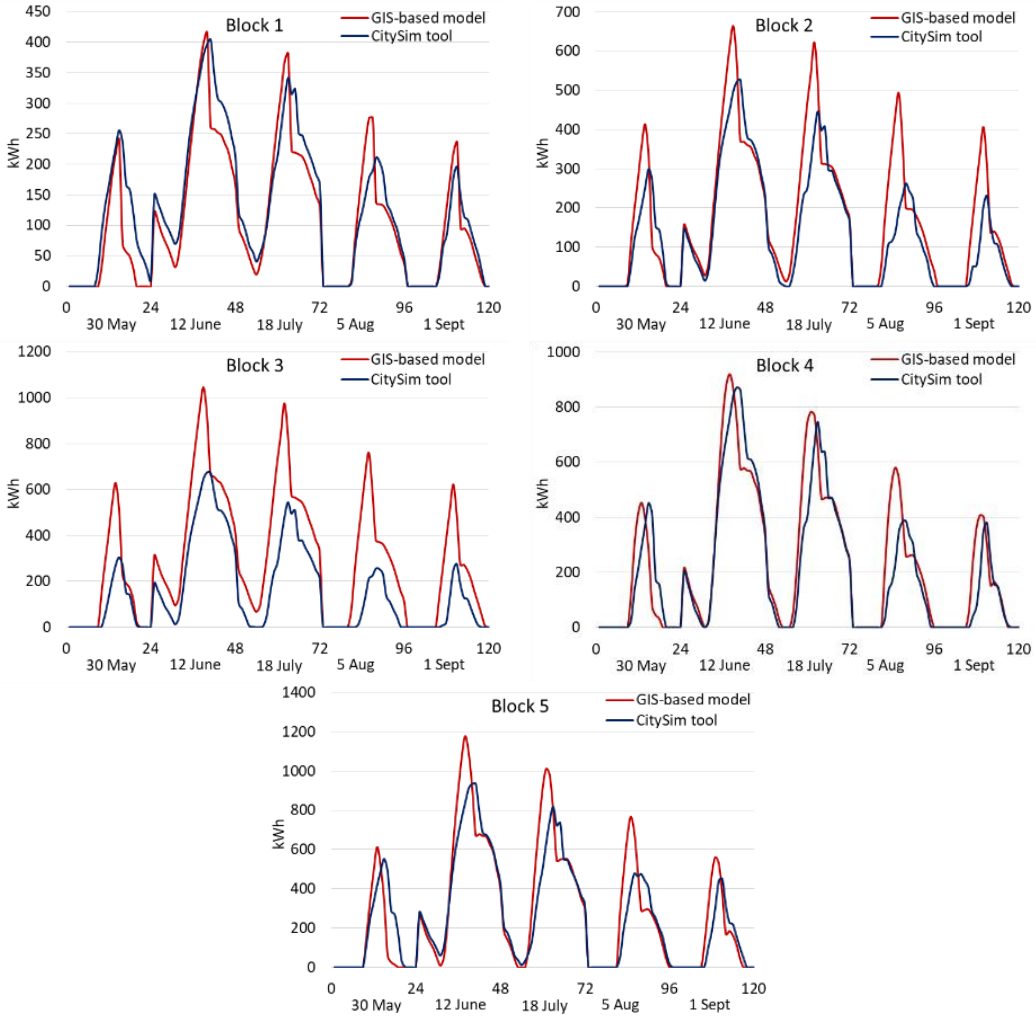

Figure 40. Comparison of hourly cooling demand at block of buildings scale for the five warmer days: GIS-based model and CitySim tool [49].

In summary, a GIS-based engineering model have been firstly validated for district-scale applications, and then used to simulate the cooling energy demand in different neighbourhoods with various morphologies.

This model uses urban variables mainly to evaluate the solar fluxes and the extra flux to the sky at block-scale. Thus, at the building scale the accuracy is low,

but at the block scale it works except for the isolated towers in block 3. The model has an accuracy that seems proportional to the number of buildings in the district.

To conclude, hourly process-driven models were designed using as a sample about 100 residential buildings connected to the DH. Thermo-physical characteristics of these buildings were defined according to the construction year. Energy simulations were carried out using an iterative procedure in Excel, and local climate data used refers to the year 2013-2014. With these models it was possible to simulate the heat flow components of the urban building energy balance and the temperatures of the three TSs (building, envelope, and glazing). Results were aggregated by creating clusters of buildings according to the construction period. Some correlations between outdoor (and sol-air) and indoor temperatures were defined in order to correct the indoor temperature in the generalization phase to the whole city. Finally, heating results were validated against measured DH data at the resolution of 1 hour, while cooling results were validated against CitySim simulation and ISO 52016 assessment. The generalized model can be applied to the whole city.

3.5 Hourly data-driven models

This section presents a data-driven model designed using machine leering techniques and compares two simplified energy models applied to the city of Fribourg in Switzerland: a process-driven model (engineering model, EN) and a data-driven model (machine learning model, ML). Hourly SH consumption for residential buildings has been simulated at urban level. The results of energy simulations are compared and evaluated against anonymized monitoring data. The investigation shows that the simulations are quite precise with an annual *MAPE* of 12.8 and 19.3% for the machine learning and the GIS-based engineering model, respectively, on residential buildings built in different periods of construction.

The novelty of this investigation is to analyse the most common simplified methods used to simulate energy consumption at different levels, from a group of buildings to city scale. The main goal of the presented study is to quantify the simulation error against calibrated SH consumption data. For privacy concerns, the measured consumption data could not be disclosed, and is therefore used to calibrate a CitySim simulation. The calibration is based on annual heat demand data, for which measurements are available on a per-building basis. The shares of this energy used for SH and DHW are estimated with the methodology contained in the Swiss norms, which consider the number of occupants. Buildings are grouped into clusters according to their normalized space heating demand and occupancy type, and a search algorithm is used to find the optimal value of the unintended air infiltration rate (*ach*) within each cluster, with which the buildings are finally simulated. The data obtained in this way retains quantitative information about the heating consumption while losing all information on user-specific dynamic behaviour.

3.5.1 Methodology

Several approaches and techniques are used by researchers and practitioners to simulate energy consumption of buildings at urban level, the bottom-up approaches are the focus of the current analysis. A data-driven model is presented, evaluated, and compared using the results of the hourly SH energy simulation at city level (Table 16). The building energy-use models used in this assessment are:

- A machine learning (ML) model based on the light gradient boosting machine algorithm [158] which makes an estimation of the hourly energy consumption of each building. Gradient boosting is chosen over other ML algorithms as it is usually among the top performers on energy load prediction comparisons [159,160] and because it provides a good balance between performance and training times.
- A place-based or GIS-based engineering (EN) model uses a bottom-up approach, and it is based on a thermal balance of buildings at urban scale to predict SH energy consumption and greenhouse gas emissions of groups of buildings in built-up context (this model is presented in section 3.4).
- CitySim (CS), an open-source simulation software that can be used to estimate the energy demand and energy-use for heating and cooling of multiple buildings, up to district scale, also considering the urban context. The simulation solver is based on the thermal-electrical analogy.

Table 16. Building energy-use models and tools investigated [47].

Models and Tools	Method	Technique	Ref.
Machine learning (ML) model	Black box	Artificial Intelligence, light gradient boosting	[155,158,159,161]
GIS-based engineering (EN) model	Gray box	Thermal balance, iterative procedure	[46,50,162]
CitySim (CS) engineering tool	White box	Thermal-electrical analogy	[29,30,163]

Figure 41 describes the main steps of this analysis. In the first phase, the input data of the Fribourg case study are collected and processed. Subsequently, according to energy models and simulation techniques used, the hourly SH consumption of residential buildings is calculated at city level. Finally, the simulated data are compared with the calibrated one by CS to evaluate the accuracy of each model. In addition, a sensitivity analysis is carried out using the Morris method.

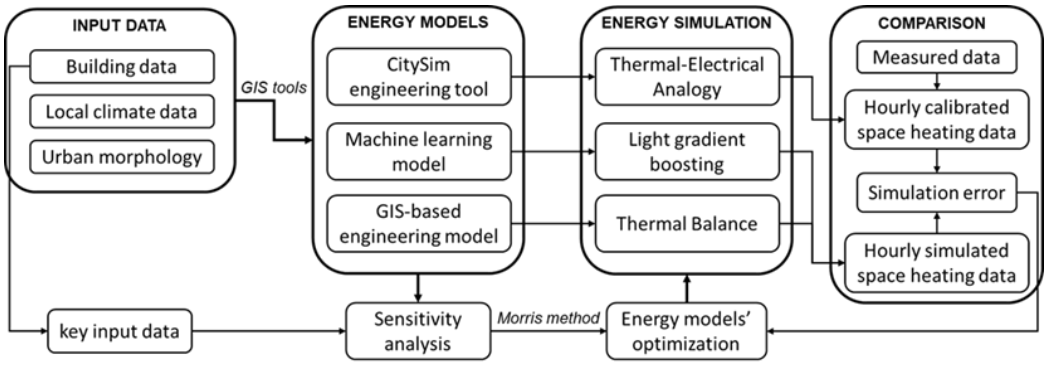

Figure 41. Urban-scale building energy modeling: flowchart methodology applied to the case study of Fribourg [47].

3.5.2 Input data

Data is essential to develop, validate and use the model. Depending on the energy-use models and tools, different input data is required. Table 17 shows the main input data used in this work for the application of the three models.

Table 17. Main input data with the source, tools used to process them and the scale of analysis [47].

Input Data	Source	Tools	Scale
Type of users and geometrical characteristics	Cadastral data	GIS	Building
Internal air temperature	norm SIA 380/1:2009	None	
Infiltration rate and thermo-physical proprieties	norm SIA 380/1:2009 and [164]	None	
Sky view factor (*SVF*)	Cadastral data and digital surface model	Relief Visualization Toolbox software, GIS	Urban
Height-to-distance ratio (*H/W*)	Cadastral data	GIS	
Meteorological data	meteonorm.com and www.meteoswiss.ch	Meteonorm software	City

The input data can be classified in building data, morphological parameters and local climate conditions.

Building data refers to (i) the type of users; (ii) the geometrical characteristics such as the heat loss surfaces, the surface-to-volume ratio (*S/V*, m^2/m^3) or non-compactness, the net and gross heated area, the opaque and transparent envelope (the glazing ratio is the windows-to-external wall ratio, %), the heated volume, the number of floors; (iii) the internal air temperature (min and max set point temperature, °C); (iv) the air changes per hour due to unintentional air infiltration rate (*ach*, h^{-1}) is an input parameter of the EN model according to the construction period, while it is used by the CS tool to calibrate the results and the ML model uses the calibrated values for tuning the model; (v) the thermo-physical proprieties assessed according to the construction period such as the thermal capacities of the

building elements (C, kJm^{-2} K^{-1}), the thermal transmittances (U, Wm^{-2} K^{-1}) and relative thermal resistances (R, m^2 KW^{-1}), the wall types (layers with thickness, conductivity, heat capacity and density); and (vi) the systems' efficiency for the space heating is assumed equal to 0.90 [164]. To consider the characteristics of a specific urban context, (i) the *SVF* (-) and (ii) the *H/W* (-) ratio were used as input data in the ML and EN models.

Local climate data refers to the year 2017. The meteorological data used are: (i) the hourly external air and sky temperature (°C); (ii) the relative humidity (%); (iii) the horizontal global irradiance (W/m^2); (iv) the wind speed (m/s) and direction (°); (v) the nebulosity (okta); and (vi) the rain fall (mm). In the EN model, the incident solar irradiance on walls is used with the hourly solar height and direction to calculate the shadow percentage on the envelope of each building as a function of its solar exposition and of the urban canyon effect [50].

In Table 18 are indicated the main input building data that depends on the construction period: the ventilation rate (*ach*, h^{-1}); the wall proprieties: thickness (*dm*, m); thermal transmittance (U_{wall}, Wm^{-2} K^{-1}) and thermal capacity (C_{wall}, kJm^{-2} K^{-1}); the thermal transmittances of roof (U_{roof}, Wm^{-2} K^{-1}) and ground slab (U_{ground}, Wm^{-2} K^{-1}) distinguishing layer with and without insulation; the windows' parameters: thermal transmittance (U_{glass}, Wm^{-2} K^{-1}), total solar energy transmittance of glazing (g_G, -) and glazing ratio (g_{ratio}, -).

Table 18. Main input building data according to the construction period [47].

Period	*ach* *	C_{wall}	*dm*	U_{wall}	U_{ground}	U_{roof}	U_{glass}	g_G	g_{ratio}
[-]	[h^{-1}]	[kJm^{-2} K^{-1}]	[m]	[Wm^{-2} K^{-1}] **				[-]	[-]
Before 1945	0.70	660	0.44	0.94	1.60	0.70	2.3	0.47	0.25
1946–1960	0.60	487	0.37	1.35	1.50				
1961–1970	0.55	355	0.27	1.03	1.30 (0.32)	0.65 (0.32)			
1971–1980	0.50	356	0.28	0.88	1.10 (0.36)	0.60 (0.34)			
1981–1990	0.40	493	0.25	0.90	0.68 (0.33)	0.43 (0.27)			
1991–2000	0.35	494	0.27	0.69	0.49 (0.33)	0.31 (0.27)			
2001–2010	0.30	495	0.30	0.51	0.35 (0.27)	0.25 (0.20)	1.7	0.49	0.35
From 2010		507	0.37		0.25 (0.20)	0.22 (0.17)			

* *ach* is the only input feature that changes between the EN model and the ML model.

** In brackets, thermal transmittances U with an additional thermal insulation layer.

3.5.3 Machine learning model

A light gradient boosting machine (LGBM) model is built and optimized in Python using the LightGBM [158] and Scikit-learn [165] libraries. LGBM is an efficient implementation of the gradient boosting algorithm—a machine learning technique where an ensemble of weak learners, typically decision trees, is used to solve a regression or classification problem. However, unlike other ensemble

algorithms, in gradient boosting, the weak learners are added to the model sequentially, so that each learner is fit to the residuals of the previous one.

The model is trained on hourly data using a combination of building features and climate data with a lag of 3 h, for a total of 20 inputs: (i) building features: footprint surface, height, net volume, heat loss surface, ach, *U* values of walls, floor, roof and glass, glazing ratio, *SVF*; (ii) climate features: air temperature, surface temperature, relative humidity, wind speed, global direct and diffuse radiation. As this approach is extremely prone to overfitting, a thorough tuning of the hyperparameters that control the generalization ability of the model is made using 3-fold cross- validation.

A list of the chosen hyperparameters for the final model is given in Table 19. The results show that reducing the amount of data on which each weak learner is trained led to a lower cross-validated error. This reduction is operated sample-wise by the bootstrap aggregating (bagging) operation and feature-wise by the feature fraction hyperparameter. Bagging fraction and bagging frequency control the number of samples that are used to train each tree and the frequency with which the sampling is updated, respectively. Bagging generally reduces the variance of the single tree and improves its stability, besides reducing overfitting [166]. In the tuned model, the bagging fraction was set to 0.95, reducing the samples used to train the trees by 5%. The feature fraction hyperparameter, on the other hand, controls the number of input features, or columns, that are sampled for each weak learner. In the case of this model, it was set to 0.6, meaning that only 60% of the features are used each time. A low value of this hyperparameter might have reduced the reliance of the model on a small subset of input features, thus improving its generalization ability. Finally, both L1 and L2 regularization terms were set at nearly the maximum tested value of 0.6. In the case of gradient boosting, the L1 and L2 regularizations are applied to the leaves (exit nodes) of each tree, so that their contribution to the prediction is smoothed to reduce overfitting.

Table 19. Hyperparameters of the machine learning model [47].

Hyperparameter	Value	Tested Range	Hyperparameter	Value	Tested Range
Bagging fraction	0.95	0.4–1	Lambda L2	0.58	0–0.6
Bagging frequency	9	1–10	Max bin	300	100–2000
Feature fraction	0.6	0.4–1	Number of estimators *	1000	100–1000
Lambda L1	0.59	0–0.6	Number of leaves	38	20–40

* Following LGBM (light gradient boosting machine) documentation, 100 estimators were used for the hyperparameter tuning and 1000 for the final model.

** The dataset was randomly divided into training and test subsets by a ratio of 80/20.

3.5.4 Model application

Case study

The city of Fribourg is in the Central-Western part of Switzerland, and it has a warm humid continental climate. The city is organized in ten zones, and there are about 3,800 heated buildings of which 84% are from the residential sector. The monitoring data is available for every zone except zone 3, which is therefore excluded from the simulations (not having the measured data, it would not have been possible to evaluate the precision of the tested models). The residential sector in Fribourg is mainly made up of large and compact condominiums (56%) with an average value of surface-to-volume (S/V) ratio of 0.33 m^2/m^3, 30% of buildings are detached houses (S/V_{avg} of 0.85 m^2/m^3) and the remaining part are row-houses. The 61% of residential buildings were built before 1970, but there is also a 12% share of new buildings, built after 2001. In Figure 42, the percentage by construction period of residential buildings is indicated for each of the ten zones. Unfortunately, for some buildings, mainly located in zones 9 and 10, the construction period is not known. Since it is a fundamental parameter for the identification of the thermo-physical characteristics of the building, these buildings have not been considered for the simulation. From over 2,000 residential buildings that will be connected to the DHN in Fribourg, about 300 of them are selected among the nine of ten zones taking into consideration: (i) the building shape, only compact condominiums, which represent the most common building typology of Fribourg, are selected for the energy simulation; (ii) and the construction periods, the buildings are classified into nine classes. A second selection is made to discard the anomalous data in which the geometric characteristics of buildings elaborated in GIS did not correspond with the CitySim database; consequently, the selected buildings used have become 200 located in eight zones (the buildings in zone 2 did not meet the requirement).

For each zone, a cluster of compact condominiums with different construction periods is selected. In accordance with the available measured space heating data, the hourly energy simulation is made for the year 2017. In Fribourg, for this year, the heating season starts on 7 October and ends on 18 May.

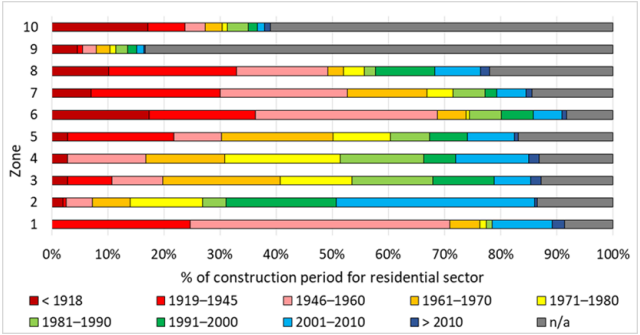

Figure 42. Distribution of construction periods for the residential sector in the ten zones of Fribourg [47].

With the support of GIS tools, a georeferenced database is created with the building characteristics, taken from satellite images, open cadastral data, and orthophotos. The geometrical characteristics are elaborated at building scale and the urban parameters were calculated at district scale for a grid with a dimension of 500 m × 500 m. Figure 43 shows the classification of heated buildings considering the type of users and the residential building typologies according to the *S/V* ratio.

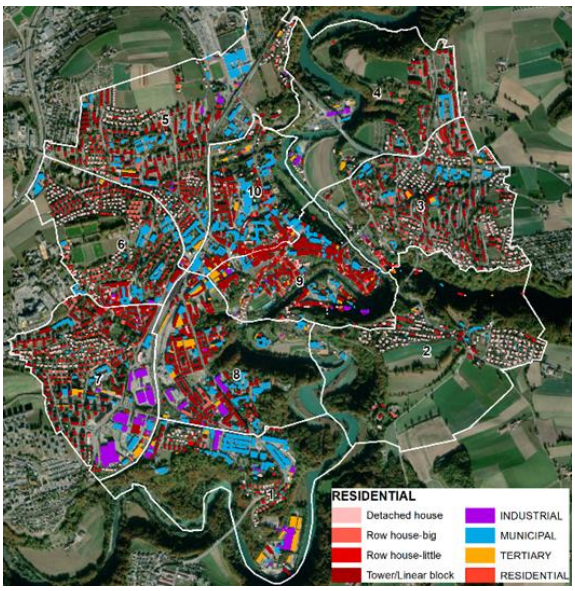

Figure 43. Buildings' characteristics: typology of heated buildings [47].

Energy simulations

The energy simulation is made for 198 residential buildings classified as compact condominiums (tower, linear block, or big row-houses) with an average *S/V* ratio of 0.41 m^2/m^3.

The construction period is known for this sample of buildings: 44% of them were built before 1970, 36% were built between 1970 and 1990, and 20% were built after 1990. Buildings that have undergone retrofit interventions were excluded. Figure 44 show the sample of residential buildings (in red) with the information of construction period for each zone.

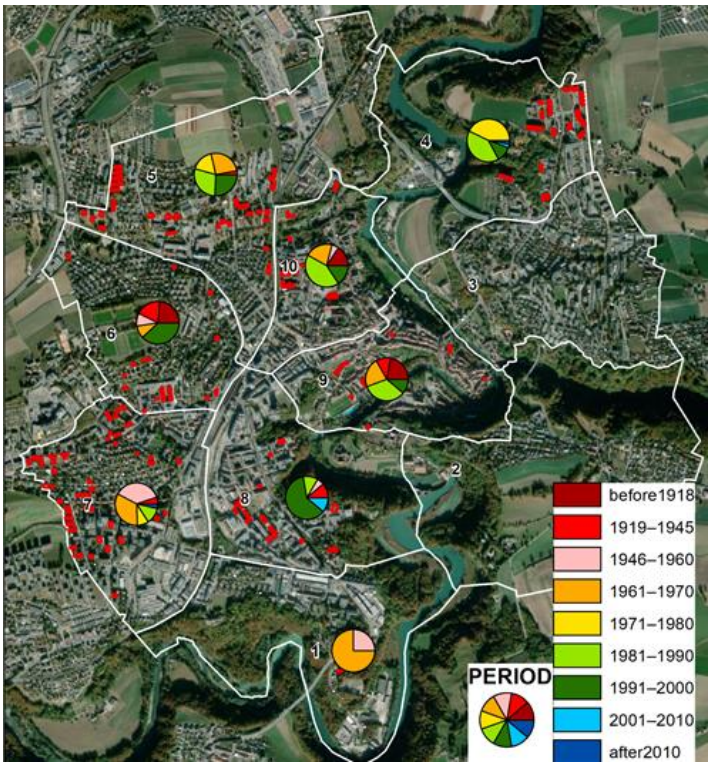

Figure 44. Construction period of residential buildings selected for the models' application: distribution in the considered eight zones [47].

3.5.5 Model results and validation

This section describes the main results obtained at multiple temporal and spatial scales. The accuracy of energy-use models has been evaluated by comparing the calculated and calibrated SH consumptions for about 200 residential buildings in Fribourg for the year 2017. The mean absolute error (MAE) and the mean absolute percentage error (MAPE), respectively, at hourly and annual levels on the heating season are calculated for the two models with respect to the CS-calibrated heating consumption.

Figure 45 and Figure 46 show the MAPE of the two models aggregated by construction period and surface-to-volume ratio *S/V* respectively. The results obtained from the preliminary analysis of the simulation errors show that the accuracy of the models depends significantly on the geometrical characteristics and the thermo-physical properties of the building. For ML and EN models, the simulations are less accurate for old buildings, built before 1919 and for new buildings, built after 2000. The MAPE is 11.44% for ML and 18.75% for EN models for buildings built between 1919 and 2000. Slightly worse performances on recent buildings were already observed for the EN model in previous studies applied to the city of Turin, where the available energy consumption data for the more recent buildings was not enough to calibrate the model [50,162].

Considering the *S/V*, it is possible to observe that the prediction error of the EN model tends to be higher on very compact buildings with values of S/V lower than

0.4 m^2/m^3, while the ML model shows a lower precision on buildings with a higher *S/V*, for which, however, there are only few test samples. In particular, the test set has 11 buildings with an *S/V* lower than 0.25 m^2/m^3, 1 of which with an *S/V* equal to 0.16 m^2/m^3 (this is due to the fact that the building is located in the historic centre with neighboring buildings), 8 with an *S/V* higher than 0.7 m^2/m^3 and the remaining 90% of buildings have an *S/V* value in between.

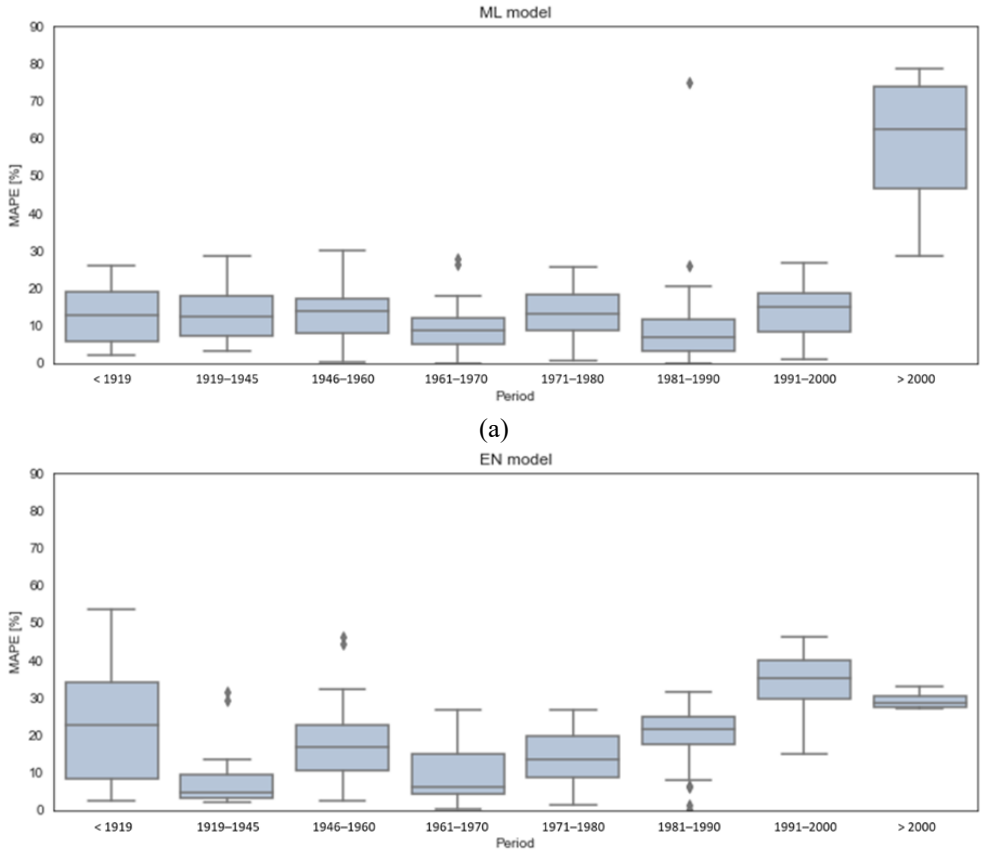

Figure 45. Error distributions of the (a) ML and (b) EN models by period of construction [47].

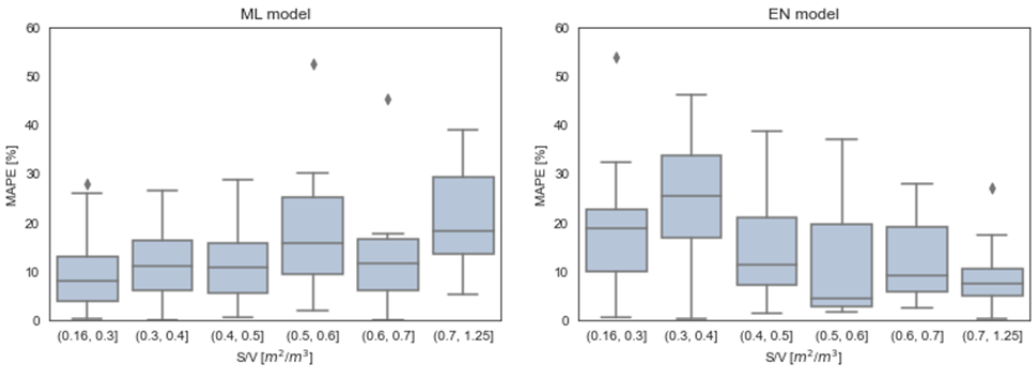

Figure 46. Error distributions of the ML and EN models by *S/V* [47].

According to the simulation errors, four buildings are selected in order to understand the reason for the difference in the energy simulation results between

the models: one building with low MAPE for both models (building ID 4397); one with high MAPE for both models (building ID 761); and two with high simulation difference between the EN and ML models (building ID 128 and ID 2724). Table 20 indicates the main characteristics of these four buildings with the hourly value of MAE in Wh. Different values of ach can be observed in Table 20: the EN model uses the ach according to the construction period; the ML model uses the calibrated values of ach used to generate the target heating demand in the CS simulation. In some cases, this discrepancy is substantial, as, for example, happens for the building with ID 761; these results will be investigated with further databases on retrofit interventions and the state of maintenance of the buildings.

Table 20. Characteristics of four selected buildings [47].

Building ID	Period of Construction	*S/V* m^2/m^3	Heated vol. m^3	*ach* h^{-1}	*ach* * h^{-1}	*SVF* -	*H/W* -	Zone	CS kWh/y	MAE_{ML} Wh	MAE_{EN} Wh
4397	1971-80	0.27	8185	0.50	0.99	0.84	0.41	4	292,713	2784	7195
761	1991-00	0.56	2802	0.35	1.025	0.88	0.25	10	167,999	10,525	8465
128	1946-60	0.30	3108	0.60	0.65	0.85	0.32	7	118,075	1436	10,196
2724	1981-90	1.24	609	0.40	0.65	0.99	0.19	5	41,014	5572	1323

* Calibrated values according to CS model.

The results of the hourly simulation for each building are shown in Figure 47. The hourly data reported are from 1 January to 31 May and from 1 October to 31 December 2017. When the annual MAPE is low, the hourly simulation is very accurate for both models. One interesting aspect of this graph is that, for buildings with high MAE, the models are more accurate with high external air temperature (T_{ae}) values of 10–15 °C, while with colder temperatures, the MAE tended to increase. In general, the energy consumption decreased as the T_{ae} increased. For these selected buildings, the ML and EN models tended to underestimate the space heating consumption for newer buildings and overestimate it for older ones.

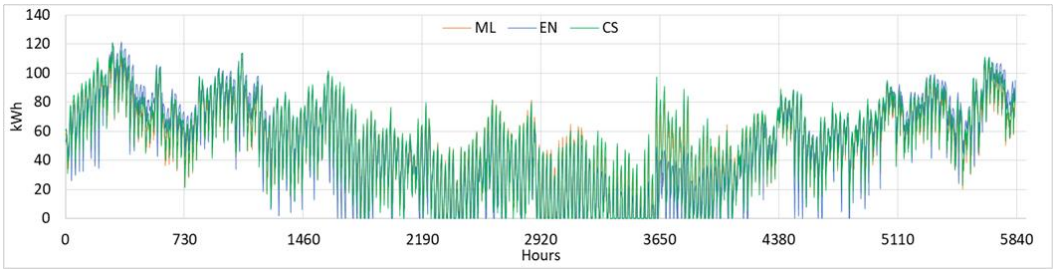

(a)

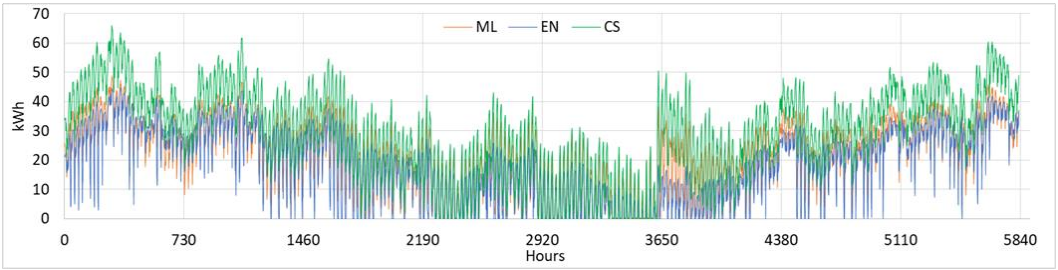

(b)

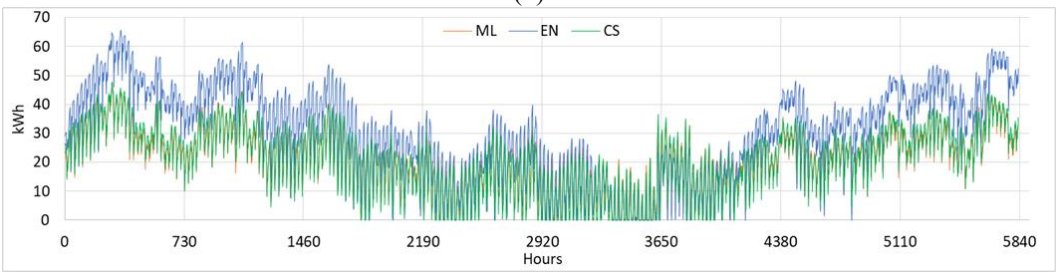

(c)

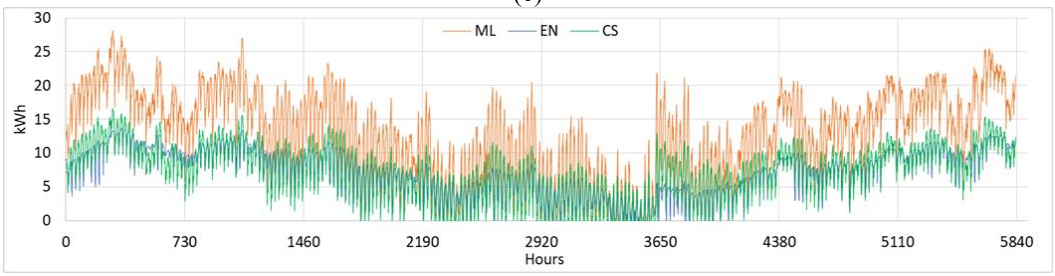

(d)

Figure 47. Building scale: Comparison of the hourly consumption profiles in 2017 from 1 January to 18 May and from 7 October to 31 December: (a) ID 4397 (period: 1971–80); (b) ID 761 (period: 1991–00); (c) ID 128 (period: 1946–60); (d) ID 2724 (period: 1981–90) [47].

Table 21. Meteorological data of 2017: Typical monthly days [47].

Typical Monthly Day	T_{ae}, °C	$T_{ae,av}$, °C	$I_{sol,avg}$, Wh/m^2/day	MAE$_{ML}$, Wh	MAE$_{EN}$, Wh
5 January	0.0	0.2	2168	7576	13,967
7 February	1.2	1.7	2973	7887	10,883
14 March	5.2	5.6	4899	5896	9827
4 April	9.2	9.3	5983	3897	8259
4 May	12.9	14.3	6655	2525	4233
16 October	10.4	10.2	3438	3292	9662
22 November	5.5	4.5	2427	6299	10,206
12 December	0.9	1.1	1570	8294	10,823

Considering the local climate condition of 2017, eight typical monthly days have been selected in order to describe the average trend as a function of the external air temperature (T_{ae}) and the horizontal global irradiance (I_{sol}). In

Table 21, the external air temperature (T_{ae}) refers to the selected day and the average values of $T_{ae,avg}$ and $I_{sol,avg}$ refer to the month.

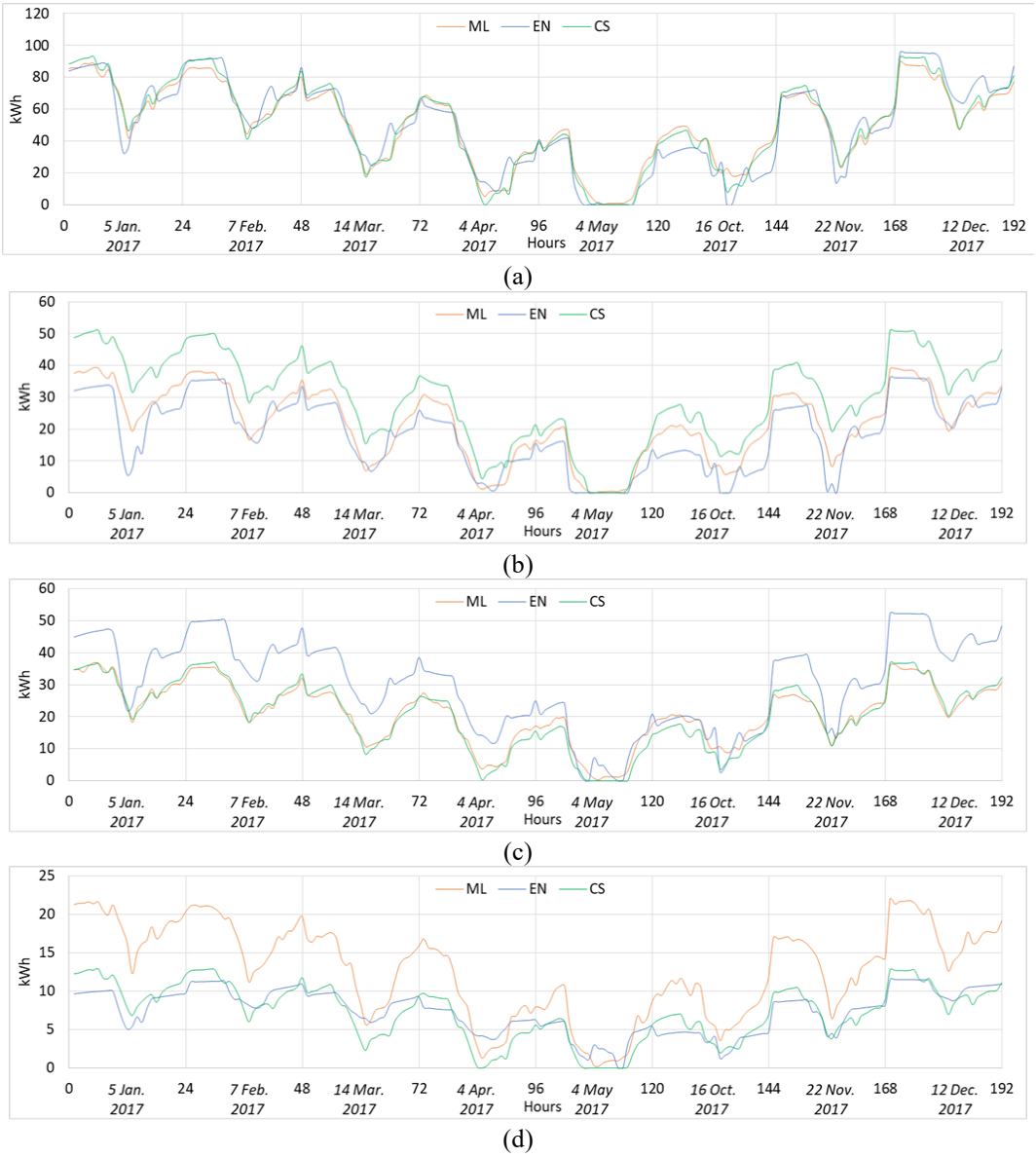

Figure 48. Building scale: Comparison of the hourly consumption profiles for the typical monthly days: (a) ID 4397 (period: 1971–80); (b) ID 761 (period: 1991–00); (c) ID 128 (period: 1946–60); (d) ID 2724 (period: 1981–90) [47].

From Figure 48, it can be observed that the hourly energy consumption profiles of the building have a typical trend. In the colder months, the heating system is always switched on, with high consumption between 11 p.m. and 6 a.m., when the solar and internal heat gains are minimal or nil. Consumption tended to decrease during the daytime, with the period of lowest consumption between midday and midnight.

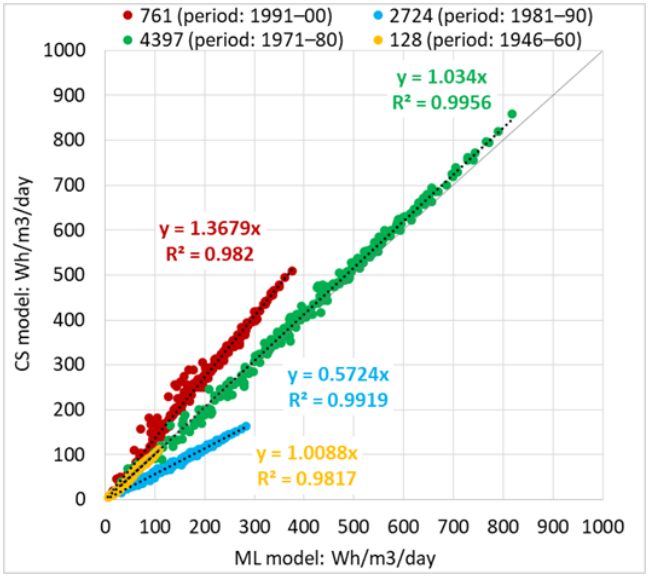

Figure 49. Building scale: Comparison of the daily consumption (kWh/m3/day) for the heating season: CS tool and ML model [47].

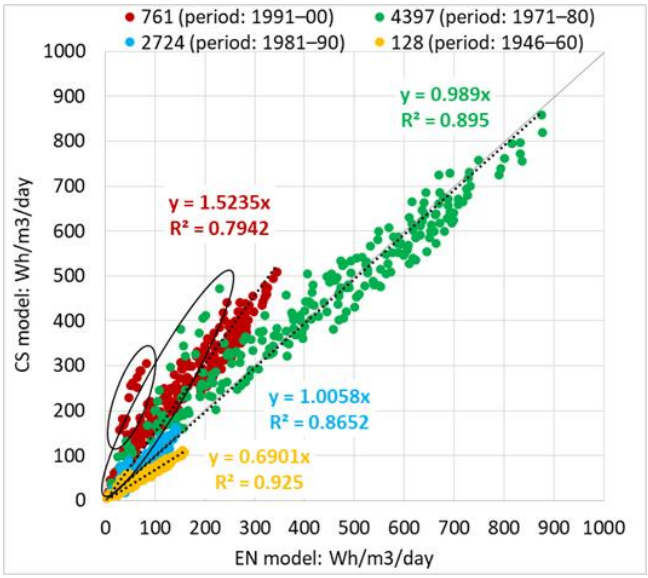

Figure 50. Building scale: Comparison of the daily consumption (kWh/m3/day) for the heating season: CS tool and EN model [47].

Figure 49 and Figure 50 show the comparison of daily consumption data (Wh/m^3/day) for the heating season between CS and ML simulations, and CS and EN simulations, distinguishing the four selected buildings. What is interesting about these graphs is that:

- Building ID 761 (built between 1991 and 2000) is problematic for both models, which tended to underestimate the real heating consumption during the whole heating season. With building ID 4397 (1971–80), on the other hand, both models showed a good accuracy and are able to approximate the behaviour of the building well.

- As had already emerged from the hourly profiles, with regards to building ID 2724 (built between 1981 and 1990), on which the ML model had a much higher error than the EN model, the heating consumption is overestimated. Similar results are obtained by the EN model, which overestimated the heating consumption of building ID 128 (built between 1946 and 1960), on which the ML model showed high precision instead.

In addition, it is possible to observe that for some days, which corresponded to non-working days, the simulation error of the EN model increased—probably, this is also a consequence of the internal gains used in the thermal balance. In the EN model, an hourly profile of internal gains is assumed according to the standards, taking into account the same intensity and profile for the whole week. This phenomenon did not occur in the ML model as it was trained on the data processed with CS, and therefore took this aspect into consideration.

Finally, Figure 51 and Figure 52 show some results at city level. The aggregated space heating consumption expressed in kWh/m^3/year according to the Fribourg zones and the construction periods have been indicated for each model.

As mentioned in the literature review, there are several factors that influence consumption (e.g., construction period, *S/V*, occupants and local climate). It is confirmed that (i) newer buildings have better energy performance than older ones (Figure 51) and (ii) urban morphology affects the energy intensity; in fact, Figure 52 shows an example on how the amount of built area influence the heating consumption (in kWh/m^3/y); in this case, the building coverage ratio (*BCR*) is used. This topic will be investigated more thoroughly in future works.

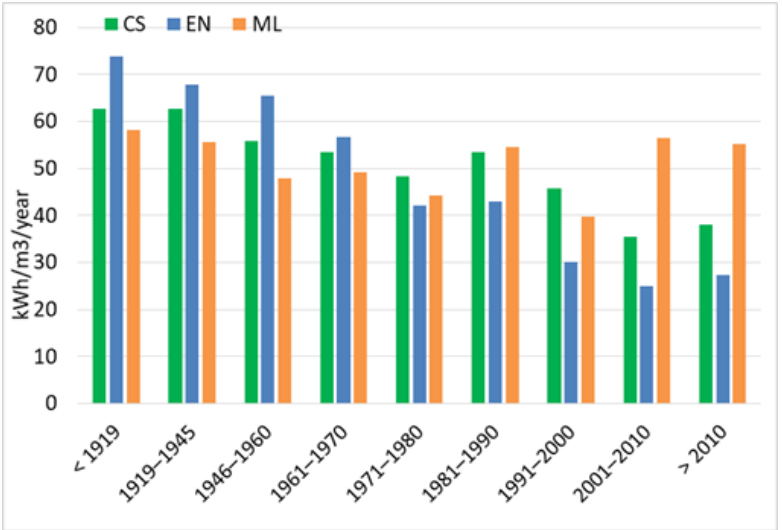

Figure 51. City scale: Comparison of the annual consumption (kWh/m3) for the heating season 2017 distinguishing: construction periods [47].

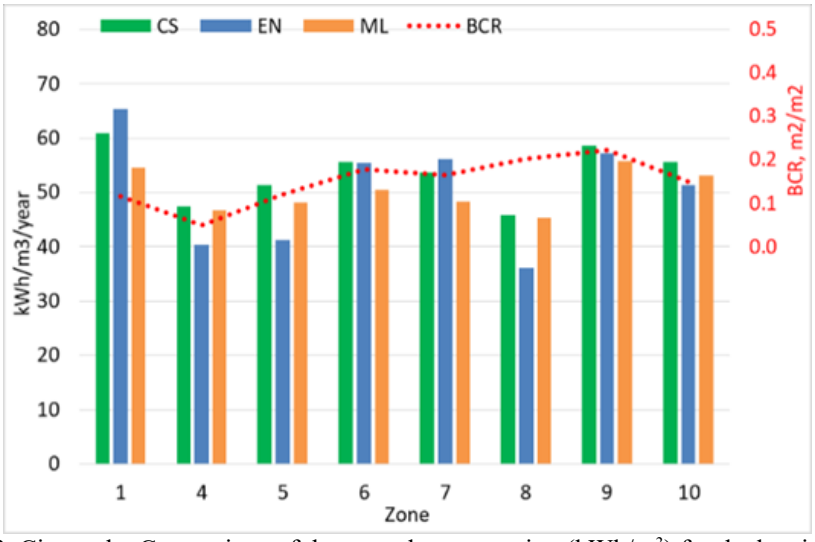

Figure 52. City scale: Comparison of the annual consumption (kWh/m^3) for the heating season 2017 distinguishing: eight zones [47].

In summary, these results show that the ML and EN models simulate hourly energy consumption on an urban scale quite accurately and with very short simulation times compared to other existing models and instruments. In particular, both these simplified models needed less than a second to simulate a single building on a mid-range consumer laptop, while a detailed CitySim simulation of the same building, modelled with nearby constructions, trees and terrain on the scene, took, on average, 10 min. The average time required to simulate an entire zone with the same level of detail in a single run grows to around two weeks with CitySim, while the simplified models are both capable of making an estimation in less than a minute. However, there are several aspects on which to intervene to improve the precision of these simplified models.

To sum up, ML and EN models were applied to 200 residential buildings in Fribourg, and energy simulation results were compared to the CS-calibrated heating consumption. Through the evaluation of the simulation errors, the study shows that these two models were quite precise with an annual mean absolute percentage error of 12.8 and 19.3% for the ML and the EN models, respectively, on buildings built in the period 1919–2000. Compared to the other models, they are less accurate, but more flexible and easily applicable to other contexts, since they use existing databases. The strong points are certainly the short simulation times and the flexibility of the models, which, since they use open input data, can be applied to other cities elsewhere in the world.

3.6 Hourly hybrid models

This section presents a first version of a hybrid model designed for some neighbourhoods in the Canton of Geneva in Switzerland. The hourly engineering model (presented in section 3.5) is optimized by adopting a data-driven correction

with a Random Forest algorithm [51]. The new model is used to study the impact of COVID-19 pandemic on the EP of the residential sector.

The unprecedented impact of the pandemic has caused the trend in energy consumption to change unexpectedly. It is essential to develop energy models to evaluate future energy trends. There are only a few studies that evaluate the impacts of the lockdown on energy heat demand. As measured energy data are often not available, energy simulation tools are used to assess the impacts of the pandemic on energy demand. Several contrasting results have been reported in the existing literature in the assessment on urban energy use; particularly in simulation-based studies. The results of the energy simulations depend on the input data set. From the literature it emerged that occupancy profiles have not been studied adequately, and this has provided contrasting results. The definition of occupancy scenarios is fundamental to take into account the resident's behaviour during the pandemic. This study introduces detailed scenarios taking into account different occupancy behaviour. As the GIS-based approach presented here is flexible, the input data can be easily updated according to the scenarios to be analyzed. In addition, the model presented allows to carry out energy assessments at urban scale, and simulation times are minimal compared to existing tools.

This investigation aims to address the aforementioned gaps by using measured and simulated data to analyze the energy trend during the COVID-19 pandemic period. More specifically, the aims of the study are as follows:

(i) Developing and verifying a bottom-up approach to explore the impacts of the COVID-19 pandemic on SH and SC demand of residential buildings using a "GIS-based engineering model".
(ii) Developing and analyzing detailed occupancy scenarios that describe the occupant's behaviour during the partial and full lockdown.
(iii) Developing a data-driven model to improve the accuracy of the GIS-based energy model using a machine learning approach.

3.6.1 Methodology

This analysis investigates the impacts of the COVID-19 pandemic on SH and SC energy performance of three residential neighbourhoods located in the Canton of Geneva in Switzerland. The proposed methodology consists of three main phases (Figure 53).

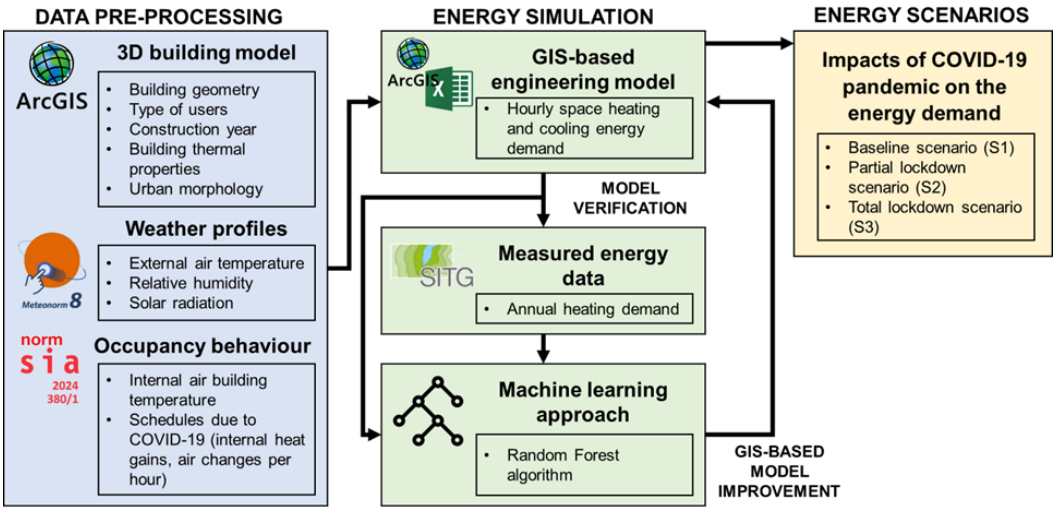

Figure 53. Flowchart of the GIS-based workflow [51].

In the first phase, the input data are processed. This methodology combines different types of data. Climate data, building data, occupancy profiles, and morphological parameters are processed and elaborated with the support of GIS tools. Energy demand in urban neighbourhoods is investigated by using a GIS-based engineering model [47,49,50]. In the energy simulation phase, the GIS-based model is verified comparing the simulated annual energy consumption with the measured data. A machine-learning algorithm is used to improve the accuracy of the model. In the third phase, the impact of the COVID-19 pandemic on the SH and SC demand is assessed by investigating three scenarios that consider the occupancy scenarios including pre-pandemic, partial and full lockdown.

Studied area

The proposed GIS-based approach is implemented in the Canton of Geneva. In this Canton, the climate is temperate with cold winters, warm summers, adequate precipitations, and a north-easterly wind (Köppen climate classification: Cfb [167]). Figure 72 shows the hourly weather data of Geneva collected from the Meteonorm 8.0.4 for the "contemporary" period from 2000 to 2019. Relative humidity (%) and external air temperature (°C) refer to a weather station in Geneva (46°25'N, 6°12'E). During the winter season, in January, the air temperature drops to -6.9 °C. In the summer season, there is the maximum temperature on 24th July at 4 pm with 34.8 °C. The coldest months are January and December, with monthly average air temperatures of 2.2 and 2.9 °C respectively. The hottest months are July with an average monthly air temperature of 20.8 °C and August with 20 °C.

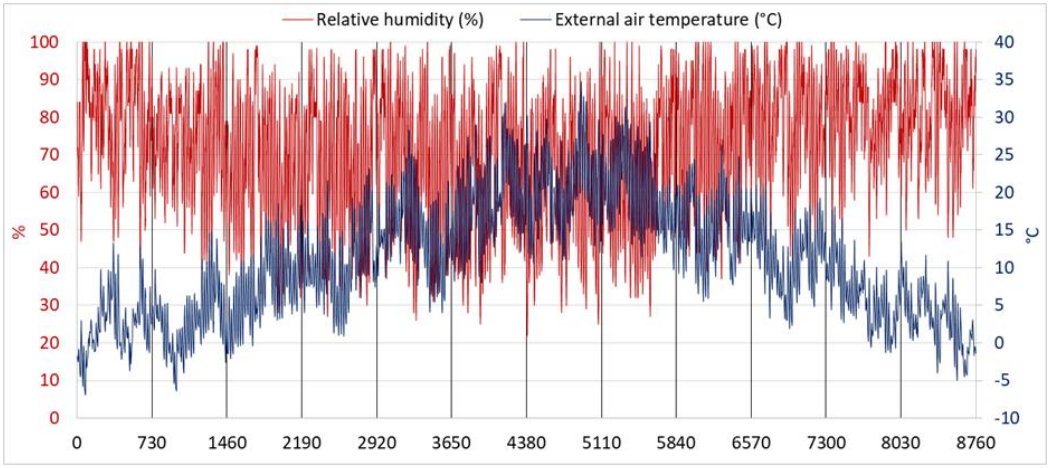

Figure 54. Hourly weather data of Geneva: relative humidity (in red) and external air temperature (in blue) [51].

Case studies

The urban morphology strongly affects the EP of buildings due to the relationship between the building and its surroundings (e.g., shading, heat exchanges between buildings) and to the type of outdoor surfaces [103,168,169]. It is possible to reduce the SH and SC energy demand of buildings by optimizing the urban morphology [170,171]. A GIS database is developed to explore the urban morphology of the three neighbourhoods in the Canton of Geneva by investigating the urban form and urban density. The 2D building characteristics and the DSM with a resolution of 0.5 meters x 0.5 meters were acquired from the Swisstopo (Federal Office of Topography) database. Several parameters, which refer to urban form and urban density, have been considered in the literature to describe urban morphology. In this study, six major parameters are considered to define the morphology of the neighbourhoods including (i) the building height (*BH*) as the average height of the buildings in the sample area, (ii) the relative height (H/H_{avg}) as an index to describe the solar exposition concerning the building heights [172], (iii) the building coverage ratio (*BCR*) as the total built area in the sample area divided by the sample area [123,173] (iv) the building density (*BD*, m^3/m^2) as the total building volume in the sample area divided by the sample area [173,174], (v) the height-to-width ratio (*H/W*) [102] which is ratio between the building height and the distance between buildings, as well as (vi) the sky view factor (*SVF*) which is used to measure the portion of sky visible from a given point [128]. The *SVF* is used in the GIS-based engineering model to count for the solar exposition of the urban morphology and to quantify the thermal radiation lost to the sky based on a 200 meters x 200 meters grid size.

A total number of 18 urban neighbourhoods in the Canton of Geneva are assessed using the aforementioned process; in which three neighbourhoods are selected based on the urban density (i.e., *BH* and *BD*) and the urban form (i.e., H/H_{avg}, *BCR*, *H/W,* and *SVF*). In this regard, for the urban density, a range of 10 to 25 m for *BH* is considered, which neighbourhood 1 is 10.8 m, neighbourhood 2 is

23.7 m and neighbourhood 3 is 15.6 m, and *BD* varies from 1.6 to 8.2 m^3/m^2. For the urban form, a range of 0.15 to 0.4 m^2/m^2 for *BCR* and a range of 0.25 to 0.8 m^2/m^2 for *H/W* are considered; *BCR* values are 0.16, 0.38 and 0.15 m^2/m^2 respectively for neighbourhood 1, 2 and 3 and *H/W* values are 0.25, 0.81 and 0.30 m^2/m^2. Finally, neighbourhoods in the Caton have similar values of H/H_{avg} and *SVF*, but they were still analyzed because are useful parameters to describe the urban form.

Another criterion used is the presence of residential buildings. Thus, considering the characteristics of the building stocks and the prevailing building sector (in this case, the residential one), three neighbourhoods have been selected. In these neighbourhoods 90% of the buildings are residential, and the energy data for annual heating consumption of most of these buildings are known. The energy simulation is carried out for residential buildings. Figure 55 shows the map of the Canton of Geneva with the location of three selected neighbourhoods (the location of neighbourhoods marked in red). Neighbourhood 1 (46° 24' N, 6° 20' E) and 2 (46° 21' N, 6° 15' E) are small urban areas in Vésenaz district and Pâquis district respectively. Neighbourhood 3 (46° 19' N, 6° 11' E) is a larger urban area in Lancy and Onex districts.

Figure 55. Map of the Canton of Geneva using the World Imagery from ESRI to show the location of three neighbourhoods as case studies [51].

Table 22 presents the value of the morphological parameters for each neighbourhood. The morphological parameters that have greater variability are *BH* and *BD*, which are used to describe the urban density, and the canyon effect evaluated as a function of the *H/W* ratio. Neighbourhoods 1 and 3 are less dense than neighbourhood 2 which is more built with higher values of *BH*, *BCR*, *BD,* and *H/W*.

Table 22. Characteristics of four selected buildings [51].

Neighbourhood		*BH* (m)	*H/H$_{avg}$* (m/m)	*BCR* (m^2/m^2)	*BD* (m^3/m^2)	*H/W* (m^2/m^2)	*SVF* (-)
1		10.79	1.32	0.16	1.61	0.25	0.82
	SD	*2.14*	*0.13*	*0.07*	*1.03*	*0.15*	*0.02*
2		23.69	1.28	0.38	8.15	0.81	0.74
	SD	*5.29*	*0.29*	*0.17*	*3.47*	*0.29*	*0.18*
3		15.60	1.51	0.15	2.02	0.30	0.81
	SD	*6.95*	*0.46*	*0.08*	*1.50*	*0.27*	*0.01*

Starting from over 3,200 buildings in the three neighbourhoods, around 1,800 buildings that have a heating/cooling system have been selected. Buildings are classified into seven categories: assembly (church, public, sports center, temple), business (service, government, offices, post office, police), commercial (commercial, retail), educational (kindergarten, school, university), industrial (manufacture, atelier), institutional (hospital), and residential (house, detached, retail house). In Figure 56 buildings are classified according to their function.

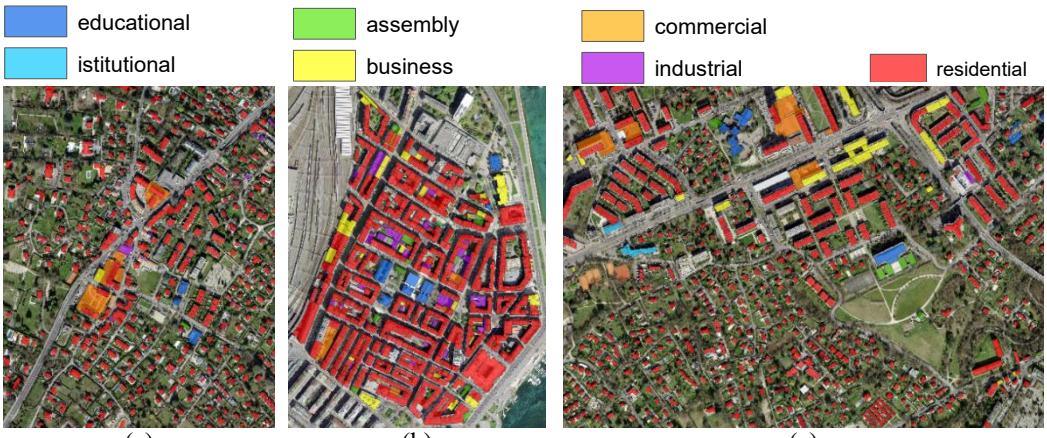

(a) (b) (c)

Figure 56. Building classification by type of users of three neighbourhoods in the Canton of Geneva: (a) neighbourhood 1, (b) neighbourhood 2, and (c) neighbourhood 3 [51].

Residential buildings are classified according to the construction year based on eight classes: before 1945 (class 1), between 1946 and 1960 (class 2), between 1961 and 1970 (class 3), between 1971 and 1980 (class 4), between 1981 and 1990 (class 5), between 1991 and 2000 (class 6), between 2001 and 2010 (class 7), and after 2010 (class 8). In Table 23 the residential buildings' characteristics of these three neighbourhoods are described (for further information [164]).

Neighbourhood 1 has over 420 heated buildings of which 95% are identified as residential users. Residential buildings have an average *S/V* ratio of 0.74 m^2/m^3 (i.e. detached house). Almost 40% of the buildings were built after 1991 and only 16% before 1945. From this database, 34 residential buildings have been selected, of which the measured energy consumption is known, to verify the accuracy of the GIS-based model. In neighbourhood 2 there are nearly 650 heated buildings of

which 84% are identified as residential users. Most of the residential buildings (42%) were built before 1945, 25% between 1946 and 1970, and there are only 4 buildings (1%) built after 2010. In this district, the measured energy consumption of 283 residential buildings is available for model validation. The third neighbourhood has over 750 heated buildings of which 92% are residential buildings with an average *S/V* of 0.71 m^2/m^3. The prevalent construction year is class 6 (21% of residential buildings were built between 1991 and 2000), 17% were built before 1945, and 7% after 2010 (47 buildings). Knowing the measured energy consumption of 134 residential buildings, these buildings have been selected to apply the model. To improve the reliability of the model, it is important to verify the simulated data by comparing it with the measured energy data. Thus, a total number of 451 buildings out of 1,640 buildings are selected based on the availability of data. For these buildings, the measured annual heating consumption and the construction year used to define the thermophysical properties of the building are known.

Table 23. Residential buildings' characteristics of the three neighbourhoods [51].

Neighbour.	Percentage of residential buildings	No. of residential buildings	Average height (m)	Average *S/V* (m^2/m^3)	Prevalent construction year
1	95	396	9.4	0.74	Class 7 (2001-2010)
2	84	542	22.1	0.36	Class 1 (before 1945)
3	92	702	11.5	0.71	Class 6 (1991-2000)

Figure 57 shows in green the residential buildings analyzed (of which the measured energy consumption is known) and in red the other residential buildings.

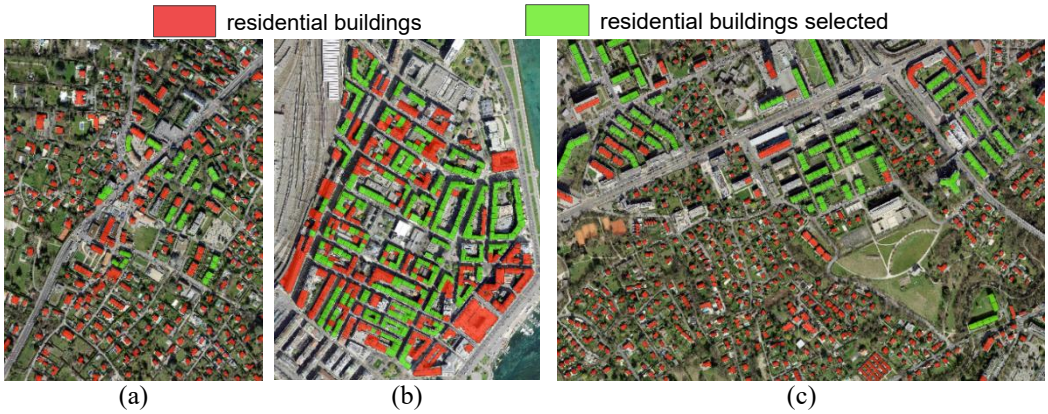

(a) (b) (c)

Figure 57. Identification of residential buildings selected (in green) and other residential buildings (in red): (a) neighbourhood 1, (b) neighbourhood 2 and (c) neighbourhood 3 [51].

3.6.2 Input data

Climate data

Hourly climate data are collected from Meteonorm 8.0.4 for the "contemporary" period from 2000 to 2019. Data recorded by the weather station and statistical interpolation of the nearby weather station (46°25'N, 6°12'E in Geneva) are elaborated for three different locations, one for each neighbourhood under analysis. Table 24 shows the main information of the three locations (cool temperate zone with sub-maritime climate). From the annual climate data, it is possible to observe that there are no significant differences between the three studied areas. The weather profiles used as input data for the GIS-based engineering model are as follows: the external air temperature (T_a in °C), the relative humidity (RH in %), the global horizontal radiation (G_h in W/m^2), the beam irradiance (B_n in W/m^2), and the diffuse horizontal irradiance (D_h in W/m^2). In this work, the wind effect on convective heat exchange was not considered.

Table 24. Measurements and annual climate data of three sites [51].

Neighbour.	Locations	Elevation	Measurements	T_a	RH	G_h	B_n	D_h
		(m)		(°C)	(%)	(kWh/m^2)		
1	46°24'N - 6°20'E	406	statistical interpolation	11.2	70	1291	1351	571
2	46°25'N - 6°12'E	420	weather station	11.2	70	1291	1309	591
3	46°19'N - 6°12'E	398	statistical interpolation	11.8	68	1292	1298	603

Comparing Heating Degree Days (HDD) and Cooling Degree Days (CDD) in the Canton of Geneva for 2019 (pre-pandemic period) for 2020 (pandemic period) no significant differences were found. The HDDs for 2019 and 2020 are 2755 and 2654 respectively, the CDDs are 298 in 2019 and 290 in 2020 (source: www.meteoswiss.admin.ch). Therefore, in this analysis, energy simulations are carried out using a typical weather year based on weather data from 2000 to 2019, taken from Meteonorm. No supplementary data related to the pandemic period are used.

Building data

The geometrical characteristics (e.g., building's footprint, number of floors, height, volume), the surface-to-volume (S/V, m^2/m^3) ratio that is a variable able to describe the compactness of the building, the construction year, and the user type (i.e., residential, school, office, industrial) of the buildings are identified and processed using different databases. These include the Swisstopo (Federal Office of Topography) database, the SITG (Système d'information du territoire à Genève) database, and Switzerland's OSM (Open Street Map) database. The first step is to identify the heated/cooled buildings. Garages and low-rise buildings lower than 3m in height and 50 m^2 total area are classified as unheated buildings (without an energy system). After identifying the buildings that have an energy system, only the

residential users are selected. Secondly, a comprehensive database is developed for residential buildings located in the neighbourhoods with the use of GIS tools. According to the construction year, the thermophysical properties of the buildings are defined using as reference a study performed for the city of Neuchâtel, Switzerland [164]. For each building thermal transmittances and thermal capacity of the windows and opaque elements, infiltration rate, total solar energy transmittance of glazing, and window-to-wall ratio (*WWR*, -) values are identified.

Occupancy scenarios

One of the aspects that affect energy consumption is the behaviour of people and their habits [118,175]. Three occupancy profiles are defined to evaluate the effect of the COVID-19 pandemic on the energy demand of residential users. Three aspects are considered: (i) the hours of operation of the energy system, (ii) the internal heat gains due to the presence and the activity of people in the buildings, (iii) the heat losses due to the windows opening. The following scenarios are defined: (i) baseline scenario (S1) simulates the energy demand considering people behaviour in a normal year, according to Swiss norm SIA 2024 [176] it is assumed that people stay at home 12 hours per day; (ii) partial lockdown scenario (S2) in which people stay at home 18 hours per day; (iii) full lockdown scenario (S3) in which people stay at home all day (24 hours per day). The heating/cooling system is always turned on to achieve a comfortable internal air temperature that is 22 °C in winter and 26 °C in summer. The heating system turns off when the internal air temperature achieves the comfortable temperature.

Figure 58, Figure 59, and Figure 60 show in blue the heating and cooling schedules for the three scenarios by distinguishing the weekdays and the weekend. In the graphs, the value 0 indicates that the internal air temperature of the building is set at 20 °C in winter and 28 °C in summer, while the value 1 indicates that the internal air temperature is set at 22 °C and 26 °C in winter and summer respectively. This means that the energy system is always in operation to keep the building temperature at 22 °C or 20 °C during the heating season and 26 °C or 28 °C during the summer season, as required by the Swiss norm SIA 2024 [176].

Internal gains depend on the number of occupants per building and the activity of the occupants. The number of occupants is calculated referring to the Swiss norm SIA 380-1 [177], which indicates that the surface area per person is 40 m^2/P for residential buildings with a *S/V* ratio equal to or less than 0.71 m^2/m^3 (typical of condominiums) or 60 m^2/P with *S/V* higher than 0.71 m^2/m^3 (typical of detached houses).

According to the type of activity, the metabolic flux is assumed as 72 W for a person who is sleeping, 108 W who is sitting, 126 W who is standing, 175 W who is cooking, 207 who is walking, and 210 who is cleaning [178]. The occupancy schedule for the baseline scenario (S1) is indicated in Figure 58 and, according to Swiss norm SIA 2024 [176], people stayed at home 12 hours. In Figure 59 and

Figure 60, it is assumed that people stayed at home 18 hours during a partial lockdown (S2) and 24 hours during the full lockdown (S3).

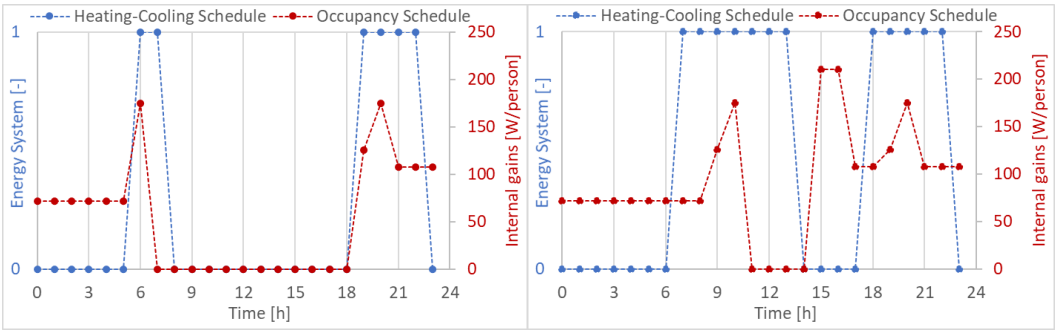

(a) (b)

Figure 58. Occupancy schedules of baseline scenario (S1): (a) weekday, (b) weekend [51].

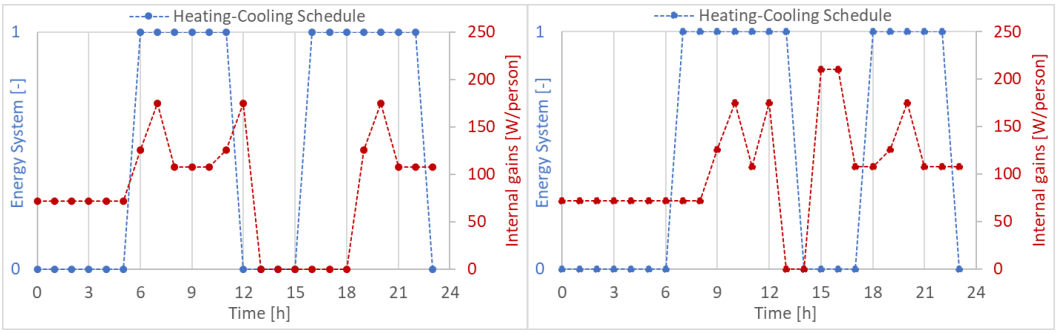

(a) (b)

Figure 59. Occupancy schedules of baseline scenario (S2): (a) weekday, (b) weekend [51].

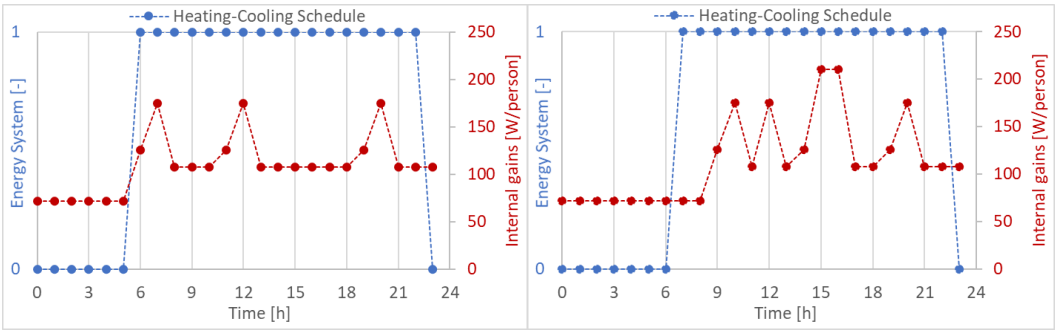

(a) (b)

Figure 60. Occupancy schedules of baseline scenario (S3): (a) weekday, (b) weekend [51].

Table 25. Air change rate (*ACH*, h^{-1}) per construction year by distinguishing three scenarios [164].

Scenario	Before 1945	1946-1960	1961-1970	1971-1980	1981-1990	1991-2000	After 2001
Baseline	0.7	0.6	0.55	0.5	0.4	0.35	0.3
Partial lockdown	0.8	0.7	0.65	0.6	0.5	0.45	0.4
Full lockdown	0.9	0.8	0.75	0.7	0.6	0.55	0.5

Heat losses are quantified according to the values of the air change rate (*ACH*, h^{-1}) for infiltration indicated in Table 25. Constant *ACH* values are assumed during the day (24 h), considering natural ventilation through infiltrations. To consider the occupancy behaviour regarding windows opening (people open windows more often staying longer at home [179]), the *ACH* values are increased in the S2 and S3 scenarios compared to the baseline scenario.

Measured energy data

The measured annual energy data for SH are used to verify the accuracy of the GIS-based engineering model. The measured energy data are obtained from the SITG (Système d'information du territoire à Genève) database. For each building the following information is acquired: the annual heat consumption for space heating and domestic hot water expressed in MJ/year and MJ/m^2/year, the share of energy used for DHW, the heated surface, the year of measurement (from 1999 to 2010) and the energy vector.

The model used in this analysis simulates the energy demand for SH under certain climatic conditions. From the measured data, only the share of energy for space heating is considered to verify the model. Residential buildings in the three neighbourhoods use natural gas as the energy vector to heat the buildings. Therefore, to calculate the energy demand, it is assumed a system efficiency of 0.85, typical of gas systems in accordance with the Swiss norm SIA 380-1 [177]. The heating degree days (HDD, °C) presented in Table 26 are used to normalize the measured energy data as for the simulations the typical weather data from Meteonorm 8.0.4 were used. In the last three columns, the HDD for the three neighbourhoods can be compared referring to the Meteonorm typical year. The relative difference between the HDD in the neighbourhoods is minimal.

Table 26. Heating Degree Days (HDD, °C) in the Canton of Geneva (source: www.meteoswiss.admin.ch) [51].

Year	**1999**	**2000**	**2001**	**2002**	**2003**	**2004**	**2005**	**2006**	**2007**	**2008**	**2009**	**2010**	**N. 1**	**N. 2**	**N. 3**
HDD	3018	2718	2812	2724	3005	2895	3163	2799	2728	2926	2781	3180	2790	2829	2718

3.6.3 Data-driven correction to the model

A machine learning approach is used to define a data-driven correction with a Random Forest (RF) algorithm in order to tune the GIS-based model results. A data-driven model is used to extract scale factors to improve the accuracy of the "GIS-based engineering model". Such scale factors are defined as the ratios between the real energy demand and the simulated one. Therefore, a RF algorithm [180] is trained (on the sample where real measurements are available) to make a data-driven prediction of the ratio between the real energy demand and the simulated one for buildings where measured values are not available. This correction is

motivated by the fact that building characteristics used to simulate the consumed energy are sometimes approximated in the GIS-based model, together with the fact that the model has its intrinsic accuracy. The model is trained using an initial set of 25 features extracted from climate databases, simulated energy data, building, and urban attributes.

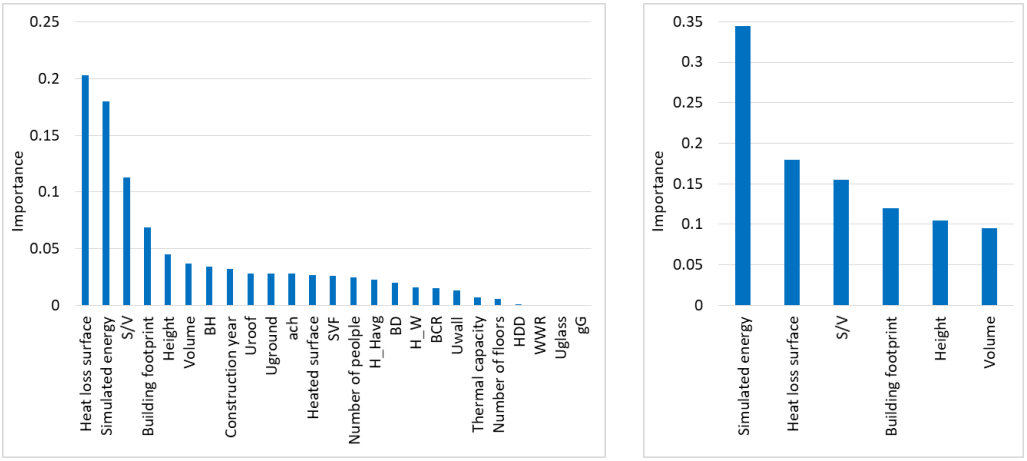

(a) (b)

Figure 61. Variables' importance: (a) all variables, (b) six variables [51].

Figure 61a depicts the relative importance of each input feature in relation to the task, extracted by an embedded function in the RF model implementation [181]. The most relevant variables are those that describe the geometric characteristics of the building (e.g. *S/V*, building footprint, heat loss surface) and the energy consumption simulated with the GIS-based model. Variables that describe the thermal properties of the building, morphological parameters, and occupancy behaviour (number of people and *ACH*) have a medium/low impact. HDDs are very similar in the three neighbourhoods and do not have a significant impact. Finally, features related to the properties of the transparent building envelope have no impact at all. Therefore, the geometrical variables have a significant impact in the prediction of scale factors. These results are due to the fact that the building database has some geometric errors (e.g., in some cases the geometries of the buildings overlap erroneously). This leads to errors in the calculation of the geometric variables of the building.

In a second step, the model is thus trained using only the six most relevant variables that are the *S/V* ratio, the heat loss surface, the simulated annual heating demand, the buildings' footprint, the height, and the volume. These are the variables that have the greatest impact in predicting the targets (i.e. the scale factor for each building). Figure 61b shows the importance of these six inputs in the performance of the model.

The dataset composed of 451 buildings is randomly divided into training and test subsets by a ratio of 75/25. The model hyperparameters are tuned using K-fold cross-validation to improve the precision of the predictions. The final RF model is

validated using the training called Out-Of-Bag (OOB) [182], and it has a mean absolute error of 15.3%, a mean squared error of 5.2%, and a root mean squared error of 22.8%. Table 27 shows the hyperparameters of the RF model.

Table 27. Hyperparameters of the RF model [51].

Hyperparameter	Description	Value	Tested range
Number of estimators	Number of trees in the forest	400	200-2000
Min samples split	Min number of data points placed in a node before the node is split	3	02-giu
Min samples leaf	Min number of data points allowed in a leaf node	4	01-apr
Max features	Max number of features considered for splitting a node	sqrt	auto, sqrt
Max depth	Max number of levels in each decision tree	85	10-160
Bootstrap	Method for sampling data points	True	True/False

In Figure 62, an example of the decision tree is indicated. The depth of trees in the forest is limited to three levels to show an understandable scheme. In the root node, the variable (i.e., simulated energy) and the value to split the node on is indicated, “mse” is the mean square error, “samples” is the number of data points in this node, and “value” is the prediction (in our case, the scale factor) for all data points in this node.

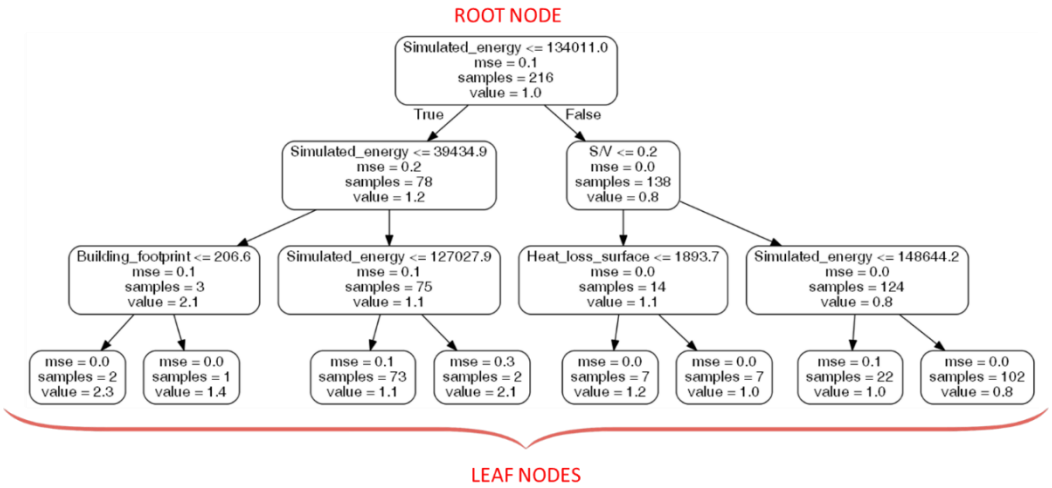

Figure 62. Decision tree: maximum depth of three levels [51].

3.6.4 Model results and validation

This section shows the main findings. The purpose of the first part of this investigation is to verify the accuracy of the model used to simulate the energy demand of residential users and to improve its precision with the integration of a machine learning model. In the second part of the results, the impacts of the COVID-19 pandemic on the energy demand are described by distinguishing three scenarios.

Model validation and improvement

The "GIS-based engineering model" is designed to simulate the energy demand of a group of buildings at the urban scale. In this work, it is applied at building scale and the energy demand is thus simulated for each building not for a group of buildings or a cluster, but with some urban variables at urban scale (not available at building scale). The energy consumption for heating and cooling of 451 residential buildings is simulated. Since the measured consumption has an annual temporal resolution, the verification is carried out using annual data. According to the baseline scenario (pre-pandemic conditions), the results of the annual heating demand are compared to the measured energy data.Despite uncertainties from input data, the developed model shows a reliable energy demand estimation. Comparison of simulated and measured energy data shows that the GIS-based model has an average mean absolute percentage error (MAPE) of 26% (the median MAPE is 20%). The MAPE varies in the three neighbourhoods. Neighbourhoods 1 (34 buildings) and 2 (283 buildings) have an average MAPE of 29%, while neighbourhood 3 (134 buildings) has a lower average MAPE equal to 18%. The results of neighbourhood 3 are more accurate, even if the model slightly overestimates the energy uses. To calculate the energy demand from measured energy consumption, it is assumed a system efficiency of 0.85 for all buildings. It is possible to define different system efficiencies depending on the construction year of the buildings, and the average MAPE could be reduced on average of 6% (in neighbourhood 1 the MAPE remains equal to 29%, in neighbourhoods 2 and 3 can be reduced on average of 9% and 1% respectively). Figure 63 shows the comparison of energy data expressed in kWh/year and the frequency distribution of the MAPE in the three neighbourhoods. In neighbourhoods 1 and 2, 61-62% of the simulated data has a MAPE lower than 30%. More accurate results are obtained in neighbourhood 3, where 85% of simulated data have a MAPE lower than 30%, and 61% of data have a MAPE lower than 20%.

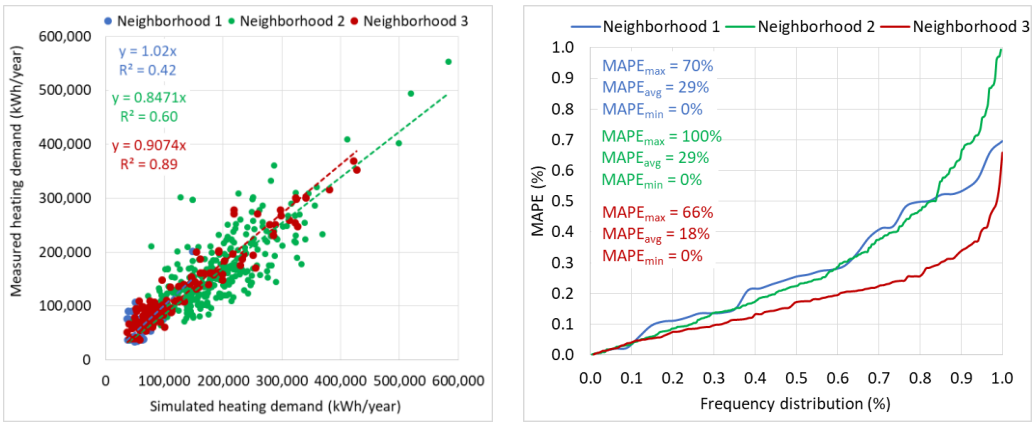

(a) (b)

Figure 63. Results of energy simulation in the three neighbourhoods: (a) comparison between measured and simulated heating demand and (b) frequency distribution of MAPE [51].

With the use of GIS tools, the MAPE is mapped at the building level in the three neighbourhoods (Figure 64).

(a) (b) (c)

Figure 64. MAPE at building level: (a) neighbourhood 1, (b) neighbourhood 2, and (c) neighbourhood 3 [51].

The scale factor, calculated as the ratio between the measured energy demand and the simulated one, is used to improve the energy simulations. This factor is calculated in two ways:

- Using a constant scale factor which is the average value calculated over the data of the 451 buildings.
- Using an ad-hoc scale factor for each building, calculated from the RF model.

Figure 65 shows the results of 113 residential buildings located in the tree neighbourhoods identified as the test set. This group of buildings has not been used for the training of the RF model. It is possible to observe that with the use of the constant correction factor the average MAPE decreases from 26% to 23%. Better results are obtained with the application of the RF model, with an average MAPE of 16%.

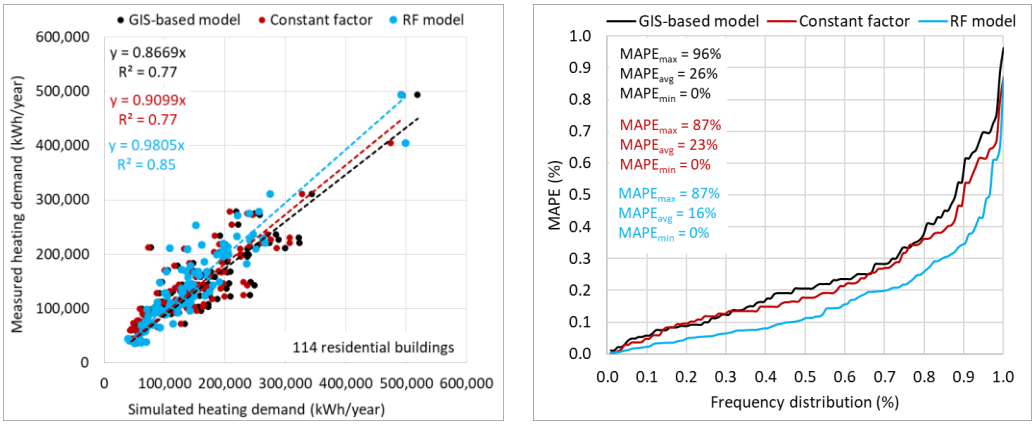

(a) (b)

Figure 65. GIS-based model, constant correction factor and RF model: (a) comparison between measured and simulated heating demand and (b) frequency distribution of MAPE [51].

The GIS-based model tends to overestimate the energy data for buildings that have a heating demand higher than 150,000 kWh/year, mainly because energy

retrofit interventions are not considered. This trend is less marked using the constant correction factor. The bias is well-corrected by the RF model.

Figure 66 shows an example of the hourly profile for heating and cooling demand for one year. These results refer to a building with a MAPE close to 0%. This building is a terrace house in neighbourhood 3. It was built between 1961 and 1970, therefore, has moderate thermal insulation. The annual heating demand is 142 kWh/m^2/y (the heating season is from 7 October to 18 May), and the annual cooling demand is 8 kWh/m^2/y (the cooling season is from 19 May to 6 October). The maximum daily demand for heating occurs in January, with an energy demand of 1,383 kWh/day and an average outdoor air temperature of -1.4 °C. During the summer season, a maximum daily cooling demand of 354 kWh/day is reached with an outdoor air temperature of 28.3 °C (on 30th June).

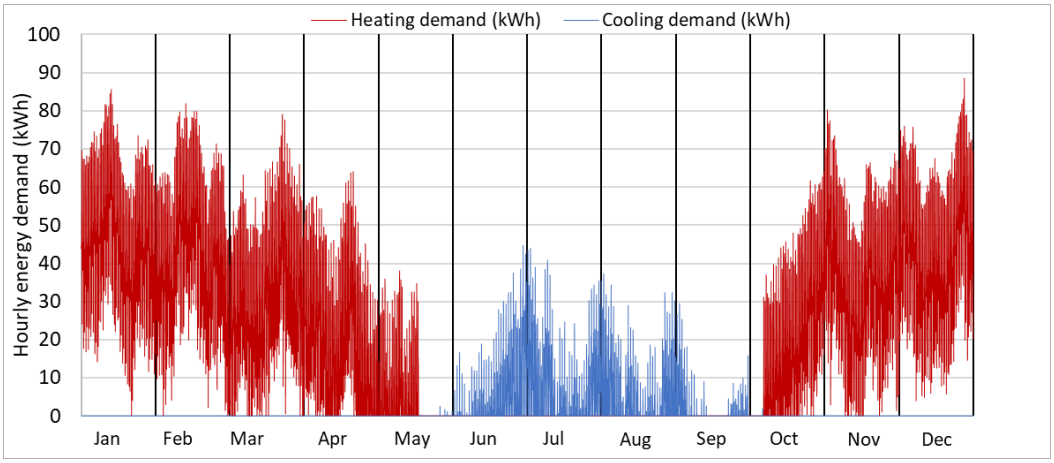

Figure 66. Hourly profiles for heating (in red) and cooling (in blue) energy demand of a terrace house built between 1961 and 1970 [51].

Impacts of COVID-19 pandemic on the energy demand

During the S1 scenario, the annual energy demand in the three neighbourhoods is 76,024 MWh/y and 5,681 MWh/y for space heating and cooling respectively. In partial lockdown conditions (S2) the energy demand increases, reaching 81,948 MWh/y (+8%) for heating and 6,625 MWh/y (+17%) for cooling. The energy demand during the full lockdown (S3) increases by 13% for heating and by 28% for cooling, compared to S1. During S3 the annual heating demand is 85,753 MWh/y (+9,729 MWh/y respect to S1 and +3,805 MWh/y respect to S2) and the annual cooling demand is 7,286 MWh/y (+1,606 MWh/y respect to S1 and +661 MWh/y respect to S2). Table 28 shows the results for each scenario. What stands out in the table is that the energy demand for cooling increases more than for heating. The internal gains due to the presence of people during the heating season partially compensate for other factors that increase heat use. During the summer, internal gains have an opposite effect with higher: human presence, use of electrical appliances, and cooling demand. In neighbourhood 1 the increase in cooling demand during restriction measures is less marked than in the other two neighbourhoods. This could depend on the construction year of the buildings, in

this zone most of the buildings were built after the year 2000 with a lower thermal capacity of envelope and building.

Table 28. Annual energy demand in the three neighbourhoods for different scenarios [51].

Neighbour.	S1 - Annual demand (MWh/y)		S2 - Annual demand (MWh/y)		S3 - Annual demand (MWh/y)	
	Heating	Cooling	Heating	Cooling	Heating	Cooling
1	2,184	511	2,406 (+10%)	550 (+7%)	2,527 (+16%)	603 (+18%)
2	54,684	3,164	58,784 (+7%)	3,773 (+19%)	61,453 (+12%)	4,202 (+33%)
3	19,156	2,005	20,758 (+8%)	2,302 (+15%)	21,773 (+14%)	2,481 (+24%)
Total	76,024	5,681	81,948 (+8%)	6,625 (+17%)	85,753 (+13%)	7,286 (+28%)

*In brackets the percentage increase in energy demand with respect to the S1 scenario is indicated.

In Figure 67 the annual heating and cooling demand expressed in kWh/m^2/y of 543 residential buildings are indicated by distinguishing for the three scenarios. What emerged from Table 28 is confirmed. Energy use in buildings increases during partial and full lockdown conditions. In addition, it can be observed that older buildings consume more in winter and less in summer compared to buildings built in recent years.

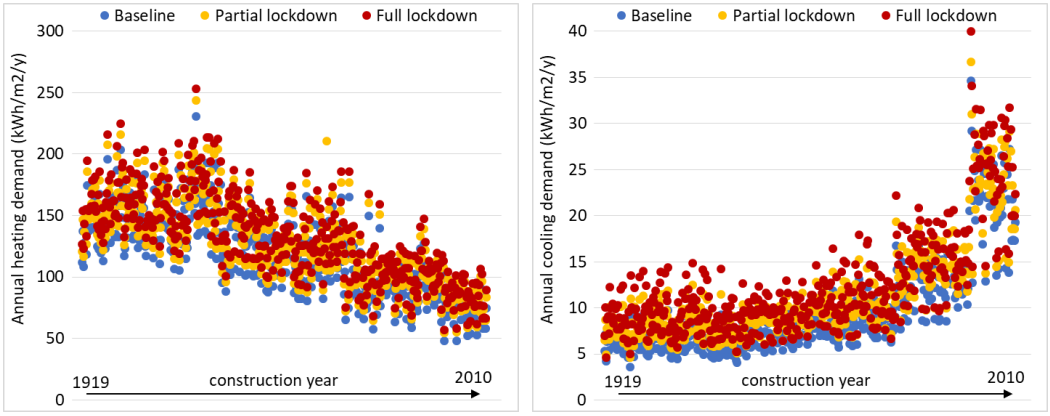

(a) (b)

Figure 67. Annual (a) heating and (b) cooling demand (kWh/m2/y) of 543 residential buildings for the three scenarios [51].

The specific heat demand for buildings built before 1945 increases by 9.7 kWh/m^2/y (+7%) during S2 and by 16.9 kWh/m^2/y (+12%) during S3 (compared to S1). For new buildings (built after 2000) the increase is relatively greater than old ones (older buildings consume more and the increase is less noticeable). The heat demand increases by 8.1 kWh/m^2/y (+11%) and 12.2 kWh/m^2/y (+17%) during S2 and S3 respectively.

In the cooling season, energy demand is higher for new buildings (due to the thermal properties of the materials, which allow good thermal insulation with low inertia, but restrictive measures have a greater impact on old buildings. For buildings built before 1945, the specific cooling demand goes from 6.6 kWh/m^2/y (S1) to 8.1 kWh/m^2/y during a partial lockdown, up to 9.4 kWh/m^2/y (S3) which is

42% more than the initial consumption. In buildings built after 2000, consumption ranges from 21.7 kWh/m^2/y (S1) to 23.1 kWh/m^2/y (S2) up to 25.1 kWh/m^2/y during a full lockdown. In this case, the cooling demand increases by 6% in S2 and by 16% in S3. These results indicate that thermophysical properties of the building have a significant impact not only on the energy performance but also on how much the COVID-19 pandemic affects final consumption. In addition, the impact of the pandemic on heating/cooling demand is not as marked as we might expect from electricity consumption.

Figure 68 shows an example of two buildings in neighbourhood 3 built in the same period (between 1961 and 1970) with different shapes. One is a terrace house that has an *S/V* of 0.34 m^2/m^3 (4 floors), and the other one is a row house that has an *S/V* of 0.25 m^2/m^3 (10 floors). The annual energy demand is indicated for each scenario. The energy demand for cooling is significantly lower than that for heating. The compact building with lower *S/V* (row house) has lower consumption, and the impact of the COVID-19 pandemic is greater in the terrace house. During the partial lockdown, the demand increased by 7-8% for heating and 18-23% for cooling. From partial to full lockdown there is always an increase but less marked, 4-5% for heating and 5-9% for cooling.

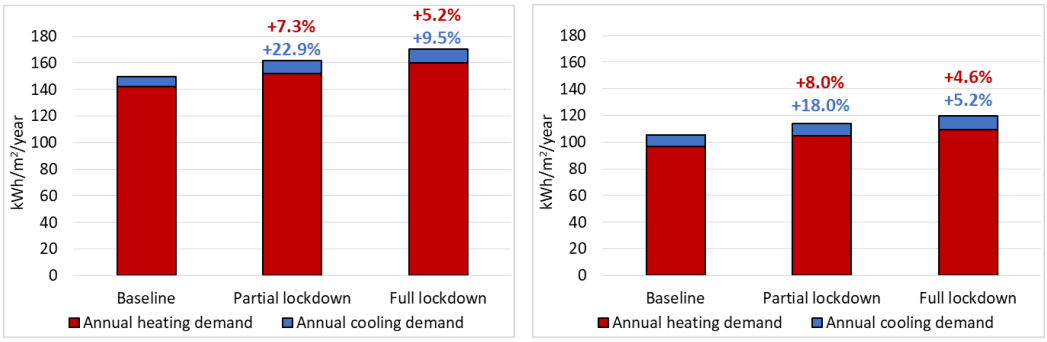

(a) (b)

Figure 68. Annual heating and cooling demand (kWh/m2/y) of two residential buildings built in 1961-1970 for the three scenarios: (a) terrace house and (b) row house [51].

In Figure 69 the hourly profiles for heating and cooling of the three scenarios during the coldest/hottest week are indicated. These results refer to the same building described in Figure 66 and Figure 68a.

As shown in Figure 69, before the lockdown and during a partial lockdown, there are two peak demands during the 24 hours, due to indoor air temperature settings. In the full lockdown conditions (S3) the internal air temperature of the building is constant during the day, it is set at 22 °C in winter and 26 °C in summer.

The energy intensity for heating is quite similar for the three scenarios. On weekdays, the daily demand for the three scenarios is 1,121 kWh/day (S1), 1,207 kWh/day (S2), and 1,273 kWh/day (S3), while on the weekend is 1,172 kWh/day (S1), 1,217 kWh/day (S2) and 1,290 kWh/day (S3). The heat demand for the entire week increases by 6% in partial lockdown conditions and by 12% with full lockdown compared to S1.

During the hottest week, the differences are more pronounced. The weekday consumption without lockdown measures is 156 kWh/day, during the weekend is

237 kWh/day. Cooling demand becomes 207 kWh/day (+33%) and 243 kWh/day (+2%) in the partial lockdown. With more restrictive measures, energy use reaches 245 kWh/day and 271 kWh/day (S3). Considering the energy use of the week, the cooling demand for the three scenarios are 1,326 kWh/week (S1), 1,588 kWh/week (S2), and 1,838 kWh/week (S3). Differences in the energy demand mainly depend on the occupancy behaviour and the external outdoor conditions.

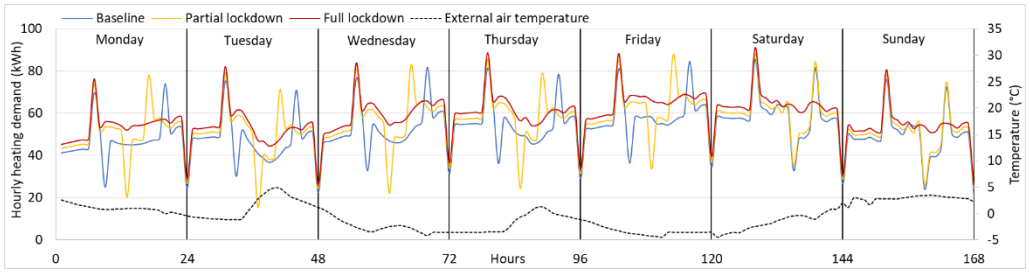

(a)

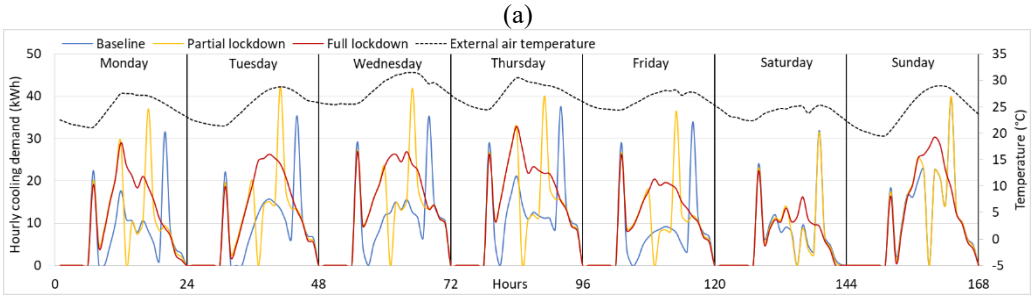

(b)

Figure 69. Hourly heating and cooling demand (kWh) of a terrace house built between 1961 and 1970 for the three scenarios: (a) coldest week and (b) hottest week [51].

Figure 70 shows the annual space heating demand expressed in kWh/m^2/y at the building level for the 3 scenarios. The results refer to a block of buildings located in neighb. 3, in which the GIS-based model is accurate with an average MAPE of 18%. In this block of buildings, the average heating demand of these 42 residential buildings is 99 kWh/m^2/y during S1, 108 kWh/m^2/y during S2, and 114 kWh/m^2/y during S3. So, there is an increase of 15 kWh/m^2/y from S1 to S3.

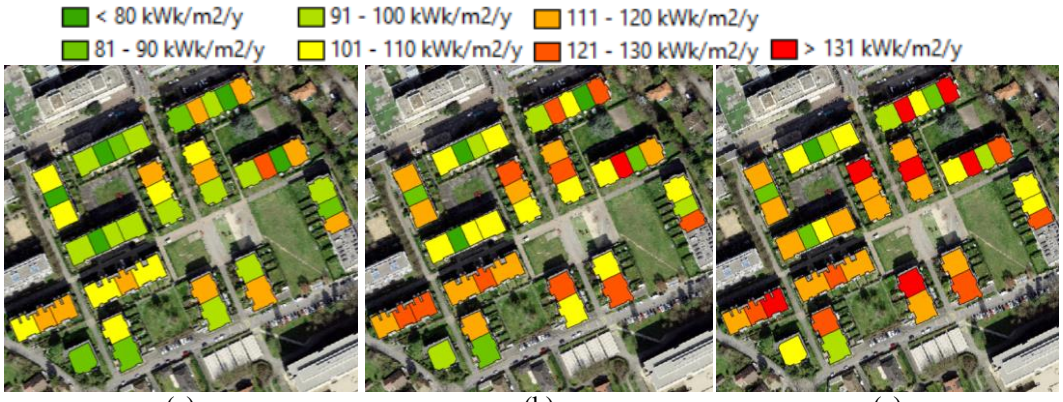

(a) (b) (c)

Figure 70. Annual space heating demand of a block of buildings in neighbourhood 3: (a) baseline; (b) partial lockdown; (c) full lockdown [51].

Together these results provide important insights into the investigation of the effect of the COVID-19 pandemic on the energy performance of residential buildings. The pandemic has caused an increase in energy demand for heating and cooling. In the three neighbourhoods analyzed, the energy use increased by 13% and 28% during the full lockdown for heating and cooling respectively. At the same time, findings on changes in the peak demand can be used in managing the energy network. To optimize the energy use of the entire system is fundamental to carry out these analyzes on a neighbourhood scale and not on a building level.

In summary, starting from 1640 residential building in Geneva, 451 were selected on the basis of the available data (measured annual heating consumption and the construction year). The GIS-based engineering model was used to simulate the energy demand. A machine learning-based method (on a subset of 451 buildings, split 75/25 as training/test sets) was used to define a data-driven correction with a random forest (RF) algorithm to tune the GIS-based model results. Through the application of the data-driven error correction it was possible to improve the precision of the energy simulations during the pre-pandemic conditions. The GIS-based model was used to investigate the impact of the COVID-19 pandemic on the energy performance of the residential neighborhoods by analyzing two scenarios (scenarios were elaborated with probable *ACH* rates based on standards, without occupant behavioral studies).

Chapter 4

Place-based energy production and productivity models

4.1 Chapter overview

The combined use of energy models, which assess energy consumption, production, and productivity from RESs, allows the demand and supply of energy for low-carbon resilient cities to be optimized.

With place-based energy production and productivity models it is possible to evaluate the potential from RESs available in the territory. Energy supply and demand can be optimized at urban scale by comparing energy productivity with energy consumption of different users. To promote a sustainable development of cities and urban areas, it is necessary to increase self-consumption and self-sufficiency through the use of RESs, such as solar energy. The Italian legislation has introduced incentives aimed at encouraging collective self-consumption and the institution of energy communities including storage systems. USEMs can be used to evaluate the feasibility of establishing energy communities, grouping producers, users and prosumers.

In this chapter (Figure 71), a monthly model to exploit the solar technologies are assessed considering the potential roofs' area with better solar exposition [52]. Subsequently, an hourly model that critically examines the energy benefits of using different orientations for PV technologies and investigates the economic costs is presented [53]. In the last part of this chapter, a methodology to promote self-consumption and self-sufficiency using the integration of solar energy with PV-battery systems that considering the new Italian economic incentives was developed [54].

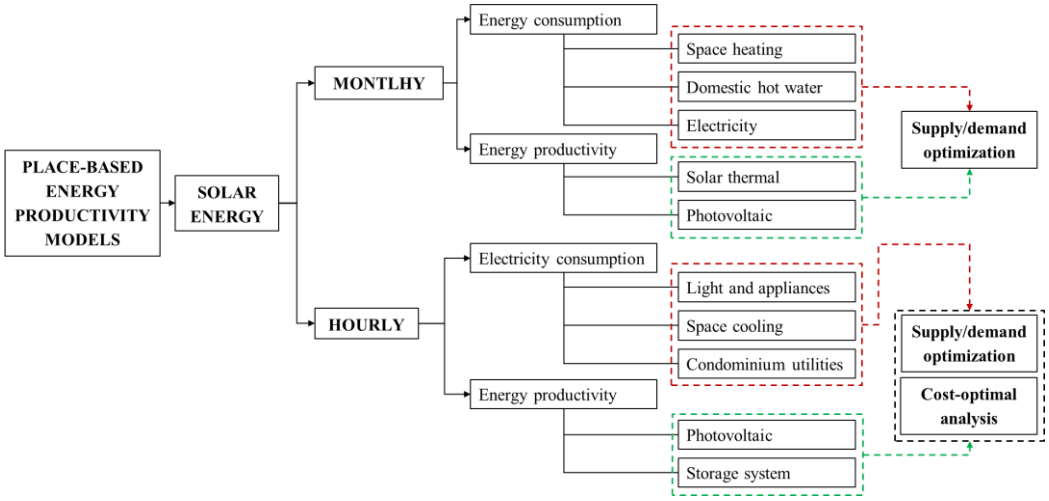

Figure 71. Flowchart of Chapter 4

4.2 Solar energy and energy communities in cities

In Europe, 70% of citizens live in urban areas and consume around 75% of the primary energy supply. The energy transition toward more sustainable and resilient energy management has become one of the principal challenges of cities today [183–185]. The goal is to plan sustainable and resilient territories, through the use of RESs that play an important role in the reduction of GHG emissions and in the promotion of energy self-sufficiency [186]. One of the main solutions is the large-scale urban generation of renewable energy [187]. Solar, biomass and wind are the most commonly available RESs that can be used in cities to promote self-consumption [188]. However, not all the sources available in urban environment are usable, due to the limited availability, or other technical or non-technical limits and constraints. In order to promote renewable energy technologies in buildings it is necessary to consider architectural, cultural, energy, technical and economic feasibility. In these cases, a strategy that facilitates the self-sufficiency is the integration of battery storage systems in connection with RES technologies which supply energy in a discontinuous way according to climatic conditions [189]. The use of a battery storage system is fundamental in the achievement of energy security at urban level where an energy mix of RESs is not available [190].

In densely built cities, the only renewable energy source that can be exploited is often solar energy [186]. North-facing roof areas are usually excluded from roof integrated solar technologies in the analysis of the technical potential [191]. Moreover, the various criteria used to evaluate the suitability of roofs can lead to significantly different results [192]. GIS tools are commonly used to evaluate the solar potential, and they are able to investigate the potential from the building scale to the city scale [193–197].

One of the limits to the promotion of solar technologies is related to the investment costs [198,199]. With the introduction of the concept of energy community (EC), it is possible to promote the use of solar technologies as a

collective self-consumption means as it reduces the investment and energy costs [200].

ECs have been introduced by two European directives: the re-cast Renewable Energy Directive n.2001/2018 (RED II) and the Internal Electricity Market Directive n.944/2019 (IEM) as part of the European Clean Energy Package. The aim is to provide the design of two new legal entities able to promote the collective self-consumption of renewable energy with the possibility of energy sharing: the "Renewable Energy Communities" (RECs) and the "Citizens Energy Communities" (CECs) [201].

In Italy, in agreement with the Clean Energy Package, the National Energy and Climate Plan (ENCP) was introduced in 2019. The five pillars are: decarbonization, energy efficiency, energy security, internal energy markets and research, innovation and competitiveness. In line with these pillars and the two EU Directives above, the National Law 8/2020 promotes some measures regarding the environment, security and energy. Especially, the article 42bis introduces two configurations for sharing renewable electricity among citizens and final users. The first one is the collective self-consumer that produces renewable electricity for its own consumption and can store or sell the surplus amount to the grid. The collective self-consumer comprises of at least two single users and one renewable plant connected to them that are located in the same building or condominium, who act collectively. The second configuration is the REC which extends the previous concept to multi-building users. Both mechanisms have the objective of increasing the efficiency in the low-carbon energy production with a hourly and seasonal matching between on-site supply and demand (i.e. high energy independence, self-sufficiency and self-consumption) so as to reduce the economic and environmental costs of energy and also combat energy poverty [202–204].

In order to establish a collective self-consumption scheme or a REC it is necessary that: (i) the *production plants*, from renewable sources, entered into operation after March 1st 2020 and the capacity of each plant should not exceed 200 kW; (ii) the production plants and the withdrawal points must be connected to the low voltage distribution grid, through the *same transformer substation*; (iii) the participants in a collective self-consumption scheme must be in the *same building or condominium*; (iv) the exchange of energy produced must take place through the *existing distribution network*; (v) *general charges* must be applied to energy withdrawn from the grid and to the shared energy.

In Italy, the Piedmont Region was the first region to promote the institution of ECs with the Regional Law 12/2018. In order to establish the ECs in the Piedmont territory, the minimum requirements that must be met by an EC have been identified in the Regional Decree n.18-8520/2019: (i) the *electrical contiguity*, the members of the EC must belong to territorially contiguous electrical "areas" (i.e. same MV/LV transformer substation); (ii) the *amount of electricity consumption*, annual electricity consumption must be at least 0.5 GWh; (iii) the annual *self-consumption* must be greater than or equal to 70%, of which at least 50% must be generated from

locally available renewable energy sources (RESs); (iv) the *plurality of actors*, there must be a plurality of energy producers and consumers.

Self-consumption is convenient for consumers if the cost of locally produced renewables is lower than retail electricity prices [205]. Economic incentives have been introduced for the promotion of energy communities and have also been extended to the installation of such technologies as storage systems [206]. The Italian legislation has introduced incentives aimed at encouraging the collective self-consumption and the institution of ECs including storage systems. The National Decree of 15th September 2020 introduces: (i) the incentives for self-consumption energy for electricity equal to 0.10 €/kWh for collective self-consumers and 0.11 €/kWh for RECs (the incentive is paid for a period of 20 years); (ii) the compensation for unused charges for the transport and distribution of energy withdrawn from the low voltage network: 0.01 €/kWh for collective self-consumers and 0.008 €/kWh for RECs.

Benefits are obtained from the establishment of energy communities, not only due to the smaller amount of energy that is taken from the grid, but also to the amount of energy that can be produced and consumed simultaneously at the local level. Through the configuration of a collective self-consumer, these incentives can promote the use of solar technologies in cities.

In order to reduce the impact of energy consumption and improve the competitiveness of local energy systems, energy communities may help to address the challenges of urban sustainability and energy security through local energy production and self-consumption.

4.2.1 Energy production models

To analyse the data of energy produced by RESs it is possible to consult portals, usually available in cities. For buildings in Italy there is the "Atlaimpianti" portal (https://atla.gse.it/atlaimpianti/project/Atlaimpianti_Internet.html). From the portal, it has emerged that 38% of the electrical consumption of residential buildings in the city of Turin is covered by a waste-to-energy plant, biogas plants, photovoltaic modules, and hydro plants. In Italy there are also regional and city-scale portals. For example, the solar portal of the Metropolitan City of Turin could be utilized for all the buildings to evaluate the productivity of roof-integrated solar technologies (i.e., photovoltaic modules and solar thermal collectors) (http://energia.sistemapiemonte.it/ittb-torino).

4.2.2 Energy productivity models

This section shows the methodology used to assess the energy productivity from solar technologies, photovoltaic modules (PV) and solar thermal (ST) collectors, at an urban level using GIS tools and the PVGIS portal (https://re.jrc.ec.europa.eu/pvg_tools/en/#PVP).

Solar potential

The solar potential of roofs is quantified at a building level for a neighbourhood in the city of Turin by analyzing the available roof area.

The annual, monthly, and hourly solar radiation values were calculated at a building level with ArcGIS using the 'Area Solar Radiation' tool ('Points solar radiation' is a similar tool) to establish the solar potential. Input data of different accuracy levels were considered to evaluate the simulation precision and the simulation time.

The urban built environment was assessed using two DSMs with different accuracies: the first one was less accurate, with a precision of 5 meters (duration of the simulation time for a block of buildings with a dimension of 150 m x 150 m: 7 seconds), while the other one was more accurate, with a precision of 0.5 meters (duration of the simulation time for a block of buildings: 25 seconds).

The local climate radiation refers to two parameters: (i) the atmospheric transparency assessed according to the linke turbidity factor (τ, -), elaborated using Meteonorm software (https://meteonorm.com/en/); (ii) the ratio of diffuse radiation to global radiation (ω, -), released from the PVGIS portal (https://ec.europa.eu/jrc/en/pvgis). The solar analysis was performed for a whole year at a monthly interval (the year 2016 was considered a typical meteorological year according to the period from 2010 to 2020 [54]). The solar analysis considered three different models of sun and sky more or less precise in terms of time periods: with annual, seasonal (three intervals) and monthly characteristics. Table 29 shows the solar radiation parameters for these three levels of analysis according to the year 2016. For the simulations the 'Area solar radiation' tool of ArcGIS was used with the following parameters: 8 zenith divisions, 8 azimuth divisions and a 'Standard overcast sky' for the diffuse model (i.e., diffuse radiation varies with zenith angle).

Table 29. Sun and sky data to evaluate the solar energy radiation (year 2016 - Turin, Italy) [53].

Months	**Monthly analysis**		**Seasonal analysis**		**Annual analysis**	
	ω	***τ***	***ω***	***τ***	***ω***	***τ***
January	0.58	0.29	0.58	0.32	0.54	0.47
February	0.68	0.31				
December	0.48	0.35				
March	0.69	0.44	0.57	0.47		
April	0.63	0.51				
May	0.60	0.53				
September	0.41	0.57				
October	0.42	0.51				
November	0.65	0.28				
June	0.58	0.54	0.44	0.60		
July	0.39	0.62				
August	0.35	0.63				

Figure 72 shows the annual solar radiation (kWh/m^2/year) obtained at a block of building scale using a DSM with a precision of 5 meters and annual average radiation parameters (one simulation to analyse the whole year, with a monthly interval out-put), and using a DSM with a precision of 0.5 meters and monthly average sun and sky data (12 simulations to analyse the whole year, one per month). In this type of analysis, the more accurate the input data, i.e., DSM of 0.5 meters and monthly sky and sun data, the better the results describe the real conditions. The average numerical value of annual solar radiation incident on the roof of the buildings has been represented. The accuracy of the outputs was improved by using more accurate input data (Figure 72b). It is possible to observe that with a coarser grain (i.e., DSM of 5 meters) the sunniest areas are together with areas that receive less solar radiation, and therefore, for example, roofs are generally less sunny (because the grid includes not only the roof but also part of the surrounding areas). In general, using a DSM with low precision and annual parameters, simulations are less accurate and tended to underestimate the solar radiation values (especially during the summer months).

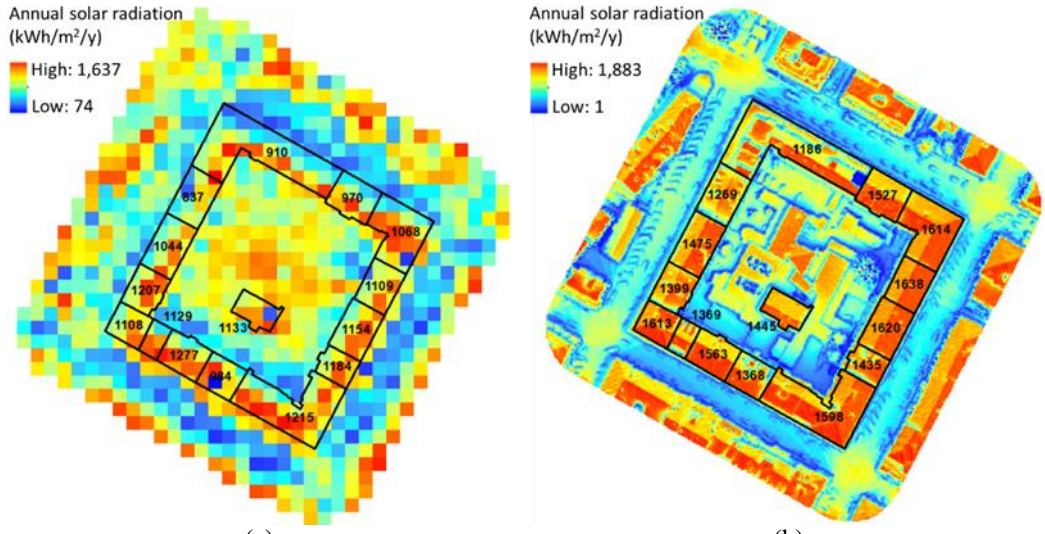

(a) (b)

Figure 72. Annual solar radiation (kWh/m^2/year) (a) using a DSM of 5 meters and annual local climatic data; (b) using a DSM with a precision of 0.5 meters and monthly local climatic data [53].

These solar radiation data processed in ArcGIS were compared with the data developed from the PVGIS portal and with data recorded by a weather station located in the city of Turin. Figure 73 compares the monthly horizontal irradiation data (kWh/m^2/month) produced using different input data and different types of simulation and tools (ArcGIS vs. PVGIS). The data indicated in the table shows the number of simulations made as a function of the input data, the simulation times, and the annual mean absolute percentage error (MAPE). The MAPE was calculated using as reference data the more accurate simulations made with the DSM of 0.5 meters and monthly sun and sky data. The ArcGIS simulations, made with monthly climatic data (12 simulations), showed a higher monthly variation than those made with the seasonal (three simulations) or annual (one simulation) sun and sky data.

The solar irradiation values resulting by the 0.5 meters DSM were higher than those of the 5 meters DSM. The data developed from PVGIS were sufficiently accurate, compared with the ArcGIS results. The MAPE shows that the PVGIS results are reasonably accurate with a MAPE of 11%.

In summary, the simulations made in ArcGIS allowed more accurate results to be obtained with higher solar irradiation values during the summer and lower ones during the winter. This is because the analysis was performed considering the monthly climatic conditions and the real characteristics of the territory with a very high precision (DSM of 0.5 m). Less accurate data were obtained from the simulations that used seasonal/annual climatic conditions (without monthly variation), PVGIS data (which refers to solar energy models and data from weather stations) and weather station measurements (with climatic data records referring to a single point on the territory).

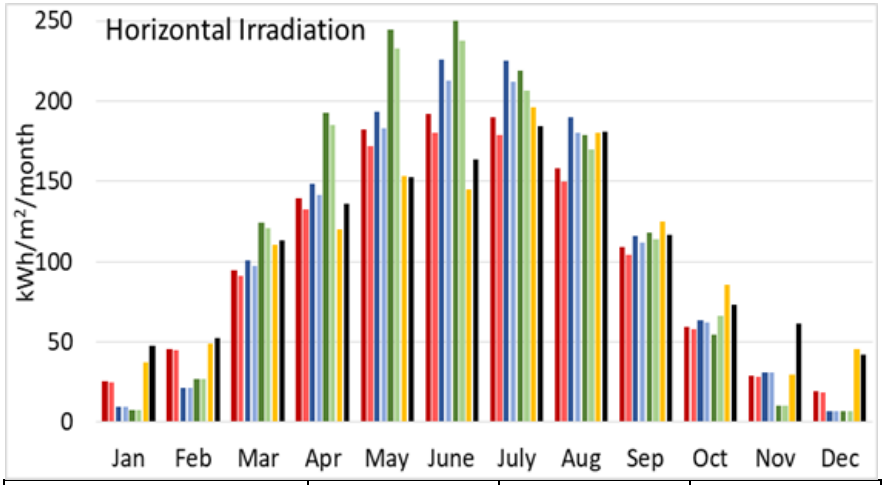

Simulations at block of buildings scale with a dimension of 150m x 150m		Number of simulations (-)	Simulation times (seconds)	Annual MAPE (%)
	DSM 0.5m, year	1	7	13
	DSM 5m, year	1	25	17
	DSM 0.5m, season	3	21	7
	DSM 5m, season	3	75	11
	DSM 0.5m, month	12	84	-
	DSM 5m, month	12	300	4
	PVGIS	-	-	11
	Weather station	-	-	8

Figure 73. Monthly horizontal irradiation values (kWh/m^2/year) on the rooftop of the buildings at block of buildings scale using different input data, types of simulation and tools: ArcGIS, PVGIS and measured data from a weather station. Down the number of simulations, the simulation times, and the annual mean absolute percentage error (MAPE) for each analysis have been indicated [53].

Subsequently, an analysis was carried out to evaluate the solar radiation according to the different orientations and inclinations of the rooftop of the buildings in Turin. Figure 74 shows an example of the comparison of the monthly solar radiation (kWh/m^2/month) considering four orientations: SE, with an azimuth of -60° (Figure 74a), SW, with an azimuth of +30° (Figure 74b), NW, with an azimuth of +120° (Figure 74c), and NE, with an azimuth of -150° (Figure 74d).

These are the typical orientations of buildings in Turin. The monthly data produced using DSMs of 0.5 and 5 meters and monthly radiation parameters were compared with data developed from the PVGIS portal. The annual relative error (RE) in the graphs is indicated to compare the PVGIS data with ArcGIS data.

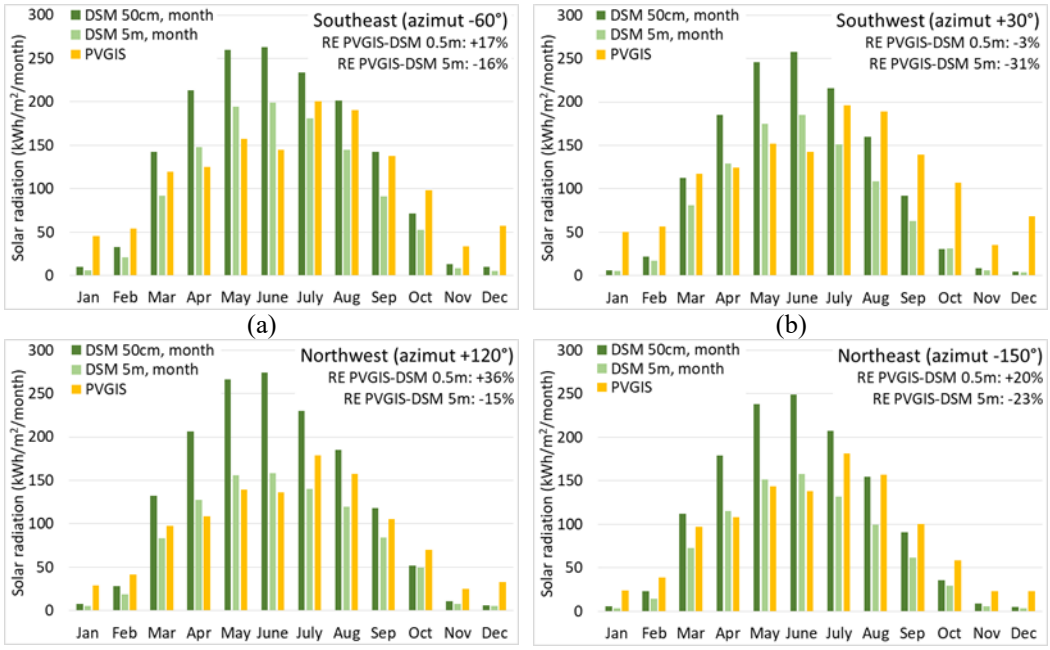

Figure 74. Comparison of the monthly solar radiation values (kWh/m^2/year) considering four orientations: (a) SE (azimuth -60°, (b) SW (azimuth +30°), (c) NW (azimuth +120°), (d) and NE (azimuth -150°) [53].

In general, it can be observed a more significant difference between the months using the monthly sun and sky data. Furthermore, depending on the orientation, the solar radiation values are greater, with azimuths of +30° and -60°, and this trend is obtained for all the analyses. PVGIS data are able to capture the differences as a function of orientations and are reasonably accurate, although are less sensitive to monthly variation. However, compared PVGIS data to the data processed using ArcGIS tools, have an average relative error of ±20%.

Therefore, several methods and tools of various degrees of accuracy that can be used to evaluate the solar PV potential of roofs are available. The simulation times and data processing times of ArcGIS are quite high, depending on the extent of the analysed area and on the accuracy of the input data (i.e., DSM precision and radiation parameters). Processing with PVGIS is fast and simple, and it is possible to collect both hourly solar radiation and PV performance values.

One of the main strengths of ArcGIS tools is that they provide outputs which de-scribe the real conditions on a city scale with greater accuracy with respect to other tools, such as PVGIS. The only real weakness is that, in carrying out this type of analysis, the more precise the input data are (a DSM of 0.5 meters and monthly climatic conditions), the more expensive the data processing is and the longer the time required for simulations, and especially for processing the outputs, is, too. The results presented in this section refer to a small area of the city of Turin (with a

dimension of 150 m x 150 m), if the analysis was carried out for the whole city, the collection and processing of the data would have required a significant effort. This is the main reason why other tools such as PVGIS are often used. They have limitations in terms of the correctness of the data but are still reasonably accurate and the processing is very simple and fast. As for the data from weather stations, they are real data measured at a specific point in the territory, therefore, depending on the location of the weather station, very different results may be obtained. This can significantly affect city-scale analyses.

Rooftop potential

The solar energy potential of roofs was quantified at a building level for a neighbourhood in the city of Turin by analyzing the available roof area, taking into account several criteria [114,194,207,208]: the shape of the roof (i.e., area and slope), the presence of disturbing elements, the roof orientation, the quota of solar radiation, as a function of the local climate conditions, and the built environment, energy and environmental regulations, heritage and aesthetic criteria.

The criteria used to identify suitable rooftops for solar panels and collectors refer to building architecture, morphological context (Table 30), building codes, and regulations. The information of buildings' architecture and morphological context were investigated using the GIS data. According to Italian Standard (UNI) 11235:2015 and to the literature review [114,207], the following criteria were identified to select the potential roofs.

Table 30. Criteria to assess rooftop renovation feasibility [56].

Criteria	Solar technology
Building height	>3.5 m (heated building)
Roof area	>50 m^2
Roof material	No disturbing element
Roof slope	≥20° and <45° (pitched roof)
Roof orientation	No North exposition*
Solar radiation	≥1200 kWh/m^2/year*

Regarding the orientation and solar radiation criteria (*) some considerations need to be made. For many years, studies that have investigated solar energy in cities have usually only considered the south-facing roof surfaces of buildings for producing energy from solar technologies [198,209–214]. Since the only RES available in densely built cities is usually solar energy, there is a need to exploit the full potential of a roof, but the question is whether this is convenient from an economic point of view.

There are relatively few studies regarding the use of different orientations to produce energy from PV panels. Azaioud et al. [215] investigated the benefits of PV installations using different orientations, and not only the southern (S) one. They confirmed that energy benefits can be achieved, such as the reduction of the

electricity peak and improvements to the SCI and SSI, by resorting to multiple orientations. In [216], the authors analysed the combination of East (E) and West (W) orientations for PV production with respect to the S one. The authors found that it is possible to reach a higher level of self-consumption and a greater degree of self-sufficiency for an E-W orientation, while the electricity costs are lower for E-W and SE-SW combinations. Lahnaoui et al. [217] confirmed that since the optimum PV orientation depends to a great extent on the hourly load profile of the users, the best solution is not always the use of South-exposed roof surfaces. Mainzer et al. [218] analysed the PV potential for residential users, taking into account a quota of north-facing roof areas that did not reduce the technical potential (even though the yield from these surfaces is lower). In [219], the authors evaluated the share of solar radiation from differently oriented surfaces. They found, regarding their seasonal analysis, that the north-facing surface had higher daily average solar radiation energy than the south-facing plane. Collectively, these studies outline a potential for the use of non-south oriented surfaces. In this chapter scenarios in which the pitch of the roofs facing north is also used are investigated.

Energy regulations

The feasibility of the installation of solar technologies is assessed considering energy and environmental regulations at national and municipal levels. According to the Italian Decree 28/2011, some requirements were considered for the installation of solar energy technologies:

- Production of thermal from ST collectors' installation: at least 50% of the annual domestic hot water consumption must be covered by the ST production.
- Production of electricity from PV panels: the installed electric power, *P,* (in kW) must be greater than or equal to the value calculated with the following equation:

$$P = (1/K) \cdot A \tag{26}$$

Where: P is the installed electric power (kW), K is a coefficient equal to 50 (m^2/kW) after 1 January 2017, and A is the footprint area of the building (m^2).

4.3 Monthly model by ST collectors and PV technologies

A place-based methodology used to evaluate the monthly productivity at urban scale is presented. The solar energy that can be produced from the monthly solar radiation has been estimated at district level for buildings in Turin. The solar energy potential has been investigated identifying the available rooftop areas, quantifying the total solar radiation on the rooftop, and considering the technical potential of buildings.

4.3.1 Methodology

The monthly models of consumption and production from solar energy were combined to evaluate the installation of solar technologies on the roofs of a neighbourhood. The consumption models were applied to calculate the thermal and electrical consumption of residential and non-residential users. The solar potential was quantified considering the existing solar technologies, and the potential as a function of the shape of the roof, and environmental/legislative constraints (see Table 30).

Energy consumption

The monthly energy consumption is simulated for a district of Turin as follow.

For the residential sector, SH consumption refers to measured data for the season 2013-2014 [46] and DHW consumption is calculated taking into account that a person needs 50 L of water per day at a temperature of 45°C (water temperature variation is 30°C). For the non-residential sector, SH and DHW consumption are quantified knowing, for different users, the specific consumption in kWh/m^3 and the heated volume (m^3) [12].

For the residential sector, electrical consumption refers to the average monthly consumption of 1,206 families for the years 2013 and 2014 [220]. For the non-residential sector, electrical consumption (kWh$_{el}$) is quantified knowing specific annual consumption in kWh$_{el}$/m^3 and the heated volume (m^3) [221].

Solar energy productivity

The GIS tool 'Area solar radiation' is used to quantify how much solar radiation each rooftop in the district receives throughout the year. The sun and sky models were elaborated, considering the monthly data of atmosphere transparency (τ) and ratio of diffuse radiation to global radiation (ω) identified from the 'Photovoltaic Geographical Information System PVGIS' of Joint Research Centre (JRC). Considering the period 2013–2014, τ was taken to equal 48%, 62%, and 72% in winter, midseason, and summer periods, respectively, and ω is taken to equal to 48%, 45%, and 35%, similarly. The quota of annual and monthly incident global solar radiation is quantified with a precision of 0.5 meters using the DSM of the entire city.

The solar technologies are assessed considering the potential roofs' area with better solar exposition.

In Italy, the most used types of low-temperature ST collectors are flat glass collectors with high efficiency and low cost and vacuum tubes, which have greater efficiency compared to flat glass collectors, due to the lower dispersions by thermal convection inside the vacuum tubes, but higher cost. On average, a solar thermal system in Italy has a monthly efficiency of 40–85% with flat collectors and 70–86% with vacuum tubes; a collection area of 0.7–1.2 m^2/person for flat collectors and 0.5–0.8 m^2/person for vacuum tubes (considering the production of DHW),

with the month of maximum solar radiation being considered for the dimensioning; and a cost of 1,000 euro/m^2 for flat collectors and 1,200 euro/m^2 for vacuum tubes.

According to European Standard (EN) 12975-2:2006 and Italian Standard (UNI) 11300-4:2016, the two typologies of ST collectors have, on average, respectively, zero-loss efficiencies *η0* of 0.94 and 0.88, linear heat loss coefficients a1 of 3.34 and 1.57 W/m^2/K, quadratic heat loss coefficients *a2* of 0.02 and 0.01 W/m^2/K, and, for the whole system, a performance ratio of 75%. Then, their monthly efficiencies vary from 0.37 to 0.87 for the flat glass collectors and from 0.69 to 0.87 for the vacuum tubes.

Regarding PV modules, the efficiency of converting solar energy into electricity varies mainly according to the type of technology chosen. The average efficiency values vary from 22% (high efficiency monocrystalline silicon) to 4% (amorphous silicon). The cost of a PV solar system depends on the installed power, which is around 2,000 euro/kWp where kWp is the peak power). The capturing surface depends on the efficiency of the module and ranges from 5.5 m^2/kWp for high efficiency monocrystalline silicon to 11 m^2/kWp for amorphous silicon. In assessing the efficiency of converting solar energy, it is also necessary to consider the energy losses of all system components, in addition to solar panels; it is estimated to be around 20–25%.

The PV modules have an efficiency of 15% (standard efficiency polycrystalline silicon module), and both PV and ST have a system performance around 75%. The hypothesized PV and ST areas are dimensioned in order to not have an overproduction during summer months.

4.3.2 Case study

The methodology presented here has been applied to ‘Pozzo Strada’ district in Turin, and the results have been calculated for a mesh with a dimension of 1 km^2 with 21,520 inhabitants.

Roofs analysis and classification

The roofs of over 700 buildings have been analysed and classified according to their geometric characteristics. Figures below show the main steps necessary for the building’s categorization: evaluation of the roof slope (Figure 75); evaluation of roof surfaces considering eight orientations (Figure 76); classification of roofs into six categories (Figure 77).

The 16% of buildings have flat roofs, only the 2% have shed roof, half-hipped and hipped/pyramid are respectively the 3% and the 8%, the gable roofs represents as much as 70% of the roofs, typical for residential buildings in Turin. In the analysed district the 79% of buildings are residential. According to four building sectors (industrial, municipal, residential and tertiary) the main results of roof orientation analysis were indicated in Table 31 and Figure 78. It is possible to

observe that a large quota of residential buildings has an optimal orientation for solar energy production (E-W).

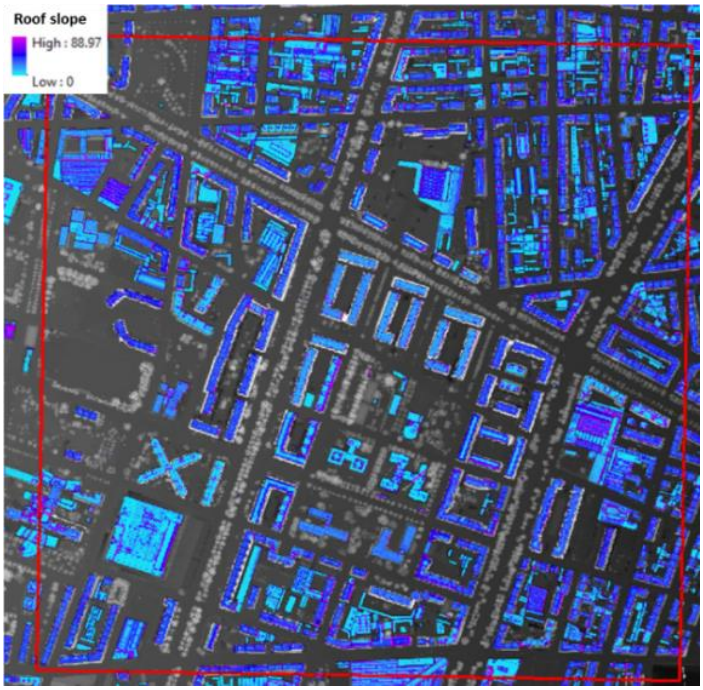

Figure 75. Roof slope analysis (slope, degree) [52].

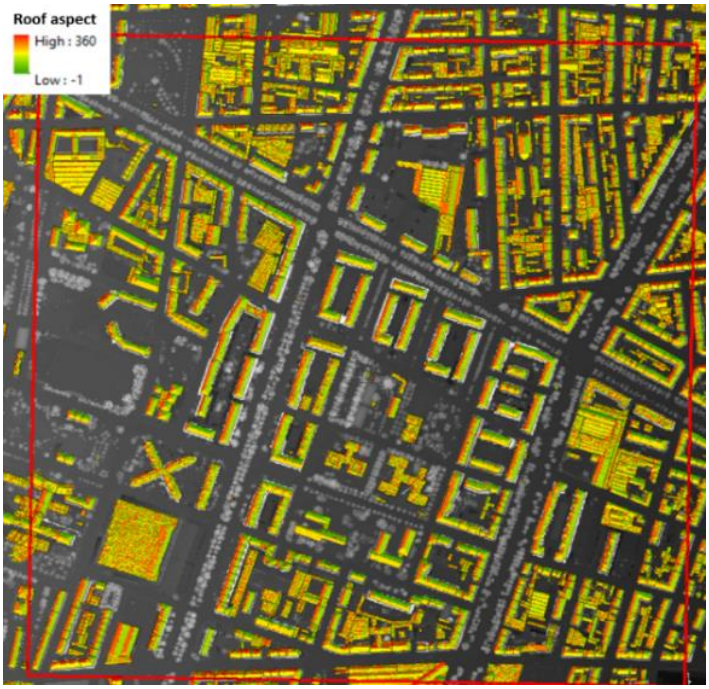

Figure 76. Roof aspect analysis (orientation, degree) [52].

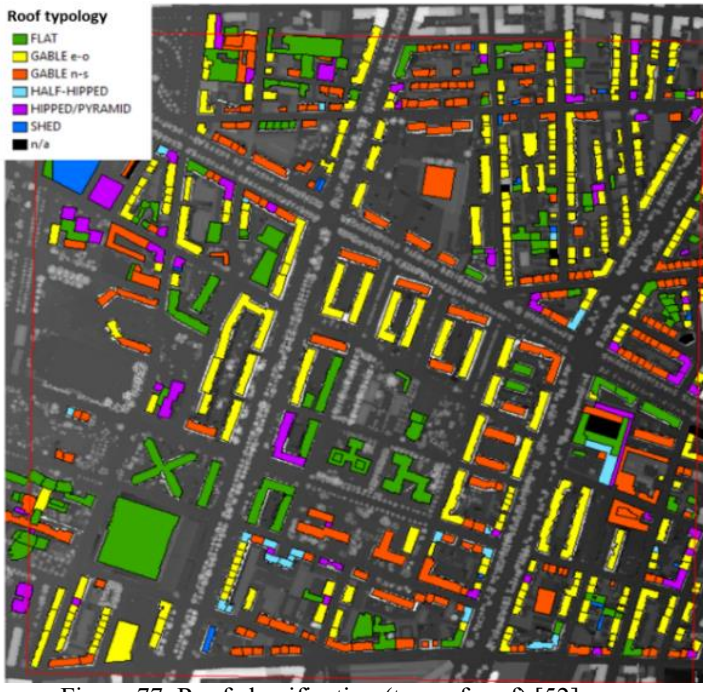

Figure 77. Roof classification (type of roof) [52].

Table 31. Roof analysis for a district in Turin (IT) with a dimension of 1 km^2 and values for the entire city are indicated in brackets [52].

Sector	No build.	Flat roof [10^3 m^2]	Pitched roof [m^2]	Slope pitch. roof [°]	Main orientation	Suitable roof areas [m^2]
Ind.	70 (4950)	17 (2,138)	17 (3,574)	17 (20)	N-S (N-S)	19,533
Mun.	53 (5561)	8 (748)	18 (1,292)	21 (24)	S-E (N-S)	15,672
Res.	572 (44224)	20 (870)	139 (8,670)	25 (25)	E-W (N-S)	93,172
Ter.	33 (4109)	20 (1,160)	8 (710)	13 (24)	S-E (N-S)	15,949

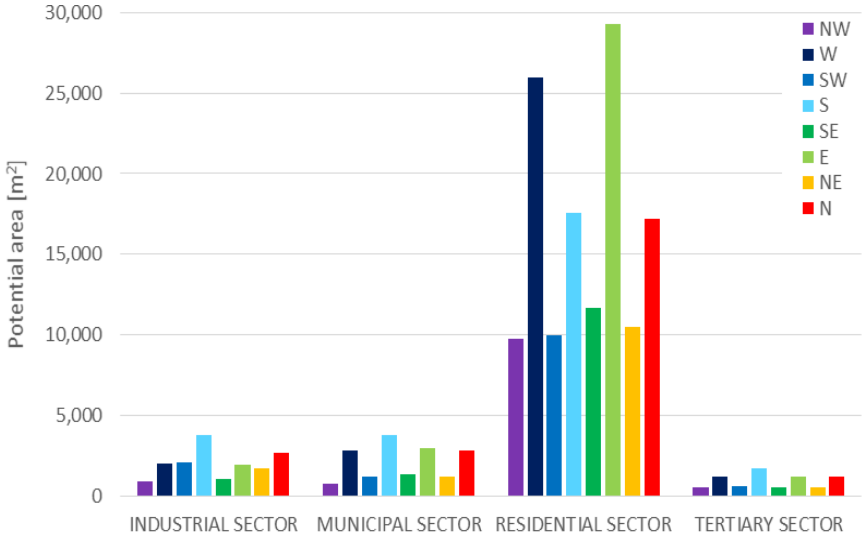

Figure 78. Areas of pitched roof distinguishing eight orientations and four building sectors [52].

Solar energy potential assessment

As previous mentioned, the sun and sky models are elaborated with the support of GIS tool 'Area solar radiation' considering the monthly data of τ and ω identified from the PVGIS portal (in Table 32).

Table 32. Monthly sun and atmosphere characteristics [52].

Month	1	2	3	4	5	6	7	8	9	10	11	12
ω [-]	0.46	0.4	0.35	0.38	0.41	0.4	0.41	0.45	0.38	0.46	0.49	0.4
τ [-]	0.46	0.58	0.64	0.66	0.71	0.74	0.73	0.69	0.66	0.56	0.46	0.42

Figure 79 shows the values of annual solar radiation (Wh/m^2/y) calculated for a district. The monthly results have been indicated for some months, where the solar radiation values are obviously higher in summer, compared to winter.

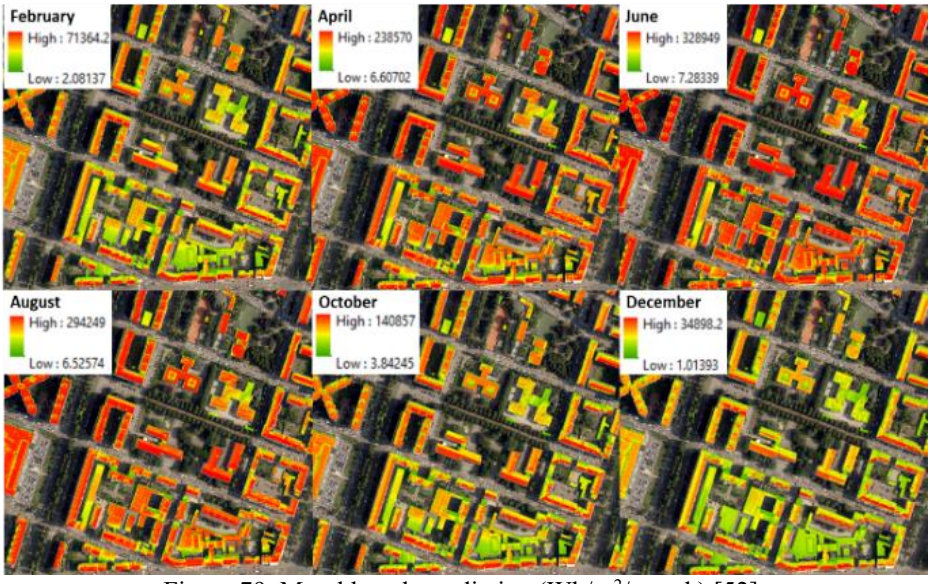

Figure 79. Monthly solar radiation (Wh/m^2/month) [52].

4.3.3 Results

After the analysis of monthly and annual solar radiation on each rooftop, taking into account 570 heated, pitched buildings and roof surface with annual solar radiation higher than 1,200 kWh/m^2/year, the ST collectors and PV modules are dimensioned according to DHW consumption and electrical consumption of residential and non-residential users.

According to the Italian Decree 28/2011, 50% of DHW consumption of residential sector is covered by ST collectors. The percentage reaches 100% in June, while in the winter months (December and January) ST production is able to cover about 7% of the residential consumption (Figure 80a). There is a GHG emission reduction of 1,958 ton/CO_2/year. The requirements indicate that 50% of

consumption must be covered; this dimensioning is appropriate, given that in July hot water can only be used to cover domestic hot water.

The PV panels can be dimensioned in two ways: (i) by covering 100% of consumption in the month of maximum irradiation or by reaching 100% of annual self-consumption, (ii) taking into account that the overproduction in the summer months that is fed into the grid will be consumed in winter. In the presented method, the PV panels were dimensioned according to the National Decree 28/2011 using the footprint area of the buildings (A), where the installed power is equal to A divided by a K coefficient = 50 (Figure 80b).

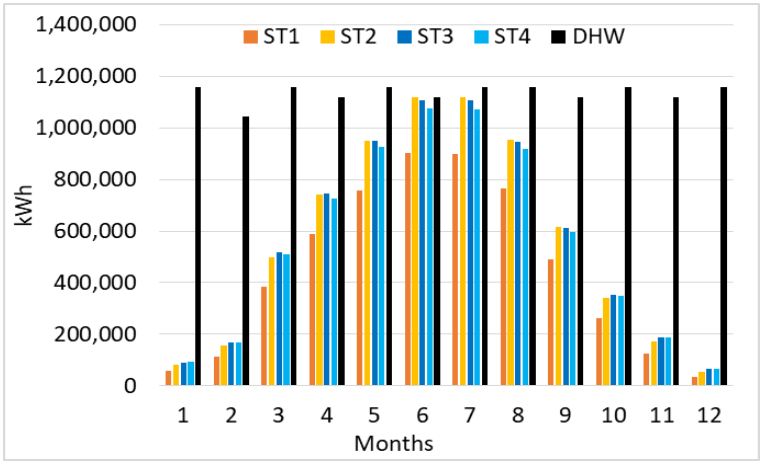

(a)

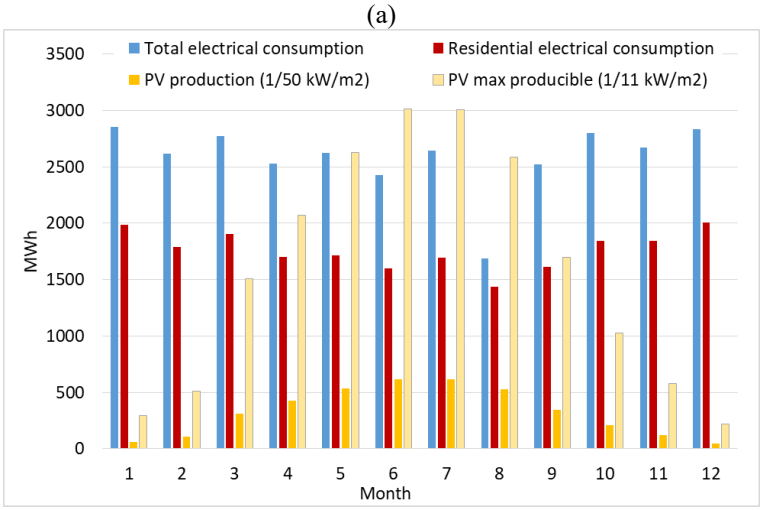

(b)

Figure 80. Solar energy technology assessment (for the 2014 year): (a) Comparison between domestic hot water (DHW) consumption of residential sector and solar thermal (ST) production considering four collector typologies (collectors' annual average efficiency: ST1 = 0.59, ST2 = 0.77, ST3 = 0.80, and ST = 0.79); (b) comparison between electrical consumption, photovoltaic (PV) production with coefficient K = 50 m^2/kW (according to the Decree 28/2011), and PV max producible [56].

According to the installed power and the annual utilization hours of use (in the Piedmont region are 1,130 h), the electricity produced from PV panels is compared to the electrical consumption. Therefore, knowing that a typical Turin family needs about 2,000 kWh_{el}/year for electricity supply and, in the district analysed, the

number of families is equal to 10,638 (ISTAT data, 2011), the 13% of the annual residential and non-residential electrical consumption has been covered with a GHG emission reduction of 1,853 ton/CO_2/year. Considering only the residential sector, PV production covers the 18% of electricity consumption. In the summer months it covers 38% and in the winter months, 2–3%.

Table 33 shows the total roof area, the quota well exposed with no disturbances (15–35%), the quota used for the ST collectors to satisfy the DHW consumptions, and the quota for the PV panels, as requested by the standards (1/50 kW/m^2). Using the maximum energy potential that can be produced from PV panels, it is possible to cover 82% of residential electrical consumption; with the reverse procedure, an optimal value of K of about 11 m^2/kW was calculated.

Table 33. Roof area for solar energy production [56].

Area	Roof	Well exposed with no disturbances (15-35%)	ST for DHW energy-use	PV 1/50 kW/m^2	PV max
m^2	172,749	101,048	4717	21,141	96,631
%	-	58	2.7	12.2	55.8

From this analysis, it emerged that to reach the 50% coverage of DHW and SH consumption, it is necessary to use not only not only the well-oriented roofs, but the producibility of the north-facing pitches must also be assessed.

In addition in some cities it is possible to use other renewable technologies, such as the energy taken from the cold source with heat pumps for heating or PV panels for cooling. Usually, there are few renewable energy sources available, but there are sources that can be exploited in public spaces, such as the PV panels on shelters, micro-power plants (of which in Turin city there are three) and mini-wind on commercial buildings, considering the acoustic impact.

4.4 Hourly model by PV technologies

This section shows a methodology that critically examines the energy benefits of using different orientations for PV technologies and investigates the economic costs. It provides new insights into the optimization of the costs and self-sufficiency of roof integrated PV technologies on residential buildings by using multiple orientations of roofs. Economic costs have been assess considering economic incentives for collective self-consumer configurations [206]. With the use of these incentives, it is possible to promote the use of PV technologies with low energy costs and a high level of the self-sufficiency index (SSI).

Thus, this research focuses on whether energy and economic benefits can be achieved by using two directions for PV installation on gable roofs for residential users configured as collective-self consumers. The presented methodology is applied to the city of Turin. In the city, only the roof areas with a predominantly south facing orientation (i.e., better-exposed roof surfaces) have generally been

used for PV production. Given that the only renewable source that can be exploited is solar energy, this section investigates whether it is possible to improve energy security and increase self-sufficiency by also using north-exposed roof surfaces (e.g. north, northeast or northwest facing orientations, considered as poorly-exposed roof surfaces).

4.4.1 Methodology

Two indicators that are used to investigate the technical-economic feasibility of an energy community are the self-consumption index (SCI) and the self-sufficiency index (SSI) [222]. These indicators have been used to assess the balance between electrical consumption and PV production.

Since the hourly load profile is compatible with PV production, the residential sector has been analysed. Seven residential buildings have been investigated and the impact of the use of two directions for PV installation has been evaluated considering electricity and SC load.

Energy consumption

This section shows details of the methodology that is used to assess the hourly load profile of residential buildings. The energy consumption is composed of electricity for light and appliances, electricity for SC, and electricity for condominium utilities (i.e., elevators).

Electricity for light and appliances

The hourly electricity consumptions for light and appliances of the residential users are calculated considering monthly electrical data measured for two consecutive years (2016 and 2017) for over 100 residential buildings located in a neighbourhood in Turin [54]. The normal distributions are investigated in order to evaluate the frequency distribution of the annual consumption of the residential users for the year 2016. Two statistical tests are run in conjunction with the distributions to observe the trend of the annual consumption of the buildings and to discard any anomalous data: the Kolmogorov-Smirnov (KS) and chi-squared (χ^2) tests. Figure 81 shows the normal distribution of the annual measured data of 107 residential users analysed for the year 2016, and both KS and χ^2 were verified. The median annual electricity consumption in this neighbourhood is 1,917 kWh/user/year, and two types of residential consumers were identified: low-consumer with 1,652 kWh/user/year (median minus the standard deviation) and high-consumer with 2,182 kWh/user/year (median plus the standard deviation). In this analysis, the number of users in each building being known, it is possible to quantify the total electrical consumption for low-consumption and high-consumption users.

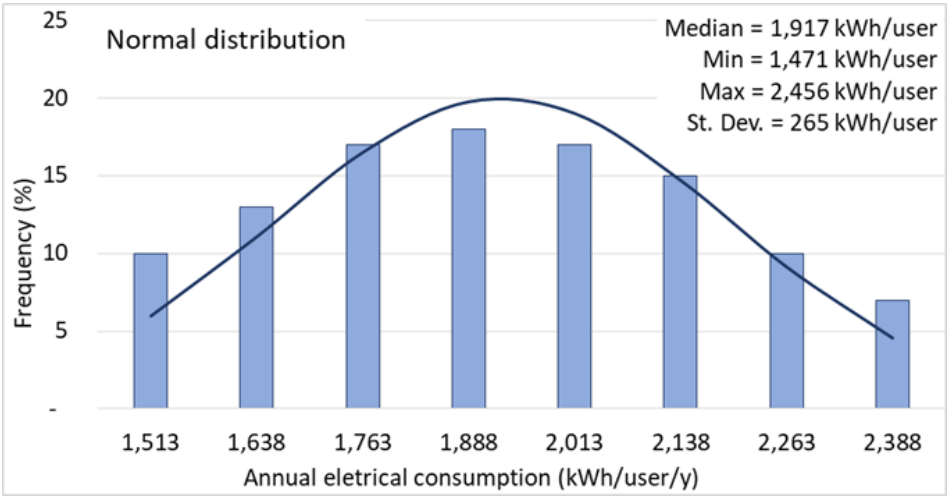

Figure 81. Distribution of the annual electrical consumption of 107 residential users for the year 2016 [53].

The seasonal hourly profile is identified using the hourly profiles of some typical days in the winter, spring, summer and autumn periods as a reference, and distinguishing between working and non-working days. The hourly profiles refer to over 400 families in the Piedmont Region with 2.15 components per family [223]. Therefore, from the monthly measured data, and the hourly profiles for one year being known, it is possible to calculate the hourly electricity for light and appliances for the year 2016 for each residential building.

Electricity for space cooling

The hourly electricity for SC of the residential buildings is quantified by applying a GIS-based engineering model [50]. The model is validated, according to a previous work [49], through a comparison of the results, using the CitySim tool and the ISO 52016 standard [29].

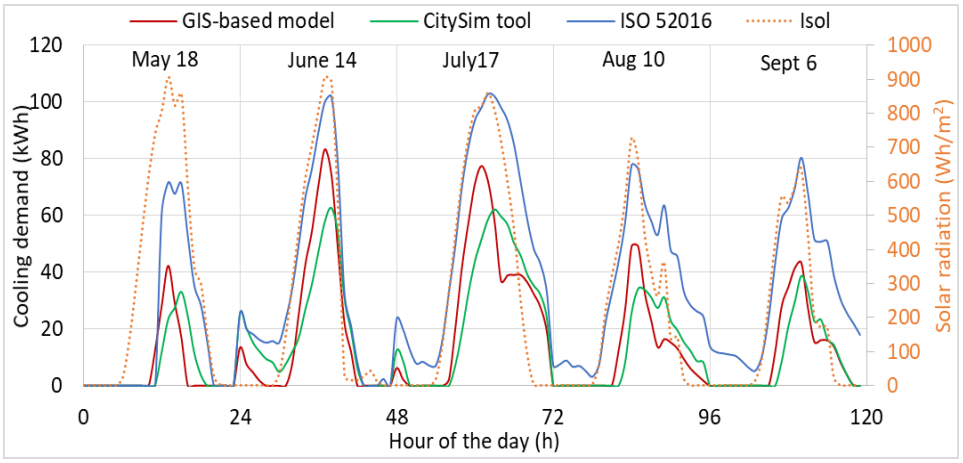

(a)

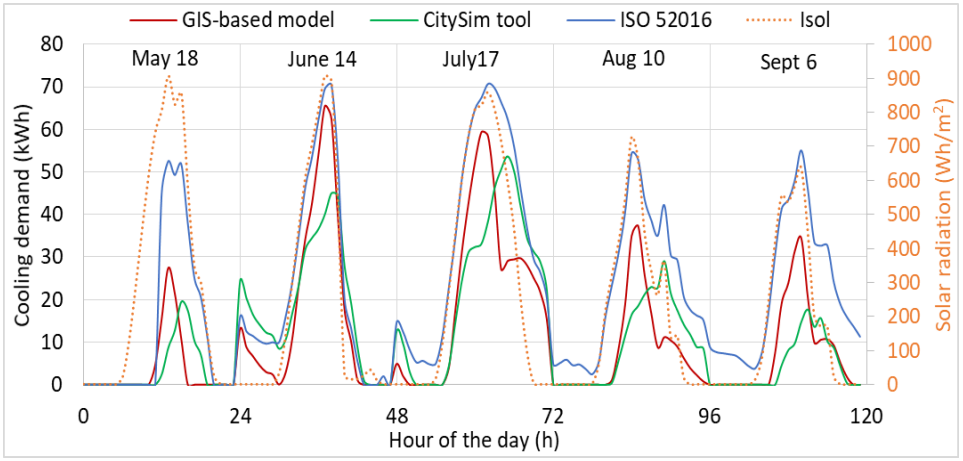

(b)

Figure 82. Comparison of the hourly cooling demands for the five typical summer days simulated with the GIS-based model (in red), the CitySim tool (in green) and the hourly method according to ISO 52016 (in blue), on the secondary axis the solar radiation expressed in Wh/m^2 is indicated (in yellow): (a) a residential building built in 1961-70 with SW (azimuth +30°) orientation; (b) a residential building built in 1919-45 with SE (azimuth -60°) orientation [53].

Figure 82 shows an example of the hourly cooling demands for the five typical summer days, simulated for two residential buildings in the neighbourhood analysed. It can be observed that the hourly cooling profiles (continuous line) have a similar trend related to the solar irradiation (dashed line). The results of the GIS-based model and the CitySim tool are very close to each other. However, the hourly ISO 52016 method simulates a higher consumption than the other two tools, especially for May and September. The daily absolute relative error for these selected days, according to the CitySim data, is on average 14% (median 7%).

Figure 83 shows the daily energy demand for SC of the two buildings described in Figure 82. As expected, the daily energy demand (kWh/day) increases as the daily external air temperature increases. However, as these models are tools that are used to perform simulations at a district scale, and not at a building scale, a 20% margin of error is compatible with neighbourhood-scale analyses.

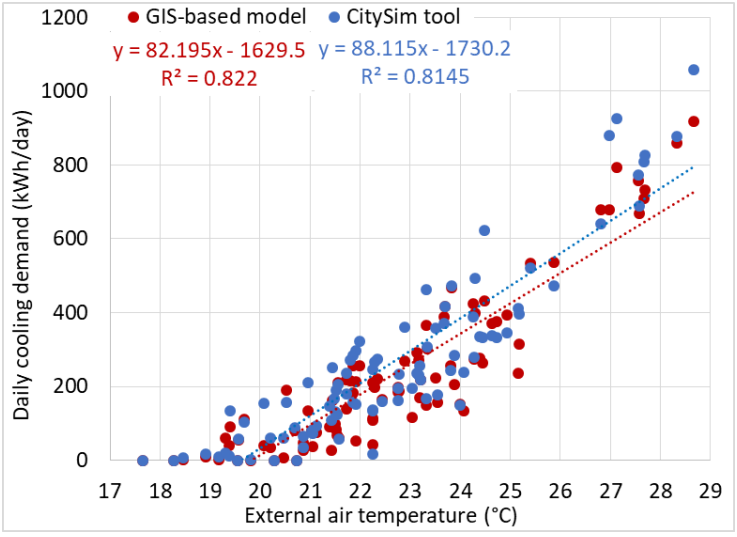

(a)

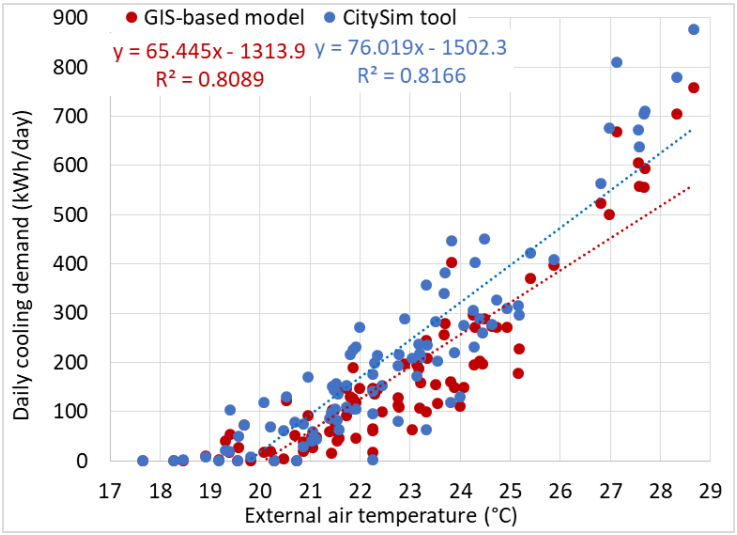

(b)

Figure 83. The influence of outdoor air temperature on daily energy demand for space cooling for: (a) residential building built in 1961-70 with SW (azimuth +30°) orientation; (b) residential building built in 1919-45 with SE (azimuth -60°) orientation [53].

The hourly electricity for SC is quantified by assuming an air-to-air electric heat pump of 35 kW with an energy efficiency ratio (EER) that varies from 6.3 (when the external air temperature is 20°C) to 4.3 (when the outdoor air temperature is 35°C).

Table 34. Correlations between EER (considering a load factor of 100%) and the external air temperature (Tae, °C) of a typical air-to-air electric heat pump available on the market [53].

Heat pump power	EER linear correlation	R^2
25 kW	$-0.1616 \cdot T_{ae} + 10.774$	0.998
35 kW	$-0.1356 \cdot T_{ae} + 8.989$	0.998

According to the EER requirements indicated in Italian Decree D.M. 26/6/09 "National guidelines for the energy certification of buildings" (and subsequent amendments and additions), the correlations between EER and the external air temperature were identified using heat pumps of 25 and 35 kW, which are typical characteristics of the heat pumps available on the market (Table 34).

Electricity for condominium utilities

In order to calculate the total load of a typical residential building, the electricity consumption of the condominium is also considered in addition to the electricity consumption for light, appliances and space cooling of the flats. The quota of energy used by the elevators is quantified for residential users to calculate the electricity consumed for condominium utilities. In Europe, elevators typically use 3-8% of the overall electricity consumption of a building [224]. This percentage mainly depends on the type of users and on the shape of the building (e.g. the number of floors and number of flats) [225,226].

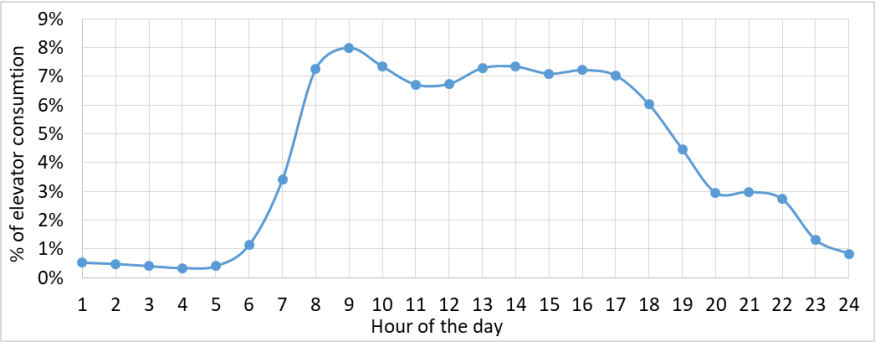

Figure 84. Typical hourly profile of elevator in residential buildings [53].

Taking into account the typology of the residential buildings, an average value of 5.5% was used to quantify the consumption of elevators. Following [227], the daily demand profile with a one-hour resolution is used to identify the hourly load profile of the elevators in the residential buildings. The differences in these energy consumptions between weekdays and holidays are minimal, therefore, only one profile is considered for the entire week. A typical hourly profile of a residential building is shown in Figure 84.

Solar energy productivity

ArcGIS tools are used to accurately describe each surface of the urban environments, and the resulting characteristics were used as input data in PVGIS. Hourly data processed from the PVGIS portal are considered accurate enough to perform the analysis. A georeferenced database was created using GIS tools, in order to evaluate the rooftop area that could be used for the installation of PV technologies, considering different orientations, inclinations and the presence of disturbing elements on the roofs. The analysis is performed on seven residential buildings located in a neighbourhood in Turin.

The hourly solar PV potential is quantified for one year using PVGIS portal, considering an inclination of PV modules of 25°. For these simulations, polycrystalline silicon modules are used with a module energy conversion efficiency in standard test conditions of 26.7% ± 0.5 [228]. PVGIS calculates the efficiency variation according to solar radiation intensity and spectrum, module temperature and wind speed. Moreover, PVGIS considers also an average value of 14% of energy losses by the cables and the inverter, and due to dirt and snow on the modules. Different scenarios are investigated, according to the maximum installable power for each roof, to identify the optimal dimension of PV modules.

Energy indexes and cost-optimal analysis

Firstly, the balance between the electrical consumption and PV production is investigated in order to examine the self-consumption and the self-sufficiency of residential users utilizing all the potential PV surfaces oriented in different directions. The variables considered to analyse the energy balance are:

- Total production (TP), which is the local energy production from new renewable energy source power plants, in our case PV plants.
- Total energy consumption (TC), which is the total energy demand of all the consumers, according to a collective self-consumer configuration.
- Uncovered demand (UD), which is the share of energy consumption that is not satisfied by the produced local energy and which must be withdrawn from the national grid.
- Over-production (OP), which is the share of energy that is not instantly self-consumed as the produced energy is greater than the energy demand: OP = TP – TC).
- Self-consumption (SC), which is the share of energy instantly self-consumed by each user (called prosumer) or, in other words, the energy produced that is used locally: SC = TP – OP or TC – UD or min(TP;TC).

Self-consumption and self-sufficiency are investigated by two indexes considering the annual data with an hourly time step calculation: (i) SCI, which is the ratio between SC and TP; (ii) and SSI, which is the ratio between SC and TC.

Secondly, a cost-optimal analysis is performed to optimize the costs and self-sufficiency of roof integrated PV technologies on residential buildings, taking into account the economic incentives for the collective self-consumer configuration [54,206]. The global cost (C_G) of the cost-optimal analysis is calculated for different PV configurations according to Equation 27. In this analysis, the cost-optimal analysis is performed considering a period of 20 years.

$$C_G = C_I + \sum_{i=1}^{\tau} \left(C_{E,i} \cdot R_{d(i)} \right) \tag{27}$$

Where:

- C_I is the initial investment cost, and in this work it refers to a cost of PV installation equal to (https://www.solareb2b.it/documenti/, in Italian):
  - 1,000 €/kW_p, if the installed PV power (P) > 20 kW.
  - 1,600 €/kW_p, if 6 kW ≤ P ≤ 20 kW.
  - 2,000 €/kW_p, if P < 6 kW.
- $C_{E,i}$ is the annual energy cost at year i, and it was calculated taking in account all the expenses for the energy taken from the grid (i.e., UD), as well as all the revenues generated by the sale of the energy to the grid (i.e., SC and OP). The average cost of the electricity taken from the grid was 0.22 €/kWh for residential users and it was applied to the UD share to calculate the expenses. The revenues were calculated considering the economic incentive for the collective self-consumer configuration in a condominium, which lasts 20 years, and were described as follows:
  - +0.10956 €/kWh to be applied to the SC share.

- +0.1 €/kWh to be applied to the OP share.

- $R_{d(i)}$ is the discount factor at year i was considered and is equal to the 2%.

4.4.2 Case study

The analysis is carried out for seven typical residential buildings with different dimensions and orientations located in a neighbourhood in Turin. The climate is continental and temperate, with 2648°C HDDs at 20 °C and 84 °C CDDs at 26 °C mainly concentrated in June, July and August (according to the UNI 10349-3:2016 Standard). About 80% of the buildings in the city are residential, and are mainly large and compact condominiums [56]. The orientation of the buildings was analysed with GIS tools using a DSM with a precision of 0.5 meters and the building footprint.

Figure 85 shows the roof surfaces as a function of the orientation, distinguishing between all the users (i.e., residential, industrial, municipal and tertiary) and residential users. A large number of the roofs are gable roofs with two prevalent orientations: SE, with the azimuth of -60° (16% of the total roof areas) and SW, with the azimuth of +30° (19% of the total roof areas). The prevalent roof pitch angle of the residential buildings is 25° and ranges from 45° to 15° for the gable and pitched roofs.

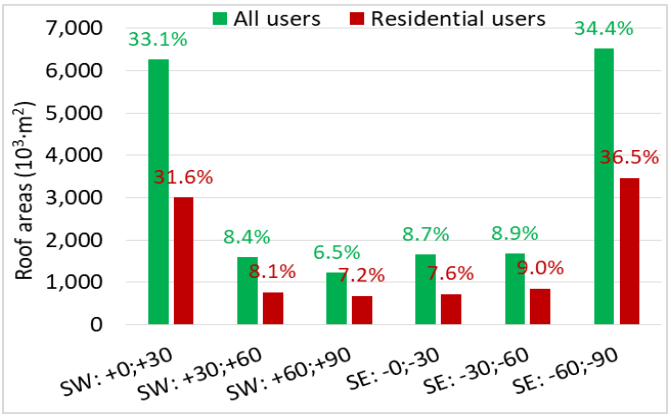

(a)

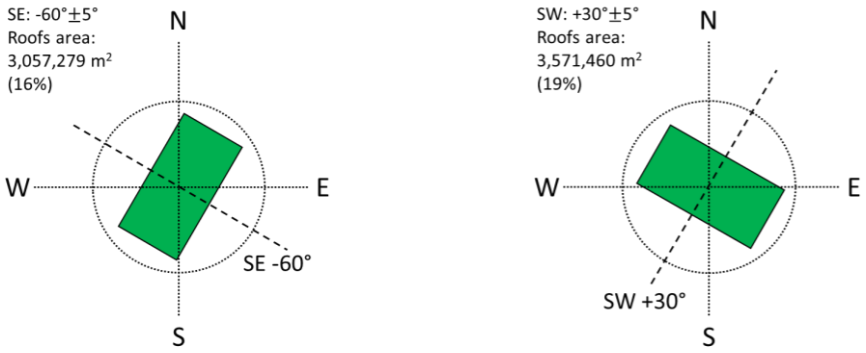

(b)

Figure 85. Orientation of the buildings in the city of Turin [53].

Selection of residential buildings

About 90% of the buildings in the analysed neighbourhood are compact residential condominiums, the number of components per family is 2.03 and the average annual electrical consumption for light and appliances is 1,928 kWh/user (according to the data measured for 2016). Seven condominiums are selected according to their orientations, dimensions (i.e., small, medium or large condominiums) and the geometrical characteristics (e.g., roof slope). In Turin, there are about 37,700 residential buildings with gable and pitched roofs and the slope of the roofs is mainly 25°, with a standard deviation of 3.77°. The seven selected residential buildings have a slope that varies between 23 and 27°. These buildings are typical of the building heritage of the historical centre of the city.

Table 35. Characteristics of the seven typical residential buildings in the considered area [53].

Building ID	Azimuth	Dimension	No. of flats	No. of floors	Roof area	Total PV area*	PV area by no. of flats
	(°)	(-)	(-)	(-)	(m^2)	(m^2)	(m^2/flat)
30	SE = -60; NW = +120	Small	10	5	210	SE = 91; NW = 87	18
91		Medium	12	5	283	SE = 156; NW = 149	20
211		Large	22	6	359	SE = 150; NW = 144	14
140	SW = +30; NE = -150	Small	10	5	285	SW = 122; NE = 120	24
258		Medium	12	5	280	SW = 125; NE = 113	20
199		Large	22	6	379	SW = 150; NE = 172	14
153	SE = -45; NW = +135	Medium	12	4	275	SE = 104; NW = 130	20

* The total photovoltaic (PV) area considers a presence of disturbing elements equal to 15% of the roof area.

Table 35 shows the main characteristics of the selected buildings:

- Small condominiums with 10 flats per building over 5 floors, and the PV area per number of flats varies from 18 to 24 m^2/flat.
- Medium condominiums with 12 flats per building over 4-5 floors, a total roof area of about 280 m^2 and a PV area of 20 m^2/flat.
- Large condominiums with 22 flats per building over 6 floors, a total roof area of about 370 m^2 and a PV area of 14 m^2/flat.

The PV area per number of flats is an interesting indicator to describe the maximum PV potential for each family.

Electrical consumption and photovoltaic potential

As mentioned before, the hourly load profile takes into account the quota for light and appliances, the quota for SC, and the quota for condominium utilities. Two types of residential consumers were investigated regarding the electricity for light

and appliances: a low-consumer with 1,652 kWh/user/year and a high-consumer with 2,182 kWh/user/year. The electricity for SC is quantified for each building by applying the GIS-based engineering model taking into account the local climate conditions for the year 2016. The electricity for condominium utilities is quantified considering that the elevator uses 5.5% of the overall electricity consumption of the condominium.

Figure 86 shows the hourly profiles of the total load, distinguishing between low-level consumers and high-level consumers, and the total PV production distinguishing between the two orientations for 12 typical days, each of which is representative of a specific month for the year 2016. It can be observed that in all the cases analysed, the PV production on the South and North orientations allows to produce energy for more hours during the day and this allows to increase generally self-consumption and energy self-sufficiency. The typical profile of the residential user is compatible with the PV production one, even if the higher consumptions of the residential user are during the evening. Then, it could be useful to consider both rooftop orientations, especially for the roof with SE-NW orientations with higher PV production in the afternoon.

Regarding the hourly load, the electricity consumption from October to April is for light, appliances and elevators with an adding quota from May to September due to SC consumption. The SC consumption allows to reach higher levels of energy self-consumption and self-sufficiency in the summer months. Since residential users have low consumption, these consumers are suitable for a spread production of low-power PV systems.

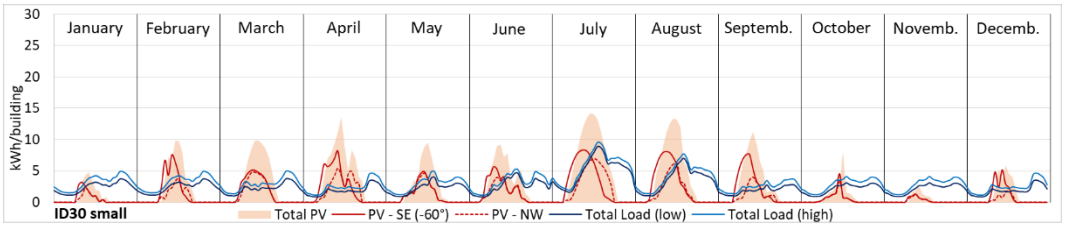

(a)

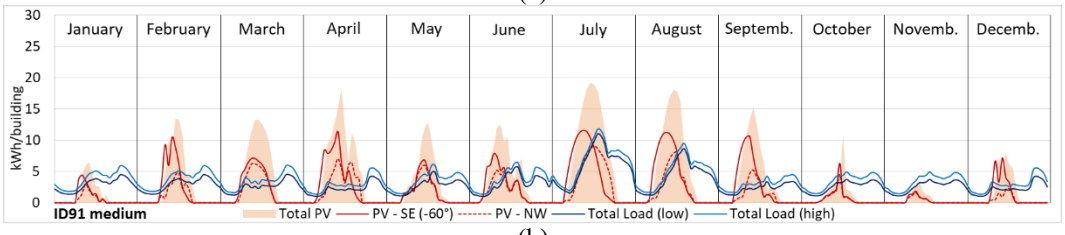

(b)

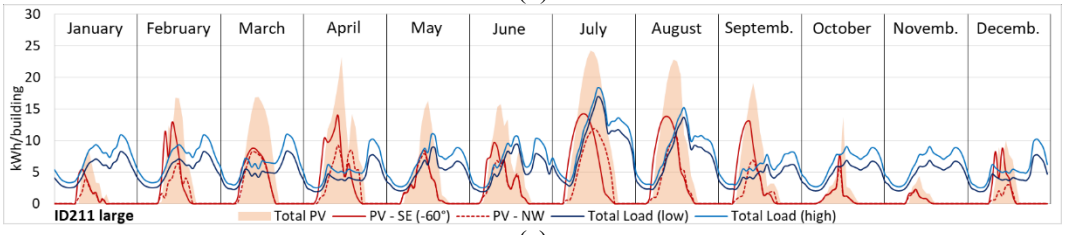

(c)

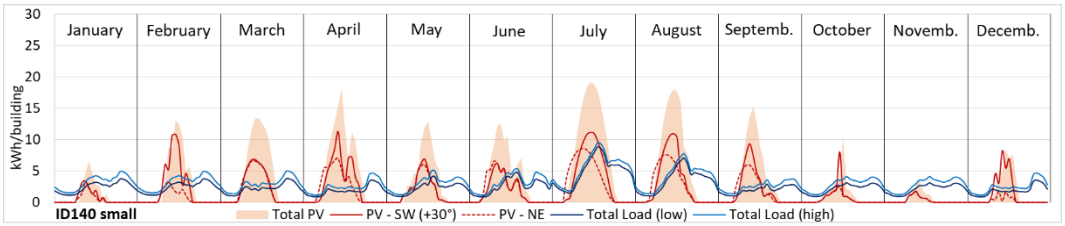

(d)

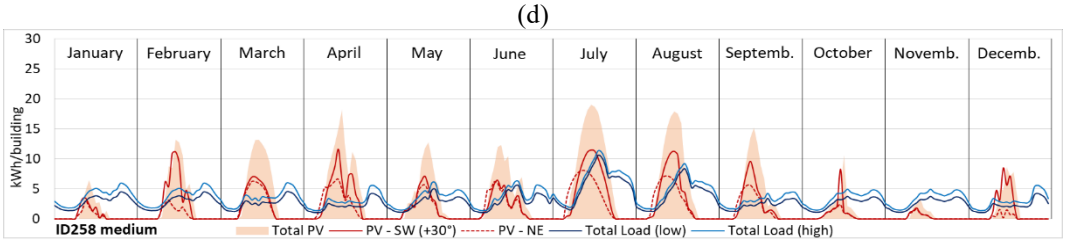

(e)

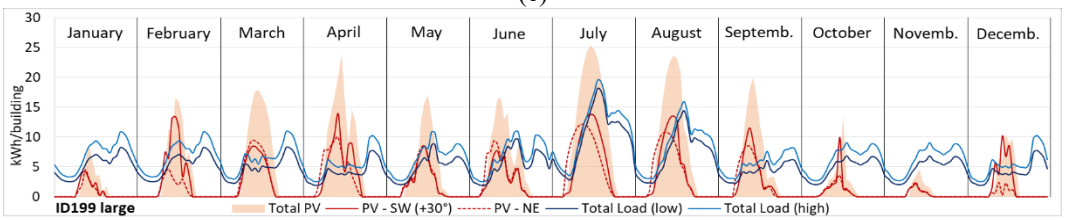

(f)

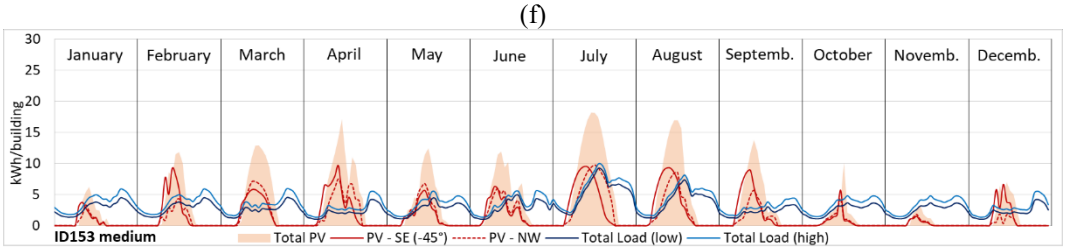

(g)

Figure 86. Hourly profiles of the load and PV production for 12 typical days, each of which is representative of a specific month of the year 2016: (a) small condominium with SE -60° orientation, (b) medium condominium with SE -60° orientation, (c) large condominium with SE -60° orientation, (d) small condominium with SW +30° orientation, (e) medium condominium with SW +30° orientation, (f) large condominium with SW +30° orientation, (g) medium condominium with SE -45° orientation [53].

Scenarios

The electrical consumption and the PV production being known, several scenarios are analysed. The results of this analysis depend on the typical energy demand of the residential users with a higher consumption during the evening. Different levels of PV production are investigated using the south-facing roof area (SE -60°, SW +30° or SE -45°) plus a quota of the north-facing roof area (NW +120°, NE -150° or NW +135°) that varied from 0 to 100%. Four electricity consumption scenarios are investigated:

- Scenario 1 (S1), which only considers electricity for light and appliances of a typical low-consumer and condominium utilities as the load (S1).

- Scenario 2 (S2), which only considers electricity for light and appliances of a typical high-consumer and condominium utilities as the load (S2).
- Scenario 3 (S3), which considers electricity for light and appliances of a typical low-consumer, condominium utilities and space cooling consumption as loads (S3).
- Scenario 4 (S4), which considers electricity for light and appliances of a typical high-consumer, condominium utilities and space cooling consumption as loads (S4).

Table 36 describes the electricity consumption, at a building level, for the year 2016 for the four scenarios and the PV power installed with reference to different percentages of used North-facing surfaces. As expected, large condominiums have a higher annual consumption (ID 211 and ID 199) and the number of installable PV panels is also greater than that of small condominiums, given that a higher roof area is available (see Table 35).

Table 36. Electricity consumption and PV power at a building level for different scenarios [53].

Build. ID	Electricity (kWh/building/year)				PV power, 100% of south + 0-100% of north roof area (kW)										
	S1	S2	S3	S4	0 %	10 %	20 %	30 %	40 %	50 %	60 %	70 %	80 %	90 %	100 %
30	17,429	23,017	20,982	26,570	11	13	14	15	16	17	18	19	20	21	22
91	20,914	27,621	25,007	31,714	16	17	19	20	22	23	24	26	27	29	30
211	38,343	50,638	44,401	56,696	20	21	23	25	27	29	31	33	34	36	38
140	17,429	23,017	20,883	26,472	15	17	18	20	21	23	24	26	27	29	30
258	20,914	27,621	24,747	31,454	16	17	18	20	21	23	24	26	27	28	30
199	38,343	50,638	44,851	57,147	19	21	23	25	27	30	32	34	36	38	40
153	20,655	27,012	24,065	30,422	13	15	16	18	19	21	23	24	26	28	29

The maximum PV power that can be installed over two orientations of roofs varies from 22 kW for small condominiums to 40 kW for large condominiums. The quota of solar energy that can be produced from PV technologies is quantified, for the year 2016, using the PVGIS portal. Crystalline silicon modules with an efficiency of 26.7% in standard test conditions, energy losses of 14%, and an average inclination of 25° were considered. Starting from these data, SCI and SSI are performed, changing the building dimensions and roof orientations, in order to evaluate how energy security can be improved. The economic benefits are quantified, at a building level, by applying the cost-optimal model, taking into account the existing incentives for the collective self-consumer configuration.

4.4.3 Results

This section shows the main findings of the SCI, SSI and cost-optimal analyses. Different values of SCI and SSI are investigated, according to the orientations, dimensions and PV productions of the residential buildings. The energy and economic benefits are quantified through a cost-optimal analysis considering a period of 20 years.

Self-sufficiency and self-consumption indexes

The first set of analyses examined the impact of the use of two directions for PV installation on SCI and SSI. These two indexes are calculated with hourly details for the year 2016. The results obtained from this first analysis are presented in Figure 10. For the roof North-facing surfaces, different scenarios are considered, using various percentages of surfaces occupied by PV modules from 0 to 100%. It can be seen that the residential buildings with low-consumers can achieve higher values of SSI and SCI than those with high-consumers. The building orientation affects both indexes, especially the SCI.

For example, the maximum achievable SCI for small condominiums, according to S2, is 57% for the building with SE orientation (azimuth of -60°) and 53% for the building with SW orientation (azimuth of +30°). These values become 66% and 61% when considering high-level consumers and the consumption for space cooling (S4). The maximum SSI values are 42 and 44% for S2 and 39 and 42% for S4. The variation in the SCI indicator is greater than in SSI. In addition, buildings with SW orientation (azimuth of +30°) have higher SSI values for buildings with the same SCI. This phenomenon is particularly evident for large condominiums (Figure 87).

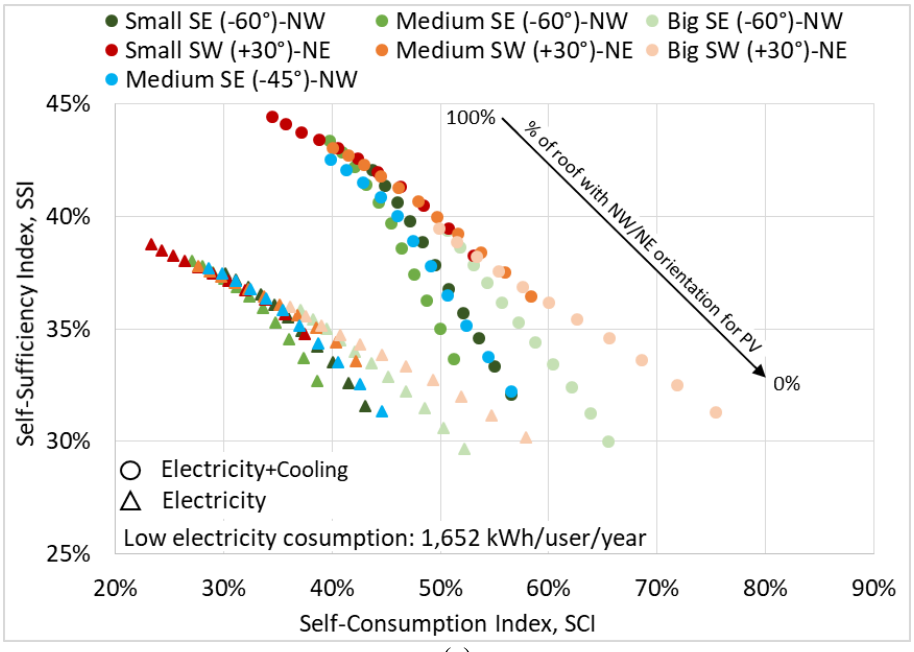

(a)

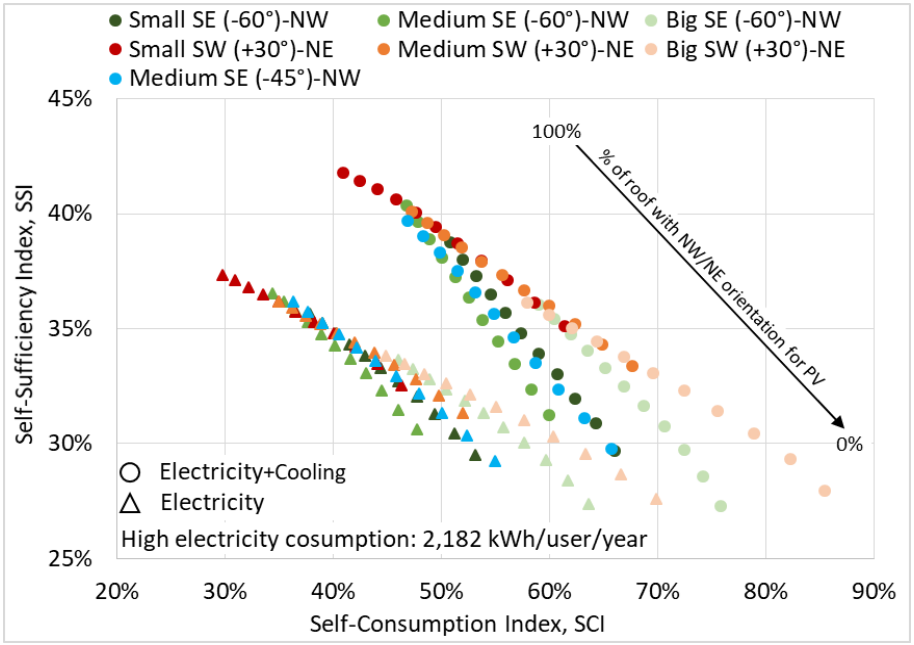

(b)

Figure 87. Analysis of SCI and SSI for condominiums with different dimensions and orientations distinguishing between (a) low-level consumers with an electricity consumption of 1,652 kWh/user/year and (b) and high- level consumers with an electricity consumption of 2,182 kWh/user/year [53].

As far as the building dimension is concerned, it is possible to confirm that small condominiums can achieve higher SSI levels than large ones and, inversely, have lower SCI values, since the SC share is lower than large condominiums that have a higher consumption. In general, increasing the amount of installed PV increases SSI, but at the same time lower SCI values can be seen. This is due to the fact that no storage systems were hypothesized in this study. In fact, it is possible to increase the installed PV power, through the use of storage systems, thereby improving not only SSI but also SCI [54].

Cost-optimal analysis

Results presented here refer to the cost-optimal analysis performed considering a period of 20 years. The initial investment cost is calculated according to the PV installation costs. This cost varies as a function of the installed PV power (*P*). The costs that were applied are: 1,600 €/kWp for 6 kW ≤ P ≤ 20 kW and 1,000 €/kWp for P > 20 kW. The annual energy cost is calculated considering the UD expenses and the SC and OP revenues to which they have been applied the economic incentives that last 20 years. Figure 88 and Figure 89 show the SSI values as a function of the global cost per flat, considering different levels of installed *P* and electricity consumption for low- level (S1, S3) and high-level consumers (S2, S4).

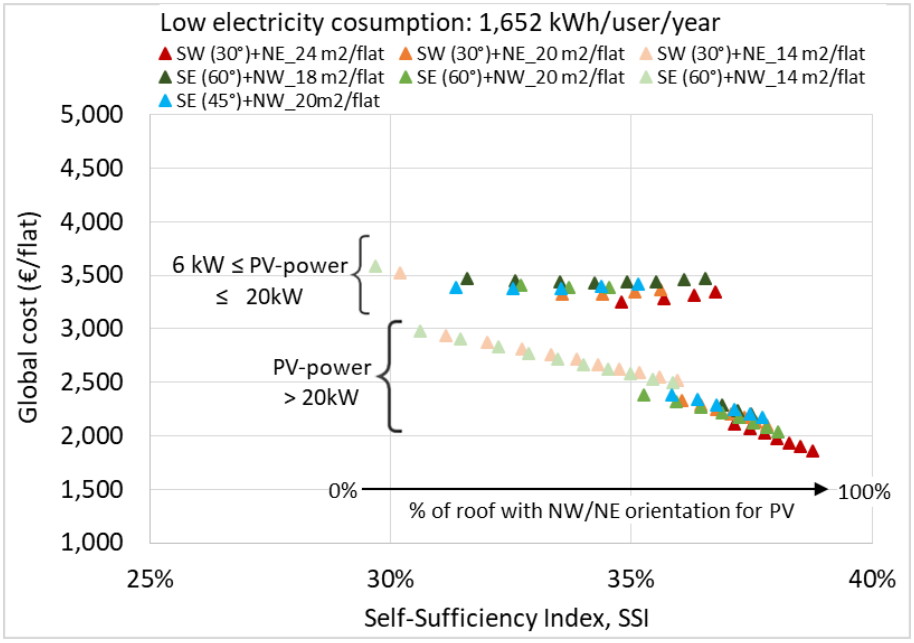

(a)

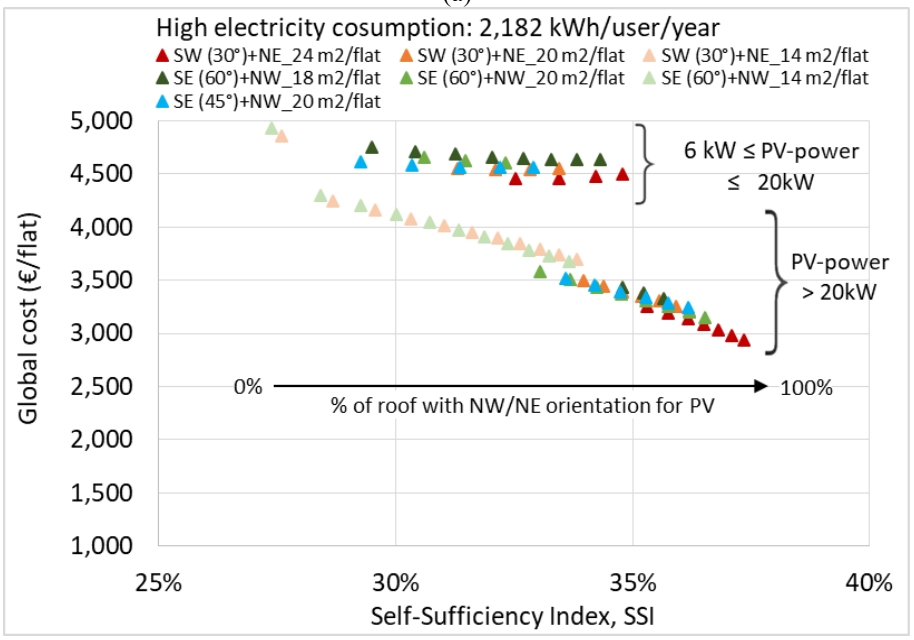

(b)

Figure 88. Global-cost analysis for residential users: SSI as a function of the global cost per flat considering different levels of in-stalled PV power and energy consumption for (a) low-level consumers (S1) and (b) high-level consumers (S2).

In general, as the share of installed PV increases, the SSI indicator increases. The question is whether it is also convenient, in terms of costs, to use two rooftop orientations for the production of solar energy. The size of the PV panels influences the results of the cost-analysis to a great extent. In fact, it is possible to observe that for a lower *P* than 20 kW, the costs are higher than for a higher *P* of 20 kW. The use of the north-facing roof surface is always convenient, from an economic point of view, for a higher *P* of 20 kW, with an improvement in energy self-sufficiency. Instead, the use of the north-facing roof surface is convenient for a lower *P* than 20 kW, where the cost of PV installation is 1,600 €/kWp more than in the other case,

if about 15% of the total surface is used. This percentage varies as a function of the type of electrical consumption (S1, S2, S3 or S4) and of the dimension and orientation of the condominiums. It is possible to observe from Figure 88 that:

- Slightly higher SSI values are achieved for low-level consumers (1,652 kWh/user/year), with a lower global cost than for high- level consumers. Small condominiums reach the highest levels of energy self-sufficiency, and the maxi-mum SSI is 39% for a *P* equal to 22 kW for the well-oriented building (SW +30°, ID30). Moreover, the quota of PV per flat affects the energy self-sufficiency; the higher the quota of PV expressed as m^2/flat is, the more SSI increases.
- It is always convenient to install PV for large condominiums, and when using 100% of the North-facing roof surface, a maximum SSI of 34-36% is achieved for a P of 38-40 kW.
- The global cost per flat varies from 3,600 to 1,850 €/flat for low electricity consumption and from 4,900 to 2,900 €/flat for high electricity consumption.

Similar trends to those described in Figure 89 can be observed when taking into account the total electricity consumption (S3 and S4). It has emerged, from Figure 89, that the global costs are higher whenever space cooling is considered, and the cost of energy in fact increases, but higher SSI values can also be achieved in this scenario. In summary, these results show that the better the orientation is, the higher the energy self-sufficiency and the lower the energy costs and those for the installation of PV technologies.

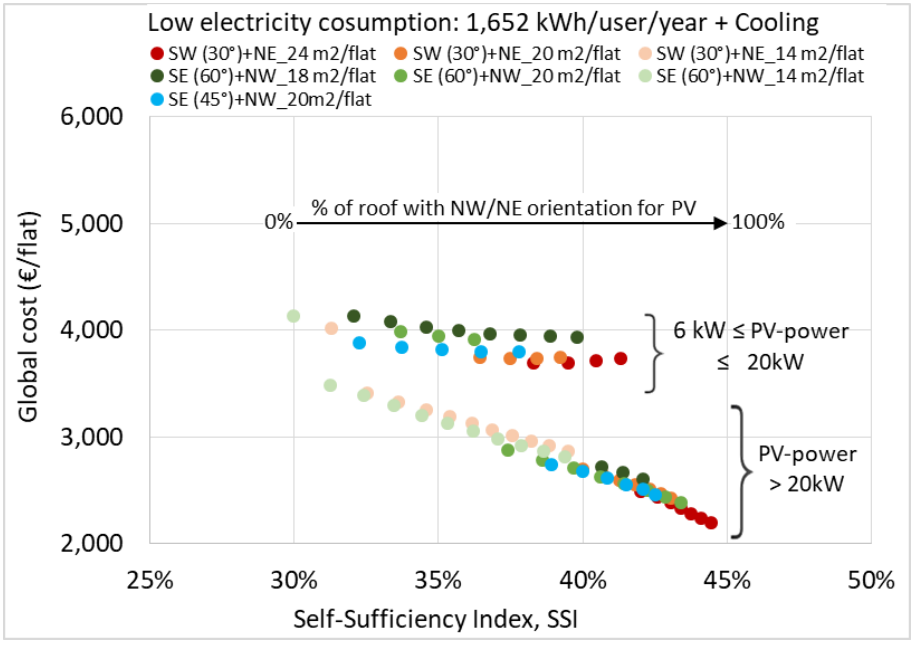

(a)

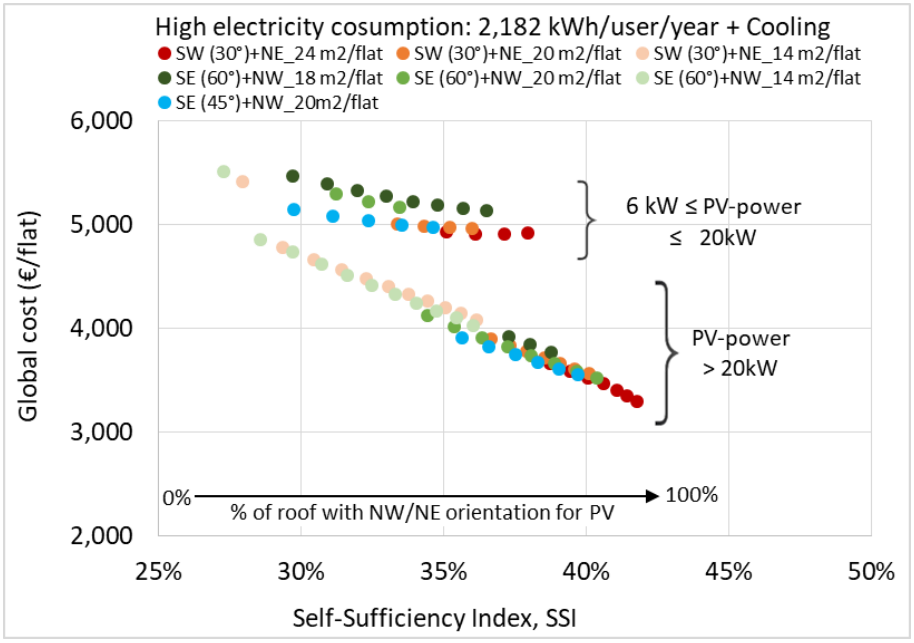

(b)

Figure 89. Global-cost analysis for residential users: SSI as a function of the global cost per flat considering different levels of in-stalled PV power and energy consumption for (a) low-level consumers (S3) and (b) high-level consumers (S4).

Table 37. Energy and economic analysis using one and two rooftop PV orientations according to scenarios S3 and S4 (see Figure 89).

User	Building ID	100% S-area and 0% N-area				100% S-area and 100% N-area				Δ
		SCI (%)	SSI (%)	P (kW)	Global cost (€/flat)	SCI (%)	SSI (%)	P (kW)	Global cost (€/flat)	SSI (%)
Low-consumer	30	57	32	11	4,133	44	42	22	2,608	10
	91	51	34	16	3,991	40	43	30	2,386	9
	211	66	30	20	4,129	51	39	38	2,809	9
	140	53	38	15	3,690	34	44	30	2,192	6
	258	58	36	16	3,740	40	43	30	2,422	7
	199	75	31	19	4,021	50	39	40	2,870	8
	153	57	32	13	3,885	70	43	29	2,457	11
High-consumer	30	66	30	11	5,468	51	39	22	3,774	9
	91	60	31	16	5,294	47	40	30	3,523	9
	211	76	27	20	5,520	59	36	38	4,032	9
	140	61	35	15	4,927	41	42	30	3,298	7
	258	68	33	16	5,012	47	40	30	3,563	7
	199	85	28	19	5,416	58	36	40	4,085	8
	153	66	30	13	5,151	47	40	29	3,550	10

Table 37 summarizes the main results obtained from the energy and economic analysis using one and two PV orientations according to S3 and S4. Small condominiums reach higher values of SSI, but have lower values of SCI than large condominiums. The costs for PV installation are lower if two rooftop orientations are used instead of one, thanks to the quota of installed P (1,600 €/kWp for 6 kW ≤

P ≤ 20 kW and 1,000 €/kWp for P > 20 kW). It can be concluded that SSI on average increases by 8.5% for the use of two PV orientations (100% of the south-area and 100% of the north-area).A last future scenario is investigated assuming a constant lower cost for the PV technologies equal to 1,600 €/kWp (independently by the PV power installed).

Figure 90 and Figure 91 show the results for the cost-optimal analysis of the scenarios: S1, S2, S3 and S4.

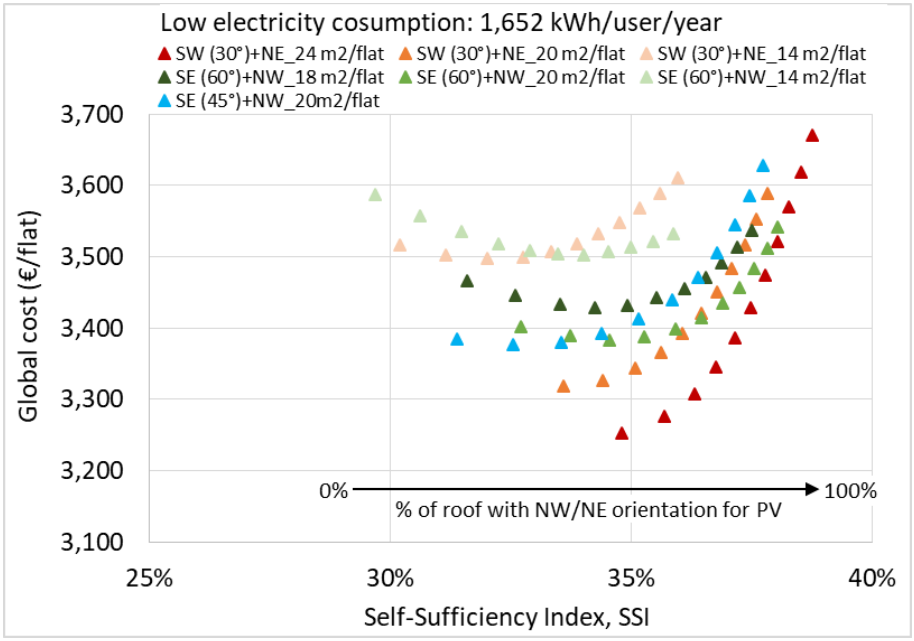

(a)

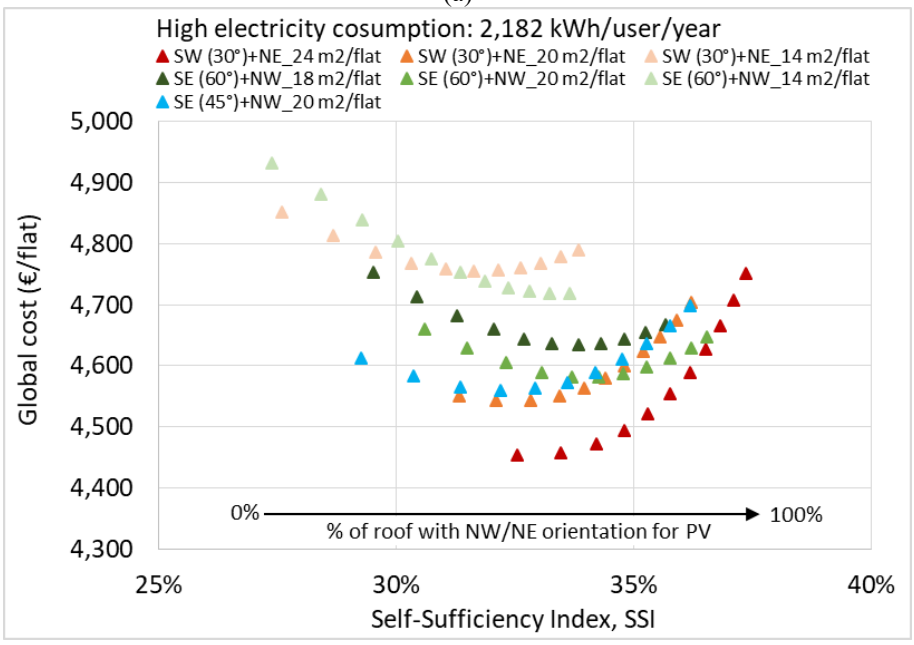

(b)

Figure 90. Global-cost analysis for residential users: SSI as a function of the global cost per flat considering different levels of in-stalled PV power and energy consumption for (a) low-level consumers (S1) and (b) high-level consumers (S2) [53].

It can be seen that the more buildings have a high consumption, the more convenient it is to use two rooftop orientations for the PV installation. In Figure 90 (as Figure 88), the global cost only refers to the energy consumption for light, appliances and condominium utilities. As previous emerged, the global cost for low-level consumers is lower than for high-level consumers and the orientation affects the convenience of the use of two orientations to a great extent. In fact, it is not always convenient to use the entire north-facing roof, especially for well-oriented buildings (SW 30°). The percentage of the north-facing roof that is convenient to use varies according to the shape of the building (e.g. PV surface/number of flats).

The results of the cost-optimal analysis, considering the energy consumption for SC (S3 and S4) are presented in Figure 91.

Again, in this case, the results de-pend on the buildings orientation:

- It is almost always convenient to also use the North surfaces for buildings with a SE-NW oriented roof (more convenient for high-level consumers).
- It is almost never convenient to use the North surfaces for buildings with a SW-NE oriented roof (always a little more convenient for high-level consumers).

With this GIS-based methodology it is possible to perform cost-benefit analyses on an urban scale but considering the specific characteristics of each single building (as for the building represented in light blue with a singular rooftop orientation).

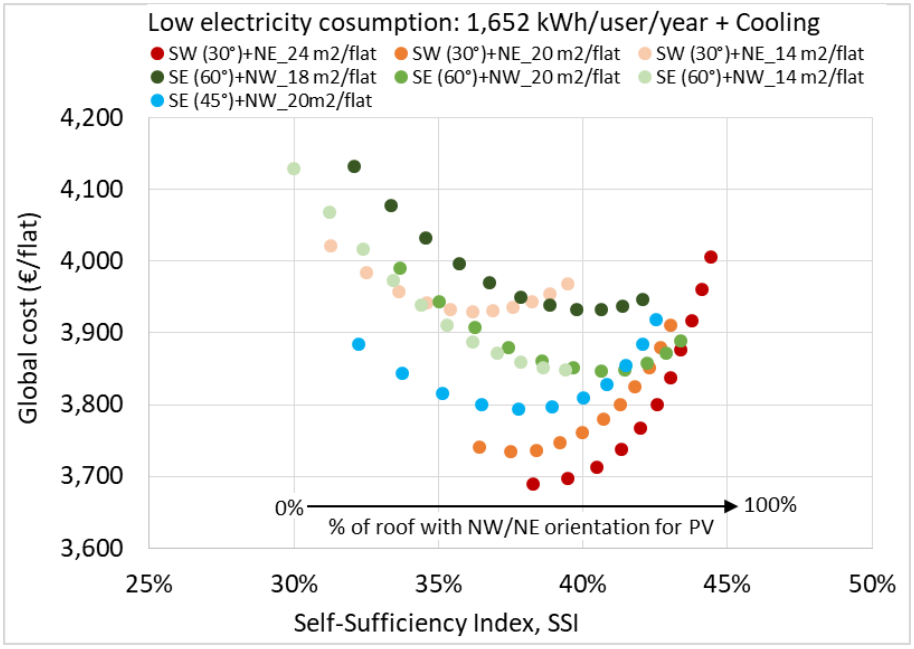

(a)

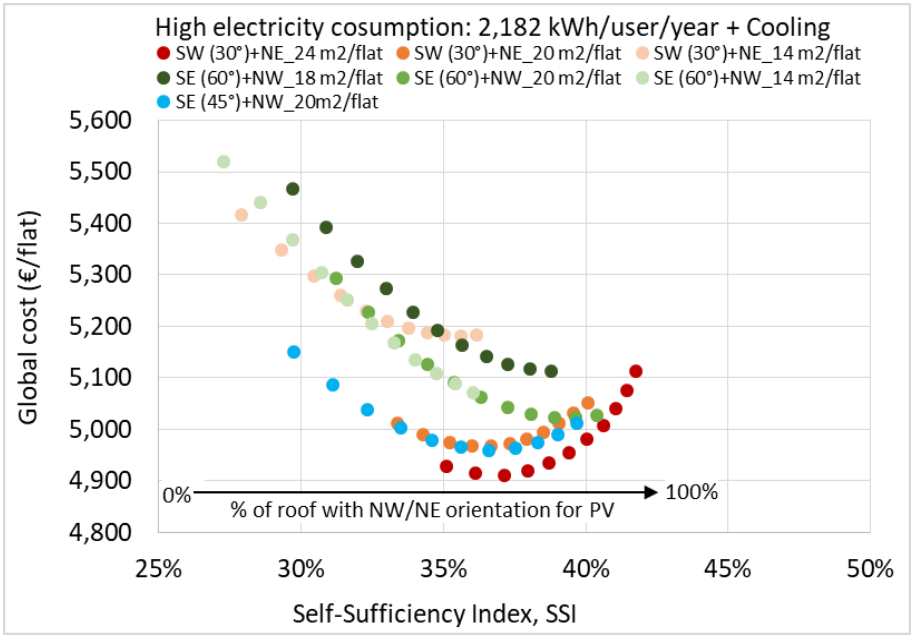

(b)

Figure 91. Global-cost analysis for residential users: SSI as a function of the global cost per flat considering different levels of in-stalled PV power and energy consumption for (a) low-level consumers (S3) and (b) high-level consumers (S4) [53].

To sum up, the results of this investigation show that the dimensions, the types of consumer and the orientations of buildings affect energy self-sufficiency. In general, without using storage systems, as the SCI increases, the SSI decreases more or less quickly as a function of the building typology. When considering the use of two roof orientations, the maximum level of achieved SSI is on average 41.8, 41.5 and 35.7% for small, medium and large condominiums, respectively. The economic benefits are investigated by applying a cost-optimal analysis, which showed that, for the investigated building stock and considering the use of two PV systems orientations, the SSI increased on average by 8.5%, with additional economic benefits for the cost of energy and the cost for the PV installation. The findings in this study provide a new understanding of how to exploit the solar energy potential in order to improve the energy performance of buildings, increase energy security and reduce energy costs.

Taken together, these results provide important insights into the investigation of costs and self-sufficiency of roof-integrated PV technologies on residential buildings using multiple orientations.

4.5 Hourly model by PV technologies and storage system

The aim of the presented methodology is to better exploit the PV production by introducing electric energy storage systems. A methodology to improve the self-consumption and self-sufficiency in high-density built context combining multiple homes at city level is assessed. More in detail, different scenarios using Li-ion battery systems are investigated. The simulation is carried out for one year with hourly time resolution, based on real monthly electricity consumption. The model

is applied to two districts located in the city of Turin with the aim of evaluating the technical feasibility of combining multiple residential users at city level. The purpose is to promote self-consumption and self-sufficiency from the network, using the integration of solar energy with PV-battery systems, and to reduce electrical losses in favour of both the single user and the distribution system. Results show that different values of self-sufficiency and self-consumption can be reached depending on the shape and dimension of each building. It is shown that it is possible to satisfy the current requirements to become an Energy Community in an urban environment with good levels of self-sufficiency.

4.5.1 Methodology

Electrical consumption of buildings depends on socio-economic aspects, on day type and on the number of occupants, but also by its surroundings and local climate conditions able to affect for example the daylight [220,229,230]. Regarding the PV production on rooftops [58], the solar energy potential depends on the suitable roof area available, on the roof slope, and on the roof orientation (south-faced tilted roofs have a higher productivity). In this investigation, two districts in the city of Turin with different socio-economic characteristics and urban environments were analysed. The balance between electrical consumption and PV production is investigated with the aim to improve the self-consumption and the self-sufficiency of residential buildings using storage systems. These two aspects are investigated using the following indexes:

- The self-consumption (SC/P) is defined as the ratio between the energy production that is locally used (SC) and the total PV production (P).
- The self-sufficiency (SC/C) is defined as the ratio between the energy production that is locally used (SC) and the total energy consumption (C).

Figure 92 shows the methodology used for the optimal design of grid connected to the PV-battery systems in urban environment.

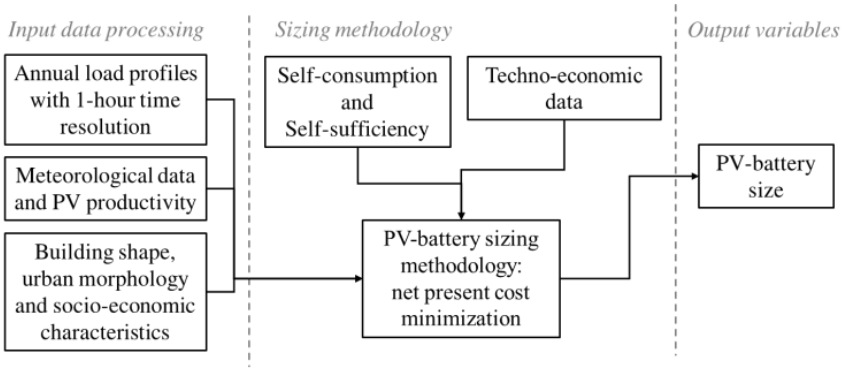

Figure 92. Flowchart of methodology [54].

In the following subsections the input data used to investigate the optimal design of grid connected to the PV-battery systems for a group of residential users are described. The annual load profiles with 1-hour time resolution and the PV productivity are assessed for each user at building level with the support of GIS.

Energy consumption

Hourly load profiles of residential buildings are obtained from monthly measured data of two consecutive years (2016 and 2017) of over 154 buildings. The annual load profile with 1-hour time resolution is generated at building level using as reference the hourly profiles of typical seasonal days (i.e. winter, spring, summer and autumn) for 380-470 residential families with 2.15 components considering both working and non-working days [223]. The average cost of withdrawing electricity from the grid (i.e. 0.22 €/kWh) and the feed-in cost (i.e. 0.10 €/kWh) for prosumers was also derived for this database. In addition, knowing the electrical consumption of each user, with the use of GIS tools, the distribution of electrical consumption at district level has been quantified.

Solar energy productivity

The potential of solar energy in the residential sector is assessed taking into account several criteria used to evaluate the rooftop suitability. The main characteristics, which affect the use of the roof for the installation of PV panels, are the roof shape, architectural characteristics, morphological context, building codes, and regulations. With the use of GIS tools, the potential rooftop area for the installation of PV technologies is identified for each building at district level taking into account the orientation (south, east and west). The hourly radiation data have been elaborated for one year using the PVGIS portal. The solar energy that can be produced on each roof is assessed considering standard PV systems with an efficiency of 14% and an inclination of 20°. Therefore, knowing the maximum installable power for each roof (according to the suitable rooftop area), a procedure to identify the optimal design of grid connected to PV-battery systems is applied.

Sizing methodology

Energy balance simulations have been performed over a reference year considering 1-hour time resolution. An energy management strategy is developed to manage the operation of the power system. The key-decision parameter for the battery operation is represented by battery SOC, which is the ratio between the stored energy and the total battery capacity.

More in detail, when the PV power is lower than the electrical demand, the battery intervenes in discharging mode until reaching the minimum state-of-charge SOC. Finally, electricity is bought from the grid when both PV and battery systems are not enough to cover the whole electrical load. In case instead the PV power is greater than the electrical demand, the surplus renewable energy is first used to

charge the battery and then (when the maximum battery SOC is reached) sold to the grid (Table 38).

The battery SOC is defined as follows:

$$SOC(t) = SOC(t-1) + \frac{P_{BT,ch}(t-1) \cdot \Delta t \cdot \eta_{BT,ch}}{Cap_{BT}} - \frac{P_{BT,dc}(t-1) \cdot \Delta t}{\eta_{BT,dc} \cdot Cap_{BT}} \quad (28)$$

Where Cap_{BT} is the battery rated capacity, $P_{BT,ch/dc}$ corresponds to the charging/discharging power of the battery, $\eta_{BT,ch/dc}$ is the battery charging/discharging efficiency and Δt is the time step of the simulation.

The optimal sizing methodology employs the particle swarm optimization (PSO) algorithm to search for the optimal system configuration (i.e. PV rated power and BT capacity), which allows to minimize the net present cost (NPC) of the power system. The metaheuristic PSO technique was adopted since it is a highly performant and robust method when dealing with the optimal design of power systems [231].

The NPC is computed in the following way:

$$NPC = CAPEX_0 + \sum_{j=1}^{n} \frac{OMC_{tot,j}}{(1+d)^j} + \frac{RC_{tot,j}}{(1+d)^j} \quad (29)$$

Where $CAPEX_{tot,0}$ represents the total initial investment cost, $OMC_{tot,j}$ and $RC_{tot,j}$ correspond respectively to the operation/maintenance and replacement costs referred to the j-the year, n is the system lifetime and finally d is the discount rate (Table 38). The $OMC_{tot,j}$ term is derived as:

$$OMC_{tot,j} = OMC_{PV,j} + OMC_{BT,j} + C_{el,buy,j} - C_{el,sell,j} \quad (30)$$

where $OMC_{PV,j}$ and $OMC_{BT,j}$ correspond to the operation/maintenance costs associated to the PV and battery component, respectively. $C_{el,buy,j}$ is the yearly cost due to electricity bought from the grid and $C_{el,sell,j}$ is the yearly revenue due to renewable electricity sold to the grid (Table 38). A constraint on the self-consumption and self-sufficiency can also be included within the optimization routine:

$$SC/P \geq (SC/P)_{target} \quad (31)$$

$$SC/C \geq (SC/C)_{target} \quad (32)$$

where $(SC/P)_{target}$ and $(SC/C)_{target}$ correspond to the target self-consumption and self-sufficiency values that the PV-battery system must achieve at the minimum system cost.

Table 38. Main techno-economic parameters used in the PV-battery optimal sizing (Li-ion battery) [222,232,233].

Parameter	Value
PV system investment cost	1,000 €/kWp if P > 20kW 1,600 if 6 ≤ P ≤ 20 2,000 €/kWp if P < 6kW*
PV O&M cost	2%/y (of Inv. cost)
BT investment cost (with extra-cost of hybrid inverter)	500 €/kWh*
BT replacement cost	250 €/kWh
BT lifetime	10 years
Maximum BT SOC	1
Minimum BT SOC	0.1
BT discharging efficiency	0.95
BT charging efficiency	0.95
Cost of PV electricity sold to the grid	0.10 €/kWh
Cost of electricity withdrawn from the grid	0.22 €/kWh
Discount rate	5%
System lifetime	20 years

*https://www.solareb2b.it/documenti/ (in Italian).

4.5.2 Case study

According to the annual report of the city [234], electricity consumption in the residential sector from 2004 to 2009 is quite constant with values close to 2.5 TWh/year; from 2010 to 2013 there was a slight decrease of 6%. This trend is presumed to be due to the increase in the energy efficiency of household appliances and electronic equipment. According to the electrical consumption data used, on average the annual electrical consumption of a Turin family is about 1,600 kWh/fam/year (reference years: 2016-2017).

Socio-economic characteristics

Starting from a database elaborated in GIS, the characteristics of the population and the characteristics of the building stock are analysed to identify homogeneous areas. One of the aims is to investigate how and at what extent the variables related to energy, social and urban morphology influence the electricity consumption and the solar energy production of the residential building stock. Two districts called Crocetta (with an extension of 199,251 m^2) and Arquata (with an extension of 108,926 m^2) are selected as homogenous zones. In these districts 80% of the buildings were built before 1945, 15% in 1946-1980, and only 5% after 1992. Crocetta is a district located near the historic city centre and is one of the most prestigious residential areas. The 90% of buildings are residential compact condominiums (with an S/V of 0.48 m^2/m^3), and there are 220 buildings with about 2,500 apartments. Arquata is a social housing district built in 1920 and includes 52 buildings (with an S/V of 0.41 m^2/m^3) for a total of about 1,070 apartments.

The characteristics of the city are described below with an in-depth investigation of the selected districts. In Figure 93 the annual per capita income distribution in €/year (updated to 2009) for 94 statistical zones of Turin (for two of them the information is not available) is indicated. The map shows that the richest areas are located in the city centre and in the hilly area East of the city, while the poorest areas are in the peripheral areas North and South of the city.

The average annual income is about 15,500 €/year, with a maximum of 23,651 €/year and a minimum of 10,122 €/year. The two zones selected for this analysis are indicated in red.

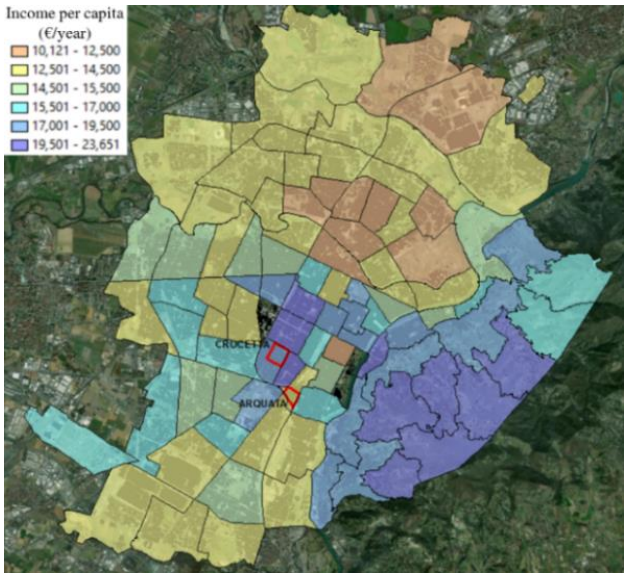

Figure 93. City of Turin: per capita income (at 2009) at statistical zone scale and identification of two case studies [54].

Table 39. Characteristics of the population in the two districts [54].

Variable	**Unit**	**Crocetta**	**Arquata**
N. of inhabitants	-	3,703	1,756
N. of families	-	1,867	937
Components for family	Inh/fam	2.03	1.88
Income per capita	€/year	18,016	14,114
Foreigners inhabitants	%	7	14
Average age	-	48	49
Old-age-dependency ratio[1]	-	242	294
Dependency ratio[2]	%	71	65
Graduates inhabitants	%	32	8
Employed inhabitants	%	95	77

[1] The old-age-dependency ratio is the ratio between the number of inhabitants aged 65 and over (age when they are generally economically inactive) and the number of inhabitants aged between 15 and 64. The value is expressed per 100 persons of working age (15-64). Values higher than 100 indicate a greater presence of elderly population than young population.

[2] The dependency ratio is an age-population ratio of those typically not in the labor force (dependents aged 0-14 and over the age of 65) and those typically in the labor force (the total population aged 15-64).

Table 39 describes the main socio-economic characteristics for these two districts. The information is elaborated using the ISTAT database (updated to 2011) at census section scale and the income database (updated to 2009) at statistical zone scale. Crocetta is a richer area with an annual income of 4,000 €/year higher than Arquata. The other indicators are quite similar, the greatest differences are the percentage of foreigners (highest in Arquata) and the percentage of graduates which is 32% in Crocetta and only 8% in Arquata.

With regard to the building stock, in Turin there are almost 60,000 buildings, of which 76% are residential. The residential buildings are mainly large and compact condominiums, with low values of surface-to-volume (*S/V*) ratio. The 55% has an *S/V* of lower than 0.45 m^2/m^3. On average, the apartments have a heated surface that varies between 75 and 95 m^2/apart; Figure 94 shows the heated surface per apartments (m^2/apart) at statistical zone scale. Comparing Figure 93 and Figure 94 it is possible to observe that, obviously, there is a relation between income and apartments surface. This is just an example of the relationships between the socio-economic variables. In a future work this aspect will be further explored by analysing other areas of the city.

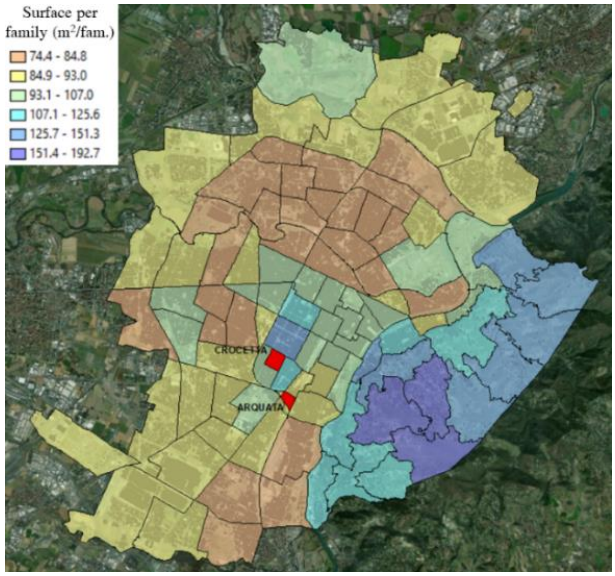

Figure 94. City of Turin: heated surface (m^2) per family at statistical zone scale and identification of two districts [54].

Table 40 describes the main characteristics of the residential building stock in the two districts. The information was elaborated using the Municipal Technical Map (updated to 2019) at building scale and the ISTAT database (updated to 2011) at census section scale. From the analysis emerged that the shape of the building is quite similar in the two districts, but there is a substantial difference, which is the heated surface per apartment. In fact, wealthy families have larger apartments, and the heated surface is 104 m^2/apart in Crocetta and 70 m^2/apart in Arquata.

Table 40. Characteristics of the residential building stock in the two districts [54].

Variable	Unit	Crocetta	Arquata
N. of buildings	-	246	52
N. of residential buildings	-	220	47
Total footprint area (residential)	m^2	55,697	19,151
Gross floor area (residential)	m^2	303,856	89,574
Surface-to-volume ratio	m^2/m^3	0.39	0.39
Heated surface per apartment	m^2/ apart	104	70
N. of apartments per building (average)	-	11	23

Electrical consumption

Starting from the database elaborated in GIS and collecting a large amount of data about the energy-use at building level, the monthly electrical consumption considering only residential users have been georeferenced with the information of the address. About 150 users are selected considering on average an annual electrical consumption of 1,500 kWh/fam/year (anomalous data were excluded from the analysis). In Crocetta and Arquata districts the measured consumption refers to 80 and 42 residential buildings respectively.

Figure 95 and Figure 96 show the residential users: in green the residential buildings selected for the analysis of which the electricity consumption are known and in red the other residential buildings are indicated.

Figure 95. Crocetta district with residential buildings [54].

Figure 96. Arquata district with residential buildings [54].

The monthly electrical consumption from January 2016 to December 2017 have been elaborated. Data are provided by the electric services company of the city, IREN. Figure 97 shows the measured monthly average daily electrical consumption per family (kWh/fam/day) referring to the period from January 1st 2017 to December 31st 2017.

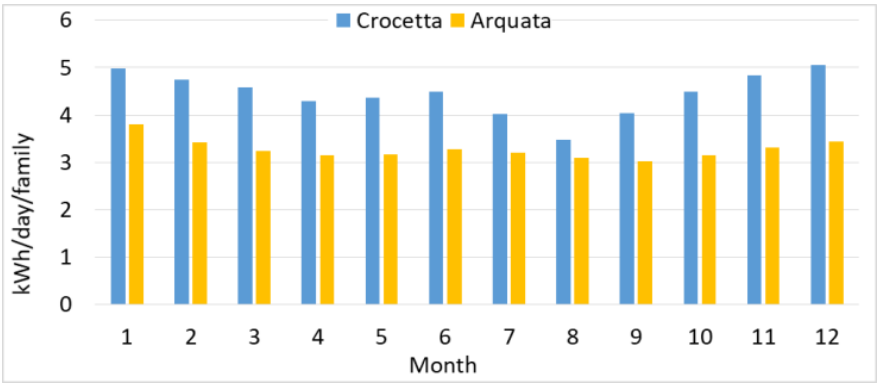

Figure 97. Measured monthly average daily electrical consumption (kWh/day/family) of 122 residential users in the two districts for the year 2017 [54].

From monthly data, and knowing the hourly profiles of some typical days, the energy demand profile for one year with 1-hour time resolution is elaborated. In Figure 98 the average hourly load profiles per family in Crocetta district for non-working days (Sunday) and working days (Monday) distinguishing winter, summer and mid-season periods are reported.

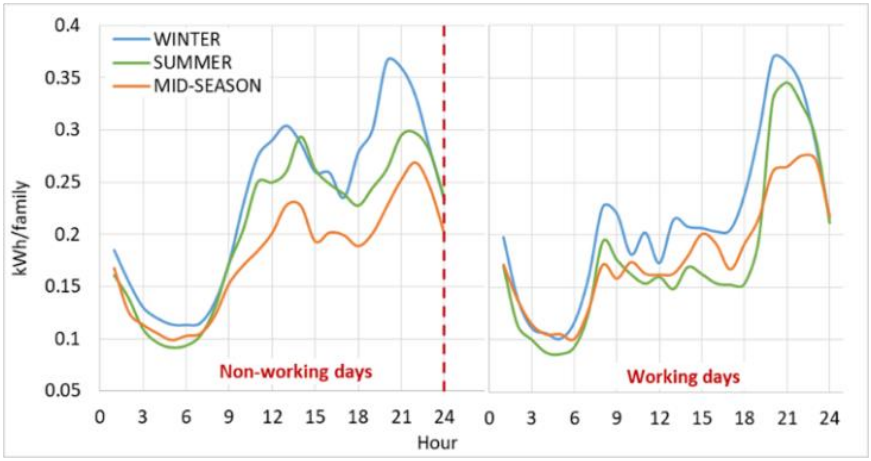

Figure 98. Electrical hourly consumption (kWh/fam) in the Crocetta district for the year 2017 [54].

Photovoltaic potential

Regarding the solar energy production, the quota of suitable rooftop area for the installation of PV technologies is analysed in GIS using the Municipal Technical Map (updated to 2019) and the DSM (updated to 2018) with a precision of 0.5 meters. The potential area is calculated for each roof according to several criteria (i.e. orientation, slope, constrains). In Crocetta and Arquata districts there are respectively 80 and 42 residential buildings with a potential PV area of 17,861 m^2 (73% of total roofs area) and 12,217 m^2 (74% of total roofs area). This potential area considers only the best-exposed solar area and the presence of disturbing elements equal to 15% of roof surface [56].

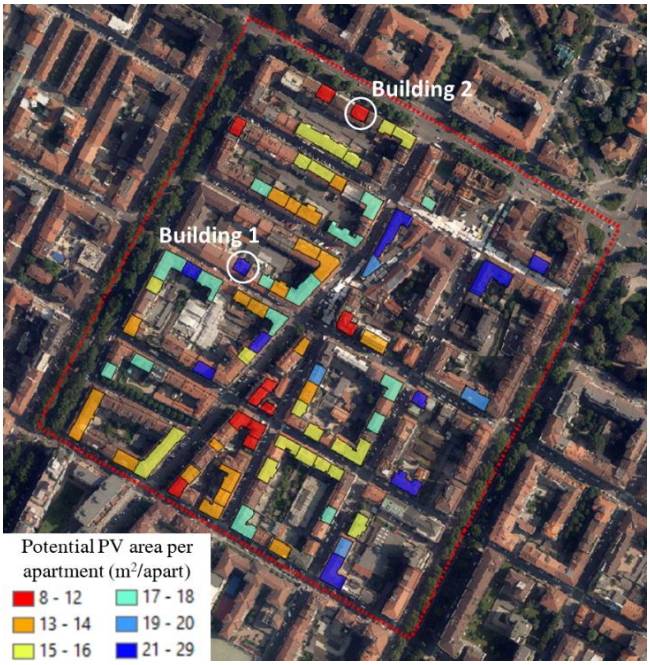

Figure 99. Crocetta district with the potential roof-integrated PV area per apartment [54].

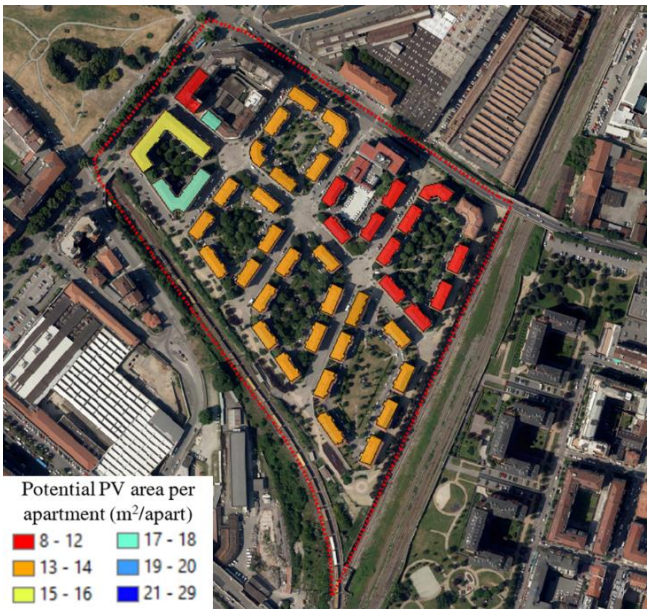

Figure 100. Arquata district with the potential roof-integrated PV area per apartment [54].

An interesting indicator calculated at building scale is the ratio between the potential area for PV installation and the number of apartments (m^2/apart). On average in Crocetta the potential PV is 16 m^2/apart (Figure 99), while is 12 m^2/apart for Arquata (Figure 100). This value is because in Crocetta the heated surface per apartment is 104 m^2/apart while in Arquata, that is a social housing zone with low-income, the heated area per apartment is 70 m^2/apart. In Figure 99 and Figure 100 the potential PV area according to the number of apartments (m^2/apart) at building level is indicated. The solar energy production depends not only on the quota of the potential PV area, but also on the area orientation; in fact, according to the exposure there are different values of solar irradiation. Table 41 shows the main information used as input data. Electrical consumption depends significantly on income, and in this case the consumption per apartment is higher in Crocetta.

Table 41. Electrical consumption and PV production data of the residential buildings in the two districts [54].

Variable	**Unit**	**Crocetta**	**Arquata**
N. of buildings	-	80	42
N. of apartments	-	1,174	976
Annual consumption per family	kWh/fam	1,660	1,180
Potential PV area	m^2	17,861	12,217
Max PV power	kW	2,223	1,527

4.5.3 Results

In this investigation, different residential districts with various building dimension and shape are investigated with the aim to improve self-consumption (SC/P) and self-sufficiency (SC/C) with roof-integrated PV technologies in the city

of Turin. At building level each house individually attempts to match energy demand and supply, and when the energy demand cannot be met by the PV-battery system of that building, it is satisfied from the grid. While at district level demand shortages are satisfied from the solar energy produced by the entire district [235], in fact with the establishment of REC it is possible to further optimize power demand and supply. Referring to the constraint in the Regional Decree n.18-8520/2019 for the establishment of ECs, the self-consumption limit of SC/P ≥ 70% is considered, and different scenarios are investigated with the aim to improve the SC/C. If the PV energy production is low, the SC/P is high, because all the self-produced energy is consumed; in this case the SC/C is low. To increase the SC/C, it is necessary to produce more PV energy, but then SC/P decreases. The ideal solution would be to have both SC/P and SC/C equal to 1, but techno-economic limitations will occur by increasing both SC/P and SC/C when reaching certain thresholds [204]. The analysis is conducted at building and district levels. Scenarios analysed in this work are indicated below:

- In scenario 1 the size of PV-battery system was identified according to the optimal configuration without limits (S1).
- In scenario 2 the PV-battery system was sized to achieve at least 70% of SC/P (according to the requirement in the Regional Decree) (S2).
- From scenario 3, considering the SC/P limit (70%), the PV-battery system was sized to achieve different levels of self-sufficiency (SC/C).

Collective self-consumer configuration

The results at building level of two buildings with different shapes located in Crocetta district are described below. Table 42 shows the main characteristics of the two buildings in Crocetta (see Figure 99).

Table 42. Characteristics of two buildings in Crocetta district [54].

Variable	Unit	Building 1	Building 2
Height	m	12	30
Surface-to-volume ratio	m^2/m^3	0.30	0.22
N. of apartments	-	6	16
Annual consumption per family	kWh/fam	1,770	2,052
Potential PV area	m^2	150	170
Max PV power	kW	19	21
Max PV area per family	m^2/fam	25	10

The buildings have the same orientation, roof type, surroundings context, type of user (i.e. residential user with high consumption), and the potential PV area is very close, with the substantial difference that 6 families live in building 1, while 16 families live in building 2. So even if the annual consumption per family is similar, the electrical demand of building 1 is 10,622 kWh/year while is 32,832

kWh/year in building 2. This difference depends on the shape and dimension of the building (or compactness), in fact the first building has only 3 floors, the other one 8 floors. Consequently, the potential area for each family to produce electricity from PV panels will be higher in the first case (with 25 m^2/fam) than in the second one (with 10 m^2/fam).

In Table 43 there are the information of PV rated power and BT capacity for different scenarios with SC/C values.

In the first scenario (S1), the model identifies the optimal system configuration without limits, and for these buildings, the two indicators SC/P and SC/C reached close values (52-51% and 32% respectively). The optimal PV size is 7 kW for building 1 and 21 kW for building 2, with which, however, 70% of SC/P is not reached. Unlike building 1, it can be notice that the maximum installable PV size – due to the shape and the dimension of the building (with greater number of families, therefore greater consumption but similar potential PV area) – is reached by building 2 in S1. As batteries are not cheap, it is found to not be required within the optimal configuration in S1. In fact, batteries are used only when constraints on SC/P and SC/C were introduced (from S3).

In the second case (S2), a self-consumption of at least 70% has been imposed, and this has reduced the quota of PV installed at the expense of self-sufficiency (SC/C equal to 27%). Also in S2, the BT is not necessary (the smaller the PV, the more SC/P increases).

From S3, different configurations have been investigated in order to have the SC/P ≥ 70% and different levels of SC/C up to the maximum achievable. The self-sufficiency constraint (from S3) introduces the need for a battery. From these results the main difference between the two buildings emerged: (i) building 1 can achieve higher values of self-sufficiency with SC/C equal to 93%; (ii) while building 2 with a high consumption compared to the installable PV potential cannot go beyond a self-sufficiency of 59%, and given that the maximum PV potential is used immediately to reach an SC/P of 70%, the PV production remains constant, and to increase the SC/C it is necessary to drastically increase the size of the BT. By increasing the SC/C of the building the BT size increases to a point where it becomes very sharp (e.g. S6 for building 1, S4-S6 for building 2); it corresponds to unfeasible solution for a technical-economic point of view.

What is interesting about the data in Table 43 is that, taking into account the limit of SC/P ≥ 70%, building 1 can achieve an SC/C of 70% with 12 kW of PV (where the maximum installable power is 19 kW, see Table 42) and 18 kWh of BT; while building 2 can achieve an SC/C of 50% with 21 kW of PV (that is the maximum installable power) and 37 kWh of BT. Obviously this depends on the electrical consumption of buildings and on the PV potential (according to the usable area and the orientation).

Table 43. Annual results at building level: comparison between two buildings in Crocetta district [54].

Scenario	Building 1			Building 2		
	Input	Output		Input	Output	
	SC/C %	PV kW	BT kWh	*SC/C* %	PV kW	BT kWh
S1	32	7	0	32	21	0
S2	27	4	0	27	13	0
S3	50	8	9	50	21	37
S4	60	10	13	55	21	71
S5	70	12	18	57	21	221
S6	97	17	1,787	59	21	1,188

In Figure 101 and Figure 102 the main hourly results of building 1 for S3 and S5 referring to 12 typical monthly days are indicated. In Figure 101a from March to October only a quota of energy demand was covered by PV and BT. In Figure 101b for the same months the energy demand is almost totally covered. In this first analysis, taking into account only the building shape, it is emerged that small buildings with lower consumption are better suited to achieve higher levels of SC/P and SC/C than large and compact condominiums. In general, SC/P and SC/C depends on building shape, roof type, solar exposition, type of user, surroundings context and local climate conditions. Therefore, in future work these aspects will be investigated comparing several areas in the city of Turin.

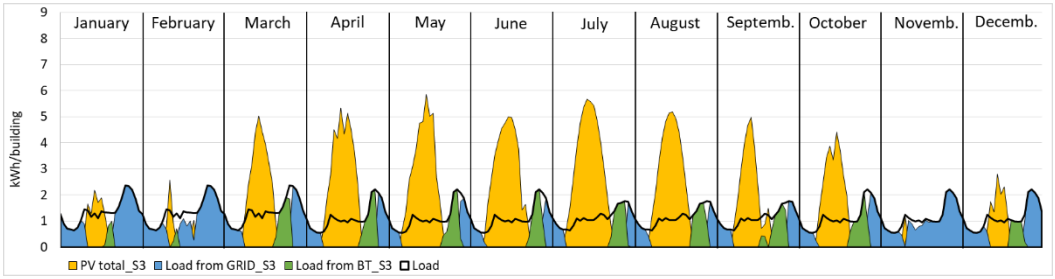

Figure 101. Hourly results for 12 typical days each representative of a specific month of the year (2017): Building 1, Scenario 3 [54].

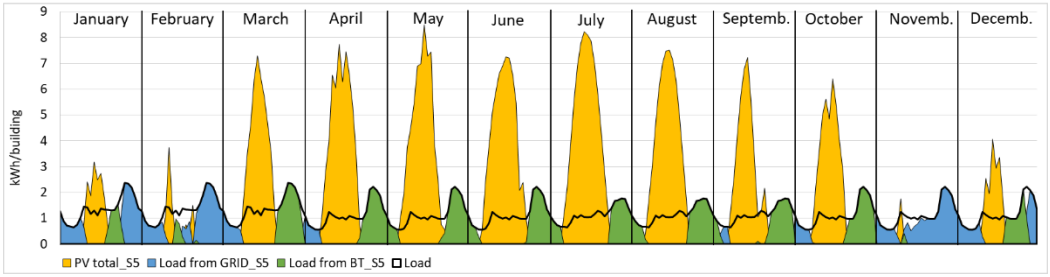

Figure 102. Hourly results for 12 typical days each representative of a specific month of the year (2017): Building 1, Scenario 5 [54].

Therefore, in case of a group of residential buildings with different shapes and electrical consumption, when willing to optimize SC/P and SC/C it is necessary to move from the building scale to the district one.

Renewable energy community

In this section the results at neighbourhood level, comparing Crocetta and Arquata districts, are described. As previous mentioned (see Table 41), a first parameter investigated is that the electricity consumption per family in the richest area, Crocetta, is higher than the other (Figure 103 and Figure 104). The analysis made at the district scale confirms that the national and regional requirements to become ECs are met. According to regional limits: (i) the electrical contiguity is verified; (ii) the amount of electricity consumption of the two districts exceeds the limit of 0.5 GWh/year (the consumption are 1.9 and 1.2 GWh/year for Crocetta and Arquata respectively); (iii) the annual self-consumption from solar energy is higher than 70%; (iv) there is a plurality of energy producers and consumers. In analogy to the analysis made at the building level, the scenarios analysed at district level were: S1 without constraints, S2 with SC/P ≥ 70%, and from S3 onwards with SC/C ≥ 50-60-… up to the maximum achievable (the BT enters the optimal configuration from S3 onwards when SC/C constraint was added).

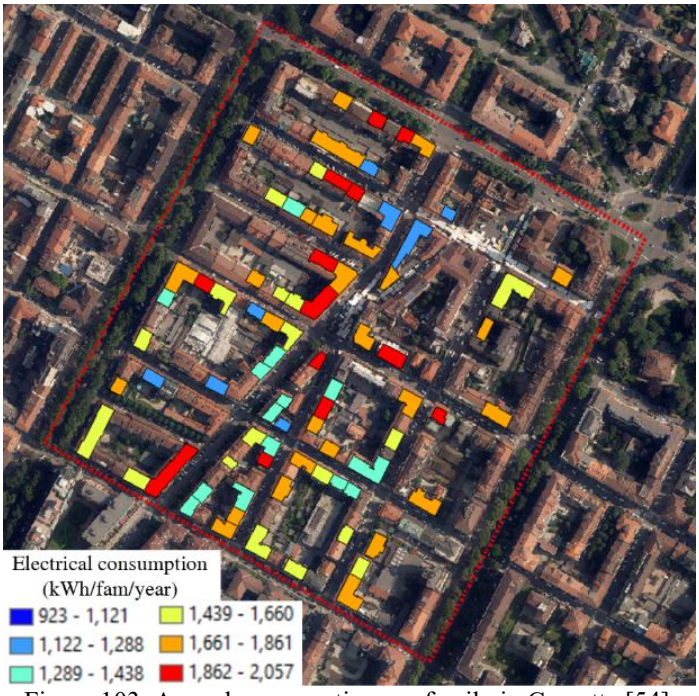

Figure 103. Annual consumption per family in Crocetta [54].

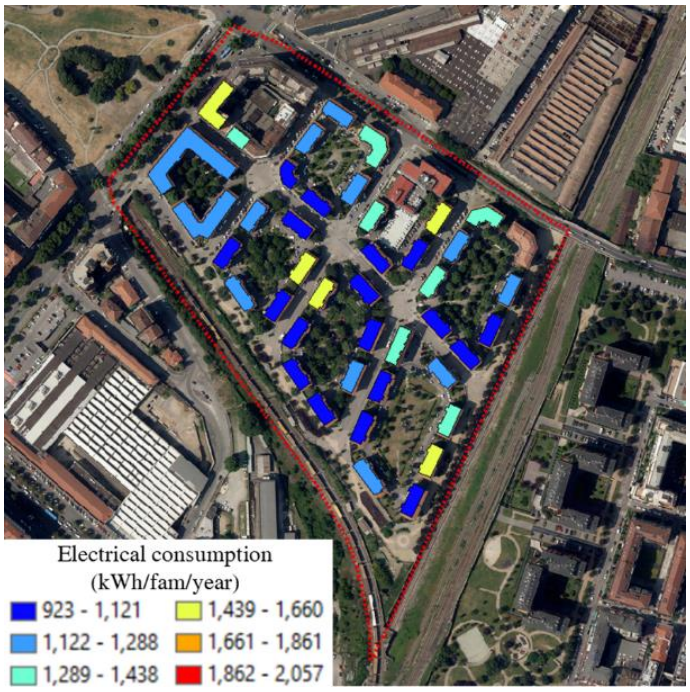

Figure 104. Annual consumption per family in Arquata [54].

Knowing that the maximum installable PV power and the annual electrical consumption are: 2,233 kW and 1,938 MWh in Crocetta and 1,527 kW and 1,185 MWh in Arquata, from Table 44 emerged that:

- In both districts, referring to scenario S2, it is not necessary to use the maximum PV power, and the SC/P constrain (70%) by installing 756 kW of PV in Crocetta and 461 kW of PV in Arquata was respected.
- In Crocetta district, imposing a constraint of at least 70% self-consumption, at most it is possible to reach an SC/C of 53%, by installing 1.36 kW/family of PV and 1.56 kWh/family of BT (S4).
- In Arquata district, imposing a constraint of at least 70% self-consumption, at most it is possible to reach an SC/C of 67%, by installing 1.31 kW/family of PV and 1.97 kWh/family of BT (S6).
- Since in Arquata district the electrical consumption per family is lower than the other district (see Table 41), it is possible to have greater self-sufficiency with the same self-consumption. At the same time, the values of potential PV area per family in Arquata are lower than in Crocetta. Therefore, in these two districts, the energy consumption has a greater influence than the potential PV area on the self-sufficiency achievable.
- Compared to the analysis at building scale, with the establishment of an EC at district level it is possible to have a self-consumption greater than 70% and good self-sufficiency (that varies between 53% and 67%) with reasonable PV and BT sizes.

Table 44. Annual results at district level [54].

	Crocetta			Arquata		
	Input	Output		Input	Output	
	SC/C %	PV kW	BT kWh	*SC/C* %	PV kW	BT kWh
S1	32	1,205	0	31	686	0
S2	27	756	0	27	461	0
S3	50	1,498	1,580	50	939	1029
S4	53	1,592	1,831	60	1,149	1,538
S5	-	-	-	66	1,237	1,962
S6	-	-	-	67	1,277	1,919

Figure 105 and Figure 106 show in detail the sizes of PV and BT installed according to different values of SC/C, maintaining the SC/P greater than or equal to 70% (from S2 to S4 or S6).

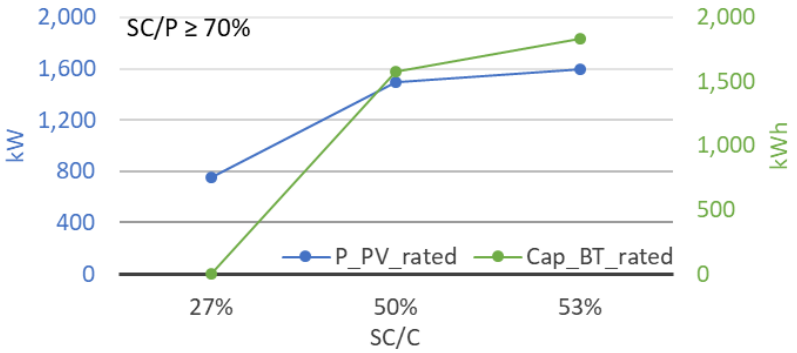

Figure 105. Crocetta district: PV installed power and BT capacity according to different SC/C values and SC/P ≥ 70% [54].

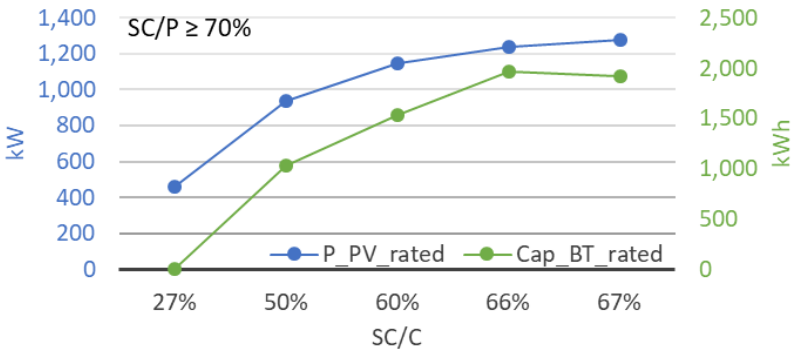

Figure 106. Arquata district: PV installed power and BT capacity according to different SC/C values and SC/P ≥ 70% [54].

Figure 107 and Figure 108 show the influence on the system operation when considering different values of SC/C for two different days of the year.

Figure 107 reports the hourly results of Crocetta district referring to December 18th 2017. In S4 it is possible to observe that from 3 to 6 pm there is no availability of PV and the energy is not taken from the grid (as in S2) but the energy demand was covered by the BT. In the summer (Figure 108), the PV production is obviously

higher than in the winter period and the BT can cover the energy demand from 6 to 11 pm (S3).

Is moving to the district level, it is possible to satisfy the EC requirements by achieving a good level of self-sufficiency for all the buildings belonging to the EC. It should also be considered that an EC can benefit from higher incentives than a configuration at single building level (National Decree of 15th September 2020). The economic aspect will be more in depth explored in future work.

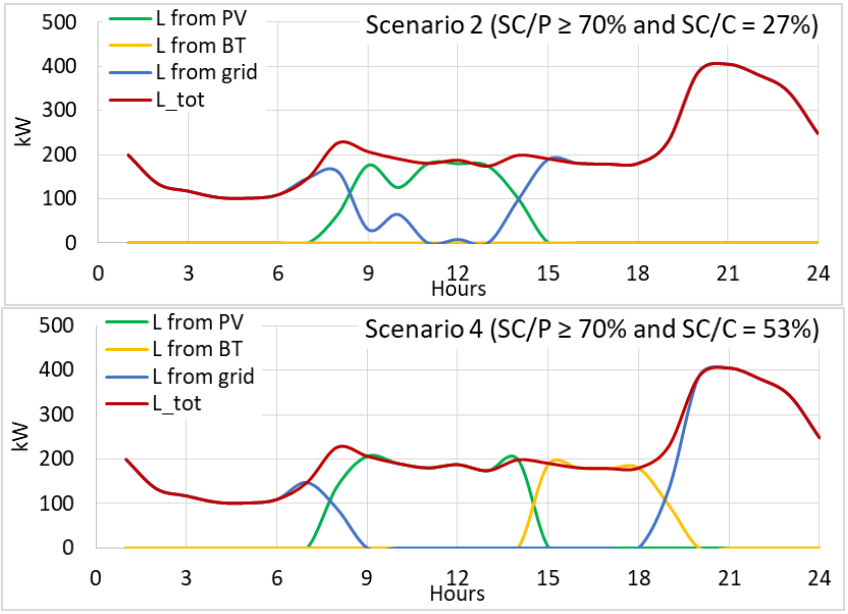

Figure 107. Crocetta district: December 18th, 2017 [54].

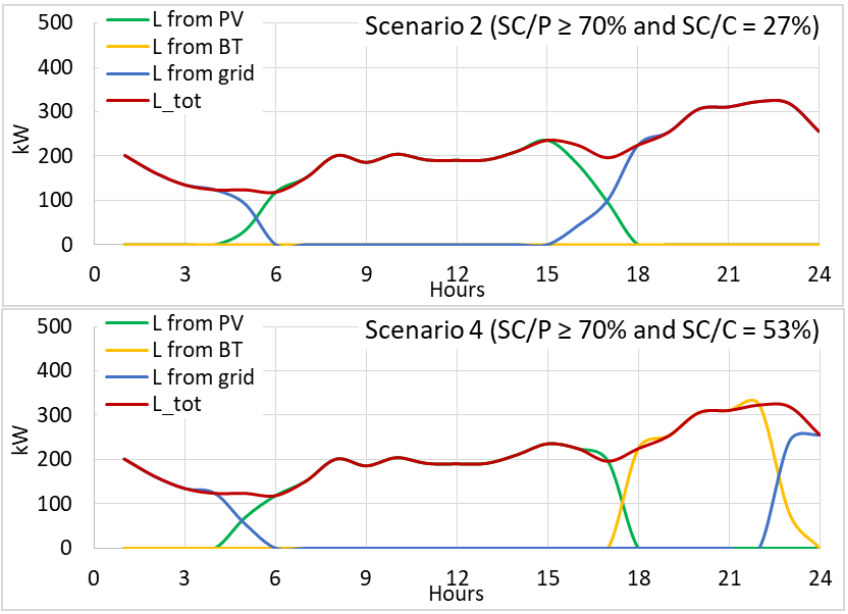

Figure 108. Crocetta district: August 24th, 2017 [54].

In summary, results show that at building level it is possible to activate the collective self-consumption mechanism, given that National and Regional requirements are respected. At the same time, at district scale it is possible to establish an REC in order to have a higher level of self-sufficiency for the whole group of residential buildings. Simulated scenarios show how imposed constraints on self-sufficiency and self-consumption rates can widely affect the optimal capacity of installed PV and storage units. Minimum targets on the self-sufficiency of buildings will drive the installation of more PV capacity and storage capacity. On the other hand, a set minimum ratio of self-consumption will lead to less solar installations and no role of batteries. In an urban environment with buildings that have the same orientation and type of user, high levels of SC/C and SC/P are more easily achieved with low and compact buildings. In cities, however, the typical form of the building is a big and compact condominium, so to improve SC/C and SC/P it is necessary to move from the building scale to the district scale. From this first investigation, it emerges that the shape of the building has a significant influence on SC/C and SC/P, therefore the urban context of a neighbourhood is fundamental to improve energy efficiency at city level. In particular, to produce energy from RESs, it is necessary to mediate the urban form with energy productivity. Urban planning policies promote a building development in height, in order to reduce permeable surfaces; but with this type of urban development, the energy productivity from solar decreases. For solar technologies, it is necessary to build volumes compatible with the available roof surface.

Chapter 5

Place-based energy efficiency models and low-carbon scenarios

5.1 Chapter overview

The aim of this chapter is to cover the gap between single-building investigation perspectives and the larger scale (neighbourhoods, districts, cities) in order to achieve energy savings, mitigate the urban heat island, and improve indoor or outdoor thermal comfort (Figure 109).

The first part of this chapter shows how to design energy efficiency models. The combined effect of DHN expansion with different buildings retrofit scenarios, using the energy performance certificate database of the Piedmont region, is investigated to reduce GHG emissions [13,55].

The shape of cities, the characteristics of outdoor surfaces and the energy performance of the built environment influence not only the energy performance of buildings but also the thermal comfort conditions and the liveability of urban spaces.

Smart solutions for the city of Turin are identified to mitigate the UHI effect and improve thermal comfort conditions. The potential of urban rooftops and outdoor surfaces are investigated, analyzing the effect of green and high-reflective roofs and solar energy technologies. The applicability of smart solutions is conducted in support of the review of the Building Annex Energy Code of Turin. This is performed within the 'Re-Coding' project, undertaken by the Research Centre Future Urban Legacy Lab (FU*LL*), which aimed to update the current building code of the city. Environmental, economic and social impacts have been assessed to identify the more effective energy efficiency measures [56,57].

Finally, applying the hourly process-driven model, the optimal shape of the buildings with low energy consumption for heating and cooling and high solar energy production has been defined for different urban neighbourhoods [49,58].

For the same neighborhoods, the outdoor thermal comfort conditions are investigated as a function of the urban form using existing climate tools [59].

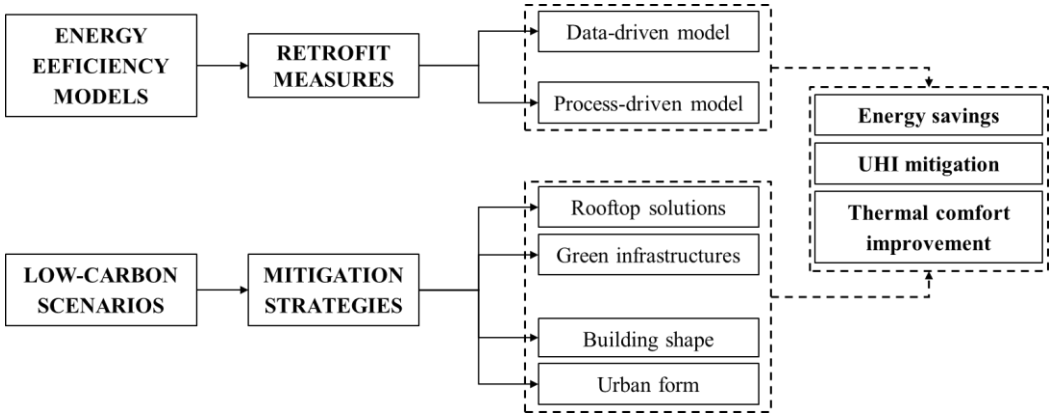

Figure 109. Flowchart of Chapter 5

5.2 Energy retrofit models

The improvement of the energy efficiency (EE) is essential to mitigate the GHG emissions, including enhanced air quality, increased social welfare, market competitiveness and creation of jobs [3]. The use of renewable energy and an increase in EE are two essential solutions to address the energy crisis. Considering the long life of buildings and the low demolition rate that characterize European building stocks, the considerable retrofit of buildings is crucial to reach successful energy saving goals [236]. Most of the building stocks in Mediterranean cities have too high energy consumption and, the Italian building stock is quite old and not adequately renovated. Data of residential buildings shows that 44% of them were built before 1961, 45% of buildings were built between 1961 and 1991, and 11% between 1991 and 2011 [237]. In order to decrease the energy consumption in the existing buildings, a diffused and effective retrofit strategy is needed. The actions of the local authorities and the effectiveness of municipal energy action plans play a crucial role. The existing European policies should be able to improve the energy performance of this housing stock promoting EE measures [238].

District heating (DH) systems can play a significant role in achieving sustainability in building related energy production and distribution [239]. DH systems are useful to reduce the impact on the environment (GHG emissions) and to decrease the fuel demands using the cogeneration combined with other efficient technologies [240,241]. Information about the existing building stock, cost-benefit analysis of EE renovation, possible reductions in energy use and socio-economic impacts on territory at different scales (regions, cities, districts and neighbourhoods) are important to facilitate policy-makers in identifying appropriate strategies and to support stakeholders [82]. The feasibility of retrofit measures in Turin, with the existing energy policies, depends mainly on: the period of construction that affects the need to renovate a building; the level of use of the

building (percentage of occupied apartments), the inhabitants' educational level, the per capita income and the employment rate.

To improve the EE of buildings it is possible to use different solutions considering the characteristics of the urban context. Individual condensing boilers represents the best solution at the single building level, but at urban level, the connection to the DH network is more advantageous due to the more efficient technological mix.

In most developed countries, heating, cooling and electricity are available in all buildings, and cost is often a driver to determine if replacing individual end-user systems to a DH system is a viable solution. In low-density context, DH system may not offer any economic advantage, due to the high costs [242,243]. In fact, DH tend to be more economic for higher density and more populated regions, and governments can facilitate greater use of the DH technology through appropriate incentives [244].

5.2.1 Retrofit measures

European Directives have introduced several instruments and tools to help achieve energy and climate targets [245–247]. The energy performance certificate (EPC) scheme was introduced, with Energy Performance Building Directive 2002/91/EC of December 16th, 2002, as a mandatory national scheme for both new buildings and some categories of already existing ones. An EPC scheme has the aim of monitoring and promoting energy performance (EP) improvements in buildings, by increasing the EE and reducing the GHG emissions of such buildings [248].

The scope and implementation details of the EPC scheme vary significantly from EU country to country. Italy introduced energy certification in 2005 with Legislative Decree no. 192 of August 9th, 2005, on the 'Implementation of Directive 2002/91/EC' related to the EP of buildings. In line with the EU directive [60], Italian legislation has adapted its EE and consumption reduction goals to European Directive EPBD 2002/91/EC. The Italian Decree introduces a number of elements, such as the minimum requirements regarding the EP of buildings and mandatory energy certification to manage energy consumption and increase EE. Article 6 on 'Energy performance certificate, release and posting' introduces certification for existing and new buildings to improve their EP. EPC –which in Italy is called 'APE' (*Attestato di Prestazione Energetica*)– certifies the EP of a building on the basis of its energy class, from A+ (more efficient) to G (less efficient). On October 1st, 2015, a new APE replaced the former certificate, and one of the novelties concerns the introduction of 10 energy classes (there were only 8 classes before October 1st, 2015). The energy class is supplied together with a numeric value that indicates he energy consumption expressed in kWh/m^2/year. APE includes information on heating and cooling systems, domestic hot water production and ventilation. EPC

generally gives information on energy consumption and the possibilities of reducing it through EE measures [249–251].

EPC is also an information instrument for the owner or buyer of a building, when a building is sold, or of the tenant, in the case of leasing a property [252,253]; in some cases, there is a positive correlation between EP and the property value of buildings. In Italy, since January 1st, 2012, APE has become mandatory when a house is put up for sale or for renting (i.e. renting a house out for more than 30 days, selling a new building, donating a house, and/or renovating a house by improving the energy performances). APE is also required to have access to tax incentives –in the form of *eco-bonus* (from 50 to 85%) or *super-bonus* (110%)– after retrofitting interventions. On June 10th, 2020, Legislative Decree no. 48, which amends Legislative Decree 192/2005, implemented EU Directive no. 844 of May 30th, 2018, on the Energy Performance of Buildings. The main changes that were introduced pertain to the calculation methodology that is adopted and the increase in sanctions in the case of buildings without any APE. Furthermore, the establishment of a national energy register, in which data should be collected related to the energy consumption of public and private buildings, was strongly recommended.

Methodology

To define energy efficiency scenarios, the EPC database of the city of Turin is georeferenced and elaborated with GIS tools. The analysed database is composed of over 55,000 certificates of which 75% referred to buildings served by the district heating network (DHN). The data are processed using a statistical analysis to discard any anomalous data, and the certificates of residential building are grouped into clusters to identify EE measures according to the type of retrofitting interventions and to the installation of renewable energy technologies.

This section describes the information obtained from the EPCs and the methodology used to process and elaborate such information. EPCs give information on the annual energy demand, including the energy requirements (energy label), and recommendations to improve EP. The main data contained in the EPCs used to elaborate the database refer to: coordinates, address, type of users, geometrical characteristics (i.e. *S/V* ratio and net heated area), construction period, motivation for the EPC release, EP and the energy label. Coordinates and addresses were used to georeference the database in the GIS; the type of users, the geometrical characteristics and the construction period are the main energy-related variables used to identify the building clusters, while the motivation for the release of an EPC was considered to assess each cluster; EP and the energy label are used to analyse the EP of the buildings of each cluster. The procedure used to process the database and discard the anomalous data is based on median values of EP intensity (kWh/m^2/year) for each type of building and homogeneous group of EPCs. In addition, the normal distributions of the EP values, U_{op}, U_g, η_H and η_{DHW}, are produced in order to implement the statistical analysis. Such processing data is in

fact fundamental; it has emerged from the literature [65,254,255] that, in order to describe the building stock, EPC databases have to be corrected by improving the accuracy and quality of the data. The following five steps are used to process the EPC database:

- *Acquisition and analysis of the EPCs*. EPCs from the regional database – from November 2009 to September 2015– pertaining to the city of Turin and to the area served by the DHN are georeferenced using information on the coordinates and the addresses indicated in the certificates. The EPCs were then classified according to the type of users. The following eight categories were considered in the EPCs:
  - E.1 (1) residential buildings used as permanent residences;
  - E.1 (2) residential buildings used for residence with occasional occupation;
  - E.1 (3) buildings used as hotels or similar activities;
  - E.2 buildings used as offices or similar activities;
  - E.3 hospitals, nursing homes and clinics;
  - E.4 buildings used for recreational, associative or religious activities or similar;
  - E.5 Buildings used for commercial activities;
  - E.6 buildings used for sports activities;
  - E.7 buildings used for school activities;
  - E.8 industrial buildings heated for the comfort of the occupants (according to Italian Decree 412/93).

The EPCs investigated only referred to buildings used as residences or similar, that is, the E.1 (1) and E.1 (2) categories.

- *Classification of the type of residential buildings*. The considered residential buildings are classified as flats or detached houses, to differentiate between the building typologies, using the *S/V* values. The *S/V* ratio is indicated in the EPCs and it is also calculated by means of GIS tools for verification purposes. Most of the EPCs located in the city were flats in condominiums (96.8% in Turin).
- *Classification of the construction period*. Eight classes are identified considering the construction period of the residential buildings: before 1918, 1919-1945, 1946-1960, 1961-1970, 1971-1980, 1981-1990, 1991-2005 and after 2006. The main characteristics of the buildings, which depend on the period of construction, are: the level of thermal insulation of the opaque and transparent envelopes (*U-values*), the type of envelope and the efficiency (η) of the energy systems.
- *Classification of the motivation for the release of the EPCs*. The following motivations are indicated in the certificates: change of ownership, renting

or other, new building, sale announcement, energy retrofitting, building renovation, important retrofitting activity, usability request, change in energy performance, extension in derogation (LR 20/2009), loan for use, usufruct and energy service contract. The motivation for the release is used to assess the EP of existing buildings (called '*generic'*) and those of retrofitted buildings (called '*retrofit'*) or after the installation of renewable energy source technologies (called '*Res'*). Three databases are identified according to this classification: *generic*, *retrofit* and *Res*. The EPCs with renewable energy technologies were also selected by checking the type of technological systems and the energy production data from RES.

- *Statistical analysis*. After the creation of the building clusters, any anomalous data in each group were discarded using the median values. In addition, in order to evaluate the frequency distribution of the values (i.e. EP), the normal distributions were evaluated. Two statistical tests are run conjunction with the distributions to observe the trend of the EP of the buildings, the thermal transmittances, and of the system efficiency value data, as well as to identify any anomalous data: the Kolmogorov-Smirnov (*KS*) and chi-squared (χ^2) tests. Therefore, the following data, which are typical of each cluster, are identified in this phase, for the three databases (*generic*, *retrofit, Res*) according to the eight construction periods: EP, U_{op}, U_g, η_H and η_{DHW} (distinguishing between the *generic*, *retrofit* and *Res* databases).
- *Analysis of the annual consumptions*. The EPCs are subdivided into homogeneous groups (only residential users) by means of the previous steps, according to the typology of the building (flat or detached house), the construction period, and the motivation for the release of the EPCs. The EP of residential buildings is evaluated using the EP_{gl} index, expressed in kWh/m^2/year, by considering the energy consumption for H and DHW. The annual energy performance EP_{gl} ($EP_{gl,generic}$, $EP_{gl,retrofit}$, $EP_{gl,Res}$), the reachable energy performance $EP_{gl,reach}$ and the annual energy savings ($E_{savings}$) after retrofitting measures and/or after the installation of RES technologies are evaluated for each group of EPCs (*generic, retrofit and Res*). Once the amount of net heated area (m^2) of the residential buildings (which is indicated in the EPCs) was known, it is possible to calculate the global consumption of the building (kWh/year) from the EP.

The equations presented below show the methodology used to calculate the current annual energy saving trends after retrofitting measures ($E_{savings,retrofit}$, Equation 33) and after the installation of RES technologies ($E_{savings,res}$, Equation 34):

$$E_{savings,retrofit} = EP_{gl,generic} - EP_{gl,retrofit} \quad (33)$$

$$E_{savings,res} = EP_{gl,generic} - EP_{gl,Res} \quad (34)$$

where:

- $EP_{gl,generic}$ (kWh/m^2/y) is the EP of a building without any energy retrofitting interventions or the installation of RES technologies elaborated according to the *generic* database;
- $EP_{gl,retrofit}$ (kWh/m^2/y) is the EP of a building after retrofitting interventions elaborated according to the *retrofit* database;
- $EP_{gl,Res}$ (kWh/m^2/y) is the EP of a building after the installation of RES technologies elaborated according to the *Res* database.

The EPCs are grouped according to the type of intervention, and the reachable EP_{gl} (kWh/m^2/y) indicator was used to quantify the energy savings (Equation 35).

$$E_{savings,int} = EP_{gl,int} - EP_{gl,reach,int} \quad (35)$$

where:

- $EP_{gl,int}$ (kWh/m^2/y) is the EP of a building after specific energy retrofitting interventions or the installation of RES technologies elaborated according to the *generic* database;
- $EP_{gl,reach,int}$ (kWh/m^2/y) is the EP calculated by the certifiers, which indicates the feasible interventions, from a technical, historical, environmental and an economic point of view (only the interventions with a payback time lower than 10 years were indicated in the EPCs used for the calculation of $EP_{gl,reach}$).

Case study

This section describes a case study of the city of Turin. A total of 182,718 EPCs, registered from 2009 to 2015, for Turin are selected from a regional database, of which 55,276 are located in the 33 districts analysed in this work, (41,848 are served by the DHN). Considering the building typology, 54,747 EPCs refer to flats (of which 41,709 are served by DHN) and only 529 EPCs refer to detached houses (of which 139 are served by the DH network).

Table 45 shows the number of EPCs, according to the *generic*, *retrofit* and *Res* typologies, for the flats and detached houses. It is possible to observe that the 33 districts selected for the analysis reflect the average characteristics of the whole city. The number of certificates (see the percentages) of the 33 districts is very close to that of the city, and the EPs of the buildings covered by the 33 districts, as characterised by their EPCs, are therefore statistically representative of the whole building stock of the entire city of Turin. Moreover, the quota of retrofitted buildings is particularly low, and to reach the European energy and climate targets it would be necessary to promote EE in buildings through the use of new financial instruments and already existing incentives [61].

Table 45. Number of EPCs in Turin and in the 33 considered meshes distinguishing between the motivations for their release [13].

Number of EPCs	Area	*Generic*		*Retrofit*		*RES*	
		Flats	**Detached Houses**	**Flats**	**Detached Houses**	**Flats**	**Detached Houses**
	Turin	167,899	5,632	5,786	760	4,030	374
		-95%	-83%	-3%	-11%	-2%	-6%
	33 districts	53,174	429	992	49	581	51
		-97%	-81%	-2%	-9%	-1%	-10%

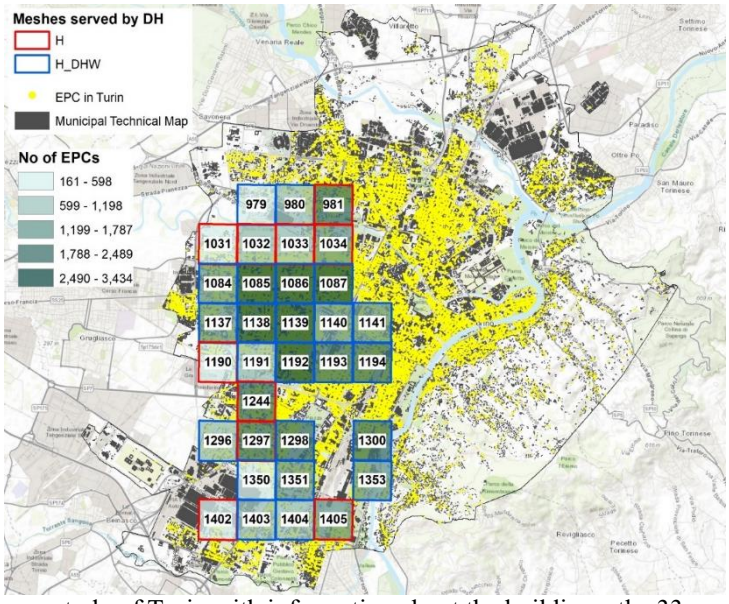

Figure 110. A case study of Turin with information about the buildings, the 33 meshes connected to the DH network (1 km x 1 km dimensions), the ID mesh, and the distribution of the EPCs [13].

Figure 110 shows the part of Turin considered with the 33 meshes served by the DH network (1 km x 1 km meshes) and the distribution of the EPCs.

The colour of the mesh outline specifies homogeneous groups of residential buildings, on the basis of the measured DH energy consumption types (H+DHW in blue or H in red). The number of EPCs in each district (33 meshes) is very important in this work because the thermo-physical characteristics of the buildings and the efficiency of the systems have been calculated for each mesh on the basis of EPC information. The calculated *U-values* and *η-values* were found to be more accurate where there was a large number of EPCs, for example, in the mesh numbers 981, 1085, 1087 and 1192.

In order to discard any anomalous data from the EPC database and assess the distributions of data, the median values and normal distributions of the EP of the buildings and the U_{op}, U_g and η values are analysed. The normal distributions are only elaborated for the flats since the detached houses did not have a sufficient number of EPCs. Figure 111 shows an example of the normal distributions for flats built before 1919, according to the *generic* database: the U_{op} and ηH values are indicated. *KS* was verified for the *U-values* and both *KS* and χ^2 tests were run for

the *η-values*. It has emerged, from the *generic* database, that most of the residential buildings were built before 1970 (69%), and the new buildings built after 2005 only represent a small percentage, that is, 2%. A total of 93% of the *retrofit* EPCs refer to buildings built before 1970, and this is because there are only a few new buildings that do not need to be retrofitted. The limited number of EPCs for some construction periods does not allow a reliable identification of all the buildings to be made, in particular for those built after 2005. This aspect does not limit the application of the models, as most of the buildings in Turin were built before 1970, and a sufficiently large data set was therefore available to carry out the analyses at an urban scale.

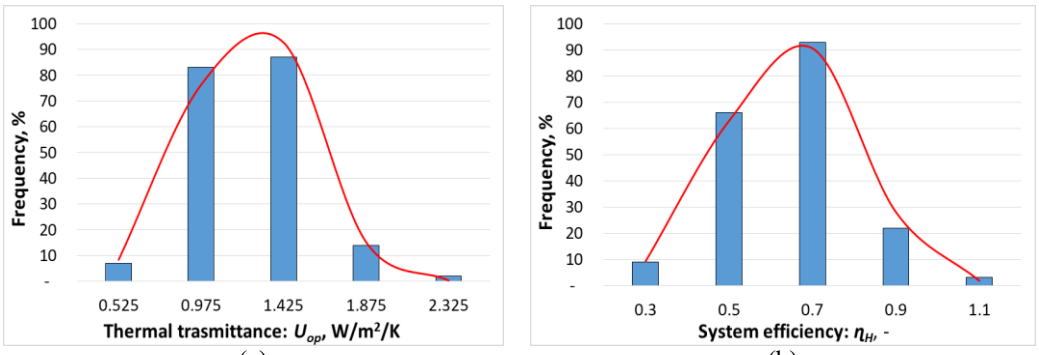

(a) (b)

Figure 111. Distributions of the thermal transmittance Uop (a) and system efficiency ηH (b) values for flats built before 1919, as taken from the generic database [13].

The type of retrofitting interventions identified from the *retrofit* database are: the installation of thermostatic valves, thermal insulation of the roof, thermal insulation of the slab/floor, the replacement of windows, thermal insulation of vertical walls and window replacements.

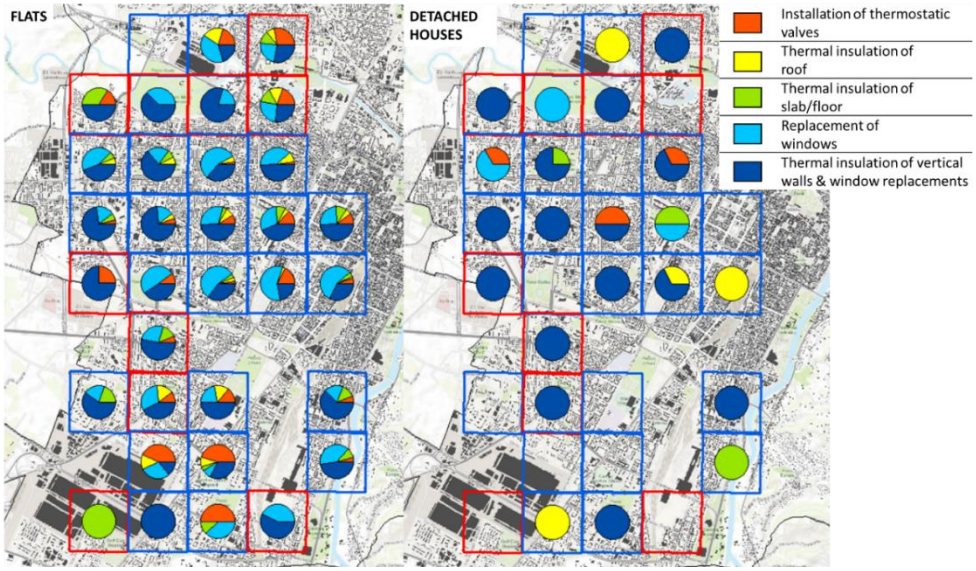

Figure 112. Typologies of retrofitting interventions in the 33 meshes connected to the DH network: (a) flats and (b) detached houses (EPC database up to September 2015) [13].

Figure 112 shows the different distributions of the typology of retrofitting for the 33 meshes of the city of Turin served by the DH network. It is possible to observe that the main interventions were the thermal insulation of walls and window replacements. No energy retrofitting measures had been carried out in some meshes. There were only 49 EPCs for the detached houses (see Figure 112) with information about retrofitting interventions.

In order to improve the accuracy of the engineering models, some new *building data* inputs are calculated at a district scale. The *U-values* of opaque envelopes (U_{op}) and glazing (U_g), and the *η-values* are calculated from the EPC database, considering the construction period and the motivation for their release (*generic* and *retrofit*).

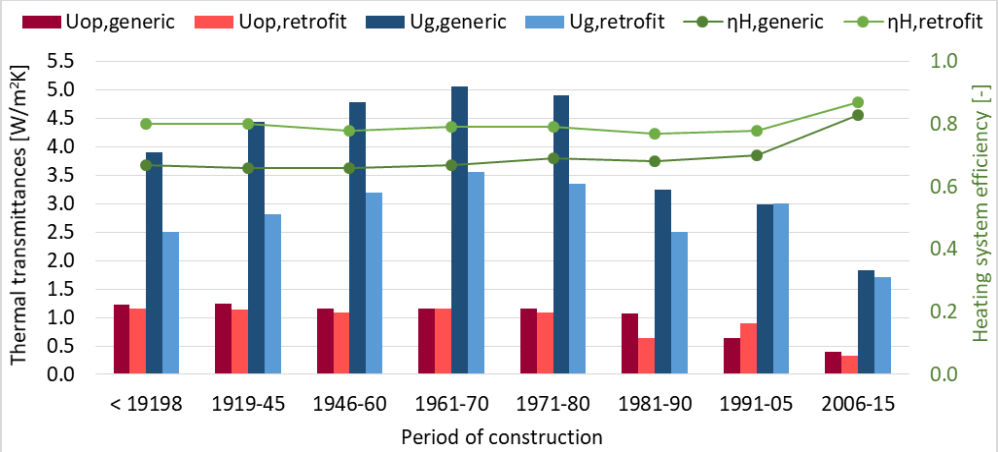

Figure 113. Thermal transmittances and system efficiency values elaborated from the EPC database distinguishing between generic and retrofit motivations (EPC database up to September 2015) [13].

It emerges, from Figure 113, that the efficiency level of residential buildings built in the 1971-1980 period, and in particular for the last three construction period classes, has improved, and shows low *U-values* and high *η-values*. This trend is more evident after energy retrofitting interventions. The obtained results are less accurate when there are fewer certificates. For example, the $U_{op,generic}$ value is lower than $U_{op,retrofit}$ for the 1991-1905 period, and the $U_{g,generic}$ value is at almost the same level as $U_{g,retrofit}$. This is due to the fact that only 88 certificates are available for buildings built in the 1991-1995 period, and this number represents 2% of the retrofitting database; in addition, as they are new buildings, they are unlikely to have been retrofitted.

Results

The adopted EE measures consider different interventions, such as thermal insulation of the building envelopes and/or the replacement of generation systems, and take into account all the constraints of the built environment and the real urban context.

Table 46 describes the data pertaining to the homogeneous groups of flats from different construction periods, as well as the median values of the energy performance index of the *generic* EPCs and *retrofit* EPCs. The difference between these two indicators allows the energy savings to be calculated considering the period of construction. It is possible to observe that the highest energy savings can be obtained for the older buildings, built before 1980. This trend emerges because residential buildings built before 1976 (the year in which the first National Law on EE was enacted) have a worse EP and a higher potential for energy savings than newer buildings. The accuracy of the energy savings also depends on the number of EPCs from which it was calculated (a higher number of EPCs makes the result more accurate).

Table 46. Characteristics of the flats according to their period of construction in 33 districts of Turin [13].

Period of construction	Number of EPCs retrofitted	Retrofit (m^2)	$EP_{gl,retrofit}$ (kWh/m^2/y) median	$EP_{gl,generic}$ (kWh/m^2/y) median	$E_{savings,retrofit}$ (kWh/m^2/y)	$E_{savings,retrofit}$ (%)
< 1918	186	15,554	142	210	68	32
1919-45	230	18,389	159	235	76	33
1946-60	336	26,060	172	227	55	24
1961-70	172	14,644	159	218	58	27
1971-80	22	2,111	137	209	72	34
1981-90*	18	1,947	157	175	18	10
1991-05*	17	1,790	123	137	14	10
> 2006*	11	680	110	114	4	4

* The number of EPCs was not sufficient to identify accurate trends for this construction period.

Table 47. Energy performance of the flats according to their renewable energy technology in 33 districts of Turin [13].

RES technology (main period)	No. of EPCs retrofitted	Retrofit (m^2)	$EP_{gl,Res}$ (kWh/m^2/y) median	$EP_{gl,generic}$ (kWh/m^2/y) median	$E_{savings,Res}$ (kWh/m^2/y)	$E_{savings,Res}$ (%)
Biomass boiler (1946-60)	24	1,714	191	226	35	16
Heat Pump (1919-45 and > 2006)	23	1,834	116	162	46	28
PV (> 2006)	31	2,194	95	114	19	30
PV – ST (>2006)	66	4,531	53	114	61	51
ST (> 2006)	437	30,977	80	114	34	38

A similar assessment has been made for the installation of the main renewable solar energy technologies (Table 47): biomass boiler, PV (photovoltaic panels), ST

(solar thermal collectors) and HP (heat pump). Because of the small number of EPCs, it was not possible to distinguish between the buildings on the basis of the period of construction and the prevalent period of construction is therefore considered for the energy saving analysis. It can be observed, in Table 47, that the greatest energy savings are obtained for two combined renewable technologies, that is, PV panels and ST collectors. The same analysis is conducted for detached houses. In this case, the results were not particularly accurate, due to the low number of EPCs available (Table 48 and Table 49).

Table 48. Characteristics of the detached houses according to their period of construction in 33 districts of Turin [13].

Period of construction	Number of EPCs retrofitted	Retrofit (m^2)	$EP_{gl,retrofit}$ (kWh/m^2/y) median	$EP_{gl,generic}$ (kWh/m^2/y) median	$E_{savings,retrofit}$ (kWh/m^2/y)	$E_{savings,retrofit}$ (%)
< 1918*	6	3,586	182	264	82	31
1919-45*	4	1,303	200	287	87	30
1946-60	23	5,942	240	267	27	10
1961-70*	10	4,299	224	280	56	20
1971-80*	1	160	152	234	82	35
1981-90*	3	359	139	191	52	27
1991-05*	1	53	98	185	87	47
> 2006*	1	57	104	112	8	7

* The number of EPCs was not sufficient to identify accurate trends for this construction period.

Table 49. Energy performance of the detached houses according to their renewable energy technology in 33 districts of Turin [13].

RES technology (main period)	Number of EPCs retrofitted	Retrofit (m^2)	$EP_{gl,retrofit}$ (kWh/m^2/y) median	$EP_{gl,generic}$ (kWh/m^2/y) median	$E_{savings,Res}$ (kWh/m^2/y)	$E_{savings,Res}$ (%)
Biomass boiler (1961-70)*	1	81	266	280	14	5
PV (1946-60)*	5	1,229	152	267	154	58
PV – ST (1946-60)*	1	99	84	267	183	69
ST (> 2006)	44	7,072	90	111	45	40

* The number of EPCs is not sufficient to identify accurate trends for this construction period.

Figure 114 shows the cumulative energy savings achieved for flats and for detached houses after retrofitting measures, while Figure 115 describes the results pertaining to cumulative energy savings after the installation of RES technologies. Although the number of detached houses in the 33 considered districts of Turin is much lower than the number of flats in condominiums, the cumulative energy

savings and the retrofitted area of the detached residential buildings still make a significant contribution on the retrofit trends in city.

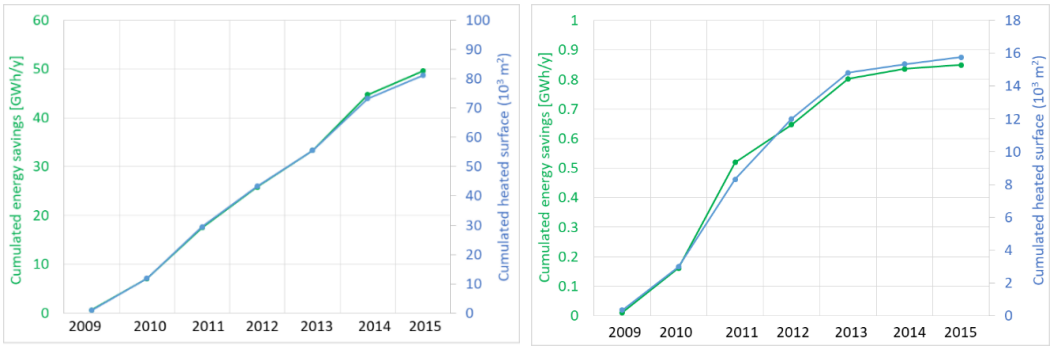

(a) (b)

Figure 114. Cumulative energy savings for (a) the flats and (b) detached houses in the 33 considered districts in Turin [13].

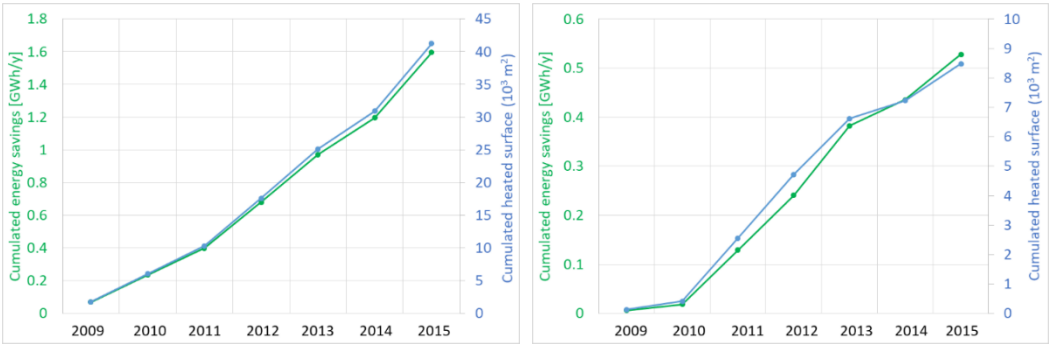

(a) (b)

Figure 115. Cumulative energy savings for renewable energy technologies for (a) the flats and (b) detached houses in the 33 considered districts in Turin [13].

Table 50. Energy consumption of the flats according to their period of construction after the main retrofitting interventions in the 33 considered districts in Turin [13].

Period	No. of EPCs	$EP_{gl,int}$ (kWh/m²/y)	EPCs %, int. roof insulation	EPCs %, int. slab/floor insulation	EPCs %, int. wall insulation and window replacements	EPCs %, int. thermostatic valves	EPCs %, int. window replacements	$EP_{gl,reach,int}$ (kWh/m²/y)	Medium term $E_{savings}$
< 1918	186	142	3%	4%	27%	6%	33%	109	23%
1919-45	230	159	8%	2%	27%	7%	27%	116	27%
1946-60	336	172	2%	5%	37%	6%	28%	133	22%
1961-70	172	159	3%	5%	32%	16%	17%	118	26%
1971-80	22	137	0%	0%	41%	5%	18%	96	30%
1981-90*	18	157	0%	0%	11%	6%	11%	143	9%
1991-05*	17	123	0%	6%	24%	12%	24%	106	13%
> 2006*	11	110	0%	0%	9%	0%	9%	89	18%

* The number of EPCs was not sufficient to identify accurate trends for this construction period.

Table 51. Energy consumption of the detached houses according to their period of construction after the main retrofitting interventions in the 33 considered districts in Turin [13].

Period	No. of EPCs	$EP_{gl,int}$ (kWh/m²/y)	EPCs %, int. roof insulation	EPCs %, int. slab/floor insulation	EPCs %, int. wall insulation and windows replacements	EPCs %, int. thermostatic valves	EPCs %, int. window replacements	$EP_{gl,reach,int}$ (kWh/m²/y)	Medium term $E_{savings}$
< 1918*	6	182	17%	0%	50%	0%	17%	128	30%
1919-45*	4	200	25%	25%	25%	25%	0%	133	33%
1946-60	23	240	9%	4%	52%	9%	9%	170	29%
1961-70*	10	224	0%	10%	80%	0%	10%	176	22%
1971-80*	1	152	0%	0%	100%	0%	0%	120	21%
1981-90*	3	139	0%	0%	33%	0%	0%	132	5%
1991-05*	1	98	0%	0%	100%	0%	0%	63	36%
> 2006*	1	125	0%	0%	0%	0%	0%	104	17%

Table 50 and

Table 51 show the main results of the energy savings, according to the construction period, and the number of EPCs for each type of renovation: thermal insulation of the roof, thermal insulation of the slab/floor, thermal insulation of vertical walls and/or window replacements, and installation of thermostatic valves. The percentage of certificates is indicated for each intervention according to the construction period, and the percentage of energy savings, calculated according to Equation 35, is reported in the last column.

The most effective interventions are the thermal insulation of vertical walls and window replacements for both flats and detached houses. Since the accuracy of the results depends on the number of EPCs, more reliable results were obtained for flats built before 1970. Certificates are not available for some construction periods, and in such cases the percentage is 0%.

5.2.2 Monthly data-driven model

The use of district heating (DH) has environmental and economic advantages in energy production and distribution for space heating consumption. In this section, the combined effect of DH expansion with different buildings retrofit scenarios using a GIS-based model is proposed.

This methodology is applied to the DH network of the city of Torino and, energy savings hypotheses were analysed, evaluating different energy saving trends starting from the current one with existing policies. A data-driven model has been developed with bottom-up and top-down approaches; then two future energy savings scenarios have been hypothesized. Energy retrofit measures have been

applied to the most critical areas with low potential of heat distribution; in a second phase, to the whole area connected to the DH network.

The results showed that intervening in the critical areas only +5% of potential buildings can be connected to the existing DH network (standard retrofit) while this percentage could grow up to +25% with advanced buildings retrofit. On the other hand, intervening on the whole city, there is a considerable reduction of consumptions and the connectable quota of buildings to the DH network reaches +42% with standard retrofit and +82% with advanced retrofit scenario with an optimization of energy distribution as well.

Methodology

The research starts from an analysis of the maximum quota of buildings connectable to the existing DH network with the existent transport pipelines not modified. This maximum quota of buildings connected to the DH network depends on territorial, economic and technical limits; technical limits consider the maximum flow rates or velocities into the pipelines. Energy consumption of buildings is evaluated by a GIS-based simplified model derived by the comparison of top-down and bottom-up models for space heating energy consumption of residential and non-residential buildings [12,145]. The GIS-based models allowed to define, with a good spatial accuracy, the energy demand and supply location while the simplified models did not required a detailed description of building geometry, thermal properties of the building envelope and heating system [256]. The bottom-up models are also useful to identify buildings that require urgent retrofit interventions and to quantify the energy savings after retrofit measures. Figure 116 shows the methodology used in this study.

In the presented research, the main data consist in characteristics of:

- Turin's buildings: the available data on the building stock provided by the Municipality and the official statistical institution, such as number of buildings, period of construction, *S/V*, heated volume, information about the type of user (residential, tertiary, municipal and industrial), occupancy, central/individual heating systems, etc. The outdoor microclimatic conditions and mainly the HDD at 20°C, registered by ARPA weather stations, have been associated to the nearer buildings.
- Turin's DHN: the local district heating company provided space heating consumption data and the heated buildings volume for 36 meshes of the size of 1 km x 1 km around the existing DH network for the city of Turin. The energy-use data have a monthly detail, for three consecutive heating seasons: 2012/2013, 2013/2014 and 2014/2015.
- Turin building retrofit interventions: the available data on building retrofit were derived from the energy performance certificates (EPC) registered in Piedmont Region from 2009 to 2015. The EPC database was created considering: 103,742 apartment buildings, of which only

4,333 are for retrofit interventions (energy efficiency renovations and installation of renewable energy technologies), and 1,841 detached houses, of which only 285 are for retrofit interventions.

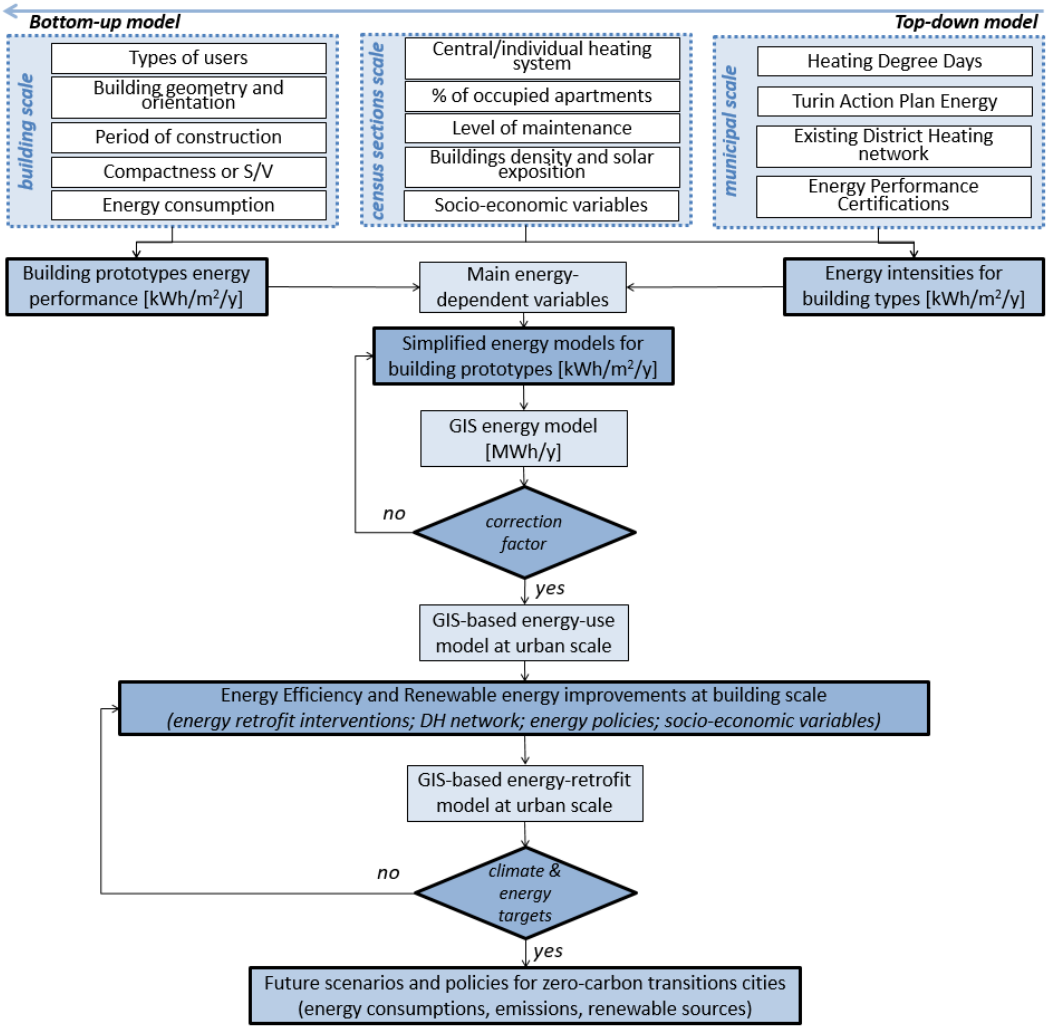

Figure 116. Flowchart of the methodology approach: energy efficiency model [55].

With the support of GIS tools, an updated database of the buildings stock in Turin was developed with all the available georeferenced information (at different scales). The GIS has the advantage to localize and to spatially describe all information to visualize, analyse and plan the energy demand and supply of buildings at local and territorial scale. The use of GIS tool supports the identification of particular buildings or clusters of buildings, with a qualitative and quantitative information on their energy performance. With these tools it is possible to identify the most promising areas to be involved in the process of energy renovation and in simulating possible energy savings scenarios [257]. The final GIS database developed in this study contains: the typological and dimensional data of buildings; the buildings spatial distribution in the city of Turin; the population distribution; the current energy demand and supply for space heating consumptions; the buildings connected to the DH network and the ones that could be connected in

the future; the distribution of buildings that need renovation; the critical areas of the DH network; the energy performance of buildings after suitable energy retrofit interventions.

Phases of the analysis

Starting from a previous study that proposed a methodology to evaluate the potential user connections in the existing DH network for the city of Turin (the goal of the model was to guarantee the maximum amount of new connections), the results shown that the average maximum quota of additional users is +25%, taking into account the territorial, economic and technical constraints of the DH network. The existing DH network is considered and the maximum thermal flux is evaluated in each pipeline fixing the temperatures gradient and the velocity limits. In this paper, to optimize the district heating network operation, a massive retrofit of connected and connectable buildings is hypnotized in order to reduce the energy required in critical pipelines increasing the DH network flexibility. This allowed a significant reduction of the additional mass flow rate of connectable buildings and thus increasing the percentage of connectable buildings. Then, the purpose of this work is to connect all the residential buildings to the existing DH network also through energy efficiency measures. In Figure 117 the main 4 phases of the procedure are represented:

Phase 1. *District heating data analysis*. With ESRI ArcGIS software, for 36 meshes with a size of 1 km2, the DH network barycenters have been localized with their respective heat flows. For each barycenter, a maximum quota of thermal flux was defined [kW; MWh/y] as the maximum heat power that can be supplied by each pipeline of the network considering all territorial, economic and technical constrains. For the 36 meshes, the real connectable quota of buildings [MWh/y] was calculated as the maximum quota minus the already connected thermal load. The connectable quota was evaluated as theoretic and real one: theoretic (corresponds to all connectable buildings and it is higher than the real quota,) considers only territorial and economic constrains, while the real quota considers also technical constrains of pipelines.

Phase 2. *Identification of critical areas*. The most critical meshes have been identified by evaluating the ratio between the real connectable quota and the theoretic connectable quota of buildings; the optimum result should be the connection to the DH network of high percentage of connectable buildings, then critical meshes have a real connectable percentage less than 20% and require urgent retrofit.

Phase 3. *Energy saving trend*. For this analysis, the data about residential buildings' energy performance certificates (EPC) have been used. The available data have been classified considering: two types of buildings (apartments or detached houses); 8 classes for the period of constructions (<1918, 1919-

1945, 1946-1960, 1961-1970, 1971-1980, 1981-1990, 1991-2005, 2006>); the reasons for the release of EPCs, distinguishing generic and the retrofit interventions. Analyzing the data of the EPCs, the annual standard and advanced energy savings trend were assessed with two future scenarios: standard and advanced energy savings scenarios.

Phase 4. *Energy Efficiency hypotheses*. With the aim of increasing the connectable buildings to the existing DH network, two hypotheses of energy efficiency measure spatial distribution were evaluated. A first hypothesis only in the critical meshes (8 meshes) considering a standard and an advanced retrofit. Then, a second hypothesis of energy efficiency renovation in all the meshes (36 meshes) with the same a standard and an advanced retrofit solutions.

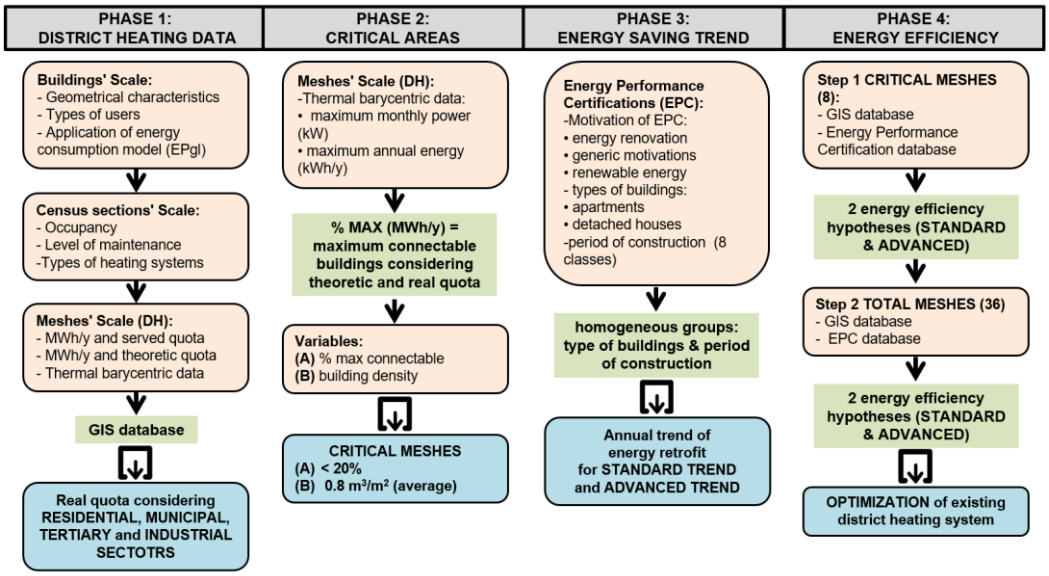

Figure 117. Flowchart of the procedure [55].

District heating data analysis

Turin consumption data [MWh/y] and heated volumes connected [m3] were provided by the DH company. Data were provided through 36 meshes of the size of 1 km x 1 km for in the South-West part of the city of Turin. With a GIS tool, 177 thermal barycenters of the DH network were georeferenced, and for 36 meshes of 1 km2 the thermal barycenters data have been associated. The connectable buildings to the DH network considering 4 types of user (residential, municipal, tertiary, industrial) [145] have been identified. In particular, in the GIS database there were information concerning: the quota of energy consumption of connected buildings [MWh/y], and the theoretic connectable quota of buildings and the relative thermal energy consumptions [MWh/y].

Using the results obtained from the fluid dynamic analysis of the DH network, the real amount of connectable buildings has been evaluated [258] and the GIS database has been implemented. Then, for each mesh the district heating data was evaluated, considering the maximum, the connected and the connectable potential

quota, the type of users, the location (microclimatic conditions) and the buildings characteristics'.

Identification of critical areas

An evaluation of the District Heating characteristics' was made to identify the critical areas with a priority of retrofit interventions. With the use of the fluid-dynamic model, values of real thermal energy flows [kW] were provided. Through the following procedure, the maximum percentage of connectable buildings to the existing DH network was calculated:

$$max\ thermal\ flow = \ connected\ thermal\ flow + \ real\ connectable\ thermal\ flow_{st} \quad (36)$$

$$real\ connectable\ thermal\ flow_{st} < theoretic\ connectable\ thermal\ flow_{st} \quad (37)$$

Where:

- *max thermal flow* [MWh/y]: maximum thermal power that can be supplied by the existing network.
- *connected thermal flow* [MWh/y]: power supplied by the network for the already connected buildings;
- *real connectable thermal flow* [MWh/y]: additional power that can be supplied by the existing network (considering also the limits due to the fluid-dynamic model of DH network);
- *theoretic connectable thermal flow* [MWh/y]: additional power that can be supplied by the existing network (considering only territorial and economic limits);
- *st*: "standard" without retrofit interventions.

Then, the critical meshes have been identified where it is possible to connect less than 20% of the connectable buildings.

Energy saving trend

The energy saving trend of the residential sector has been evaluated, considering the available data on building renovations derived from the energy performance certificates (EPC) from September 2009 to 2015. For this analysis, disregarding the first partial and anomalous years, only EPCs of 2011-2015 were considered. Homogeneous groups of EPCs have been identified, considering: the type of buildings, the period of construction and the motivation for the release of the EPCs. For each group, the annual energy performance, the energy savings and the reachable energy performance [kWh/m^2/y] were calculated. The energy performance was evaluated from the *EPgl* index considering the energy consumptions for space heating and hot water production.

Subsequently, two future scenarios for standard and advanced retrofits were hypothesized applying the energy saving models. The current annual energy saving trends was also evaluate. This procedure was based on median values of energy intensities for each type of buildings and homogeneous group of EPCs.

Energy efficiency hypotheses

A priority of retrofit interventions has been evaluated, initially with the hypothesis to intervene only in the most critical areas of Turin (identified in phase 2) and then on the whole urban area.

1. Energy efficiency interventions in the most critical areas, that are the meshes in which it is not possible to connect to the existing network more than 20% of the theoretic quota; evaluation of the energy savings achievable with the retrofit of the: the *connectable buildings;* the *connectable buildings and the connected portion.*
2. Energy efficiency measures in the whole city of Turin; evaluation of the energy savings achievable with the retrofit of: *the connectable buildings*; *the connectable buildings and the connected portion*.

Through the following procedure, the connectable buildings quota was calculated using the energy savings models with the existing energy policies (standard) and with more deep retrofit interventions (advanced). The current annual energy savings was calculated deducting the energy intensities of EPCs released for generic interventions and the ones of EPCs for retrofit interventions. The advanced annual energy savings instead was calculated deducting the energy intensities of EPCs released for retrofit interventions and the reachable energy intensities.

In particular, comparative analysis of the energy assessment results of the residential area before and after the application of sustainable retrofitting strategies have been made, calculating the improvement potential with the real building stock. The results of the energy assessment of residential buildings were uploaded with GIS, with the spatial distribution of energy consumptions.

Case study

The energy efficiency model was applied to the city of Turin, then the different retrofit measures and the reduction of CO_2 emissions were analysed. To promote the potential expansion of DH network, a study on the optimization of the heat flow distribution has been provided. This analysis could be useful to support a sustainable urban energy plan.

Characteristics of Turin's buildings

Turin has about 60 thousand of buildings equal to 232 Mm3, considering the four different types of users:

- Residential sector has more than 45 thousand of buildings, equal to 164 Mm^3 (70%).
- Municipal sector consists in 6 thousand of buildings, equal to 23 Mm^3 (10%).

- Tertiary sector is constituted by 4 thousand of buildings, equal to 20 Mm^3 (9%).
- Industrial sector with more than 4 thousand of buildings, equal to 25 Mm^3 (11%).

The residential buildings of Turin have an average surface to volume ratio *S/V* equal to 0.63 m^{-1}, with mainly big and compact condominiums (*S/V* ≤ 0.45 m^{-1}). Although, most of the buildings were built before 1960 (57%) and the 62% have a good level of maintenance (26% excellent and only 11% are in mediocre condition). Considering the existing district heating network, the theoretic connectable buildings consist of 43 thousand heated buildings equal to 196 Mm^3. To identify the environmental limits, the localization (hills, Po river, historical centre and LTZ) and the type of heating systems (centralized and autonomous systems) have been considered. The residential sector is the most critical for energy consumption analyses; it has almost 32 thousand of heated buildings equal to 136 Mm^3 (70%). The municipal, the tertiary and the industrial sectors have 11 thousand of heated buildings, specifically 4 thousand (17 Mm^3), 3 thousand (18 Mm^3) and 4 thousand (25 Mm^3).

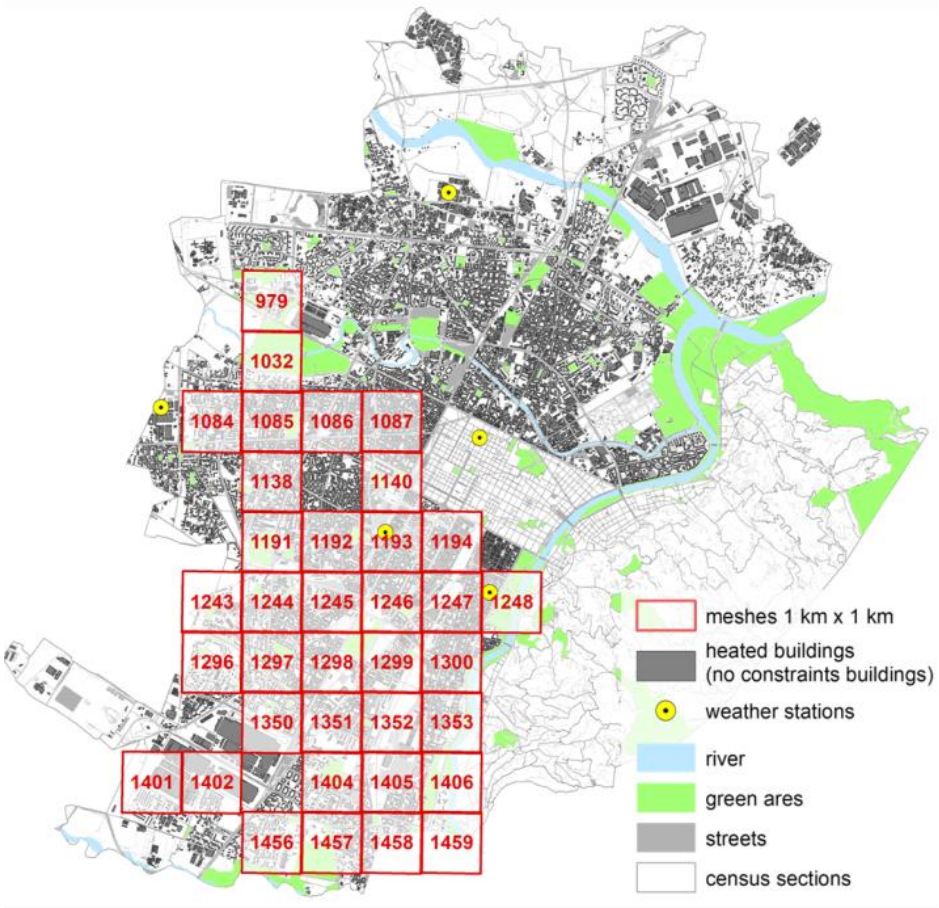

(a)

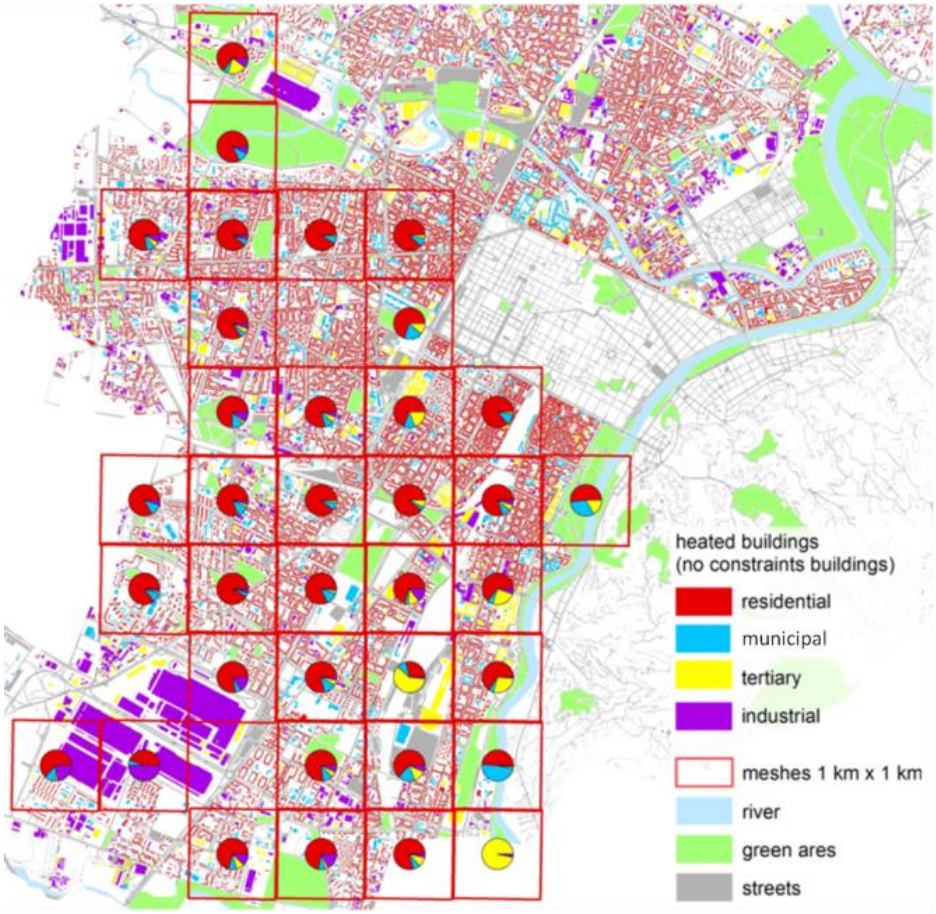

(b)

Figure 118. (a) The 36 square meshes of 1 km2 with ID code (red), weather stations (yellow) and connectable buildings to the DH network; (b) Urban distribution of types of users for the 36 meshes: residential, municipal, tertiary and industrial [55].

In this investigation, energy consumption data were provided on 36 meshes of 1 km x 1 km on the urban territory (with monthly period). The 36 meshes, used in this study, are represented in Figure 118 in the South-West part of the city with 20 thousand of heated buildings equal to 105 Mm^3 and the residential sector represents a significant share, with 16 thousand of heated buildings (almost 80 Mm3). The residential sector accounts for 76%, the municipal sector is 10%, the tertiary sector is 9% and the industrial sector is 5%.

In this area, residential buildings are mainly large condominiums, with an average *S/V* equal to 0.52 m^{-1}. The prevailing level of maintenance is good, specifically 32% of buildings have an excellent level, 43% good, 19% mediocre and 6% bad. Most of the buildings were built before 1960 (53%) and only 21% of the residential buildings were built after 1970, so this buildings stock can represent the general characteristics of the building heritage in the whole city.

The characteristics of buildings in the 36 meshes of Turin (number buildings, heated volume, surface to volume factor, occupancy, types of users, period of construction, main level of conservation, weather station, space heating energy consumptions) have been implemented with a GIS tool to all the analysed buildings with the Municipal Technical Map of Turin (2015) and the ISTAT Census Data (2011). In particular, the following average characteristics have been calculated for

each mesh: the number of buildings, the main period of construction, the S/V_{avg}, the heated volumes, the types of buildings (residential or non-residential), the main level of maintenance and the level of the apartments used. Data on energy space heating consumption (*EPgl*) were evaluated by the use of simplified energy models at urban scale for the city of Turin [12] considering also the urban heat island (UHI) phenomenon that influences the microclimate with significantly higher temperatures in the city centre and the lowest temperatures in the suburbs and in the surrounding rural and hilly areas. To take into account the UHI effect and its influence on space heating consumptions, different microclimate characteristics were analysed considering the nearest weather station on the average heating season of 2011/2012. In Figure 118a also the territorial constrains are shown with the hills on the South-East part of the city across the Po river and the historical centre. Figure 118b represents the types of user considered in the simplified energy models at urban scale for the evaluation of the energy consumptions.

Characteristics of the district heating network

The Turin DHN serves about half of the users located in the urban area, for a total value of about 60 Mm^3 of buildings. In particular, for the analysed 36 meshes, 51 Mm^3 of buildings were connected to the DH network corresponding to more than 48% of users. Furthermore the potentially theoretic connectable buildings are 42 Mm3 (40% of users), but the real potential expansion allows the connection of only 25% of users taking into account also the technical limits of the pipelines (i.e. maximum mass flow or velocity).

Table 52. Connected portion, connectable buildings of DH network and additional deliverable power/consumption: heated volume (% and m3) and thermal energy consumptions (MWh/y) [55].

ID mesh	Connected quota		Connected thermal consumption	Connectable buildings theoretic quota		Connectable buildings theoretic consumption	Additional deliverable power (real quota)	Additional deliverable consumption (real quota)
	[%]	[m^3]	[MWh/y]	[%]	[m^3]	[MWh/y]	[MW]	[MWh/y]
979	49.09	586,681	51,315	33.28	397,748	17,080	52	30,783
1032	22.77	189,027	38,581	57.53	477,595	22,197	6	3,327
1084	21.75	593,715	127,303	53.73	1,467,010	68,400	7	4,007
1085	29.22	1,224,495	183,795	56.42	2,363,999	103,690	13	7,505
1086	26.83	1,160,967	186,026	52.69	2,279,739	98,017	20	11,680
1087	32.06	1,886,912	246,982	50.27	2,958,534	124,160	20	11,899
1138	64.88	3,026,070	212,264	28.76	1,341,488	61,051	58	34,291
1140	54	2,008,939	140,404	35.45	1,318,749	49,773	50	29,706
1191	37.82	876,846	108,339	42.74	990,957	46,305	15	9,065
1192	34.99	1,346,974	169,325	42.1	1,620,288	71,278	22	12,774
1193	56.36	2,874,301	198,200	36.85	1,879,377	65,969	69	40,376
1194	31.63	1,393,934	184,482	45.84	2,020,053	84,567	12	6,865

1243	74.42	790,217	50,322	17.19	182,493	8,649	7	4,120
1244	62.78	2,057,371	151,878	28.01	917,834	42,540	37	21,655
1245	47.88	1,575,241	139,346	41.87	1,377,608	58,346	30	17,729
1246	53.29	2,095,972	164,742	40.43	1,589,902	66,598	36	21,334
1247	18.18	969,026	228,418	67.17	3,579,794	153,436	10	5,875
1248	2.26	49,000	75,811	72.98	1,581,516	55,327	0	159
1296	100	2,676,882	114,403	0	0	0	32	18,623
1297	61.27	2,354,104	173,446	35.35	1,358,196	61,312	42	24,996
1298	84.29	2,915,578	145,110	13.91	481,125	20,184	49	29,003
1299	43.12	1,116,560	123,083	48.99	1,268,435	60,294	18	10,566
1300	63.98	2,967,762	208,930	28.19	1,307,837	58,907	52	30,822
1350	49.46	994,865	104,846	39.57	795,867	41,485	10	6,182
1351	59.84	2,112,957	153,030	32.93	1,162,573	50,386	56	33,109
1352	81.12	2,350,986	88,239	17.14	496,799	15,127	12	7,354
1353	75.18	2,026,351	119,412	18.6	501,258	22,209	41	24,366
1401	36.08	372,317	53,020	40.78	420,808	21,620	11	6,520
1402	19.7	227,236	78,423	63.17	728,553	49,542	6	3,605
1404	53.55	1,572,648	131,574	37.73	1,108,070	49,643	41	24,102
1405	46.41	1,182,307	105,699	44.48	1,133,150	47,018	29	16,867
1406	100	839,804	30,481	0	0	0	47	27,594
1456	46.79	993,775	102,225	41.62%	883,987	42,550	24	13,919
1457	46.49	801,192	85,847	40.13%	691,634	34,450	15	8,549
1458	29.55	500,411	75,537	53.59%	907,489	40,479	20	12,018
1459	3.26	19,778	16,475	77.19%	468,591	12,716	9	5,115

In Table 52 the data of the potential expansion of the DH network are shown for all the 36 analysed meshes; in particular there were reported: the data of the buildings connected to the DH network and the data of theoretic and real connectable quota (heated volumes and their relative thermal energy consumptions). In Table 52, it is possible to observe that two meshes (i.e. 1296 and 1406 in grey) don't have a potential connectable quota because in those areas all connectable buildings are already connected to the existing DH network. In the last columns, the additional deliverable power/consumption (i.e. real connectable quota) was obtained through the knowledge of the design mass flow rates and temperature gap at the primary side of the heat exchangers installed in the substations knowing the already connected quota. Because the delivery temperature at the thermal plant is fixed at 120 °C and assuming a temperature gradient due to losses of 3 °C, a temperature gap of 50 °C was assumed (taking into account that these temperatures can vary a lot during the year).

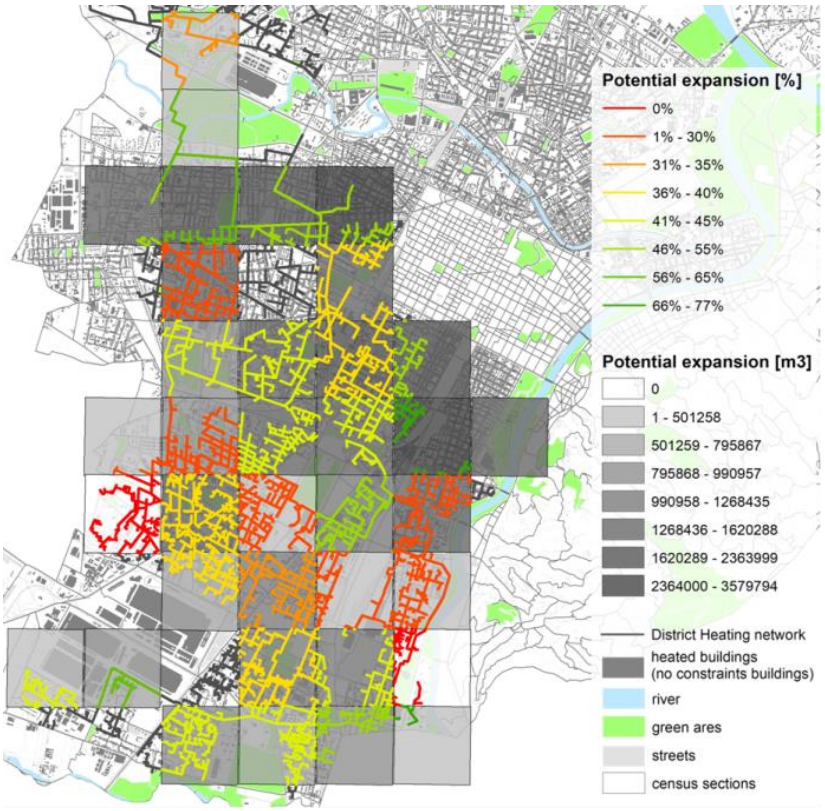

(a)

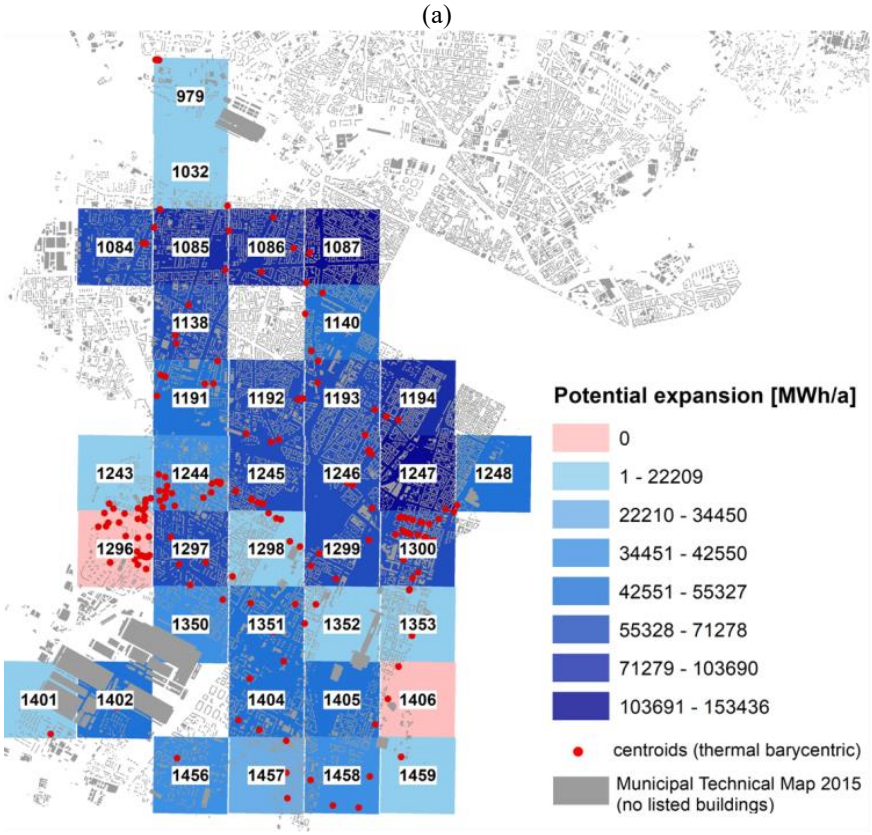

(b)

Figure 119. (a) Total potential expansion of the existing DH network: theoretic connectable quota [% and m3]; (b) Total potential expansion of the existing DH network: thermal energy consumptions [MWh/y] [55].

In Figure 119 the 36 meshes were represented with the information of the total potential expansion considering the theoretic connectable quota [% and m3] and the relative thermal energy consumptions [MWh/y]. Figure 119a shows that areas with low buildings densities are already saturated and then with low potential expansion of the existing DH network. On the other hand, in Figure 119b it can be observed that in the northern peripheral areas of the network, the higher potential expansion corresponds to the higher buildings densities zones of the city.

Results

For each mesh, the characteristics of the residential buildings were analysed by collecting data and classifying the buildings according to the period of construction and building typology with a GIS tool (Figure 120a). In the historical centre of the city, buildings were built mainly before 1945, while in the other parts, buildings were mainly built in 1961-80. Only in three meshes, there is a high percentage of buildings built in 1981-90.

For each homogeneous group of buildings the following parameters have been calculated: the number of buildings, heated area [m^2], heated volume [m^3], specific consumption [$kWh/m^3/y$], annual consumption [MWh/y], connected portion, theoretic connectable portion and real connectable portion [MWh/y].

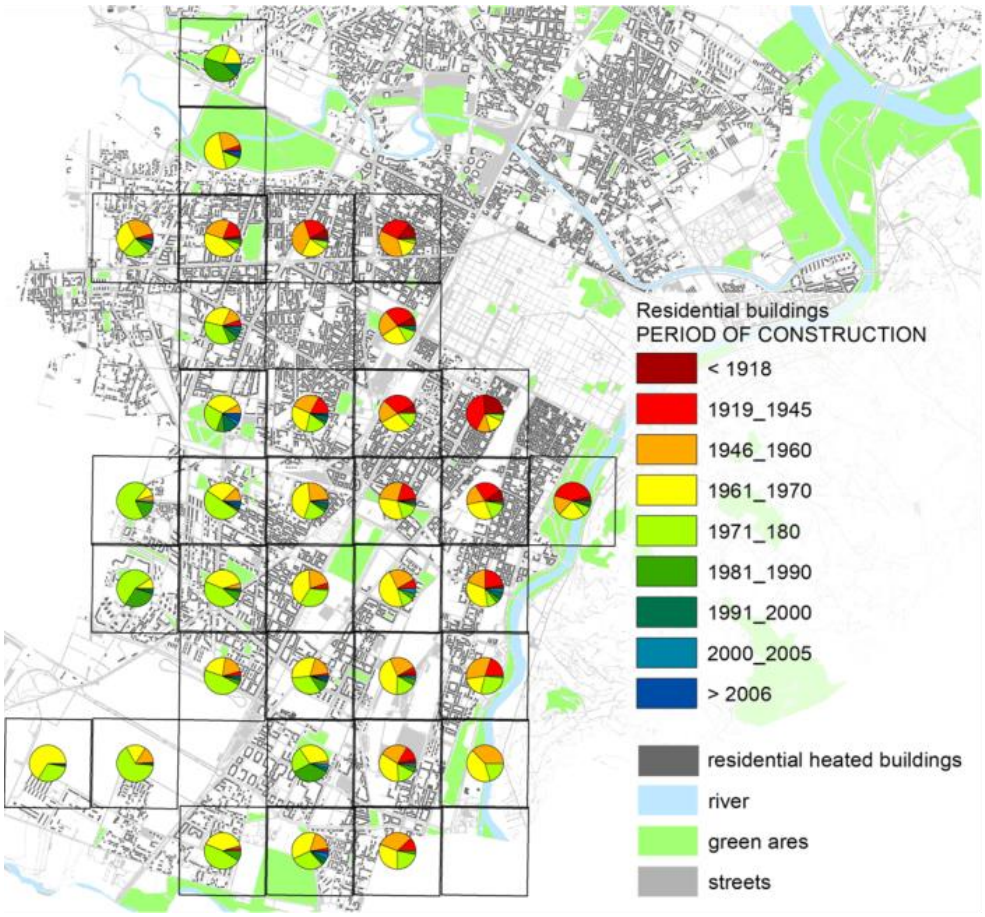

(a)

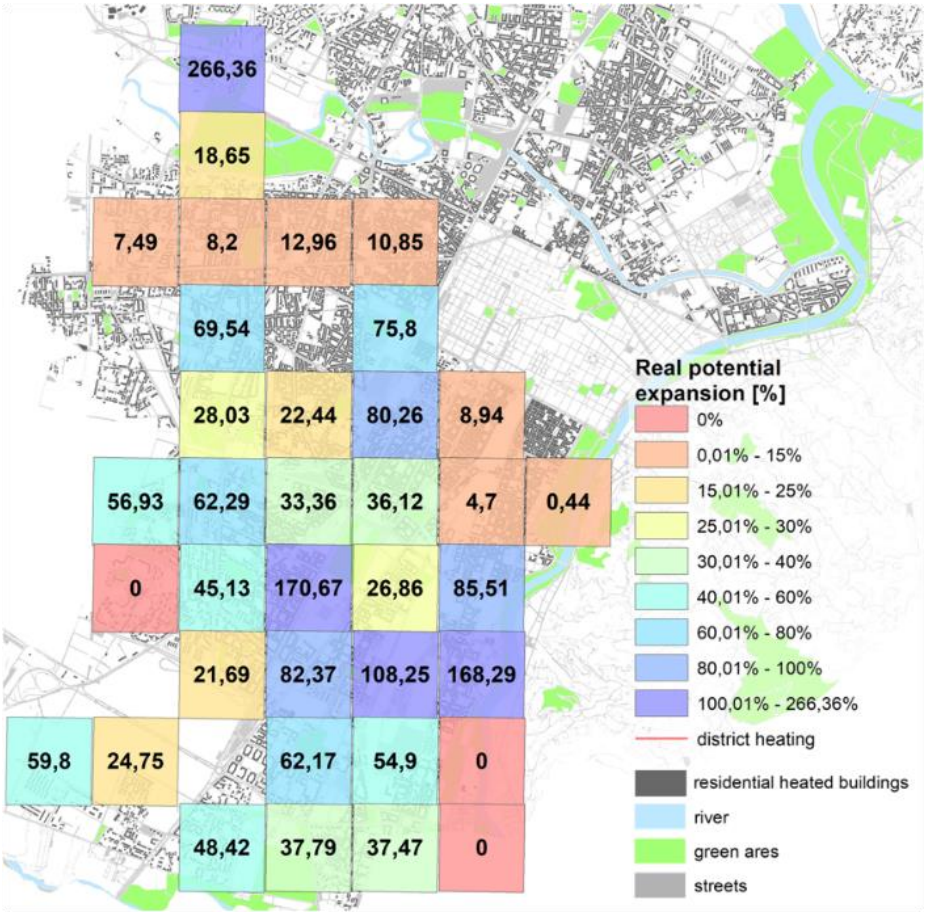

(b)

Figure 120. (a) Distribution of residential buildings considering the period of construction; (b) Real connectable buildings with a potential expansion of the existing DH network (considering the residential sector) [55].

Considering the load losses in the DH network and the energy consumption of the connected buildings, the real connectable quota of residential buildings for each thermal barycenter and mesh was evaluated. Figure 120b shows the real quota of residential buildings that can be connected to the existing DH network; an expansion of 0% indicates that the meshes are saturated with all potential residential buildings already connected. The last mesh in the lower right corner is saturated as no residential building is still connectable.

The expansion of the DH network also depends on the number of buildings present in the meshes and therefore on their relative buildings density. Therefore, in the evaluation of the critical meshes (with real connectable quota < 20% than the theoretic quota and excluding the saturated meshes), the average building density of these 8 meshes (in Figure 121a) was calculated: 0.7 m^3/m^2.

Figure 121 shows that the critical meshes are located in peripheral areas where the network is less dense. The building density is greater than 0.85 m^3/m^2 for six critical meshes, on the other hand two meshes (1032 and 1248) have a very low density (0.2-0.25m^3/m^2) but are nevertheless considered critical because in those areas the potential expansion is less than 20%.

Figure 121b also shows that there are two saturated meshes, 1296 and 1406. For these two meshes the connectable quotas, equal to 18,622 MWh/y and 27,593 MWh/y, are considered as surplus and the supplied energy could be used to serve other buildings. In addition, the mesh n. 1459 has a potential quota (5,115 MWh/y) that could be used to serve non-residential buildings because in this area there are tertiary and industrial buildings (with an energy required of 12,716 MWh/y).

With the application of the energy savings models, two future group of scenarios were assumed considering a standard and advanced building retrofit. For the first group of scenarios, only a retrofit of connectable residential buildings was proposed; while the second group of scenarios presented a retrofit for all buildings (connectable plus connected residential buildings). Moreover, these scenarios were also subdivided in more scenarios with these interventions only on the critical meshes (phase one) and on the whole area (phase two).

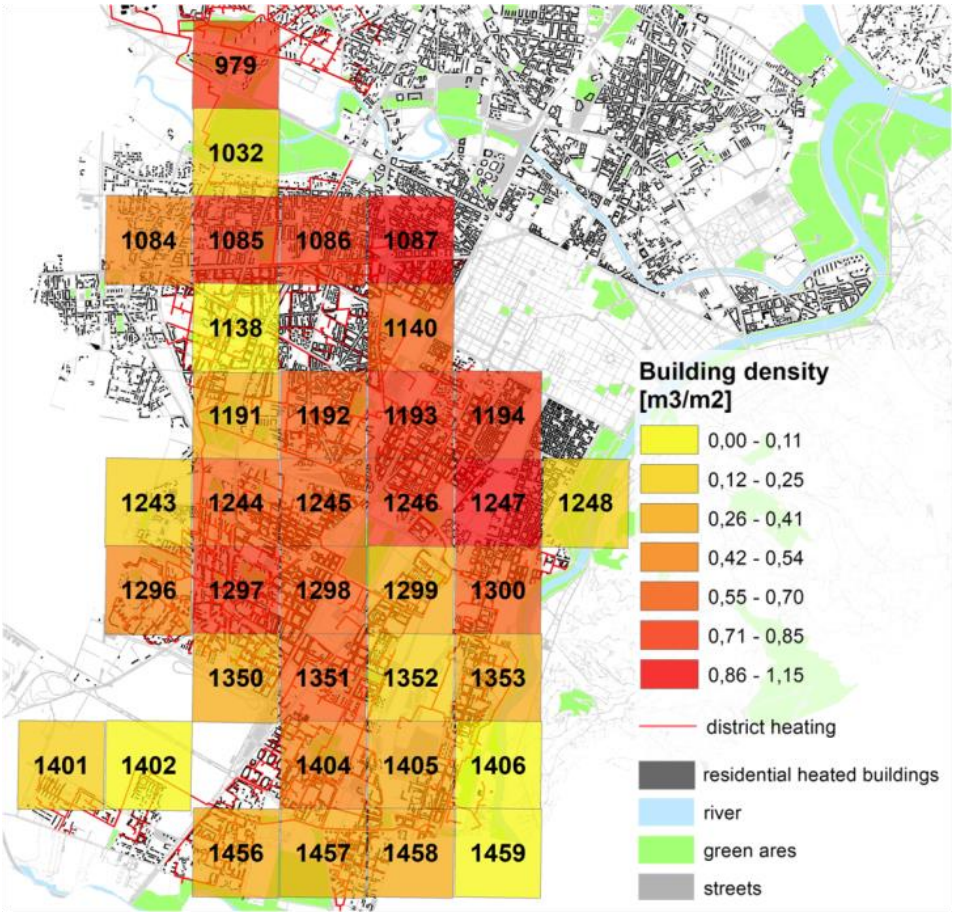

(a)

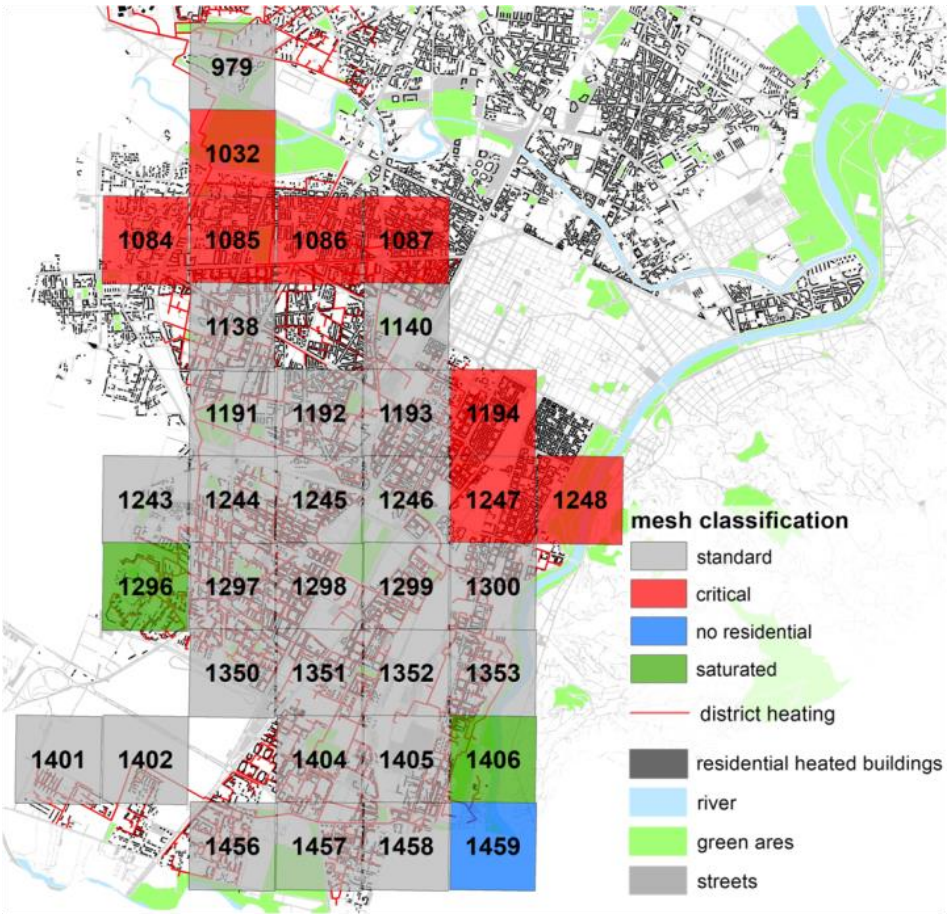

(b)

Figure 121. (a) Distribution of residential building density; (b) Classification of 36 meshes: standard, critical, not-residential buildings, saturated [55].

The scenarios analysed, that evaluate the energy savings (ES) through the hypotheses of energy efficiency, are the following:

- Group of scenarios 1. Energy savings (ES) assessment considering: 1a. ES trend *of residential apartments* without other energy retrofit interventions; 1b. ES trend *of residential apartments* plus a standard retrofit for the real connectable buildings; 1c. ES trend *of residential apartments* plus advanced retrofit for real connectable buildings.
- Group of scenarios 2. Energy saving assessment considering: 2a. ES trend *of residential apartments* plus standard retrofit for real connectable buildings and connected buildings; 2b. ES trend *of residential apartments* plus advanced retrofit for the real connectable buildings and connected buildings.

In the first phase, the energy savings hypotheses were evaluated only for the most critical meshes and the buildings that need an urgent retrofit have been identified in order to optimize the heat distribution in the DH network. Then, energy savings of residential buildings were evaluated considering the 8 critical meshes represented in Figure 121b.

Table 53 shows for each scenario the average real connectable quotas of buildings in the 8 critical meshes [%, MWh/y] and the energy savings [MWh/y] taking into account standard and advanced retrofit applied to connectable and connected buildings. Intervening only on the critical meshes there is a moderate energy savings; in particular, the real connectable quota in the first scenarios varies from 8.5 % in scenario 1a to 16.3 % with advanced retrofit in scenario 1c. In scenario 2, intervening with retrofit measures on all buildings (connected and connectable) the percentage of real connectable quota reaches 57.9 % (scenario 2b), with the advanced retrofit.

Table 53. Energy savings assessment of Turin critical areas (8 meshes, phase 1) [55].

Number meshes	Scenario	Average real connectable quotas in the 8 meshes [%]	Theoretic connectable quota [MWh/y]	Real connectable quota [MWh/y]	Energy savings [MWh/y]
8	1a	8.5	601,012	51,318	0
	1b	11.1		66,925	139,482
	1c	16.3		98,153	286,886
	2a	25,1		151,010	203,457
	2b	57.9		348,240	416,897

In phase two, the energy savings of residential buildings were evaluated considering the whole district heating area (36 meshes). In this case, the surplus of energy obtained with retrofit interventions is significant, especially with the advanced retrofit measures applied to all buildings (scenario 2b).

In Table 54 the results of phase 2 are shown with the surplus quota in brackets. The results shown a considerable reduction of thermal energy consumptions, with the possibility to connect almost all the potential buildings. In particular, in scenario 1 it is possible to connect 34.3% (40.5%) of potential residential buildings without energy retrofit (1a) and 53% (71%) with an advanced retrofit of the residential building stock (1c). In scenario 2, there is a connectable quota equal to 58% (79%) of the total through a standard retrofit, but with scenario 2b it is possible to reach 82% (168%).

Table 54. Energy savings (ES) assessment of whole Turin areas (36 meshes, phase 2) [55].

Number meshes	Scenario	Average of real connectable quotas (global with surplus) [%]	Theoretic connectable quota [MWh/y]	Real connectable quota [MWh/y]	Energy savings (ES) [MWh/y]	Surplus (energy savings, ES) [MWh/y]	Maximum energy required [MWh/y]
36	1a	34.3 (40.5)	1,410,985	483,446	0	87,899	2,169,097
	1b	41.5 (49.7)		585,557	294,786	116,126	2,140,870
	1c	52.5 (71.3)		741,369	650,375	264,897	1,992,099
	2a	57.8 (79.0)		815,559	626,842	298,679	1,958,317
	2b	81.7 (167.6)		1,152,841	1,407,373	1,211,706	1,045,290

The maximum energy supplied for the whole DH area is equal to 2,256,996 MWh/y, of which 1,680,536 MWh/y are connected buildings and 87,899 is a surplus. Taking into account the energy savings for the different scenarios, the energy supplied can be considerably reduced from 2,169,097 MWh/y (scenario 1a) to 1,045,290 MWh/y (scenario 2b). The energy required through an advanced retrofit of all residential buildings is reduced by 52%.

Figure 122 shows the maximum energy required for the different scenarios. For each mesh the energy quota required to cover the energy consumption was indicated (% and MWh/y) considering the current situation (scenario 1a), the standard retrofit (scenarios 1b and 2a) and the advanced retrofit (scenarios 1c and 2b).

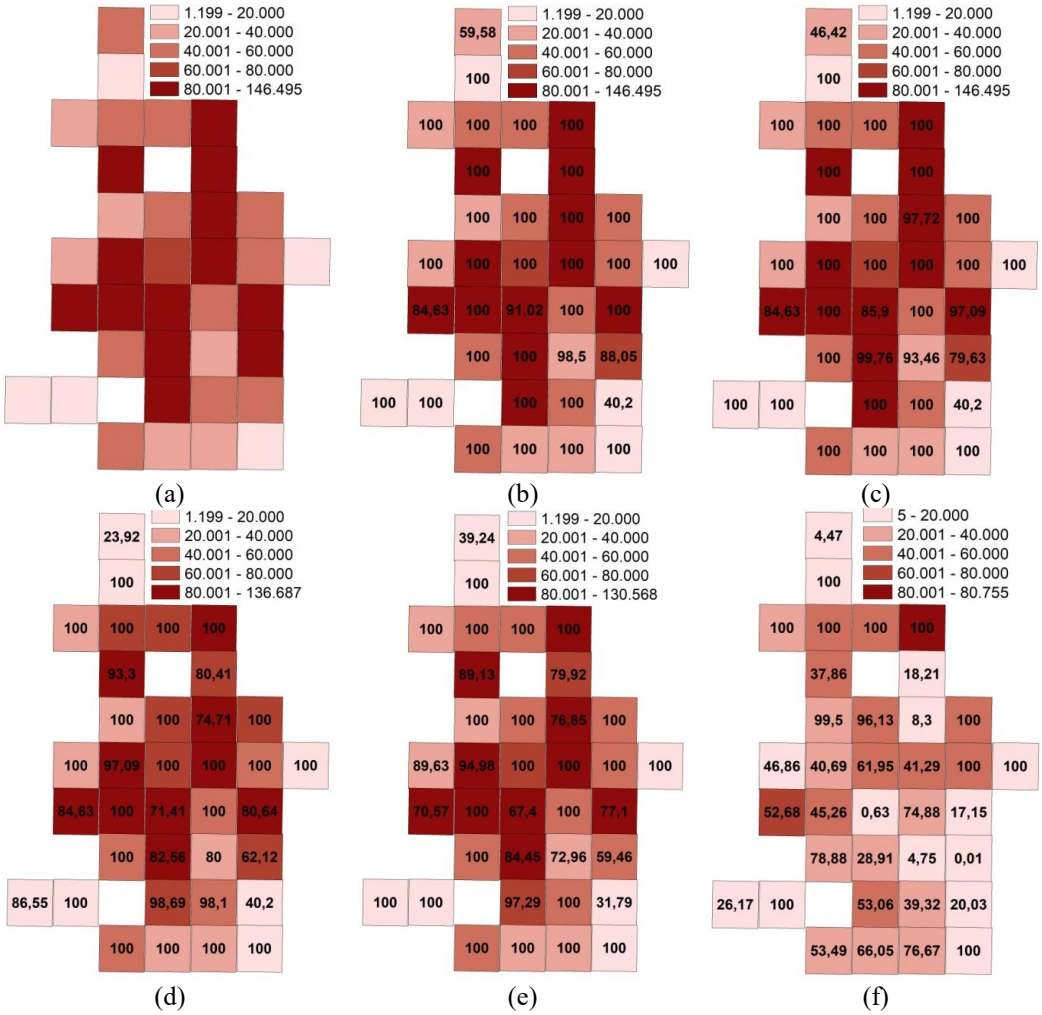

Figure 122. Maximum energy supplied [MWh/y] for: (a) case study; (b) 1a, energy savings (ES) without energy retrofit; (c) 1b, ES with standard retrofit of residential connectable buildings; (d) 1c, ES with advanced retrofit of residential connectable buildings; (e) 2a, ES with standard retrofit of residential connectable & connected buildings; (f) 2b, ES with an advanced retrofit of residential connectable & connected buildings [55].

The retrofitting measures lead to a change in the water dynamic within the network. The evaluation of the effects on the water velocities within the pipelines is here performed through a fluid-dynamic model of the district heating network.

The model is based on the application of mass and momentum to respectively the nodes and the branches of the network; the network topology is expressed through a graph approach. The model allows evaluating the pressure and the mass flow rates in all the nodes and branches of the network. It has been validated [259,260] and it has already been used with the aim of pumping cost reduction [261] and thermal peak shaving [262]. All the scenarios analysed in this study (1a, 1b, 1c, 2a and 2b) are simulated through the fluid-dynamic model and the results obtained are shown in Figure 123. In the figure, the velocity in all the branches is plotted for all the scenarios considered. The velocity of the water is always lower than 4.5 m/s, thus acceptable. The velocity values tent to decrease while the retrofitting measure become more significant, i.e. the energy required by the user decreases. In case 2b, which is the scenario presenting the most effective retrofitting measures, the higher velocity value is about 3 m/s. The values progressively increases until 4.5 m/s in case 1a. The mean velocity value in the network also decreases, with increased weight of the retrofitting measures; in particular, the scenario 1a presents a mean velocity of 1.4 m/s, while the value is 0.9 m/s in the scenario 2b.

Then, the results show that in future scenarios with retrofit interventions there will be a decrease of the energy consumption with an improvement in the operation of the DH network and an over energetic potential (surplus) that could be used to serve other nearby areas; the reduction of energy consumption will determine also a consequent decrease of greenhouse gas emissions and the possibility to connect more users with therefore an increase of the liveability or urban spaces and probably an improvement of social life.

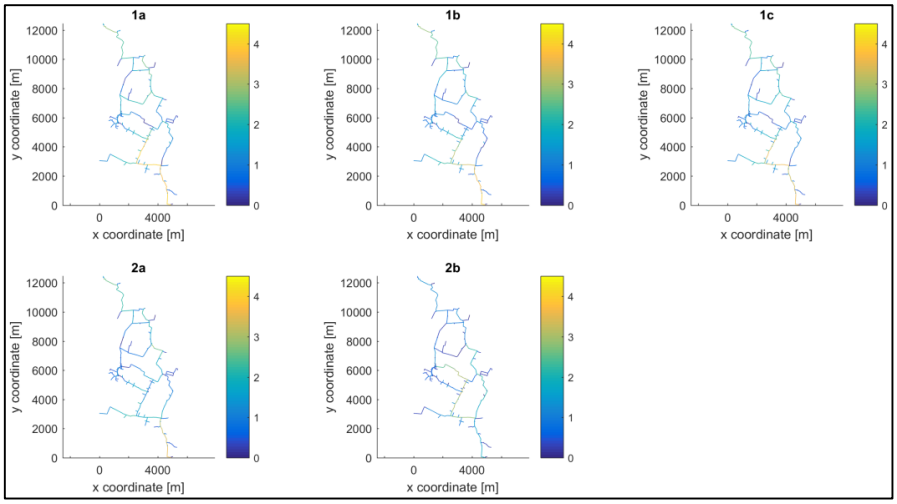

Figure 123. Comparison of velocity values [m/s] in the branches of the network between standard and advanced retrofit [55].

Considering the energy consumptions and the mix of the energy sources, the greenhouse gas emissions were also evaluate (in Table 55) in tCO_2/MWh [10]: gas oil = 0.280, LPG = 0.240, carbon = 0.370, fuel oil = 0.290, electricity energy = 0.460, natural gas = 0.210, solar thermal = 0.0; for the DH, the results of Data4Action project for Turin with 0.153 tCO_2/MWh. In the 36 meshes connected

to the DH network, the buildings with centralized heating system are 78 %, of which most of the buildings use natural gas (79.1 %), a small portion uses gas oil (14.6 %) and electricity energy (5 %). Buildings with autonomous heating systems (22 %) also use mainly natural gas (91.1 %) and electricity energy (4.6 %). Then, most of the residential buildings use natural gas for space heating and the distribution of the use of energy sources is consistent with the national residential energy consumption by source. The existing emissions, considering the current state, amounted to 676.547 tonCO2, then the emissions decrease by 19% with an advanced retrofit only for the real connectable buildings (scenario 1c) and they decrease up to 54% with an advanced retrofit for the real connectable and connected buildings (scenario 2b).

Table 55. Greenhouse gas emissions for each scenario [55].

Num. meshes	Scenario	Energy consumptions (DH) [MWh/y]	Energy consumptions (centralized systems) [MWh/y]	GHG emissions (DH) [tonCO2]	GHG emissions (centralized systems) [tonCO2]	GHG emissions (autonomous systems) [tonCO2]	Total emissions [tonCO2]
36	0	1,680,536	1,410,985	257,122	329,270	90,155	676,547
	1a	2,169,097	927,471	331,872	216,436		638,463
	1b	2,140,870	825,024	327,553	192,529		610,237
	1c	1,992,099	669,848	304,791	156,317		551,263
	2a	1,958,317	595,204	299,622	138,898		528,675
	2b	1,045,290	257,896	159,929	60,183		310,267

This investigation is useful for future hypotheses of energy efficiency policies, to understand how to exploit the energy surplus achieved thanks to the retrofit of the residential sector and to evaluate a possible retrofit of other sectors (municipal, tertiary and industrial). Furthermore, the socio-economic variables that influence the energy consumption trend could be taken into consideration, such as the characteristics of the inhabitants and the income and engineering models at district scale will be developed to take into account also the hourly energy profiles.

5.2.3 Monthly process-driven model

Starting from previous research [46], the EPC database is used to improve the accuracy simulation of two monthly USEMs (the ‘H+DWH’ model and ‘H’ model) and to update an existing urban-energy atlas of the city.

The aim of this assessment is to promote the sustainable development of cities by defining potential retrofitting strategies according to: the EPC database, the distribution of space heating (SH) and domestic hot water (DHW) consumptions, and the real characteristics of the built-up environment. The main objectives of this analysis can be summarised as follows:

- This method optimizes the simulation accuracy of an engineering model by improving the input data. The model simulates SH and DHW consumption at an urban scale, with monthly details, considering the real characteristics of the buildings and their surroundings.
- An urban energy atlas is presented, it uses a GIS-mapping tool, gives information on EE trends, and creates energy consumption and energy saving maps of buildings at different territorial scales, for both individual buildings and aggregated data. This update has been possible thanks to the use of GIS tools and to the flexibility of the methodology. The GIS-based engineering model mainly uses open data, and it is possible to easily apply it to different cities. The impact of EE measures on the EP of buildings can easily be assessed by integrating the atlas with an EPC database and applying energy models.
- An in-depth analysis of the energy retrofitting of buildings provides possible low-carbon emission energy scenarios for a more resilient and sustainable city. The reduction in energy consumption and, consequently, in GHG emission has been assessed.

Methodology

Since an EPC scheme is an important tool to support EE in buildings and to give information on the EP of a building, an EPC database has been used to identify retrofitting scenarios for residential buildings, to improve the input data of a GIS-based energy model and to update an energy atlas by creating a new retrofitting database. Figure 124 shows the main steps:

1. *Analysis of the EPC database* (see section 5.2.1). The EPC database of residential buildings in the Piedmont Region has been processed and elaborated to support energy retrofitting strategies and to assess the EP of buildings. After the acquisition and analysis of the EPC, homogenous groups were identified. The residential buildings were classified as flats or detached houses using the *S/V* ratio. Since the main characteristics of a building depend on the construction period, eight classes of buildings were created. Three databases were created according to the motivation for the release of the EPC: generic for existing buildings, retrofit for retrofitted buildings and Res for buildings that have undergone the installation of renewable energy technologies. The EP of residential buildings and the energy savings were calculated, for each homogenous group, on the basis of the retrofitting intervention and the installation of renewable energy technologies.
2. *Input data improvement* of an existing monthly engineering model, using the real characteristics of buildings. An existing GIS-based monthly engineering model [46] was updated to assess residential energy consumption at different territorial scales, using real input data of the

thermal transmittance values of the opaque envelope (*Uop*, W/m^2/K) and glazing (*Ug*, W/m^2/K) of the buildings, and the space heating (η_H, -) and domestic hot water (η_{DHW}, -) system efficiency. The thermal transmittance values and system efficiencies in the first version of the engineering model referred to literature reviews and Italian standards (standard operating conditions) and did not take into account the share of retrofitted buildings. Therefore, the accuracy of the previous model has been improved using new input variables (*Uop*, *Ug*, η_H and η_{DHW}) that are the result of EPC data processing.

3. *Identification of EE scenarios.* EE assumptions were made considering the most frequently used energy retrofitting measures. The thermal consumption was simulated, before and after the use of EE measures, for non-retrofitted residential buildings, to assess the energy and environmental impacts.
4. *Design of an urban-energy atlas* of the city of Turin [15] –which is able to map and visualise, for example, the energy retrofitting trends– with the EPC database of residential buildings. The main information that was added was: the energy label, EP, and the reachable EP of residential buildings, the used energy retrofitting measures, and presence of RES technologies.

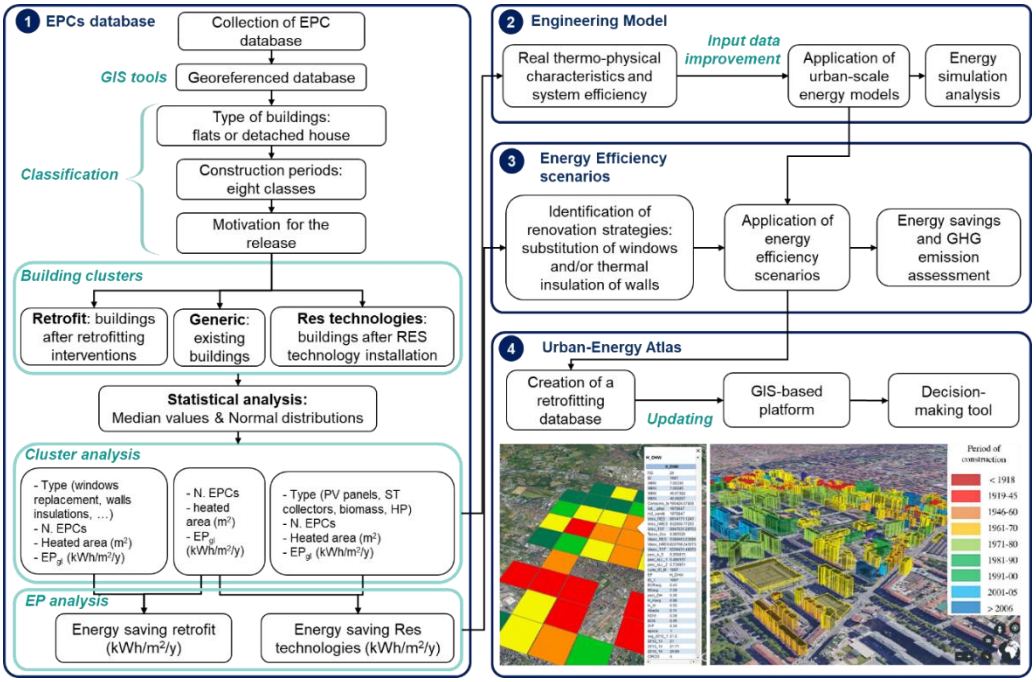

Figure 124. Flowchart of the methodology: EPC database processing, engineering model application, identification of energy efficiency scenarios, and urban-energy atlas updates as a decision-making tool [13].

Monthly engineering model

As previous mentioned, this study proposes an improvement in the input data of an engineering model at an urban scale, and investigates EE scenarios as taken from an EPC database. Energy consumptions for the space heating (H) and

domestic hot water (DHW) of residential buildings, with monthly details, were simulated at a district level (1 km^2 mesh) for three consecutive heating seasons (2012/2013, 2013/2014 and 2014/2015). The existing urban-scale energy models for H+DHW and H were optimised using new *U-vales* and *η-values* elaborated from an EPC database (2009-2015).

The presented GIS-based engineering model was based on a thermal balance at an urban scale. The H and DHW consumptions of residential buildings served by the DHN were simulated for a 1 km x 1 km mesh. In a previous work [46], the model was validated using the real energy consumption of three consecutive heating seasons (2012/2013, 2013/2014 and 2014/2015). The measured consumption data for H and DHW were aggregated data and referred to residential users located in 1 km x 1 km meshes. For this reason, the engineering model was designed according to this scale, but being flexible, it can also be applied to the building scale or the entire city [47]. The model was designed according to the ISO EN 52016-1:2017 and ISO EN 52017-1:2017 standards for residential buildings, and the main input data, elaborated with GIS tools (ArcGIS, ESRI) at building and district scales, were indicated as follows:

- *Building data*: type of user, construction period, maintenance level, net/gross heated area, net/gross heated volume, internal building air temperature (T_{ai}, °C), *U-values* of the opaque envelope and glazing ($W/m^2/K$), compactness or *S/V* (m^2/m^3) ratio, and η (-). Some new input building data were calculated at a district scale (*U-values* and *η-values*) from the EPC database to improve the simulation accuracy.
- *Local climate data*: air *temperature* (T_{ae}, °C) and relative humidity (*UR*, %), solar irradiance (I_{sol}, W/m^2) and heating degree days (*HDD*, °C).
- *Urban parameters*: the *orientation* of the main streets (*MOS*, -), the sky view factor (*SVF*, -), the relative height (H/H_{avg}, m^2/m^2) and the canyon effect, which is described as the height-to-width (*H/W*, m^2/m^2) ratio. These parameters were calculated at an urban level for each mesh.

In order to apply the urban balance, specific values of *U* and η were identified for each construction period, and an average value was given with each district (1 km^2), considering the percentage distribution of the buildings with different construction periods and the quota of heated volume served by the DHN. The thermal transmittances of the opaque envelope (U_{op}) and glazing (U_g), and the *η-values* were calculated from the EPC database of the city of Turin, according to the motivation for the release of the EPC (*generic* or *retrofit*). The median values of U_{op}, U_g, η_H and η_{DHW} were then calculated for each mesh. The conversion factors for the energy supplied as primary energy from the Turin DH system were used.

Energy Efficiency scenarios

In the third part of this work, EE scenarios were hypothesised considering the real characteristics of the existing building heritage. The following retrofitting

measures were identified from an analysis of the EPC database (*retrofit*) of the city: installation of thermostatic valves; thermal insulation of the roof; thermal insulation of the slab and/or floor; replacement of windows; thermal insulation of the opaque envelope and window replacement.

Once the most common retrofitting measures were known, and the real characteristics of the buildings were taken into account, EE scenarios were hypothesized. In this work, two energy efficiency scenarios were applied for each mesh in the district heating area: (i) thermal insulation of the opaque envelope, (ii) and thermal insulation of the opaque envelope and window replacements. The monthly energy models were used to evaluate the H and DHW consumptions before and after the energy retrofitting of the residential buildings. The energy savings and GHG emission reductions were assessed for each mesh. Furthermore, an analysis on the cost implications of retrofitting measures was carried out.

Case study

Specific values of U_{op}, U_g, η_H *and* η_{DHW} were then calculated, according to the EPCs in the DH area, from the EPC database for each mesh (column 1 indicates the ID mesh code, see Table 56) for the different construction periods and considering the quota of heated volumes served by the DHN.

Table 56 shows a comparison between the old (i) and the new (ii) values of U_{op}, U_g, η_H *and* η_{DHW} for each mesh. The number of EPCs in each mesh, the percentage of heated volumes of EPCs served by the DH network, the prevalent period of construction and the prevalent energy class (from A+ to G) with the percentage, distinguishing between the *generic* database with 41,190 EPCs and the *retrofit* database with only 658 EPCs, are also indicated in Table 56. It is possible to observe that the energy class of *generic* buildings is worse in almost all the meshes, and is equal to G. On the one hand, this is negative from an energy point of view, but at the same time it can represent a possibility of promoting EE measures, as only 2% of the buildings had been retrofitted by 2015, with a no significant improvement in the energy class.

Table 56. Comparison of the input data for the old version (i) and the new updated (ii) monthly model: U-values (Uop and Ug), heating (ηH) and domestic hot water (ηDHW) system efficiencies [13].

ID mesh	No. of EPCs	Heated volume (EPCs)	Heated volume (EPCs) served by DH	Prevalent period*	U_{op} (i)	U_{op} (ii)	U_g (i)	U_g (ii)	η_H (i)	η_H (ii)	η_{DHW} (i)	η_{DHW} (ii)	Prevalent energy class (from A+ to G) with the % of EPCs	
		m^3	%	-	$W/m^2/K$				-		-		*generic*	*retrofit*
979	80	20,414		1981-90	0.91	1.18	4.02	4	0.81	0.78	0.6	0.71	G, 50%	-
980	631	177,535	22.9	1961-70	1.07	1.13	4.48	4.15	0.74	0.8	0.6	0.6	G, 62%	A+, 57%
981	1,454	332,024	100	1961-70	1.07	1.15	4.48	4.27	0.74	0.89	-	-	G, 65%	F, 43%

1031	309	89,364	30	1971-80	1.05	1.05	4.5	3.29	0.68	0.91	-	-	G, 50%	E, 50%
1032	712	183,767	100	1961-70	1.13	1.14	4.67	4.21	0.68	0.83	-	-	G, 60%	G, 39%
1033	768	206,097	79.7	1946-60	1.2	1.17	4.58	4.24	0.79	0.81	-	-	G, 64%	D, 50%
1034	1,141	310,701	58.2	1961-70	1.15	1.16	4.53	4.48	0.68	0.83	-	-	G, 64%	G, 75%
1084	1,277	341,294	50.7	1946-60	1.09	1.14	4.43	4.26	0.71	0.79	0.6	0.6	G, 60%	F, 50%
1085	2,387	740,149	55.1	1961-70	1.16	1.15	4.61	4.41	0.71	0.78	0.6	0.6	G, 63%	G, 37%
1086	2,365	714,115	54.9	1946-60	1.2	1.17	4.58	4.3	0.71	0.76	0.6	0.6	G, 64%	F, 45%
1087	2,538	846,345	40.2	1946-60	1.25	1.21	4.62	4.41	0.71	0.79	0.6	0.68	G, 65%	F, 49%
1137	1,282	312,468	27.5	1961-70	1.05	1.15	4.43	4.35	0.68	0.78	0.6	0.6	G, 63%	G, 68%
1138	2,219	632,729	19.7	1961-70	1.05	1.13	4.33	4.28	0.76	0.77	0.6	0.6	G, 52%	F, 24%
1139	1,963	487,375	26.5	1919-45	1.19	1.19	4.55	4.35	0.72	0.81	0.6	0.6	G, 65%	F, 34%
1140	890	311,087	13.5	1919-45	1.2	1.15	4.58	4.19	0.76	0.78	0.6	0.61	G, 56%	F, 50%
1141	1,075	480,434	100	< 1918	1.31	1.15	4.64	3.85	0.76	0.82	0.6	0.6	G, 64%	G, 41%
1190	427	99,970	100	1961-70	1.06	1.05	4.49	3.86	0.68	0.78	-	-	G, 62%	D, 50%
1191	482	119,178	13.1	1961-70	1	1.14	4.15	4.41	0.7	0.75	0.6	0.6	G, 52%	E, 72%
1192	1,871	447,703	30	1946-60	1.14	1.17	4.49	4.44	0.73	0.8	0.6	0.6	G, 59%	G, 72%
1193	1,874	744,487	22.8	1919-45	1.22	1.18	4.7	4.33	0.85	0.8	0.6	0.6	G, 60%	F, 35%
1194	1,387	568,806	34.6	1919-45	1.3	1.2	4.73	4.18	0.81	0.8	0.6	0.75	G, 68%	F, 49%
1244	1,798	453,581	23.5	1971-80	1.07	1.13	4.53	4.45	0.68	0.78	-	-	G, 49%	G, 50%
1296	828	254,071	11.7	1971-80	0.95	1.18	4.23	4.39	0.69	0.8	0.6	0.6	G, 42%	C, 43%
1297	2,032	521,107	22.7	1961-70	1.05	2.11	4.54	4.31	0.8	0.8	-	-	G, 51%	F, 59%
1298	1,821	491,805	16.2	1961-70	1.11	1.13	4.64	4.35	0.79	0.77	0.6	0.6	G, 52%	G, 40%
1300	1,569	427,182	13.7	1946-60	1.13	1.16	4.42	4.37	0.79	0.8	0.6	0.72	G, 53%	E, 21%
1350	466	129,190	12.6	1946-60	1.08	1.2	4.48	4.56	0.67	0.82	0.6	0.77	G, 56%	E, 50%
1351	1,621	452,981	20.3	1961-70	1.07	1.17	4.49	4.34	0.68	0.79	0.6	0.63	G, 47%	F, 46%
1353	1,114	288,540	14.7	1946-60	1.17	1.2	4.6	4.19	0.79	0.79	0.6	0.6	G, 56%	G, 55%
1402	357	94,866	68.7	1971-80	1.07	1.21	4.53	3.74	0.68	0.89	-	-	G, 57%	C, 100%
1403	1,038	268,546	25.9	1971-80	0.96	1.11	4.14	4.22	0.69	0.77	0.6	0.6	G, 46%	F, 80%
1404	1,095	299,132	18.7	1961-70	0.95	1.15	4.21	4.46	0.69	0.82	0.6	0.6	G, 49%	F, 50%
1405	977	255,431	23.3	1961-70	1.13	1.2	4.52	4.06	0.68	0.78	-	-	G, 54%	F, 58%

Results

This assessment has analysed the EPCs database of residential buildings in the Piedmont Region (Italy). The EPCs have been elaborated through the use of a GIS tool to assess the distribution of building characteristics and EE measures in the city of Turin. The residential energy consumptions (H+DHW and H) have been simulated through the use of a monthly engineering model of buildings served by

the DHN. The model was only applied to the district heading area of the city, since the accuracy of the modal had already been validated using district heating consumption. The energy simulations of these models have been improved using EPC information as input data, and the validation has been made by comparing the measured and simulated data of three consecutive heating seasons (2012/2013, 2013/2014 and 2014/2015). An urban-energy atlas has been implemented for the city and EE scenarios have been elaborated according to the EPC database.

Engineering model application

The presented engineering model is able to predict the energy consumptions, with monthly time steps, for H and DHW. The accuracy of these models depends not only on the input data but also on: (i) the distribution of the type of users, since the model simulates residential consumption at a district scale, and the percentage and number of residential buildings in each district; (ii) the percentage of heated volume served by the DH network, and the models were in fact validated using the DH consumptions at a district scale; (iii) and the dimension of the used territorial unit [15,46]. A total of 26 meshes were selected from the original 33 to show the obtained results; some meshes were excluded due to the presence of erroneous data in the input database. Figure 125 shows a comparison of the measured (x-axis) and the simulated data (y-axis) for the old (i) and the new updated (ii) engineering models. The global consumptions (of three consecutive heating seasons) are indicated for each mesh, distinguishing between the H+DHW model (Figure 125a) and the H model (Figure 125b). It is possible to observe a general improvement in the accuracy for both models, especially for the H+DHW model.

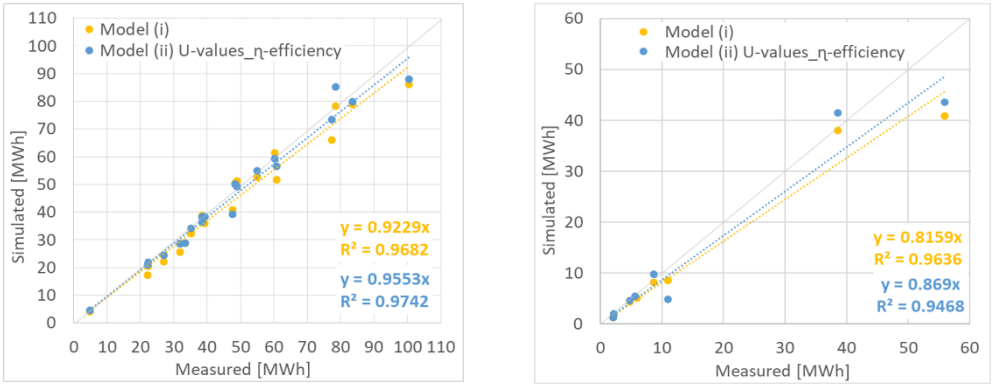

Figure 125. Comparison of the measured and simulated energy consumptions for three consecutive heating seasons (2012-13, 2013-14 and 2014-15) for the old (i) and new (ii) USEMs: (a) the H+DHW model and (b) the H model [13].

The relative error, E_r, (calculated as the difference between the measured and simulated data, divided by the measured data) was used to assess the precision of the model. Figure 126 and Figure 127 show the global relative error ($E_{r,global}$, %) of the H+DHW and H models for each mesh. The errors for the updated models (ii) were generally lower, although this was not observed in some meshes where there

were only a few EPCs and only a few flats were served by the DHN (see Table 56). In this case, the number of EPCs and/or the quota served by the DHN were not sufficient to describe the real characteristics of the residential building stock. Regarding the H+DHW model (Figure 126), no improvement was observed in the energy simulation in meshes 1298 and 1404, which showed an average $E_{r,global}$ of 16%. In this case, the increase in error depends on the quota served by the DHN; in fact, only 16% of the EPCs located in the district are served by the DHN in mesh 1298 and this percentage is about 19% in mesh 1404 (see Table 56). As far as the H model is concerned, an $E_{r,global}$ of 13 and 8%, respectively, can be observed in meshes 1033 and 1297 (Figure 127). There are just over 700 EPCs in mesh 1033 (see Table 56), and only 23% of the EPCs in mesh 1297 are served by the DHN. The number of EPCs in each mesh and the quota of EPCs served by the DHN are important t to describe the characteristics of the buildings; when the EPC quota was not sufficient, the input data optimisation was invalidated. However, the input data improvement in all the other meshes has given an important contribution to the assessment of the EP of buildings at an urban scale.

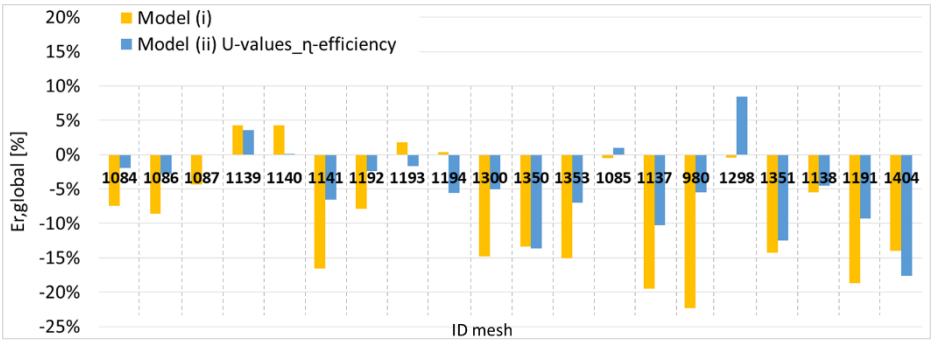

Figure 126. Comparison of the global relative error (Er,global - %) for the old (i) and new (ii) monthly H+DHW models [13].

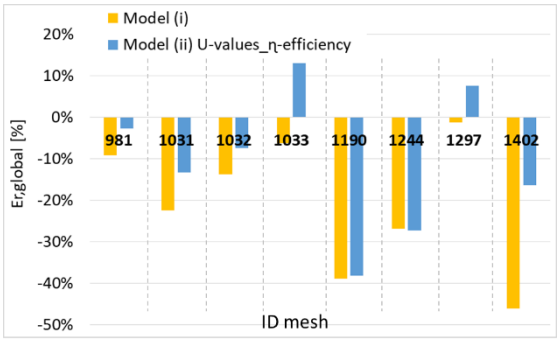

Figure 127. Comparison of the global relative error (Er,global - %) for the old (i) and new (ii) monthly H models [13].

Energy efficiency scenarios

In line with the most common efficiency measures used in the city and taking into account the real characteristics of the considered buildings, two EE scenarios have been hypothesised in the district heating area of Turin: (i) thermal insulation of the opaque envelope; (ii) thermal insulation of the opaque envelope and window

replacements. Effective energy retrofitting measures can be identified using these models and considering the most critical areas with the worst air quality conditions and highest building energy consumptions.

Figure 128 shows the monthly space heating consumption of meshes 1086 and 1193 for the 2014-2015 heating season. The measured data (in grey) were compared with the simulated ones (in red), distinguishing between the old model (i) and the optimised model (ii). The seasonal relative error decreases from 8.6 to 7.4% for mesh 1086 as a result of the optimisation, and from 3.4 to 0.1% for mesh 1193. Two retrofitting scenarios were investigated (in blue) considering the most common EE measures: the thermal insulation of the opaque envelope of residential buildings was hypothesised in the first one (S1), while window replacement was added to S1 in the second scenario (S2). The greatest energy savings occur during the winter months, when the energy consumption for heating is higher. An annual energy saving of 4,400 MWh/year is observed in mesh 1086, and the energy saving is 5,072 MWh/year in mesh 1193.

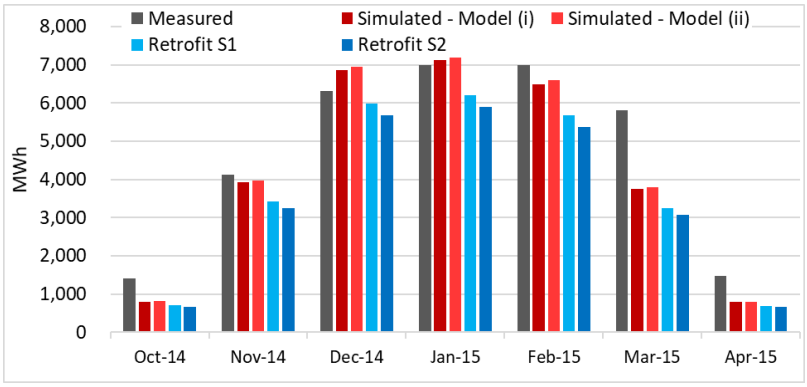

(a)

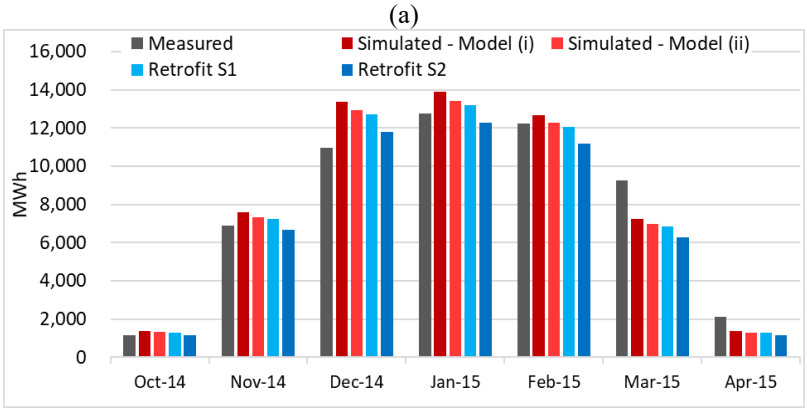

(b)

Figure 128. Monthly results of DH consumption: measured, simulated (models i and ii), with retrofitting measures (scenario 1 with thermal insulation of the opaque envelope and scenario 2 with thermal insulation of the opaque envelope and window replacements) for (a) mesh 1086 and (b) mesh 1193 [13].

The monthly H and DHW models were then used to quantify the energy savings of residential buildings served by the DHN, and the GHG emission reduction was assessed using 0.154 tonCO_2/MWh for district heating [10] (that is, the conversion emission factors of the DHN). In the first scenario, the thermal transmittance values

of the opaque envelope after retrofitting interventions were used as input data, considering the quota of residential buildings already renovated and the main construction period. In this case, an energy saving of 22,251 MWh/y is obtained and a consequent reduction in GHG emissions of 3,404 tonCO_{2eq}/y. On the other hand, it is possible to achieve an annual energy saving of 79,064 MWh/y with a GHG reduction of 12,097 tonCO_{2eq}/y for the thermal insulation of the opaque envelope and window replacements.

With this place-based tool, it is possible to visualise the distribution of energy savings and GHG emission reductions at a territorial level. Figure 129 shows an example of the results of the two scenarios at a district scale (1 km x 1 km mesh). The annual energy saving (MWh·10^3/y) is indicated for each mesh. From the results of this work, it has emerged that it would be possible to reduce the energy consumption of residential buildings with low energy performance served by the DHN by thermally insulating the opaque envelope and replacing the windows. Other measures could be used to further reduce the energy consumption of these buildings, for example, the installation of thermostatic valves and the use of RES technologies. The impact of these measures will be investigated in future work using an updated EPC database.

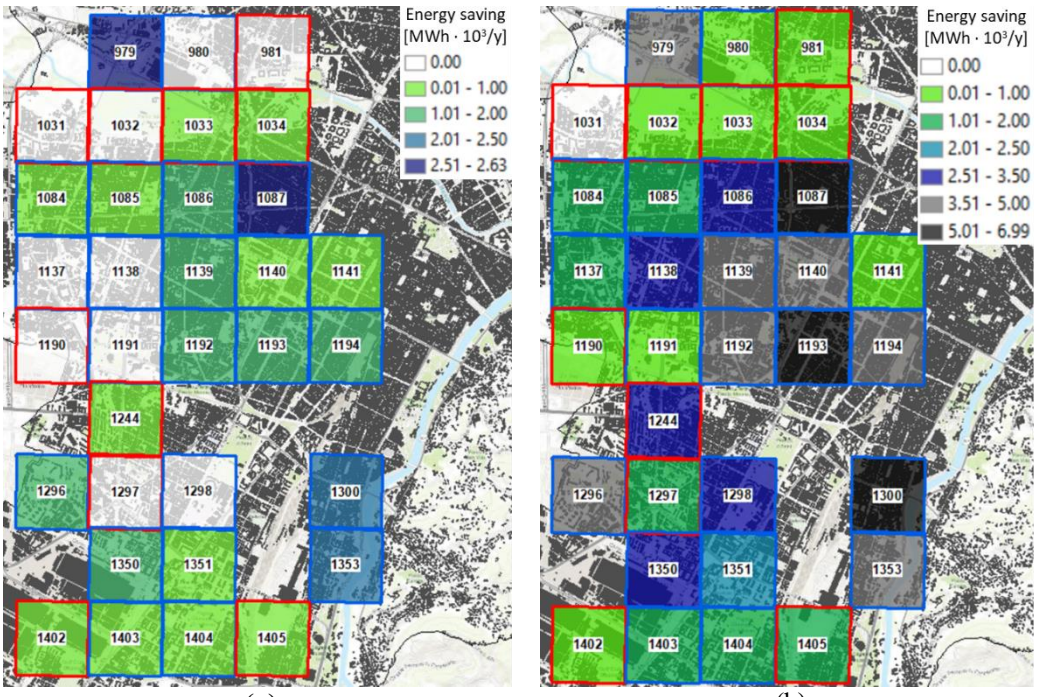

(a) (b)

Figure 129. Annual energy savings at a district scale after energy retrofitting strategies: (a) thermal insulation of the opaque envelope (b) thermal insulation of the opaque envelope and window replacements [13].

Costs analysis

In this section, a new retrofitting database has been created using EPCs data. It was necessary to perform a statistical analysis of the EPC data when working at an urban scale in order to discard anomalous data and to find characteristic data of the

buildings. Summarising: (i) the input data of an engineering model were improved using the EPC data; (ii) the energy savings that could be attained as a result of retrofitting interventions were investigated with the same database considering the characteristics of the buildings; (ii) thanks to these assessments, the EE interventions that can be done in the city have been identified and the energy saving have been quantified.

It is necessary to consider the costs of the interventions for the application of EE scenarios. An analysis on the costs of EE measures, in which National trends are taken into account, is described in this section. Four retrofitting interventions have been considered to improve the EP of building: thermal insulation of the roof, thermal insulation of the slab/floor, window replacements, and thermal insulation of vertical walls and window replacements. Table 57 shows the cost of such interventions, as elaborated from the ENEA (Italian National Agency for New Technologies, Energy and Sustainable Economic Development) Report on EE, to monitor and evaluate developments of national energy policies (updated to 2019) and energy savings (%) based on the EPC database.

Table 57. Costs of the retrofitting measures and the energy saving (%) of residential flats [13].

Retrofitting measure	**Costs of retrofitting measure (€/m²)**	**Range of energy saving (%)**
Thermal insulation of the roof	105* €/m² (m² refers to the roof/slab/floor area)	11-25%
Thermal insulation of the slab/floor		5-7%
Window replacements	890 €/m² (m² refers to the surface of windows)	11-25%
Thermal insulation of vertical walls	92 €/m² (m² refers to the surface of walls)	24-34%

* The ENEA Report only indicated an average cost for the roof and slab/floor interventions.

The costs of the interventions indicated in Table 57 were applied to the city of Turin, and Figure 130 shows the costs of the EE scenarios for each mesh (expressed in M€) applied to the whole district heating area considering the two analysed scenarios. Higher costs in general correspond to areas with more significant energy savings (see Figure 13). Multi-criteria analyses will be carried out in future works to identify effective financial schemes to promote EE in buildings and to assess the cost-effectiveness of EE measures, considering the existing tax incentives [263].

This investigation shows how an improvement of input data can reduce the output errors of an energy model by approximately 4%. This has been possible thanks to the processing and elaboration of the EPC data and the creation of a GIS retrofitting database. The EE scenarios were hypothesised considering the real characteristics of the existing building heritage. Further improvements can be introduced to optimise the model, which is, adding other variables that affect the evaluation of thermal consumption to the methodology. Socio-economic factors, such as income level, type of income, number of occupants and their age, are in fact known to influence the energy consumption in buildings and the applicability and

efficacy of energy policies [264]. If fuel prices increase, consumers with a low income tend to decrease their consumption (by changing their behaviour) more than wealthy families [265]. Since socio-economic factors affect energy consumption, urban scale energy models will be implemented, taking into consideration the real characteristics of the population, in order to identify effective energy measures. In addition, the education level also seems to have an impact on energy savings and behaviour [266].

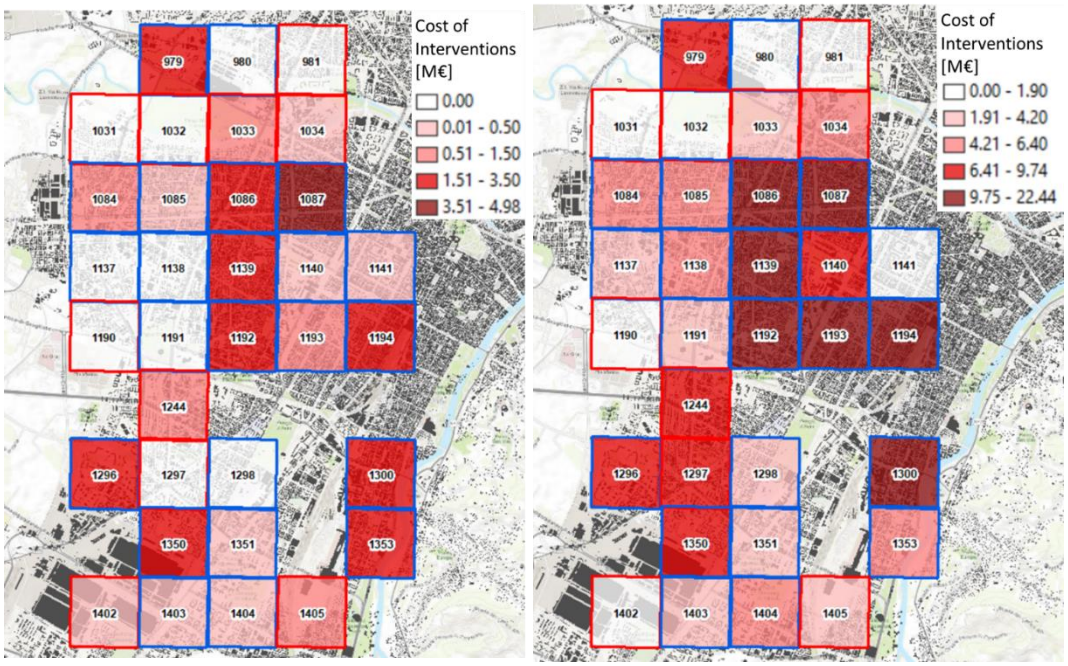

(a) (b)

Figure 130. Costs of the interventions at a district scale when applying energy retrofitting strategies: (a) thermal insulation of the opaque envelope (b) thermal insulation of the opaque envelope and window replacements [13].

The limitations of these types of models are that the necessary data are often not available, but the here presented monthly engineering models mainly simulate consumptions using open data, and it is therefore possible to apply such models easily to different cities with a sufficient degree of accuracy to be able to evaluate the distribution of consumption at a city scale. Urban planners, stakeholders, and policy makers could make use of these tools to identify effective EE strategies and smart-green solutions, and energy saving policies could incorporate this place-based approach. In addition, in this way, it would be possible to inform citizens about the energy consumption of their buildings, thus encouraging them to improve their EP.

5.3 Smart rooftop solutions and green infrastructures

The decrease of energy consumptions in buildings is one of the measures to improve the liveability and quality of cities reducing greenhouse gas emissions (GHG) and mitigating the urban heat island (UHI) effect [134,267]. These

emissions are in most part from non-renewable energy sources and the use of smart green technologies has become a viable cleaner alternative [268]. Therefore, the role of RESs such as the solar energy for sustainable energy production in cities is of the utmost importance [115]. These technologies are able to promote the liveability of cities, to improve the quality of life reducing the energy consumption and GHGs in buildings, exploiting the RES, and mitigating the UHI effect [269,270]. In addition, green-roof technologies, which have high thermal inertia technology, guarantee an excellent thermal behaviour in both heating and cooling seasons with consequent good thermal comfort conditions [271,272]. Moreover, the combination of green roof and green walls improves buildings performance with a significant reduction in thermal consumptions [273].

Urban rooftops are a potential source of water, energy, and food that contribute to make cities more resilient and sustainable. The use of smart technologies such as solar panels or cool roofs helps to reach energy and climate targets [274,275].

This section examines the roofs' potential in a densely built-up context, analyzing the effects of smart green technologies on energy savings and thermal comfort conditions at district scale. The methodology presented can be used to accurately estimate green roof potential on existing building stock at national, municipal, district and building level, with direct application in energy efficiency policy design. With the support of a place-based approach, the methodology is applied to the city of Turin in Italy, a 3D roof model was designed, some scenarios were investigated, and priorities of interventions were established, taking into account the conditions of the urban landscape. The applicability of smart solutions was conducted as a support to the review of the Building Annex Energy Code of Turin, within the project 'Re-Coding', which aimed to update the current building code of the city. In the Turin context, using an insulated green roof, there was energy saving in consumption for heating up to 88 kWh/m^2/year and for cooling of 10 kWh/m^2/year, with a reduction in greenhouse gas emissions of 193 tCO_{2eq}/MWh/year and 14 tCO_{2eq}/MWh/year, respectively. This approach could be a significant support in the identification and promotion of energy efficiency solutions to exploit also renewable energy resources with low greenhouse gas emissions.

5.3.1 Methodology

The methodology described in this section was applied to the city of Turin. The city is located in the north-western part of Italy and has a continental climate and almost 900,000 inhabitants. The aim was to assess the applicability of rooftop renovation strategies in a built-up context at district level, investigating environmental, social, and economic impacts of smart roof solutions. Figure 131 describes in detail materials, methods, and tools used.

A place-based model has been developed to improve energy management of buildings using smart green technologies – solar panels, collectors, and green roofs

– on the top of buildings in order to identify low-carbon infrastructure strategies. Energy consumptions of buildings sector with monthly detail have been assessed at districts scale, and roofs suitability has been investigated to evaluate usable solar energy and potential green roofs.

This methodology has been proven to be flexible and easily applicable in different districts and neighbourhoods. On one hand, some neighbourhoods and/or buildings are better suited for solar active technologies, where energy that can be produced using PV panels and ST collectors. On the other hand, some areas are more suited for installing green technologies like intensive and extensive green roofs.

The creation of a 3D-roof model is useful to assess solar energy and green roofs potential. The potential of roof retrofitting depends on: the structural static capacity of the buildings, the cover material and the physical aspects of the roof, such as the available surface and inclination [208]. In addition, the local built environment plays a significant role in urban areas, due to the shadowing effects of the surrounding buildings [276].

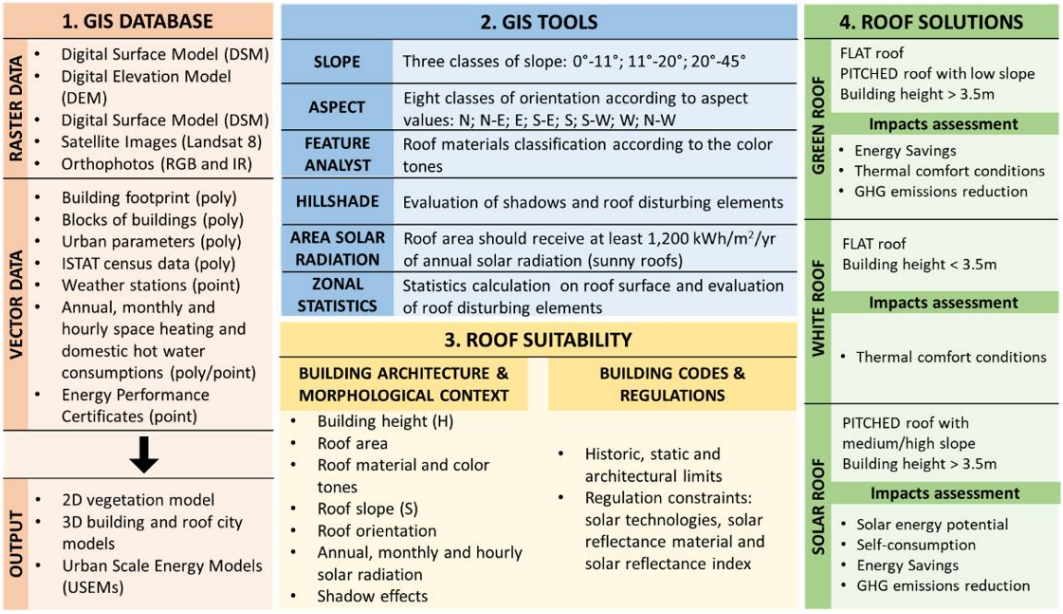

Figure 131. Flowchart of materials, methods, and tools [56].

Input data

A georeferenced territorial database (DBT) was organized using ArcGIS 10.7, and a 3D-roof model for buildings has been created. The DBT includes:

- Remote sensing images from Landsat 8 (OLI/TIRS) with a precision 30 meters that have used to analyse the land cover types (territorial scale).
- Orthophotos with RGB (red, green, blue) and IR (infrared) spectral bands with a precision of 0.1 meters (building scale) useful to evaluate colour tones.

- Digital Surface Models (DSM) with a precision of 0.5 and 5 meters, represents the earth's surface and includes all objects (surfaces of trees, buildings), have been used for roof analysis and solar radiation assessment on the rooftop (building scale).
- Building data from Municipal Technical Map that gives information on a building's footprint, area, volume, number of floors and type of users (building scale).
- Local climate data from weather stations (WS) with monthly and hourly precision: air temperature, relative humidity, vapor pressure, wind velocity and the solar radiation.
- District heating (DH) energy consumptions of residential buildings with monthly and hourly precision (building and districts scale).
- Energy Performance Certificates (EPC) database from Piedmont Region.
- Socio-economic data from ISTAT census section and urban variables (building blocks scale) with the characteristics of technological systems.

Rooftop potential

This section presents the criteria used to evaluate the feasibility of rooftop renovation and to identify the correct rooftop strategy as a function of urban environment.

These criteria refer to building architecture, morphological context (Table 58), building codes, and regulations. The information of buildings' architecture and morphological context were investigated using the DBT presented in Section x. According to Italian Standard (UNI) 11235:2015 and to the literature review [277,278], the following criteria were identified to select the potential roofs.

- Building height had to be higher than 3.5 m for green roofs, while for albedo strategies (high-reflectance roof) it had to be less than 3.5 m in order to have the greatest effect on near-surface air temperatures.
- Roof area had to be greater than 100 m^2 for green roofs; for high-reflectance roofs, greater than 20 m^2.
- Roof material and colour tones for green and high-reflectance roofs were excluded; roofs with high reflectance and vegetated roofs, solar roofs, roofs with red tiles and/or disturbing elements, such as dormers and/or antennas, were excluded.
- Roof slope had to be less than 11° (flat roofs) for intensive green roofs and between 11° and 20° for extensive green roofs. There is no limit for high-reflectance roofs.
- Shadow effects: More than 3 h of sunlight for green roofs are necessary to allow the growth of vegetation. Therefore, the shaded roofs (less than 3 h of sunlight) were excluded. In addition, the shadowing effects are important for the selection of the most appropriate plant species for green roofs.

Table 58. Criteria to assess rooftop renovation feasibility.

Criteria	Green roof	High-reflectance roof
Building height	>3.5 m (heated building)	≤3.5 m (low building)
Roof area	>100 m^2	>20 m^2
Roof material/colour tones	No high-reflectance, vegetated and red-tiled roofs	No high-reflectance, vegetated and red-tiled roofs
Roof slope	<11° intensive (flat) ≥11° and <20° extensive (pitched)	<8.5° low sloped ≥8.5° steep sloped
Roof orientation	No limit	No limit
Solar radiation	Related to shadow criterion	No limit
Shadow effects	Sunny roofs with more than 3 h of sunlight	No limit

*Criteria for solar technologies are described in section 4.2.2.

The feasibility of energy efficiency interventions was assessed considering energy and environmental regulations at national and municipal levels. For roofing structures of buildings, verification of the effectiveness, in terms of cost–benefit ratio, was assessed referring to (according to Italian Decree 28/2011):

- Materials with high reflectance of roofs, assuming for the latter a solar reflectance value of not less than 0.65 in the case of flat roofs and 0.30 in the case of pitched roof.
- Passive cooling technologies (e.g., night ventilation and green roofs).

Furthermore, the Solar Reflectance Index (*SRI*) is used in the main international certification protocols for comparing the coolness of roof surfaces. In Italy some voluntary environmental protocols have been introduced, such as the ITACA (Institute for Innovation and Transparency of Procurement and Environmental Compatibility) protocol, Casaclima Nature certification, and the Green Building Council (GBC) Italia, in which *SRI* levels for roofs have been specified. In addition, from the enactment of the Italian Decree 11/01/2017, the Ministry for the Environment, Land and Sea has established the "Adoption of minimal environmental criteria (CAM) for the awarding of design services and new construction, renovation and maintenance work on buildings for management of construction sites of the public administration and minimal environmental criteria for the supply of incontinence aids", thus aligning itself with environmental protection strategies adopted at an international level. The section "Reduction of impact on the microclimate and atmospheric pollution" establishes the requirement of materials with a high *SRI* (Table 59).

The Municipality of Turin regulates the roof elements through a number of rules, as shown in the image below. Current regulations determine rules to design roofs in relation to geometry, structural characteristics, heights, and architectural appearance. Such regulations also define restrictions to design intervention and uses according to functions and zoning of the masterplan, limiting, in particular, changes

in the historical centre of the city. Moreover, while the Building Annex Energy Code in place calls for environmental awareness by setting compulsory requirements for thermal insulation and derogations to enable the installation of solar and photovoltaic panels, the conversion into green surfaces is only mentioned within the voluntary requirements, leaving the economic burden to the private owners and the limitation of opportunities to out-of-date regulations.

To overcome such limitations, and after the identification of criteria to evaluate rooftops' renovation feasibility, the rooftops' potential was investigated for a district in Turin and the impact of smart-green technologies was evaluated and quantified using several indicators.

Table 59. Italian voluntary protocols and requirements [56].

Documents	Credits	Application	*SRI* threshold value
LEED 2009 Itaca	1 point	Roofs	At least 75% of the roof surface must consist of material having: $SRI \geq 78$ for low sloped roofs (<8.5°) and $SRI \geq 29$ for steep sloped roofs
GBC HOME	2 points	Roofs	At least 50% of the roof surface must consist of material having: $SRI \geq 82$ for low sloped roofs and $SRI \geq 29$ for steep sloped roofs (>8.5°)
GBC HISTORIC BUILDING	2 points	High-reflectance roofs	
Ministerial Decree 11/01/2017	-	Roofs	$SRI \geq 29$ for roofs with slope greater than 8.5° and $SRI \geq 76$ for roofs with slope less than or equal to 8.5°

Impact of rooftop solutions

From the literature review [275,279–282], it emerged that the main roof technologies able to obtain a positive impact on the urban heat island (UHI) mitigation, on the energy consumptions and savings, on the outdoor and indoor thermal comfort conditions, and on social and economic aspects are green and cool (high-reflectance) roofs and walls and the energy production from PV panels and ST collectors.

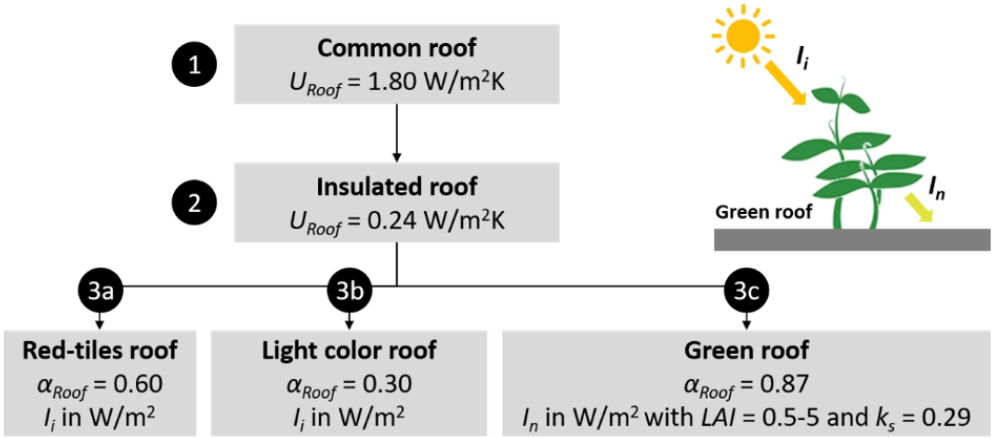

Figure 132. Energy efficiency solutions' scheme [56].

To evaluate the energy savings after the rooftop renovation, the assessment of heat fluxes through the roof were quantified during the heating and cooling seasons. Different thermo-physical properties of the roofs, indicated in Figure 132, were used according to roof type: Common roof, common insulated roof (red tiles), insulated high-reflectance roof, and insulated green roof.

The roofs have different values of thermal transmittance (U_{Roof}) that depend on the type of insulations. U_{Roof} is taken to equal 1.80 W/m^2/K for common roofs and 0.24 W/m^2/K for insulated roofs (according to Italian standard) and has different solar absorption coefficients (α_{Roof}) that depend on the roof-covering materials. The α_{Roof} is equal to 0.6 for common roofs with red tiles, 0.3 for light-color roofs, and 0.87 for green roofs. The quota of solar radiation changes according to the presence of vegetation, the incident global solar radiation (I_i), was calculated according to global solar radiation recorded by weather stations, while the quota of incident solar radiation entering a green roof (I_n) depends on the Leaf Area Index (LAI), which is the ratio between the green area and the underneath soil area [281], and on the short-wave extinction coefficient (k_s) [283].

Using green roof technology, the heat flow of solar radiation that enters the system is a net contribution taking into account the solar reflection and green absorption. Equation (38) describes the exponential law developed by Palomo Del Barrio [284] used in this work to assess the effect of green roofs on incident global solar radiation:

$$I_n = I_i^{-k_s \cdot LAI} \tag{38}$$

Where: solar irradiance entering the system (W/m^2); I_i is the incident solar irradiance (W/m^2); k_s is the short-wave extinction coefficient (-), which was assumed to equal 0.29 (values proposed for similar vegetation characteristics in [284]); and LAI is the ratio between the green area and the underneath soil area (-), which was assumed to equal 5 in summer, 3.5 in spring, 3 in autumn, and 0.5 in winter [281,283].

To assess the energy savings of a building, due to the roof component, some simplified assumptions were made: (1) The heat flow rate from internal gains was constant; (2) the heat flow rate dispersed by ventilation was constant; (3) the evapotranspiration of green roofs was not considered; and (4) and the thermal capacity of different roof typologies was equal.

The energy savings for space heating and cooling were quantified calculating the hourly heat flow rates before and after the rooftop retrofit interventions with the following equations [283]:

$$\frac{\Delta Q_H}{A} = U_1 \cdot \left(T_{ai,H} - T_{sa,1}\right) - U_2 \cdot \left(T_{ai,H} - T_{sa,2}\right) \tag{39}$$

with:

$$T_{si} = T_{ai,H} - R_{si} \cdot U \cdot \left(T_{ai,H} - T_{ae} + \alpha \cdot \frac{I}{h_e}\right)$$

$$\frac{\Delta Q_C}{A} = U_1 \cdot \left(T_{sa,1} - T_{ai,C}\right) - U_2 \cdot \left(T_{sa,2} - T_{ai,C}\right) \quad (40)$$

with:

$$T_{si} = T_{ai,C} + R_{si} \cdot U \cdot \left(T_{ae} + \alpha \cdot \frac{I}{h_e} - T_{ai,C}\right)$$

Where: ΔQ_H is the energy savings during the heating season (Wh); ΔQ_C is the energy savings during the cooling season (Wh); A is the roof area (m^2); U is the thermal transmittance of the roof ($W/m^2/K$); R_{si} is the thermal resistance of the roof (m^2K/W); $T_{ai,H}$ is the internal air temperature during the heating season equal to 20 °C; $T_{ai,C}$ is the internal air temperature during the cooling season equal to 26 °C; T_{sa} is the sol–air temperature, which was introduced to take into account not only the external air temperature but also the incident solar irradiation absorbed by the roof (°C); T_{si} is the internal surface temperature of the roof (°C); T_{ae} is the external air temperature (°C); α is the solar absorption of the roof (-); I_i is the incident solar irradiance (W/m^2), which with green roof was equal to I_n (see Equation (38)); and h_e is the external thermal adductance ($W/m^2/K$).

The primary energy savings for space heating and cooling were quantified as the sum of the hourly energy savings during, respectively, the heating and cooling seasons divided by the efficiency of the systems:

$$\frac{\Delta Q_{P,H}}{A} = \frac{\sum \Delta Q_H}{A} \cdot \eta_{HS}^{-1} \qquad \frac{\Delta Q_{P,C}}{A} = \frac{\sum \Delta Q_C}{A} \cdot EER^{-1} \quad (41)$$

where: $\Delta Q_{P,H}$ is the primary energy savings during the heating season (Wh); $\Delta Q_{P,C}$ is the primary energy savings during the cooling season (Wh); η_H is the average seasonal efficiency of the heating system (in Italy, for residential buildings, this value varies between 0.65 and 0.75 (-)); and EER is the average seasonal energy efficiency ratio, which depends on the efficiency of air conditioners (in Italy, for a typical heat pump (air/air) this value is about 3).

Following the energy savings obtained from the retrofit of the rooftop, the GHG emissions' reduction was quantified.

Green roof technology

Green roofs alleviate UHI effect through the raising of surface albedo [285] and, so, can reduce the air temperature through evaporation [286] and thermal insulation [287,288]. Therefore, green roofs and walls help in the reduction of energy consumption and guarantee an excellent thermal behaviour in both heating and cooling seasons with consequent good thermal comfort conditions, thanks to the high thermal inertia technology [272,289,290].

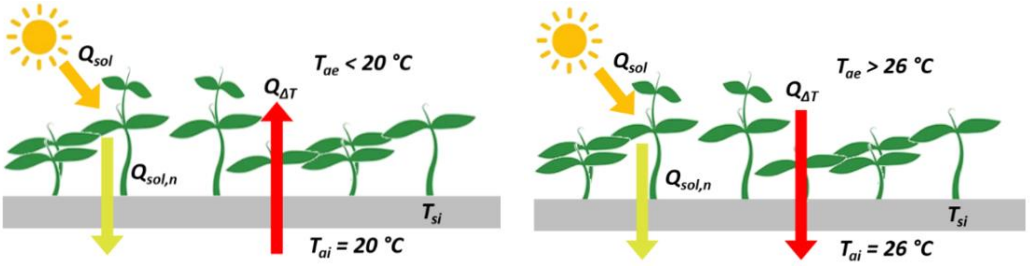

(a) (b)

Figure 133. Schematic diagram of green roof during (a) heating season and (b) cooling season [56].

Figure 133 shows the heat flows through the roof during the heating and cooling seasons, where Q_{sol} is the quota of solar gains and $Q_{sol,n}$ is the quota of solar gains that enters the system.

The thermal conditions of buildings and urban environments were investigated at urban scale using two parameters: The 'Normalized Difference Vegetation Index' (*NDVI)* and the 'Land Surface Temperature' (*LST)*. According to recent studies, the *LST* and the external air temperature decrease more or less rapidly as the green areas increase, depending also on the type of urban morphology. The local climate conditions were assessed before and after the installation of green technologies.

Cool roof strategy

High reflectance of roofs, identified as albedo strategy, is able to maximize the diffuse reflection of solar radiation, reducing the overheating of buildings and the surrounding urban context and maintaining lower surface temperatures [291,292]. From past studies on UHI mitigation, it has become accepted that a high level of albedo (as white roofs) has the potential to cool cities by 1–3 °C, cooling the lower states/layers of the atmosphere [293–295]. In particular, since in the urban canyon white roof has the greatest effect on air temperatures when used on buildings of 1–2 stories' height [291], in this work low buildings were identified as suitable for this strategy. Moreover, the beneficial effects are greater in a mixed urban morphology context, such as the case of the Turin district analysed in this work.

As previously mentioned, the *SRI*, used in the main international certification protocols, is a metric for comparing the coolness of roof surfaces. The higher the *SRI*, the cooler the roof will be in the sun [278]. For example, a clean black roof usually has an *SRI* of about 0 (with a solar reflectance of 0.05 and an infrared emittance of 0.90), while a clean white roof could have an *SRI* of about 100 (with a solar reflectance of 0.80 and a thermal emittance of 0.90). In general, dark roofs have an *SRI* less than 20 [296].

In this work, the effect of albedo strategy on thermal conditions was investigated calculating the *SRI* and the roof surface temperature (T_s) based on solar reflectance (ρ) and infrared emittance (ε). According to ASTM E1980-11(2019) standard, *SRI* can be defined as:

$$SRI = 100 \cdot \frac{T_b - T_s}{T_b - T_w} \tag{42}$$

with:

$$T_s = 310.04 + 82.49 \cdot \alpha - 2.82 \cdot \sigma - 54.33 \cdot \alpha \cdot \sigma + 21.72 \cdot \alpha \cdot \sigma^2$$

where: T_b is the steady-state temperature of a black surface (K) with solar reflectance of 0.05 and infrared emittance of 0.9, under the standard solar and ambient conditions with a solar flux of 1000 Wm^{-2}, ambient air temperature of 310 K, convective coefficient of 12 $Wm^{-2} \cdot K^{-1}$ surfaces, and apparent sky temperature of 300 K; T_w is the steady-state temperature of a white surface (K) with solar reflectance of 0.80 and infrared emittance of 0.9, under standard solar and ambient conditions; T_s is the temperature of the roof surface (K) under the standard solar and ambient conditions; α is the solar absorptance of the roof surface (-) equal to $1 - \rho$; ρ is the solar reflectance of the roof surface (-); and σ is the Stefan–Boltzmann constant, 5.67×10^{-8} ($Wm^{-2} \cdot K^{-4}$). Table 60 shows typical roofing materials with solar absorption (α), solar reflectance (ρ), and infrared emittance (ε) values used in this work to quantify *SRI* and T_s before and after roof renovation using the albedo strategy.

In the analysed district, the values of roofing material properties refer to 'generic black shingle' for dark and black roofs, 'gray Ethylene-Propylene Diene Monomer (EPDM)' for medium roofs, and 'white EPDM' for white and renovated roofs. The values of *SRI* and T_s were calculated both at building scale and at blocks-of-building scale to evaluate the external conditions.

The main problem of this strategy is that over time the solar reflectance values of high- reflectance roofs decrease due to the accumulation of surface dirt and the degradation of the material by about 0.15 mainly during the first year [297]. The emission, however, does not decrease significantly, and washing the roof surfaces could restore the roof solar reflectance to 70%–100% of the original values [298].

Since most roofs are not washed frequently, it is necessary to evaluate aged values of solar reflectance and infrared emittance values to predict energy savings. If aged values of a roof are unknown, it is possible to estimate the aged solar reflectance ($Aged_\rho$) based on the initial solar reflectance ($Initial_\rho$) by using the following equation:

$$Aged_\rho = 0.7 \cdot \left(Initial_\rho - 0.2\right) + 0.2 \tag{43}$$

Table 60. Solar performance of roofing materials [292].

Roof material	**α (-)**	**ρ (-)**	**ε (-)**	**T_s (°C)**	***SRI* (-)**
Smooth bitumen	0.94	0.06	0.86	83	-0.1
Generic black shingle	0.95	0.05	0.91	82	0.1
Vegetated field	0.90	0.10	0.76	83	-0.2
Grey EPDM	0.77	0.23	0.87	68	0.21
Red clay tile	0.67	0.33	0.90	69	0.36

Red concrete tile	0.82	0.18	0.91	76	0.17
Shasta white shingle	0.74	0.26	0.91	64	0.27
Light gravel	0.66	0.34	0.90	57	0.37
Aluminum	0.39	0.61	0.25	48	0.56
White EPDM	0.31	0.69	0.87	25	0.84
White coating on shingle	0.29	0.71	0.91	23	0.87
White PVC	0.17	0.83	0.92	11	1.04

Referring to LEED (Leadership in Energy and Environmental Design) environmental protocol is also possible to assess mixed non-roof and roof measures, using the following relation as a function of area surfaces (A):

$$\frac{A_{nonroof\ measures}}{0.5} + \frac{A_{high\ reflectance\ roof}}{0.75} + \frac{A_{vegetated\ roof}}{0.75} \geq A_{total\ site} + A_{total\ roof} \quad (44)$$

5.3.2 Case study

The methodology presented was applied to a district of the city of Turin, 'Pozzo Strada'. Turin is located in the northwest of Italy, in the Po valley, and it is characterized by a temperate-continental climate, with cold winters and a shorter but hot summer. According to Italian standard UNI 10349:2016, Turin's climate is characterized by 2648 heating degree day (HDD) at 20 °C and 84 cooling degree day (CDD) at 26 °C. The results of this study were presented for a district with a dimension of 1 km^2 with 21,520 inhabitants and more than 1000 buildings.

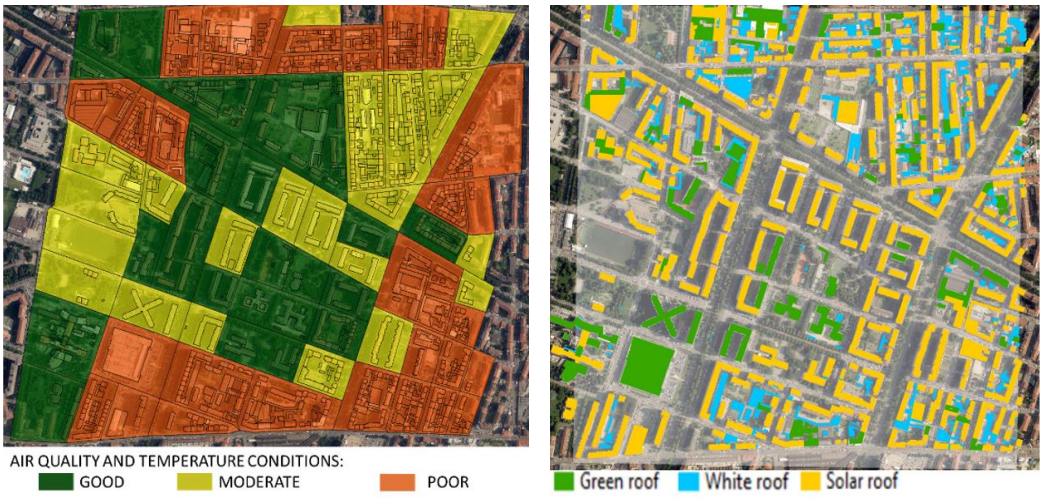

(a) (b)

Figure 134. District of Turin with a dimension of 1 km2: (a) Building block classification according to three classes of air quality conditions (green, good; yellow, acceptable, red, bad); (b) analysis of roof potential and feasibility of smart solutions: Green, high-reflectance, and solar roofs [56].

In the selected district, 1,228 buildings were analysed. Of these buildings, 1,097 were classified as potential rooftop renovation opportunities, distinguishing three

types of smart solutions: green roof technology, high-reflectance strategy (cool roof), and energy production from ST collectors and PV modules.

In order to give a priority of interventions, critical areas with the worst air quality conditions were identified as priority areas for the installation of green roof technologies (Figure 134a, orange areas) to mitigate the UHI effect. The other areas, with mainly residential buildings, were considered for solar energy production using ST collectors and PV panels. Solar technologies were dimensioned considering residential and non-residential demand. Figure 134b shows the rooftop classification, distinguishing these three types of smart solutions.

The main characteristics of the buildings selected as potential are indicated in Table 61. It is possible to observe that, thanks to the typical urban mix of Turin, the retrofit measures are well distributed within the district and, moreover, there is a consistent potential. For this reason, it is important to encourage the buildings' renovation – in this case the rooftop renovation – especially in consolidated urban contexts where energy efficiency measures to intervene on buildings are limited.

Table 61. Buildings' characteristics [56].

Roof solutions	No buildings	Height$_{avg}$ (m)	Potential roof area (m^2)	Slope$_{avg}$ (°)
Green roof	110	13.6	64,712	0
High reflectance roof	417	3.6	44,956	9
Solar roof	570	19.3	172,749	36

Figure 135 shows the total area (m^2) of flat roofs identified as potential is equal to 64,458 m^2, and pitched roofs' area with a slope less than 20° representing a small quota of 254 m^2.

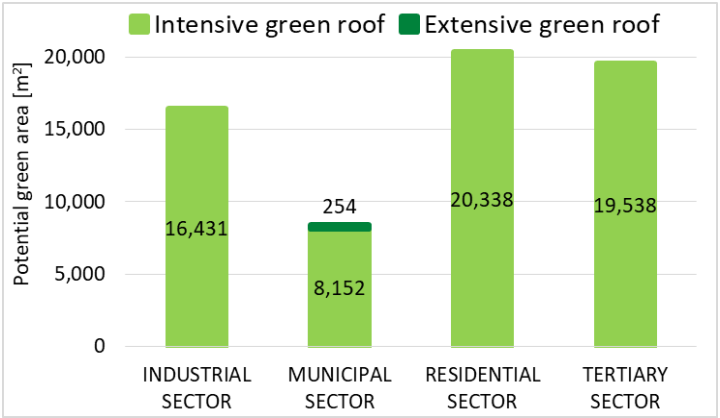

Figure 135. Analysis results of the potential intensive (flat roof) and extensive (pitched roof) green roofs [57].

The social effect of green roofs is not included in this study but is interesting to underline that the creation of green roofs can be integrated in the urban farming concept, as well as in the creation of "park roof" (e.g. playgrounds) dedicated to social activities.

5.3.3 Results

This subsection describes the main results obtained from the use of three smart solutions: green roof technology and high-reflectance roof strategy (cool roof). Results regarding solar energy technologies are described in Chapter 4.

The feasibility of green roof technology was assessed considering requirements the Ministerial Decree 26/06/2015. The roofs' albedo in the district analysed varied between 0.05 and 0.26 (for a few buildings, mainly industrial, the albedo was around 0.33). After retrofit measures with green roofs, the roof albedo criterion was respected due to the installation of passive cooling technology.

The feasibility of high-reflectance roof strategy was assessed according to the Italian Decree 11/01/2017 and the environmental protocols. The *SRI* prerequisites (*SRI* > 0.29) were respected.

Energy savings

In the district analysed, 64,712 m^2 of roofs were identified as potential green roofs. Referring to Equations (39) and (40), the energy savings for heating and cooling seasons were quantified for a district in Turin. In this scenario, potential roofs were renovated using green roof technologies. The thermal transmittance with green technologies is equal to 0.24 $W/m^2/K$ (according to Italian Decree 26/6/2015) and the solar absorptance of a green roof surface is 0.87 [299]. The energy savings after the installation of green roofs was equal to 5669 MWh/year, which corresponds to 8.4% of space heating consumptions of residential buildings. The energy savings during cooling season was equal to 662 MWh/year. Figure 136 describes the energy savings at block-of-building scale, distinguishing heating and cooling seasons.

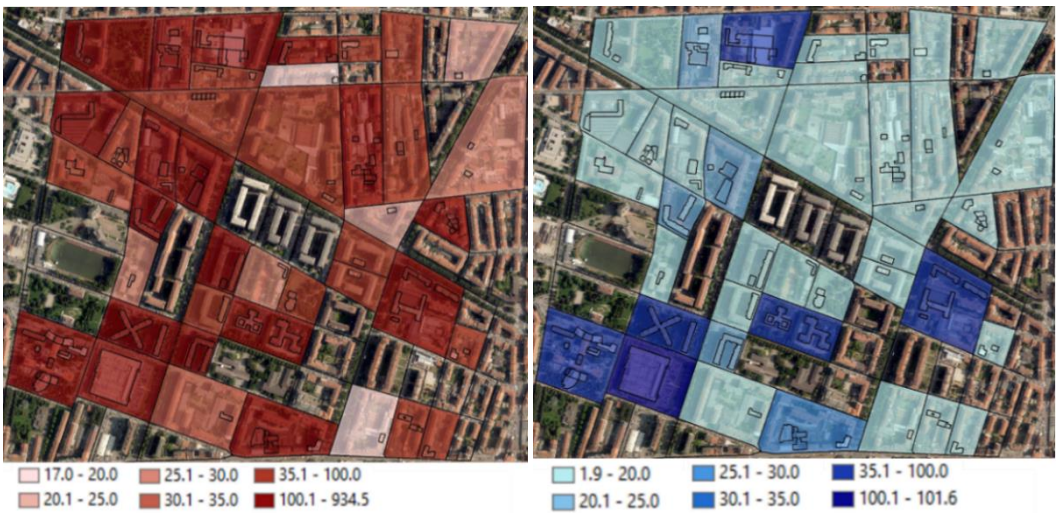

(a) (b)

Figure 136. Green roofs' potential assessment at block-of-building scale: (a) Heating and (b) cooling primary energy savings in MWh/year [56].

Green and high-reflectance roofs (cool roofs) have a significant effect in reducing energy consumption during cooling and heating seasons. In accordance with literature review [281,300–304], from this work it emerged that cool roofs are more effective in reducing heat gain in the cooling (C) season from 15 April to 14 October, than heat loss in the heating (H) season from 15 October to 14 April (Figure 137).

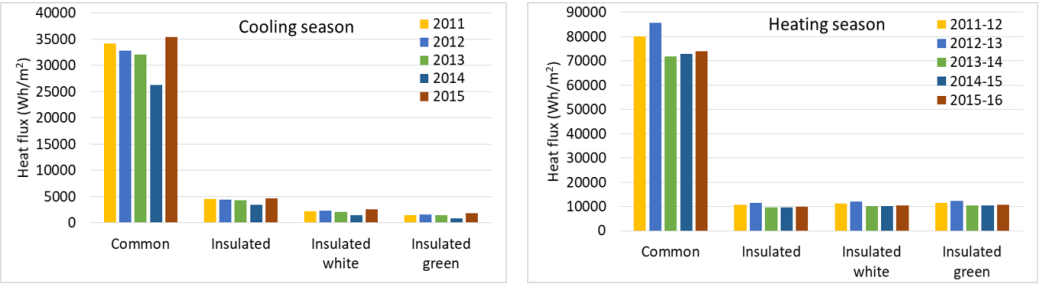

(a) (b)

Figure 137. Comparison of heat fluxes (Wh/m^2) between common roof, insulated common roof, insulated high-reflectance roof, and insulated green roof: (a) Cooling season; (b) heating season [56].

This analysis was carried out using weather data measurement recorded by Politecnico weather station (WS) for the period from 2011 to 2016. The thermal performance of a refurbished roof was compared to the typical common roof. In particular, three roof solutions were taken into account: (1) Insulated common roof, (2) insulated high-reflectance roof, and (iii) insulated green roof. The heat flux (Q) in the roof was quantified according to Equations (53) and (54). Table 62 describes the characteristics of roof solutions and the main energy efficiency results. GHG emissions were quantified using 0.210 tonCO_2/MWh for natural gas and 0.46 tonCO_2/MWh for electricity.

Table 62. Characteristics of roof solutions and energy efficiency results [56].

Roof solution	**A (-)**	**U (W/m^2/K)**	**Q_H (Wh/m^2)**	**Q_C (Wh/m^2)**	**ΔQ_H (Wh/m^2)**	**ΔQ_C (Wh/m^2)**	**GHG_H (tCO_2/MWh)**	**GHG_C (tCO_2/MWh)**
Common	0.60	1.80	76,838	32,135	-	-	1,333	319
Common insulated	0.60	0.24	10,245	4,285	88,790	9,284	178	43
Insulated white	0.30	0.24	10,874	2,147	87,951	9,996	189	21
Insulated green	0.87	0.24	11,130	1,457	87,611	10,226	193	14

Figure 138 and Figure 139 show the results for three consecutive hot days (21–23 July 2015) and cold days (15–17 January 2012). From the comparison of hourly heat fluxes (W/m^2) between common roof, insulated common roof, insulated high-reflectance roof, and insulated green roof, it emerged that using an insulated green

roof there was less heat gain during the summer season and with an insulated roof there was less heat loss in the winter season.

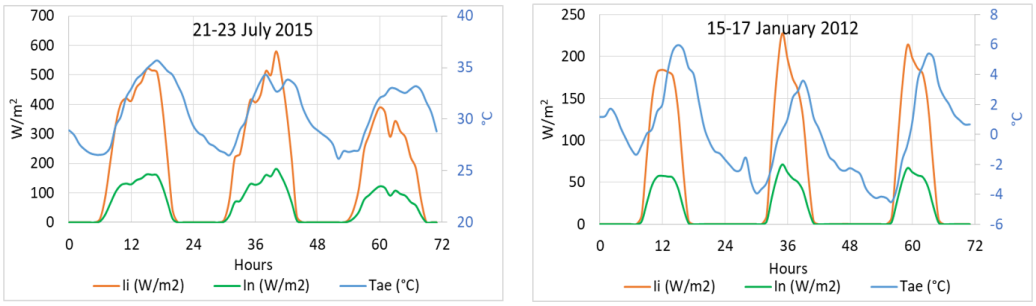

(a) (b)

Figure 138. Hourly values of global solar radiation (Ii), solar radiation entering in the system (In), and the external air temperature (Tae) for three consecutive days: (a) 21–23 July 2015; (b) 15–17 January 2012 [56].

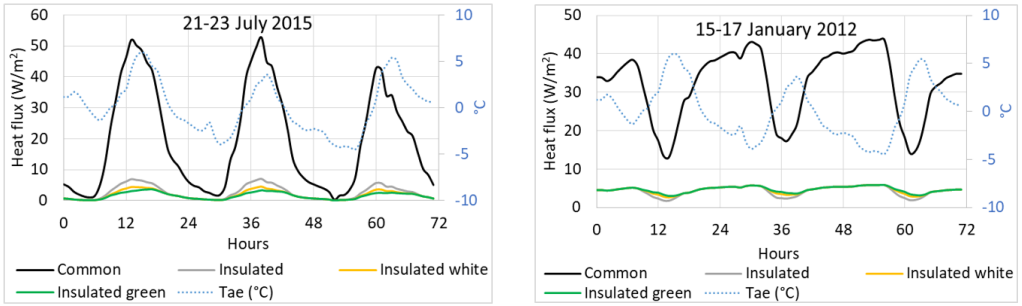

(a) (b)

Figure 139. Comparison of hourly heat fluxes (W/m2) between common roof, insulated common roof, insulated high-reflectance roof, and insulated green roof for three consecutive days: (a) 21–23 July 2015; (b) 15–17 January 2012 [56].

The potential green roofs identified are 26 % of the total roof areas (249,609 m^2). Thermal energy saving after the use of vegetated roofs, –calculated with the application of GIS-based engineering models– is 1,610 MWh/year, which corresponds to 1.5 % of thermal consumptions of residential and non-residential buildings for space heating and DHW consumption. Cooling energy saving was computed in CitySim for the area object of the comfort analysis. Considering the typical hot summer day of 7th August 2015, the cumulative energy saving for the buildings including a green roof is 14 $Wh/m^3_{gross\ volume}$ (-12 %).

It is important to compute the impact of the greening in the urban local climate; indeed, the presence of grass decreases the air temperature. This phenomenon has consequently an important impact on the UHI effect and the assessments of this aspect are presented in the following section.

Outdoor thermal comfort conditions

Firstly, thermal conditions were investigated using some parameters calculated at block-of-building scale from satellite images. These parameters are the *NDVI* and the *LST* and allow us to describe the UHI effect and the local-climate characteristics of the urban environment. An analysis at blocks-of-building scale was made, and

Figure 140a shows the variation of *LST* before and after the installation of green roof technologies. According to the literature review [279,280], the *LST* and the air temperature tend to decrease more or less rapidly as the green areas increase, depending also on the type of urban morphology. Increasing the green roofs' areas of 64,712 m^2, on average, the *LST* in the district tends to decrease by 1 °C (Figure 140b).

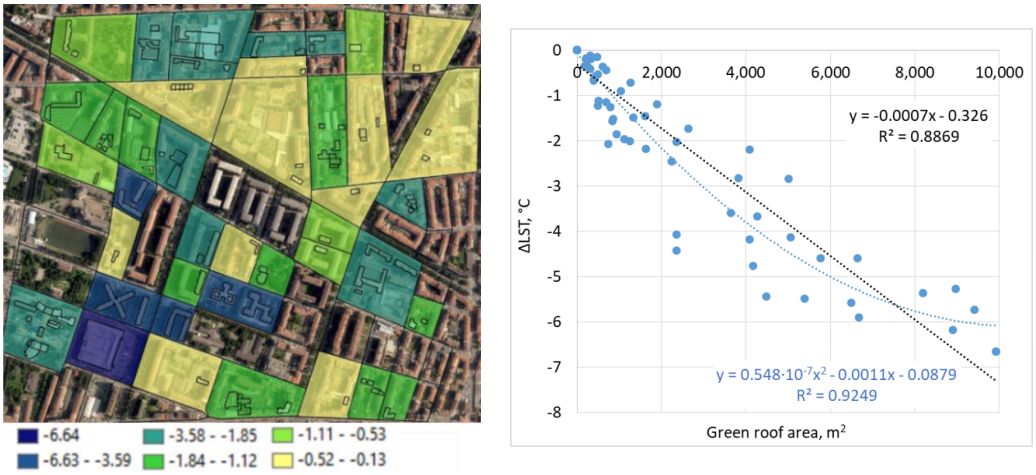

(a) (b)

Figure 140. Green roofs' potential assessment at block-of-building scale: (a) Thermal condition assessment, Land Surface Temperature (LST) variation before and after the installation of green roof technologies; (b) correlation between the LST variation and the quota of green roof area [56].

Starting with 500 low buildings located in the district of Turin, 417 were selected as potential for the renovation of rooftop with white colour (high-reflectance roof). Of these 417 potential buildings, which corresponded to an area of almost 45,000 m^2, 313 had a slope less than 8.5° and 104 had a higher slope (on average, had slope of 8.8°, see Table 61).

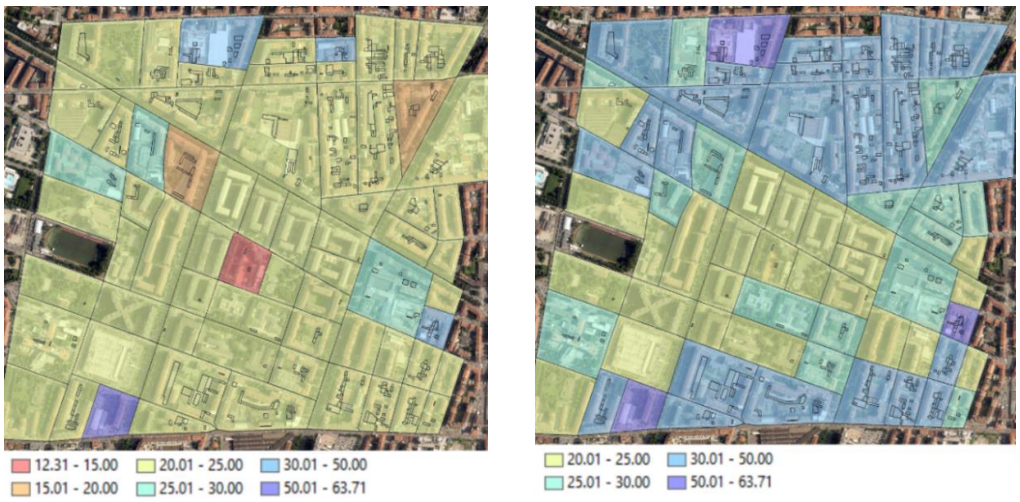

(a) (b)

Figure 141. Solar Reflectance Index (*SRI* , %) values of existing roof at block-of-building scale: (a) Before (b) and after high-reflectance strategy [56].

Figure 141 shows the *SRI* values calculated for each block of buildings before (Figure 141a) and after (Figure 141b) the use of high-reflectance roof strategy on 417 potential roofs. From the results, it emerged that it is possible to obtain an increase in *SRI* of almost 30 and a reduction of T_s of over 10 °C. Therefore, these indicators could help designers and consumers to choose the proper materials for sustainable buildings and communities.

Secondly, existing urban climate tools were used to investigate outdoor thermal comfort conditions in the case-study area. In the analysed district, a smaller site was selected (Figure 142) and two scenarios were investigated: (a) the business as usual S_{BAU} with standard insulated roof in red, and (b) the installation of roof-integrated green technologies with standard insulated roof in red, green roof with a substrate of 10 cm in dark green and the use of cold or cool surfaces in light green in the courtyards (S_{GREEN}).

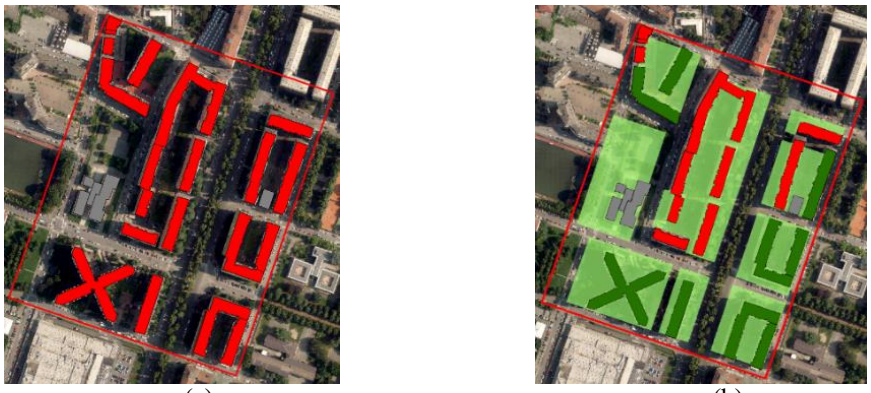

(a) (b)

Figure 142. The two scenarios of roof retrofit intervention: (a) Business as usual; (b) Green roofs and surfaces [57].

The simulation was done taking into account the local climate conditions of one of the warmest days of the years 2014 and 2015: August 7th, 2015 (Figure 143): the average daily temperature was 31.4 °C, with a daily solar irradiation of 6,680 (Wh/m^2/day). The air temperature reaches its maximum values between 5 and 6 p.m., with 36.5 °C. The wind speed is quite constant, with a maximum of 2.7 m/s and a minimum of 0.4 m/s, and the air relative humidity varies between 30 and 70%.

The analysis was done using ENVI-met and SOLWEIG. In ENVI-met thermal comfort indices (*PMV*/*PPD*, *PET*, *UTCI*, and *SET*) were calculated at 1 meter above the ground (this software does not consent a major accuracy of this height) for a grid of 10 m x 10 meters considering the following data (ISO 7730:2005):

- Human body parameters: 35 years old, male, weight of 75 kg, height of 1.75 m, surface area of 1.91 m^2.
- Clothing insulation: 0.5 clo or 0.08 m^{2}K/W (typical summertime daily wear clothing).
- Metabolic rate: 1 met or 58 W/m^2 (seated relaxed) and 1.9 met or 110 W/m^2 (walking at 2 km/h).

In SOLWEIG, *PET* and *UTCI* thermal indices were simulated using the same human body parameters, clothing insulation and metabolic rate used in ENVI-met, but the urban environment was described with a DSM and a DEM with a precision of 1 meter.

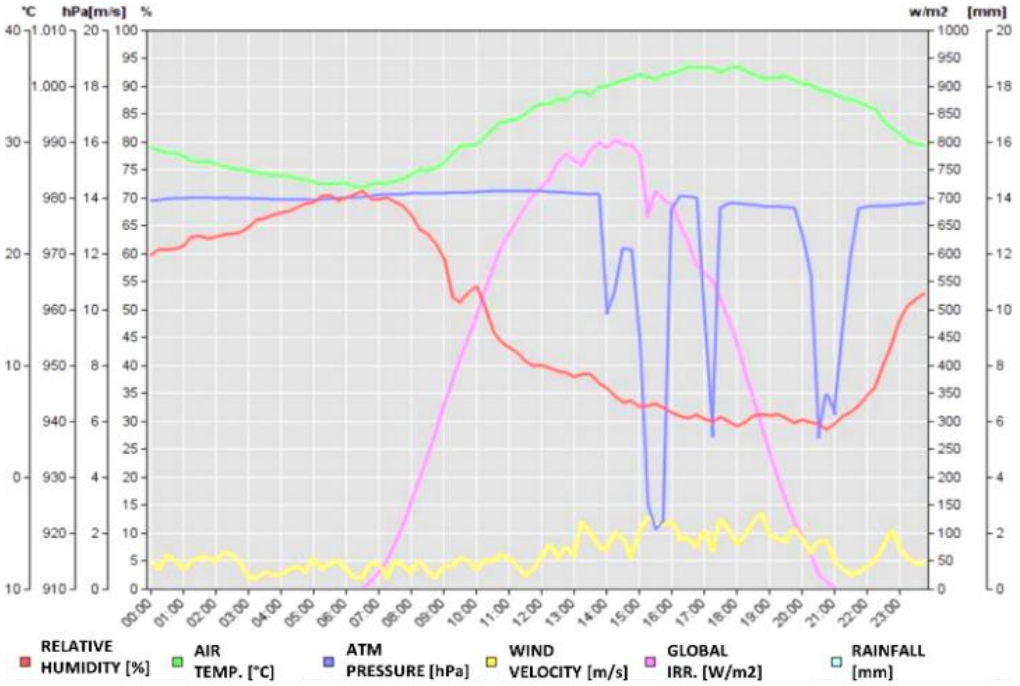

Figure 143. Local climate data for a typical summer day: August 7th, 2015 [57].

Additional simulations were conducted using CitySim, to compute the T_{mrt} on a 10 x 10 meters grid, using 1.5 meter high virtual pedestrians. CitySim's model provides the longwave exchanges within the model (including the buildings), as well as the evapotranspiration of the green surfaces. However, the air temperature, relative humidity, and wind speed and direction are assumed constant within the area. The nebulosity was assumed constant (4 Octas).

The results include the comparison of the T_{mrt} computed by CitySim, ENVI-met, SOLWEIG and GIS-based model analysed for the selected hot summer day, distinguishing two scenarios of retrofit intervention for the buildings' roofs (S_{BAU} and the S_{GREEN}).

Outdoor thermal comfort conditions were assessed using existing simulation models and tools: ENVI-met, SOLWEIG, CitySim and GIS-based model. In order to quantify the effect of greening in the urban microclimate, the same area was simulated with and without the installation of green roofs and the use of green areas. The comparisons of mean radiant temperature and *PET* (with seated relaxed activity) shows an improvement of outdoor thermal comfort conditions due to the use of green mitigation strategies (in Figure 144). Improvements were especially visible in the new sunny green areas, while in the shaded areas the difference was minimal.

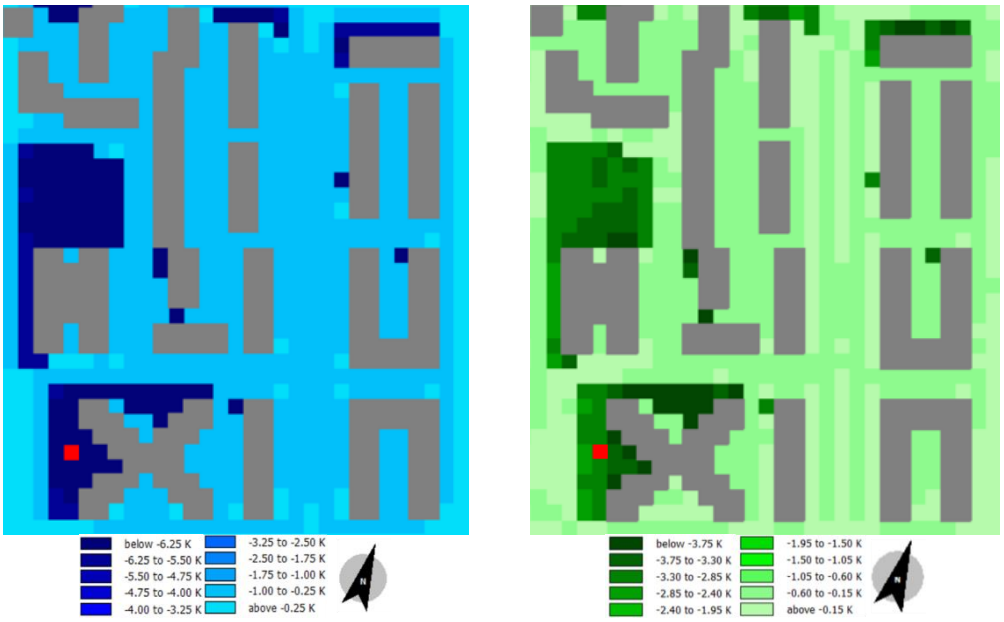

(a) (b)

Figure 144. ENVI-met: comparison between SBAU and SGREEN at 6 pm on August 7th , 2015: (a) Absolute difference MRT (K); (b) Absolute difference PET (K) [57].

Figure 145 shows a reduction in the external surface temperature. In the scenario S_{BAU} the temperature varies between 33.3°C and 60.8°C, while in the scenario S_{GREEN} the lower temperature of the grass surfaces corresponds to 27.9°C. Indeed, the grass temperature follows the air temperature path but taking into account the evapotranspiration process. Finally, the reduction of the outdoor surface temperature of the roof affects the internal surface temperature and then comforts conditions resulting also in energy savings for space cooling.

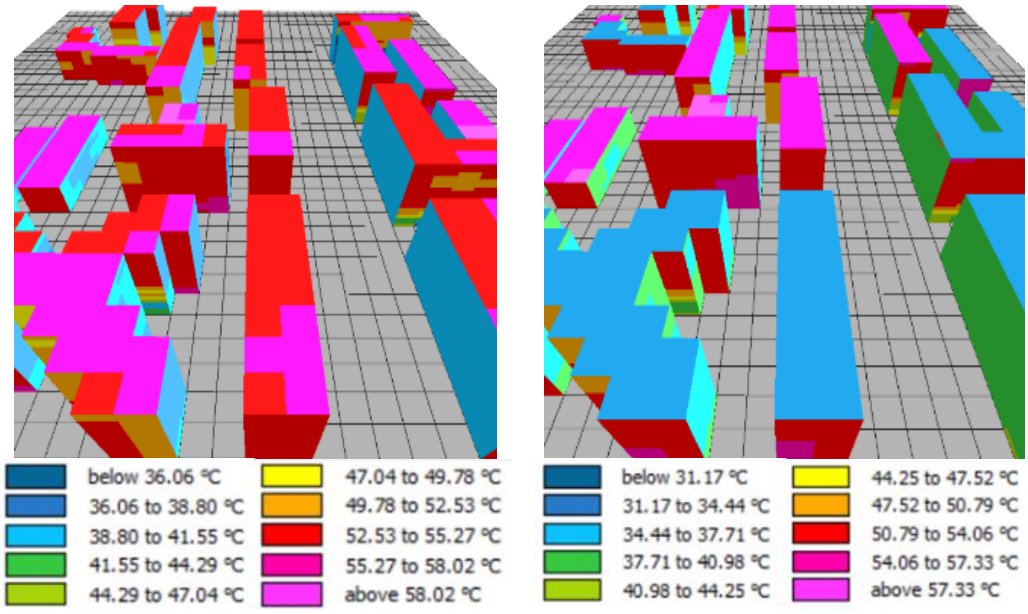

(a) (b)

Figure 145. ENVI-met: Temperature of buildings' surfaces at 1 pm on August 7th, 2015: (a) Business as usual with standard flat roof; (b) Intensive green flat roof and green surfaces [57].

Figure 146 shows an example of the hourly results for a building: outdoor roof surface temperature T_{roof} (S_{BAU} and S_{GREEN}), external air temperature (T_{ae}) and global solar irradiance. The impact that can be seen is extremely important in the fight against climate changes (e.g. IPCC projections for 2050 and 2100) and against the increase of summer hot events.

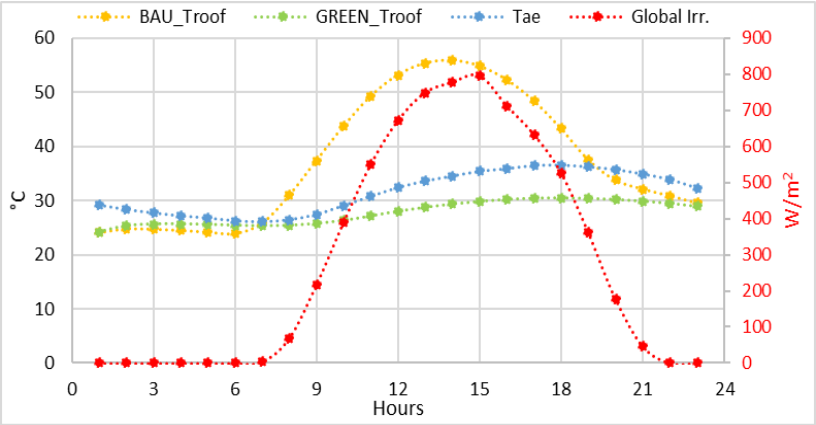

Figure 146. ENVI-met: comparison of external roof temperature between scenarios SBAU and SGREEN on August 7th , 2015 [57].

Figure 147 and Figure 148 show *PET* (°C) and *UTCI* (°C) indexes calculated in ENVI-met and SOLWEIG on August 7th, 2017 (with hourly precision) for a single point indicated in Figure 144 (red point).

In general, it is possible to observe an improvement in comfort conditions with green surfaces also at pedestrian level. Regarding *PET* index, the results of two urban climate tools were very close: SOLWEIG perceives a greater difference between the two scenarios S_{BAU} and S_{GREEN} with a maximum *PET* difference of 4.5°C at 4 pm; in ENVI-met there was a max *PET* difference of 2.8°C at 6 pm. For both scenarios maximum *PET* values were reached between 3 pm and 5 pm. Similar trend can be observed for *UTCI* index, where the maximum UTCI difference of scenarios S_{BAU} and S_{GREEN} was 2°C at 5 pm in SOLWEIG and 1.4 °C at 4 pm in ENVI-met.

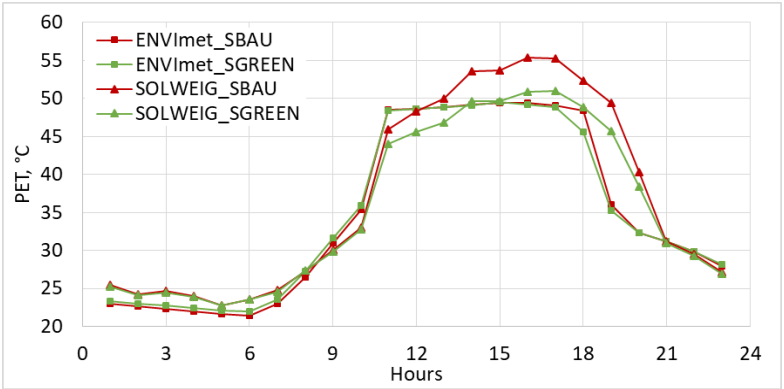

Figure 147. ENVI-met and SOLWEIG: comparison between SBAU and SGREEN on August 7th , 2015 for the red point indicated in Figure 144 [57].

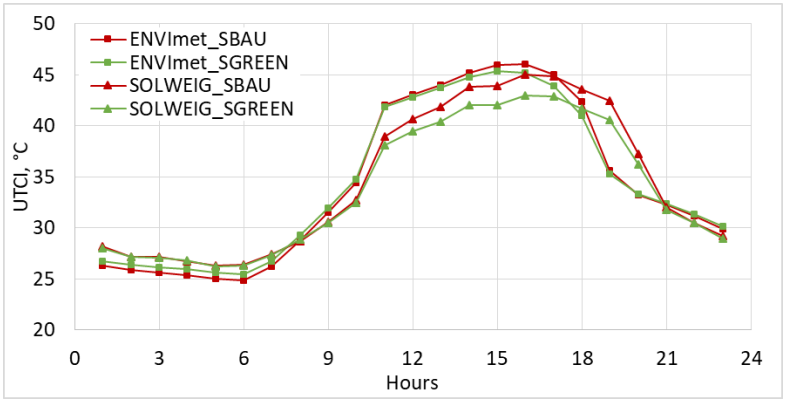

Figure 148. ENVI-met and SOLWEIG: comparison between SBAU and SGREEN on August 7th , 2015 for the red point indicated in Figure 144 [57].

ENVI-met, SOLWEIG, CitySim and GIS-based model results were compared using the hourly profile of the T_{mrt}. Figure 12 shows the T_{mrt} (°C) comparison for August 7th, 2015 distinguishing the two scenarios on a specific point indicated in Figure 149.

The results of T_{mrt}, computed by the three software and the GIS-based model (only for scenario S_{BAU}) were within similar temperature range. ENVI-met simulated higher values at midday (about +15°C) compared to CitySim and GIS-based model, while SOLWEIG simulates intermediate values; this result is consistent with previous studies [37]. The difference between the two scenarios was also of similar magnitude, but with CitySim a greater difference between the two scenarios at midday can be observed. The effect of the thermal inertia seems also more significant in CitySim, where the difference between the two scenarios is still noticeable later in the evening. In this work, no calibration or confrontation with measured values has been conducted. However, it is important to notice that simulations conducted using two different validated models both show an appreciable reduction of the T_{mrt} thanks to the proposed intervention scenario S_{GREEN}. Future investigations will be made to implement the GIS-based model.

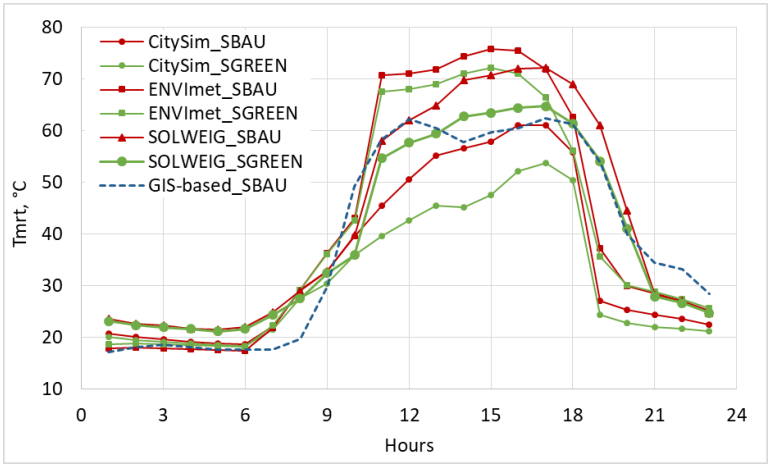

Figure 149. ENVI-met, SOLWEIG, CitySim and GIS-based model: comparison between SBAU and SGREEN on August 7th, 2015 for the red point indicated in Figure 144 [57].

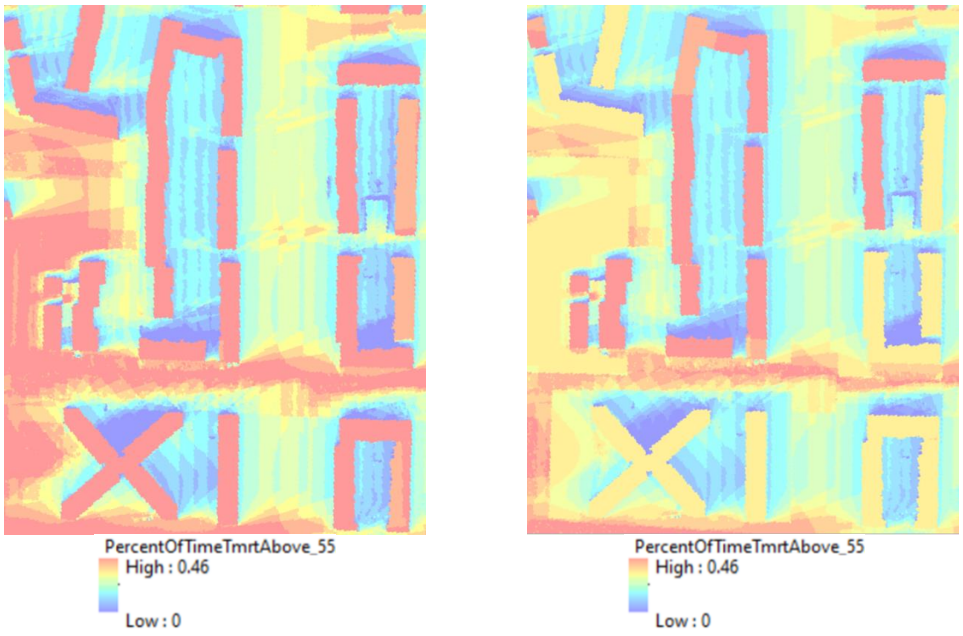

(a) (b)

Figure 150. SOLWEIG: percentage of time in which Tmrt is above 55 °C base on 24 hours for August 7th, 2015: (a) Business as usual with standard flat roof; (b) Intensive green flat roof and green surfaces [57].

Figure 150 shows statistical maps elaborated in SOLWEIG, for both scenarios, that indicates the percentage of time in which the T_{mrt} was above 55 °C based on the whole analysis time (24 hours for August 7th, 2015). It is possible to see a reduction in percentage after the installation of green roofs and the use of green surfaces (from 46% to 33%). This type of map can be used to identify critical areas under thermal heat stress.

In conclusion, to promote a sustainable and resilient development of cities, there is no one solution, but different low-carbon strategies and smart green technologies can be used in the different urban environments.

The methodology presented in this section evaluates the solar potential energy on the building's roofs, the existing and potential green roofs, and the relationship between the local climate and the new vegetated areas. This analysis is useful to discover the effect of smart green technologies to reduce dependence on energy from hydrocarbons and fossil fuels harnessing solar energy, and the impact of green roofs and green surfaces on urban microclimate improving thermal comfort and energy savings. From the results, it is emerged that the use of green technologies can improve liveability and quality of a district in Turin.

5.4 Building shape and urban form

The energy performance of buildings is affected not only by geometrical and thermophysical characteristics of the building, but also by its surroundings and local climate conditions [46]. There are several parameters used to assess the correlation between urban form and environmental performance [305]. These parameters are

able to describe the distance between buildings, the urban building density, the presence of greening, the built-up surfaces, the urban canyon, the material and use patterns of urban spaces [306]. Recently, researchers have shown an increased interest in the energy optimization of urban and building design. The energy consumption of building can be quantified at district or city level with the use of urban-scale energy models and tools that consider urban climate and morphology [22]. In addition, by designing the neighbourhood according to the exposure, solar energy can be used both passively for heating and daylighting and actively for electricity and domestic hot water production [307–310]. Investigations on solar availability in urban environments are very complex; however, recent progress has been made thanks to the use of 3D urban models of cities [172]. The relation between urban morphology, energy performance and solar energy potential of buildings are central to help urban planners and designers in improving the energy efficiency of new or existing urban areas [311–314].

Therefore, building geometry, urban morphology and local climate are crucial aspects to optimize the energy performance of buildings at neighbourhoods scale [155]. In addition, urban form is a key parameter in modifying solar availability in densely built-up areas. This section explores relationships between urban form and energy performance with implications for solar energy production on building roofs.

In the first part of this section, six neighbourhoods in Turin have been analysed considering the urban morphology and the solar potential, taking into account the urban block typologies found across the city. From the energy simulations –made with the use of an urban-scale energy model– it has been found that in densely urban context, the optimal shape of the building –with low energy consumption and high solar energy production– must have a *S/V* ratio that varies between 0.37 m^2/m^3 for favourable orientated buildings and 0.35 m^2/m^3 for unfavorable oriented ones. These results could help in the design phase of new neighbourhoods or in the reuse of existing buildings and empty spaces to promote the transition to low-carbon energy.

5.4.1 Energy performance and solar potential

The assessment presented investigates the relationship between urban form and its energy performance with implications for solar availability in urban areas, to optimize solar gains and to harnessing solar energy as renewable resource for local energy production in densely built-up context. A flexible methodology to analyse urban morphology using several parameters such as the building density, to simulate energy consumption at neighbourhood scale and to assess the solar potential considering the expositions and roof geometry is described. The results of this study provide new insights into the identification of the optimal urban form with low energy consumption and high solar energy productivity.

Methodology

Heating energy demand

The hourly process-driven (i.e., engineering) model for residential buildings has been used to assess the relationship between urban form and the energy performance. The model, used to simulate the SH consumption of residential buildings, considers the real characteristics of the urban context. The *SVF*, the *H/W* and the solar exposition have been used as input data.

The model has been applied to 13 residential buildings –located in the six neighbourhoods– that are representative of the neighbourhoods and with typical characteristics. Since the building-scale variables that mainly affect the energy consumption of buildings are the thermophysical characteristics (which are identified as a function of the construction period) and the *S/V* ratio, the sample of buildings selected has an *S/V* ratio ranging from 0.23 to 0.46 m^2/m^3 with different construction periods from 1919 to 1971. The simulated consumption has been compared to the measured one according to the season 2013-14. To evaluate the influence of the construction period on the energy performance, the heating consumption has been also simulated by modifying the thermo-physical characteristics of the building according to four construction periods: 1919-45, 1946-60, 1961-70 and 1971-80.

Solar energy potential

To assess to potential of solar energy production from solar thermal (ST) collectors and photovoltaic (PV) panels in urban built-up areas, the better solar exposition and the quota of monthly solar radiation on the rooftop have been taken into consideration. The solar radiation on each rooftop has been quantified for the season 2013-14 using the ArcGIS tool 'Area solar radiation'. The sun and sky models were elaborated considering the monthly data of atmosphere transparency (τ) and the ratio of diffuse radiation to global radiation (ω) identified from the 'Photovoltaic Geographical Information System PVGIS' of JRC (Table 63).

Table 63. Solar radiation analysis: input data [58].

	Month											
	1	**2**	**3**	**4**	**5**	**6**	**7**	**8**	**9**	**10**	**11**	**12**
τ	0.43	0.43	0.43	0.43	0.42	0.4	0.38	0.39	0.4	0.56	0.46	0.37
ω	0.49	0.56	0.63	0.66	0.71	0.75	0.71	0.69	0.67	0.53	0.5	0.49

Cooling energy demand

Energy models and tools are used to simulate SC energy demand. The hourly cooling energy demand of residential buildings was simulated for five blocks of buildings located in the six neighbourhoods of Turin (Figure 151).

The hourly engineering model has been applied to evaluate how the urban form influences the demand for SC considering also different types of buildings as a

function of the relative construction periods (until 1918, 1961-70, 1981-90, and after 2006).

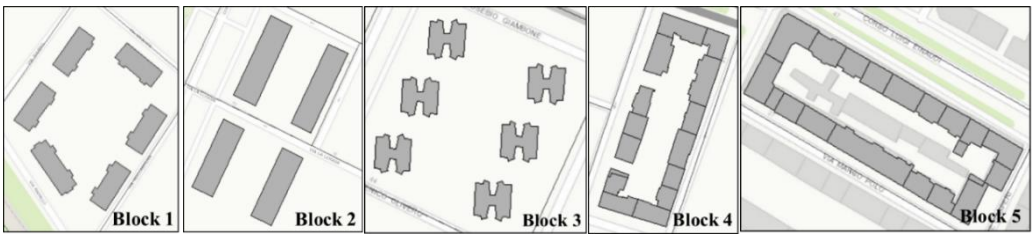

Figure 151. Blocks of buildings [49].

Case study

The relationship between urban form, energy performance and solar productivity has been investigated for six neighbourhoods –homogenous zones– in the city. Figure 152 shows the six homogeneous zones, the measured heating consumption and the census parcels.

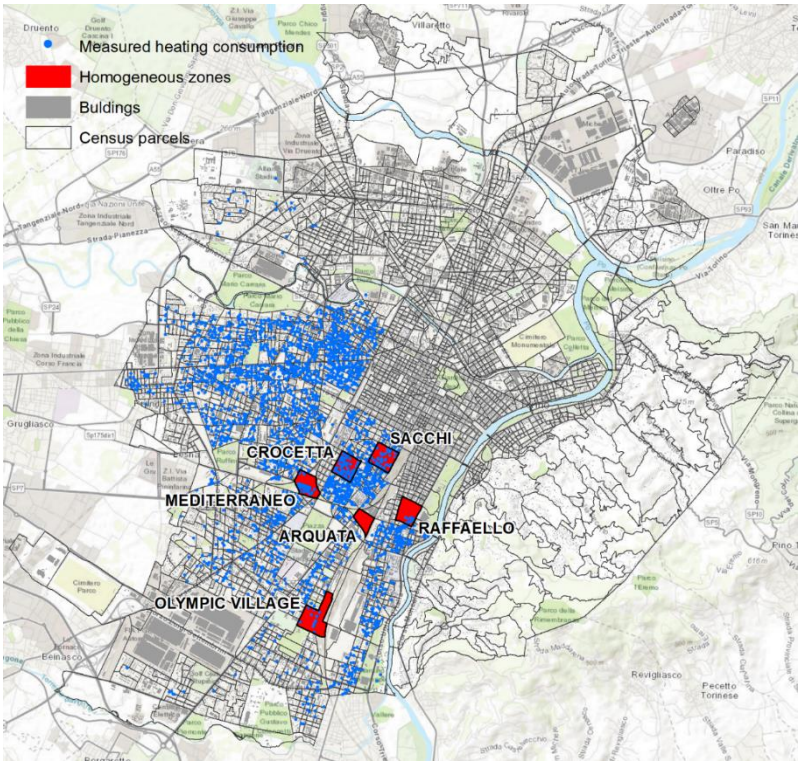

Figure 152. Map of the city of Turin: identification of six homogeneous zones [58].

Table 64 shows the average value of the urban parameters for each zone. The urban parameters that have greater variability are the *BCR* and *BD*, which are used to describe the urban building density, and the canyon effect evaluated as a function of the *H/W* ratio. Arquata and Olympic Village neighbourhoods are those with the greatest green areas with low urban density, in fact they have the low values of *BCR*, *BD* and *H/W*, while the *A* is slightly higher (close to 0.17 indicates the presence of green areas [151]).

Table 64. Homogenous zones of Turin (IT) [58].

Zone	Building variables and urban parameters					
	BCR	***MOS***	***BD***	***H/W***	H/H_{avg}	***A***
Arquata	0.18	0.59	3.56	0.27	1.01	0.19
Crocetta	0.28	0.45	5.86	0.52	0.97	0.15
Raffaello	0.38	0.45	8.1	0.57	0.95	0.15
Sacchi	0.4	0.54	7.72	0.6	0.95	0.14
Mediterraneo	0.24	0.58	6.96	0.62	1.01	0.15
Olympic Village	0.16	0.29	4.13	0.34	1.02	0.16

Figure 153 shows the six neighbourhoods. In Crocetta, Raffaello and Sacchi most of the residential buildings were built before 1946 and there are no new buildings. In Crocetta 80% of the buildings were built before 1960, 15% in 1961-1970, and only 6% after 1971; in Raffaello 86% of the buildings were built before 1970 (of which 67% before 1960); and in Sacchi 77% of the buildings were built before 1945, while 15% between 1946 and 1960.

Figure 153. Construction year of residential buildings located in the six neighbourhoods: (a) Arquata; (b) Crocetta; (c) Raffaello; (d) Sacchi; (e) Mediterraneo; (f) Villaggio Olimpico [58].

In the Arquata neighbourhood the entire residential buildings heritage was built between 1961 and 1970. Only in the Mediterraneo and Olympic Village there are recently built areas: in the first neighbourhood, most of the buildings are built between 1946 and 1960 (37%), but there is a 10% built after 2001; the second one is the newest neighbourhood, in fact 73% of the buildings were built after 2001 and 5% between 1981 and 1990.

From the analysis of land use, it emerges that the most built areas are Sacchi, Raffaello and Crocetta, followed by the Mediterraneo, Arquata and Olympic Village.

Raffaello, Sacchi and Mediterraneo have the highest population density, with an average value of 245 in./hectare, in fact in these areas the *BD* (which varies between 7.6 and 8.1 m3/m2) is greater than in the other three areas, in which there is a population density of about 140 in./hectare and an average *BD* of 4.5 m^3/m^2.

Results

Since the relationship between urban form and buildings affects the energy performances, it is therefore possible to obtain a lower energy demand by improving the morphology of the built environment [125]. The shape and height of buildings may affect their solar exposition, with consequences on the solar heat gains and the energy produced by envelope-integrated PV modules and ST collectors [126]. Compact urban configurations (with low values of *S/V*) reduce the heat exchanges between the buildings and the outdoor environment, but also reduce the solar heat gains. The *H/W* ratio describes the typical urban microclimates around the buildings, with urban canyons having a higher solar radiation absorption and consequently higher air temperatures, lower wind speeds and worse air quality [124]. The *MOS* also influences the solar absorption in an urban canyon, with limited shade for an East-West orientation and more shade for a North-South orientation. When an East-West orientation is not attainable, achieving high compactness, by keeping the *S/V* ratio low, becomes an important low-energy design strategy [127].

Heating energy demand and solar potential

The results from the energy simulations of 13 residential buildings confirm that energy consumption tends to increase with increasing *S/V* (less compact buildings consume more) and older buildings consume more than new ones. Figure 154 shows the energy consumption and energy savings from ST production of eight residential buildings with favourable orientation (E-W), while Figure 155 shows the results of five residential buildings with unfavorable orientation (N-S), taking into account the construction period and the *S/V* ratio. It is emerged that with an E-W orientation, it is possible to have a higher *S/V* (less compact buildings), so even having higher consumption, there is greater solar gains and therefore more productivity from solar energy. Depending on the construction period, the *S/V* can be increased for newer buildings: for example, *S/V* varies from 0.353 m^2/m^3 for

buildings built in 1919-45 to 0.375 m2/m3 for buildings built in 1971-80 (well-oriented buildings). These values tend to decrease for buildings with an unfavorable orientation, with an *S/V* ranging from 0.339 to 0.355 m^2/m^3.

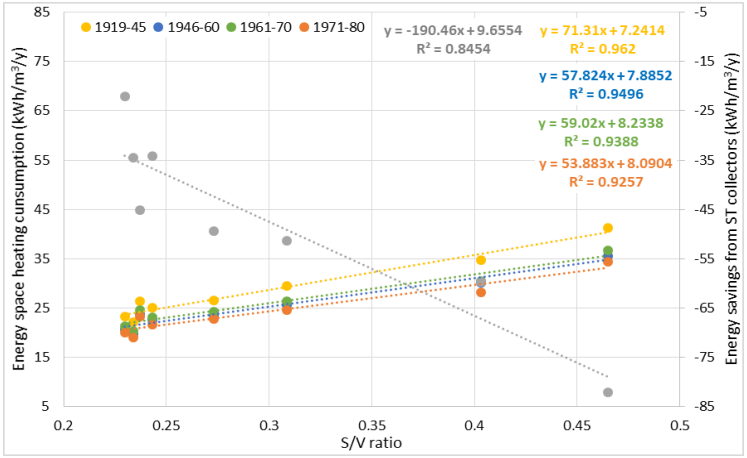

Figure 154. Energy consumption and energy savings from ST production depending on the S/V ratio: residential buildings with E-W orientation [58].

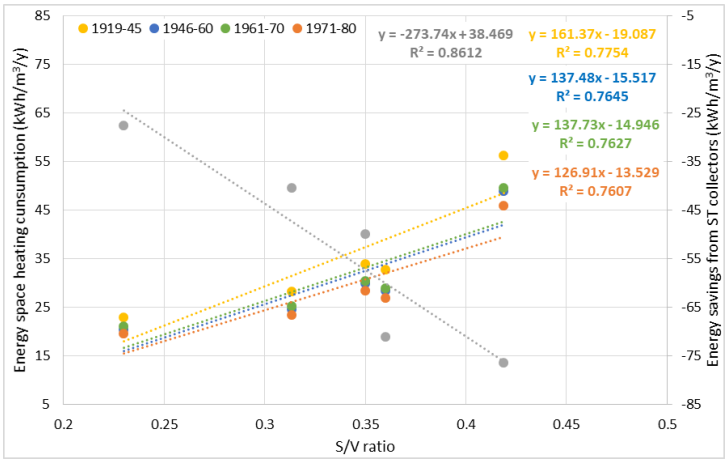

Figure 155. Energy consumption and energy savings from ST production depending on the S/V ratio: residential buildings with N-S orientation [58].

To investigate the potential of ST and PV energy generation in urban built areas, an energy indicator 'P/C' has been used to assess the self-energy; that is the ratio between the production and the consumption. This value bigger than one mean the building achieves and energy surplus.

To do this kind of analysis, the monthly consumption of heating, DHW and electricity have been simulated [52] and compared with the energy production from ST collectors and PV panels. Figure 156 shows an example of one residential building located in Sacchi neighbourhood. Thanks to the favourable orientation, this building has an electrical P/C of 1.11 (annual average value), so there is a surplus due to overproduction in the warmer months.

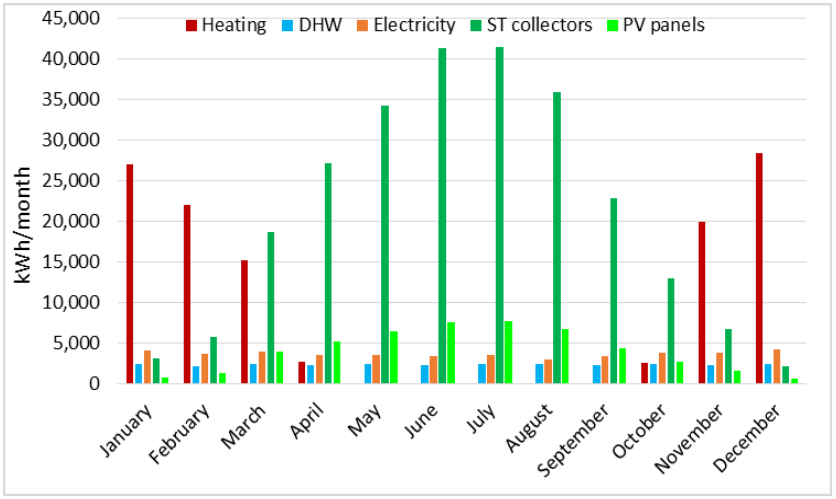

Figure 156. Monthly consumption and production of residential building with E-W orientation [58].

From the analysis of the relationship between urban form, energy consumption and solar energy, it is emerged that the main parameters that affect the energy performance and the solar energy productivity of buildings are the thermo-physical characteristics, the *S/V* ratio, the *BO*, the *BCR* and the *BD*.

From Figure 157 it is possible to observe that the heating consumption (in kWh/m^3/y) depends on the built area –quantified using the *BCR*– and on the compactness of the building, that is the *S/V* ratio. For example, less compact buildings, with high *S/V* values (close to 0.4 m^2/m^3), have higher consumptions.

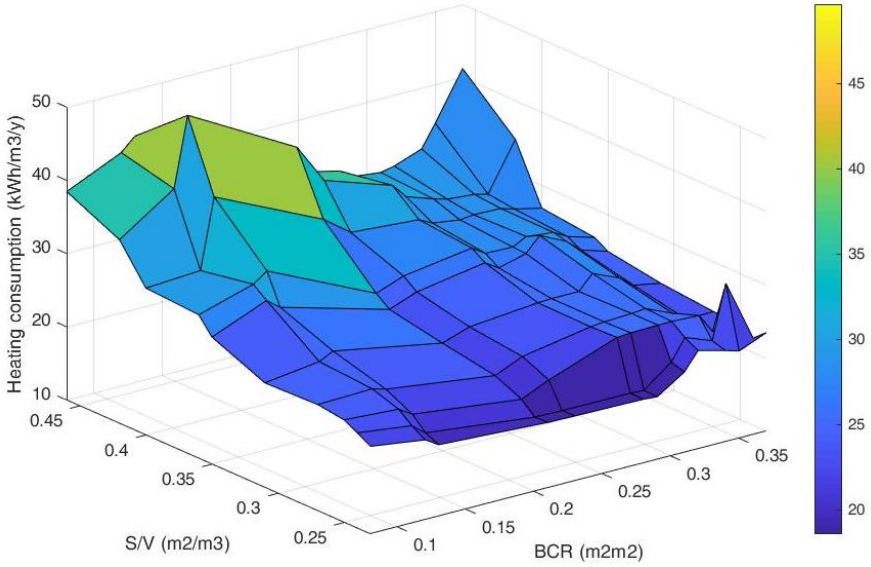

Figure 157. Relationship between urban form and energy consumption [58].

Figure 158 shows the trend of electricity P/C as a function of *BO* and *S/V* ratio. These results confirm that the solar energy potential depends on the building exposure and on the compactness of the building: well-exposed buildings (with *BO* values close to 1) have a higher P/C, moreover buildings with low *S/V* values mean that the number of families per building is lower (consequently, electricity

consumption is lower). With a favourable orientation and low electricity consumption, there is a consistent annual surplus.

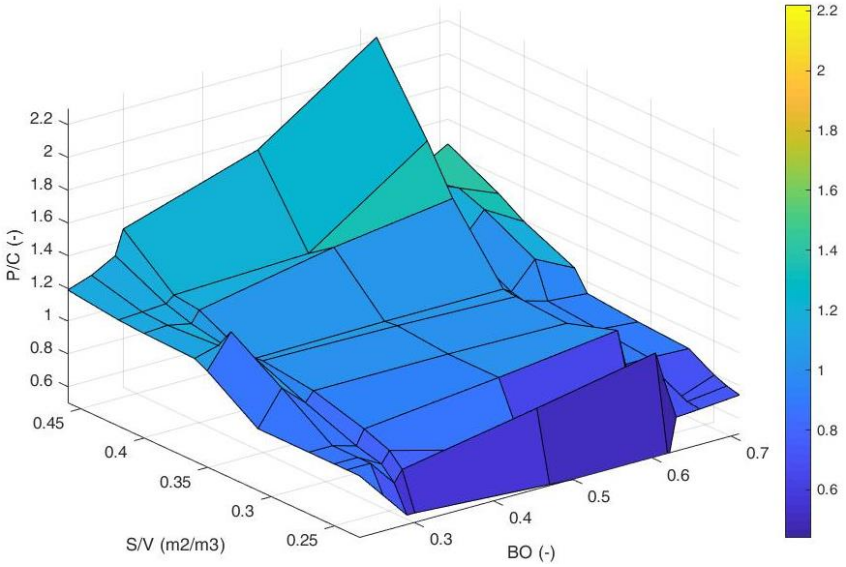

Figure 158. Relationship between urban form and solar energy [58].

Cooling energy demand

The effect of urban forms on cooling energy performance has been investigated using the hourly engineering model according to four different construction periods. The effect of urban form on cooling energy demand has been analysed by investigating the energy performance of five blocks of buildings (in Figure 159).

This analysis takes into account different thermo-physical properties according to four construction periods: until 1918, 1961-70, 1980-90, and after 2006. The four construction periods have been selected considering a consistency variation of the thermal transmittance values of the opaque and transparent components and of the thermal capacities of the envelope that characterizes the buildings.

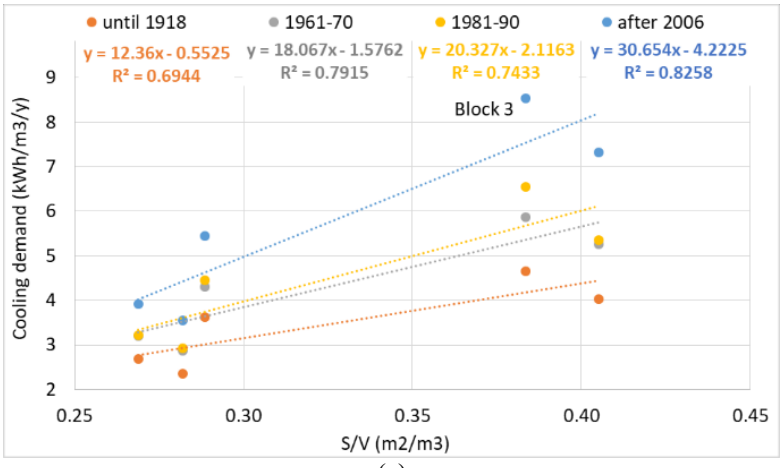

(a)

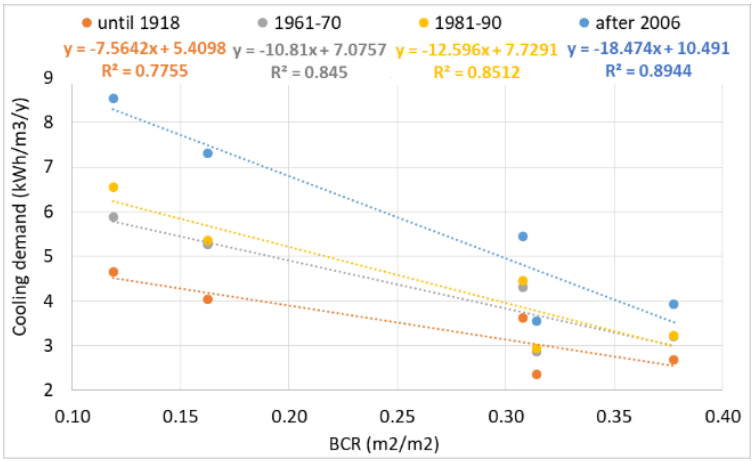

(b)

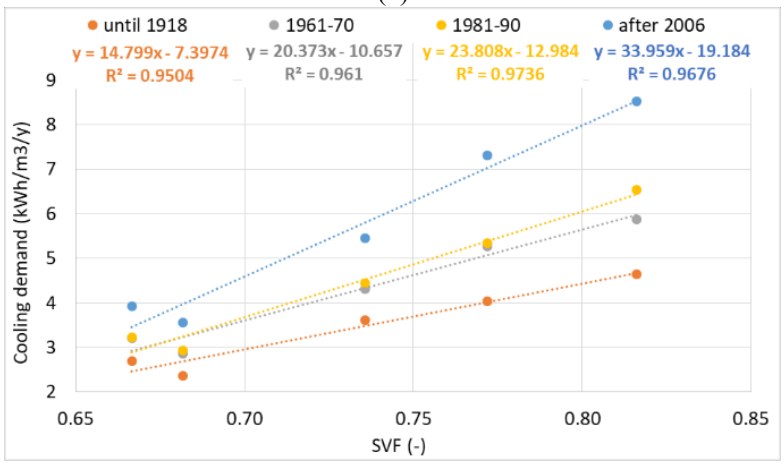

(c)

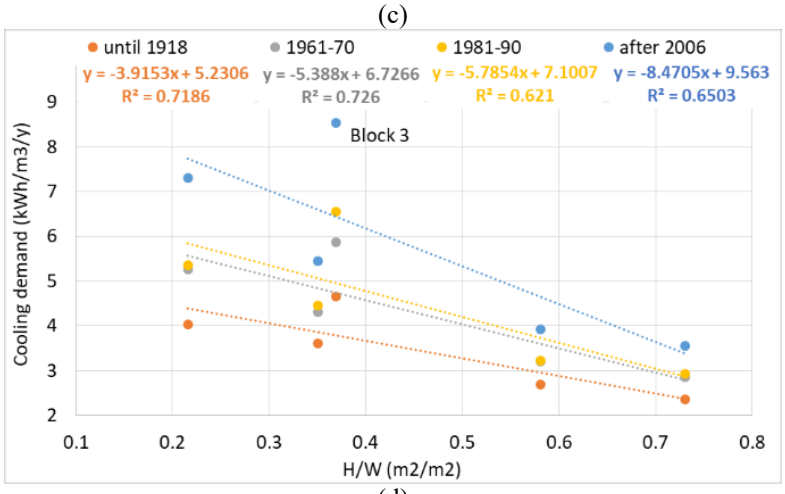

(d)

Figure 159. Simulation at block of buildings scale using the GIS-based engineering model for different urban forms and construction periods: correlation between the cooling demand and (a) the surface-to-volume ratio (*S/V*), (b) the building coverage ratio (*BCR*), (c) the sky view factor (*SVF*), and (d) the height-to-width ratio (*H/W*) [49].

The main findings were summarised as follows: (i) in all blocks of buildings investigated, older buildings have lower cooling energy demand, probably due to the higher thermal capacity values; (ii) cooling energy demand increases as *S/V* and *SVF* increase, and decreases with high values of *H/W* and *BCR*; (iii) the courtyard block (typical urban form in historical Turin districts), and the South-North

orientation (block 4 in Mediterraneo) has the lowest cooling demand; (iv) the towers, behave abnormally and the GIS model is not accurate with this urban shape (block 3 in Villaggio Olimpico).

5.4.2 Outdoor thermal comfort conditions

In this section, the outdoor thermal comfort are in the six neighbourhoods located in the city of Turin that have different urban morphologies.

Methodology

According to the literature review, ENVI-met is based on CFD models and it is one of the most used tools to analyse thermal comfort conditions in urban environment, since it is able to consider the effect of vegetation and evapotranspiration.

Therefore, ENVI-met is used to investigate the local climate conditions and the outdoor thermal comfort in six neighbourhoods identified as case studies. The analysis is carried out on neighbourhoods with different urban characteristics. Each neighbourhood was designed in ENVI-met using grid cells with a resolution of 10 x 10 meters. This resolution is accurate enough to describe the six zones but not too detailed to increase too much the simulation times. Since ENVI-met it is a "holistic" three-dimensional model, it takes a long time to simulate outdoor thermal comfort conditions and in this work each neighbourhood simulation required from 9 to 11 hours. The simulations are done taking into account the hottest day (summer), the coldest day (winter) and an average reference day for spring and for autumn. The first simulation aims to describe the business-as-usual (S_{BAU}) scenario; then, after mitigation interventions, such as green roofs, the effect of vegetation and green roofs (S_{GREEN}) on outdoor thermal comfort is quantified by calculating T_{mrt}, *PMV*, *PET* and *UTCI*. The output of these simulations can allow to analyse the liveability in different neighbourhoods and how it depends on the urban form and on the use of mitigation measures.

Case study

The analysis is carry out in six neighbourhoods identified as homogeneous zones with different building characteristics and urban contexts (see Section 5.4.1). By analyzing these neighbourhoods –with a dimension of about 400 x 400 meters– it is possible to identify the sustainable urban form that ensures higher thermal comfort conditions. The neighbourhoods that have been analysed are Arquata, Crocetta, Raffaello, Sacchi, Mediterraneo and Villaggio Olimpico.

In addition, in each neighbourhood three points with different urban characteristics have been identified –points in urban courtyards (UC, in red), points in green areas (GR, in blue) and points in squares (SQ, in yellow)– in which the comfort conditions have been analysed. In Table 65 the main characteristics of each neighbourhood, such as quantities of the type of soil and the presence of trees, have

been indicated. Recent neighbourhoods (Arquata, Mediterraneo and Villaggio Olimpico) present more grass coverage and a low footprint of the built-up area, vice versa the neighbourhoods with a more traditional conformation (Crocetta, Raffaello and Sacchi) are more densely urbanized. In general, it is possible to observe for all districts, the high values of street surfaces covered with asphalt between (between 36 and 51%), even in the historical districts of Crocetta, Sacchi and Raffaello.

Table 65. Neighbourhoods characteristics (in brackets the number of trees per 10,000 m^2 was indicated) [59].

Neighbourhoods	Arquata	Crocetta	Mediterraneo	Raffaello	Sacchi	Villaggio Olimpico
Inhabitants	1,756	3,703	4,718	4,827	4,223	2,803
Extension of the area [m²]	108,925	199,250	182,461	182,418	204,717	294,409
Building density (BD) [m³/m²]	3.56	5.86	6.96	8.10	7.72	4.13
Height-to-width ratio (H/W) [m/m]	0.27	0.52	0.62	0.57	0.60	0.34
Concrete light pavement [%]	6.13	0.00	11.64	0.00	0.00	4.27
Concrete grey pavement [%]	20.63	24.28	13.24	28.60	27.76	14.37
Asphalt [%]	43.50	51.24	49.72	36.44	35.92	45.47
Grass [%]	10.31	1.28	8.08	2.36	1.72	18.40
Buildings [%]	19.44	23.20	17.32	32.60	34.60	17.49
Building coverage ratio (BCR) [%]	0.18	0.28	0.24	0.38	0.40	0.16
Trees with height of 15 m * [%]	1.9 (2.75)	4.6 (5.77)	3.9 (5.37)	2.0 (2.69)	2.9 (3.52)	3.4 (4.31)
Trees with height of 5 m * [%]	6.0 (8.81)	1.4 (1.71)	0.8 (1.10)	1.7 (2.36)	2.4 (2.88)	1.2 (1.56)

Regarding local climate conditions, a set of hourly meteorological data from the 'Politecnico di Torino' weather station was used to investigate local climate conditions. Turin has a moderately continental climate, characterized by cold and humid winters, and hot and humid summers. The assessment was done for the hottest day (summer, August 7th), the coldest day (winter, January 1st) and an average reference day for spring and for autumn (March 27th and November 9th) in 2015 (Figure 160). The hottest day and the coldest day of the year have been selected to evaluate the outdoor thermal comfort conditions in extreme conditions. Different trend and intensity of solar irradiance affects the air temperature. The hotter the air the lower the relative humidity and vice versa, in the case of the summer day, where temperatures are higher, the accumulation in the air of water vapor is favored, raising the absolute humidity for evaporation and evapotranspiration from moist soil and vegetation. In all four days that have been chosen, the wind speed always presents low values (varies between 0.9 and 1.9

m/s), this is due to the geographical position in which the city of Turin is located: in the Po Valley and surrounded by the Alps.

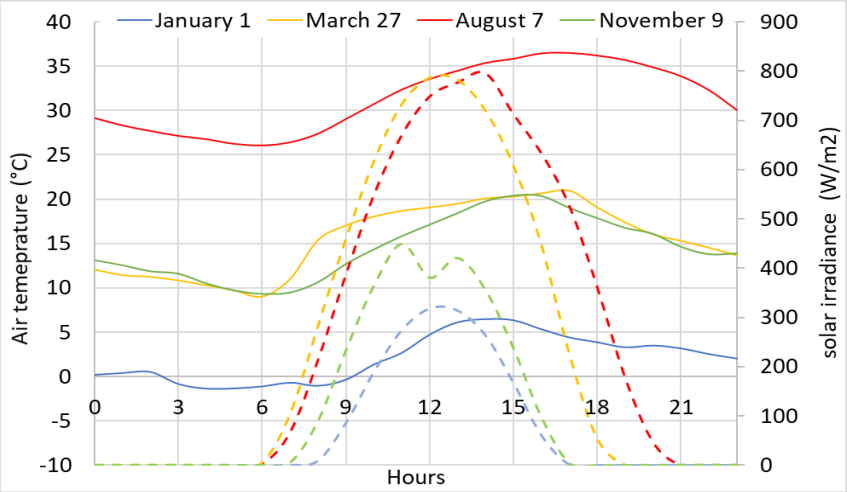

Figure 160. Air temperature (primary axis, solid line) and solar radiation (secondary axis, dashed line) with hourly detail for typical days (year 2015) [59].

Results

Thermal comfort analysis at a neighbourhood scale

Thermal comfort simulations were carried out for four typical days. In ENVI-met, with the support of Bio-met, the T_{mrt} and three thermal comfort indices (*PMV*, *PET* and *UTCI*) were calculated at 1 meter above the ground for a person with 35 years old, male, weight of 75 kg, height of 1.75 m, taking into account the following input data: *clothing insulation*: 0.5 clo or 0.08 m^2K/W (typical summertime clothing), 1 clo or 0.015 m^2K/W (typical midseason clothing), 1.5 clo or 0.23 m^2K/W (typical wintertime clothing); *metabolic rate*: 1.9 met or 110 W/m^2 (walking at 0.56 m/s).

In order to investigate the local climate conditions during summer, winter and mid-season, ENVI-met was used to describe the spatial distribution of the T_{mr} in different urban contexts. Figure 161 shows an example of the analysis made in Mediterraneo. Three points were selected to evaluate the outdoor thermal comfort in winter and summer, and in three different areas (GR is a point located in green area surrounded by buildings, SQ is a point located in an open space (without shading), UC is a point located in area with concrete pavement area surrounded by buildings).

In Figure 161, it is possible to observe how the T_{mrt} vary depending on the location in the neighbourhood. GR and UC points, which were surrounded by buildings, have lower temperatures in some hours of the day (mainly in the morning and the afternoon) due to shading. In addition, the variations of T_{mrt} depend on the reference season and in particular the greater incidence of shading in summer, where at 3 pm the temperature drops drastically and then rises again around 5 pm. By contrast, during the winter day there is no variation.

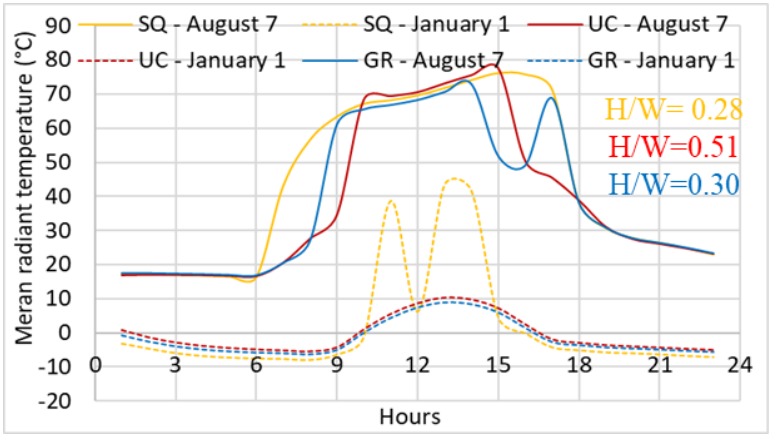

Figure 161. Hourly values of the Tmr in 'Mediterraneo' [59].

One of the strategies to mitigate the urban heat island effects and improve the liveability and quality of urban environments is the use of greenings in built-up areas. There are many benefits from the use of greenery in neighbourhoods: air temperature reductions, outdoor thermal comfort improvements, energy savings for space cooling, lower greenhouse gas emissions, better air quality and urban space liveability improvements, storm-water run-off reductions, and aesthetic and social benefits [269].

(a) Arquata

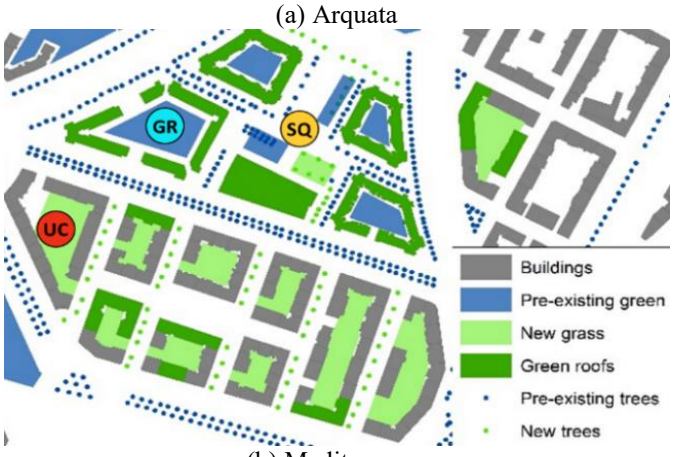

(b) Mediterraneo

Figure 162. Mitigation strategies: SBAU and SGREEN [59].

Since urban context significantly affects thermal comfort, two neighbourhoods that had different urban morphologies (Mediterraneo and Arquata, see Table 65) have been selected to evaluate the effect of mitigation strategies (Figure 162).

Table 66. Analysis of outdoor thermal comfort condition using mitigation strategies. In brackets the maximum difference between SBAU and SGREEN is indicated [59].

Neighbourhood	Green areas (%)	Green roofs (%)	Trees (%)	PET (°C)	PMV (-)	UTCI (°C)	Simulation time
Mediterraneo	+7.8	+29.3	+2.0	−1.47 (−2.20)	−0.12 (−0.17)	−0.36 (−0.68)	11 hours
Arquata	+1.1	+22.2	+2.6	−0.57 (−1.05)	−0.09 (−0.15)	−0.35 (−0.59)	9 hours

Table 66 shows the increase of green surfaces and trees (in %) comparing the S_{BAU} and the S_{GREEN}, and the consequent improvements of outdoor thermal comfort conditions by evaluating *PET*, *PMV* and *UTCI*. The average daily variation of *PET*, *PMV* and *UTCI* for August 7th, 2015 (from 8 am to 6 pm) for two points (in Arquata and in Mediterraneo UC points, see Figure 162) was shown in Table 66. Greater improvement of the indexes are visible in Mediterraneo neighbourhood due to more relevant mitigation action. Figure 163 shows how *PET* changes during the day by comparing the S_{BAU} and S_{GREEN} scenarios for different points (see Figure 162).

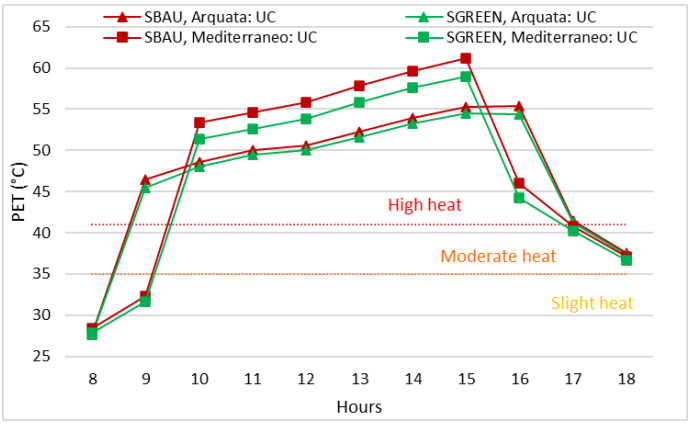

Figure 163. Comparison between SBAU and SGREEN on August 7th, 2015: hourly values of PET (°C) at specific points (UC) [59].

With Envi-met it is possible to map the urban thermal comfort indices to observe where the main changes occur. Figure 164 shows the absolute difference of UTCI and PET of the two scenarios at 1 pm in Mediterraneo (taking into account a person that is walking at 2 km/h) for August 7th, 2015. There was a slight overall improvement throughout the neighbourhood, and the main progresses were particularly visible where the new green areas were inserted. PET is more effective because UTCI as used in the software is limited to a wind speed and this does not allow us to see the improvements in comfort within the courtyards.

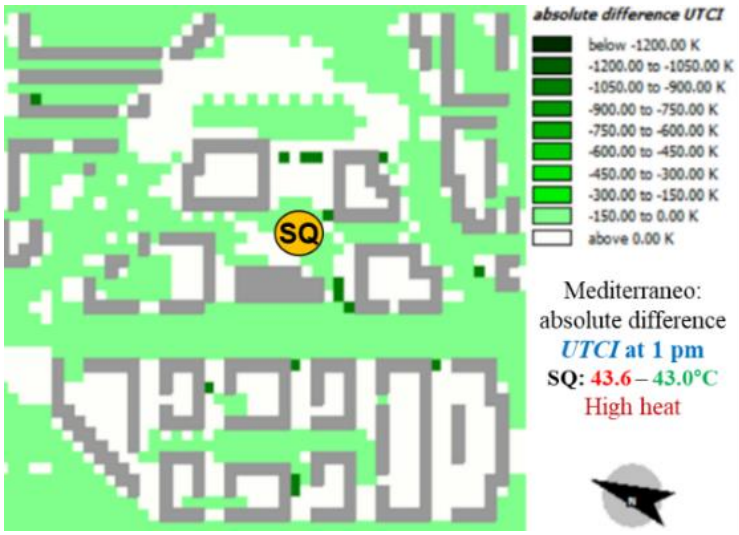

(a) Mediterraneo: absolute difference *UTCI* at 1 pm

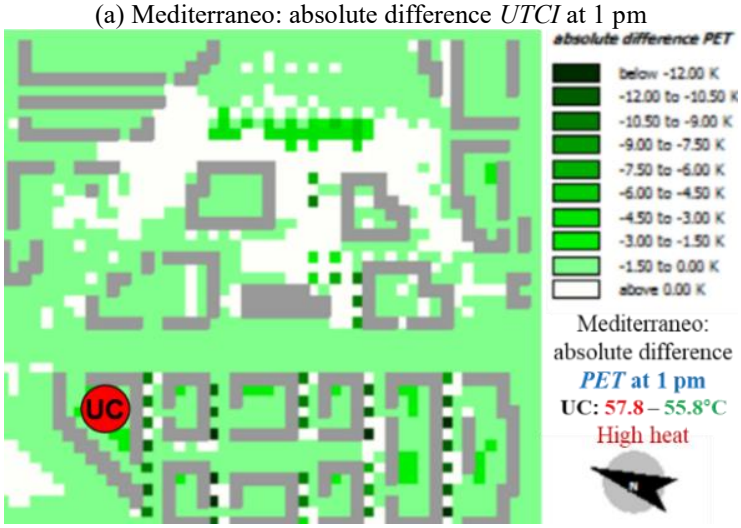

(b) Mediterraneo: absolute difference *PET* at 1 pm

Figure 164. Comparison between SBAU and SGREEN on August 7th, 2015 [59].

Impact of urban morphology on thermal comfort

The relation between outdoor thermal comfort conditions and urban morphology was investigated by analyzing the orientation, the building density (*BD*) that is the ratio between the total volume of the buildings and the building block area, and the urban canyons height-to-width ratio (*H/W*) that is the ratio between the building height and the distance between buildings.

In the first part of this analysis, the results on thermal comfort conditions with different types of outdoor surfaces, urban contexts and orientations have been investigated for August 7th, 2015. Figure 165 shows the T_{mrt} in two courtyards with *H/W* of 0.6 m/m (orange line) and 0.4 m/m (blue line). The summer comfort conditions are better with East-West orientation and *H/W* of 0.6 m/m, this is due to the fact that the hours in which the courtyard is sunny are from 10 am to 1 pm (3 hours). With North-South orientation and *H/W* of 0.4 m/m the hours of sunshine range from 11 am to 3 pm (4 hours), hours in which the solar irradiation has a maximum intensity. Similar trend can be observed in Figure 7b, which shows the

T_{mrt} in an urban canyon with *H/W* of 0.7 m/m. Considering the urban canyon without tress (red line), the summer comfort is better with the East-West orientation, and the hours of sunshine are from 9 am to 1 pm (with North-South orientation from 12 am to 4 pm). Using trees (green line) it is possible to reduce the T_{mrt} in a few hours during the day.

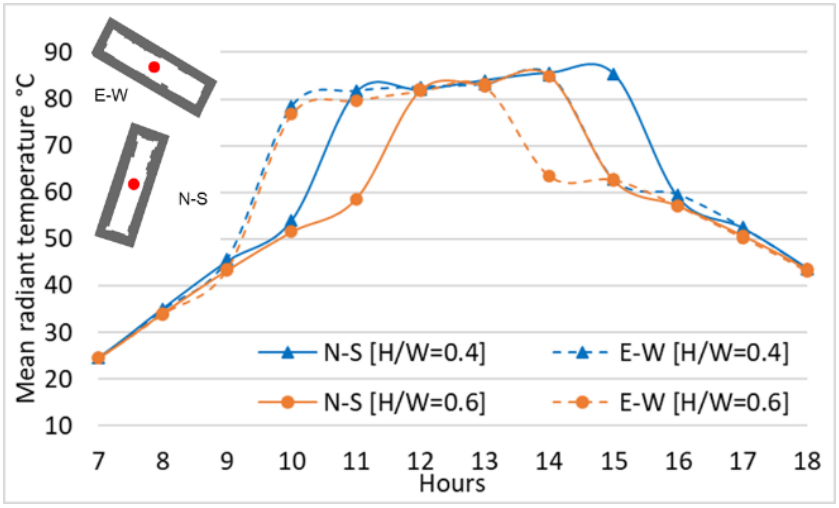

(a) courtyards with *H/W* = 0.6 and *H/W* = 0.4

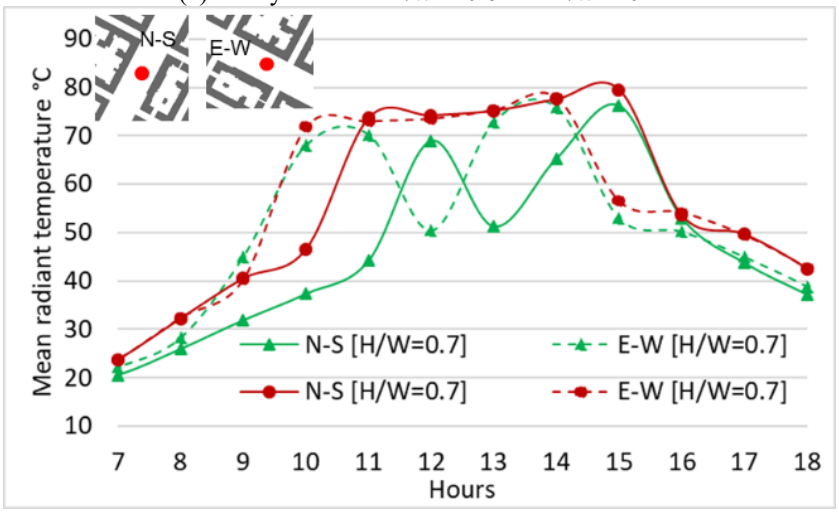

(b) urban canyon with *H/W* = 0.7

Figure 165. The mean radiant temperature (Tmrt) from 7 am to 6 pm for August 7th, 2015 [59].

In the second part of this analysis, average values of the *BD* and *H/W* were calculated for each neighbourhood, and Figure 166 shows the correlations between the urban parameters and the average T_{mrt} on August 7th, 2015 and on January 1st, 2015 for the six neighbourhoods. From these findings it has emerged that neighbourhoods that have a prevalent East-West orientation, *BCR* of 6-8 m^3/m^2 and *H/W* of 0.55-0.6 m/m (Raffaello, Mediterraneo and Crocetta) can achieve higher levels of summer and winter comfort conditions. Sacchi has characteristics similar to the previous neighbourhoods, but the characteristics that define the neighbourhood are “not optimal”; in this case it is necessary to improve the winter

comfort with compensatory measures. Finally, Arquata and Villaggio Olimpico neighbourhoods, that have low values of *H/W* and *BCR*, are less dense with higher summer temperatures. Therefore in these neighbourhoods it is necessary to intervene with compensatory measures in order to improve the summer comfort.

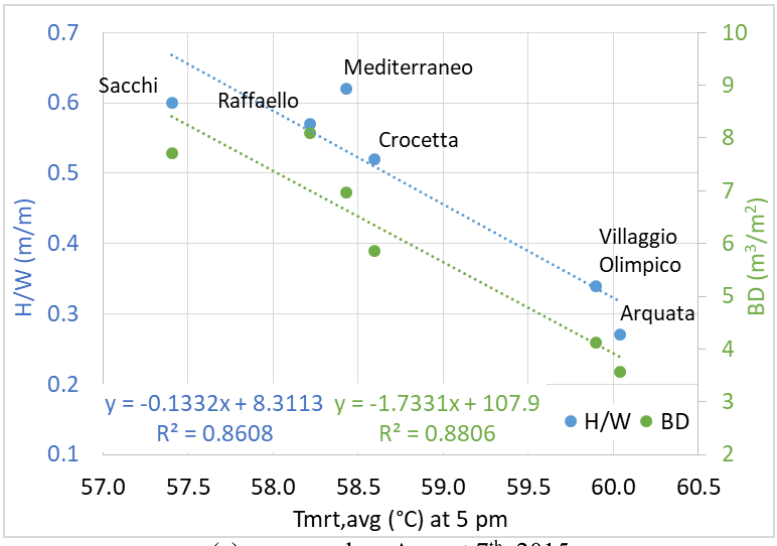

(a) summer day: August 7th, 2015

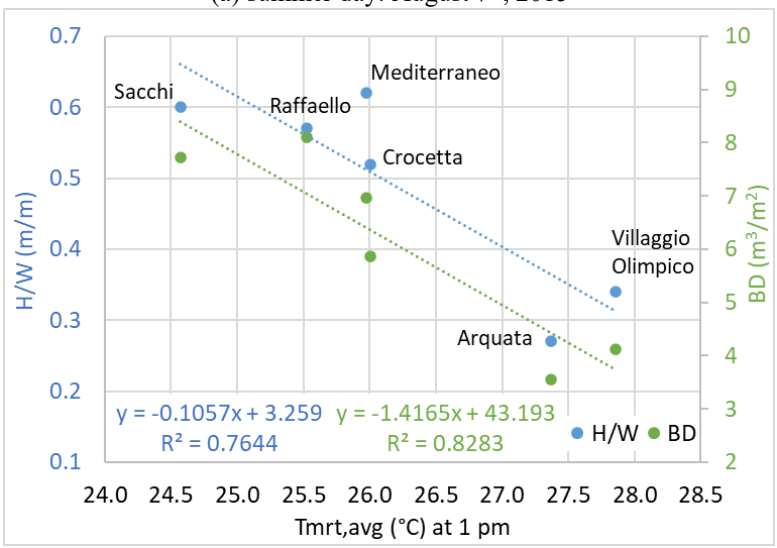

(b) winter day: January 1st, 2015

Figure 166. Correlations between urban parameters (BD and H/W) and the mean radiant temperature (Tmrt) [59].

Chapter 6

Energy efficiency policies and financial instruments

6.1 Chapter overview

To address the issue of underinvestment in energy efficiency, revisions in 2018 to the Energy Performance of Buildings Directive 2010/31/EU and Energy Efficiency Directive 2012/27/EU, have strengthened the existing policy and financial framework.

New elements include the reinforcement of existing financial instruments, establishment of new financial models or supporting mechanisms and a more active participation of financial institutions. In line with these actions, the European Commission launched the Smart Finance for Smart Buildings Initiative in 2016, with the aim to further mobilize private financing for sustainable energy in buildings. This initiative stresses the importance of more effective use of public EU funding and the need to de-risk energy efficiency investments in buildings by giving investors and private financiers a better understanding of the risks and benefits of energy efficiency.

A solid financial component has also been underlined as a prerequisite for the successful implementation of the long-term building renovation strategies set up by the EU Member States in accordance with the Energy Performance of Buildings and Energy Efficiency Directives.

This chapter gives an overview of energy efficiency policies of EU for buildings [60] and describes financial instruments and mechanisms at European level for each country used to promote energy retrofit in buildings [61,62] (Figure 167).

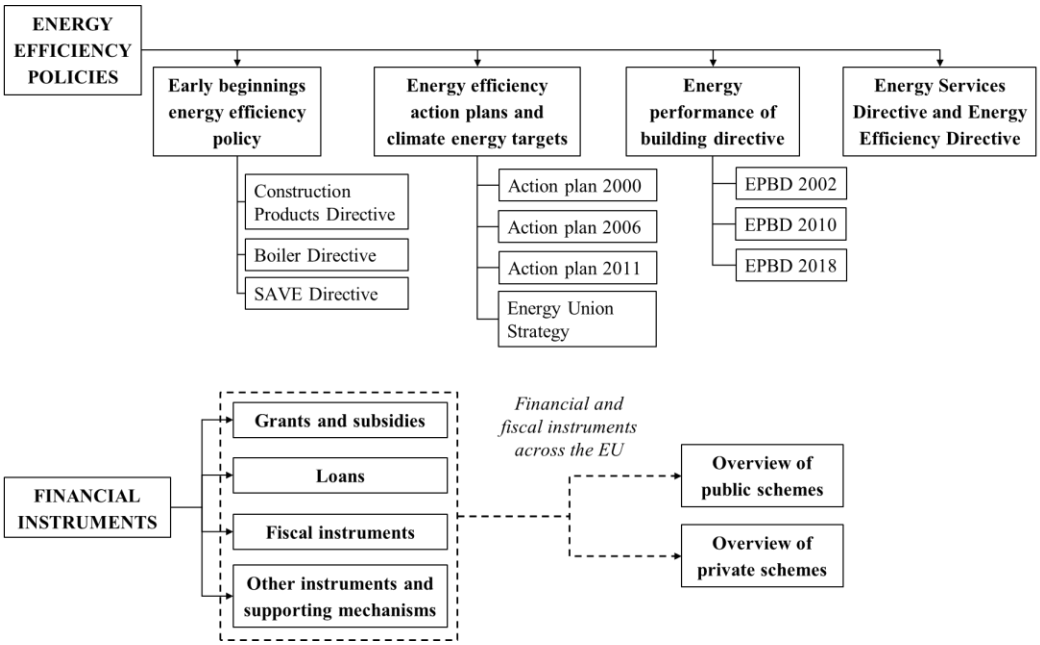

Figure 167. Flowchart of Chapter 6

6.2 Energy efficiency policies of EU for buildings

In order to understand how the EU policies have been effective in transforming the building stock and in reducing the energy consumption in new and existing buildings, this section investigates EU energy efficiency policy initiatives affecting the building sector.

6.2.1 Early beginnings energy efficiency policy

The development of energy policy was at the heart of the European project, with the ECSC Treaty (establishing the European Coal and Steel Community) in 1951 and the Euratom Treaty (establishing the European Atomic Energy Community) in 1957. In the 1970s and 1980s, the initial emphasis of energy policies was on the security of energy supply as result of the Oil Embargo in the 1970s [315–317]. Following the oil crisis in OECD countries in the 1973-1974, energy efficiency started to emerge as an important policy response to enhance oil security [245,318,319]. At the time, energy security was associated with "security of oil supply", but was later evolved to focus on other energy carriers including natural gas and renewable energy [320].

Following the first oil crisis, the European Council adopted a Resolution promoting energy savings in 1974 with the goal of reducing the rate of energy consumption growth and reach by 1985 a level 15% below the January 1973 estimates (Council Resolution of 17th December 1974, OJ C 153/2). In 1980, the European Council introduced a target for energy intensity and adopted policies including energy pricing measures (Council Resolution of 9th June 1980, OJ C 149/1). The Council Resolution of 16th September 1986 (86/C 241/01, concerning

new Community energy policy objectives for 1995 and convergence of the policies of the Member States[3]) emphasized the need to search for balanced solutions as regards energy and the environment, make use of the best available and economically justified technologies and improve energy efficiency. This Council Resolution represented the first EU policy initiative adopting an EE target with the aim to achieve greater energy efficiency in all sectors and to tap into various energy saving possibilities. The EE target was defined as a minimum 20% improvement in the "efficiency of final energy demand" ―defined as the ratio of final energy demand to gross national product― by 1995.

In 1987, the Commission Communication entitled "Towards a continuing policy for energy efficiency in the European Community" (COM(1987)223 final) proposed fourteen EE measures to Member States to help achieve the 1995 target. Seven out of the fourteen recommended policies were related to the provision of consumer information, seen as essential element to trigger investments in energy efficiency in a period of low oil prices.

In 1990, the climate change issue started to emerge and in the same year the European Council of Environment and Energy Ministers agreed on 29 October 1990 to stabilize total CO_2 emissions in 2000 at the 1990 levels.

Following the first Intergovernmental Panel on Climate Change (IPCC) Assessment report and establishment of the UNFCCC at the Rio Summit in 1992, the mitigation of climate change impacts became a key component of the EU energy policy along with the security of energy supply and competitiveness of energy users [321–323]. It was highlighted that EE contributed to three pillars of energy policy: the reduction of energy demand (and the related CO_2 emissions), the reduction of energy imports to meet energy service demand, and the cheaper energy services due to the reduction in energy use [324].

In the field of energy performance of buildings, the existence of large variations in energy performance levels and norms at Member State level gave a reason to consider policy action at the EU level [325,326]. The early EU energy efficiency policies for buildings constituted the "Construction Products Directive" in 1989, the "Boiler Directive" in 1992 and the "SAVE Directive" in 1993 [327].

6.2.2 Energy efficiency action plans and climate energy targets

Since 2000 the Commission has published several Energy Efficiency Action Plans laying out its strategic vision and proposing actions such as new policies or strengthened existing measures.

The 2000 Action Plan [324,328] proposed several reinforced actions, building on the SAVE Directive provisions on buildings. The Action Plan acknowledged the fact that different implementation and enforcement approaches of the SAVE Directive led to mixed results. The Commission in its 2000 Action Plan highlighted

3 https://eur-lex.europa.eu/legal-content/EN/TXT/PDF/?uri=CELEX:31986Y0925(01)&from=IT.

the need to amend the SAVE Directive, define more concrete measures and strengthen reporting and compliance procedures. While a more coordinated and harmonized approach was recommended in the Action Plan, the freedom for Member States to set their own efficiency requirements was also stressed. This Action Plan has nonetheless served as a key trigger that shaped the policy cycle leading to the development of the EPBD in 2002.

In 2006 the European Commission published its second Energy Efficiency Action Plan[4] [329–331]. Its scope was to control and reduce energy demand and to take targeted action on consumption and supply with the intention to save 20% of annual consumption of primary energy by 2020 compared to baseline energy consumption forecasts for 2020. This objective corresponded to achieving approximately a 1.5% saving per year up to 2020. Following the 2006 Action Plan in March 2007, EU leaders committed Europe to become a highly energy-efficient, low carbon economy and agreed on the targets, known as the "20-20-20" targets, by 2020 [332], which were formulated as: a 20% reduction in greenhouse gas emissions compared to 1990 levels; an increase in the share of energy from renewable energy sources to 20%; improvements in energy efficiency that lead to 20% EU primary energy savings.

In 2011 the new Commission presented the Roadmap for moving to a competitive low carbon economy in 20505 introducing new far-reaching targets to promote energy security, energy equity, and environmental sustainability: a cut in GHG emissions of 40% in 2030, 60% in 2040 and 80-95% in 2050 compared to 1990 levels [333]. At the same time the Commission adopted a new Energy Efficiency Action Plan [331]. Given the large energy saving potential of building renovations, the Plan stressed the need of more energy renovations in private and public sectors and introduced energy efficiency criteria for public buildings. Some measures introduced by the Plan were directed towards addressing the issue of 'split incentives', promoting the use of cogeneration combining electricity generation and district heating systems (wherever possible) and facilitating the use of tools such as energy performance contracting, energy audits, and ESCOs.

In 2014, the EU adopted energy and climate targets for 2030 as part of the Intended nationally determined contributions (INDC) to UNFCCC process leading to the Paris agreement. These were defined as: a 40% reduction in GHG emissions compared to 1990 levels, a minimum 27% share of renewable energy consumption, and at least 27% energy savings [321,334]. In 2018, following the discussions on setting the legal basis for the targets, the renewable and energy efficiency targets were modified to 32% and 32.5%, respectively.

4 https://eur-lex.europa.eu/legal-content/EN/TXT/?uri=LEGISSUM:l27064.
5 COM(2011) 112 final (https://eur-lex.europa.eu/LexUriServ/LexUriServ.do?uri=COM:2011:0112:FIN:EN:PDF).

6.2.3 Energy performance of building directive

The first cohesive European legal act on energy policy in buildings was the Energy Performance of Buildings Directive (EPBD, 2002/91/EC). Introduced in 2002, it aimed to tap into the large cost-effective saving potential of the sector (namely 22% in a 10-year period) underlined by several Commission Communications6. With this initiative, the European Union transposed a key article of its founding Treaty7 (new Article 191 on environmental protection), based on the idea to, inter-alia, improve the security of energy supply, increase employment and eliminate large differences observed between Member States.

In compliance with the EPBD Article 11, after the official transposition by the Member States (due by 4th January 2006) and the first years of implementation, the Commission started to evaluate the Directive in light of the experience gained during its application. Following this evaluation, the EPBD underwent a recast procedure in order to clarify and strengthen several provisions, the result of which was the adoption of the EPBD recast 2010/31/EU of 19th May 2010. Overall, the EPBD policy framework laid down the foundation for: setting minimum energy performance standards in new buildings and existing buildings under major renovation; ensuring that prospective buyers or renters are well informed and thereby encouraged to choose higher than minimum standards in their decision making processes; speeding up the rate at which investors engage in energy efficiency projects (including through finance).

The following sections give an overview of the first EPBD (2002) and describe the re-cast of EPBD in 2010 and its amendment in 2018.

EPBD 2002

With the Directive 2002/91/EC of 16th December 2002, the European Parliament and the Council introduced a joint energy performance calculation methodology for buildings. The following main areas of action were identified:

1. National minimum requirements and specific energy performance measures for new buildings and large (more than 1000m^2) existing buildings undergoing major renovation;
2. Specific provisions for the set-up of mandatory national energy performance certificate (EPC) schemes for both new and some categories of existing buildings, including the need to display EPCs together with recommended indoor temperatures in large public buildings;
3. Revised conditions for the inspection of boilers and heating/cooling systems, made by qualified and accredited experts.

6 COM (2001) 226, COM (2000) 769 of 29 November 2000 and COM (2000) 247 of 26 April 2000.
7 https://eur-lex.europa.eu/collection/eu-law/treaties/treaties-force.html.

In accordance with the European subsidiarity principle and considering the local peculiarities and climatic differences, Member States were asked to transpose the EPBD provisions within a three year period. Given the novelty of the Directive, in particular in relation to building codes and certification schemes [335,336], the progress of the transposition in several Member States was rather slow [335,337,338]. Member States were therefore given the possibility to apply for an additional period of three years (until 2009) to comply with the provisions of the Directive.

EPBD 2010

In 2009 the European Commission presented the recast of the EPBD[8] (2010/31/EC, EPBD Recast) with the aim to strengthen some original EPBD provisions and capture additional energy savings as stated in the 2006 Action Plan. The main purpose of the EPBD recast was to ensure that national Minimum Energy Performance Requirements adopted by Member States had similar ambition levels in terms of energy savings and greenhouse gas emissions reduction. This is because some national standards were not ambitious and cost-effective enough [339]. To this end, Article 5 of the EPBD recast introduced the cost-optimal methodology as the guiding principle for setting building energy requirements and Article 9 introduced the concept of "nearly zero-energy buildings" (NZEBs) according to which all new private buildings will have to comply with nationally defined NZEB standards by January 2021.

The new EPBD also eliminated the threshold of 1,000 m^2 for existing buildings under renovation to meet energy performance standards and installation requirements. In addition, energy performance requirements were introduced for technical building systems (heating, hot water, ventilation, cooling, air conditioning). The provisions related to the EPCs and inspection of heating and air-conditioning systems were reinforced to make them more effective. The EPBD recast aimed to raise the importance of financial incentives to promote energy renovations and required Member States to identify and submit to the Commission national financial measures to improve energy efficiency. From the Commission's side, support was made available in terms of structural funds, European Investment bank funds and other EU funds.

EPBD 2018

In order to implement the Energy Union Strategy[9], in November 2016 the Commission adopted a package of measures (the Winter Package) to revise the EED and EPBD and align them to the new 2030 energy and climate targets. The EPBD amendment procedure started at the end of 2016 and ended on 30 May 2018

8 https://eur-lex.europa.eu/legal-content/EN/TXT/?uri=CELEX%3A32010L0031.
9 COM/2015/080 final.

with the approval of Directive 2018/844/EU. The Commission also launched a new buildings database – the EU Building Stock Observatory[10] – to track the EP of buildings across Europe. In order to stimulate and increase the level of direct investment towards the renovation of the building stock, the Commission launched the 'Smart Finance for Smart Buildings' initiative, which aims to unlock an additional EUR 10 billion of public and private funds.

On 19th June 2018 the new Directive (2018/844/EU, EPBD) was published and the revised provisions entered into force on 9th July 2018. This revision introduces targeted amendments to the current EPBD aimed at accelerating the cost-effective renovation of existing buildings, with the aim of a decarbonized building stock by 2050 and the mobilization of investments to reach this goal [340]. The revision also supports electro-mobility diffusion by mandating electro-mobility infrastructure deployment in buildings' car parks. It also introduces new provisions to enhance smart technologies and technical building systems, including building automation.

Member States have 20 months to transpose the Directive into national laws (namely by 10th March 2020).

6.2.4 Energy Services Directive and Energy Efficiency Directive

The Energy Services Directive (ESD - 2006/32/EC) is broadly considered as successor of the SAVE Directive and the predecessor of the EED. Adopted in 2006, the ESD laid out the foundation for setting indicative national targets equivalent to at least 9% energy savings by 2016 and introduced reporting obligations through the preparation of National Energy Efficiency Plans (NEEAPs) [341,342]. Whilst the ESD did not have any specific focus on buildings, it included some provisions on metering and billing, financing and energy performance contracts. These provisions were strengthened in the subsequent EED, discussed below.

The legal basis of the 2020 targets and other provisions stipulated in the 2011 Energy Efficiency Action Plan was established in the Energy Efficiency Directive (EED, 2012/27/EU) which was adopted in December 2012 as part of the European Energy and Climate Package [343].

The Directive quantified the 20% energy efficiency target in terms of absolute primary and final energy consumption levels by 2020 and required MSs to contribute to the overarching EU target by setting their own energy efficiency targets at national level. While these targets are of indicative nature, the Directive set several mandatory EE policy measures to help reach the target, focusing on all stages of the energy chain from production to end use. The most important EED articles on buildings included the requirement for the public sector to renovate its central government building stock (Article 5), the setup of metering and billing requirements measures (Articles 9-11) [344] and establishment of long-term strategies for national building stock renovation (Article 4). The Directive also

10 https://ec.europa.eu/energy/topics/energy-efficiency/energy-efficient-buildings/eu-bso_en.

included provisions to promote energy performance contracting in the public sector (Article 18) [345], to remove split incentives (Article 19a) and to establish mandatory audits for large companies (Article 8) [346]. Lastly, the Directive pushed to open up energy markets to demand response (Article 15) and establish Energy Efficiency Obligation Schemes mandating energy companies to achieve 1.5% annual energy savings for final consumers every year (Article 7) [329,347]. In 2018 the EED was amended (2018/2002/EU) to provide a legal frame for the 2030 energy efficiency targets and extend article 7 to 2030.

6.3 Financial and fiscal instruments

A solid financial component on energy efficiency has a key role in the transition towards climate-neutral buildings, with a need for more targeted financial mechanisms, new financial models and more active participation of financial institutions.

To accelerate energy efficiency investments in buildings, the European Commission has intensified its efforts in recent years, with specific calls to strengthen the existing financial framework, increase funding levels, diversify types of financial models and explore new supporting mechanisms. Various private and public financial and fiscal mechanisms for energy renovations in buildings are currently available in Europe in the form of non-repayable rewards, debt financing, equity financing.

6.3.1 Grants and subsidies

Grant schemes can be useful at stimulating the market by subsidizing energy efficiency investments for households and businesses, which otherwise cannot be fully supported by the market alone due to high upfront costs. They directly fill an immediate financial gap and thus enable a temporary shift in the market. They typically rely on limited resources and can, therefore, neither offer a sustainable solution nor support massive market uptake programs.

Grants mainly serve as direct investment subsidies which may partially or fully cover renovation costs including acquisition of material/equipment, advice, certification and installation. Across EU Member States, grants are offered for projects with investment size ranging from a few thousand to over EUR 1 million, reflecting the varying nature and scope of the eligible projects [348]. Any remaining costs are either self-financed or covered by a loan. The grant intensity (subsidy level) may vary with the following parameters:

- Energy performance: e.g. subsidy is linked to amount of energy or costs saved meaning more support is provided for more ambitious projects;
- Household income: more favourable conditions may apply for low income households or customers subject to fuel poverty;

- Specific target group: e.g. condominiums or rented properties may have access to higher grant intensity;
- Intervention measure: e.g. some harder-to-implement interventions such as insulation may be associated with higher intensity;
- Innovativeness of technology: new and emerging technologies may receive more support to help their entry to the market.

Although grants generally score low on the continuity and funding sustainability criteria (Table 67), they constitute the most commonly found mechanism that EU countries currently use to encourage energy efficiency improvements in the building stock. They are typically associated with high uptake rates, but even the most prominent instruments cannot offer a real widespread implementation. If public grant schemes rely on EU funds, e.g. ERDF, there is often a significant delay and uncertainty in setting up follow-up schemes which may have a negative impact on market players. In addition, grant schemes often attract recipients who would have carried out the investments even without the incentive, the so-called free riders. Grant schemes are often designed in a way to crowd out any other viable commercial schemes. A more careful design of grant schemes can reduce the effects of free ridership. For example, eligible interventions can be restricted to renovations leading to state-of-art energy performance or can be limited only to a specific target group, e.g. low income households, tenants, and small and medium enterprises. Compatibility of these grant schemes with energy performance certificates could also leverage in private investments.

Table 67. Overview of grant schemes as a vehicle for financing energy efficiency investments [62].

Strengths	Weaknesses
- Can support initial stage of a new market/diffusion of new promising technologies and deep renovations which may be perceived risky by investors. - Can be used to provide financial assistance to vulnerable groups or low-income households meeting political priorities such as health or social inclusion - Can support energy efficiency projects that normally would be too small to get attention from commercial banks	- Cannot offer massive uptake rates - Typically more suitable for individual interventions which may lead to energy saving "locking-in" effect - Public budget restrictions may threaten its continuation due to high costs - May attract free riders - May discourage the use of other forms of financing such as commercial loans or energy performance contracts - Can be associated with significant paperwork or bothersome application processes - May have a negative impact on the market as a result of manufacturers or contractors raising prices (e.g. equipment or services) in anticipation

6.3.2 Loans

Debt financing in the form of loans can be a more sustainable means of up-scaling energy efficiency investments as they can provide liquidity and direct access to capital. Loans can be more relevant for energy efficiency measures attached to high upfront costs, especially in deep renovation projects which comprise a package of multiple intervention measures. Despite this, private debt financial products designed specifically for energy renovations in buildings are currently not fully developed as financial institutions are often unfamiliar with these investments and thus perceive energy efficiency loans as high-risk investments. High transaction costs for relatively small projects and failure to offer financing for terms long enough to support deeper measures are additional factors hindering market uptake.

To address some of these issues, international financial institutions and governments can intervene to fill the debt gap where local and traditional banking sector actors are not active. This can be done through various mechanisms, e.g. preferential loans offered by public banks, dedicated credit lines, third party financing etc. An example of the latter includes the regional "Ile-de-France Energies" third party finance scheme for condominium association supported by a EUR 100 million European Investment Bank loan. Given the nature of energy efficiency, there are different repayment methods, beyond what is considered "traditional". Traditional schemes refer to any loan and soft loan schemes which are attached to conventional repayment methods: that is, a lump sum of money is lent which is then periodically repaid through instalments that cover interest and principal over a fixed period of time. Repayments can also take the form of energy performance contract bills, property tax and utility bill. All these options are discussed below.

Table 68. Overview of loan schemes as a vehicle for financing energy efficiency investments [62].

Strengths	Weaknesses
- Represents a more sustainable means of financing than grants as capital is preserved and can be re-lent as soon as loan repayments are partly or fully made - Can be combined with various support mechanisms such as a revolving fund mechanism which ensures that loan funds are cycled back into the fund for more energy efficiency projects - Can be easily implemented by banking institutions, reducing long bureaucratic processes often linked with government grant schemes	- Households and other target recipients may be unwilling to take on (additional) debt - Lack of understanding of value of energy efficiency projects by financial institutions remains a key barrier - Acquiring a second loan (e.g. on top of existing mortgage) may be complicated - Not suitable for vulnerable groups as credit worthiness of certain target groups would reduce their eligibility - Small projects may not be attractive for bankers

Traditional loan and soft loan schemes

Various international financial institutions and EU governments have begun experimenting with loan schemes that offer attractive terms to customers for energy efficient projects. In most cases, preferential or soft loans —government supported loans offered at below market interest rates— are delivered through public-private partnerships where the government provides financial support to a bank, which in turn offers a loan scheme with preferential interest rate to its customers. Typically credit lines are extended to financial institutions as low interest rate loans by a donor or a government. The recipient institution then on-lends the funds to customers (e.g. private individuals, condominium association, commercial customers, public authorities, energy service companies, etc.) to invest in energy efficiency projects. They can be an alternative or a complementary measure to subsidies.

Low interest rates are a common feature of most of national loan schemes in the EU targeting energy efficiency investments. In certain cases, zero interest rate loans are available such as in Belgium, Croatia and France. These are typically directed towards the most vulnerable groups such as low income households. In France, the cost difference between the normal- and zero-rate loans is paid by the government through a tax credit scheme offered to participating banks. The combination of loans and grants in order to partially offset project costs are also a common practice. For example, the Bulgarian Energy Efficiency and Renewable Source Fund offers incentive payments of 20-35% with a funding cap of EUR 9,000. The Bulgarian scheme also provides Energy Service Companies (ESCOs) portfolio guarantee, and thereby undertakes some of the risk associated with disruptions in the flow of receivables of the ESCO. The Estonian Renovation loan for apartment buildings, which is designed based on the concept of revolving fund, also provides guarantees. In Germany, German public bank KfW receives a subsidy from the government to lower the interest rate at which it lends to the commercial banks, which can thus propose energy efficiency loans to homeowners under market rates.

Loans with performance contract bill repayment model

Under an energy performance contract (EPC), an energy services company (ESCO) undertakes a project to deliver energy efficiency improvements in the premises of the client. It then partially or fully uses the stream of income from the cost savings to repay the costs of the project. Following the end of the contract all energy savings are transferred to the client.

There are two main types of energy performance contracts with different loan arrangements:

1. Guaranteed savings: The ESCO guarantees a certain level of energy savings and in this way shields the client from any performance risk. The loan goes on the client's balance sheet and the ESCO assumes full project performance risk.

2. Shared savings: The savings are split in accordance with a pre-arranged percentage between the client and the ESCO, i.e. the loan goes on the ESCO's balance sheet. The ESCO finances the project and assumes debt obligation on balance sheet. The ESCO assumes both (partial) project performance and credit risks. There is no standard split of the share of the ESCO vs. the client, as it depends on the length of the contract, payback time and underlying risks taken.

ESCO projects[11] can either be financed through internal funds of customers or ESCOs, or alternatively through third-party financing. While financing is not supposed to be part of the key ESCO activities, they may often provide or arrange for the financial terms of the project in the case of the shared savings EPC model. In the customer financing model, the ESCO does not participate in the financial solution of the project, but instead its role is restrained to the technical and managerial aspects. Project financing may also come from a third party, typically a financial institution, instead of internal funds of the ESCO or of the customer.

Table 69. Overview of energy performance contracts as a vehicle for financing energy efficiency investments [62].

Strengths	Weaknesses
- Reduces or eliminates performance risk of energy efficiency measures - Eliminates need for internal technical expertise and packages all services in a single contract/source of accountability - Avoids upfront capital expenditure in case of shared model - Incentivizes ESCOs to provide optimised and state-of-the-art solutions to maximize energy savings	- Uncertainty of baseline measurement and ex-post measurement challenges - Difficulty to access finance by ESCOs who may become very indebted - Not suitable for small projects due to high transaction costs - Difficulty to promote ESCO models in markets which are not yet mature

Loans with on-tax repayment model

Property Assessed Clean Energy (PACE) is a means of financing energy renovations through the use of specific bonds offered by municipal governments to investors. The governments use the funds raised by these bonds to loan money towards energy renovations in residential or commercial buildings. The loans are repaid over the assigned term – typically 15 or 20 years – via an annual assessment on their property tax bill. The long repayment term attached to PACE programmes allows for investments with long payback times to be considered in the renovation. This additional tax assessment is placed on the property rather the property owner which means that PACE assessments are also transferable. In other words, it is possible to recoup the investment upon sale thereby reducing the concern about

[11] A large database of good practices on ESCO projects can be found here: https://guarantee-project.eu/bestpractice/

investment recovery during sale transactions. PACE programmes are secured by a senior lien on the owner's property, which avoids repayment security to be attached to the borrower's creditworthiness and is therefore more attractive to financiers. The loan is attached to the property, so it can be transferred and paid off by the next owner.

PACE programmes are mainly implemented in the United States with a reported $150 million in federal grant funds initially allocated (LBNL, 2011). Currently, there are 36 US states with PACE enabling legislation, 12 with active programmes and others in the process of programme development. It should be noted that PACE programmes were suspended in 2010 due to the fact that U.S. mortgage authorities Freddie Mac and Fannie Mae refused to finance mortgages with PACE liens. This occurred because PACE loans are generally assigned first lien status; that is, in cases of default, they are paid off to the municipality before the main mortgage is paid to the lender [349].

Despite this issue, in the US there is still growing interest around the PACE mechanism. PACE financing is not yet available in the EU, however, pilot project, EuroPACE[12] is testing the concept in Olot, a municipality in Catalunya. The EuroPACE project aims to adopt best practices from the US PACE market and enhance its impact in the European market.

Table 70. Overview of On-Tax repayment schemes as a vehicle for financing energy efficiency investments [62].

Strengths	Weaknesses
- Avoided upfront capital expenditure - Can be paid off over extended periods of time - Can be transferred to next owner if property is sold - Associated with lower probability of default than in standard loans due to reduced red tape for lenders in case of default (it is the tax collector who carries the burden) - Can be combined with technical assistance	- Selling the property might be challenging if buyers don't want the loan - Effective only if national tax collection is well-structured and transparent. Not all countries collect property taxes in the way that is suitable for PACE

Loans with on-utility bill repayment model

On-bill financing is a mechanism that reduces upfront cost barriers by linking repayment of energy efficiency investments to the utility bill and thereby allowing customers to pay back part or all costs of energy efficiency investments over time. The funds can originate from utilities, the state or third parties. Savings made by energy efficiency investments under this mechanism can be higher than the cost to make the investment, ensuring the total post-renovation utility bill does not exceed the pre-renovation bill. They can be particularly useful for small businesses with

[12] https://www.europace2020.eu/

limited capital to spend as well multi-family or rented properties where split incentive deter such investments. On-bill finance programmes can be categorized into: (1) on-bill loans and (2) on-bill tariffs. The main difference between the two is that on-bill loans must be paid off in case of ownership transfer while on-bill tariffs assign the obligation to the property, thus allowing for a transfer of the repayments to the next tenant or buyer.

Utility on-bill financing programmes, typically administrated by utilities, have been used in the US for many years. The US experience shows that while on-bill financing can successfully overcome important barriers such as upfront cost and split incentives, there are still issues that need to be addressed such as the need to modify billing systems, role of utilities as financial institutions, risks of no payment, handling transfer of property, diversifying sources of capital, etc. In the European context, the first on-bill financing scheme was implemented in the UK in 2013 with the introduction of the Green Deal, which enabled owners and occupants to install EE improvements at no up-front cost. The scheme initially gained momentum before it was effectively ended due a number of key barriers including uncompetitive interest rates in comparison with general home improvement loans or traditional commercial bank loans.

Table 71. Overview of On-Utility Bill repayment schemes as a vehicle for financing energy efficiency investments [62].

Strengths	Weaknesses
- Avoided upfront capital expenditure - Ease of repayment linked to bill neutrality concept - Access to finance for customers who are not able to qualify for traditional financing options - Can be transferred to the next owner	- Challenging design elements such as modification of billing systems, role of utilities as financial institutions, risks of no payment, handling transfer of property, diversification sources of capital - Difficulties in assessing credit risk of customers through their historical payments - Customer risk of power shut-off or repayment issues when customers partially pay their bills

6.3.3 Fiscal instruments

Tax incentives can increase demand for energy efficiency projects by reducing the cost of the energy efficiency improvement through reduced taxes for households and businesses. They can be less costly than grant schemes and are considered a popular instrument promoting energy efficiency in certain EU countries. They may work well alongside a taxation scheme, whereby the tax loss attributed to the tax incentive scheme is offset by revenues from taxation for energy intensive industries. They are effective if the tax collection rate is sufficiently high and can be useful at promoting new technologies that lack profitability at current stage. They can take various forms, such as accelerated depreciation, tax exemptions, income tax or VAT reduction (Table 72). As in the case of grant schemes, tax incentives are

susceptible to free ridership issues and therefore careful design of this policy is needed.

Table 72. Types of tax incentives [350].

Tax deduction	Eligible investment costs relating to energy efficiency measures can be deducted (fully or in part) from income or revenues liable to taxation
Tax credit	Similar to tax deductions but investment costs are deducted (fully or in part) from respective taxes due to be paid
Tax reduction	Purchase taxes or sales taxes are reduced for qualifying equipment or services, e.g. reduced value added taxes for insulation material and installation services. This is either done directly at the point of sale (tax reductions) or applications for tax refund must be filed after the purchase (tax rebates);
Accelerated depreciation	It allows purchasers to depreciate the costs of their energy efficiency investments more rapidly than standard investments, thus effectively reducing the after tax total cost of the equipment;
Tax or customs duty exemptions	They relieve purchasers from paying customs duties or import taxes on qualifying imported equipment or excise tax on consumption or purchase of specified products, e.g. highly efficient appliances.

Income tax credits/deductions

Income tax credits or deductions form the most common type of tax incentive scheme across the EU. Tax schemes directed towards energy renovations of buildings are currently favored in Belgium, Denmark, Netherlands, France, Italy and Greece. The schemes are often designed with a specific technology focus, which mean that they are designed to stimulate investments in specific technologies/measures rather than set overall energy performance criteria. An exception is the Italian tax credit scheme which offers the option of a comprehensive retrofit package in addition to their list of individual measures. France, in its recently enacted law on Energy Transition for Green Growth (2015) has announced rebates for home renovations, whereby taxpayers will receive a tax credit corresponding to 30% of renovation costs incurred to make their homes more energy efficient. In the Netherlands, the Dutch Energy Allowance investment scheme offers innovators a stimulus to develop new technologies that have a better energy efficiency performance than reference technologies. By allowing for frequent updates of the eligible measure list, the schemes can facilitate the market introduction phase of new technologies. Selected schemes are described in more detail below, as they can provide examples of how to effectively design a potential tax incentive scheme in case this type of instrument is to be considered in the future by the Cypriot authorities. While tax incentives can be expensive due to reduced government income as a result of lowered collected tax, these should be considered in conjunction with new tax revenues as a direct impact of the scheme. The latter has been possible in the case of the French and Italian schemes.

Table 73. Overview of tax incentive schemes as a vehicle for financing energy efficiency investments [62].

Strengths	Weaknesses
- Can work well if the tax collection rate is sufficiently high - Can be useful at promoting new technologies that lack profitability at current stage - In certain cases, they can increase tax revenues to the government	- Usually have a poor performance in an economy in recession or in transition - Less effective if tax evasion is easy high or tax collection rates are low - Can be subject to the problem of the "free rider" - Tax savings to households and businesses typically mean reduced tax revenue to the government

Property taxation

Incorporating the building energy class in the evaluation of property tax, which currently mostly depends on the real estate value of the building, can give an incentive to property owners to invest in energy saving measures in order to reduce their tax burden. For instance the property tax could be modified as to reflect the current efficiency standard of a building; the better the standard the lower the tax. The adjustment can be revenue-neutral —i.e. tax levels are increased for inefficient buildings and decreased for efficient ones— or revenue-generating where taxes are increased for inefficient buildings only [351]. The generated revenue of the latter could feed a public support fund which would provide incentives to groups with low creditworthiness or limited capital to invest (e.g. low income households or SMEs). A careful design modification of current property tax system to incorporate the efficiency level of the building into property tax paid by owners can incentive property owners of very inefficient buildings to invest in energy efficiency upgrades in order to reduce their tax burden rate. As in the case of other types of fiscal instruments, success highly depends on the effectiveness of tax collection mechanism.

Table 74. Overview of property taxation schemes as a vehicle for financing energy efficiency investments [62].

Strengths	Weaknesses
- Incentives to homeowners to reduce tax burden - Can work well if the tax collection rate is sufficiently high	- Less effective if tax evasion is easy high or tax collection rates are low - Can result to loss of tax revenue for government - May not be sufficient to incentive homeowners - May have an adverse effect on poor/vulnerable households

Value added tax reduction

Value added tax (VAT) reduction schemes on energy efficiency offer lower VAT rates for the purchase and/or installation of various energy efficiency intervention measures, ranging from thermal insulation materials to heat pumps and biomass boilers. These schemes are diffused in a few EU countries such as Belgium, France and Netherlands, with reduced VAT rate being as low as 5% in certain cases. Governments can generally use this type of scheme to lower VAT rates for either the purchase or installation costs of energy efficiency products and materials as well as renewable energy technologies. They aim to influence the choice made by consumers and have the advantage of being directly perceived by the consumer at the point of purchase. However, there often fail to promote comprehensive energy efficiency upgrades at building level and the total amount of the reduction is limited by the amount of tax applicable to the product.

Table 75. Overview of VAT reduction schemes as a vehicle for financing energy efficiency investments [62].

Strengths	Weaknesses
- VAT reduction mechanism enables immediate reduction in investment costs - VAT reduction can be cumulated with the tax reduction and/or the subsidies for energy efficiency investments	- May be less effective at promoting comprehensive energy efficiency upgrades at building level

6.3.4 Other instruments and supporting mechanisms

Energy efficiency obligation schemes

Energy Efficiency Obligations (EEOs) are a market-based instrument enacted by governments in order to stimulate energy efficiency investments through obligations placed on energy companies. Under an Energy Efficiency Obligation scheme, energy distributors or retail energy sales companies are required to achieve a certain amount of energy savings in a pre-defined time. For example, the Energy Efficiency Directive requires Member States to establish energy efficiency obligations, mandating energy companies to achieve yearly energy savings of 1.5% of annual sales to final consumers. Once implemented, energy efficiency obligations have the advantage of boosting the market for energy efficiency investments by stimulating the development of new business models such as ESCOs. Whilst energy companies may choose to deliver their savings in various sectors of the economy such as industry, residential and commercial customers may also be targeted in energy efficiency obligation schemes through specific interventions in buildings. Following the introduction of the Energy Efficiency Directive in 2012 the number of EEOs in Europe has grown from 5 schemes (prior to the implementation of the EED) to 16 EEOs [352,353].

Energy efficiency feed in tariffs

Feed-in Tariffs can be another relevant type of market-based instrument introduced by governments to promote the use of specific technologies. Energy efficiency feed-in tariffs (EE FITs) represent an innovative instrument inspired from the concept of Feed in Tariffs for small-scale renewable and low-carbon electricity generation technologies. In the case of energy efficiency, consumers are encouraged to reduce their energy use through a reward-based system. The exact price for a kWh of energy saved is indicated and the market is allowed to determine the quantity of energy savings to be delivered. One of the limits of this instrument is the set-up of the price of energy savings and associated risk of a fixed price system favoring cheap energy efficiency interventions [354]. As EE FITs are a new concept, there are no practical examples from which experiences can be drawn.

One-stop shops

The revised Energy Performance in Buildings Directive (EU) 2018/844 introduces the concept of one-stop-shops. With the establishment of long-term renovation strategies (Article 2a of Directive (EU) 2018/844), Member States are called to consider advisory tools such as one-stop-shops to inform and assist consumers in relation to energy efficiency renovations and relevant financial instruments. Article 20(2) also requires Member States to provide information to owners and tenants through accessible and transparent advisory tools such as one-stop-shops.

One-stop-shops (OSSs) can be defined as advisory tools that facilitate access to financial mechanisms, assist consumers in relation to technical and financial issues and guide them through a number of key stages in the renovation process. OSSs are transparent and accessible advisory tools from the client perspective and new, innovative business models from the supplier perspective [355].

Assistance through OSSs can help address a number of barriers, such as the difficulty in accessing financial incentives, fragmentations of energy efficiency interventions, high transaction costs due to small individual investments, insufficient understanding of complex energy efficiency interventions, lack of reliable and credible information about costs and benefits.

Homeowners are often engaged in simple or routine works, such as replacement of appliances, or modernization projects that are geared towards enhanced comfort or aesthetics levels. OSSs promote integrated energy renovation solutions (that is, full home renovation, which address energy efficiency in a holistic way) wherever possible. They represent a building-related service that facilitates a dialogue between building users/owners and suppliers in order to identify solutions throughout all stages of the renovation process. The role of OSSs can be thus defined as an intermediary point of contact.

From a practical point of view, OSSs can help clients in selecting appropriate contractors and suppliers, taking into account their previous experiences. OSSs

often guarantee the quality of the service, and have a few basic packages tailored to specific cases. These cover detailed information about what each renovation package entails, including possible interventions, solutions and benefits. At the same time, from the supplier's point of view (planners, engineers, installers, manufacturers, financial partners), OSSs help the provider to simplify interactions with single private clients, as OSSs guide clients through visits, decision-making processes and other cumbersome processes.

OSSs overcome market fragmentation on both the demand side and the supply side by offering holistic, whole-value-chain renovation solutions [356].

The OSS service providers usually are organizations, projects, and independent experts or advisors that deal with technical assistance, structuring and provision of financial support, helping the client to apply for public funding. OSSs target residential buildings, mostly within the private stock. In Europe, several examples of OSSs have been identified in Nordic countries, France and Benelux countries [355]. Some notable examples of OSSs include the Rhodoshop Programme Development Unit in Bulgaria, the Småland-Blekinge pilot OSS in Sweden, the Ile-de-France Energies13 for residential buildings in France and the Energy Investment Unit at Cambridgeshire County Council for public buildings in the UK14. The EU programme Horizon 2020 supports establishment of OSSs, recognizing their value to mobilize energy efficiency finance.

Technical assistance

The European Commission has set up a series of facilities funding Project Development Assistance (PDA) to support public authorities and bodies in developing bankable sustainable energy projects.

The European Local Energy Assistance (ELENA) facility, a joint initiative by the EIB and the European Commission under the Horizon 2020 programme, provides grants for technical assistance on the implementation of energy efficiency, distributed renewable energy and urban transport programmes. Established in 2009, the ELENA facility has awarded more than EUR 130 million of EU support triggering an estimated investment of around EUR 5 000 million on the ground. ELENA supports programmes above EUR 30 million with a three-year implementation period for energy efficiency and four-year for urban transport and mobility. It can cover up to 90% of technical assistance/project development costs. The main objective of ELENA is to help private individuals and homeowner associations prepare and implement energy renovations in private and public residential buildings.

[13] https://www.iledefranceenergies.fr/
[14] https://www.mlei.co.uk/

6.4 Public and private schemes in EU

6.4.1 Overview of public schemes

Table 76 provides an EU28 overview of the main public financial and fiscal instruments supporting energy renovations in buildings. Many countries have chosen to deploy a combination of different instruments, each tailored to address different barriers, specific segments and recipient groups within the building sector.

Financial support is predominantly offered in the form of grants/subsidies, followed by loans and tax incentives. Grants and subsidies is a type of instrument deployed in all Member States. This is a particularly popular instrument in Austria, Croatia, Ireland, Cyprus, Estonia, Latvia, Greece, and Poland. Grants and subsidies represent the main type of public support for energy renovations in buildings in these countries. Loans and soft loans are available in over half of the EU countries, namely Austria, Belgium, Bulgaria, Czech Republic, Estonia, France, Germany, Hungary, Italy, Latvia, Lithuania, Luxembourg, Malta, Portugal, Romania, Slovakia, Slovenia, Spain and the UK. Some of these schemes are supported by state guarantees such as in Bulgaria, Estonia, France, Italy and Romania. In addition, several of these schemes have been designed as revolving funds. Examples include the Energy Efficiency and Renewable Sources Fund in Bulgaria, the Kredex Fund in Estonia, the National Revolving Fund for Energy Savings in the Netherlands and the SALIX scheme in the UK. Tax incentives have been found to be active in Belgium, Denmark, Finland, France, Italy, Malta, Sweden, the Netherlands and the UK. These are typically offered in the form of income tax incentives (e.g. Belgium, France and Italy) or VAT reduction schemes such as in Belgium, France and the Netherlands.

France, Belgium, Italy and Portugal have enacted all types of instruments for all types of buildings covered in our study: residential, commercial and public. For all other countries, the main focus is the residential sector, with some instruments also targetting commercial buildings and/or public buildings or a different combination of building types. In Finland, Ireland, Estonia, and Romania, public support is given for residential buildings only. Many of the instruments examined herein have been designed to work together with other instruments or be part of a policy package. Energy Efficiency Obligation Schemes (EEOs) have been used for years in Denmark, Belgium, France, Italy, and United Kingdom and more recently in compliance with Article 7 of the Energy Efficiency Directive 2012/27/EU in many other countries. In Denmark, France, Luxembourg, Poland and the UK, these schemes, inter-alia, cover energy efficiency upgrades in buildings.

Figure 168 provides a snapshot of all public financial and fiscal instruments in this study. In summary, there are 129 instruments supporting energy renovations in buildings across the EU, 61% of which are grants/subsidies, 19% loans/soft loans, 10% tax incentives and the remaining 10% a combination of the above. Our results show that around EUR 15 billion are roughly spent by public resources on an annual

basis across the EU[15]. This analysis is based on budget-related information collected for 85% of instruments covered in our study. The findings of this study showed that the largest schemes in terms of public resources spent are the Italian Eco-bonus tax rebate scheme, the French Energy Transition Tax Credit scheme, the German KfW Energy Efficient Refurbishment Programme and the Austrian Regional subsidies for energy efficiency in residential buildings.

Table 76. Overview of main public instruments identified in this study that support energy renovations of residential, tertiary and public buildings in EU Member States [62].

Member State	Sectors covered	Measure Type			Number of measures	Notable Examples
		Grants/ Subsidies	Loans/Soft Loans	Tax Exemption/ Reduction		
AUSTRIA (AT)	Residential	■	■		4	1) Residential building subsidy("Wohnbauförderung")
	Commercial	■			2	2) Austrian Federal Government's Renovation Drive ("Sanierungsscheck")
	Public	■			2	
BELGIUM (BE)	Residential	■	■	■	11	1) Green loans for energy efficiency investments by households (Brussels)
	Commercial	■	■	■	4	2) Property Tax Reduction (Flanders)
	Public	■	■	■	4	3) Financial incentives for RUE investments in buildings (Wallonia)
BULGARIA (BG)	Residential	■	■		4	1) National Energy Efficiency Program for Multifamily Residential Buildings renovation
	Commercial	■	■		2	2) Residential Energy Efficiency Credit Line REECL
	Public		■		1	
CROATIA (HR)	Residential	■			3	1) Programme of energy renovation of commercial non-residential buildings 2014-2020 (B.4)
	Commercial	■			1	2) Programme of energy renovation of multifamily housing
	Public	■			1	
CYPRUS (CY)	Residential	■			3	1) Grant scheme "Save & Upgrade" for residential sector
	Commercial	■			1	
	Public					
CZECH REPUBLIC (CZ)	Residential	■	■		5	1) Operational Programme Environment (2014-2020): Sustainable Use of Energy Sources
	Commercial	■	■		4	2) New Green Savings Programme 2014-2020
	Public	■			2	
	Residential	■		■	2	

[15] It is important to note that these figures do not refer to any specific period, but rather represent a generic year during the duration of the given scheme. Depending on data availability for each scheme, this was taken as the average value over a specified period (preferred option) or the value given for a specific year or a typical year on average (alternative option).

DENMARK (DK)	Commercial			■	1	1) Green BoligJobordning household employment scheme
	Public			■	1	
ESTONIA (EE)	Residential		■		1	1) Reconstruction of private residences and apartment buildings
	Commercial					
	Public					
FINLAND (FI)	Residential	■		■	2	1) Energy Grants for Residential Buildings/Housing Finance and Development Centre of Finland
	Commercial					
	Public					
FRANCE (FR)	Residential	■	■	■	6	1) Energy Transition Tax Credit (CITE)
	Commercial	■	■	■	3	2) Social Housing eco-loan
	Public	■	■	■	4	3) Energy Saving Certificates
GERMANY (DE)	Residential	■	■		4	1) CO2-Gebäudesanierungsprogramm
	Commercial	■	■		4	2) Market Incentive Programe for Renewable Energies (MAP)
	Public	■	■		4	4) Energy Incentive Programme (APEE)
GREECE (EL)	Residential	■			1	1) "Saving at home" Programme
	Commercial					2) Energy savings in Local Self-Governments
	Public	■			1	
HUNGARY (HU)	Residential	■	■		4	1) Warmth at Home Programme (WAH) (funded from carbon credits)
	Commercial	■			1	2) Energy Efficiency subsidies for public and local governmental buildings
	Public	■			2	
IRELAND (IE)	Residential	■			5	1) Better Energy Homes (Residential Retrofit)
	Commercial					2) Warmer Homes Scheme (Low Income Housing Programme)
	Public					
ITALY (IT)	Residential	■	■	■	5	1) Ecobonus 2017 tax deduction scheme
	Commercial	■	■	■	3	2) Renewable Energy for Heating and Cooling and Small Interventions Increasing Energy Efficiency Support Scheme (Conto Termico 2.0)
	Public	■	■	■	4	
LATVIA (LV)	Residential	■	■		2	1) Energy efficiency improvement in residential buildings
	Commercial	■			2	2) Energy efficiency improvement in public buildings
	Public	■			4	3) Energy efficiency in manufacturing industry
LITHUANIA (LT)	Residential	■	■		3	1) Programme for the renovation/upgrading of multi-apartment buildings
	Commercial	■			2	2) Programme for Improving Energy Efficiency in Public Buildings
	Public	■			1	
LUXEMBOURG (LU)	Residential	■	■		4	1) Promotion of energy renovation of residential buildings
	Commercial		■		1	2) Klimabank loans
	Public		■		1	

MALTA (MT)	Residential	■	■	■	1	1) Financing Schemes and instruments and fiscal incentives
	Commercial			■		
	Public					
NETHERLANDS (NL)	Residential	■	■	■	5	1) Subsidy schemes (IRE, MEI, UKR, Clean and Efficient Demonstration Projects)
	Commercial	■		■	3	2) Energy Investment Allowance (EIA)
	Public					
POLAND (PL)	Residential	■			3	1) Subsidised loans for the construction of energy efficient houses
	Commercial					2) Operational Programme Infrastructure and Environment 2014-2020
	Public	■			1	
PORTUGAL (PT)	Residential	■	■	■	6	1) Energy Efficiency National Fund
	Commercial	■	■	■	3	2) 1 Direito
	Public	■	■	■	3	
ROMANIA (RO)	Residential	■	■		2	1) National Programme for Improvement of Energy Performance in Apartment Blocks
	Commercial					
	Public					
SLOVAKIA (SK)	Residential	■	■		7	1) State Housing Development Fund
	Commercial	■			1	2) SlovSEFF II and III (for renovation of multifamily buildings)
	Public	■			1	
SLOVENIA (SI)	Residential	■	■		3	1) Financial incentives for energy-efficient renovation and sustainable construction of residential buildings
	Commercial		■		2	2) Financial incentives for the energy efficient heating systems in residential and Commercial buildings
	Public	■			1	
SPAIN (ES)	Residential	■	■		3	1) PAREER programme
	Commercial	■			1	2) PIMA SOL programme
	Public	■			2	
SWEDEN (SE)	Residential	■		■	2	1) EU financial support for energy efficiency in buildings
	Commercial			■	1	2) Aid for improvement and increases in energy efficiency of rental accommodation
	Public			■	1	
UNITED KINGDOM (UK)	Residential	■	■	■	7	1) Energy Efficiency Loan Scheme (SALIX)
	Commercial	■			1	2) Energy Company Obligation (ECO)
	Public		■		1	

Our findings are in line with data stemming from other reports. Blom, Vergeer and Forster (2018) confirmed around 16 billion per year for net public costs committed in public schemes (i.e. grants/subsidies, tax rebate, debt finance) — considering all sectors (not only residential, commercial and public). Historical data showed that public funding for energy efficiency in the EU grew from 6 billion in

2012 —when the Energy Efficiency Directive (2012/27/EU) was approved— to about 7 billion in 2014 [358].

While private investments are not included in these figures, achieving the goals set out by the EU in 2030 would require significantly higher levels of funding. The IEA estimates that 60-100 billion of annual investment is needed in buildings to achieve Europe's 2020 energy efficiency targets alone (considering both public and private funds) [359]. Looking out to 2040, the IEA estimates showed that an average of 178 billion needs to be invested annually to keep the EU on track to the well below 2°C goal [360].

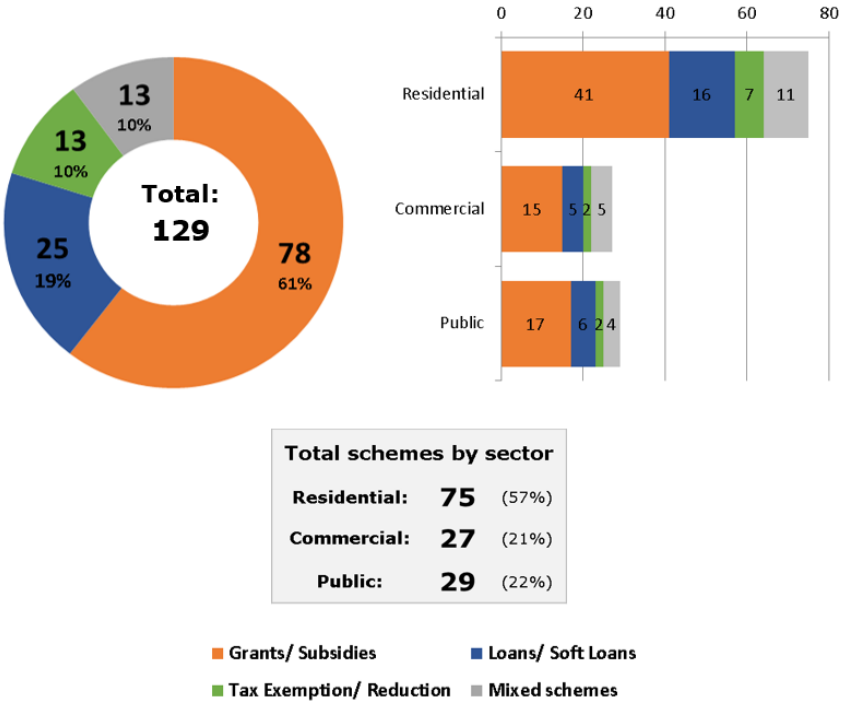

Figure 168. Snapshot of financial instruments supporting energy renovations in buildings across the EU [62].

The main instruments identified in each country are summarised below. Multiple sources were used to collect the latest information about financial support for energy renovations in buildings: the latest National Energy Efficiency Action Plans submitted in 2017 by Member States in accordance with Article 24 of Directive 2012/27/EU, the long-term renovation strategies submitted in 2017 by Member States to comply with the requirements of Article 4 of the same Directive and the new draft Energy and Climate Plans submitted in 2018 by Member States in the framework of the Energy Union Governance Regulation. Databases such as the MURE database on energy efficiency policies and Energy Efficiency Database of the International Energy Agency were also consulted.

6.4.2 Overview of private schemes

The landscape of private financing on energy efficiency is complex, involving various mechanisms, business models and actors. Many private households, companies, project developers and ESCOs decide to invest their own resources to improve the energy efficiency of their own or their clients' premises. In addition, energy renovations often happen “behind the scenes” of many maintenance, modernization and routine restoration works. All these factors mean that it is extremely difficult to get a complete picture of private financing practices in the area of energy efficiency investments.

In recent years, financial institutions have been more active in offering specialized financial products geared towards energy efficiency investments. At the same time, new models based on non-conventional methods of raising funds are being explored as a vehicle to drive more investments.

As discussed earlier, private and public funds are often blended to establish financial products with more attractive terms. To make a clear distinction between private and public, it was decided to explore financial products which may be partially or fully covered by private funds and are dispersed by private intermediaries in this chapter[16].

Table 77. List of private schemes in EU Member States [62].

MSs	Type	Name of scheme	Timing
IT	Commercial loans on energy efficiency	Condominium Financing ("Finanziamento Condominio")	Since 2019
HR		Green Housing Loans by Zagrebacka Bank	n/a
BE		Belifus housing retrofit programme	Since 2018
*Mult		EBRD Sustainable Energy Financing Facilities schemes	Since 2006
PL		Financing energy efficiency by BOŚ commercial bank	Since 2012
UK	Energy Efficiency Mortgages	Eon-BNP Paribas green mortgage product	Since 2018
*Mult		Green home ("Casa Ta Verde"), Raiffeisen bank	Since 2018
SE		Nordea Green Mortgages	Since 2018
DE		MünchenerHyp sustainability loans	Since 2015
DE	Crowdfunding and energy cooperatives	Bettervest	Since 2013
*Mult		CitizenEnergy	Since 2014
DE		Econeers	Since 2013

[16] Instead, financial schemes which are partly or fully supported by public sources and have been made available to end users through public intermediaries (e.g. a public bank) have been covered in Chapter 3.

ES		Fundeen	Since 2017
UK	Specialised funds	Mayor's London Energy Efficiency Fund	Since 2018
LV		Latvian Baltic Energy Efficiency Facility	Since 2016
*Mult		SUSI Energy Efficiency Fund	Since 2009
UK	Energy efficiency insurance	HSB Engineering Insurance	Since 2014
DE		Energie Einspar Protect (EEP) KlimaProtect	n/a
*Mult		Energy Savings Insurance	Since 2015

The collected information on private schemes was obtained from desk research, and complemented by interviews carried out with national experts. Based on our research, we were able to identify 19 private schemes which have been divided into the following subgroups: commercial loans on energy efficiency; energy efficiency mortgages; crowdfunding and energy cooperatives; specialized funds; energy efficiency insurance.

Commercial loans on energy efficiency

To scale up energy efficiency investments, commercial banks must take a prominent role in tapping into the energy efficiency market. Credit lines established by banks can help mitigate the perceived high financial risk of energy efficiency projects and lower transaction costs through the establishment of standardized project appraisal and loan processing processes. These are often combined with technical assistance to improve understanding of the fundamentals of energy efficiency projects and eliminate the perceived risks of energy efficiency investments. For project developers and/or energy service companies, credit lines can expand the pool of commercial debt financing for their projects.

Energy efficiency credit lines make funds available to participating financial institutions including local banks. Typically credit lines are extended to financial institutions as a low interest rate loan by a donor (such as a multilateral development bank or other international financial institutions) or by government. The recipient institution then on-lends the funds to borrowers (private or legal persons) to invest in energy efficiency projects.

Table 78. Main strengths and weaknesses of commercial loans on energy efficiency [62].

Strengths	Weaknesses
- More sustainable means of financing than public funds; - Support to deeper/more ambitious renovations	- Down-payment may be high; - Unwillingness to take on additional - debt; - High transaction costs for small projects

Energy Efficiency Mortgages

Energy efficient (or green) mortgages are an attractive way of tapping into the mainstream mortgages market. An energy efficient mortgage (EEM) is a loan product that allows borrowers to reduce their utility bill costs by allowing them to finance the cost of energy-efficient upgrades into a new housing purchase or the refinancing of existing housing. Preferential mortgage terms may be offered to efficient properties, or existing mortgages can be extended in order to finance efficiency improvements. Energy efficient mortgages give the opportunity to obtain better borrowing terms, finance upgrades as part of a single mortgage, increase debt-to-income qualifying ratios and allow consumers to qualify for a larger loan amount. Energy efficient mortgages can credit a home's energy efficiency in the mortgage itself and thereby increase the home buying power of consumers and capitalize the energy savings in the appraisal. Alternatively, they are used to purchase or re-finance existing homes that will undergo energy efficiency upgrades. In other words, they allow borrowers to include the cost of energy-efficiency improvements to an existing home in the mortgage without increasing the down-payment by using the money saved in utility bills.

In the EU, the pilot projects EeMAP and EeDaPP were recently launched with the aim to create a standardized framework and data collection architecture for energy efficient mortgages. These are funded by the European Commission's Horizon 2020 Programme and supported by 40 major European banks. The pilot scheme EeMAP[17] is aimed at creating new European standardized criteria for energy efficiency mortgages under the EU funded Energy Efficient Mortgages Initiative. Some of Europe's largest banks are participating in the pilot, including BNP Paribas, ING Bank, Nordea Bank and Société Générale. Given the rapidly growing investor demand for green mortgage-backed bonds, the business case for lenders to provide more attractive mortgages to those opting for greener homes has received more attention in recent years. Lower utility costs and their ability to hold their value better over time mean green homes are increasingly recognized as less risky investments for both borrowers and lenders.

Table 79. Main strengths and weaknesses of energy efficiency mortgages [62].

Strengths	Weaknesses
- Access to low cost capital; - Enhanced borrower ability to pay monthly instalments; - Long repayment period	- High transaction costs for small projects; - High collateral requirements

[17] https://eedapp.energyefficientmortgages.eu/.

Crowdfunding and energy cooperatives

Crowdfunding is a term used to describe the collective effort made by a large number of individuals (investors) with the aim to pool funds together and support a project, cause, business idea or loan initiated by other people or organizations through an online web-based platform [361]. With annual growth rates exceeding 100%, crowdfunding has expanded exponentially over the last years, attracting the interest of professional financial institutions, institutional investors, venture capitalists and angel investors.

Investments in energy efficiency and renewable energy projects through crowdfunding have also gained some popularity, even though they currently account only for a considerably small share of the sector. While the two largest crowdfunding platforms Kickstarter and Indiegogo focus on innovations in consumer products such as energy management or small scale renewable energy generation systems, new platforms are designed to give funders the opportunity to provide capital in exchange for equity or future return on investments in energy efficiency and/or renewable projects. The fastest growth of crowdfunding platforms in this area is linked to renewable energy projects. Few other crowdfunding platforms have started supporting energy efficiency projects, such as Bettervest, ECONEERS and CitizenEnergy but most platforms cover both energy efficiency and renewable energy projects.

Crowdfunding uses a wide range of models. There are 4 different types of models supported by crowdfunding: donation crowdfunding, reward crowdfunding, debt (peer-to-peer lending) and equity crowd-funding. For energy efficient projects, debt (peer-to-peer lending) is the most common type which involves requesting support and resources from other investors to meet a certain crowd-investment target in exchange for interest. The size of the crowd-investment target can range from very small (e.g. a few hundreds) to several hundred thousands or more. Crowdfunding for energy efficiency can be used when there is a lack of affordable financing or high upfront costs for implementing or scaling up cost-effective energy efficiency measures, e.g. in commercial buildings. Crowdfunding removes the involvement of financial institutions and helps projects get off the ground with the help of crowd investors, who then expect return on their investment through interest payments or equity. In addition, crowdfunding can lead to better awareness and support for energy efficiency projects, and offer market outreach and validation for new energy efficiency technologies. With the help of the internet, crowdfunding can draw support from people across entire countries and increasingly internationally.

Energy cooperatives, on the other hand, rely on members in local communities to group together and support projects that would be difficult to get started otherwise. Energy cooperatives can cover small districts, entire cities, regions or even operate a variety of projects on a national level. Several energy cooperatives focusing on renewable energy exist in Europe, many of which are hosted on the website of REScoop.eu, the European federation of renewable energy cooperatives.

The main difference between energy cooperatives and crowdfunding lies in the fact that crowdfunding platforms may have multiple different projects in different countries and offer various types of participation as discussed above, while energy cooperatives are single organizations typically raising money to fund their own projects. Increasingly though, the lines are becoming blurred: cooperatives can make their own investment offers or can even make use of crowdfunding platforms to fund part of their goals. Ultimately, both cooperatives and crowdfunding take advantage of support from individual members of the public to get projects up and running.

Table 80. Main strengths and weaknesses of crowdfunding platforms [62].

Strengths	Weaknesses
- Access to finance for consumers not eligible for traditional financing options; - Awareness raising and wide market outreach through the help of the internet	- May be difficult to reach funding target; - Investments may be risk given weak regulatory framework protecting participants

Energy efficiency insurance

Energy efficiency (or energy savings) insurance is an innovative product in which policies protect the installer or owner of an energy efficiency project from under-achievement of predicted energy savings. One of the main barriers of the energy efficiency investments in buildings is the uncertainty associated with risks in terms of the assets installed, the revenues resulting from the project, and the energy savings generated. Specialised insurance solutions are useful to scaling up energy efficiency investments and to remove these uncertainties. Insurance companies also facilitate the flow of financing for these technology solutions and address the untapped market potential.

Leading insurance companies have been developing a number of specialized solutions in order to transfer risks from client to the insurance company. The main specialized energy efficiency insurance products and services are shown below:

1. Energy Performance Guarantee (EPG): EPGs cover the financial risk when energy efficiency improvements do not lead to projected levels of energy savings. EPGs can cover performance risks and/or technology risks.
2. Energy Efficiency (EE) services: Insurance companies offer EE services to existing and new clients such as technical assistance, advisory services, and business development, in order to exploit their existing relationships.
3. Add-on coverage: Insurance companies offer their clients add-ons that extend the coverage of existing insurance policies to take into account value increases resulting from EE investments.

Services and products are offered to energy efficiency stakeholders, from manufacturers of technology solutions to ESCOs, project hosts and project sponsors.

Table 81. Main strengths and weaknesses of energy efficiency insurance [62].

Strengths	Weaknesses
- Overcoming technical uncertainty and improvement of credit risk; - Confidence on the customer side; - Improved credit worthiness, availability and cost of loans	- Sometimes, investments are limited to small projects due to very short payback periods

Chapter 7

Conclusions and outlook

7.1 Main findings

USEMs are fundamental tools for assessing and managing the distribution of energy at territorial scale. They can be used to improve the resilience of a city by guaranteeing an affordable, reliable, sustainable and modern energy system from different points of view: energetic, economic, environmental and social [362,363]. With these models it is also possible to promote EE measures [363] (e.g., for building energy codes that can play an important role in energy savings [364]) and to exploit the RESs that are available locally [365].

This doctoral thesis has described how to design urban-scale energy models based on GIS tools. Firstly, different place-based approaches were presented. Subsequently, data-driven and process-driven models were designed, validated and applied to different cities in order to promote smart solutions for sustainable and resilient cities. In particular, the place-based energy consumption models designed have annual, monthly and hourly resolutions and use statistical, engineering, machine learning and hybrid techniques. Finally, having assessed the distribution of energy consumption, productivity and energy efficiency models were designed and applied. These models could be used to optimize energy supply and demand, considering the use of RES technologies, from an energy community perspective. The goal is to achieve the energy independence of municipalities by reducing their energy use, improving their energy performance, and exploiting the available RESs.

One of the main objectives of the place-based models presented is to create a decision-making support system for citizens, designers and policy makers. These models are purposely designed: (i) to draw up new neighborhoods by optimizing the EP of buildings according to urban characteristics; (ii) to identify the most effective EE measures for existing neighborhoods by considering the real characteristics of their buildings, population, and urban morphology; (iii) to create an easily upgradable energy atlas for buildings, related to the existing territorial databases; (iv) to evaluate the feasibility of establishing energy communities and

grouping private and public entities, considering their energy consumption and production to achieve energy security with a low environmental impact and equitable socio-economic effects.

As the place-based models presented are simplified models, the simulation times are significantly lower than with existing tools. Even if they are simplified models, they are sufficiently accurate and able to simulate energy consumption from the building block scale to the city scale. They use open data, so are easily applicable to different urban contexts. Therefore, the results of this research could provide a significant contribution to overcoming the limits of existing energy models at urban scale, such as the simulation times, the need to use a lot of accurate input data to obtain sufficiently precise results, their flexibility, and their applicability to blocks of buildings and not to the entire city.

Strengths and weaknesses of models and tools

From the analysis and application of models that use top-down and bottom-up approaches, the strengths and weaknesses of these approaches have been identified and summarized in Table 82.

Table 82. Strengths and weaknesses of top-down and bottom-up approaches.

Approach	Strengths	Weaknesses
Top-down	- Based on historical data series and aggregated data, available on public online databases, ensuring an ever easier and faster data collection. - High flexibility and adaptability of simplified energy models with the place-based approach and georeferenced data.	- Georeferenced results are linked to the average energy consumption at urban scale (model output). - Difficulties in determining the spatial variability of the results in relation to different urban forms, contexts and population, even though these are georeferenced information.
Bottom-up	- Based on disaggregated data representative of individual energy end-use. - Possibility to described energy-related parameters considering spatial specificities (climatic, socio-economic condition and urban form). - High flexibility in evaluating the impact of energy-related factors (adaptability and scalability). - Can be used to evaluate the energy saving potential after retrofit interventions.	- Need for extensive empirical data at a detailed level. - Data collection often long, difficult, onerous and sometimes is not possible.

There are different methods and technique used to design place-based energy models. As for the approaches, Table 83 describes the main strengths and weaknesses of engineering (EN) models (or process-driven models), statistical models and machine learning (ML) models.

Table 83. Strengths and weaknesses of the engineering, statistical and machine learning models [47].

USEM	Strengths	Weaknesses
EN model	- Fewer energy consumption data are needed. - Mathematical relationships between input and the output are known, it is possible to improve the accuracy of the results adding/updating the input data. - The model is based on the thermal balance equations, and can be used to simulate for future scenarios.	- Real consumption data to calibrate the model. - The model at urban scale is based on simplified thermal balance, it is less precise, as it fails to consider some aspects (i.e., natural ventilation variability, diffuse component of solar gains, geometrical interactions with the surroundings). - Human related factors are difficult to be simulated.
Statistical model	- Smaller sample of observations than ML model. - Widely applied, user-friendly methods. - Very short simulation times (almost instantaneous).	- Real consumption data to calibrate the model. - Difficult to take into account complex patterns as human related factors. - Specific range of application: the model is trained on a very specific space and sample of buildings; it lacks the ability to generalize (adaptability/replicability).
ML model	- It is more specialized on the considered case study and therefore more precise. - It is able to learn aspects deeply related to the case study affecting consumption (i.e., average behavior of the occupants). - Human related factors can be simulated. - Very short simulation times (almost instantaneous).	- A big database of real consumption data is needed to train and test the model. - Specific range of application: low adaptability/replicability.

There is no one methodology to design USEMs. Based on the data available and the type of analysis to be carried out, one approach is better than another. Within this doctoral research different approaches and techniques to design place-based models were presented. The models presented allow (i) to use existing databases, so as to be able to apply the models to different contexts; (ii) to compare different phenomena (e.g., energy saving but also liveability of outdoor spaces); (iii) and to carry out analyzes on a block, neighborhood and city scale.

Place-based consumption models

Annual data-driven models described in this research are simple linear regressions that give useful information on the distribution of annual energy consumption at city scale. The application of these simplified models can help to optimize energy demand and supply of buildings at urban level. Critical areas with high consumption can be identified as priority areas to apply mitigation strategies. Consequently, the adopted methodology can help policy makers in defining

effective energy policies to improve the liveability in cities. The main limitation of these annual models is that they are not very flexible and for example do not allow to evaluate how consumption changes according to seasonal climate conditions. Therefore this doctoral research focused mainly on the definition of process-driven (i.e., engineering) models, that are more flexible and are able to take into account the effect of seasonal conditions on the EP of buildings.

A first version of the engineering model presented was able to simulate the consumption of SH and DHW with monthly detail. The model was designed, applied and validated for residential buildings served by the DHN in the city of Turin. The novelty of this model was the introduction of a number of urban parameters in the thermal balance, in order to tune it from the building to the urban level (the missing data of the buildings were substituted by similar variables at block of building scale). The results of this investigation show that the simplified quasi-steady state heat balance can produce good results at an urban scale, especially for areas with old buildings, with a MAPE of 4-17%. The methodology has been verified using the SH and DHW consumption data for three consecutive heating seasons of thirty-three districts in the Turin urban context. Since the model is very flexible, it is also possible to apply it to other large urban contexts [15]. The results of these models should help to improve predictions of the impact of an urban context on the energy consumption of buildings.

To assess the peak demand, more accurate models have been developed and can simulate the hourly consumption for SH and SC. Different methods and case studies were investigated. A process-driven model that uses an engineering approach is designed for the city of Turin, a data-driven model based on machine learning techniques is applied to city of Fribourg in Switzerland, and finally a hybrid model is developed for the city of Geneva using the engineering model that was optimized using a data-driven correction with a Random Forest algorithm [180].

Comparing these hourly models to the other existing energy tools, it has emerged that they are less accurate, but more flexible and easily applicable to other contexts since they use existing databases. In fact, existing tools are more accurate but do not allow analysis on cities, have much longer calculation times, and need data that is often not available. The strong points of these models are certainly the short simulation times and their flexibility, which, since they use open input data, can be applied to other cities elsewhere in the world.

Place-based productivity models from RESs

Place-based productivity models that use solar energy were applied to the city of Turin. Different scenarios were investigated by using ST collectors, PV panels and battery systems are investigated. The GIS-based methodology presented can help in the identification of the optimal level of self-sufficiency as a function of the costs of the PV power installed and of the energy. For example, in Turin it could be convenient to exploit all the potential rooftop surfaces (south-facing and north-

facing) with PV panels to considerably improve energy self-sufficiency, as well as to provide significant economic benefits for the residential users. These findings could contribute to our understanding to identify the optimum solution for PV systems installation. They may also provide a basis for the establishment of collective self-consumers and energy communities in urban environments. It is also emerged that the shape of the building and the roof orientation influence the availability of solar energy and the EP of buildings.

Place-based energy efficiency models

Energy efficiency models were applied to the city of Turin to investigate the potential expansion of the DH network and the future scenarios of building retrofit hypotheses for a more sustainable city. From the energy retrofit of buildings, there are economic and environmental advantages, and with the optimization of the DHN it is possible to connect more users, in order to reduce polluting emissions and to reduce energy consumptions.

Low-carbon scenarios were investigated using smart rooftop solutions. For example, the installation of green rooftop technologies helps to reach energy and climate targets by reducing energy consumption and improving outdoor thermal comfort conditions.

As already mentioned, the building shape and urban form influence the EP of buildings. The relationship between the built environment and the EP was examined to identify the optimal urban shape with low energy consumption and high solar energy productivity. In addition, a methodology to assess the impact of urban form and green mitigation actions on the outdoor thermal comfort was applied. It has been found that comfort conditions are strongly influenced by urban morphology. The use of urban geometries together with the use of greenery can help urban planners and architects to design better outdoor spaces whose use is strongly influenced by winter and summer thermal comfort conditions. The results obtained could be used as a tool to support the master plan proposals and the identification of actions concerning urban regulations guidelines and building codes.

In conclusion, USEMs should be used to identify smart energy solutions for sustainable cities and policies, and to support energy and environmental goals. Energy efficiency measures such as cool roofs can be identified as accounting for real characteristics of the urban environment. Therefore, these models provide insights to inform city decision making on sustainability, efficiency, and resilience.

7.2 Future outlook

Concerning energy consumption modes, it has emerged that place-based engineering models have strong potential in the analysis of energy distribution on a territorial scale. The accuracy of these models can be improved by implementing the input data and/or using a hybrid approach. In future works the accuracy of these engineering models will be improved by adding new urban energy-related

variables. For example, the effect of evapotranspiration will be considered in the urban thermal balance.

With the application of productivity models from RESs, a methodology to promote self-consumption and self-sufficiency using the integration of solar energy with PV-battery systems was developed. Another investigation could involve evaluating the energy and economic benefits of the combined installation of PV and ST technologies [366]. Local climate conditions also affect the production and consumption of PV energy [367,368], and this will also be further evaluated. In the results of this research, a city in the North-West of Italy was used as a case study, but it would be interesting to evaluate how the benefits, in terms of costs and EP, vary for cities located in southern Italy, with its warmer climate with greater solar radiation intensity. Finally, the hourly PV potential has been evaluated using data elaborated from the PVGIS portal, since the processing is fast and simple. However, from the analysis of the existing methods and tools used to evaluate the PV potential, it has emerged that GIS-based methodology tools allow much more accurate investigations to be performed with respect to using only the PVGIS portal. The complexity of GIS tools lies in the processing times of the input and output data and in the simulation times. The analyses carried out with GIS tools are more accurate because the real urban environment is taken into account, thanks to the use of DSMs (e.g., the presence of disturbing elements). The description of the context is important to obtain reliable results, as the more accurate the input data are (e.g. the precision of the DSM), the better the outputs are able to return real data.

Regarding thermal comfort conditions, in future works, simplified correlations for thermal comfort conditions will be investigated using GIS-based models that require, at urban scale, less input data with lower simulation times. Evaluations will be made in cities with different urban morphologies and climates, comparing thermal comfort indexes in different climate conditions, especially as regard urban canyon dimension, orientation and ventilation.

References

[1] Peron F, De Maria MM, Spinazzè F, Mazzali U. An analysis of the urban heat island of Venice mainland. Sustain Cities Soc 2015;19:300–9. https://doi.org/10.1016/j.scs.2015.05.008.

[2] Reinhart CF, Cerezo Davila C. Urban building energy modeling – A review of a nascent field. Build Environ 2016;97:196–202. https://doi.org/10.1016/j.buildenv.2015.12.001.

[3] UNEP. Emissions Gap Report 2018. 2018.

[4] Dogan T, Reinhart C. Shoeboxer: An algorithm for abstracted rapid multi-zone urban building energy model generation and simulation. Energy Build 2017;140:140–53. https://doi.org/10.1016/j.enbuild.2017.01.030.

[5] Sokol J, Cerezo Davila C, Reinhart CF. Validation of a Bayesian-based method for defining residential archetypes in urban building energy models. Energy Build 2017;134:11–24. https://doi.org/10.1016/j.enbuild.2016.10.050.

[6] International Energy Agency (IEA). Perspectives for the Clean Energy Transition. The Critical Role of Buildings. Paris: 2019.

[7] Grove-Smith J, Aydin V, Feist W, Schnieders J, Thomas S. Standards and policies for very high energy efficiency in the urban building sector towards reaching the 1.5°C target. Curr Opin Environ Sustain 2018;30:103–14. https://doi.org/10.1016/J.COSUST.2018.04.006.

[8] Huang B, Xing K, Pullen S, Liao L, Huang K. Ecological–economic assessment of renewable energy deployment in sustainable built environment. Renew Energy 2020;161:1328–40. https://doi.org/10.1016/j.renene.2020.08.004.

[9] Su Y. Smart energy for smart built environment: A review for combined objectives of affordable sustainable green. Sustain Cities Soc 2020;53:101954. https://doi.org/10.1016/j.scs.2019.101954.

[10] Mutani G, Todeschi V. Energy resilience, vulnerability and risk in urban spaces. J Sustain Dev Energy, Water Environ Syst 2018;6:694–709. https://doi.org/10.13044/J.SDEWES.D6.0211.

[11] Mutani G, Todeschi V, Kampf J, Coors V, Fitzky M. Building energy consumption modeling at urban scale: Three case studies in Europe for residential buildings. INTELEC, Int. Telecommun. Energy Conf., vol. 2018-Octob, 2019. https://doi.org/10.1109/INTLEC.2018.8612382.

[12] Mutani G, Todeschi V. Space heating models at urban scale for buildings in the city of Turin (Italy). ENERGY PROCEDIA, vol. 122, 2017, p. 841–6. https://doi.org/10.1016/j.egypro.2017.07.445.

[13] Mutani G, Todeschi V. GIS-based urban energy modelling and energy efficiency scenarios using the energy performance certificate database. Energy Effic 2021;14:47. https://doi.org/10.1007/s12053-021-09962-z.

[14] Lauzet N, Rodler A, Musy M, Azam M-H, Guernouti S, Mauree D, et al. How building energy models take the local climate into account in an urban context – A review. Renew Sustain Energy Rev 2019;116:109390. https://doi.org/10.1016/J.RSER.2019.109390.

[15] Mutani G, Todeschi V. An urban energy atlas and engineering model for resilient cities. Int J Heat Technol 2019;37. https://doi.org/10.18280/ijht.370402.
[16] Li W, Zhou Y, Cetin K, Eom J, Wang Y, Chen G, et al. Modeling urban building energy use: A review of modeling approaches and procedures. Energy 2017;141:2445–57. https://doi.org/10.1016/j.energy.2017.11.071.
[17] Ryan EM, Sanquist TF. Validation of building energy modeling tools under idealized and realistic conditions. Energy Build 2012;47:375–82. https://doi.org/10.1016/j.enbuild.2011.12.020.
[18] Nageler P, Zahrer G, Heimrath R, Mach T, Mauthner F, Leusbrock I, et al. Novel validated method for GIS based automated dynamic urban building energy simulations. Energy 2017;139:142–54. https://doi.org/10.1016/J.ENERGY.2017.07.151.
[19] Alhamwi A, Medjroubi W, Vogt T, Agert C. GIS-based urban energy systems models and tools: Introducing a model for the optimisation of flexibilisation technologies in urban areas. Appl Energy 2017;191:1–9. https://doi.org/10.1016/J.APENERGY.2017.01.048.
[20] Caputo P, Pasetti G. Boosting the energy renovation rate of the private building stock in Italy: Policies and innovative GIS-based tools. Sustain Cities Soc 2017;34:394–404. https://doi.org/10.1016/j.scs.2017.07.002.
[21] Sola A, Corchero C, Salom J, Sanmarti M. Simulation tools to build urban-scale energy models: A review. Energies 2018;11. https://doi.org/10.3390/en11123269.
[22] Sola A, Corchero C, Salom J, Sanmarti M. Multi-domain urban-scale energy modelling tools: A review. Sustain Cities Soc 2019:101872. https://doi.org/10.1016/J.SCS.2019.101872.
[23] Ferrando M, Causone F, Hong T, Chen Y. Urban building energy modeling (UBEM) tools: A state-of-the-art review of bottom-up physics-based approaches. Sustain Cities Soc 2020;62. https://doi.org/10.1016/j.scs.2020.102408.
[24] Bruse M, Nouvel R, Wate P, Kraut V, Coors V. An Energy-Related CityGML ADE and Its Application for Heating Demand Calculation. Int J 3D Inf Model 2015;4:59–77. https://doi.org/10.4018/IJ3DIM.2015070104.
[25] Chen Y, Hong T, Piette MA. Automatic generation and simulation of urban building energy models based on city datasets for city-scale building retrofit analysis. Appl Energy 2017;205:323–35. https://doi.org/10.1016/J.APENERGY.2017.07.128.
[26] Luo X, Hong T, Tang Y-H. Modeling Thermal Interactions between Buildings in an Urban Context. Energies 2020;13:2382. https://doi.org/10.3390/en13092382.
[27] Zhu P, Yan D, Sun H, An J, Huang Y. Building Blocks Energy Estimation (BBEE): A method for building energy estimation on district level. Energy Build 2019;185:137–47. https://doi.org/10.1016/J.ENBUILD.2018.12.031.
[28] Chen Y, Hong T. Impacts of building geometry modeling methods on the simulation results of urban building energy models. Appl Energy 2018;215:717–35. https://doi.org/10.1016/j.apenergy.2018.02.073.
[29] Walter E, Kämpf JH. A verification of CitySim results using the BESTEST and monitored consumption values. Proc 2nd Build Simul Appl Conf 2015:215–22.

[30] Robinson D, Haldi F, Leroux P, Perez D, Rasheed A, Wilke U. CITYSIM: Comprehensive Micro-Simulation of Resource Flows for Sustainable Urban Planning. Proc Elev Int IBPSA Conf 2009:1083-1090-1083-1090 PP-Glasgow.
[31] Robinson D. Computer Modelling for Sustainable Urban Design. 1st Editio. London: 2011. https://doi.org/10.4324/9781849775403.
[32] Reinhart C, Dogan T, Jakubiec J, Rakha T, Sang A. Umi-an urban simulation environment for building energy use, daylighting and walkability. Proc. BS2013 13th Conf. IBPSA (International Build. Perform. Assoc., Building simulation; 2013, p. 476–83.
[33] Quan SJ, Wu J, Wang Y, Shi Z, Yang T, Yang PP-J. Urban Form and Building Energy Performance in Shanghai Neighborhoods. Energy Procedia 2016;88:126–32. https://doi.org/10.1016/j.egypro.2016.06.035.
[34] Monsalvete P, Robinson D, Eicker U. Dynamic Simulation Methodologies for Urban Energy Demand. Energy Procedia 2015;78:3360–5. https://doi.org/10.1016/j.egypro.2015.11.751.
[35] Nouvel R, Zirak M, Coors V, Eicker U. The influence of data quality on urban heating demand modeling using 3D city models. Comput Environ Urban Syst 2017;64:68–80. https://doi.org/10.1016/j.compenvurbsys.2016.12.005.
[36] Nouvel R, Brassel K-H, Bruse M, Duminil E, Coors V, Eicker U, et al. SimStadt, a new workflow-driven urban energy simulation platform for CityGML city models. Proc Int Conf CISBAT 2015 Futur Build Dist – Sustain from Nano to Urban Scale 2015:889–94. https://doi.org/10.5075/epfl-cisbat2015-889-894.
[37] Naboni E, Meloni M, Coccolo S, Kaempf J, Scartezzini J-L. An overview of simulation tools for predicting the mean radiant temperature in an outdoor space. Energy Procedia 2017;122:1111–6. https://doi.org/10.1016/j.egypro.2017.07.471.
[38] Mauree D, Naboni E, Coccolo S, Perera ATD, Nik VM, Scartezzini J-L. A review of assessment methods for the urban environment and its energy sustainability to guarantee climate adaptation of future cities. Renew Sustain Energy Rev 2019;112:733–46. https://doi.org/10.1016/j.rser.2019.06.005.
[39] Lindberg F, Grimmond CSB. The influence of vegetation and building morphology on shadow patterns and mean radiant temperatures in urban areas: model development and evaluation. Theor Appl Climatol 2011;105:311–23. https://doi.org/10.1007/s00704-010-0382-8.
[40] Al Savafi M.K. PM V. RayMan and SkyHelios as tools of urban climatology simulation. Interact Sci 2018:8–12. https://doi.org/10.21661/r-472891.
[41] Lindberg F, Grimmond CSB, Gabey A, Huang B, Kent CW, Sun T, et al. Urban Multi-scale Environmental Predictor (UMEP): An integrated tool for city-based climate services. Environ Model Softw 2018;99:70–87. https://doi.org/10.1016/j.envsoft.2017.09.020.
[42] Hedegaard RE, Kristensen MH, Pedersen TH, Brun A, Petersen S. Bottom-up modelling methodology for urban-scale analysis of residential space heating demand response. Appl Energy 2019;242:181–204. https://doi.org/10.1016/j.apenergy.2019.03.063.
[43] Perera ATD, Coccolo S, Scartezzini J-L, Mauree D. Quantifying the impact of urban climate by extending the boundaries of urban energy system

modeling. Appl Energy 2018;222:847–60. https://doi.org/10.1016/J.APENERGY.2018.04.004.
[44] Buckley N, Mills G, Reinhart C, Berzolla ZM. Using urban building energy modelling (UBEM) to support the new European Union's Green Deal: Case study of Dublin Ireland. Energy Build 2021;247:111115. https://doi.org/10.1016/j.enbuild.2021.111115.
[45] Abbasabadi N, Ashayeri M. Urban energy use modeling methods and tools: A review and an outlook. Build Environ 2019;161:106270. https://doi.org/10.1016/J.BUILDENV.2019.106270.
[46] Mutani G, Todeschi V. Building energy modeling at neighborhood scale. Energy Effic 2020. https://doi.org/10.1007/s12053-020-09882-4.
[47] Todeschi V, Boghetti R, Kämpf JH, Mutani G. Evaluation of Urban-Scale Building Energy-Use Models and Tools—Application for the City of Fribourg, Switzerland. Sustainability 2021;13. https://doi.org/10.3390/su13041595.
[48] Mutani G, Todeschi V, Novo R, Mattiazzo G, Tartaglia A. LE ISOLE MINORI TRA SOLE, MARE E VENTO. LIBRO BIANCO ANCIM-ENEA. 2019.
[49] Mutani G, Todeschi V, Santantonio S. Urban-Scale Energy Models: the relationship between cooling energy demand and urban form. 38th UIT Heat Transf. Conf. 21st-23rd June 2021, J. Phys. Conf. Ser. (IOP), Press, 2021.
[50] Mutani G, Todeschi V, Beltramino S. Energy Consumption Models at Urban Scale to Measure Energy Resilience. Sustain 2020. https://doi.org/10.3390/su12145678.
[51] Todeschi V, Javanroodi K, Castello R, Mohajeri N, Mutani G, Scartezzini J-L. The impact of COVID-19 pandemic on the energy performance of residential neighbourhoods and their occupancy behaviour. Sustain Cities Soc n.d. https://doi.org/10.1016/j.scs.2022.103896.
[52] Mutani G, Todeschi V. Low-Carbon Strategies for Resilient Cities: A Place-Based Evaluation of Solar Technologies and Green Roofs Potential in Urban Contexts. Tec Ital J Eng Sci 2020;64:193–201. https://doi.org/10.18280/ti-ijes.642-410.
[53] Mutani G, Todeschi V. Optimization of Costs and Self-Sufficiency for Roof Integrated Photovoltaic Technologies on Residential Buildings. Energies 2021;14. https://doi.org/10.3390/en14134018.
[54] Todeschi V, Marocco P, Mutani G, Lanzini A, Santarelli M. Towards Energy Self-consumption and Self-sufficiency in Urban Energy Communities. Int J Heat Technol 2021;39:1–11. https://doi.org/10.18280/ijht.390101.
[55] Mutani G, Todeschi V, Guelpa E, Verda V. Building Efficiency Models and the Optimization of the District Heating Network for Low-Carbon Transition Cities. In: Bertoldi P, editor. Improv. Energy Effic. Commer. Build. Smart Communities, Springer, Cham; 2020. https://doi.org/10.1007/978-3-030-31459-0_14.
[56] Todeschi V, Mutani G, Baima L, Nigra M, Robiglio M. Smart Solutions for Sustainable Cities — The Re-Coding Experience for Harnessing the Potential of Urban Rooftops. Appl Sci 2020;10:1–27. https://doi.org/10.3390/app10207112.
[57] Mutani G, Todeschi V. Roof-integrated green technologies, energy saving and outdoor thermal comfort: insights from a case study in urban

environment. Int J Sustain Dev Plan 2021. https://doi.org/10.18280/ijsdp.160102.
[58] Mutani G, Todeschi V, Carozza M, Rolando A. Urban-Scale Energy Models: relationship between urban form and energy performance. 2020 IEEE 3rd Int. Conf. Work. Óbuda Electr. Power Eng., 2020, p. 185–90. https://doi.org/10.1109/CANDO-EPE51100.2020.9337760.
[59] Mutani G, Todeschi V, Beltramino S. How to Improve the Liveability in Cities: The Effect of Urban Morphology and Greening on Outdoor Thermal Comfort. Tec Ital J Eng Sci 2021;65:361–70. https://doi.org/10.18280/ti-ijes.652-433.
[60] Economidou M, Todeschi V, Bertoldi P, D'Agostino D, Zangheri P, Castellazzi L. Review of 50 years of EU energy efficiency policies for buildings. Energy Build 2020;225:110322. https://doi.org/10.1016/j.enbuild.2020.110322.
[61] Bertoldi P, Economidou M, Palermo V, Boza-Kiss B, Todeschi V. How to finance energy renovation of residential buildings: Review of current and emerging financing instruments in the EU. WIREs Energy Environ 2021;10:e384. https://doi.org/10.1002/wene.384.
[62] Economidou M, Todeschi V, Bertoldi. Accelerating energy renovation investments in buildings - Financial andfiscalinstrumentsacross the EU. Luxembourg: Publications Office of the European Union; 2019. https://doi.org/10.2760/086805.
[63] D'Alonzo V, Novelli A, Vaccaro R, Vettorato D, Albatici R, Diamantini C, et al. A bottom-up spatially explicit methodology to estimate the space heating demand of the building stock at regional scale. Energy Build 2020;206:109581. https://doi.org/10.1016/j.enbuild.2019.109581.
[64] Buffat R, Froemelt A, Heeren N, Raubal M, Hellweg S. Big data GIS analysis for novel approaches in building stock modelling. Appl Energy 2017;208:277–90. https://doi.org/10.1016/j.apenergy.2017.10.041.
[65] Hjortling C, Björk F, Berg M, Klintberg T af. Energy mapping of existing building stock in Sweden – Analysis of data from Energy Performance Certificates. Energy Build 2017;153:341–55. https://doi.org/10.1016/j.enbuild.2017.06.073.
[66] Groppi D, de Santoli L, Cumo F, Astiaso Garcia D. A GIS-based model to assess buildings energy consumption and usable solar energy potential in urban areas. Sustain Cities Soc 2018;40:546–58. https://doi.org/10.1016/J.SCS.2018.05.005.
[67] Pillot B, Al-Kurdi N, Gervet C, Linguet L. An integrated GIS and robust optimization framework for solar PV plant planning scenarios at utility scale. Appl Energy 2020;260:114257. https://doi.org/10.1016/j.apenergy.2019.114257.
[68] Dall'O' G, Galante A, Torri M. A methodology for the energy performance classification of residential building stock on an urban scale. Energy Build 2012;48:211–9. https://doi.org/10.1016/j.enbuild.2012.01.034.
[69] Martínez-Molina A, Tort-Ausina I, Cho S, Vivancos J-L. Energy efficiency and thermal comfort in historic buildings: A review. Renew Sustain Energy Rev 2016;61:70–85. https://doi.org/10.1016/J.RSER.2016.03.018.
[70] Streicher KN, Padey P, Parra D, Bürer MC, Schneider S, Patel MK. Analysis of space heating demand in the Swiss residential building stock: Element-

based bottom-up model of archetype buildings. Energy Build 2019;184:300–22. https://doi.org/10.1016/J.ENBUILD.2018.12.011.

[71] Camporeale PE, Mercader-Moyano P. A GIS-based methodology to increase energy flexibility in building cluster through deep renovation: A neighborhood in Seville. Energy Build 2021;231:110573. https://doi.org/10.1016/j.enbuild.2020.110573.

[72] Gupta R, Gregg M. Targeting and modelling urban energy retrofits using a city-scale energy mapping approach. J Clean Prod 2018;174:401–12. https://doi.org/10.1016/j.jclepro.2017.10.262.

[73] Exner D, D'Alonzo V, Paoletti G, Pascuas R, Pernetti R. Building-Stock Analysis for the Definition of an Energy Renovation Scenario on the Urban Scale. Smart Sustain. Plan. Cities Reg., 2017, p. 33–54. https://doi.org/10.1007/978-3-319-44899-2_3.

[74] Ben H, Steemers K. Modelling energy retrofit using household archetypes. Energy Build 2020;224:110224. https://doi.org/10.1016/j.enbuild.2020.110224.

[75] Meha D, Dragusha B, Thakur J, Novosel T, Duić N. A novel spatial based approach for estimation of space heating demand saving potential and CO2 emissions reduction in urban areas. Energy 2021;225:120251. https://doi.org/10.1016/j.energy.2021.120251.

[76] Droutsa KG, Kontoyiannidis S, Dascalaki EG, Balaras CA. Mapping the energy performance of hellenic residential buildings from EPC (energy performance certificate) data. Energy 2016;98:284–95. https://doi.org/10.1016/j.energy.2015.12.137.

[77] Ali U, Shamsi MH, Bohacek M, Purcell K, Hoare C, Mangina E, et al. A data-driven approach for multi-scale GIS-based building energy modeling for analysis, planning and support decision making. Appl Energy 2020;279:115834. https://doi.org/10.1016/j.apenergy.2020.115834.

[78] Cozza S, Chambers J, Deb C, Scartezzini J-L, Schlüter A, Patel MK. Do energy performance certificates allow reliable predictions of actual energy consumption and savings? Learning from the Swiss national database. Energy Build 2020;224:110235. https://doi.org/10.1016/j.enbuild.2020.110235.

[79] Ahern C, Norton B. Energy Performance Certification: Misassessment due to assuming default heat losses. Energy Build 2020;224:110229. https://doi.org/10.1016/j.enbuild.2020.110229.

[80] Fan Y, Xia X. Building retrofit optimization models using notch test data considering energy performance certificate compliance. Appl Energy 2018;228:2140–52. https://doi.org/10.1016/j.apenergy.2018.07.043.

[81] van Dronkelaar C, Dowson M, Burman E, Spataru C, Mumovic D. A Review of the Energy Performance Gap and Its Underlying Causes in Non-Domestic Buildings . Front Mech Eng 2016;1:17.

[82] Johansson T, Olofsson T, Mangold M. Development of an energy atlas for renovation of the multifamily building stock in Sweden. Appl Energy 2017;203:723–36. https://doi.org/10.1016/J.APENERGY.2017.06.027.

[83] Ang YQ, Berzolla ZM, Reinhart CF. From concept to application: A review of use cases in urban building energy modeling. Appl Energy 2020;279:115738. https://doi.org/10.1016/j.apenergy.2020.115738.

[84] Filippi Oberegger U, Pernetti R, Lollini R. Bottom-up building stock retrofit

based on levelized cost of saved energy. Energy Build 2020;210:109757. https://doi.org/10.1016/j.enbuild.2020.109757.

[85] Cerezo C, Sokol J, AlKhaled S, Reinhart C, Al-Mumin A, Hajiah A. Comparison of four building archetype characterization methods in urban building energy modeling (UBEM): A residential case study in Kuwait City. Energy Build 2017;154:321–34. https://doi.org/10.1016/j.enbuild.2017.08.029.

[86] Hong T, Chen Y, Luo X, Luo N, Lee SH. Ten questions on urban building energy modeling. Build Environ 2020;168:106508. https://doi.org/10.1016/J.BUILDENV.2019.106508.

[87] Foucquier A, Robert S, Suard F, Stéphan L, Jay A. State of the art in building modelling and energy performances prediction: A review. Renew Sustain Energy Rev 2013;23:272–88. https://doi.org/10.1016/j.rser.2013.03.004.

[88] Koulamas C, Kalogeras AP, Pacheco-Torres R, Casillas J, Ferrarini L. Suitability analysis of modeling and assessment approaches in energy efficiency in buildings. Energy Build 2018;158:1662–82. https://doi.org/10.1016/j.enbuild.2017.12.002.

[89] Wei Y, Zhang X, Shi Y, Xia L, Pan S, Wu J, et al. A review of data-driven approaches for prediction and classification of building energy consumption. Renew Sustain Energy Rev 2018;82:1027–47. https://doi.org/10.1016/J.RSER.2017.09.108.

[90] Chalabi ZS, Bailey BJ. Sensitivity analysis of a non-steady state model of the greenhouse microclimate. Agric For Meteorol 1991;56:111–27. https://doi.org/10.1016/0168-1923(91)90107-2.

[91] Corrado V, Fabrizio E. Assessment of building cooling energy need through a quasi-steady state model: Simplified correlation for gain-loss mismatch. Energy Build 2007;39:569–79. https://doi.org/10.1016/j.enbuild.2006.09.012.

[92] Veken J, Saelens D, Verbeeck G, Hens H. Comparison of steady-state and dynamic building energy simulation programs, Computer Science; 2004.

[93] Swan LG, Ugursal VI. Modeling of end-use energy consumption in the residential sector: A review of modeling techniques. Renew Sustain Energy Rev 2009;13:1819–35. https://doi.org/10.1016/j.rser.2008.09.033.

[94] Ali U, Shamsi MH, Hoare C, Mangina E, O'Donnell J. Review of urban building energy modeling (UBEM) approaches, methods and tools using qualitative and quantitative analysis. Energy Build 2021;246:111073. https://doi.org/10.1016/j.enbuild.2021.111073.

[95] Li Y, Wang C, Zhu S, Yang J, Wei S, Zhang X, et al. A Comparison of Various Bottom-Up Urban Energy Simulation Methods Using a Case Study in Hangzhou, China. Energies 2020;13. https://doi.org/10.3390/en13184781.

[96] Brøgger M, Wittchen KB. Estimating the energy-saving potential in national building stocks – A methodology review. Renew Sustain Energy Rev 2018;82:1489–96. https://doi.org/10.1016/j.rser.2017.05.239.

[97] Nouvel R, Mastrucci A, Leopold U, Baume O, Coors V, Eicker U. Combining GIS-based statistical and engineering urban heat consumption models: Towards a new framework for multi-scale policy support. Energy Build 2015;107:204–12. https://doi.org/10.1016/j.enbuild.2015.08.021.

[98] Caldera M, Corgnati SP, Filippi M. Energy demand for space heating through a statistical approach: application to residential buildings. Energy

Build 2008;40:1972–83. https://doi.org/10.1016/j.enbuild.2008.05.005.
[99] Yang X, Hu M, Heeren N, Zhang C, Verhagen T, Tukker A, et al. A combined GIS-archetype approach to model residential space heating energy: A case study for the Netherlands including validation. Appl Energy 2020;280:115953. https://doi.org/10.1016/j.apenergy.2020.115953.
[100] Filogamo L, Peri G, Rizzo G, Giaccone A. On the classification of large residential buildings stocks by sample typologies for energy planning purposes. Appl Energy 2014;135:825–35. https://doi.org/10.1016/j.apenergy.2014.04.002.
[101] Loga T, Stein B, Diefenbach N. TABULA building typologies in 20 European countries—Making energy-related features of residential building stocks comparable. Energy Build 2016;132:4–12. https://doi.org/10.1016/j.enbuild.2016.06.094.
[102] Martin M, Wong NH, Hii DJC, Ignatius M. Comparison between simplified and detailed EnergyPlus models coupled with an urban canopy model. Energy Build 2017;157:116–25. https://doi.org/10.1016/j.enbuild.2017.01.078.
[103] Ahn Y, Sohn D-W. The effect of neighbourhood-level urban form on residential building energy use: A GIS-based model using building energy benchmarking data in Seattle. Energy Build 2019;196:124–33. https://doi.org/10.1016/J.ENBUILD.2019.05.018.
[104] Muniz-Gäal LP, Pezzuto CC, de Carvalho MFH, Mota LTM. Urban geometry and the microclimate of street canyons in tropical climate. Build Environ 2019:106547. https://doi.org/10.1016/J.BUILDENV.2019.106547.
[105] Luo Q, Yang L, Liu N, Xia J. Comparative Study on Thermal Environment and Energy Consumption of Urban Residential Houses in Beijing. Procedia Eng 2015;121:2141–8. https://doi.org/10.1016/j.proeng.2015.09.085.
[106] Vuckovic M, Kiesel K, Mahdavi A. Toward Advanced Representations of the Urban Microclimate in Building Performance Simulation. Energy Procedia 2015;78:3354–9. https://doi.org/10.1016/j.egypro.2015.11.750.
[107] Dochev I, Gorzalka P, Weiler V, Estevam Schmiedt J, Linkiewicz M, Eicker U, et al. Calculating urban heat demands: An analysis of two modelling approaches and remote sensing for input data and validation. Energy Build 2020;226:110378. https://doi.org/10.1016/j.enbuild.2020.110378.
[108] Romero Rodríguez L, Duminil E, Sánchez Ramos J, Eicker U. Assessment of the photovoltaic potential at urban level based on 3D city models: A case study and new methodological approach. Sol Energy 2017;146:264–75. https://doi.org/10.1016/J.SOLENER.2017.02.043.
[109] Kaden R, Kolbe TH. Simulation-Based Total Energy Demand Estimation of Buildings Using Semantic 3D City Models. Int J 3D Inf Model 2014;3:35–53. https://doi.org/10.4018/ij3dim.2014040103.
[110] Rosser JF, Long G, Zakhary S, Boyd DS, Mao Y, Robinson D. Modelling Urban Housing Stocks for Building Energy Simulation Using CityGML EnergyADE. ISPRS Int J Geo-Information 2019;8. https://doi.org/10.3390/ijgi8040163.
[111] Wate P, Coors V. 3D Data Models for Urban Energy Simulation. Energy Procedia 2015;78:3372–7. https://doi.org/10.1016/j.egypro.2015.11.753.
[112] Ferrari S, Zagarella F, Caputo P, Dall'O' G. Mapping Buildings' Energy-Related Features at Urban Level toward Energy Planning. Buildings

2021;11. https://doi.org/10.3390/buildings11080322.
[113] Li C. 2.09 - GIS for Urban Energy Analysis. In: Huang BBT-CGIS, editor. Earth Syst. Environ. Sci., Oxford: Elsevier; 2018, p. 187–95. https://doi.org/10.1016/B978-0-12-409548-9.09652-4.
[114] Suomalainen K, Wang V, Sharp B. Rooftop solar potential based on LiDAR data: Bottom-up assessment at neighbourhood level. Renew Energy 2017;111:463–75. https://doi.org/10.1016/J.RENENE.2017.04.025.
[115] Khan J, Arsalan MH. Estimation of rooftop solar photovoltaic potential using geo-spatial techniques: A perspective from planned neighborhood of Karachi – Pakistan. Renew Energy 2016;90:188–203. https://doi.org/10.1016/J.RENENE.2015.12.058.
[116] Erdélyi R, Wang Y, Guo W, Hanna E, Colantuono G. Three-dimensional SOlar RAdiation Model (SORAM) and its application to 3-D urban planning. Sol Energy 2014;101:63–73. https://doi.org/10.1016/J.SOLENER.2013.12.023.
[117] Goy S, Maréchal F, Finn D. Data for Urban Scale Building Energy Modelling: Assessing Impacts and Overcoming Availability Challenges. Energies 2020;13. https://doi.org/10.3390/en13164244.
[118] Buttitta G, Finn DP. A high-temporal resolution residential building occupancy model to generate high-temporal resolution heating load profiles of occupancy-integrated archetypes. Energy Build 2020;206:109577. https://doi.org/10.1016/j.enbuild.2019.109577.
[119] Martinaitis V, Zavadskas EK, Motuzienė V, Vilutienė T. Importance of occupancy information when simulating energy demand of energy efficient house: A case study. Energy Build 2015;101:64–75. https://doi.org/10.1016/j.enbuild.2015.04.031.
[120] Dong B, Liu Y, Fontenot H, Ouf M, Osman M, Chong A, et al. Occupant behavior modeling methods for resilient building design, operation and policy at urban scale: A review. Appl Energy 2021;293:116856. https://doi.org/10.1016/j.apenergy.2021.116856.
[121] Wu W, Dong B, Wang Q (Ryan), Kong M, Yan D, An J, et al. A novel mobility-based approach to derive urban-scale building occupant profiles and analyze impacts on building energy consumption. Appl Energy 2020;278:115656. https://doi.org/10.1016/j.apenergy.2020.115656.
[122] Xu X, Yin C, Wang W, Xu N, Hong T, Li Q. Revealing urban morphology and outdoor comfort through genetic algorithm-driven urban block design in dry and hot regions of China. Sustain 2019;11. https://doi.org/10.3390/su11133683.
[123] Wei R, Song D, Wong NH, Martin M. Impact of Urban Morphology Parameters on Microclimate. Procedia Eng 2016;169:142–9. https://doi.org/10.1016/J.PROENG.2016.10.017.
[124] Afiq WM, Azwadi CSN, Saqr KM. Effects of buildings aspect ratio, wind speed and wind direction on flow structure and pollutant dispersion in symmetric street canyons: a review. Int J Mech Mater Eng 2012;7:158–65.
[125] Gobakis K, Kolokotsa D. Coupling building energy simulation software with microclimatic simulation for the evaluation of the impact of urban outdoor conditions on the energy consumption and indoor environmental quality. Energy Build 2017;157:101–15. https://doi.org/10.1016/J.ENBUILD.2017.02.020.

[126] Shi Z, Fonseca JA, Schlueter A. A review of simulation-based urban form generation and optimization for energy-driven urban design. Build Environ 2017;121:119–29. https://doi.org/10.1016/j.buildenv.2017.05.006.
[127] Vartholomaios A. A parametric sensitivity analysis of the influence of urban form on domestic energy consumption for heating and cooling in a Mediterranean city. Sustain Cities Soc 2017;28:135–45. https://doi.org/10.1016/j.scs.2016.09.006.
[128] Middel A, Lukasczyk J, Maciejewski R, Demuzere M, Roth M. Sky View Factor footprints for urban climate modeling. Urban Clim 2018;25:120–34. https://doi.org/10.1016/J.UCLIM.2018.05.004.
[129] Nasrollahi N, Namazi Y, Taleghani M. The effect of urban shading and canyon geometry on outdoor thermal comfort in hot climates: A case study of Ahvaz, Iran. Sustain Cities Soc 2021;65:102638. https://doi.org/10.1016/j.scs.2020.102638.
[130] Liang S. Narrowband to broadband conversions of land surface albedo I: Algorithms. Remote Sens Environ 2001;76:213–38. https://doi.org/10.1016/S0034-4257(00)00205-4.
[131] Dodoo A, Tettey UYA, Gustavsson L. Influence of simulation assumptions and input parameters on energy balance calculations of residential buildings. Energy 2017;120:718–30. https://doi.org/10.1016/j.energy.2016.11.124.
[132] Taha H, Sailor D, Municipal S. High-Albedo Materials for Reducing Building Cooling Energy Use. Energy 1992. https://doi.org/10.2172/7000986.
[133] Zaitunah A, Samsuri S, Ahmad AG, Safitri RA. Normalized difference vegetation index (ndvi) analysis for land cover types using landsat 8 oli in besitang watershed, Indonesia. IOP Conf Ser Earth Environ Sci 2018;126. https://doi.org/10.1088/1755-1315/126/1/012112.
[134] Faroughi M, Karimimoshaver M, Aram F, Solgi E, Mosavi A, Nabipour N, et al. Computational modeling of land surface temperature using remote sensing data to investigate the spatial arrangement of buildings and energy consumption relationship. Eng Appl Comput Fluid Mech 2020;14:254–70. https://doi.org/10.1080/19942060.2019.1707711.
[135] Daramola M, Eresanya E. Land Surface Temperature Analysis over Akure. J Environ Earth Sci 2017;7.
[136] Palme M, Inostroza L, Villacreses G, Lobato-Cordero A, Carrasco C. From urban climate to energy consumption. Enhancing building performance simulation by including the urban heat island effect. Energy Build 2017;145:107–20. https://doi.org/10.1016/j.enbuild.2017.03.069.
[137] Akbari K, Jolai F, Ghaderi SF. Optimal design of distributed energy system in a neighborhood under uncertainty. Energy 2016;116:567–82. https://doi.org/10.1016/j.energy.2016.09.083.
[138] Ferrari S, Zagarella F, Caputo P, D'Amico A. Results of a literature review on methods for estimating buildings energy demand at district level. Energy 2019;175:1130–7. https://doi.org/10.1016/j.energy.2019.03.172.
[139] Al-Shammari ET, Keivani A, Shamshirband S, Mostafaeipour A, Yee PL, Petković D, et al. Prediction of heat load in district heating systems by Support Vector Machine with Firefly searching algorithm. Energy 2016;95:266–73. https://doi.org/10.1016/j.energy.2015.11.079.
[140] Nutkiewicz A, Yang Z, Jain RK. Data-driven Urban Energy Simulation

(DUE-S): A framework for integrating engineering simulation and machine learning methods in a multi-scale urban energy modeling workflow. Appl Energy 2018;225:1176–89. https://doi.org/10.1016/j.apenergy.2018.05.023.
[141] Belussi L, Danza L, Ghellere M, Guazzi G, Meroni I, Salamone F. Estimation of building energy performance for local energy policy at urban scale. Energy Procedia 2017;122:98–103. https://doi.org/10.1016/j.egypro.2017.07.379.
[142] Monteiro CS, Pina A, Cerezo C, Reinhart C, Ferrão P. The Use of Multi-detail Building Archetypes in Urban Energy Modelling. Energy Procedia 2017;111:817–25. https://doi.org/10.1016/J.EGYPRO.2017.03.244.
[143] Li X, Yao R, Liu M, Costanzo V, Yu W, Wang W, et al. Developing urban residential reference buildings using clustering analysis of satellite images. Energy Build 2018;169:417–29. https://doi.org/10.1016/J.ENBUILD.2018.03.064.
[144] Mutani G, Todeschi V. Urban Building Energy Modeling: hourly energy balance model of residential buildings at district scale. 37th UIT Heat Transf. Conf. Padova, 24-26 June 2019, 2019, p. 1–9.
[145] Guelpa E, Mutani G, Todeschi V, Verda V. A feasibility study on the potential expansion of the district heating network of Turin. Energy Procedia, vol. 122, 2017. https://doi.org/10.1016/j.egypro.2017.07.446.
[146] ISO-52016-1:2017(en). Energy performance of buildings — Energy needs for heating and cooling, internal temperatures and sensible and latent heat loads — Part 1: Calculation procedures 2017.
[147] ISO-52017-1:2017(en). Energy performance of buildings — Sensible and latent heat loads and internal temperatures — Part 1: Generic calculation procedures 2017.
[148] 13790:2008(en) I. Energy performance of buildings — Calculation of energy use for space heating and cooling 2008.
[149] AA. VV. - TABULA. Typology Approach for Building Stock Energy Assessment - TABULA. 2012.
[150] Zakšek K, Oštir K, Kokalj Ž. Sky-View Factor as a Relief Visualization Technique. Remote Sens 2011;3:398–415. https://doi.org/10.3390/rs3020398.
[151] Mutani G, Todeschi V. The Effects of Green Roofs on Outdoor Thermal Comfort , Urban Heat Island Mitigation and Energy Savings. Atmosphere (Basel) 2020;11:1–32. https://doi.org/10.3390/atmos11020123.
[152] Kikegawa Y, Genchi Y, Yoshikado H, Kondo H. Development of a numerical simulation system toward comprehensive assessments of urban warming countermeasures including their impacts upon the urban buildings' energy-demands. Appl Energy 2003;76:449–66. https://doi.org/10.1016/S0306-2619(03)00009-6.
[153] Duffie JA, Beckman WA. Wiley: Solar Engineering of Thermal Processes, 4th Edition - John A. Duffie, William A. Beckman. 2013.
[154] Miguel AF. Constructal design of solar energy-based systems for buildings. Energy Build 2008;40:1020–30. https://doi.org/10.1016/J.ENBUILD.2007.08.005.
[155] Boghetti R, Fantozzi F, Kämpf J, Mutani G, Salvadori G, Todeschi V. Building energy models with Morphological urban-scale parameters : a case study in Turin. Proc. 4th Build. Simul. Appl. Conf. - BSA 2019, 2019, p. 1–

8.
[156] Mutani G, Perino M. Ventilazione naturale mediante apertura controllata di finestre: implicazioni sul comfort interno. 41° Convegno AICARR, 2000, p. 1049–65.
[157] Mutani G, Santantonio S, Todeschi V. Evaluation of ventilation loads in buildings energy modelling at urban scale. 2021 IEEE 4th Int. Conf. Work. Óbuda Electr. Power Eng., 2021, p. 37–42. https://doi.org/10.1109/CANDO-EPE54223.2021.9667547.
[158] Ke G, Meng Q, Finley T, Wang T, Chen W, Ma W, et al. LightGBM: A Highly Efficient Gradient Boosting Decision Tree. In: Guyon I, Luxburg U V, Bengio S, Wallach H, Fergus R, Vishwanathan S, et al., editors. Adv. Neural Inf. Process. Syst., vol. 30, Curran Associates, Inc.; 2017, p. 3146–54.
[159] Wang Z, Hong T, Piette MA. Building thermal load prediction through shallow machine learning and deep learning. Appl Energy 2020;263:114683. https://doi.org/10.1016/j.apenergy.2020.114683.
[160] Miller C, Arjunan P, Kathirgamanathan A, Fu C, Roth J, Park JY, et al. The ASHRAE Great Energy Predictor III competition: Overview and results. Sci Technol Built Environ 2020;26:1427–47. https://doi.org/10.1080/23744731.2020.1795514.
[161] Boghetti R, Fantozzi F, Kämpf JH, Salvadori G. Understanding the performance gap: a machine learning approach on residential buildings in Turin, Italy. J Phys Conf Ser 2019;1343:12042. https://doi.org/10.1088/1742-6596/1343/1/012042.
[162] Mutani G, Todeschi V, Pastorelli M. Thermal-Electrical Analogy for Dynamic Urban-Scale Energy Modeling. Int J Heat Technol 2020;38:571–82. https://doi.org/10.18280/ijht.380301.
[163] Kämpf JH, Robinson D. A simplified thermal model to support analysis of urban resource flows. Energy Build 2007;39:445–53. https://doi.org/10.1016/j.enbuild.2006.09.002.
[164] Perez D. A framework to model and simulate the disaggregated energy flows supplying buildings in urban areas 2014. https://doi.org/10.5075/epfl-thesis-6102.
[165] Pedregosa F, Varoquaux G, Gramfort A, Michel V, Thirion B, Grisel O, et al. Scikit-Learn: Machine Learning in Python. J Mach Learn Res 2011;12:2825–2830.
[166] Büchlmann P, Yu B. Analyzing Bagging. Ann Stat 2002;30:927–61.
[167] Peel MC, Finlayson BL, McMahon TA. Updated world map of the Köppen-Geiger climate classification. Hydrol Earth Syst Sci 2007;11:1633–44. https://doi.org/10.5194/hess-11-1633-2007.
[168] Mangan SD, Koclar Oral G, Erdemir Kocagil I, Sozen I. The impact of urban form on building energy and cost efficiency in temperate-humid zones. J Build Eng 2021;33:101626. https://doi.org/10.1016/j.jobe.2020.101626.
[169] Leng H, Chen X, Ma Y, Wong NH, Ming T. Urban morphology and building heating energy consumption: Evidence from Harbin, a severe cold region city. Energy Build 2020;224:110143. https://doi.org/10.1016/j.enbuild.2020.110143.
[170] Perera ATD, Javanroodi K, Wang Y, Hong T. Urban cells: Extending the energy hub concept to facilitate sector and spatial coupling. Adv Appl

Energy 2021;3:100046. https://doi.org/10.1016/j.adapen.2021.100046.
[171] Javanroodi K, Mahdavinejad M, Nik VM. Impacts of urban morphology on reducing cooling load and increasing ventilation potential in hot-arid climate. Appl Energy 2018;231:714–46. https://doi.org/10.1016/j.apenergy.2018.09.116.
[172] Chatzipoulka C, Compagnon R, Nikolopoulou M. Urban geometry and solar availability on façades and ground of real urban forms: using London as a case study. Sol Energy 2016;138:53–66. https://doi.org/10.1016/J.SOLENER.2016.09.005.
[173] Mohajeri N, Upadhyay G, Gudmundsson A, Assouline D, Kämpf J, Scartezzini J-L. Effects of urban compactness on solar energy potential. Renew Energy 2016;93:469–82. https://doi.org/10.1016/j.renene.2016.02.053.
[174] Quan SJ, Economou A, Grasl T, Yang PP-J. An exploration of the relationship between density and building energy performance. URBAN Des Int 2020;25:92–112. https://doi.org/10.1057/s41289-020-00109-7.
[175] Csoknyai T, Legardeur J, Akle AA, Horváth M. Analysis of energy consumption profiles in residential buildings and impact assessment of a serious game on occupants' behavior. Energy Build 2019;196:1–20. https://doi.org/10.1016/j.enbuild.2019.05.009.
[176] SIA Zurich. SIA 2024 Conditions D'utilisation Standard Pour L'énergie Et Les InstallationsDu Bâtiment 2006.
[177] SIA Zurich. SIA 380/1 L'énergie thermique dans le bâtiment 2009.
[178] Cvetković D, Nešović A, Terzić I. Impact of people's behavior on the energy sustainability of the residential sector in emergency situations caused by COVID-19. Energy Build 2021;230:110532. https://doi.org/10.1016/j.enbuild.2020.110532.
[179] Lepore E, Aguilera Benito P, Piña Ramírez C, Viccione G. Indoors ventilation in times of confinement by SARS-CoV-2 epidemic: A comparative approach between Spain and Italy. Sustain Cities Soc 2021;72:103051. https://doi.org/10.1016/j.scs.2021.103051.
[180] Breiman L. Random Forests. Mach Learn 2001;45:5–32. https://doi.org/10.1023/A:1010933404324.
[181] Breiman L, Friedman JH, Olshen RA, Stone CJ. Classification And Regression Trees. Routledge; 1984. https://doi.org/10.1201/9781315139470.
[182] Liaw A, Wiener M. Classification and Regression by randomForest. R News 2002;2:18–22.
[183] Benasla M, Hess D, Allaoui T, Brahami M, Denaï M. The transition towards a sustainable energy system in Europe: What role can North Africa's solar resources play? Energy Strateg Rev 2019;24:1–13. https://doi.org/10.1016/j.esr.2019.01.007.
[184] Collier MJ, Nedović-Budić Z, Aerts J, Connop S, Foley D, Foley K, et al. Transitioning to resilience and sustainability in urban communities. Cities 2013;32. https://doi.org/10.1016/j.cities.2013.03.010.
[185] Gielen D, Boshell F, Saygin D, Bazilian MD, Wagner N, Gorini R. The role of renewable energy in the global energy transformation. Energy Strateg Rev 2019;24:38–50. https://doi.org/10.1016/j.esr.2019.01.006.
[186] Delponte I, Schenone C. RES Implementation in Urban Areas: An Updated

Overview. Sustainability 2020;12. https://doi.org/10.3390/su12010382.
[187] Perea-Moreno M-A, Hernandez-Escobedo Q, Perea-Moreno A-J. Renewable Energy in Urban Areas: Worldwide. Energies 2018;11:1–19. https://doi.org/10.3390/en11030577.
[188] Pavani P, Bak-Jensen B, Pillai JR. Maximizing the self-consumption of Solar-PV using Battery Energy Storage System in Samsø-Marina. 2019 IEEE PES Innov. Smart Grid Technol. Eur., 2019, p. 1–5. https://doi.org/10.1109/ISGTEurope.2019.8905498.
[189] Gagliano A, Nocera F. Analysis of the performances of electric energy storage in residential applications. Int J Heat Technol 2017;35:41–8. https://doi.org/10.18280/ijht.35Sp0106.
[190] Struth J, Kairies K-P, Leuthold M, Aretz A, Bost M, Gährs S, et al. PV-Benefit: A Critical Review of the Effect of Grid Integrated PV-Storage-Systems. Proc. Int. Renew. Energy Storage Conf. (IRES), Berlin, 18.-20. Novemb. 2013, 2013.
[191] Defaix PR, van Sark WGJHM, Worrell E, de Visser E. Technical potential for photovoltaics on buildings in the EU-27. Sol Energy 2012;86:2644–53. https://doi.org/10.1016/j.solener.2012.06.007.
[192] Tröndle T, Pfenninger S, Lilliestam J. Home-made or imported: On the possibility for renewable electricity autarky on all scales in Europe. Energy Strateg Rev 2019;26:100388. https://doi.org/10.1016/j.esr.2019.100388.
[193] Boulahia M, Djiar KA, Amado M. Combined Engineering—Statistical Method for Assessing Solar Photovoltaic Potential on Residential Rooftops: Case of Laghouat in Central Southern Algeria. Energies 2021;14. https://doi.org/10.3390/en14061626.
[194] Thebault M, Clivillé V, Berrah L, Desthieux G. Multicriteria roof sorting for the integration of photovoltaic systems in urban environments. Sustain Cities Soc 2020;60:102259. https://doi.org/10.1016/j.scs.2020.102259.
[195] Wong MS, Zhu R, Liu Z, Lu L, Peng J, Tang Z, et al. Estimation of Hong Kong's solar energy potential using GIS and remote sensing technologies. Renew Energy 2016;99:325–35. https://doi.org/10.1016/J.RENENE.2016.07.003.
[196] Ruiz HS, Sunarso A, Ibrahim-Bathis K, Murti SA, Budiarto I. GIS-AHP Multi Criteria Decision Analysis for the optimal location of solar energy plants at Indonesia. Energy Reports 2020;6:3249–63. https://doi.org/10.1016/j.egyr.2020.11.198.
[197] Firozjaei MK, Nematollahi O, Mijani N, Shorabeh SN, Firozjaei HK, Toomanian A. An integrated GIS-based Ordered Weighted Averaging analysis for solar energy evaluation in Iran: Current conditions and future planning. Renew Energy 2019;136:1130–46. https://doi.org/10.1016/j.renene.2018.09.090.
[198] Mansouri Kouhestani F, Byrne J, Johnson D, Spencer L, Hazendonk P, Brown B. Evaluating solar energy technical and economic potential on rooftops in an urban setting: the city of Lethbridge, Canada. Int J Energy Environ Eng 2019;10:13–32. https://doi.org/10.1007/s40095-018-0289-1.
[199] Bódis K, Kougias I, Jäger-Waldau A, Taylor N, Szabó S. A high-resolution geospatial assessment of the rooftop solar photovoltaic potential in the European Union. Renew Sustain Energy Rev 2019;114:109309. https://doi.org/10.1016/j.rser.2019.109309.

[200] Pontes Luz G, e Silva R. Modeling Energy Communities with Collective Photovoltaic Self-Consumption: Synergies between a Small City and a Winery in Portugal. Energies 2021;14. https://doi.org/10.3390/en14020323.
[201] Lowitzsch J, Hoicka CE, van Tulder FJ. Renewable energy communities under the 2019 European Clean Energy Package – Governance model for the energy clusters of the future? Renew Sustain Energy Rev 2020;122:109489. https://doi.org/10.1016/j.rser.2019.109489.
[202] Wang C, Cheng X, Shuai C, Huang F, Zhang P, Zhou M, et al. Evaluation of energy and environmental performances of Solar Photovoltaic-based Targeted Poverty Alleviation Plants in China. Energy Sustain Dev 2020;56:73–87. https://doi.org/10.1016/j.esd.2020.04.003.
[203] Li J, Wang Z, Cheng X, Shuai J, Shuai C, Liu J. Has solar PV achieved the national poverty alleviation goals? Empirical evidence from the performances of 52 villages in rural China. Energy 2020;201:117631. https://doi.org/10.1016/j.energy.2020.117631.
[204] Luthander R, Nilsson AM, Widén J, Åberg M. Graphical analysis of photovoltaic generation and load matching in buildings: A novel way of studying self-consumption and self-sufficiency. Appl Energy 2019;250:748–59. https://doi.org/10.1016/j.apenergy.2019.05.058.
[205] Dehler J, Keles D, Telsnig T, Fleischer B, Baumann M, Fraboulet D, et al. Chapter 27 - Self-Consumption of Electricity from Renewable Sources. In: Europe's Energy Transition, editor. Eur. Energy Transit. Insights Policy Mak., Academic Press; 2017, p. 225–36. https://doi.org/10.1016/B978-0-12-809806-6.00027-4.
[206] Mutani G, Santantonio S, Beltramino S. Indicators and Representation Tools to Measure the Technical-Economic Feasibility of a Renewable Energy Community . The Case Study of Villar Pellice (Italy). Int J Sustain Dev Plan 2021;16:1–11. https://doi.org/10.18280/ijsdp.160101.
[207] Hong T, Lee M, Koo C, Jeong K, Kim J. Development of a method for estimating the rooftop solar photovoltaic (PV) potential by analyzing the available rooftop area using Hillshade analysis. Appl Energy 2017;194:320–32. https://doi.org/10.1016/J.APENERGY.2016.07.001.
[208] Zheng Y, Weng Q, Zheng Y. A hybrid approach for three-dimensional building reconstruction in indianapolis from LiDAR data. Remote Sens 2017;9:1–24. https://doi.org/10.3390/rs9040310.
[209] Gómez-Navarro T, Brazzini T, Alfonso-Solar D, Vargas-Salgado C. Analysis of the potential for PV rooftop prosumer production: Technical, economic and environmental assessment for the city of Valencia (Spain). Renew Energy 2021;174:372–81. https://doi.org/10.1016/j.renene.2021.04.049.
[210] Gagnon P, Margolis R, Melius J, Phillips C, Elmore R. Estimating rooftop solar technical potential across the US using a combination of GIS-based methods, lidar data, and statistical modeling. Environ Res Lett 2018;13:24027. https://doi.org/10.1088/1748-9326/aaa554.
[211] Singh D, Gautam AK, Chaudhary R. Potential and performance estimation of free-standing and building integrated photovoltaic technologies for different climatic zones of India. Energy Built Environ 2020. https://doi.org/10.1016/j.enbenv.2020.10.004.
[212] Yang Y, Campana PE, Stridh B, Yan J. Potential analysis of roof-mounted

solar photovoltaics in Sweden. Appl Energy 2020;279:115786. https://doi.org/10.1016/j.apenergy.2020.115786.
[213] Oh M, Kim J-Y, Kim B, Yun C-Y, Kim CK, Kang Y-H, et al. Tolerance angle concept and formula for practical optimal orientation of photovoltaic panels. Renew Energy 2021;167:384–94. https://doi.org/10.1016/j.renene.2020.11.096.
[214] Hartner M, Ortner A, Hiesl A, Haas R. East to west – The optimal tilt angle and orientation of photovoltaic panels from an electricity system perspective. Appl Energy 2015;160:94–107. https://doi.org/10.1016/j.apenergy.2015.08.097.
[215] Azaioud H, Desmet J, Vandevelde L. Benefit Evaluation of PV Orientation for Individual Residential Consumers. Energies 2020;13. https://doi.org/10.3390/en13195122.
[216] Mubarak R, Weide Luiz E, Seckmeyer G. Why PV Modules Should Preferably No Longer Be Oriented to the South in the Near Future. Energies 2019;12. https://doi.org/10.3390/en12234528.
[217] Lahnaoui A, Stenzel P, Linssen J. Tilt Angle and Orientation Impact on the Techno-economic Performance of Photovoltaic Battery Systems. Energy Procedia 2017;105:4312–20. https://doi.org/10.1016/j.egypro.2017.03.903.
[218] Mainzer K, Fath K, McKenna R, Stengel J, Fichtner W, Schultmann F. A high-resolution determination of the technical potential for residential-roof-mounted photovoltaic systems in Germany. Sol Energy 2014;105:715–31. https://doi.org/10.1016/j.solener.2014.04.015.
[219] Ng KM, Adam NM, Inayatullah O, Kadir MZAA. Assessment of solar radiation on diversely oriented surfaces and optimum tilts for solar absorbers in Malaysian tropical latitude. Int J Energy Environ Eng 2014;5:75. https://doi.org/10.1007/s40095-014-0075-7.
[220] Mutani G, Pastorelli M, de Bosio F. A model for the evaluation of thermal and electric energy consumptions in residential buildings: The case study in Torino (Italy). 2015 Int. Conf. Renew. Energy Res. Appl., 2015, p. 1399–404. https://doi.org/10.1109/ICRERA.2015.7418637.
[221] Mutani G, Beltramino S, Forte A. A Clean Energy Atlas for Energy Communities in Piedmont Region (Italy). Int J Des Nat Ecodynamics 2020;15:343–53. https://doi.org/10.18280/ijdne.150308.
[222] Schopfer S, Tiefenbeck V, Staake T. Economic assessment of photovoltaic battery systems based on household load profiles. Appl Energy 2018;223:229–48. https://doi.org/10.1016/j.apenergy.2018.03.185.
[223] Mutani G, Santantonio S, Brunetta G, Caldarice O, Demichela M. An energy community for territorial resilience: Measurement of the risk of an energy supply blackout. Energy Build 2021;240:110906. https://doi.org/10.1016/j.enbuild.2021.110906.
[224] De Almeida A, Hirzel S, Patrão C, Fong J, Dütschke E. Energy-efficient elevators and escalators in Europe: An analysis of energy efficiency potentials and policy measures. Energy Build 2012;47:151–8. https://doi.org/10.1016/j.enbuild.2011.11.053.
[225] Tukia T, Uimonen S, Siikonen M-L, Donghi C, Lehtonen M. High-resolution modeling of elevator power consumption. J Build Eng 2018;18:210–9. https://doi.org/10.1016/j.jobe.2018.03.008.
[226] Tukia T, Uimonen S, Siikonen M-L, Hakala H, Donghi C, Lehtonen M.

Explicit method to predict annual elevator energy consumption in recurring passenger traffic conditions. J Build Eng 2016;8:179–88. https://doi.org/10.1016/j.jobe.2016.08.004.

[227] Tukia T, Uimonen S, Siikonen M-L, Donghi C, Lehtonen M. Modeling the aggregated power consumption of elevators – the New York city case study. Appl Energy 2019;251:113356. https://doi.org/10.1016/j.apenergy.2019.113356.

[228] Gracia-Amillo AM, Bardizza G, Salis E, Huld T, Dunlop ED. Energy-based metric for analysis of organic PV devices in comparison with conventional industrial technologies. Renew Sustain Energy Rev 2018;93:76–89. https://doi.org/10.1016/j.rser.2018.04.029.

[229] Wang Z, Hong T. Generating realistic building electrical load profiles through the Generative Adversarial Network (GAN). Energy Build 2020;224:110299. https://doi.org/10.1016/j.enbuild.2020.110299.

[230] Serrano-Guerrero X, Escrivá-Escrivá G, Roldán-Blay C. Statistical methodology to assess changes in the electrical consumption profile of buildings. Energy Build 2018;164:99–108. https://doi.org/10.1016/j.enbuild.2017.12.059.

[231] Maleki A, Askarzadeh A. Comparative study of artificial intelligence techniques for sizing of a hydrogen-based stand-alone photovoltaic/wind hybrid system. Int J Hydrogen Energy 2014;39:9973–84. https://doi.org/10.1016/j.ijhydene.2014.04.147.

[232] Marocco P, Ferrero D, Gandiglio M, Ortiz MM, Sundseth K, Lanzini A, et al. A study of the techno-economic feasibility of H2-based energy storage systems in remote areas. Energy Convers Manag 2020;211:112768. https://doi.org/https://doi.org/10.1016/j.enconman.2020.112768.

[233] Moretti L, Polimeni S, Meraldi L, Raboni P, Leva S, Manzolini G. Assessing the impact of a two-layer predictive dispatch algorithm on design and operation of off-grid hybrid microgrids. Renew Energy 2019;143:1439–53. https://doi.org/10.1016/j.renene.2019.05.060.

[234] Pavone F. NONO RAPPORTO SULL' ENERGIA: Provincia di Torino. 2014.

[235] Goy S, Sancho-Tomás A. 4 - Load management in buildings. In: Eicker UBT-UES for L-CC, editor., Academic Press; 2019, p. 137–79. https://doi.org/10.1016/B978-0-12-811553-4.00004-4.

[236] Delmastro C, Mutani G, Corgnati SP. A supporting method for selecting cost-optimal energy retrofit policies for residential buildings at the urban scale. Energy Policy 2016;99:42–56. https://doi.org/10.1016/j.enpol.2016.09.051.

[237] Caputo P, Pasetti G. Overcoming the inertia of building energy retrofit at municipal level: The Italian challenge. Sustain Cities Soc 2015;15:120–34. https://doi.org/10.1016/j.scs.2015.01.001.

[238] Martínez-Hervás M, Sendra JJ, Suárez R. Towards an Energy Assessment on an Urban Scale for Retrofitting the Housing Stock in Mediterranean Cities. Procedia Environ Sci 2017;38:688–95. https://doi.org/10.1016/j.proenv.2017.03.150.

[239] Olsthoorn D, Haghighat F, Mirzaei PA. Integration of storage and renewable energy into district heating systems: A review of modelling and optimization. Sol Energy 2016;136:49–64. https://doi.org/10.1016/j.solener.2016.06.054.

[240] Lund H, Möller B, Mathiesen B V, Dyrelund A. The role of district heating in future renewable energy systems. Energy 2010;35:1381–90. https://doi.org/10.1016/j.energy.2009.11.023.
[241] Sperling K, Möller B. End-use energy savings and district heating expansion in a local renewable energy system – A short-term perspective. Appl Energy 2012;92:831–42. https://doi.org/10.1016/j.apenergy.2011.08.040.
[242] Nielsen S, Möller B. GIS based analysis of future district heating potential in Denmark. Energy 2013;57:458–68. https://doi.org/10.1016/j.energy.2013.05.041.
[243] Gils HC, Cofala J, Wagner F, Schöpp W. GIS-based assessment of the district heating potential in the USA. Energy 2013;58:318–29. https://doi.org/10.1016/j.energy.2013.06.028.
[244] Rezaie B, Rosen MA. District heating and cooling: Review of technology and potential enhancements. Appl Energy 2012;93:2–10. https://doi.org/10.1016/j.apenergy.2011.04.020.
[245] Papadopoulos AM. Forty years of regulations on the thermal performance of the building envelope in Europe: Achievements, perspectives and challenges. Energy Build 2016;127:942–52. https://doi.org/10.1016/J.ENBUILD.2016.06.051.
[246] Serrano S, Ürge-Vorsatz D, Barreneche C, Palacios A, Cabeza LF. Heating and cooling energy trends and drivers in Europe. Energy 2017;119:425–34. https://doi.org/10.1016/J.ENERGY.2016.12.080.
[247] Thomas S, Rosenow J. Drivers of increasing energy consumption in Europe and policy implications. Energy Policy 2020;137:111108. https://doi.org/https://doi.org/10.1016/j.enpol.2019.111108.
[248] Bull R, Chang N, Fleming P. The use of building energy certificates to reduce energy consumption in European public buildings. Energy Build 2012;50:103–10. https://doi.org/10.1016/J.ENBUILD.2012.03.032.
[249] Beerepoot M, Sunikka M. The Contribution of the EC Energy Certificate in Improving Sustainability of the Housing Stock. Environ Plan B Plan Des 2005;32:21–31. https://doi.org/10.1068/b3118.
[250] Cerin P, Hassel LG, Semenova N. Energy Performance and Housing Prices. Sustain Dev 2014;22:404–19. https://doi.org/10.1002/sd.1566.
[251] Davis PT, McCord JA, McCord M, Haran M. Modelling the effect of energy performance certificate rating on property value in the Belfast housing market. Int J Hous Mark Anal 2015;8:292–317. https://doi.org/10.1108/IJHMA-09-2014-0035.
[252] Fregonara E, Rolando D, Semeraro P. Energy performance certificates in the Turin real estate market. J Eur Real Estate Res 2017;10:149–69. https://doi.org/10.1108/JERER-05-2016-0022.
[253] Fregonara E, Rolando D, Semeraro P, Vella M. The impact of Energy Performance Certificate level on house listing prices. First evidence from Italian real estate. Aestimum 2014;65:143–63. https://doi.org/10.13128/Aestimum-15459.
[254] Las-Heras-Casas J, López-Ochoa LM, López-González LM, Paredes-Sánchez JP. A tool for verifying energy performance certificates and improving the knowledge of the residential sector: A case study of the Autonomous Community of Aragón (Spain). Sustain Cities Soc 2018;41:62–72. https://doi.org/10.1016/j.scs.2018.05.016.

[255] Hardy A, Glew D. An analysis of errors in the Energy Performance certificate database. Energy Policy 2019;129:1168–78. https://doi.org/10.1016/j.enpol.2019.03.022.
[256] Chalal ML, Benachir M, White M, Shrahily R. Energy planning and forecasting approaches for supporting physical improvement strategies in the building sector: A review. Renew Sustain Energy Rev 2016;64:761–76. https://doi.org/10.1016/j.rser.2016.06.040.
[257] Caputo P, Pasetti G. GIS tools towards a renovation of the building heritage. Energy Procedia 2017;133:435–43. https://doi.org/10.1016/j.egypro.2017.09.388.
[258] Guelpa E, Mutani G, Todeschi V, Verda V. Reduction of CO2 emissions in urban areas through optimal expansion of existing district heating networks. J Clean Prod 2018;204. https://doi.org/10.1016/j.jclepro.2018.08.272.
[259] Guelpa E, Toro C, Sciacovelli A, Melli R, Sciubba E, Verda V. Optimal operation of large district heating networks through fast fluid-dynamic simulation. Energy 2016;102:586–95. https://doi.org/10.1016/j.energy.2016.02.058.
[260] Guelpa E, Sciacovelli A, Verda V. Thermo-fluid dynamic model of large district heating networks for the analysis of primary energy savings. Energy 2019;184:34–44. https://doi.org/10.1016/j.energy.2017.07.177.
[261] Sciacovelli A, Guelpa E, Verda V. Pumping Cost Minimization in an Existing District Heating Network. vol. Volume 6A:, 2013. https://doi.org/10.1115/IMECE2013-65169.
[262] Guelpa E, Barbero G, Sciacovelli A, Verda V. Peak-shaving in district heating systems through optimal management of the thermal request of buildings. Energy 2017;137:706–14. https://doi.org/10.1016/j.energy.2017.06.107.
[263] Baldini M, Brøgger M, Jacobsen HK, Wittchen KB. Cost-effectiveness of energy efficiency improvements for a residential building stock in a Danish district heating area. Energy Effic 2020;13:1737–61. https://doi.org/10.1007/s12053-020-09889-x.
[264] van den Brom P, Meijer A, Visscher H. Performance gaps in energy consumption: household groups and building characteristics. Build Res Inf 2018;46:54–70. https://doi.org/10.1080/09613218.2017.1312897.
[265] Bhattacharjee S, Reichard G. Socio-Economic Factors Affecting Individual Household Energy Consumption: A Systematic Review 2011:891–901. https://doi.org/10.1115/ES2011-54615.
[266] O'Neill BC, Chen BS. Demographic Determinants of Household Energy Use in the United States. Popul Dev Rev 2002;28:53–88.
[267] Li X, Zhou Y, Yu S, Jia G, Li H, Li W. Urban heat island impacts on building energy consumption: A review of approaches and findings. Energy 2019;174:407–19. https://doi.org/10.1016/J.ENERGY.2019.02.183.
[268] Lukač N, Seme S, Dežan K, Žalik B, Štumberger G. Economic and environmental assessment of rooftops regarding suitability for photovoltaic systems installation based on remote sensing data. Energy 2016;107:854–65. https://doi.org/10.1016/J.ENERGY.2016.04.089.
[269] Santamouris M, Ban-Weiss G, Osmond P, Paolini R, Synnefa A, Cartalis C, et al. Progress in urban greenery mitigation science – assessment methodologies advanced technologies and impact on cities. J Civ Eng Manag

2018;24:638–71. https://doi.org/10.3846/jcem.2018.6604.
[270] Aram F, Solgi E, García EH, Mosavi A, Várkonyi-Kóczy AR. The cooling effect of large-scale urban parks on surrounding area thermal comfort. Energies 2019;12:1–21. https://doi.org/10.3390/en12203904.
[271] Ng E, Chen L, Wang Y, Yuan C. A study on the cooling effects of greening in a high-density city: An experience from Hong Kong. Build Environ 2012;47:256–71. https://doi.org/10.1016/J.BUILDENV.2011.07.014.
[272] Cascone S, Catania F, Gagliano A, Sciuto G. A comprehensive study on green roof performance for retrofitting existing buildings. Build Environ 2018;136:227–39. https://doi.org/10.1016/J.BUILDENV.2018.03.052.
[273] Wilkinson S, Feitosa RC, Kaga IT, Franceschi IH de. Evaluating the Thermal Performance of Retrofitted Lightweight Green Roofs and Walls in Sydney and Rio de Janeiro. Procedia Eng 2017;180:231–40. https://doi.org/10.1016/J.PROENG.2017.04.182.
[274] Schindler BY, Blaustein L, Lotan R, Shalom H, Kadas GJ, Seifan M. Green roof and photovoltaic panel integration: Effects on plant and arthropod diversity and electricity production. J Environ Manage 2018;225:288–99. https://doi.org/10.1016/J.JENVMAN.2018.08.017.
[275] Shafique M, Kim R, Rafiq M. Green roof benefits, opportunities and challenges – A review. Renew Sustain Energy Rev 2018;90:757–73. https://doi.org/10.1016/J.RSER.2018.04.006.
[276] Sturiale L, Scuderi A. The role of green infrastructures in urban planning for climate change adaptation. Climate 2019;7. https://doi.org/10.3390/cli7100119.
[277] Santos T, Tenedório JA, Gonçalves JA. Quantifying the city's green area potential gain using remote sensing data. Sustain 2016;8:1–16. https://doi.org/10.3390/su8121247.
[278] Urban B, Roth K. Guidelines for selecting cool roofs. US Dep Energy 2010:1–23.
[279] Yang J, Bou-Zeid E. Scale dependence of the benefits and efficiency of green and cool roofs. Landsc Urban Plan 2019;185:127–40. https://doi.org/10.1016/J.LANDURBPLAN.2019.02.004.
[280] Dong J, Lin M, Zuo J, Lin T, Liu J, Sun C, et al. Quantitative study on the cooling effect of green roofs in a high-density urban Area—A case study of Xiamen, China. J Clean Prod 2020;255:120152. https://doi.org/10.1016/J.JCLEPRO.2020.120152.
[281] He Y, Yu H, Ozaki A, Dong N. Thermal and energy performance of green roof and cool roof: A comparison study in Shanghai area. J Clean Prod 2020;267:122205. https://doi.org/10.1016/j.jclepro.2020.122205.
[282] Canto-Perello J, Martinez-Garcia MP, Curiel-Esparza J, Martin-Utrillas M. Implementing sustainability criteria for selecting a roof assembly typology in medium span buildings. Sustain 2015;7:6854–71. https://doi.org/10.3390/su7066854.
[283] D'Orazio M, Di Perna C, Di Giuseppe E. Green roof yearly performance: A case study in a highly insulated building under temperate climate. Energy Build 2012;55:439–51. https://doi.org/10.1016/j.enbuild.2012.09.009.
[284] Barrio EP Del. Analysis of the green roofs cooling potential in buildings. Energy Build 1998;27:179–93. https://doi.org/10.1016/S0378-7788(97)00029-7.

[285] Sanchez L, Reames TG. Cooling Detroit: A socio-spatial analysis of equity in green roofs as an urban heat island mitigation strategy. Urban For Urban Green 2019;44:126331. https://doi.org/10.1016/j.ufug.2019.04.014.
[286] Suter I, Maksimović Č, van Reeuwijk M. A neighbourhood-scale estimate for the cooling potential of green roofs. Urban Clim 2017;20:33–45. https://doi.org/10.1016/j.uclim.2017.02.007.
[287] Hoelscher MT, Nehls T, Jänicke B, Wessolek G. Quantifying cooling effects of facade greening: Shading, transpiration and insulation. Energy Build 2016;114:283–90. https://doi.org/10.1016/j.enbuild.2015.06.047.
[288] Mahmoud AS, Asif M, Hassanain MA, Babsail MO, Sanni-anibire MO. Energy and Economic Evaluation of Green Roofs for Residential Buildings in Hot-Humid Climates. Buildings 2017;7:14. https://doi.org/10.3390/buildings7020030.
[289] Zhang L, Deng Z, Liang L, Zhang Y, Meng Q, Wang J, et al. Thermal behavior of a vertical green facade and its impact on the indoor and outdoor thermal environment. Energy Build 2019;204. https://doi.org/10.1016/j.enbuild.2019.109502.
[290] Peng LLH, Jiang Z, Yang X, He Y, Xu T, Chen SS. Cooling effects of block-scale facade greening and their relationship with urban form. Build Environ 2020;169:106552. https://doi.org/10.1016/J.BUILDENV.2019.106552.
[291] Botham-Myint D, Recktenwald GW, Sailor DJ. Thermal footprint effect of rooftop urban cooling strategies. Urban Clim 2015;14:268–77. https://doi.org/10.1016/J.UCLIM.2015.07.005.
[292] Krarti M. Chapter 8 - Integrated Design of Energy Efficient Cities. In: Krarti Communities, and Urban Centers MBT-OD and R of EEB, editor., Butterworth-Heinemann; 2018, p. 471–545. https://doi.org/10.1016/B978-0-12-849869-9.00008-9.
[293] Akbari H, Pomerantz M, Taha H. Cool surfaces and shade trees to reduce energy use and improve air quality in urban areas. Sol Energy 2001;70:295–310. https://doi.org/10.1016/S0038-092X(00)00089-X.
[294] Oleson KW, Bonan GB, Feddema J. Effects of white roofs on urban temperature in a global climate model. Geophys Res Lett 2010;37. https://doi.org/10.1029/2009GL042194.
[295] Macintyre HL, Heaviside C. Potential benefits of cool roofs in reducing heat-related mortality during heatwaves in a European city. Environ Int 2019;127:430–41. https://doi.org/10.1016/j.envint.2019.02.065.
[296] Akbari H, Levinson R. Evolution of cool-roof standards in the US. Adv Build Energy Res 2008;2:1–32. https://doi.org/10.3763/aber.2008.0201.
[297] Berdahl P, Akbari H, Rose LS. Aging of reflective roofs: soot deposition. Appl Opt 2002;41:2355–60. https://doi.org/10.1364/AO.41.002355.
[298] Akbari H, Berhe A, Levinson R, Graveline S, Foley K, Delgado A. Aging and weathering of cool roofing membranes. Report Lawrence Berkeley Natl Lab Berkeley, CA 2005.
[299] Akbari H, Berdahl P, Levinson RM, Wiel S, Miller WA, Desjarlais A. Cool Color Roofing Materials. 2006.
[300] La Roche P, Berardi U. Comfort and energy savings with active green roofs. Energy Build 2014;82:492–504. https://doi.org/10.1016/j.enbuild.2014.07.055.
[301] Rakotondramiarana HT, Ranaivoarisoa TF, Morau D. Dynamic Simulation

of the Green Roofs Impact on Building Energy Performance, Case Study of Antananarivo, Madagascar. Buildings 2015:497–520. https://doi.org/10.3390/buildings5020497.

[302] Costanzo V, Evola G, Marletta L. Energy savings in buildings or UHI mitigation? Comparison between green roofs and cool roofs. Energy Build 2016;114:247–55. https://doi.org/10.1016/j.enbuild.2015.04.053.

[303] Silva CM, Gomes MG, Silva M. Green roofs energy performance in Mediterranean climate. Energy Build 2016;116:318–25. https://doi.org/10.1016/j.enbuild.2016.01.012.

[304] Bevilacqua P, Bruno R, Arcuri N. Green roofs in a Mediterranean climate: energy performances based on in-situ experimental data. Renew Energy 2020;152:1414–30. https://doi.org/10.1016/j.renene.2020.01.085.

[305] Natanian J, Aleksandrowicz O, Auer T. A parametric approach to optimizing urban form, energy balance and environmental quality: The case of Mediterranean districts. Appl Energy 2019;254:113637. https://doi.org/10.1016/j.apenergy.2019.113637.

[306] Strømann-Andersen J, Sattrup PA. The urban canyon and building energy use: Urban density versus daylight and passive solar gains. Energy Build 2011;43:2011–20. https://doi.org/10.1016/j.enbuild.2011.04.007.

[307] Sanaieian H, Tenpierik M, Linden K van den, Mehdizadeh Seraj F, Mofidi Shemrani SM. Review of the impact of urban block form on thermal performance, solar access and ventilation. Renew Sustain Energy Rev 2014;38:551–60. https://doi.org/10.1016/j.rser.2014.06.007.

[308] Vartholomaios A. The residential solar block envelope: A method for enabling the development of compact urban blocks with high passive solar potential. Energy Build 2015;99:303–12. https://doi.org/10.1016/j.enbuild.2015.04.046.

[309] Martins TA de L, Adolphe L, Bastos LEG, Martins MA de L. Sensitivity analysis of urban morphology factors regarding solar energy potential of buildings in a Brazilian tropical context. Sol Energy 2016;137:11–24. https://doi.org/10.1016/j.solener.2016.07.053.

[310] van Esch MME, Looman RHJ, de Bruin-Hordijk GJ. The effects of urban and building design parameters on solar access to the urban canyon and the potential for direct passive solar heating strategies. Energy Build 2012;47:189–200. https://doi.org/10.1016/j.enbuild.2011.11.042.

[311] Martellotta F, Cannavale A, Ayr U. A Machine Learning Approach to Predict Energy Consumptions in Office and Industrial Buildings as a Function of Weather Data. Tec Ital J Eng Sci 2019;63:452–8. https://doi.org/10.18280/ti-ijes.632-449.

[312] Sarralde JJ, Quinn DJ, Wiesmann D, Steemers K. Solar energy and urban morphology: Scenarios for increasing the renewable energy potential of neighbourhoods in London. Renew Energy 2015;73:10–7. https://doi.org/10.1016/j.renene.2014.06.028.

[313] Zhang J, Xu L, Shabunko V, Tay SER, Sun H, Lau SSY, et al. Impact of urban block typology on building solar potential and energy use efficiency in tropical high-density city. Appl Energy 2019;240:513–33. https://doi.org/10.1016/j.apenergy.2019.02.033.

[314] El Kontar R, Jin X. A Framework for Optimal Placement of Rooftop Photovoltaic: Maximizing Solar Production and Operational Cost Savings in

Residential Communities. ASME J Eng Sustain Build Cities 2020;1. https://doi.org/10.1115/1.4049135.
[315] Alpanda S, Peralta-Alva A. Oil crisis, energy-saving technological change and the stock market crash of 1973–74. Rev Econ Dyn 2010;13:824–42. https://doi.org/10.1016/J.RED.2010.04.003.
[316] Bluszcz A. European economies in terms of energy dependence. Qual Quant 2017;51:1531–48. https://doi.org/10.1007/s11135-016-0350-1.
[317] Vivoda V. Diversification of oil import sources and energy security: A key strategy or an elusive objective? Energy Policy 2009;37:4615–23. https://doi.org/10.1016/J.ENPOL.2009.06.007.
[318] Blumstein C, Krieg B, Schipper L, York C. Overcoming social and institutional barriers to energy conservation. Energy 1980;5:355–71. https://doi.org/10.1016/0360-5442(80)90036-5.
[319] Brown SPA, Huntington HG. OPEC and world oil security. Energy Policy 2017;108:512–23. https://doi.org/10.1016/J.ENPOL.2017.06.034.
[320] Månsson A, Johansson B, Nilsson LJ. Assessing energy security: An overview of commonly used methodologies. Energy 2014;73:1–14. https://doi.org/10.1016/J.ENERGY.2014.06.073.
[321] Bertoldi P. The Paris Agreement 1 . 5 ° C goal: what it does mean for energy efficiency? 2018 ACEEE Summer Study Energy Effic. Build., 2018.
[322] Sovacool BK, Saunders H. Competing policy packages and the complexity of energy security. Energy 2014;67:641–51. https://doi.org/10.1016/J.ENERGY.2014.01.039.
[323] Wiel S, Martin N, Levine M, Price L, Jayant Sathaye. The role of building energy efficiency in managing atmospheric carbon dioxide. Environ Sci Policy 1998;1:27–38. https://doi.org/https://doi.org/10.1016/S1462-9011(98)00004-5.
[324] Geller H, Harrington P, Rosenfeld AH, Tanishima S, Unander F. Polices for increasing energy efficiency: Thirty years of experience in OECD countries. Energy Policy 2006;34:556–73. https://doi.org/10.1016/J.ENPOL.2005.11.010.
[325] Elagöz A. Legal and administrative measures for energy savings in non-industrial buildings in the member states of the EC. Renew Energy 1994;4:109–12. https://doi.org/https://doi.org/10.1016/0960-1481(94)90071-X.
[326] Swisher JN. Regulatory and Mixed Policy Options for Reducing Energy Use and Carbon Emissions. Mitig Adapt Strateg Glob Chang 1996;1:23–49. https://doi.org/10.1023/B:MITI.0000027538.90774.a8.
[327] Axelrod RS. Reconciling energy use with environmental protection in the European Community. Int Environ Aff 1992;4:185–202.
[328] ZGAJEWSK T. ENERGY EFFICIENCY: THE EVER NEGLECTED PRIORITY OF THE EUROPEAN ENERGY STRATEGY. Egmont Institute, Egmont Paper; 2014.
[329] Fawcett T, Killip G. Re-thinking energy efficiency in European policy: Practitioners' use of 'multiple benefits' arguments. J Clean Prod 2019;210:1171–9. https://doi.org/10.1016/J.JCLEPRO.2018.11.026.
[330] Dineen D, Ó Gallachóir BP. Modelling the impacts of building regulations and a property bubble on residential space and water heating. Energy Build 2011;43:166–78.

https://doi.org/https://doi.org/10.1016/j.enbuild.2010.09.004.
[331] Backlund S, Thollander P, Palm J, Ottosson M. Extending the energy efficiency gap. Energy Policy 2012;51:392–6. https://doi.org/https://doi.org/10.1016/j.enpol.2012.08.042.
[332] Dehousse F, Zgajewski T. The EU Climate Policy after the Climate Package and Copenhagen - Promises and Limits. vol. 38. 2010.
[333] da Graça Carvalho M. EU energy and climate change strategy. Energy 2012;40:19–22. https://doi.org/https://doi.org/10.1016/j.energy.2012.01.012.
[334] Veum K, Bauknecht D. How to reach the EU renewables target by 2030? An analysis of the governance framework. Energy Policy 2019;127:299–307. https://doi.org/10.1016/J.ENPOL.2018.12.013.
[335] Fokaides PA, Polycarpou K, Kalogirou S. The impact of the implementation of the European Energy Performance of Buildings Directive on the European building stock: The case of the Cyprus Land Development Corporation. Energy Policy 2017;111:1–8. https://doi.org/10.1016/J.ENPOL.2017.09.009.
[336] Santamouris M. Energy Performance of Residential Buildings: A Practical Guide for Energy Rating and Efficiency. 1st ed. London: Routledge; 2004. https://doi.org/10.4324/9781849776059.
[337] Dascalaki EG, Balaras CA, Gaglia AG, Droutsa KG, Kontoyiannidis S. Energy performance of buildings—EPBD in Greece. Energy Policy 2012;45:469–77. https://doi.org/10.1016/J.ENPOL.2012.02.058.
[338] Blumberga A, Cilinskis E, Gravelsins A, Svarckopfa A, Blumberga D. Analysis of regulatory instruments promoting building energy efficiency. Energy Procedia 2018;147:258–67. https://doi.org/10.1016/J.EGYPRO.2018.07.090.
[339] Ó Broin E, Nässén J, Johnsson F. Energy efficiency policies for space heating in EU countries: A panel data analysis for the period 1990–2010. Appl Energy 2015;150:211–23. https://doi.org/10.1016/J.APENERGY.2015.03.063.
[340] Thonipara A, Runst P, Ochsner C, Bizer K. Energy efficiency of residential buildings in the European Union – An exploratory analysis of cross-country consumption patterns. Energy Policy 2019;129:1156–67. https://doi.org/10.1016/J.ENPOL.2019.03.003.
[341] Ringel M, Knodt M. The governance of the European Energy Union: Efficiency, effectiveness and acceptance of the Winter Package 2016. Energy Policy 2018;112:209–20. https://doi.org/https://doi.org/10.1016/j.enpol.2017.09.047.
[342] Bertoldi P, Economidou M. EU member states energy efficiency policies for the industrial sector based on the NEEAPs analysis. Eceee Ind Summer Study Proc 2018;2018-June:117–27.
[343] Rosenow J. The need for comprehensive and well targeted instrument mixes to stimulate energy transitions: The case of energy efficiency policy. Energy Res Soc Sci 2017;33:95–104. https://doi.org/10.1016/J.ERSS.2017.09.013.
[344] Zangheri P, Serrenho T, Bertoldi P. Energy savings from feedback systems: A meta-studies' review. Energies 2019;12. https://doi.org/10.3390/en12193788.
[345] Bertoldi P, Boza-Kiss B. Analysis of barriers and drivers for the development

of the ESCO markets in Europe. Energy Policy 2017;107:345–55. https://doi.org/10.1016/j.enpol.2017.04.023.
[346] Nabitz L, Hirzel S. Transposing The Requirements of the Energy Efficiency Directive on Mandatory Energy Audits for Large Companies: A Policy-Cycle-based review of the National Implementation in the EU-28 Member States. Energy Policy 2019;125:548–61. https://doi.org/10.1016/J.ENPOL.2017.12.016.
[347] Malinauskaite J, Jouhara H, Ahmad L, Milani M, Montorsi L, Venturelli M. Energy efficiency in industry: EU and national policies in Italy and the UK. Energy 2019;172:255–69. https://doi.org/https://doi.org/10.1016/j.energy.2019.01.130.
[348] Economidou M, Bertoldi P. Financing building energy renovations. Luxembourg: Publications Office of the European Union; 2014. https://doi.org/10.2790/28141.
[349] Bird S, Hernández D. Policy options for the split incentive: Increasing energy efficiency for low-income renters. Energy Policy 2012;48:506–14. https://doi.org/10.1016/J.ENPOL.2012.05.053.
[350] Hilke A, Ryan L. Mobilising investment in energy efficiency: Economic instruments for low-energy buildings. Paris: 2012.
[351] Bürger B. Overview and assessment of new and innovative integrated policy sets that aim at the nZEB standard. 2013.
[352] Rosenow J, Bayer E. Costs and benefits of Energy Efficiency Obligations: A review of European programmes. Energy Policy 2017;107:53–62. https://doi.org/10.1016/J.ENPOL.2017.04.014.
[353] Tsemekidi-Tzeiranaki S, Labanca N, Cuniberti B, Toleikyte A, Zangheri P, Bertoldi P. Analysis of the Annual Reports 2018 under the Energy Efficiency Directive – Summary report. Luxembourg: 2019.
[354] Eyre N. Energy saving in energy market reform—The feed-in tariffs option. Energy Policy 2013;52:190–8. https://doi.org/10.1016/J.ENPOL.2012.07.042.
[355] Boza-Kiss B, Bertoldi P. One-stop-shops for energy renovations of buildings - case studies. Ispra: European Commission,; 2018.
[356] Boza-Kiss B, Bertoldi P. One-stop shops for residential building renovation in the EU - Part 2: Analysis. Luxembourg: Publications Office of the European Union; 2019. https://doi.org/10.2760/XXXXX.
[357] Blom M, Vergeer R, Forster D. Mapping , analysing and benchmarking of Energy Efficiency schemes in the EU. Eur Comm DG Energy 2018.
[358] Maio J, Zinetti S, Rod J. Energy Efficiency Policies in Buildings- the Use of Financial Instruments at Member State Level 2012:1–44.
[359] IEA. Global Status Report 2017. Towards a zero-emission, efficient, and resilient buildings and construction sector. 2017.
[360] Amon A, Holmes I. Energy Efficiency as Infrastructure: Leaping the Investment Gap 2016:1–16.
[361] Ordanini A, Miceli L, Pizzetti M, Parasuraman A. Crowd-funding: transforming customers into investors through innovative service platforms. J Serv Manag 2011;22:443–70.
[362] Bertheau P, Blechinger P. Resilient solar energy island supply to support SDG7 on the Philippines: Techno-economic optimized electrification strategy for small islands. Util Policy 2018;54:55–77.

https://doi.org/10.1016/J.JUP.2018.07.005.
[363] Zou J, Chang Q, Ou X, Arinez J, Xiao G. Resilient adaptive control based on renewal particle swarm optimization to improve production system energy efficiency. J Manuf Syst 2019;50:135–45. https://doi.org/10.1016/J.JMSY.2018.12.007.
[364] Baniassadi A, Heusinger J, Sailor DJ. Energy efficiency vs resiliency to extreme heat and power outages: The role of evolving building energy codes. Build Environ 2018;139:86–94. https://doi.org/10.1016/J.BUILDENV.2018.05.024.
[365] Bagheri M, Delbari SH, Pakzadmanesh M, Kennedy CA. City-integrated renewable energy design for low-carbon and climate-resilient communities. Appl Energy 2019;239:1212–25. https://doi.org/10.1016/J.APENERGY.2019.02.031.
[366] Ul Abdin Z, Rachid A. A Survey on Applications of Hybrid PV/T Panels. Energies 2021;14. https://doi.org/10.3390/en14041205.
[367] Beccali M, Bonomolo M, Di Pietra B, Leone G, Martorana F. Solar and Heat Pump Systems for Domestic Hot Water Production on a Small Island: The Case Study of Lampedusa. Appl Sci 2020;10. https://doi.org/10.3390/app10175968.
[368] Staffell I, Pfenninger S. The increasing impact of weather on electricity supply and demand. Energy 2018;145:65–78. https://doi.org/10.1016/j.energy.2017.12.051.